

Innate immune dysregulation: a driving force of autoimmunity and chronic inflammation

Edited by

Jens Y. Humrich, Tamas Nemeth, Kyle T. Amber
and Reza Akbarzadeh

Published in

Frontiers in Immunology



FRONTIERS EBOOK COPYRIGHT STATEMENT

The copyright in the text of individual articles in this ebook is the property of their respective authors or their respective institutions or funders. The copyright in graphics and images within each article may be subject to copyright of other parties. In both cases this is subject to a license granted to Frontiers.

The compilation of articles constituting this ebook is the property of Frontiers.

Each article within this ebook, and the ebook itself, are published under the most recent version of the Creative Commons CC-BY licence. The version current at the date of publication of this ebook is CC-BY 4.0. If the CC-BY licence is updated, the licence granted by Frontiers is automatically updated to the new version.

When exercising any right under the CC-BY licence, Frontiers must be attributed as the original publisher of the article or ebook, as applicable.

Authors have the responsibility of ensuring that any graphics or other materials which are the property of others may be included in the CC-BY licence, but this should be checked before relying on the CC-BY licence to reproduce those materials. Any copyright notices relating to those materials must be complied with.

Copyright and source acknowledgement notices may not be removed and must be displayed in any copy, derivative work or partial copy which includes the elements in question.

All copyright, and all rights therein, are protected by national and international copyright laws. The above represents a summary only. For further information please read Frontiers' Conditions for Website Use and Copyright Statement, and the applicable CC-BY licence.

ISSN 1664-8714
ISBN 978-2-8325-6481-3
DOI 10.3389/978-2-8325-6481-3

Generative AI statement

Any alternative text (Alt text) provided alongside figures in the articles in this ebook has been generated by Frontiers with the support of artificial intelligence and reasonable efforts have been made to ensure accuracy, including review by the authors wherever possible. If you identify any issues, please contact us.

About Frontiers

Frontiers is more than just an open access publisher of scholarly articles: it is a pioneering approach to the world of academia, radically improving the way scholarly research is managed. The grand vision of Frontiers is a world where all people have an equal opportunity to seek, share and generate knowledge. Frontiers provides immediate and permanent online open access to all its publications, but this alone is not enough to realize our grand goals.

Frontiers journal series

The Frontiers journal series is a multi-tier and interdisciplinary set of open-access, online journals, promising a paradigm shift from the current review, selection and dissemination processes in academic publishing. All Frontiers journals are driven by researchers for researchers; therefore, they constitute a service to the scholarly community. At the same time, the *Frontiers journal series* operates on a revolutionary invention, the tiered publishing system, initially addressing specific communities of scholars, and gradually climbing up to broader public understanding, thus serving the interests of the lay society, too.

Dedication to quality

Each Frontiers article is a landmark of the highest quality, thanks to genuinely collaborative interactions between authors and review editors, who include some of the world's best academicians. Research must be certified by peers before entering a stream of knowledge that may eventually reach the public - and shape society; therefore, Frontiers only applies the most rigorous and unbiased reviews. Frontiers revolutionizes research publishing by freely delivering the most outstanding research, evaluated with no bias from both the academic and social point of view. By applying the most advanced information technologies, Frontiers is catapulting scholarly publishing into a new generation.

What are Frontiers Research Topics?

Frontiers Research Topics are very popular trademarks of the *Frontiers journals series*: they are collections of at least ten articles, all centered on a particular subject. With their unique mix of varied contributions from Original Research to Review Articles, Frontiers Research Topics unify the most influential researchers, the latest key findings and historical advances in a hot research area.

Find out more on how to host your own Frontiers Research Topic or contribute to one as an author by contacting the Frontiers editorial office: frontiersin.org/about/contact

Innate immune dysregulation: a driving force of autoimmunity and chronic inflammation

Topic editors

Jens Y. Humrich — University Hospital Schleswig-Holstein, Campus Lübeck, Germany

Tamas Nemeth — Semmelweis University, Hungary

Kyle T. Amber — Rush University, United States

Reza Akbarzadeh — University of Lübeck, Germany

Citation

Humrich, J. Y., Nemeth, T., Amber, K. T., Akbarzadeh, R., eds. (2025). *Innate immune dysregulation: a driving force of autoimmunity and chronic inflammation*. Lausanne: Frontiers Media SA. doi: 10.3389/978-2-8325-6481-3

Table of contents

05	Editorial: Innate immune dysregulation: a driving force of autoimmunity and chronic inflammation Reza Akbarzadeh, Jens Y. Humrich, Tamás Németh and Kyle T. Amber
10	Mincle receptor in macrophage and neutrophil contributes to the unresolved inflammation during the transition from acute kidney injury to chronic kidney disease Cui Wang, Yilin Zhang, Anran Shen, Taotao Tang, Ning Li, Chuanhui Xu, Bicheng Liu and Linli Lv
24	An early regulatory mechanism of hyperinflammation by restricting monocyte contribution Megumi Akiyama, Masashi Kanayama, Yoshihiro Umezawa, Toshikage Nagao, Yuta Izumi, Masahide Yamamoto and Toshiaki Ohteki
40	Dysregulated complement activation during acute myocardial infarction leads to endothelial glycocalyx degradation and endothelial dysfunction via the C5a:C5a-Receptor1 axis Carl Vahldieck, Samuel Löning, Constantin Hamacher, Benedikt Fels, Bettina Rudzewski, Laura Nickel, Joachim Weil, Henry Nording, Lasse Baron, Marie Kleingarn, Christian Marcel Karsten and Kristina Kusche-Vihrog
59	Increased neutrophil extracellular trap formation in oligoarticular, polyarticular juvenile idiopathic arthritis and enthesitis-related arthritis: biomarkers for diagnosis and disease activity Hongxia Tang, Yucheng Zhong, Yali Wu, Yanmei Huang, Yi Liu, Jing Chen, Ting Xi, Yini Wen, Ting He, Shanshan Yang, Fan Liu, Runji Xiong and Runming Jin
74	The emerging role of neutrophil extracellular traps in the progression of rheumatoid arthritis Jingjing Chen, Yang Cao, Jing Xiao, Yujie Hong and Yan Zhu
85	The role of cGAS-STING signaling in rheumatoid arthritis: from pathogenesis to therapeutic targets Qiugang Zhu and Huimin Zhou
97	Molecular mechanisms of obesity predisposes to atopic dermatitis Dajin Shang and Shengnan Zhao
108	Inflammasomes and idiopathic inflammatory myopathies Rui Sun, Jiyan Chu and Ping Li
127	Nanoparticles containing intracellular proteins modulate neutrophil functional and phenotypic heterogeneity Leonore Raudszus, Farbod Bahreini, Susanne Allan, Kai-Uwe Kalies, Charles C. Caldwell and Kathrin Kalies

- 143 **ARHGAP25: a novel player in the Pathomechanism of allergic contact hypersensitivity**
Domonkos Czárán, Péter Sasvári, Kende Lőrincz, Krisztina Ella, Virág Gellén and Roland Csépanyi-Kömi
- 160 **Current perspectives and trends of neutrophil extracellular traps in organ fibrosis: a bibliometric and visualization study**
Yanbo Li, Zhengmin Cao, Jing Liu, Rui Qiang, Jiuchong Wang and Wenliang Lyu
- 173 **IRAK3 is upregulated in rheumatoid arthritis synovium and delays the onset of experimental arthritis**
Federica Borghese, Richard O. Williams and Felix I. L. Clanchy
- 183 **Fbxo16 mediates degradation of NF- κ B p65 subunit and inhibits inflammatory response in dendritic cells**
Akiko Sugimoto-Ishige, Aya Jodo and Takashi Tanaka



OPEN ACCESS

EDITED AND REVIEWED BY
Francesca Granucci,
University of Milano-Bicocca, Italy

*CORRESPONDENCE
Reza Akbarzadeh
✉ r.akbarzadeh@uni-luebeck.de

RECEIVED 21 May 2025
ACCEPTED 26 May 2025
PUBLISHED 09 June 2025

CITATION

Akbarzadeh R, Humrich JY, Németh T
and Amber KT (2025) Editorial: Innate
immune dysregulation: a driving force of
autoimmunity and chronic inflammation.
Front. Immunol. 16:1632416.
doi: 10.3389/fimmu.2025.1632416

COPYRIGHT

© 2025 Akbarzadeh, Humrich, Németh and
Amber. This is an open-access article
distributed under the terms of the [Creative
Commons Attribution License \(CC BY\)](#). The
use, distribution or reproduction in other
forums is permitted, provided the original
author(s) and the copyright owner(s) are
credited and that the original publication in
this journal is cited, in accordance with
accepted academic practice. No use,
distribution or reproduction is permitted
which does not comply with these terms.

Editorial: Innate immune dysregulation: a driving force of autoimmunity and chronic inflammation

Reza Akbarzadeh^{1*}, Jens Y. Humrich¹, Tamás Németh^{2,3,4,5}
and Kyle T. Amber⁶

¹Department of Rheumatology and Clinical Immunology, University of Lübeck, Lübeck, Germany,

²Department of Physiology, Semmelweis University School of Medicine, Budapest, Hungary, ³MTA-SE
"Lendület" Translational Rheumatology Research Group, Hungarian Academy of Sciences and
Semmelweis University, Budapest, Hungary, ⁴Department of Rheumatology and Immunology,
Semmelweis University, Budapest, Hungary, ⁵Department of Internal Medicine and Oncology,
Semmelweis University, Budapest, Hungary, ⁶Department of Dermatology, Rush University Medical
Center, Chicago, IL, United States

KEYWORDS

innate immunity, immune dysregulation, autoimmunity, chronic inflammation,
inflammatory mechanisms

Editorial on the Research Topic

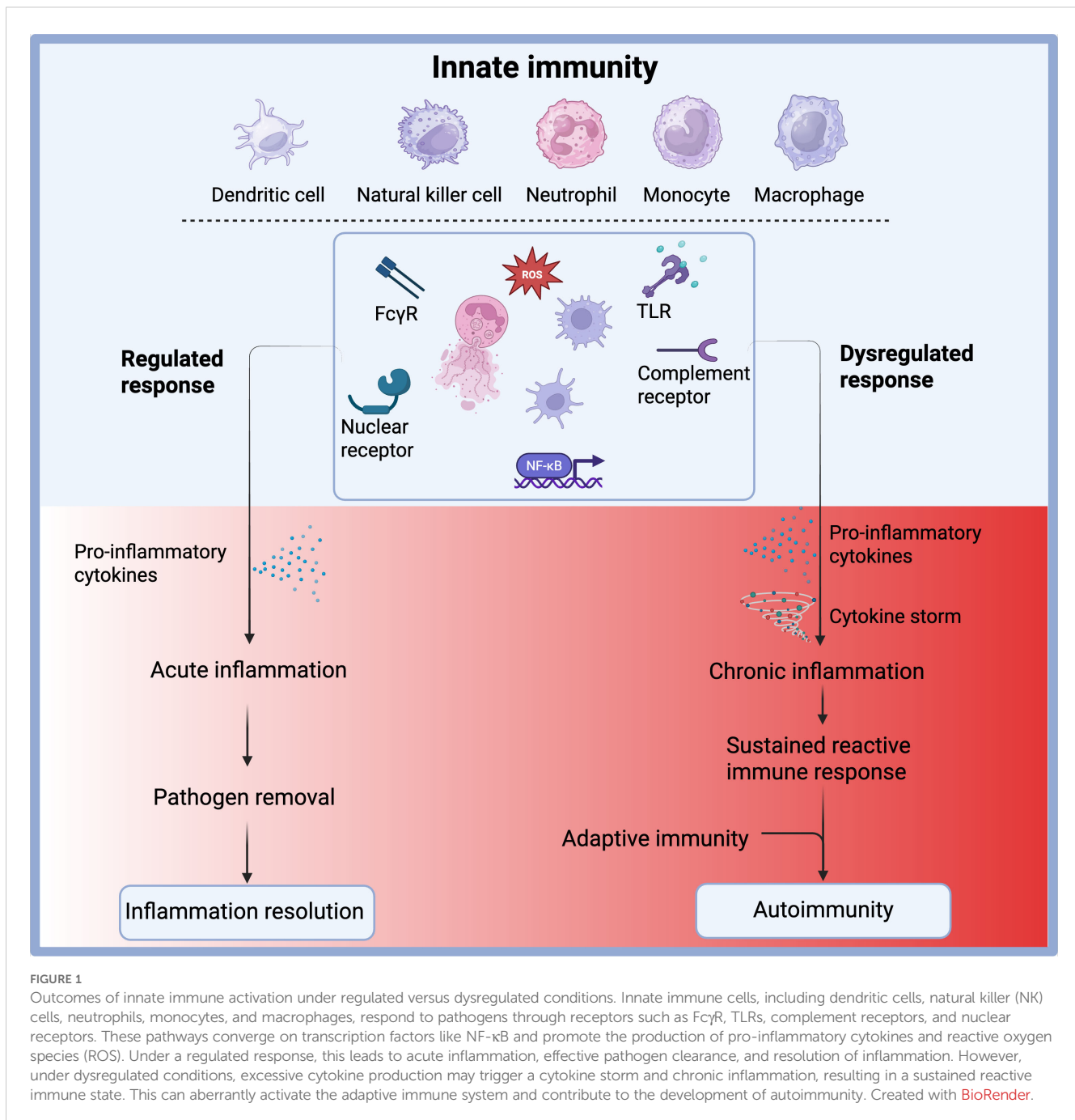
**Innate immune dysregulation: a driving force of autoimmunity and
chronic inflammation**

1 Introduction

Innate immunity plays a critical role in protecting the host against infections, tumors, and tissue damage by initiating inflammatory responses, recruiting immune cells, and orchestrating the production of both pro- and anti-inflammatory mediators (1). Traditionally considered the first line of defense, emerging evidence reveals that innate immunity operates through far more complex mechanisms. It not only responds to a wide array of pathogens but also engages in intricate crosstalk with the adaptive immune system (2). Importantly, its dysregulation is increasingly linked to various pathological conditions.

The initiation, activation, and resolution of innate inflammatory responses must be tightly controlled to ensure effective pathogen clearance and preservation of tissue homeostasis, while preventing excessive or prolonged inflammation. When this regulation fails, it can lead to autoinflammatory diseases and significantly contribute to chronic inflammation and autoimmune disorders (Figure 1) (3) such as systemic lupus erythematosus (SLE), rheumatoid arthritis (RA), and juvenile idiopathic arthritis (JIA). Although autoimmune diseases are typically characterized by a breakdown in self-tolerance associated with the adaptive immune system, the innate immune system plays a fundamental role in their onset, progression, and chronicity.

Over recent decades, autoimmune and chronic inflammatory diseases have become a growing clinical challenge, marked by rising incidence and a lack of effective, long-term treatments (4, 5). Despite advances in understanding their underlying mechanisms, current



therapies largely rely on non-specific immunosuppressants, which are limited by suboptimal efficacy and potential safety concerns. These limitations often result in high disease burden, morbidity, and, in many cases, mortality. There is, therefore, an urgent unmet medical need for precisely modulating innate immune responses that reduce pathological inflammation without compromising overall immune function. Given the significant role of innate immune dysregulation in driving autoimmune and chronic inflammatory conditions, fostering scientific insights into the mechanisms by which innate immunity contributes to

autoimmunity and chronic inflammation holds promise for identifying new therapeutic targets.

2 Molecular mechanisms of inflammation regulation

While the activation of immune responses is necessary to defend the body, unchecked or prolonged inflammation can lead to tissue damage and chronic disease. A central component of this

regulation is the transcription factor NF- κ B, which orchestrates the expression of pro-inflammatory genes during infections or tissue injury. However, NF- κ B must be swiftly inactivated once the threat is resolved. This is where proteins like PDLIM2, an E3 ubiquitin ligase, come into play. PDLIM2 targets the p65 subunit of NF- κ B for degradation, effectively silencing the inflammatory signal. Recent research by Sugimoto-Ishige et al. revealed that the F-box protein Fbxo16 is critical in this process. Fbxo16 enables PDLIM2 to interact with p65 within the nucleus. Without Fbxo16, p65 accumulates, prolonging cytokine production and increasing the risk of chronic inflammation (6).

Another important checkpoint is provided by IRAK3, a negative regulator of Toll-like receptor (TLR) and interleukin-1 receptor (IL-1R) signaling. Borghese et al. demonstrated that mice lacking IRAK3 exhibit more severe inflammatory arthritis. They produce higher levels of IL-1 β and show reduced numbers of regulatory T cells, suggesting impaired immune tolerance. Moreover, IRAK3 expression is often diminished in autoimmune conditions such as SLE and inflammatory bowel disease, highlighting its relevance in human disease (7, 8).

In a different regulatory context, ARHGAP25, a Rho GTPase-activating protein, controls cytoskeletal dynamics and cell migration (9). Czárán et al. found that mice deficient in ARHGAP25 had significantly milder allergic contact dermatitis, associated with reduced immune cell migration and activation. This suggests that manipulating cytoskeletal signaling could represent a novel approach to treating chronic inflammation.

3 Innate immune cells and components in disease progression

Innate immune components are crucial regulators of inflammation. In JIA, Tang et al. reported an increased NET formation correlates with disease activity. Anti-TNF therapies reduce NET formation, indicating that NETs may serve as both biomarkers and therapeutic targets (10, 11). It has also been shown that the complement system, particularly the C5a-C5aR1 axis, is another potent driver of inflammation. An original article published by Vahldieck et al. indicated that in acute myocardial infarction, C5a disrupts the endothelial glycocalyx, reduces nitric oxide bioavailability, and recruits inflammatory cells, contributing to tissue injury. C5aR1 antagonists show therapeutic potential by preserving vascular integrity and reducing inflammation (12).

Besides these molecules, innate immune cells such as monocytes and macrophages play a key role in immune regulation. In the article by Akiyama et al., it has been shown that during hyperinflammatory conditions, such as cytokine release syndrome, monocytes undergo apoptosis to prevent overwhelming cytokine production. Disruption of this process, as shown in mouse models, leads to exaggerated immune responses and higher mortality. Maintaining monocyte homeostasis through controlled cell death or immunomodulation is emerging as a critical strategy in

preventing systemic inflammatory damage (13, 14). Furthermore, Wang et al. identified that marked expression of Mincle receptors, transmembrane pattern recognition receptors on macrophages and neutrophils, exert pro-inflammatory and pro-fibrotic effects, involved in persistence of renal inflammatory microenvironment and accelerated renal fibrosis progression by inducing TNF production (15, 16).

4 Neutrophils in immunity and autoimmunity: balancing host defense and inflammation

Neutrophils are among the first responders in innate immunity, essential for eliminating pathogens. However, their prolonged activation can exacerbate inflammation, especially in sterile conditions. One key process is the formation of neutrophil extracellular traps (NETs), webs of DNA, histones, and granule proteins that capture microbes but also stimulate autoimmunity if dysregulated (10, 11). Li et al. reviewed the involvement of NETs in fibrotic and sterile inflammatory diseases. In conditions such as RA, NETs release modified self-antigens that provoke adaptive immune responses. Chen et al. showed that citrullinated proteins within NETs activate dendritic cells, encouraging T cell activation and the production of autoantibodies, thereby fueling the autoimmune cycle.

Given the dual nature of neutrophils, new strategies aim to reprogram rather than eliminate them. Raudszus et al. used cell-derived nanoparticles (CDNPs) to modulate neutrophil function. These CDNPs induced an anti-inflammatory phenotype, marked by increased IL-10 production and programmed cell death, facilitating inflammation resolution without compromising microbial defense. Such approaches reflect a growing interest in using nanomedicine to selectively steer immune cell function (17).

5 Inflammasomes and cytosolic DNA sensors as central drivers of chronic inflammation

Inflammasomes are multiprotein complexes that detect intracellular threats and activate caspase-1, leading to the release of IL-1 β and IL-18 and triggering pyroptosis, a highly inflammatory form of cell death. The NLRP3 and AIM2 inflammasomes are the most studied and are increasingly implicated in chronic inflammatory diseases (18, 19). In idiopathic inflammatory myopathies, Sun et al. found that overactivation of NLRP3 and AIM2 correlates with disease severity. Inhibitors like MCC950, which specifically block NLRP3 activation, reduced inflammation in preclinical models and are being investigated in clinical trials (20, 21).

Parallel to inflammasomes, the cytosolic DNA sensing pathway, particularly cGAS-STING, is another major contributor to chronic inflammation. The article by Zhu and Zhou explained that while

this pathway is vital in recognizing viral DNA, it can be aberrantly triggered by self-DNA released during cellular stress or apoptosis. The result is the chronic production of type I interferons and pro-inflammatory cytokines, a hallmark of diseases like SLE and dermatomyositis (22, 23). Small-molecule inhibitors of STING are currently under development, aiming to mitigate this persistent immune activation (24).

6 Metabolic and systemic influences on immune function

Beyond molecular signaling, immune function is tightly linked to systemic metabolic cues. Obesity, for instance, promotes chronic low-grade inflammation and can exacerbate inflammatory disorders. Shang and Zhao demonstrated that obesity impairs skin barrier integrity, alters the microbiome, and increases inflammatory mediators such as TNF- α and leptin. These changes worsen conditions like atopic dermatitis and reduce treatment efficacy (25, 26).

In contrast, nuclear receptors such as PPAR- γ serve as anti-inflammatory regulators. PPAR- γ activation inhibits pro-inflammatory gene transcription and promotes lipid metabolism, improving epithelial integrity and immune tolerance. Agonists targeting PPAR- γ have shown promise in reducing inflammation, particularly in obesity-related immune disorders (27, 28). This highlights the therapeutic potential of integrating metabolic interventions into inflammatory disease management.

References

- Janeway CA, Medzhitov R. Innate immune recognition. *Annu Rev Immunol*. (2002) 20:197–216. doi: 10.1146/annurev.immunol.20.083001.084359
- Takeuchi O, Akira S. Pattern recognition receptors and inflammation. *Cell*. (2010) 140:805–20. doi: 10.1016/j.cell.2010.01.022
- Xiong T, Turner JE. Innate lymphoid cells in autoimmunity and chronic inflammatory diseases. *Semin Immunopathol*. (2018) 40:393–406. doi: 10.1007/s00281-018-0670-4
- Miller FW. The increasing prevalence of autoimmunity and autoimmune diseases: an urgent call to action for improved understanding, diagnosis, treatment, and prevention. *Curr Opin Immunol*. (2023) 80:102266. doi: 10.1016/j.coi.2022.102266
- Schultze JL, Rosenstiel P. Systems medicine in chronic inflammatory diseases. *Immunity*. (2018) 48:608–13. doi: 10.1016/j.immuni.2018.03.022
- Tanaka T, Grusby MJ, Kaisho T. PDLIM2-mediated termination of transcription factor NF- κ B activation by intranuclear sequestration and degradation of the p65 subunit. *Nat Immunol*. (2007) 8:584–91. doi: 10.1038/ni1464
- Kobayashi K, Hernandez LD, Galán JE, Janeway CA, Medzhitov R, Flavell RA. IRAK-M is a negative regulator of Toll-like receptor signaling. *Cell*. (2002) 110:191–202. doi: 10.1016/S0092-8674(02)00827-9
- Ban T, Sato GR, Nishiyama A, Akiyama A, Takasuna M, Umehara M, et al. Lyn kinase suppresses the transcriptional activity of IRF5 in the TLR-myd88 pathway to restrain the development of autoimmunity. *Immunity*. (2016) 45:319–32. doi: 10.1016/j.immuni.2016.07.015
- Csepányi-Kömi R, Sirokmány G, Geiszt M, Ligeti E. ARHGAP25, a novel Rac GTPase-activating protein, regulates phagocytosis in human neutrophilic granulocytes. *Blood*. (2012) 119:573–82. doi: 10.1182/blood-2010-12-324053
- Khandpur R, Carmona-Rivera C, Vivekanandan-Giri A, Gizinski A, Yalavarthi S, Knight JS, et al. NETs are a source of citrullinated autoantigens and stimulate inflammatory responses in rheumatoid arthritis. *Sci Transl Med*. (2013) 5:178ra40. doi: 10.1126/scitranslmed.3005580
- Llood C, Blanco LP, Purmalek MM, Carmona-Rivera C, De Ravin SS, Smith CK, et al. Neutrophil extracellular traps enriched in oxidized mitochondrial DNA are interferogenic and contribute to lupus-like disease. *Nat Med*. (2016) 22:146–53. doi: 10.1038/nm.4027
- Noris M, Remuzzi G. Overview of complement activation and regulation. *Semin Nephrol*. (2013) 33:479–92. doi: 10.1016/j.semnephrol.2013.08.001
- Weber GF, Chousterman BG, He S, Fenn AM, Nairz M, Anzai A, et al. Interleukin-3 amplifies acute inflammation and is a potential therapeutic target in sepsis. *Science*. (2015) 347:1260–5. doi: 10.1126/science.aaa4268
- Hotchkiss RS, Monneret G, Payen D. Sepsis-induced immunosuppression: from cellular dysfunctions to immunotherapy. *Nat Rev Immunol*. (2013) 13:862–74. doi: 10.1038/nri3552
- Ishikawa E, Ishikawa T, Morita YS, Toyonaga K, Yamada H, Takeuchi O, et al. Direct recognition of the mycobacterial glycolipid, trehalose dimycolate, by C-type lectin Mincle. *J Exp Med*. (2009) 206:2879–88. doi: 10.1084/jem.20091750
- Ly LL, Tang PM, Li CJ, You YK, Li J, Huang XR, et al. The pattern recognition receptor, Mincle, is essential for maintaining the M1 macrophage phenotype in acute renal inflammation. *Kidney Int*. (2017) 91:587–602. doi: 10.1016/j.kint.2016.10.020
- Fattal E, Fay F. Nanomedicine-based delivery strategies for nucleic acid gene inhibitors in inflammatory diseases. *Adv Drug Delivery Rev*. (2021) 175:113809. doi: 10.1016/j.addr.2021.05.019
- Fernandes-Alnemri T, Yu JW, Juliana C, Solorzano L, Kang S, Wu J, et al. The AIM2 inflammasome is critical for innate immunity to *Francisella tularensis*. *Nat Immunol*. (2010) 11:385–93. doi: 10.1038/ni.1859
- Chen Y, Ye X, Escames G, Lei W, Zhang X, Li M, et al. The NLRP3 inflammasome: contributions to inflammation-related diseases. *Cell Mol Biol Lett*. (2023) 28:51. doi: 10.1186/s11658-023-00462-9
- Coll RC, Robertson AA, Chae JJ, Higgins SC, Muñoz-Planillo R, Inerra MC, et al. A small-molecule inhibitor of the NLRP3 inflammasome for the treatment of inflammatory diseases. *Nat Med*. (2015) 21:248–55. doi: 10.1038/nm.3806

Author contributions

RA: Writing – original draft, Writing – review & editing. JH: Writing – review & editing. TN: Writing – review & editing. KA: Writing – review & editing.

Conflict of interest

The authors declare that the research was conducted in the absence of any commercial or financial relationships that could be construed as a potential conflict of interest.

Generative AI statement

The author(s) declare that no Generative AI was used in the creation of this manuscript.

Publisher's note

All claims expressed in this article are solely those of the authors and do not necessarily represent those of their affiliated organizations, or those of the publisher, the editors and the reviewers. Any product that may be evaluated in this article, or claim that may be made by its manufacturer, is not guaranteed or endorsed by the publisher.

21. Mangan MSJ, Olhava EJ, Roush WR, Seidel HM, Glick GD, Latz E. Targeting the NLRP3 inflammasome in inflammatory diseases. *Nat Rev Drug Discov.* (2018) 17:588–606. doi: 10.1038/nrd.2018.97
22. Crowl JT, Gray EE, Pestal K, Volkman HE, Stetson DB. Intracellular nucleic acid detection in autoimmunity. *Annu Rev Immunol.* (2017) 35:313–36. doi: 10.1146/annurev-immunol-051116-052331
23. Motwani M, Pesiridis S, Fitzgerald KA. DNA sensing by the cGAS-STING pathway in health and disease. *Nat Rev Genet.* (2019) 20:657–74. doi: 10.1038/s41576-019-0151-1
24. Haag SM, Gulen MF, Reymond L, Gibelin A, Abrami L, Decout A, et al. Targeting STING with covalent small-molecule inhibitors. *Nature.* (2018) 559:269–73. doi: 10.1038/s41586-018-0287-8
25. Hotamisligil GS. Inflammation, metaflammation and immunometabolic disorders. *Nature.* (2017) 542:177–85. doi: 10.1038/nature21363
26. Egawa G, Kabashima K. Barrier dysfunction in the skin allergy. *Allergol Int.* (2018) 67:3–11. doi: 10.1016/j.alit.2017.10.002
27. Széles L, Töröcsik D, Nagy L. PPARgamma in immunity and inflammation: cell types and diseases. *Biochim Biophys Acta.* (2007) 1771:1014–30 doi: 10.1016/j.bbali.2007.02.005.
28. Glass CK, Saijo K. Nuclear receptor transrepression pathways that regulate inflammation in macrophages and T cells. *Nat Rev Immunol.* (2010) 10:365–76. doi: 10.1038/nri2748



OPEN ACCESS

EDITED BY

Jia Xiao,
Jinan University, China

REVIEWED BY

Bin Yang,
University of Leicester, United Kingdom
Li Wang,
Southwest Medical University, China

*CORRESPONDENCE

Linli Lv
✉ lvlinli@seu.edu.cn

[†]These authors have contributed
equally to this work and share
first authorship

RECEIVED 13 February 2024

ACCEPTED 10 April 2024

PUBLISHED 17 May 2024

CITATION

Wang C, Zhang Y, Shen A, Tang T, Li N, Xu C,
Liu B and Lv L (2024) Mincle receptor in
macrophage and neutrophil contributes to
the unresolved inflammation during the
transition from acute kidney injury to chronic
kidney disease.
Front. Immunol. 15:1385696.
doi: 10.3389/fimmu.2024.1385696

COPYRIGHT

© 2024 Wang, Zhang, Shen, Tang, Li, Xu, Liu
and Lv. This is an open-access article
distributed under the terms of the [Creative
Commons Attribution License \(CC BY\)](#). The
use, distribution or reproduction in other
forums is permitted, provided the original
author(s) and the copyright owner(s) are
credited and that the original publication in
this journal is cited, in accordance with
accepted academic practice. No use,
distribution or reproduction is permitted
which does not comply with these terms.

Mincle receptor in macrophage and neutrophil contributes to the unresolved inflammation during the transition from acute kidney injury to chronic kidney disease

Cui Wang[†], Yilin Zhang[†], Anran Shen, Taotao Tang, Ning Li,
Chuanhui Xu, Bicheng Liu and Linli Lv*

Institute of Nephrology, Zhongda Hospital, Southeast University School of Medicine, Nanjing,
Jiangsu, China

Background: Recent studies have demonstrated a strong association between acute kidney injury (AKI) and chronic kidney disease (CKD), while the unresolved inflammation is believed to be a driving force for this chronic transition process. As a transmembrane pattern recognition receptor, Mincle (macrophage-inducible C-type lectin, Clec4e) was identified to participate in the early immune response after AKI. However, the impact of Mincle on the chronic transition of AKI remains largely unclear.

Methods: We performed single-cell RNA sequencing (scRNA-seq) with the unilateral ischemia-reperfusion (UIR) murine model of AKI at days 1, 3, 14 and 28 after injury. Potential effects and mechanism of Mincle on renal inflammation and fibrosis were further validated *in vivo* utilizing Mincle knockout mice.

Results: The dynamic expression of Mincle in macrophages and neutrophils throughout the transition from AKI to CKD was observed. For both cell types, Mincle expression was significantly up-regulated on day 1 following AKI, with a second rise observed on day 14. Notably, we identified distinct subclusters of Mincle^{high} neutrophils and Mincle^{high} macrophages that exhibited time-dependent influx with dual peaks characterized with remarkable pro-inflammatory and pro-fibrotic functions. Moreover, we identified that Mincle^{high} neutrophils represented an “aged” mature neutrophil subset derived from the “fresh” mature neutrophil cluster in kidney. Additionally, we observed a synergistic mechanism whereby Mincle-expressing macrophages and neutrophils sustained renal inflammation by tumor necrosis factor (TNF) production. Mincle-deficient mice exhibited reduced renal injury and fibrosis following AKI.

Conclusion: The present findings have unveiled combined persistence of Mincle^{high} neutrophils and macrophages during AKI-to-CKD transition, contributing to unresolved inflammation followed by fibrosis via TNF- α as a central pro-inflammatory cytokine. Targeting Mincle may offer a novel therapeutic strategy for preventing the transition from AKI to CKD.

KEYWORDS

unresolved inflammation, Mincle, macrophage, neutrophil, acute kidney injury, chronic kidney disease

Introduction

As a widespread clinical syndrome with acute renal dysfunction, acute kidney injury (AKI) could progress to chronic kidney disease (CKD) with high risk, which is characterized with fibrotic structural lesions (1). However, the mechanism underlies the progression from AKI to CKD remains unclear. Inflammation plays a dual role, being essential for renal repair while also acting as a potential driver of sustained kidney damage leading to CKD (2–5). Therefore, depicting the mechanism of unresolved inflammation during this chronic transition process is of great significance.

The onset of AKI prompts an immediate and robust innate inflammatory response characterized by rapid recruitment of neutrophils and natural killer cells followed by infiltration and activation of monocytes/macrophages and resident dendritic cells, which further stimulate the adaptive immune responses (3, 6). The innate immunity triggered by AKI produce a spectrum of inflammatory mediators, meanwhile, damage-associated molecular patterns (DAMPs) facilitate the recruitment and/or persistence of various inflammatory cells (3, 7). As the disease progresses, if injury is not resolved, prolonged inflammation can result in maladaptive repair and subsequent uncontrolled fibrosis (8–10). However, the precise mechanism driving the formation of the inflammatory milieu and the role of innate immune cells in the unresolved situation have yet to be completely delineated. Phenotypic and functional plasticity of innate immune cells increase the complexity of the context. Recently, emerging single-cell genomic studies have provided novel insights into the heterogeneity of innate immune cells during the process of renal inflammation and fibrosis (11–14).

Mincle (macrophage-inducible C-type lectin, Clec4e), recognized as a pattern recognition receptor is mainly expressed in innate immune cells including monocytes/macrophages, neutrophils and dendritic cells (15–17). Previous researches have uncovered the significant involvement of Mincle in both infectious diseases and sterile inflammation, wherein it prompts the secretion of pro-inflammatory cytokines and chemokines upon activation by its ligands encompassing pathogen-associated molecular patterns (PAMPs) or DAMPs (18–20). We have previously reported that Mincle could induce aggravated renal inflammation in the context of AKI by maintaining pro-inflammatory phenotype of macrophages, thereby contributing to the deterioration of kidney injury (21, 22). Importantly, Mincle was suggested to recognize β -glucosylceramide and free cholesterol released from dead tubular cells, thereby contributing to the cell death-induced sustained inflammation and renal atrophy (23). However, given the diversity and heterogeneity of innate immune cells, the dynamic profiling of Mincle in distinct populations of these cells and their contribution to the chronic progression of AKI after the initial kidney injury remains poorly understood.

Here, we applied single-cell RNA sequencing (scRNA-seq) and spatial transcriptomics in a unilateral ischemia-reperfusion (UIR) murine model of AKI at days 1, 3, 14 and 28 after injury. This study unveiled the combined persistence of Mincle^{high} neutrophils and macrophages during AKI-to-CKD transition, contributing to unresolved inflammation followed by fibrosis via tumor necrosis

factor (TNF) as a central pro-inflammatory cytokine. Mincle-deficient mice showed improved renal pathology and reduced extracellular matrix deposition, suggesting that targeting Mincle may offer a novel therapeutic avenue for halting chronic progression of AKI.

Materials and methods

Preparation of single-cell suspension

Each kidney sample from three mice was minced and digested using the Multi Tissue dissociation kit (Miltenyi, 130-110-203), followed by homogenization through syringe-based mechanical disruption. The kidney tissue was enzymatically digested using a mixture of collagenase I, collagenase IV, and hyaluronidase in 1640 medium (Gibco, USA) at 37°C for 40 minutes while suppressing the response with 10% fetal bovine serum (FBS). The resulting dissociated solution was passed through 70- μ m cell strainer and then was centrifuged at 400g for 5min at 4°C to collect the cell pellet. To remove any remaining erythrocytes, the red blood cell (RBC) lysis solution (Miltenyi, 130-094-183) was applied on ice. Finally, the single-cell suspension was obtained with over 90% viability as detected by Countstar (Alit Biotech, Rigel S2).

Single-cell RNA-seq library generation and sequencing

This process was performed by CapitalBio Technology in Beijing. The harvested cell suspension was processed with the Chromium single-cell controller (10x Genomics, GCG-SR-1) and the Single Cell G Chip Kit (10x Genomics, 1000120) to generate the single-cell gel beads in the emulsion. The reverse transcription was performed with the S1000TM Touch Thermal Cycler (Bio Rad) following a procedure of 53°C for 45 minutes, 85°C for 5 minutes and a subsequent hold at 4°C. The official library kit (Single Cell 3' Library and Gel Bead Kit V3.1) was applied to construct the libraries intended for single-cell RNA-seq analysis. After the cDNA synthesis and amplification, the cDNA quality assessment was analyzed using Agilent 4200 instrument, and then sequenced on an Illumina Novaseq 6000 sequencer with paired-end reads of length 150 bp. The minimum sequencing depth per cell required was set at 100,000 reads.

Analysis of single-cell RNA-seq data

Alignment and quality control

The cleaned raw FASTQ files underwent alignment to the mm10 (Ensembl GRCm38.93) reference genome and quantification using Cell Ranger (Version 6.0). Following data quality control, preprocessing, and dimensional reduction analysis performed by Seurat, a merged gene-cell data matrix was generated from all 15 matrices, comprising 12 UIR samples and 3 control samples. Prior to downstream analysis, low-quality cells with fewer

than 200 expressed genes or mitochondrial gene percentages exceeding 25% were excluded. The remaining high-quality cell barcodes were exported.

Identification of marker genes and differentially expressed genes (DEGs)

For subsequent analysis, the remaining 60,010 high-quality single cells underwent a repeated Seurat process to generate the final dataset. The identification of DEGs in cell clusters was performed using the FindAllMarkers function implemented in the Seurat package. A comprehensive list of cell markers was employed for cell type annotation of all identified clusters in the final dataset.

Cell sub-clustering analysis

For cell sub-clustering, the entire Seurat pipeline was re-executed with identical parameters only in the barcodes of cells labeled as monocyte/macrophage and neutrophil. As a result, a total of 7 distinct subclusters of the monocyte/macrophage populations and 3 distinct subclusters of the neutrophil populations were identified.

Enrichment analysis

The GO (gene ontology) pathway enrichment analysis was conducted by the KOBAS software incorporating the Benjamini-Hochberg multiple testing adjustment. The top 50 DEGs ([Supplementary Table S1](#)) of each cluster were used as input for the enrichment. The obtained results were visualized using the R package.

The scoring of gene sets in scRNA-seq data

Gene sets comprising relevant markers were collected from previously relevant literatures in combination with GO database ([Supplementary Table S2](#)). The Seurat package's "AddModuleScore" function was used for gene set scores of each cell cluster.

Cell trajectory analysis

The inference of cell developmental trajectory was conducted using RNA velocity according to the instructions (24). The state of mRNA over time can be inferred by RNA Velocity through the analysis of dynamic changes in alternative splicing of mRNA. Specifically, by incorporating both spliced and unspliced data, we employed the Python-based Velocity command-line tool and the Velocity.R package to calculate the RNA velocity and visualize it on the uniform manifold approximation and projection (UMAP) graph.

Ligand–receptor interaction analysis

The CellChat library was utilized to analyze cell-to-cell communication based on single-cell transcriptome data, enabling an investigation into inter-cellular cross-talk among diverse cell types (25). To forecast ligand-receptor interactions specific to each cell type, we employed the Python package CellChat with database v1.1.3. We considered only receptors and ligands expressed in over 5% of cells for analysis and visualization.

Spatial transcriptome sequencing

This process was performed by CapitalBio Technology in Beijing. The kidney cryosections (10 μm thickness) were carefully positioned on the Thermocycler Adaptor with the active surface facing upwards and incubated at 37°C for 1 minute. Subsequently, they were fixed in -20°C methyl alcohol for 30 minutes. The Visum spatial gene expression slide and Reagent Kit (10x Genomics, PN-1000184) were utilized for processing the Visum spatial gene expression analysis. A volume of 70 μl of permeabilization enzyme was introduced and incubated at 37°C for 30 minutes. A total volume of 100 μl of SSC was used to rinse each well, after which 75 μl of reverse transcription Master Mix was added for cDNA synthesis. Upon completion of first-strand synthesis, the RT Master Mix was removed from the wells. A subsequent step involved incubating each well with 75 μl of a solution containing 0.08 M KOH at room temperature for 5 minutes, followed by removal of KOH and washing with EB buffer (100 μl). In the process of second-strand synthesis, each well received an addition of Second Strand Mix (75 μl). The cDNA amplification procedure was conducted using a Bio Rad S1000TM Touch Thermal Cycler. The Visum spatial libraries were generated utilizing the Visum spatial Library construction kit (10x Genomics, PN-1000184) and sequenced on Illumina Novaseq 6000 sequencer with at least 100,000 reads per spot and paired-end reads of length 150 bp. The gene list for calculation of fibrosis score and inflammation score was based on [Supplementary Table S2](#).

Animals

The Mincle genetic (WT&KO) mice, bred on the C57BL/6J genetic background, were generously provided by Dr. Sho Yamasaki from Osaka University in Osaka, Japan (26). Male C57BL/6J mice, aged 6–8 weeks and weighing 20–25g, were obtained from Beijing Vital River Laboratory Animal Technology Co., Ltd. The mice were housed in a pathogen-free environment under a 12-hour light/dark cycle and provided with standard mouse diet and water ad libitum. All animal experiments conducted in this study received ethical approval from the Committee on the Ethics of Animal Experiments at Southeast University.

Renal unilateral ischemic reperfusion injury model

The mice were allocated into distinct groups at random, and the same researchers carried out every surgical procedure. The abdomen was surgically opened under anesthesia to establish the UIR model. The warm renal ischemia was initiated by applying arterial clips on the left renal pedicle for 35 minutes on a 37°C-warming pad, while maintaining the integrity of the right kidney. Throughout the procedure, strict measures were taken to maintain a consistent core body temperature of mice at 36.8–37.2°C using a rectal probe for monitoring purposes. Sham-operated mice underwent identical surgical procedures, excluding the application

of microaneurysm clamps. Kidney samples were collected on days 1, 3, 14, and 28 following UIR induction.

Histopathological analysis

The kidney sections (4μm) that had been fixed in formalin and embedded in paraffin were processed for periodic acid-Schiff (PAS), and Masson's trichrome staining according to a standardized protocol. Two experienced pathologists performed the renal histopathological analysis in a blinded manner. The evaluation of renal histopathological damage included assessment of brush border loss, tubular dilation, cast formation, and tubular necrosis in 10 randomly selected tissue sections per mouse. The extent of tubular damage was evaluated using a semiquantitative scoring method to assess renal injury as a percentage: 0, no damage; 1, 10%; 2, 10–25%; 3, 25–75%; 4, >75%. Interstitial fibrosis was indicated by blue area observed in Masson staining. Renal fibrosis was quantified in at least five sections per mouse by Image J software.

Cell experiments

A mouse macrophage cell line Raw264.7 (ATCC) was used for *in vitro* study. Raw264.7 cells were cultured in Dulbecco's Modified Eagle Medium (DMEM; Gibco) supplemented with 1%(v/v) penicillin-streptomycin (P/S, Gibco) and 10% FBS (10099141C, Gibco). *Clec4e* knockdown in Raw264.7 cell was achieved by using lentivirus shRNA (Target sequence: CCTTTGAACTGGAAACATT) targeting the *Clec4e* gene purchased from GeneChem (Shanghai, China). Non-silencing lentivirus shRNA was used as a nonsense control (NC). Lentiviruses expressing *Clec4e* and nonsense control (NC') constructed in the GV492 vector were purchased from Genechem (Shanghai, China). Raw264.7 cells infected with lentivirus (MOI=100) were stimulated with LPS (100ng/ml, L2630, Sigma) for 12h and then were applied for the following detection through RT-qPCR and immunofluorescence.

Immunofluorescence staining

Prior to immuno-staining, antigen retrieval for all paraffin-embedded kidney sections was conducted using the microwave heating method in EDTA (MVS-0098, MXB Biotechnologies, Foochow, China). For immunofluorescence staining, formaldehyde-fixed kidney sections were incubated with primary antibodies against Mincle (CLEC-4E (B-7): sc-390806, Santa Cruz, USA), CD68 (ab125212, Abcam, UK), Ly6G (GB11229-100, Servicebio, CN), TNF-α (ab1973, Abcam, UK), Megalin (sc-515772, Santa Cruz, USA), α-SMA (ab5694, Abcam, UK). Raw264.7 cells seeded on the cover glasses were incubated with primary antibody against TNF-α (ab1973, Abcam, UK). Subsequently secondary antibodies were applied and DAPI was employed to stain cell nuclei. Immunostained samples were observed under a confocal microscope (FV3000, Olympus).

Flow cytometry analysis

The Mincle-positive immune cell population in UIR kidney was quantified using flow cytometry. In brief, kidney samples were minced and enzymatically digested using the gentleMACS™ octo dissociator (Miltenyi Biotec) along with the multi tissue dissociation kit (Miltenyi, 130-110-203), followed by a 30-minute incubation at 37°C. The resulting cell suspension was filtered through 70-μm cell strainers and washed with wash buffer (PBS containing 2% FBS and 2 mM EDTA). Erythrocytes were eliminated using RBC lysis buffer (00-4333-57, eBioscience™), and cell viability was detected with Live/Dead-Fixable Viability Stain 780 (BD Biosciences, Cat. No. 565388). After blocking nonspecific Fc binding with FC Block (553141, BD Biosciences), cell suspensions were then incubated with CD45-BV510 (103138, Biolegend), CD11b-FITC (101206, Biolegend), F4/80-BV421 (565411, BD Biosciences), Ly6G-PerCP-cy5.5 (127615, Biolegend) for 30min at 4°C. For Mincle, we applied the primary anti-Mincle antibody (D266-3, MBL) and then incubated with the Alexa Fluor 647-conjugated second antibody (ab150167, abcam, UK). Flow cytometry was performed on FACSymphony A5 SORP (BD Biosciences) and data was analyzed with FlowJo software.

Quantitative real-time PCR

The total RNA was extracted from mouse kidney samples and Raw264.7 cell lysate using RNAiso Plus (Vazyme, Nanjing, China) following the manufacturer's protocols. Subsequent reverse transcription and quantitative real-time PCR were performed using 5× HiScript III qRT SuperMix and 2× ChamQ SYBR qPCR Master Mix (Vazyme, Nanjing, China). The expression levels of β-actin were used for data normalization, and the primers utilized in RT-qPCR were listed in [Supplementary Table S3](#).

Statistical analysis

The data were presented as the mean ± standard deviation (SD). Statistical analysis was conducted using t-test or one-way analysis of variance (ANOVA) with GraphPad Prism 9.0 software. A significance threshold of $P < 0.05$ indicated statistical significance.

Results

The expression of Mincle exhibited a biphasic pattern during the progression of renal fibrosis

To explore the dynamics and functional role of Mincle in the progression of AKI to CKD, we established a UIR-induced mouse model ([Figure 1A](#)). We observed remarkable renal interstitial collagen deposition on day 14, indicating the development of renal fibrosis which was aggravated on day 30 ([Figures 1B, D](#)).

Meanwhile, a time-dependent dynamic expression of Mincle during the AKI-to-CKD transition process was noted by immunofluorescence staining (Figures 1C, E). We observed a biphasic pattern of Mincle expression following AKI, characterized by a sharp increase on the first day and a subsequent second peak at day 14. The Pearson correlation coefficient analysis indicated a positive association between Mincle and the extent of fibrosis suggesting potential involvement of Mincle in the chronicity of AKI (Figure 1F).

The single-cell transcriptional analysis revealed the comprehensive landscape of Mincle expression in macrophages and neutrophils

Single-cell RNA sequencing analysis was performed to investigate the landscape of Mincle expression in cell clusters (Figure 1A). Our findings revealed that Mincle was mainly expressed in the populations of monocytes/macrophages and neutrophils in the kidney displaying a time-dependent pattern (Figures 2A, B). The Mincle expression in monocytes/macrophages and neutrophils exhibited a rapid increase on the first day post-UIR injury. However, the expression of Mincle was observed to be down-regulated in total monocytes/macrophages as disease progressed (Figures 2A, B), which may attribute to the decreased expression in monocyte cluster (Supplementary Figures S1A, B). Interestingly, unlike monocytes/macrophages, Mincle in neutrophils exhibited a sustained elevation and demonstrated a secondary peak of up-regulation on day 14 (Figures 2A, B). The biphasic pattern of Mincle expression on day 1 and 14 suggested their critical role in the acute phase as well as the transition point towards chronicity.

To validate the findings of single-cell sequencing data, we employed flow cytometry analysis and identified a notable increase in the recruitment of Mincle-positive F4/80⁺ macrophages and neutrophils on day 1 following AKI, which further augmented on day 14 (Figures 2C–F). Immunofluorescence staining also displayed a large number of macrophages and neutrophils expressing Mincle in renal interstitium on day 14 (Figure 2G). Overall, single-cell RNA sequencing analysis unveiled a dynamic profile of Mincle expression, predominantly exhibited by macrophages and neutrophils, throughout the process of AKI-to-CKD transition.

High Mincle-expressing neutrophils and macrophages were characterized with pro-inflammatory and pro-fibrotic signatures

Further analysis was subsequently conducted to delineate the characteristics of cell clusters expressing Mincle. By performing sub-clustering analysis, neutrophils were partitioned into 3 subsets displayed in UMAP plots (Figure 3A). The cell fraction of neutrophil cluster 1 and cluster 2 (referred to as Neu 1 and Neu 2) exhibited a significant increase on day 1, followed by obvious decline by day 3. However, with disease progression, they displayed

a peak on day 14 (Figure 3B). Next, gene set scores were established in regard to cell maturation, activation, aging, apoptosis, phagocytosis, and chemotaxis (related genes in Supplementary Table S2). Neu 1 and Neu 2 were identified as mature neutrophil subsets with phagocytic function (Figure 3C). Neu 2 displayed early activation and chemotaxis characteristics while Neu 1 was more likely to represent an “aged” subset of neutrophils characterized with high level of *Cxcr4* and low level of *Sell* (27) (Figure 3C). However, Neu 3 may represent a small subset of immature or renal-resident neutrophils with undefined function (Figure 3C). Therefore, we focused on Neu 1 and Neu 2 in the following analysis.

Through gene ontology (GO) pathway enrichment analysis, Neu 1 (high expression of *Clec4e*, *Ccl3*, *Ccl4*, *Tnf*, *Siglec*, *Il1rn*, *Icam1*, *Il1a*, *Ccr12*, *Ctsb*) and Neu 2 (high expression of *Retnlg*, *Slpi*, *S100a8*, *S100a9*, *Lcn2*, *Ccl6*, *Mmp8*, *Lrg1*) were found to be involved in inflammatory responses (Figure 3D). RNA velocity analysis further elucidated the trajectory of neutrophils, revealing that Neu 2 (as a fresh mature subset) differentiated into Neu 1 (as an aged mature subset) (Figure 3E), which aligned well with the observed dynamic changes in neutrophil proportions as well as the defined gene set functions (Figures 3B, C). In addition, it turned out that Mincle was significantly up-regulated in Neu 1 (Figure 3F). Meanwhile, unsupervised clustering identified seven distinct cell subpopulations of mononuclear phagocytes (including monocyte and Mac 1–6). Notably, a remarkable Mincle expression was observed in two specific subsets, monocyte and Mac1 (Figure 3F). The Neu 1 and Mac 1 clusters presenting with dual peak expression of Mincle were identified as Mincle^{high} neutrophils and Mincle^{high} macrophages, respectively. Functional assessments revealed that these Mincle^{high} neutrophils and Mincle^{high} macrophages exhibited prominent pro-inflammatory and pro-fibrotic properties (Figure 3G). Moreover, spatial transcriptomics data showed a pronounced expression of Mincle at the outer-stripe of outer medulla in the kidney, with similar distribution for myeloid cells (indicated by *Itgam*) as well as inflammatory regions (indicated by inflammation score) and fibrotic regions (indicated by *Acta2* expression and fibrosis score) (Figure 3H). Persistent chronic renal inflammation was revealed by inflammation score peaked on day 14 after AKI (Figure 3H).

Therefore, Mincle was highly expressed in specific subsets of neutrophils and macrophages, displaying remarkable pro-inflammatory and pro-fibrotic properties crucial for driving CKD progression following the initial kidney injury.

Mincle^{high} neutrophils and Mincle^{high} macrophages synergistically promote the production of TNF

To further elucidate the mechanisms driving AKI-to-CKD transition mediated by Mincle-expressing macrophages and neutrophils, we identified 54 common genes from the up-regulated genes of these two cell subsets (Figure 4A). GO terms of these 54 genes were predicated to be implicated in immune-inflammatory responses and extracellular matrix synthesis (Figure 4B). In addition, protein-protein interaction (PPI)

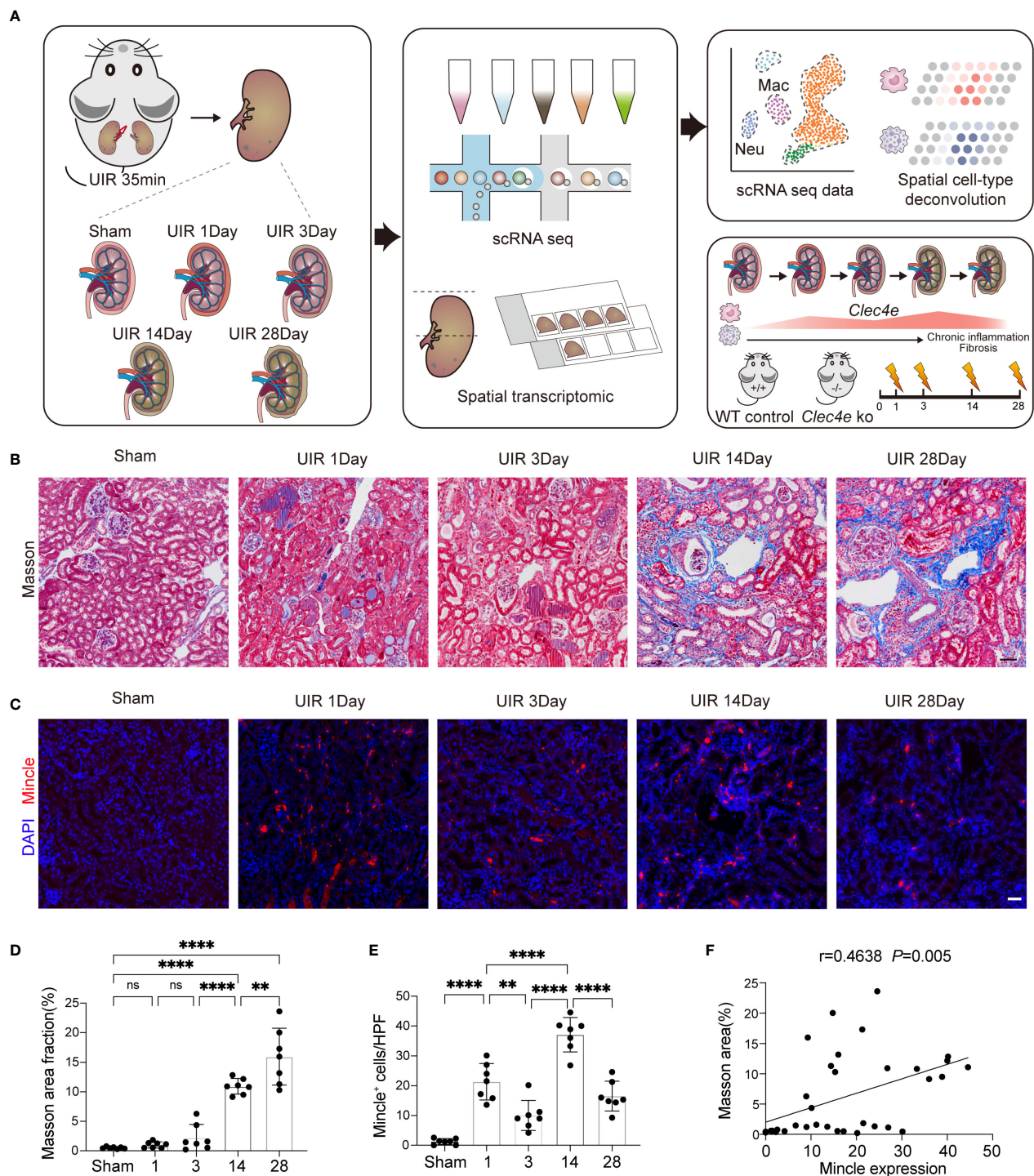


FIGURE 1

The expression of Mincle exhibited a significant correlation with kidney fibrosis. **(A)** Design and workflow of this study. The transition from AKI to CKD was experimentally induced in mice through UIR. Kidney samples collected at days 1, 3, 14, and 28 post-UIR, along with sham kidneys, were subjected to the 10x chromium single-cell and visium spatial transcriptomic procedures. Validation experiments were conducted in Mincle WT and KO mice. **(B, D)** Masson staining and quantification of kidney at various time points post-UIR. $n=7$. Scale bar, 50 μ m. **(C, E)** Representative immunofluorescent images and quantification of Mincle (labeled in red) in kidney at various time points post-UIR. $n=7$. Scale bar, 50 μ m. **(F)** The correlation analysis between fibrosis severity, as indicated by masson area fraction, and Mincle expression was conducted. $n=35$. Data were presented as mean \pm SD. ns, no significance, $**p < 0.01$, $****p < 0.0001$.

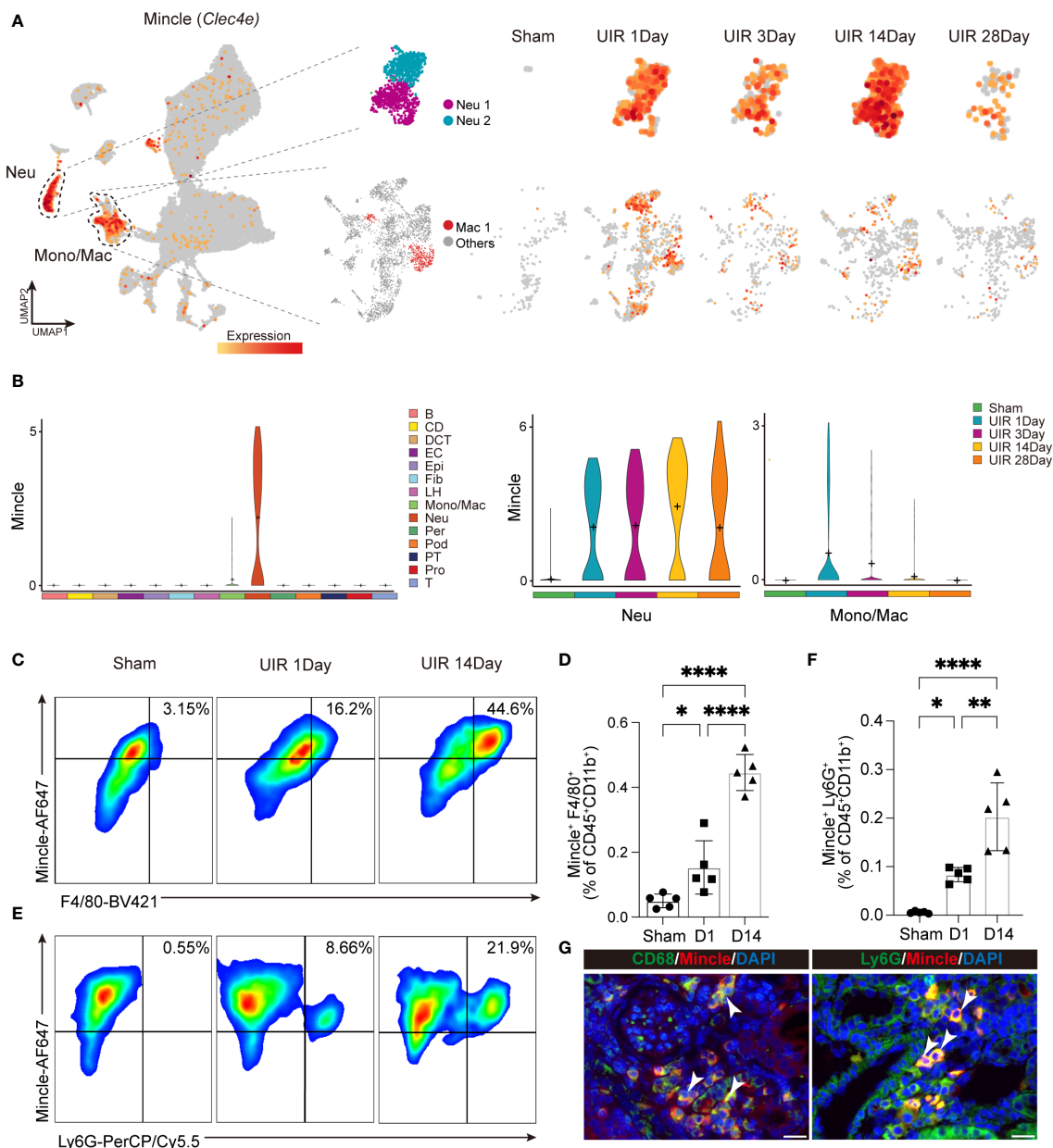


FIGURE 2

Dynamic expression of Mincle in macrophage and neutrophil. (A, B) The UMAP projection and violin plot suggesting expression of Mincle (*Clec4e*) in all different identified cell clusters and specific expression in neutrophil and monocyte/macrophage at different time points post injury. B, B cell; CD, collecting duct; DCT, distal convoluted tubule; EC, endothelial cell; Epi, epithelial cell; Fib, fibroblast; LH, loop of Henle; Mono/Mac, monocyte/macrophage; Neu, neutrophil; Per, pericyte; Pod, podocyte; PT, proximal tubule; Pro, proliferation cell; T, T cell. (C–F) Flow cytometry analysis revealing the quantification of Mincle-positive macrophages and neutrophils in the kidney from AKI to CKD (Sham, day 1 and day 14). n=5. (G) Representative immunofluorescence staining of CD68⁺Mincle⁺ and Ly6G⁺Mincle⁺ cells in kidney of day 14 post-UIR. CD68/Ly6G, green; Mincle, red. Scale bar, 20μm. Data were presented as mean ± SD. *p < 0.05, **p < 0.01, ****p < 0.0001.

analysis showed that *Tnf* emerged as the hub gene closely related to the up-regulated genes in both Mincle^{high} neutrophils and Mincle^{high} macrophages (Figure 4C). Gene expression correlation analysis demonstrated a strong association between *Tnf* and *Clec4e* in these two Mincle^{high} immune cell subsets (Figure 4D). The CellChat algorithm-based inter-cellular communication analysis revealed important contribution of Mincle^{high} neutrophils and Mincle^{high} macrophages as ligand sources in the TNF signaling pathway network (Figure 4E). Correspondingly, a prominent

increase in *Tnf* expression primarily in macrophages and neutrophils, particularly on day 14 was observed (Figure 4F). Furthermore, the *in vitro* validation confirmed a decrease in TNF expression following Mincle knockdown, while an increase was observed after overexpression of Mincle in LPS-stimulated Raw264.7 cells (Supplementary Figures S2A–D). Meanwhile, TNF-α expression was reduced in macrophages and neutrophils on day 14 in Mincle knockout (KO) mice (Figure 4G). Hence, we identified that Mincle^{high} myeloid cells (specifically macrophages

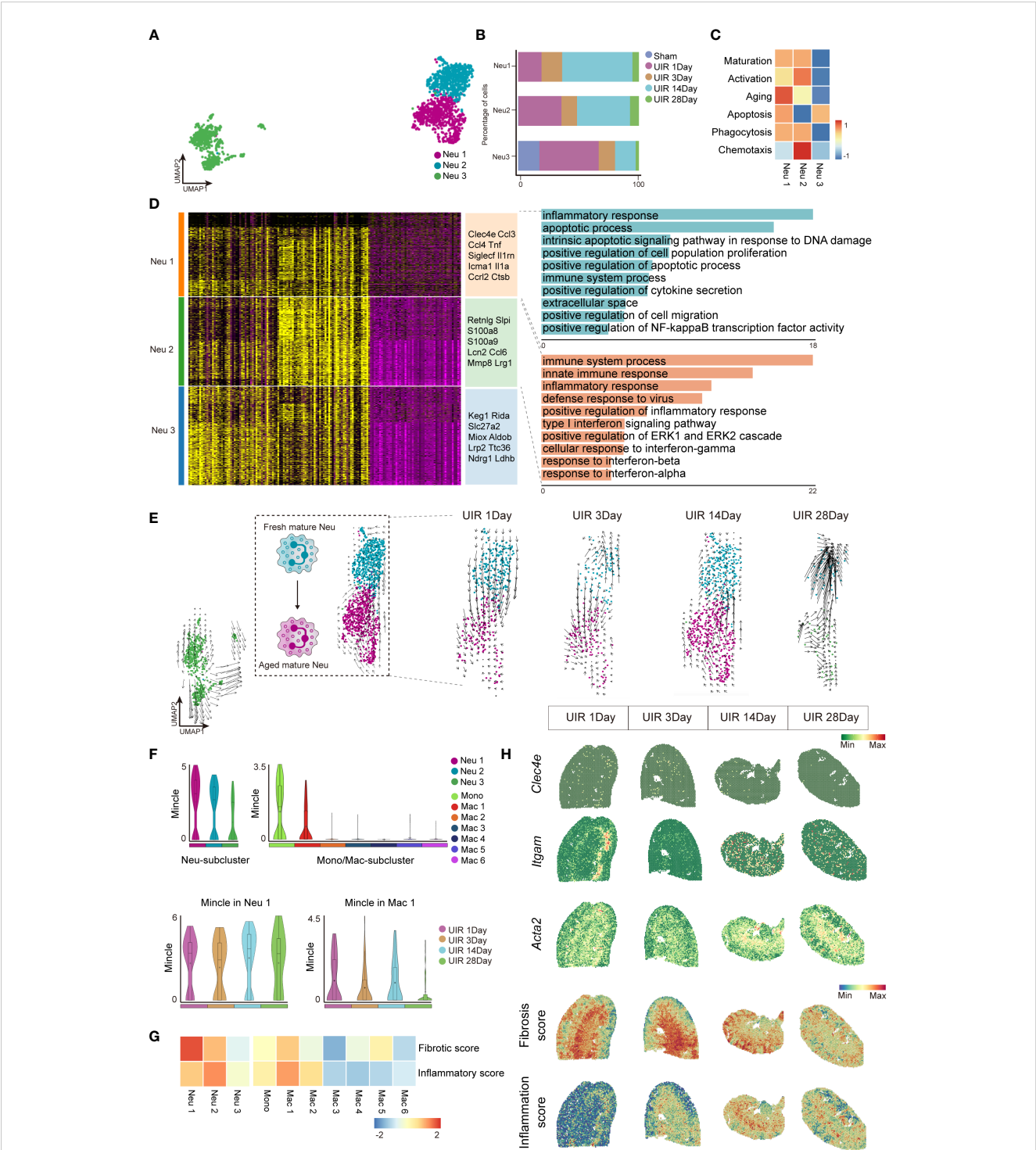
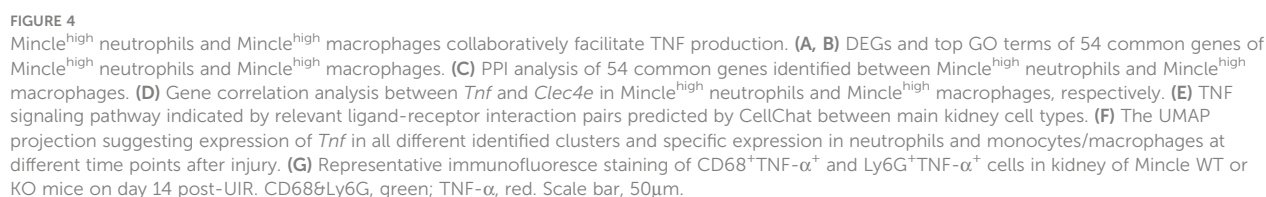


FIGURE 3 Neutrophils and macrophages expressing high levels of Mincle exhibited pro-inflammatory and pro-fibrotic signatures. **(A)** UMAP plot of all clusters of neutrophils. **(B)** The proportion of each subgroup of neutrophils at different time points. **(C)** Heatmap of phenotype and function score (including maturation, activation, aging, apoptosis, phagocytosis and chemotaxis) for each neutrophil cluster. **(D)** Heatmap of each sub-cluster of neutrophils based on DEGs and their top marker genes were listed. Top GO pathway enrichment analysis of Neu1 and Neu 2 subtypes were presented. **(E)** The UMAP plot depicting the developmental transition of neutrophil clusters in Neu 1-2 following injury, as revealed by RNA velocity analysis. **(F)** Violin plot suggesting Mincle expression in all macrophage sub-clusters and neutrophil sub-clusters, as well as the dynamics of Mincle in clusters of Neu1 and Mac1 at each time point after injury. **(G)** Heatmap of fibrotic score and inflammatory score in sub-clusters of Neu1-3 and Monocyte and Mac1-6. **(H)** Temporal and spatial gene expression patterns of *Clec4e*, *Itgam* and *Acta2*, along with fibrosis score and inflammation score, were elucidated using 10x Visium spatial transcriptomics.



and neutrophils) synergistically contributed to TNF production during the chronic transition of AKI.

Mincle deficiency protect kidney from aggravated injury and fibrosis post-UIR

Due to the distinctive expression pattern of renal myeloid-derived Mincle during both early and chronic stages of kidney injury, along with its pro-inflammatory and pro-fibrotic properties, we further investigated the renal manifestations in Mincle knockout mice. In wild-type (WT) mice, obvious tubular epithelial cell (TEC) flattening, loss of the brush border and epithelial cell nuclei, and tubular cast formation were observed after AKI, which could not be completely repaired in the late stage of the disease and was accompanied by a substantial interstitial immune cell infiltration (Figures 5A, B). However, Mincle knockout resulted in significant amelioration in renal pathological damage at different time points during the process of AKI to CKD (Figures 5A, B). Additionally, α -SMA immunofluorescence staining indicated a notable attenuation of renal fibrosis in Mincle-deficient mice (Figures 5A, C). In Mincle WT mice, Mincle mRNA expression confirmed a biphasic up-regulation pattern following AKI (Figure 5D). Quantitative analysis of kidney weight and megalin staining revealed more pronounced renal atrophy and tubular loss in WT mice than those observed in KO mice (Figures 5E–G). Remarkably, compared to WT group, Mincle KO mice exhibited significant down-regulation in the mRNA expression of pro-inflammatory factors (TNF- α , IL-1 β , Ccl2) and fibrosis-associated factors (TGF- β , α -SMA, COL1A1) especially on day 14 (Figures 5H–M). Collectively, our findings demonstrated that Mincle played a critical role in renal injury and fibrosis progression after AKI probably by mediating the unresolved inflammation.

Discussion

While Mincle has been extensively characterized as a key mediator of inflammation in AKI, further investigation is warranted to elucidate its role in the transition from AKI to CKD. In this research, we offered a comprehensive single-cell analysis of Mincle behavior during the progression from AKI to CKD. Using mouse models of UIR, we delineated the detrimental involvement of Mincle in the unresolved inflammation and subsequent renal fibrosis across the acute and chronic phase after AKI (Figure 6).

Initially, we identified biphasic pattern of Mincle expression during the progression of renal fibrosis which potentially contributed to the chronicity of inflammation. Previous research predominantly emphasized the pathogenic role of Mincle-expressing macrophages in AKI, confirming the initiation and exacerbation of renal inflammation by Mincle (21, 22, 28). Here, we observed a rapid up-regulation of Mincle in the initial stage of kidney injury, followed by a second peak during the chronic progression of AKI, accompanied by recruitment of immune cells and sustained inflammatory status, which exhibited a strong

association with late-stage renal fibrosis. Inflammatory processes are pivotal in kidney fibrosis, involving diverse innate immune cells in establishing renal interstitial inflammation environment (2, 5). Innate immune cells not only initiate and exacerbate inflammation in the early stage, but also contribute to the progression of kidney fibrosis through sustained chronic inflammation driven by the activation of innate immune pathways (5, 7). Furthermore, in conjunction with the implementation of spatial transcriptome technology, some innate immune cells were identified in anatomical regions adjacent to fibrotic areas and were deemed to be implicated in the establishment of the renal fibrosis microenvironment (29, 30). Xu et al. recently elucidated that the sustained macrophages infiltration, along with subsequent activation of T-cells and neutrophils leading to a pro-inflammatory immune response, facilitated secondary kidney injury during AKI-to-CKD transition (11). Therefore, Mincle derived from macrophages and neutrophils may not only exacerbate early inflammatory responses but also involved in the chronic transformation of kidney injury.

Further study identified two distinct sub-clusters of Mincle^{high} macrophages and Mincle^{high} neutrophils, both exhibiting pro-inflammatory and pro-fibrotic characteristics during kidney injury progression. The recognition of functional diversity and time-dependent infiltration of immune cell signifies a critical facet in the complex pathogenesis of renal interstitial inflammation and chronic injury (7). The phenotypic heterogeneity and functional plasticity of macrophages have gained increasing interest (31). Macrophages not only participate in the early inflammatory and repair process, but also can be transformed into pro-fibrotic phenotype to mediate the collagen matrix deposition in the kidney. Utilizing single-cell RNA sequencing technology, a plethora of novel subsets of macrophages have been identified to exert distinct roles in both AKI and CKD. In the ischemia-reperfusion-induced AKI mouse model, a specific subset of monocyte-derived macrophages marked by S100a8/S100a9 expression triggered and intensified kidney inflammation (32). Additionally, an early-emerging Arg1⁺ monocyte subset displayed a pro-inflammatory and pro-fibrotic phenotype, while Ccr2⁺ macrophages appeared in late phase of injury (14). In the current study, we identified a specific Mincle^{high} macrophage population that possesses both M1 and M2 phenotypes exhibiting pro-inflammatory and pro-fibrotic characteristics, potentially sustaining renal inflammatory and fibrogenic processes. Neutrophils, recognized as primary responders in early renal injury (3, 7), have garnered increased attention in the AKI-to-CKD transition in recent researches. Persistent infiltration of specific neutrophils, such as Siglec-F⁺ or MMP-9⁺ neutrophils, is crucial for creating a pro-fibrotic microenvironment that facilitates the progressive renal fibrosis (11, 33, 34). In addition, previous report showed that the “aged” neutrophils (Cxcr4^{hi} & Icam1^{hi}Cxcr1^{lo}) presented in the renal tissue were associated with a pro-inflammatory phenotype (35). Here, we systematically characterized three neutrophil subpopulations in UIR-induced AKI-to-CKD model. Specifically, the Mincle^{high} neutrophils were found as an “aged” sub-cluster with pro-inflammatory and pro-fibrotic signatures, prominently infiltrating during late renal UIR

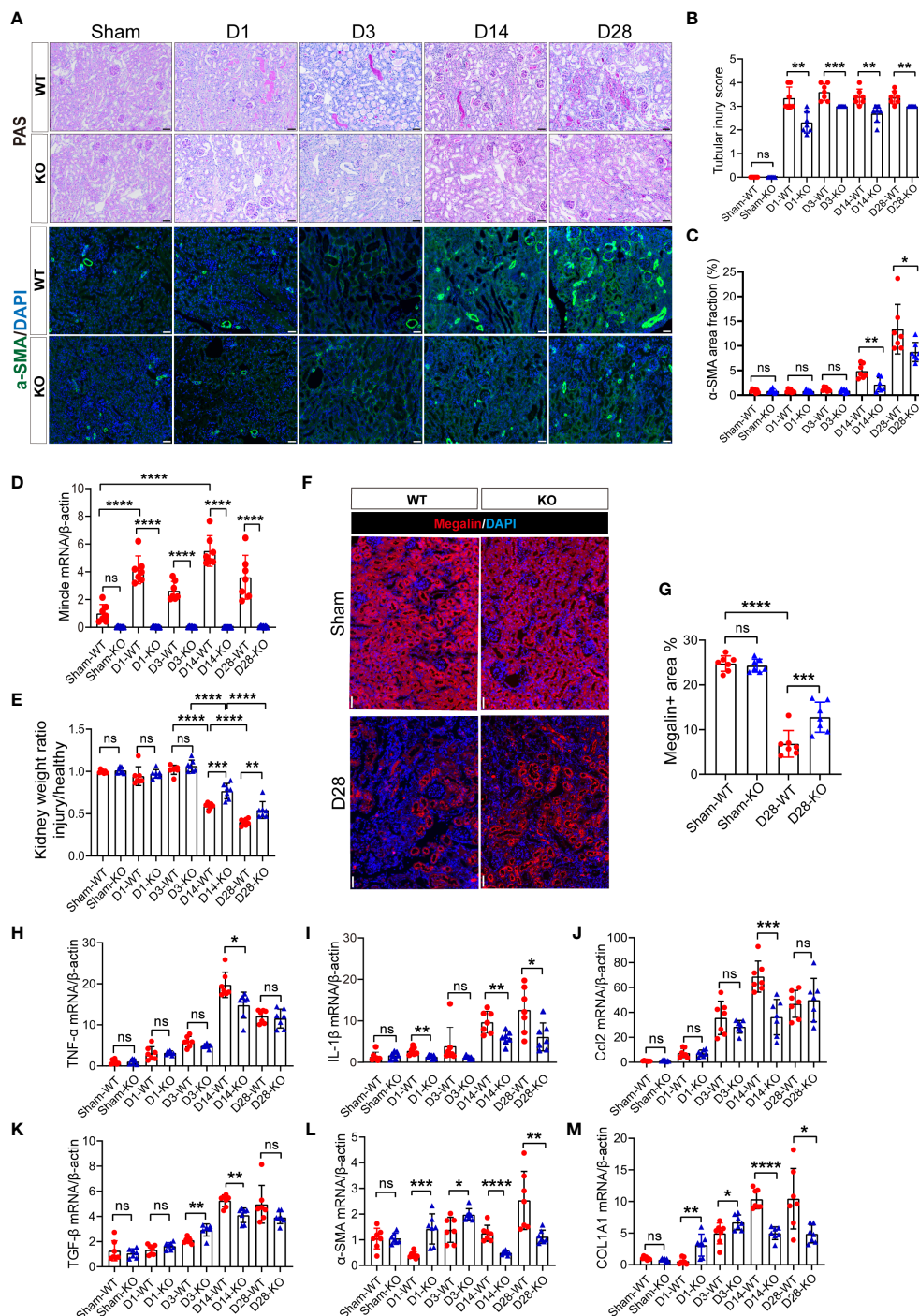


FIGURE 5

The absence of Mincle provides protection by mitigating exacerbated injury and fibrosis following UIR. (A–C) Acute kidney injury was induced by UIR in Mincle WT or KO mice. Renal tubular injury score was calculated according to PAS staining at each time point (Sham, day1, day3, day14 and day28) post-UIR. Representative immunofluorescent staining of α -SMA (green) in kidney at each time point after UIR. n=7. Scale bar, 50 μ m. (D) RT-qPCR analysis of Mincle mRNA in kidney from Mincle WT and KO mice. n=7. (E) The ratio of the weight of the injured kidney to that of the healthy (sham group) kidney. n=7. (F–G) Immunofluorescence staining of megalin (red) in kidney sections (Sham and day 28) after UIR with representative images. Megalin-positive areas were quantified. n=7. Scale bar, 50 μ m. (H–M) RT-qPCR analysis for the indicated inflammation and fibrosis related factors was performed on sham kidney and injured kidney samples harvested on day1, 3, 14, and 28 after injury. n=7. Data were presented as mean \pm SD. ns, no significance, *p < 0.05, **p < 0.01, ***p < 0.001, ****p < 0.0001.

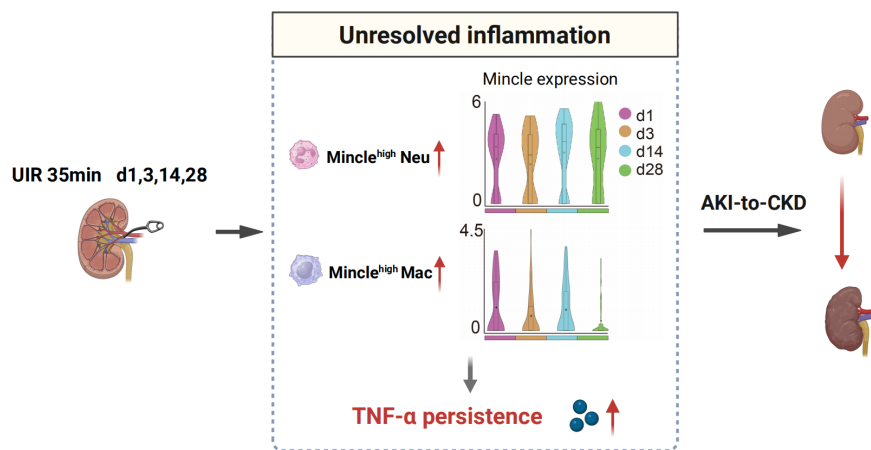


FIGURE 6

Schematic illustration depicting the involvement of Mincle in the AKI-to-CKD transition. Mincle^{high} neutrophils and macrophages contribute to unresolved inflammation by up-regulating TNF- α production, thereby driving the progression of AKI towards CKD. UIR, unilateral ischemia-reperfusion; Neu, neutrophil; Mac, macrophage; AKI, acute kidney injury; CKD, chronic kidney disease.

stages, suggesting its significant role in fibrosis progression. Therefore, Mincle^{high} macrophages and Mincle^{high} neutrophils may represent a distinct myeloid cell population implicated in inflammation and fibrosis during AKI to CKD transition. Interestingly, the expression of Mincle in neutrophils was significantly higher than that in macrophages. Nevertheless, further validation utilizing macrophage-specific Mincle-deficient mice and neutrophil-specific Mincle-deficient mice is warranted to determine whether neutrophil-derived Mincle plays a predominant role in the AKI-to-CKD progression.

Next, we found that Mincle^{high} macrophages and Mincle^{high} neutrophils contributed to the production of TNF, which was reduced significantly in Mincle knockout mice. The pathogenic role of TNF signaling pathway in kidney disease has been extensively reported. Wen et al. found that the KLF4 deficiency in myeloid cells augmented TNF- α production, thereby exacerbating necroptosis of TECs and renal interstitial fibrosis in two murine models of CKD induced by nephrotoxic serum nephritis and unilateral ureteral obstruction, however, this effect was mitigated by macrophage-specific TNF deletion (36). Utilizing single-cell transcriptomics, TNF from activated leukocytes drove Gli1⁺ cell proliferation and fostered renal fibrosis by elevating Indian Hedgehog (IHH) release from TECs (37). Moreover, an unbiased transcriptomic approach revealed shared molecular signatures of an activated kidney TNF pathway and unfavorable clinical outcomes among patients diagnosed with either minimal change disease or focal segmental glomerulosclerosis, highlighting TNF as a pivotal driver in the progression of these diseases (38). Considering the impact of TNF on renal injury and fibrosis, the dynamic infiltration of these two Mincle-expressing immune cell subsets collectively facilitates TNF production which may act as the critical contributor to the chronic transition of AKI.

Finally, we identified that Mincle deficiency protect kidney from aggravated injury and fibrosis post-UIR. New anti-inflammation therapies against renal fibrosis have been well discussed (39, 40). It

has proven that targeting the endogenous ligands of Mincle represents a promising approach for alleviating renal inflammation (22, 28). Moreover, Syk inhibitors and a variety of Chinese patent medicine compounds have demonstrated the ability to suppress Mincle/Syk/NF- κ B signaling pathway, consequently mitigating acute kidney inflammation induced by various etiologies (41–43). Furthermore, modulating Mincle activation via targeted manipulation of Mincle gene (23, 44) or protein receptor (45, 46) emerged as potential therapeutic avenues. Nevertheless, a limitation of this study lies in its exclusive utilization of a murine model of UIR induced AKI. Given the intricate etiologies of AKI in humans (47), it is imperative to explore alternative kidney disease models to unveil the complex mechanistic actions of Mincle in different disease contexts.

In conclusion, we have elucidated the dynamic expression of Mincle with a second peak in a UIR-mediated AKI-to-CKD model through sc-RNA seq analysis. We identified distinct Mincle^{high} macrophages and neutrophils exerting pro-inflammatory and pro-fibrotic effects, which synergistically contributed to the persistence of renal inflammatory microenvironment and accelerated renal fibrosis progression by promoting TNF production. Precisely targeting Mincle or its downstream pathways may provide a promising therapeutic avenue to impede AKI-to-CKD transition.

Data availability statement

The data presented in the study are deposited in the GEO repository, accession number GSE267242.

Ethics statement

The animal study was approved by The Committee on the Ethics of Animal Experiments at Southeast University (Permit No.

20210302023). The study was conducted in accordance with the local legislation and institutional requirements.

Author contributions

CW: Writing – original draft, Visualization, Validation, Software, Resources, Methodology, Investigation, Formal analysis, Data curation, Conceptualization. YZ: Writing – review & editing, Visualization, Software, Resources, Methodology, Investigation, Formal analysis, Data curation, Conceptualization. AS: Writing – review & editing, Validation. TT: Writing – review & editing, Investigation. NL: Writing – review & editing, Software, Formal analysis. CX: Writing – review & editing, Investigation. BL: Writing – review & editing, Supervision, Project administration, Funding acquisition. LL: Writing – review & editing, Supervision, Project administration, Funding acquisition, Conceptualization.

Funding

The author(s) declare financial support was received for the research, authorship, and/or publication of this article. This study was supported by grants from the National Natural Science Foundation of China (Grant No. 82241045, 82122011) and the National Key Research and Development Program of China (Grant No. 2022YFC2502503).

Acknowledgments

We express our sincere gratitude to Dr. Sho Yamasaki (Osaka University, Osaka, Japan) for generously providing us with Mincle WT and KO mice.

References

- Kalantar-Zadeh K, Jafar T, Nitsch D, Neuen B, Perkovic V. Chronic kidney disease. *Lancet*. (2021) 398:786–802. doi: 10.1016/s0140-6736(21)00519-5
- Meng X, Nikolic-Paterson D, Lan H. Inflammatory processes in renal fibrosis. *Nat Rev Nephrol*. (2014) 10:493–503. doi: 10.1038/nrneph.2014.114
- Tang P, Zhang Y, Chan M, Lam W, Chung J, Kang W, et al. The emerging role of innate immunity in chronic kidney diseases. *Int J Mol Sci*. (2020) 21:4018. doi: 10.3390/ijms21114018
- Huen S, Cantley L. Macrophages in renal injury and repair. *Annu Rev Physiol*. (2017) 79:449–69. doi: 10.1146/annurev-physiol-022516-034219
- Speer T, Dimmeler S, Schunk S, Fliser D, Ridker P. Targeting innate immunity-driven inflammation in CKD and cardiovascular disease. *Nat Rev Nephrol*. (2022) 18:762–78. doi: 10.1038/s41581-022-00621-9
- Jang H, Rabb H. Immune cells in experimental acute kidney injury. *Nat Rev Nephrol*. (2015) 11:88–101. doi: 10.1038/nrneph.2014.180
- Xu L. The role of myeloid cells in acute kidney injury and kidney repair. *Kidney360*. (2021) 2:1852–64. doi: 10.34067/kid.0000672021
- Lee S, Noel S, Sadasivam M, Hamad A, Rabb H. Role of immune cells in acute kidney injury and repair. *Nephron*. (2017) 137:282–6. doi: 10.1159/000477181
- Rabb H, Griffin M, McKay D, Swaminathan S, Pickers P, Rosner M, et al. Inflammation in AKI: current understanding, key questions, and knowledge gaps. *J Am Soc Nephrol*. (2016) 27:371–9. doi: 10.1681/asn.2015030261
- Puthumana J, Thiessen-Philbrook H, Xu L, Coca S, Garg A, Himmelfarb J, et al. Biomarkers of inflammation and repair in kidney disease progression. *J Clin Invest*. (2021) 131:e139927. doi: 10.1172/jci139927
- Xu L, Guo J, Moledina D, Cantley L. Immune-mediated tubule atrophy promotes acute kidney injury to chronic kidney disease transition. *Nat Commun*. (2022) 13:4892. doi: 10.1038/s41467-022-32634-0
- Balzer M, Doke T, Yang Y, Aldridge D, Hu H, Mai H, et al. Single-cell analysis highlights differences in druggable pathways underlying adaptive or fibrotic kidney regeneration. *Nat Commun*. (2022) 13:4018. doi: 10.1038/s41467-022-31772-9
- Melo Ferreira R, Sabo A, Winfree S, Collins K, Janosevic D, Gulbranson C, et al. Integration of spatial and single-cell transcriptomics localizes epithelial cell-immune cross-talk in kidney injury. *JCI Insight*. (2021) 6:e147703. doi: 10.1172/jci.insight.147703
- Conway B, O'Sullivan E, Cairns C, O'Sullivan J, Simpson D, Salzano A, et al. Kidney single-cell atlas reveals myeloid heterogeneity in progression and regression of kidney disease. *J Am Soc Nephrol*. (2020) 31:2833–54. doi: 10.1681/asn.2020060806
- Lee W, Kang J, Yan J, Lee M, Jeon B, Cho S, et al. Neutrophils promote mycobacterial trehalose dimycolate-induced lung inflammation via the mincle pathway. *PLoS Pathog*. (2012) 8:e1002614. doi: 10.1371/journal.ppat.1002614
- Matsumoto M, Tanaka T, Kaisho T, Sanjo H, Copeland N, Gilbert D, et al. A novel LPS-inducible C-type lectin is a transcriptional target of NF-IL6 in macrophages. *J Immunol*. (1999) 163:5039–48.

Conflict of interest

The authors declare that the research was conducted in the absence of any commercial or financial relationships that could be construed as a potential conflict of interest.

Publisher's note

All claims expressed in this article are solely those of the authors and do not necessarily represent those of their affiliated organizations, or those of the publisher, the editors and the reviewers. Any product that may be evaluated in this article, or claim that may be made by its manufacturer, is not guaranteed or endorsed by the publisher.

Supplementary material

The Supplementary Material for this article can be found online at: <https://www.frontiersin.org/articles/10.3389/fimmu.2024.1385696/full#supplementary-material>

SUPPLEMENTARY FIGURE 1

The dynamics of monocytes and Mincle-derived from the monocyte cluster. (A) The monocyte cluster highlighted in the UMAP projection was markedly increased on day 1 after injury. (B) The violin plot suggesting expression of Mincle in Mono cluster at different time points post-injury. Mono, monocyte; Mac, macrophage.

SUPPLEMENTARY FIGURE 2

Expression of TNF- α in Raw264.7 cell with Mincle knockdown or overexpression. (A, B) RT-qPCR analysis for Mincle and TNF- α mRNA was performed in lentivirus-infected Raw264.7 cells after stimulation with LPS. (C, D) Immunofluorescence staining of TNF- α (red) in Raw264.7 stimulated with LPS with representative images. The mean fluorescence intensity (MFI) of TNF- α was quantified by Image J software. $n=3$. Scale bar, 20 μ m. NC/NC', nonsense control; KD, knockdown; OE, overexpression. Data were presented as mean \pm SD. * $p < 0.05$, ** $p < 0.01$, *** $p < 0.001$.

17. Iborra S, Martínez-López M, Cueto F, Conde-Garrosa R, Del Fresno C, Izquierdo H, et al. Leishmania uses mincle to target an inhibitory ITAM signaling pathway in dendritic cells that dampens adaptive immunity to infection. *Immunity*. (2016) 45:788–801. doi: 10.1016/j.immuni.2016.09.012
18. Ishikawa E, Ishikawa T, Morita Y, Toyonaga K, Yamada H, Takeuchi O, et al. Direct recognition of the mycobacterial glycolipid, trehalose dimycolate, by C-type lectin Mincle. *J Exp Med*. (2009) 206:2879–88. doi: 10.1084/jem.20091750
19. Yamasaki S, Ishikawa E, Sakuma M, Hara H, Ogata K, Saito T. Mincle is an ITAM-coupled activating receptor that senses damaged cells. *Nat Immunol*. (2008) 9:1179–88. doi: 10.1038/ni.1651
20. Huang X, Yu Q, Zhang L, Jiang Z. Research progress on Mincle as a multifunctional receptor. *Int Immunopharmacol*. (2023) 114:109467. doi: 10.1016/j.intimp.2022.109467
21. Lv L, Tang P, Li C, You Y, Li J, Huang X, et al. The pattern recognition receptor, Mincle, is essential for maintaining the M1 macrophage phenotype in acute renal inflammation. *Kidney Int*. (2017) 91:587–602. doi: 10.1016/j.kint.2016.10.020
22. Lv L, Wang C, Li Z, Cao J, Zhong X, Feng Y, et al. SAP130 released by damaged tubule drives necroinflammation via miRNA-219c/Mincle signaling in acute kidney injury. *Cell Death Dis*. (2021) 12:866. doi: 10.1038/s41419-021-04131-7
23. Tanaka M, Saka-Tanaka M, Ochi K, Fujieda K, Sugiura Y, Miyamoto T, et al. C-type lectin Mincle mediates cell death-triggered inflammation in acute kidney injury. *J Exp Med*. (2020) 217:e20192230. doi: 10.1084/jem.20192230
24. La Manno G, Soldatov R, Zeisel A, Braun E, Hochgerner H, Petukhov V, et al. RNA velocity of single cells. *Nature*. (2018) 560:494–8. doi: 10.1038/s41586-018-0414-6
25. Jin S, Guerrero-Juarez C, Zhang L, Chang I, Ramos R, Kuan C, et al. Inference and analysis of cell-cell communication using CellChat. *Nat Commun*. (2021) 12:1088. doi: 10.1038/s41467-021-21246-9
26. Yamasaki S, Matsumoto M, Takeuchi O, Matsuzawa T, Ishikawa E, Sakuma M, et al. C-type lectin Mincle is an activating receptor for pathogenic fungus, *Malassezia*. *Proc Natl Acad Sci U.S.A.* (2009) 106:1897–902. doi: 10.1073/pnas.0805177106
27. Grieshaber-Bouyer R, Nigrovic P. Neutrophil heterogeneity as therapeutic opportunity in immune-mediated disease. *Front Immunol*. (2019) 10:346. doi: 10.3389/fimmu.2019.00346
28. Li S, Zhang Y, Lu R, Lv X, Lei Q, Tang D, et al. Peroxiredoxin 1 aggravates acute kidney injury by promoting inflammation through Mincle/Syk/NF- κ B signaling. *Kidney Int*. (2023) 104:305–23. doi: 10.1016/j.kint.2023.04.013
29. Abedini A, Ma Z, Frederick J, Dhillion P, Balzer MS, Shrestha R, et al. Spatially resolved human kidney multi-omics single cell atlas highlights the key role of the fibrotic microenvironment in kidney disease progression. *bioRxiv*. (2022). doi: 10.1101/2022.10.24.513598. 2022.10.24.513598.
30. Lake B, Menon R, Winfree S, Hu Q, Melo Ferreira R, Kalhor K, et al. An atlas of healthy and injured cell states and niches in the human kidney. *Nature*. (2023) 619:585–94. doi: 10.1038/s41586-023-05769-3
31. Tang P, Nikolic-Paterson D, Lan H. Macrophages: versatile players in renal inflammation and fibrosis. *Nat Rev Nephrol*. (2019) 15:144–58. doi: 10.1038/s41581-019-0110-2
32. Yao W, Chen Y, Li Z, Ji J, You A, Jin S, et al. Single cell RNA sequencing identifies a unique inflammatory macrophage subset as a druggable target for alleviating acute kidney injury. *Adv Sci (Weinh)*. (2022) 9:e2103675. doi: 10.1002/advs.202103675
33. Ryu S, Shin J, Kwon S, Lee J, Kim Y, Bae Y, et al. Siglec-F-expressing neutrophils are essential for creating a profibrotic microenvironment in renal fibrosis. *J Clin Invest*. (2022) 132:e156876. doi: 10.1172/jci156876
34. Wang H, Gao M, Li J, Sun J, Wu R, Han D, et al. MMP-9-positive neutrophils are essential for establishing profibrotic microenvironment in the obstructed kidney of UUO mice. *Acta Physiol (Oxf)*. (2019) 227:e13317. doi: 10.1111/apha.13317
35. Skopelja-Gardner S, Tai J, Sun X, Tanaka L, Kuchenbecker J, Snyder J, et al. Acute skin exposure to ultraviolet light triggers neutrophil-mediated kidney inflammation. *Proc Natl Acad Sci USA*. (2021) 118:e2019097118. doi: 10.1073/pnas.2019097118
36. Wen Y, Lu X, Ren J, Privratsky J, Yang B, Rudemiller N, et al. α KLF4 in macrophages attenuates TNF-mediated kidney injury and fibrosis. *J Am Soc Nephrol*. (2019) 30:1925–38. doi: 10.1681/asn.2019020111
37. O'Sullivan E, Mylonas K, Xin C, Baird D, Carvalho C, Docherty M, et al. Indian Hedgehog release from TNF-activated renal epithelia drives local and remote organ fibrosis. *Sci Transl Med*. (2023) 15:eabn0736. doi: 10.1126/scitranslmed.abn0736
38. Mariani L, Eddy S, AlAkwa F, McCown P, Harder J, Nair V, et al. Precision nephrology identified tumor necrosis factor activation variability in minimal change disease and focal segmental glomerulosclerosis. *Kidney Int*. (2023) 103:565–79. doi: 10.1016/j.kint.2022.10.023
39. Liu F, Zhuang S. New therapies for the treatment of renal fibrosis. *Adv Exp Med Biol*. (2019) 1165:625–59. doi: 10.1007/978-981-13-8871-2_31
40. Tang T, Wang B, Lv L, Dong Z, Liu B. Extracellular vesicles for renal therapeutics: State of the art and future perspective. *J Control Release*. (2022) 349:32–50. doi: 10.1016/j.jconrel.2022.06.049
41. Tan R, Li J, Liu J, Lei X, Zhong X, Wang C, et al. BAY61-3606 protects kidney from acute ischemia/reperfusion injury through inhibiting spleen tyrosine kinase and suppressing inflammatory macrophage response. *FASEB J*. (2020) 34:15029–46. doi: 10.1096/fj.202000261RRR
42. Hui D, Rui-Zhi T, Jian-Chun L, Xia Z, Dan W, Jun-Ming F, et al. Astragalus propinquus Schischkin and Panax notoginseng (A&P) compound relieved cisplatin-induced acute kidney injury through inhibiting the mincle maintained macrophage inflammation. *J Ethnopharmacol*. (2020) 252:112637. doi: 10.1016/j.jep.2020.112637
43. Lei X, Tan R, Jia J, Wu S, Wen C, Lin X, et al. Artesunate relieves acute kidney injury through inhibiting macrophagic Mincle-mediated necroptosis and inflammation to tubular epithelial cell. *J Cell Mol Med*. (2021) 25:8775–88. doi: 10.1111/jcmm.16833
44. Xue V, Chung J, Tang P, Chan A, To T, Chung J, et al. USMB-shMincle: a virus-free gene therapy for blocking M1/M2 polarization of tumor-associated macrophages. *Mol Ther Oncolytics*. (2021) 23:26–37. doi: 10.1016/j.omto.2021.08.010
45. Stephens M, Keane K, Roizes S, Liao S, Weid P. Mincle-binding DNA aptamer demonstrates therapeutic potential in a model of inflammatory bowel disease. *Mol Ther Nucleic Acids*. (2022) 28:935–47. doi: 10.1016/j.omtn.2022.05.026
46. Tan R, Zhong X, Han R, Xie K, Jia J, Yang Y, et al. Macrophages mediate psoriasis via Mincle-dependent mechanism in mice. *Cell Death Discovery*. (2023) 9:140. doi: 10.1038/s41420-023-01444-8
47. Kellum J, Romagnani P, Ashuntantang G, Ronco C, Zarbock A, Anders H. Acute kidney injury. *Nat Rev Dis Primers*. (2021) 7:52. doi: 10.1038/s41572-021-00284-z



OPEN ACCESS

EDITED BY

Paola Italiani,
National Research Council (CNR), Italy

REVIEWED BY

Ivana Kawikova,
University of Hartford, United States
Till Adhikary,
University of Marburg, Germany

*CORRESPONDENCE

Toshiaki Ohteki
✉ ohteki.bre@mri.tmd.ac.jp

[†]These authors have contributed equally to this work

RECEIVED 09 March 2024

ACCEPTED 06 June 2024

PUBLISHED 08 July 2024


CITATION

Akiyama M, Kanayama M, Umezawa Y, Nagao T, Izumi Y, Yamamoto M and Ohteki T (2024) An early regulatory mechanism of hyperinflammation by restricting monocyte contribution.
Front. Immunol. 15:1398153.
doi: 10.3389/fimmu.2024.1398153

COPYRIGHT

© 2024 Akiyama, Kanayama, Umezawa, Nagao, Izumi, Yamamoto and Ohteki. This is an open-access article distributed under the terms of the [Creative Commons Attribution License \(CC BY\)](#). The use, distribution or reproduction in other forums is permitted, provided the original author(s) and the copyright owner(s) are credited and that the original publication in this journal is cited, in accordance with accepted academic practice. No use, distribution or reproduction is permitted which does not comply with these terms.

An early regulatory mechanism of hyperinflammation by restricting monocyte contribution

Megumi Akiyama^{1,2†}, Masashi Kanayama^{1†},
Yoshihiro Umezawa², Toshikage Nagao², Yuta Izumi¹,
Masahide Yamamoto² and Toshiaki Ohteki^{1*} 

¹Department of Biodefense Research, Medical Research Institute, Tokyo Medical and Dental University (TMDU), Tokyo, Japan, ²Department of Hematology, Graduate School of Medical and Dental Sciences, TMDU, Tokyo, Japan

Innate immune cells play a key role in inflammation as a source of pro-inflammatory cytokines. However, it remains unclear how innate immunity-mediated inflammation is fine-tuned to minimize tissue damage and assure the host's survival at the early phase of systemic inflammation. The results of this study with mouse models demonstrate that the supply of monocytes is restricted depending on the magnitude of inflammation. During the acute phase of severe inflammation, monocytes, but not neutrophils, were substantially reduced by apoptosis and the remaining monocytes were dysfunctional in the bone marrow. Monocyte-specific ablation of *Casp3/7* prevented monocyte apoptosis but promoted monocyte necrosis in the bone marrow, leading to elevated levels of pro-inflammatory cytokines and the increased mortality of mice during systemic inflammation. Importantly, the limitation of monocyte supply was dependent on pro-inflammatory cytokines *in vivo*. Consistently, a reduction of monocytes was observed in the peripheral blood during cytokine-release syndrome (CRS) patients, a pathogen-unrelated systemic inflammation induced by chimeric antigen receptor-T cell (CAR-T cell) therapy. Thus, monocytes act as a safety valve to alleviate tissue damage caused by inflammation and ensure host survival, which may be responsible for a primitive immune-control mechanism that does not require intervention by acquired immunity.

KEYWORDS

monocyte, apoptosis, inflammation, cytokine, CRS - cytokine release syndrome

1 Introduction

Inflammation is a basic biological phenomenon that is mediated by the immune system and therefore has been studied for a long time. Although inflammatory responses are necessary to maintain homeostasis (1), they can be a serious risk to life and health if inappropriately driven and sustained. Before the COVID-19 pandemic, about 19.7% of deaths were related to sepsis, a life-threatening multiple organ failure induced by infection-mediated inflammation (2), in the world (3). After the pandemic, the mortality of COVID-19 patients with severe sepsis reached up to 48% (4). In addition to infection-induced inflammation, immune therapies such as chimeric antigen receptor-T cell (CAR-T cell) treatment of patients with hematological malignancies often cause an acute systemic inflammation known as cytokine release syndrome (CRS), which sometimes threatens the lives of patients. Thus, regardless of pathogen involvement, controlling severe systemic inflammation remains the biggest challenge even today.

Innate immunity plays a critical role in host protection by phagocytosing pathogens, producing cytokines and inducing adaptive immunity. However, at the same time, the production of systemic cytokines by activated innate immune cells causes tissue damage and the dysfunction of multiple organs during systemic infection, which could be a life-threatening risk (5–7). Especially in the early stage of inflammation, the mechanism of innate immunity to regulate the balance between host protection and inflammation-mediated tissue damage has not been fully understood.

Monocytes are a unique immune cell population that can differentiate into multiple cell lineages such as macrophages and dendritic cells (8), even though they are constantly provided to the periphery through circulating blood (9). Classical monocytes, a major subset of monocytes, are related to the pathogenesis of various diseases such as cancer, infection and inflammation by producing cytokines and differentiating into pro-inflammatory and into anti-inflammatory cell populations (10–15). In the early stage of infection, monocytes are recruited from the bone marrow (BM) to infected sites and play roles in inflammation and pathogen clearance (10, 16). Indeed, genetic deletion of *Ccr2*, a gene encoding a critical chemokine receptor for monocyte exit from the BM to the periphery, decreased the severity of sepsis after cecal ligation and puncture (CLP) induction with reduced systemic cytokine production, suggesting that existing monocytes in the periphery are important for the progression of inflammation (17). In addition, the tolerance and trained memory of monocytes modify the secondary immune responses at the late phase of inflammatory responses including microbial infections (18). However, the early regulatory mechanism of excessive inflammation that affects the fate of monocytes has remained unclear.

In this study, we found that the fate of monocytes is dramatically changed to maintain homeostasis depending on the intensity of systemic inflammation. At early stages of severe systemic inflammation, the number of monocytes was significantly reduced in peripheral organs although neutrophils were successfully supplied to the periphery. This was because half of the monocytes were immediately killed by apoptosis, and the remaining monocytes were dysfunctional and failed to migrate into the periphery. Importantly, the mechanism to prevent monocyte

supply was pro-inflammatory cytokine-dependent and driven only when severe inflammation was induced. The monocyte-specific ablation of *Casp3* and *Casp7* prevented their apoptosis but promoted monocyte necrosis, which increased both the production of pro-inflammatory cytokines and the mortality of mice during sepsis. Finally, we collected blood samples of CRS patients who received CAR-T cell therapy and confirmed that the classical monocyte counts in their blood were reduced at early phases of inflammation. Collectively, monocytes sense the severity of inflammation to decide whether to participate in the inflammatory responses or commit suicide or dysfunction to reduce the tissue damage and ensure the host's survival.

2 Materials and methods

2.1 Mice

C57BL/6J (B6) mice were obtained from Japan Slc Inc. (Hamamatsu, Japan). B6.SJL-ptprca (B6.SJL, Strain #: 4007) mice congenic at the CD45 locus (CD45.1⁺CD45.2⁻), CAG-EGFP mice (Strain#: 006567), *Ccr2*^{-/-} mice (Strain#: 004999) and *Ccr2-creERT2* mice (Strain #: 035229) were obtained from Jackson Laboratories (Bar Harbor, ME, USA). *Casp3*^{flox/flox} mice and *Casp7*^{-/-} mice were generated as shown in [Supplementary Figures 3A, B](#). *Casp3-flox* and *Casp7* Knockout (KO) mice were generated using the CRISPR/Cas system as previously reported (19) with slight modifications. For *Casp3-flox*, two crRNAs were synthesized (Fasmac, Kanagawa, Japan) to target the 5'-CAACAACCTCAAGTTAAGTAC-3' and 5'-GTCTCATCTTGAGGCCAAGG-3' sequences in introns flanking the *Casp3* exon2 containing the start codon. The plasmid vector used to generate the floxed allele of *Casp3* was constructed with the 5'- and 3'-homology arms of 1500 bases long loxP sequences (5'-ATAACTTCGTATAGCATACATTATACGAAGTTAT-3') placed at the cleavage sites by Cas9 and restriction sites (Sall and NotI). For *Casp7* KO, two crRNAs targeting the 5'-AAGCAGCCCA CAGAACAGCT-3' sequence in the intron between exons 4 and 5 and the 5'-TGTTTCCTTGCCCCGCCAAG-3' sequence in the intron between exons 6 and 7 were synthesized (Fasmac) to delete exons 5 and 6. To generate the KO allele with a precisely designed DNA sequence, a 150-mer single-stranded oligodeoxynucleotide (ssODN) was synthesized (5'-CACCTCTTTATAGAGAGAG AAGAAAATGGAGGTTAGCCAACCTCTCTCTGCTGTCA CAAAGCAGCCCA CAGAACAAAGGGGACCTGGCTCAGTGGG CAAGCTACTTG CAGTACAAGCAATGAGGACCCAAGA CCGAATCCCCAGCATCTA-3' by Hokkaido System Science (Sapporo, Japan). A mixture of Cas9 protein (final concentration of 30 ng/μl, NEB), crRNAs (8.7 ng/μl each), tracrRNA (28.6 ng/μl, Fasmac), the plasmid vector (10 ng/μl) and the ssODN (15 ng/μl) was injected into the pronuclei of C57BL/6J zygotes produced by *in vitro* fertilization. Zygotes surviving after the injection were transferred into the ampullae of the oviducts of pseudopregnant female mice. After natural delivery or caesarean section, newborn pups were genotyped using PCR primer pairs (5'-GTAAGCTA ACCGAGCCAATG-3' and 5'-AGTCAGGTAGATCAGAGGTC-3' for *Casp3-flox*, 5'-GACGGAGCACACCTTTAATCC-3' and 5'-

CAGTCTGTCGGAATTTGGAGC-3' for *Casp7* KO), restriction enzymes and Sanger sequencing. Founder mice with the expected genetic modifications were used for further experiments.

2.2 Study design for CAR-T cell therapy

We performed an analysis of patients with relapse/refractory diffuse large B cell lymphoma (DLBCL), B-cell lymphoid leukemia (B-ALL), who were treated with CD19-targeted CAR T-cell therapy. We prospectively collected blood samples on CRS patients in Tokyo medical and dental university hospital. Samples were collected from 22 patients between July 2020 and April 2023 and 3 patients were excluded from the analysis of this study according to the reasons shown in [Supplementary Figure 4E](#). Nineteen patients were treated with a lymphocyte-depletion regimen (Fludarabine 25 mg/m² + Cyclophosphamide 250 mg/m²; Flu+CY) from Day -5 to Day -3 and CD19-specific CAR-T cells (tisagenlecleucel, tisa-cel) (Novartis, Basel, Switzerland) were infused at Day 0. Blood samples were collected before CAR-T cell administration until Day 14. All patients were enrolled in this study with protocols approved by the Institutional Review Board of the Tokyo Medical and Dental University, and written informed consent was obtained from a legally authorized representative as per the Declaration of Helsinki. CRS grading was defined by clinicians blinded to the results of the analysis based on Penn CRS grading ([Supplementary Table 1](#)) (20). Blood samples were collected in vacutainer tubes containing heparin. Sample tubes were delivered to the laboratory within 4 hours of the sample draw. Peripheral blood mononuclear cells (PBMCs) were purified via density gradient centrifugation and were processed for flow cytometry analysis. Lymphocyte separation solution ($d = 1.077$, $d = 1.119$) (Nacalai Tesque Inc., Kyoto, Japan) was used. The blood samples were placed at room temperature for 30–60 min after the blood collection and then kept on ice for all experimental steps until FACS analysis, except for density gradient centrifugation. Plasma samples were stored at -80°C.

Patients' medical records were reviewed for laboratory data and outcomes. All data were collected from documentation in the medical records. Clinical laboratory studies, including complete blood count (CBC) with differential, C-reactive protein (CRP), lactate dehydrogenase (LDH) and fibrinogen (Fbg) were performed in the Tokyo Medical and Dental University Hospital.

2.3 Flow cytometry and cell sorting

After staining with specific antibodies, cells were analyzed using a FACS AriaTM III (BD Bioscience, Franklin Lakes, NJ, USA) and then by FlowJo software (Treestar Inc., Ashland, OR, USA). For sorting of monocytes, BM cells were stained with PE/Cy5-conjugated antibodies against TER119, B220, Ly6G, CD4, CD3e, CD8a (Thermo Fisher Scientific), NK1.1 and CD19 (Biolegend). After washing, cells were incubated with anti-Cy5 microbeads (Miltenyi Biotec, Bergisch Gladbach, Germany) and monocytes were briefly isolated by negative isolation with Auto MACS (Miltenyi Biotec). Monocytes were then stained with a specific

antibody and the Ly6C^{hi} monocyte fraction was isolated using a FACS AriaTM III. For counting cell numbers, CountBrightTM absolute counting beads (Thermo Fisher Scientific) were used.

2.4 Real-time PCR

Total mRNAs were reverse-transcribed to cDNAs and gene expression levels were determined using a Light Cycler 480 and SYBR Green I Master (04707516001, Roche Diagnostics, Basel, Switzerland). The values were normalized according to the expression of β -actin. Specific primers used for real-time PCR are shown in [Supplementary Table 4](#).

2.5 Quantification of cytokines

To measure cytokine production from monocytes, BM monocytes obtained from wild type (WT) mice before and 12 hours after lipopolysaccharide (LPS, L2880–100mg, Sigma-Aldrich, Saint Louis, MO, USA) treatment (5 mg/kg) were cultured overnight with RPMI-1640 containing 10% FBS in the absence or presence of LPS (100 ng/ml). Supernatants were collected and analyzed using a LEGENDplexTM Mouse Macrophage/Microglia Panel kit (BioLegend, San Diego, CA, USA). *Casp3/7*^{Amono} and their littermate control mice were treated with 20 mg/kg LPS and plasma was collected 2 hours after the LPS injection to evaluate the levels of TNF- α , IL-6, IL-1 β and IL-10 using ELISA kits (R&D Systems, Minneapolis, MN, USA and Biolegend). For blood samples of CRS patients, a LEGENDplexTM Human Inflammation Panel 1 kit (Biolegend) was used to measure the levels of cytokines.

2.6 Cytological analysis

CD11b⁺Ly6C^{hi}Ly6G⁻ monocytes were obtained from the BM 12 hours after treatment (5 mg/kg). Cells were stained with Diff Quik (Sysmex, Kobe, Japan) and the diameters of nuclei in each population were evaluated using Image J.

2.7 Evaluation of apoptosis

Cells were obtained from the BM, peripheral blood, and spleen 2, 4, 6 and 12 hours after LPS injection (5 mg/kg). After staining cell surface markers for neutrophils and monocytes, cells were stained with a PE-conjugated anti-Annexin V antibody (Thermo Fisher Scientific, Waltham, MA, USA) and propidium iodide (PI) and were analyzed by flow cytometry. For the detection of cells expressing active caspase-3/7, cells were stained with CellEventTM Caspase-3/7 Detection Reagents (Thermo Fisher Scientific) after the cell surface marker staining. For detection of cells expressing active caspase-1, cells were stained with a FAM-FLICA^(R) Caspase 1 Assay Kit (Immunochemistry Technologies, Davis, CA, USA) after the cell surface marker staining.

2.8 *In vitro* stimulation of BM cells

Monocytes, neutrophils, and B cells isolated from naïve WT mice were cultured with LPS (10–1000 ng/ml) and/or cytokines (50 ng/ml, Biolegend) at 37°C for 3 hours. For caspase-blockade, cells were pre-cultured with inhibitors for Caspase-1 (Z-YVAD-FMK), Caspase-3 (Z-DEVD-FMK), Caspase-8 (Z-IETD-FMK) or Caspase-9 (Z-LEHD-FMK) (1–100 μ M) (R&D Systems) before the stimulation. After stimulation, live cell numbers were counted by flow cytometry using CountBright™ absolute counting beads (Thermo Fisher Scientific).

2.9 Cecal ligation and puncture model

Mice were anesthetized by intraperitoneal injection of an anesthetic mixture of medetomidine, midazolam and butorphanol. The abdomen of each mouse was then shaved and a laparotomy was performed. The cecum was exposed and tightly ligated 1.0 cm from the distal end. The ligated cecum was then perforated twice with a 26G or 19G needle. The cecum was returned to the peritoneal cavity after gentle squeezing to extrude a small amount of feces from the perforated sites. The peritoneum was sutured, and the skin was closed using a clip. Twelve hours after CLP induction, the mice were sacrificed and the frequencies and absolute numbers of neutrophils and monocytes in the BM and the peritoneal cavity were determined using flow cytometry.

2.10 Cytokine administration

Carrier-free recombinant mouse TNF- α and IFN- γ (10 μ g/mouse each) (Biolegend, endotoxin level: <0.1 EU/ μ g protein) were mixed and administered intraperitoneally to WT C57BL/6J mice after which the numbers, PI⁺ dead cell ratio, and active caspase3/7-expressing apoptotic cell ratio in monocytes and neutrophils obtained from the BM and peripheral blood were evaluated 6 hours after the cytokine treatment.

2.11 Intra-BM transplantation

Mice were anesthetized by an intraperitoneal injection of an anesthetic mixture of medetomidine, midazolam and butorphanol, after which monocytes obtained from the BM of CAG-EGFP mice were transplanted into the tibias of recipient B6.SJL mice. After the intra-BM transplantation, mice were quickly recovered by an injection of atipamezole. The mice were then treated with LPS (5 mg/kg) 1 hour after the transplantation. Eighteen hours after treatment, the distribution, expression of monocyte markers and cell death of donor cells were analyzed using FACS. To examine the apoptosis in monocytes, monocytes sorted from the BM of naïve TLR4-deficient or sufficient mice were transplanted into the BM of B6.SJL mice. Then, LPS (5 mg/kg) was intraperitoneally injected into the recipient mice and the apoptotic cell ratio was determined in the BM donor monocytes 6 hours after the LPS-treatment.

2.12 Transwell migration assay

To evaluate the migration capacity of monocytes toward CCL2, Transwell migration assays (3- μ m pores, Corning, Pittsburgh, PA, USA, #3402) were performed. Monocytes (3×10^5 cells) obtained from the BM before and after LPS treatment (5 mg/kg) were placed in the upper chamber and different doses of recombinant CCL2 (0, 2.5, 10, 50 ng/ml) (Biolegend) were added in the lower chamber. The cells were then cultured 12 hours at 37°C with 5% CO₂. Cells that had migrated from the lower chamber were counted by FACS with cell counting beads (Thermo Fisher Scientific).

2.13 Western blot analysis

Western blotting was performed as previously described (21). *Casp3/7^{Δmono}* mice were treated with 100 mg/kg tamoxifen intraperitoneally for 5 days. Two days after the last injection of tamoxifen, monocytes ($2\text{--}3 \times 10^5$ cells) were sorted from the BM of WT mice and of *Casp3/7^{Δmono}* mice and were lysed in lysis buffer containing 1% Triton X-100, 20 mM Tris-HCl (pH 7.5), 150 mM NaCl, 1 mM EDTA, 1 mM sodium orthovanadate, 1 mM phenylmethylsulfonyl fluoride, 10 μ g/ml aprotinin and 10 μ g/ml leupeptin. The lysates were incubated on ice for 15 minutes and the supernatants were collected after centrifugation at 15,000 rpm, 4 °C for 20 min. The supernatants were mixed with 1 volume of 2x Laemmli sample buffer and were separated by electrophoresis on SDS-PAGE gels (Biorad, Hercules, CA, USA). The proteins were transferred to Immobilon P membranes (Millipore, Darmstadt, Germany) using a wet transfer method. Western blotting was performed using specific antibodies against β -actin (Sigma-Aldrich), Caspase3 (Cell Signaling Technology, Danvers, MA, USA, #14220T) and Caspase7 (Cell Signaling #12827T) and the proteins detected by those antibodies were visualized using a chemiluminescence kit (Western Lightning Plus-ECL, PerkinElmer, Waltham, MA, USA).

2.14 Statistical analysis

Statistical analyses were performed using Microsoft Excel or Prism software version 3 (GraphPad, San Diego, CA, USA). A two-tailed Student's t-test was used for statistical analyses of two-group comparisons. Multigroup comparisons were performed using one-way analysis of variance (ANOVA) followed by the Tukey–Kramer multiple comparisons test. The criterion of significance was set at $p < 0.05$. Results are expressed as means \pm standard error of the mean (SEM). For analysis of survival of the high dose LPS challenge, each group was subjected to Kaplan-Meier analysis and comparisons were performed using the log-rank test. CRS grading was defined by clinicians blinded to the results of analysis based on Penn CRS grading (Supplementary Table 1). Samples from 3 patients were excluded from the analysis as shown in Supplementary Figure 4E. Randomization of the groups was not performed. No statistical methods were used to estimate sample size.

3 Results

3.1 Disappearance of monocytes at early phase of systemic inflammation

To examine the kinetics of monocytes in acute systemic inflammation, we intraperitoneally administered a sublethal dosage of LPS (5 mg/kg) to WT C57BL/6 mice to induce sepsis. After LPS treatment, the upregulation of chemoattractants for monocytes (*Ccl2*, *Ccl3*, *Ccl4*, *Ccl6*, *Ccl7* and *Ccl8*) and neutrophils (*Cxcl1* and *Cxcl2*) was examined in various peripheral organs (Supplementary Figure 1A). Consistent with previous reports, major monocyte and neutrophil chemoattractants such as CCL2, CCL7, and CXCL1/2 were substantially elevated (Supplementary Figure 1A), which are driven by common transcription factors NF- κ B and/or AP-1 both in mice and in humans (22–24). We then examined the kinetics of monocytes in the BM, peripheral blood, spleen, and peritoneal cavity of mice after LPS treatment and found that about half of classical monocytes (hereafter referred to as “monocyte”) and neutrophils were lost in the BM within 12 hours after sepsis induction (Figures 1A–C; gating strategy is shown in Supplementary Figure 1B). Interestingly, the increase of monocytes was not observed in the blood and spleen until 72 hours after LPS treatment (Figures 1A, B), although neutrophils were greatly increased in the peripheral blood 12 hours after sepsis induction (Figure 1C). Thus, we investigated where the monocytes that were lost in the BM went. However, LPS injection did not increase the number of monocytes in most peripheral organs at 12 hours after treatment (Figure 1D). In some organs, such as the peritoneal cavity and kidney, an increase of monocytes was observed within 12 or 24 hours after LPS treatment (Figures 1A, D). Consistent with previous reports (25, 26), monocytes accumulated transiently in the lungs 2 hours after the injection of LPS. However, those effects were too small to explain the decrease of monocytes in the BM (Figures 1A, D, Supplementary Figure 1C). We transferred Ly6C^{hi} monocytes from CAG-EGFP mice (CD45.2) into the BM of B6.SJL mice (CD45.1) and examined the donor-derived monocytes in the BM and spleen 12 hours after LPS treatment (Figure 1E). Compared to naïve conditions, the LPS treatment significantly decreased the ratio of splenic monocytes/BM monocytes (Figure 1F), suggesting that BM monocytes do not distribute to the periphery at the early stage of LPS-induced sepsis. To further demonstrate that the LPS-induced monocyte reduction in the BM was unlikely due to the egress of monocytes from the BM, we induced LPS-induced sepsis in CCR2-deficient mice (Figure 1G). As the decrease of monocytes in the BM was observed even in CCR2-deficient mice 12 hours after LPS treatment (Figure 1G), the egress of monocytes from the BM seems not to be a cause of the monocyte reduction in the BM at the early stage of sepsis. To further examine whether LPS treatment altered the expression of monocyte markers, which would make monocyte identification difficult, we transferred BM-derived monocytes from CAG-EGFP mice into the BM of recipient mice and examined the expression of monocyte markers 12 hours after LPS treatment (Figures 1E, H). The expression of CD11b and Ly6C was maintained and Ly6G was not expressed in the donor-derived monocytes regardless of LPS-injection (Figure 1H), ruling out the possible alteration of monocyte markers.

3.2 Monocytes are eliminated by apoptosis early after systemic inflammation

To examine the reason for the disappearance of monocytes in peripheral organs after LPS treatment, we evaluated cell death in monocytes and neutrophils 12 hours after LPS treatment. Staining with propidium iodide (PI) and Annexin V revealed that the frequency of dead cells (PI⁺ Annexin V⁺) in monocytes was increased immediately after LPS treatment (Figure 2A), and the increase of cell death in monocytes was significantly higher than that in neutrophils (Figure 2B). When monocytes isolated from the BM of CAG-EGFP mice were transferred into the BM of recipient mice (as shown in Figure 1E), the frequency of PI⁺ dead cells was increased in donor monocytes after LPS treatment (Figure 2C). Staining for active caspase-3/7 demonstrated that apoptosis is selectively induced in monocytes, but not in neutrophils or other leukocytes in the BM, spleen and peripheral blood after LPS treatment (Figures 2D, E), which suggests that monocyte apoptosis was induced in both the BM and the periphery. In contrast, the frequencies of active caspase-1-expressing cells were comparable between monocytes and neutrophils after LPS treatment (Figure 2F), suggesting that pyroptosis could not explain the selective disappearance of monocytes in peripheral organs after sepsis induction.

We next examined whether inflammatory stimuli cause the cell death of monocytes *in vitro*. We isolated Ly6C^{hi} monocytes from the BM of naïve WT mice and cultured them with LPS or with inflammatory cytokines for 3 hours (Figure 2G) and found that LPS and inflammatory cytokines such as IFN- γ and TNF- α but not IL-6, quickly decreased the number of live monocytes (Figure 2H). In contrast, the impact of the stimulation with LPS or with cytokines in the cell death of neutrophils and B cells was much lower than that of monocytes (Figure 2I), which suggests that the monocyte-specific cell death program is driven by infection/inflammation. Consistent with the low induction of apoptosis in B cells, we recently showed that the number of B cells was not decreased in the BM within 12 hours after a high dose LPS injection (27). To demonstrate how monocytes were killed by inflammatory stimuli, we pre-cultured monocytes in the presence of inhibitors for caspases-3, 8, 9 or 1 for 30 minutes and then stimulated them with LPS. Live cell counts revealed that only the caspase-3 inhibitor suppressed the cell death (Figure 2J), which indicates that monocytes are eliminated by apoptosis. Taken together, microbial and/or inflammatory signals eliminate monocytes by inducing apoptosis early after the onset of sepsis.

3.3 Functional alteration of monocytes in the BM during systemic inflammation

Half of the monocytes were eliminated by apoptosis early after sepsis, meaning that the other half of the monocytes survived (Figures 1A, B). We characterized the surviving monocytes in the BM. The monocytes from LPS-treated mice and from naïve monocytes showed kidney-shaped nuclei, a representative monocyte morphology (Figure 3A). However, the LPS-treated

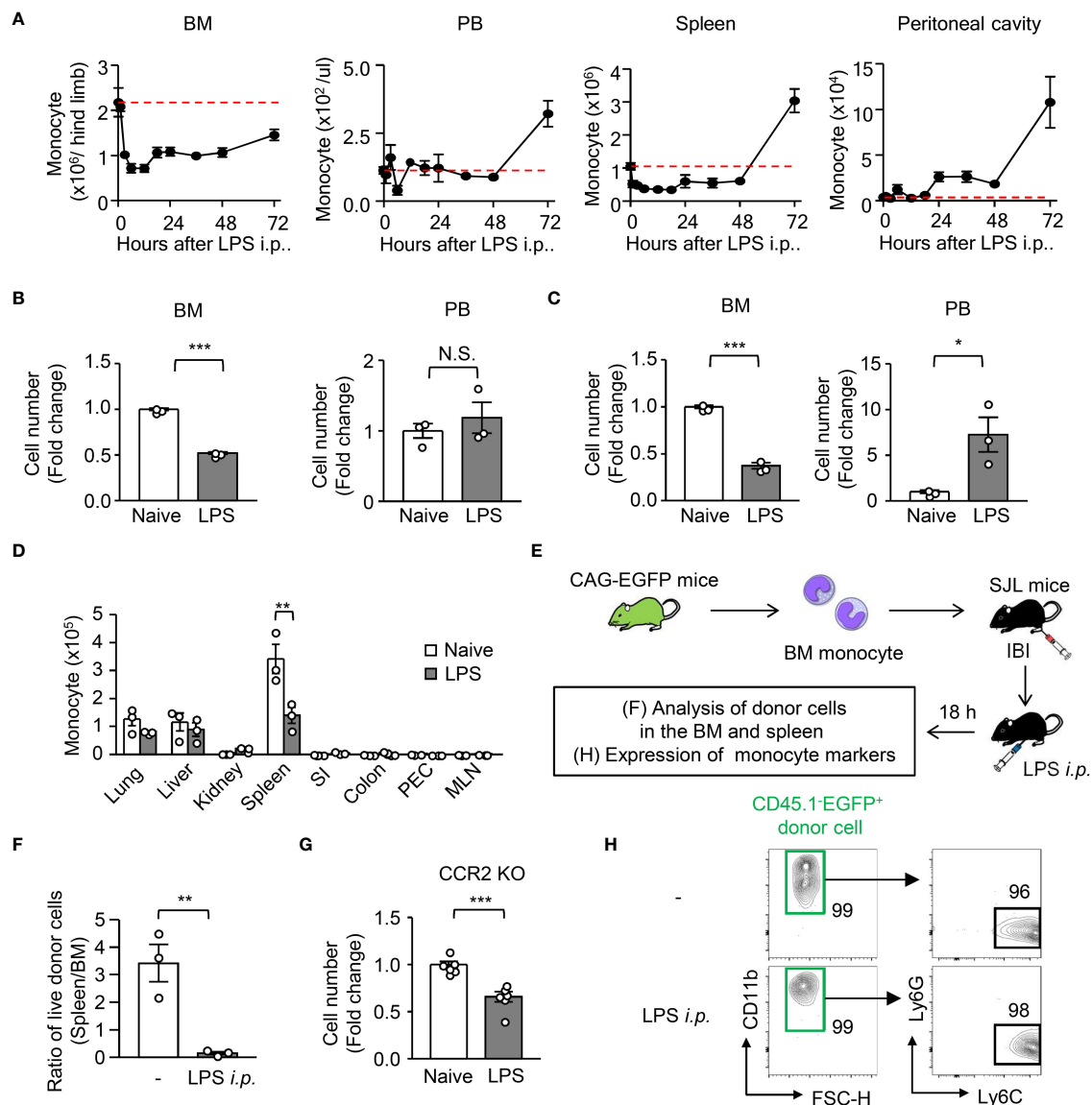


FIGURE 1

Kinetic analysis of monocytes and neutrophils during LPS-induced inflammation. LPS (5 mg/kg) was intraperitoneally injected into WT C57BL/6J mice to mimic systemic inflammation caused by a systemic bacterial infection. **(A)** Kinetics of monocytes (Mo) in the BM, peripheral blood (PB), spleen and peritoneal cavity from 0 to 72 hours after treatment with LPS; red dotted lines indicate monocyte numbers at naive conditions. **(B–D)** Numbers of monocytes (**B**, **D**) and neutrophils (**C**) in the BM and PB (**B**, **C**) and/or lung, liver, kidney, spleen, small intestine (SI), colon, peritoneal cavity (PEC) and mesenteric lymph node (MLN) (**D**) 12 hours after LPS treatment; n=3 each group. **(E, F, H)** Experimental strategy for intra-BM injection of monocytes obtained from CAG-EGFP mice (**E**). Monocytes obtained from the BM of naive CAG-EGFP mice were transferred into the BM of B6.SJL mice after which the mice received LPS treatment. The ratio of monocyte number between spleen and BM (**F**) and the expression of monocyte markers (**H**) were examined 18 hours after LPS treatment; n=3 each group. The numbers on the FCM plots indicate the frequencies of the gated populations. **(G)** Monocyte number in the BM of CCR2-deficient mice before and 12 hours after LPS treatment; n=3 each group. *p<0.05, **p<0.01, ***p<0.001, N.S., not significantly different (Student's t-test). Data are representative of two independent experiments (error bars, SEM).

monocytes were significantly larger in size than the naive monocytes (Figure 3B). Monocyte egress from the BM is dependent on CCR2, a receptor for CCL2, during infection (28). The BM monocytes from LPS-treated mice maintained their CCR2 expression even after LPS treatment (Figures 3C–E). However, they showed an impaired migration ability toward CCL2 compared to BM monocytes from naive mice (Figures 3F, G), which suggested that surviving monocytes in the BM after sepsis had lost their capacity to migrate out of the BM.

M-CSF-mediated signaling promotes monocyte differentiation into macrophages, and LPS treatment induces ADAM17-dependent shedding of CD115, a receptor for M-CSF (29). In this context, CD115 expression on the surface of BM monocytes was largely abolished within 3 hours after LPS treatment (Supplementary Figure 2A). To examine the differentiation capacity of monocytes *in vivo*, we obtained BM monocytes before and after LPS treatment and transferred them into the peritoneal cavity of naive B6.SJL mice, after which flow cytometry was used to examine the generation of

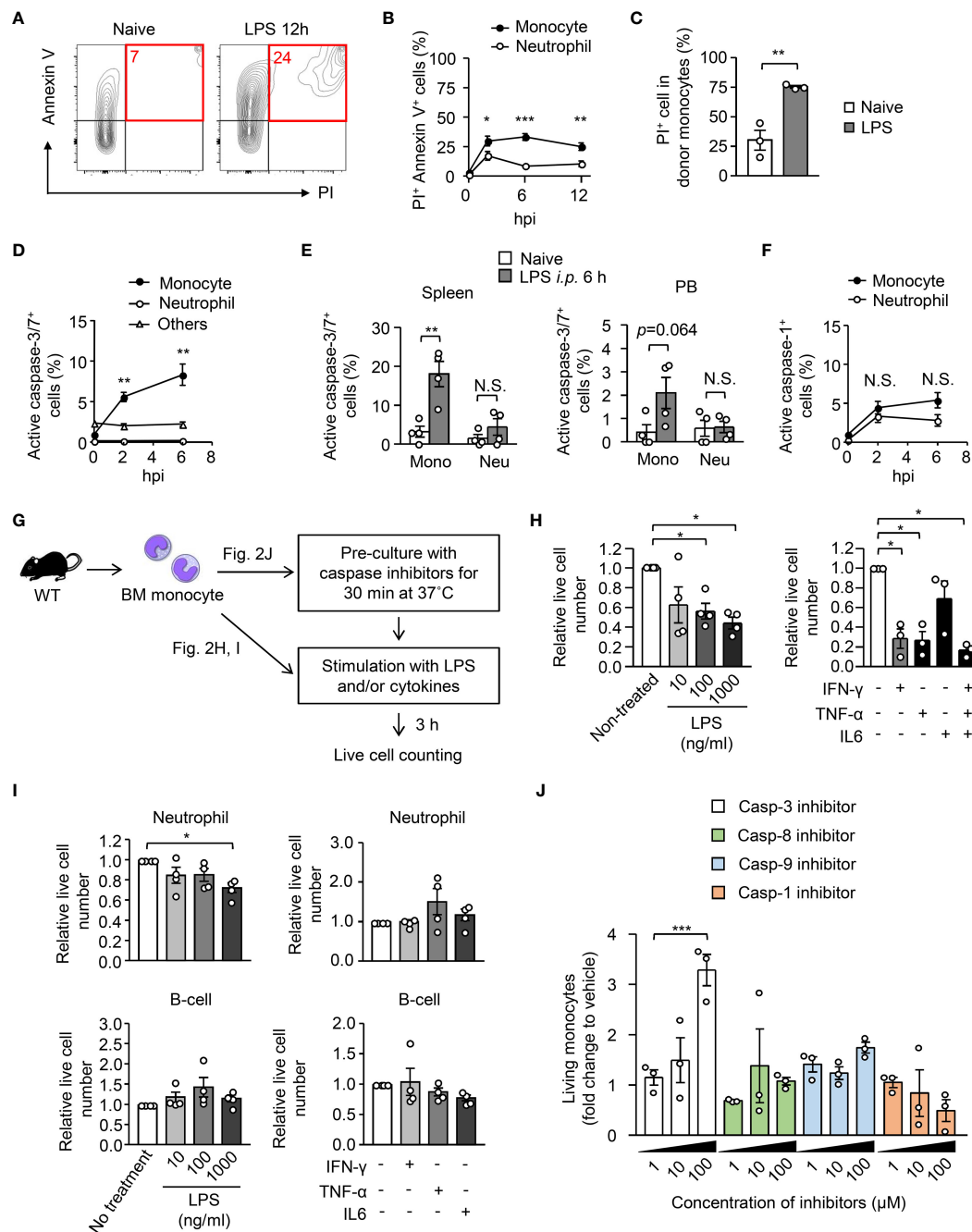


FIGURE 2

Exclusion of monocytes by apoptosis early after systemic inflammation. (A, B) Evaluation of cell death of BM monocytes before and after intraperitoneal injection of LPS (5 mg/kg). BM cells were obtained before and 6 or 12 hours after LPS treatment and the frequencies of the PI⁺ AnnexinV⁺ fraction were measured using FACS; representative FACS plots are shown in (A). (C) EGFP⁺ monocytes were transferred to B6.SJL mice as shown in Figure 1E and the frequency of PI⁺ dead cells was examined in donor monocytes 18 hours after LPS treatment; n=4 per group. (D, E) Frequencies of apoptotic cells in monocytes obtained from the BM (D), spleen and PB (E) were evaluated by counting active caspase-3/7-expressing cells; n=4 per group for (D, E). (F) Frequencies of active caspase-1-expressing cells in BM monocytes before and after LPS administration; n=4 per group. (G–I) Induction of apoptosis in monocytes by *ex vivo* stimulation with LPS or cytokines. Monocytes (H), neutrophils and B cells (I) obtained from the BM of naive WT mice were stimulated with LPS or indicated cytokines for 3 hours, and surviving cell numbers were counted by FACS with cell counting beads; n=4 per group. The experimental strategy is shown in (G). (J) BM monocytes obtained from naive WT mice were pre-cultured in the presence of caspase inhibitors at various concentrations as indicated for 30 minutes and then were stimulated with LPS (10 ng/ml) for 3 hours. Surviving cell numbers were examined by FACS with cell counting beads. *p<0.05, **p<0.01, ***p<0.001, N.S., not significantly different (one-way ANOVA). Data are representative of two independent experiments (error bars, SEM).

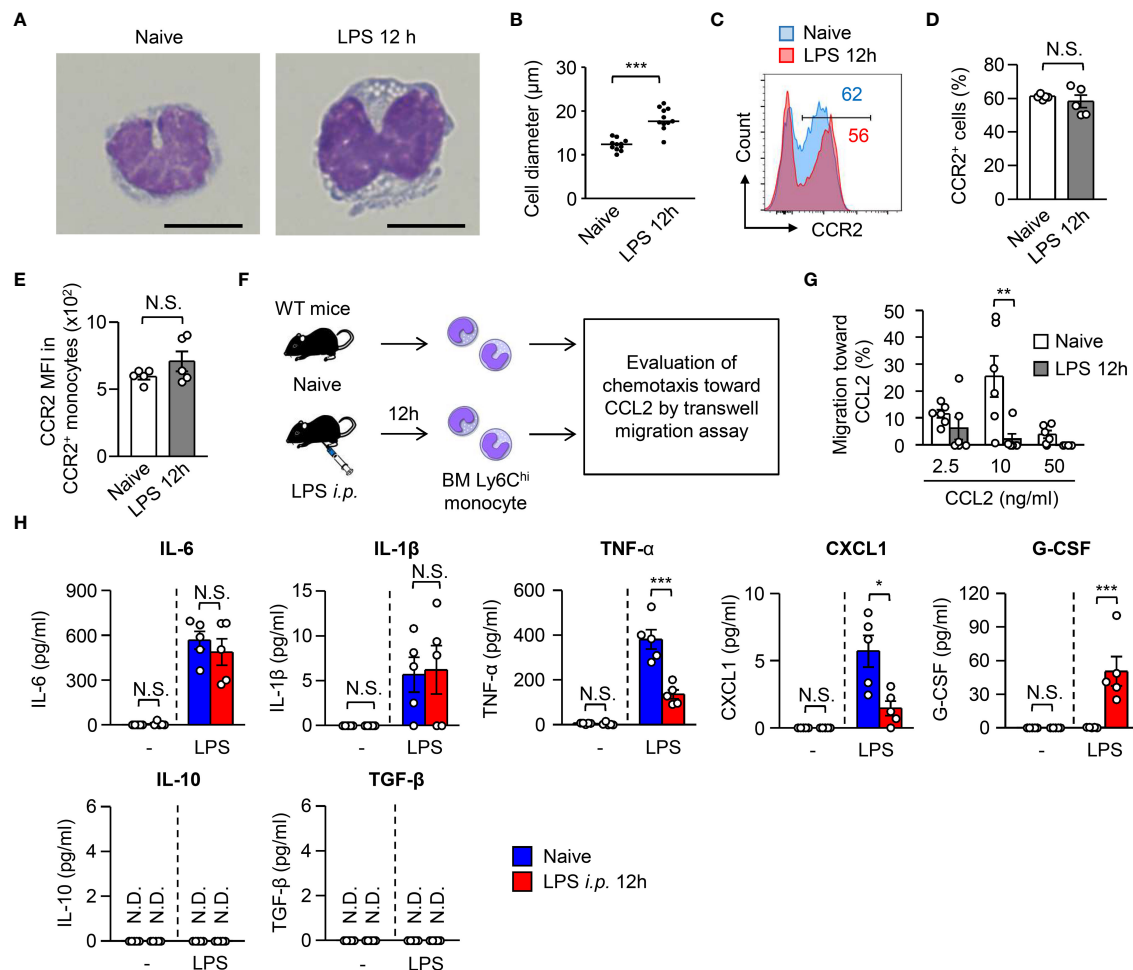


FIGURE 3

Monocytes surviving in the BM after LPS treatment lose their functions. (A, B) Morphology of monocytes obtained from the BM of WT C57BL/6 mice before and 12 hours after LPS treatment (5 mg/kg). Representative images and the maximum diameter of BM monocytes are shown in (A, B), respectively; scale bars indicate 5 μ m. (C–E) Expression of CCR2 on monocytes obtained from the BM of WT C57BL/6 mice before and 12 hours after LPS treatment (5 mg/kg). Representative FACS plots are shown in (C) and statistical analysis of the frequencies of CCR2⁺ cells (D) and the CCR2 mean fluorescence intensity (MFI) (E) of BM monocytes is shown in (D); n=5 per group. (F, G) Transwell migration assay for BM monocytes. Monocytes were obtained from the BM of naive or LPS-treated WT C57BL/6 mice (3×10^5 cells/well) and were added to the upper chamber with the indicated concentration of recombinant mouse CCL2 added in the lower chamber. The cells were then incubated at 37°C overnight, after which the number of migrated monocytes was counted by FACS with cell-counting beads. The experimental strategy is shown in (F) and statistical analysis of specific migration toward CCL2 is shown in (G); n=6 per group. (H) Cytokine production by monocytes obtained from the BM of naive or LPS-treated mice. BM monocytes were obtained from WT mice before and 12 hours after LPS treatment (5 mg/kg) and were cultured (5×10^5 cells/ml) in the presence of LPS (100 ng/ml) for 24 hours. N.S., not significantly different. Supernatants were collected and the production of cytokines was evaluated using Legendplex. *p<0.05, **p<0.01, ***p<0.001, N.S., not significantly different; N.D., not detectable [Student t-test (D, E) and one-way ANOVA (G)]. Data are representative of two independent experiments (A–E) or pooled from two independent experiments (G) (error bars, SEM).

F4/80⁺Ly6C⁺ macrophages from F4/80⁺Ly6C⁺ monocytes (Supplementary Figure 2B). As expected, the monocytes obtained from LPS-treated mice showed impaired differentiation into macrophages (Supplementary Figures 2C, D).

Monocytes act as a source of cytokines during infections (17, 28). Thus, we evaluated the cytokine production ability of BM monocytes from naive and from LPS-treated mice (Figure 3H, Supplementary Figure 2E) and found that BM monocytes from LPS-treated mice showed significantly lower production of TNF- α , a representative cytokine involved in sepsis induction, and CXCL1 (Figure 3H). In contrast, monocytes from LPS-treated mice, but not from naive mice, were able to produce G-CSF (Figure 3H).

Together with the defects in migration, differentiation, and cytokine production, the surviving monocytes in the BM after LPS treatment are dysfunctional in terms of sepsis induction.

3.4 Severe inflammation prevents an increase of monocytes in the periphery

A previous report suggested that administration of high-dose LPS does not increase circulating monocytes, although low-dose LPS does that (26). However, the mechanism and physiological meaning of that are unknown. In this context, our results from

monocyte cultures revealed that the stronger the inflammatory stimulus, the greater the apoptosis of monocytes (Figure 2H), which implies that severe inflammation more efficiently suppresses monocyte appearance *in vivo*. Using a cecal ligation and puncture (CLP) infection model, we induced mild and severe sepsis with 26G and 19G needles, respectively. Severe sepsis-induced mice showed significantly higher plasma levels of TNF- α compared to mild sepsis-induced mice (Figure 4A). In both settings, the numbers of monocytes and neutrophils were similarly decreased in the BM within 12 hours after CLP-induction (Figure 4B). However, the frequency and number of monocytes that migrated into the peritoneal cavity were significantly higher in mice with mild sepsis compared to mice with severe sepsis (Figures 4C, D). In contrast, the number of neutrophils was comparable between the severe and mild CLP settings (Figures 4C, D). As we observed in the LPS injection model (Figures 2D, E), the apoptotic cell ratio in BM monocytes of severe sepsis-induced mice was significantly higher than that of mild sepsis-induced mice (Figures 4E, F). Since it has been reported that the injection of low-dose LPS (20 ng/body) increases monocytes in the periphery (26), we also tested the impact of treatment with low-dose (20 ng/body) and high-dose (100 μ g/body) LPS in the apoptosis of monocytes (Supplementary

Figure 2F). Consistent with our results with the CLP model, low-dose LPS injection did not induce apoptosis, although high-dose LPS injection did induce apoptosis. Thus, monocytes are eliminated by apoptosis only when the inflammation is excessive.

3.5 Inhibition of apoptosis in monocytes exacerbates systemic inflammation during sepsis

A CCR2-deficiency improved the severity of sepsis and a supply of peripheral monocytes restores sepsis in CCR2-deficient mice (17), suggesting that the existence of monocytes in the periphery enhances systemic inflammation. To further examine if the apoptosis-mediated reduction of monocytes alters the magnitude of inflammation, we generated *Casp3*^{-/-}; *Casp3*^{flax/flax}; *CCR2-CreERT2* (*Casp3*/ γ ^{*A*mon}) mice (Supplementary Figures 3A–C). We injected tamoxifen (2 mg/mouse/day) into *Casp3*/ γ ^{*A*mon} mice and their littermate control mice (*Casp3*^{fl/fl}; *Casp3*^{-/-} mice) for 5 consecutive days (Figure 5A) and confirmed that monocytes from *Casp3*/ γ ^{*A*mon} mice after that treatment lacked Caspase-3 and 7 by western blotting (Supplementary Figure 3D). The frequency of Annexin⁺ PI⁻ early

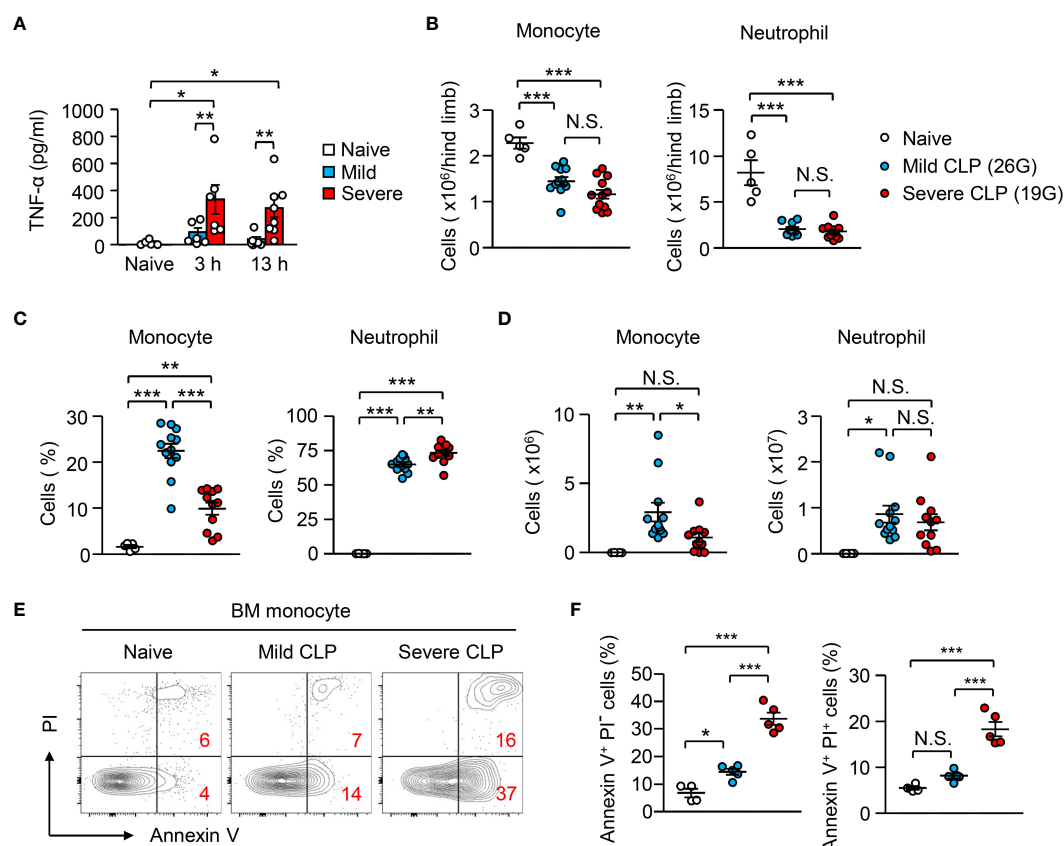


FIGURE 4

Peripheral monocyte supply is dependent on the magnitude of inflammation. (A–F) Mild and severe CLP was performed in WT mice using 26G and 19G needles, respectively; $n=5$ for naive, $n=12$ for mild CLP and $n=11$ for severe CLP. (A) Levels of plasma TNF- α were evaluated 3 or 13 hours after the induction of mild or severe CLP. (B–D) Number (B, D) and frequency (C) of monocytes and neutrophils in the BM (B) and peritoneal cavity (C, D) 13 hours after CLP-induction. (E, F) Frequencies of early apoptotic cells (Annexin V⁺ PI⁻) and dead cells (Annexin V⁺ PI⁺) in BM monocytes before and 13 hours after CLP induction; representative FACS plots are shown in (E). * $p<0.05$, ** $p<0.01$, *** $p<0.001$, N.S., not significantly different [one-way ANOVA (A–D, F)]. Data are pooled from two (A) or five (B–F) independent experiments (error bars, SEM).

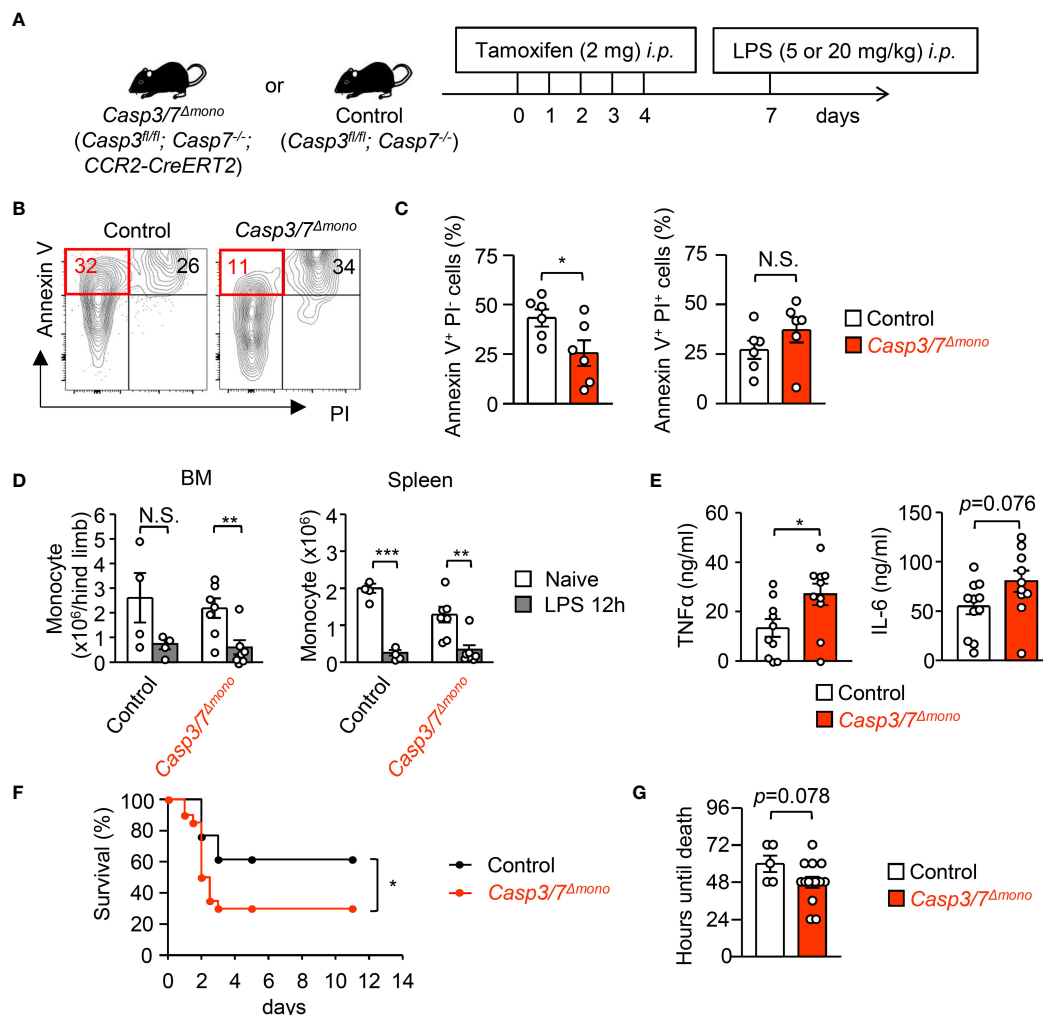


FIGURE 5

Casp3/7-deficiency in monocytes exacerbates systemic inflammation during sepsis. **(A)** Experimental strategy with *Casp3/7^{Δmono}* mice (*Casp3^{fl/fl}; Casp7^{-/-}; CCR2-CreERT2*) and their littermate control (*Casp3^{fl/fl}; Casp7^{-/-}*) mice. **(B, C)** Frequencies of early apoptotic cells (Annexin V⁺ PI⁻) and dead cells (Annexin V⁺ PI⁺) in monocytes obtained from the BM of *Casp3/7^{Δmono}* and control mice 12 hours after LPS treatment (5 mg/kg); n=6 per group. **(D)** Numbers of monocytes in the BM and spleens of *Casp3/7^{Δmono}* and control mice before and 12 hours after LPS treatment (5 mg/kg); n=4 for control, n=7 for *Casp3/7^{Δmono}*. **(E)** Concentration of TNF-α and IL-6 in the plasma of *Casp3/7^{Δmono}* mice and control mice 2 hours after LPS treatment (5 mg/kg); n=10 per group. **(F, G)** LPS (20 mg/kg) was administered to *Casp3/7^{Δmono}* mice and control mice and their mortality was monitored for 11 days. Kaplan-Meier survival curve and the life times of mice are shown in **(F, G)**, respectively; n=20 for *Casp3/7^{Δmono}* mice, n=13 for control mice. *p < 0.05, **p < 0.01, ***p < 0.001, N.S., not significantly different [Student's t-test (**C, E, G**), one-way ANOVA (**D**) or log-rank test (**F**)]; data are pooled from two (**B–E**) or three (**F, G**) independent experiments (error bars, SEM).

apoptotic cells was also successfully decreased in monocytes by the genetic ablation of *Casp3/7* after LPS treatment (Figures 5B, C). On the other hand, the frequency of the Annexin-V⁺ PI⁺ fraction, which is a mixture of necrotic cells and late apoptotic cells, was not significantly changed (Figures 5B, C), which suggests that the monocyte death was induced by non-apoptotic cell death such as necrosis in *Casp3/7^{Δmono}* mice. Consistently, the blockade of apoptosis results in the induction of necroptosis (30–32). Indeed, the number of monocytes was equally reduced in control and in *Casp3/7^{Δmono}* mice (Figure 5D). In this context, there was no significant difference in the frequency of monocytes expressing active caspase-1, an indicator of pyroptosis, between control and *Casp3/7^{Δmono}* mice (Supplementary Figure 3E). Collectively, these results imply the necrosis-mediated clearance of monocytes in *Casp3/7^{Δmono}*

mice. To evaluate the importance of monocyte death by apoptosis in fine-tuning the magnitude of inflammation, we examined blood cytokine levels 2 hours after LPS treatment and found that the levels of TNF-α and IL-6 were increased in *Casp3/7^{Δmono}* mice compared to control mice (Figure 5E). In contrast, the levels of IL-1β and IL-10 were comparable between the two groups (Supplementary Figure 3F). Reflecting the severe inflammation, the weight and size of the spleens in *Casp3/7^{Δmono}* mice were slightly increased (Supplementary Figure 3G). In addition, the mortality of *Casp3/7^{Δmono}* mice was significantly increased compared to control mice during sepsis induced by treatment with a lethal dosage of LPS (20 mg/kg) (Figures 5F, G). These results suggested that the apoptosis-dependent reduction of monocytes is crucial for fine-tuning excessive inflammation during sepsis.

3.6 Cytokine-mediated stimulation is sufficient to induce monocyte disappearance in periphery

In contrast to immune paralysis, which is induced at a later phase of sepsis (33), we showed that monocyte apoptosis at an early stage of sepsis protects the host from excessive inflammation, implying that this mechanism might work independently of microbial stimuli. To examine that hypothesis, TLR4-deficient or TLR4-sufficient monocytes were mixed with monocytes from TLR4-sufficient CAG-EGFP mice at a 1:1 ratio and were directly transplanted into the BM of B6.SJL mice. When we examined the ratio between EGFP⁺ and EGFP⁻ donor (TLR4-deficient or TLR4-sufficient) monocytes 12 hours after LPS treatment (Figure 6A), the TLR4-deficiency did not alter that ratio (Figure 6B). Next, we administrated LPS (5 mg/kg) into SJL mice that received an intra-BM transplantation of WT or TLR4-deficient monocytes (Figure 6C). Importantly, the TLR4-deficiency did not alter the ratio of Annexin V⁺PI⁺ dead cells, Annexin V⁺PI⁻ early apoptotic cells (Figures 6D, E) or active caspase3/7-expressing cells in donor monocytes (Figure 6F). These results suggested that TLR4-mediated signaling is not required to trigger monocyte apoptosis *in vivo* and implied the importance of pro-inflammatory cytokine-mediated signaling. To directly test this *in vivo*, we treated WT mice with recombinant TNF- α and IFN- γ as reported previously (34) (Figure 6G), which caused monocyte cell death *in vitro* (Figure 2H), and found that the numbers of monocytes and neutrophils were significantly reduced in the BM 6 hours after the treatment (Figure 6H). Importantly, monocytes simultaneously disappeared from the peripheral blood, while the number of neutrophils was greatly increased (Figures 6H, I). At this time, the increases in dead cells, which were evaluated by PI staining, and caspase3/7-expressing cells were pronounced in monocytes compared with neutrophils and CD11b⁻ cells in the BM (Figures 6J–L). Collectively, these results suggested that a microbial stimulus is not required while a pro-inflammatory cytokine stimulation is sufficient to induce monocyte apoptosis, which resulted in the selective disappearance of monocytes in the periphery.

3.7 The monocyte disappearance during human cytokine release syndrome

As pro-inflammatory cytokines are sufficient to induce apoptosis-mediated monocyte disappearance in mice (Figure 6), we aimed to determine whether it is also observed in human patients during pathogen-unrelated systemic inflammation. To this end, we focused on cytokine-release syndrome (CRS), which is caused by the release of large amounts of cytokines accompanying an excessive immune response not only during systemic infection but also during CAR-T cell immunotherapy. It should be emphasized that CAR-T cell administration has the advantage of monitoring CRS from the starting point of inflammation, which is not feasible in patients with infectious diseases or other inflammatory diseases because the symptoms are already present at the time the patient is seen in the hospital. In the CAR-T cell-induced CRS model with humanized mice and human CAR-T cells, human monocytes act as a major

source of cytokines (35). We monitored the kinetics of CD14⁺CD16^{low} classical monocytes, neutrophils, c-reactive protein (CRP), and fibrinogen (FBG) in the blood of 19 patients until day 14 after CAR-T cell administration (Figure 7A, the gating strategy of classical monocytes and neutrophils is shown in Supplementary Figure 4A). The severity of CRS was graded based on the Penn grading scale (Supplementary Table 1). All patients who received CAR-T cell therapy developed CRS (n=19), but only four patients developed severe CRS (grade 3 and 4, 15.8%). Patient characteristics with each CRS grade were shown in Supplementary Table 2. The peak of blood neutrophil count almost coincided with the peaks of the inflammation markers CRP and FBG (Figure 7B). In contrast, the peak of classical monocyte count was later than the peaks of CRP and FBG, implying the suppression of monocyte appearance in the periphery during systemic inflammation in humans. In this context, the duration between the peak of monocytes, but not neutrophils, and the peak of CRP or FBG became larger in patients with severe CRS (grades 3 and 4) compared to those with relatively mild CRS (grades 1 and 2) (Figures 7C, D). Thus, the more severe the inflammation, the more delayed the appearance of classical monocytes in the blood during CRS. Related to this, patients with higher counts of classical monocytes before CAR-T therapy had a more severe CRS after receiving CAR-T therapy (day 0) (Figure 7E). On the other hand, the blood levels of cytokines, neutrophils and clinical indicators of inflammation at day 0 did not affect the severity of CRS (Supplementary Figures 4B–D; Supplementary Table 3), implying that the counts of classical monocytes in the blood before starting CAR-T therapy may serve as a biomarker to predict the severity of subsequent CRS after the treatment. Importantly, compared to day 0, the counts of monocytes in the blood were significantly increased at the peak of CRS in grade 1/2 patients, whereas grade 3/4 patients showed a decrease of monocytes in their blood at that time (Figures 7F, G). Those results obtained from patients are consistent with results obtained from mice (Figure 4), and the magnitude of inflammation is critical for changing monocyte behavior both in mice and in humans.

4 Discussion

Monocytes are a unique population of cells that have the potential to differentiate into multiple cell lineages while existing in the periphery. The variability of monocytes is suitable for maintaining homeostasis flexibly according to the situation. In this study, we found that apoptosis and functional alterations are induced in monocytes early after systemic inflammation, which effectively suppresses the appearance of monocytes in peripheral tissues. During excessive inflammation, this could be a mechanism to attenuate monocyte-mediated acceleration of systemic inflammation and tissue damage and instead assure host survival. Indeed, suppression of monocyte appearance was observed during severe inflammation both in mice and in humans.

Apoptosis maintains homeostasis by silently removing unwanted or harmful cells during various biological processes such as development, inflammation, and aging (36–38). Importantly, the impaired apoptotic cell death selectively in

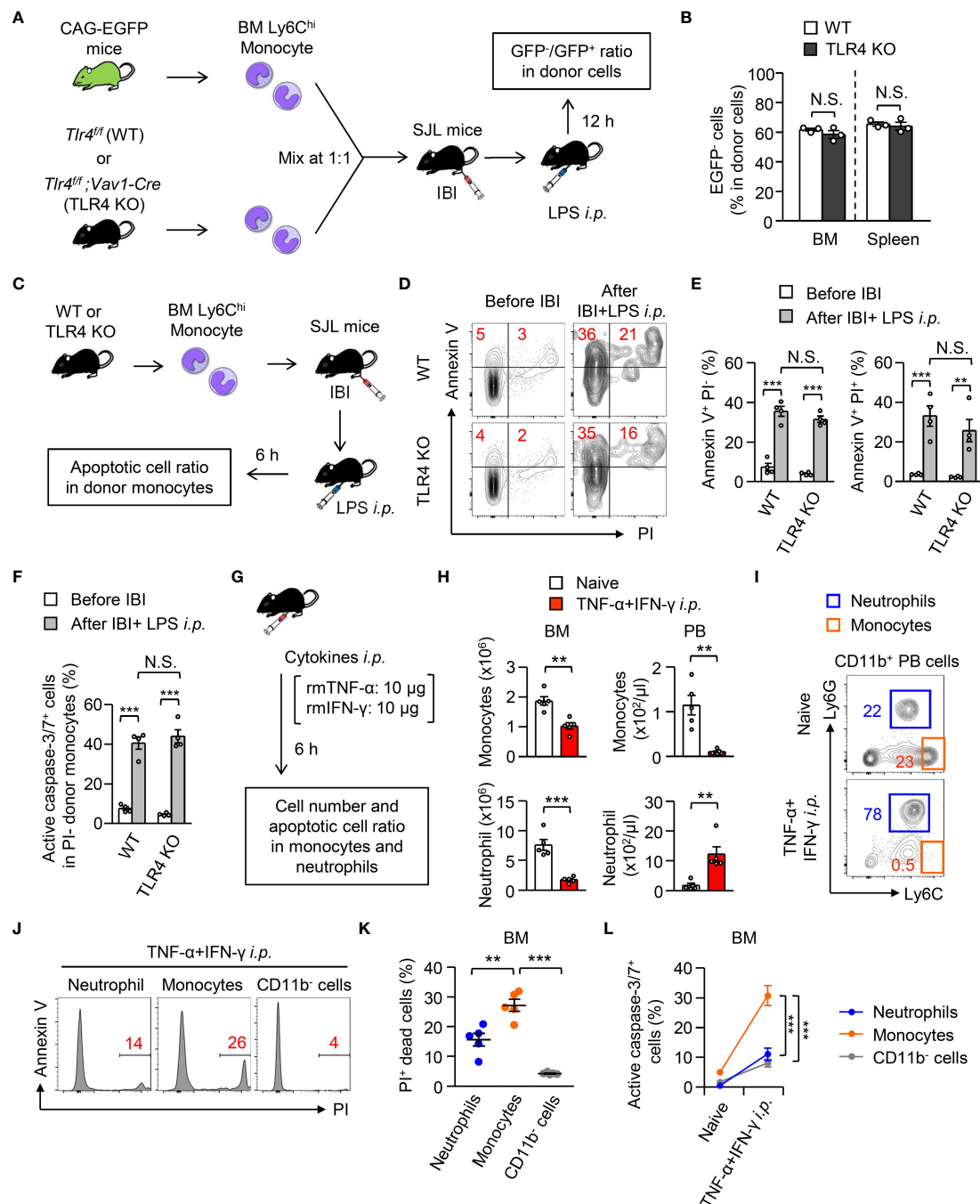


FIGURE 6

Importance of TLR4-mediated signaling to trigger monocyte cell death during systemic inflammation. (A, B) Experimental strategy for co-IBI of TLR4-sufficient or TLR4-deficient monocytes and EGFP-expressing monocytes (A). Monocytes were obtained from the BM of naive *Tlr4^{fllox/fllox}; Vav1-Cre* mice (TLR4 KO) or their littermate control (*Tlr4^{fllox/fllox}*; WT) mice and were mixed with monocytes obtained from naive CAG-EGFP mice at a 1:1 ratio. The mixed monocytes were transferred into the BM of recipient SJL mice and the recipient mice received an intraperitoneal injection of LPS (5 mg/kg). Twelve hours after treatment, the ratio of GFP⁺ and GFP⁺ cells in CD45.2⁺CD45.1⁺ donor cells was examined (B). (C–F) BM monocytes were obtained from TLR4 KO or control mice were injected into the BM of B6.SJL mice after which the mice were treated with LPS (5 mg/kg) as shown in (C). Six hours after the treatment, the frequencies of Annexin V⁺PI⁺ dead cells, Annexin V⁺PI⁻ early apoptotic cells (D, E), and active caspase3/7-expressing cells (F) in donor monocytes were examined. Representative FACS plots are shown in (D). (G–L) A mixture of recombinant mouse TNF- α and IFN- γ (10 μ g/mouse each) was injected intraperitoneally to WT B6 mice and the numbers (H), dead cell ratio (J, K), and active caspase3/7-expressing cell ratio (L) of monocytes, neutrophils and/or CD11b⁺ cells in the BM and PB were examined 6 hours after the cytokine administration. The experimental strategy is shown in (G). Representative FACS plots for CD11b⁺ cells in the PB and monocytes and neutrophils in the BM are shown in (I, J), respectively. ***p* < 0.01, ****p* < 0.001, N.S., not significantly different [Student *t*-test (B, H), one-way ANOVA (D, E, K, L)]. Data are pooled from two independent experiments (Error bars, SEM).

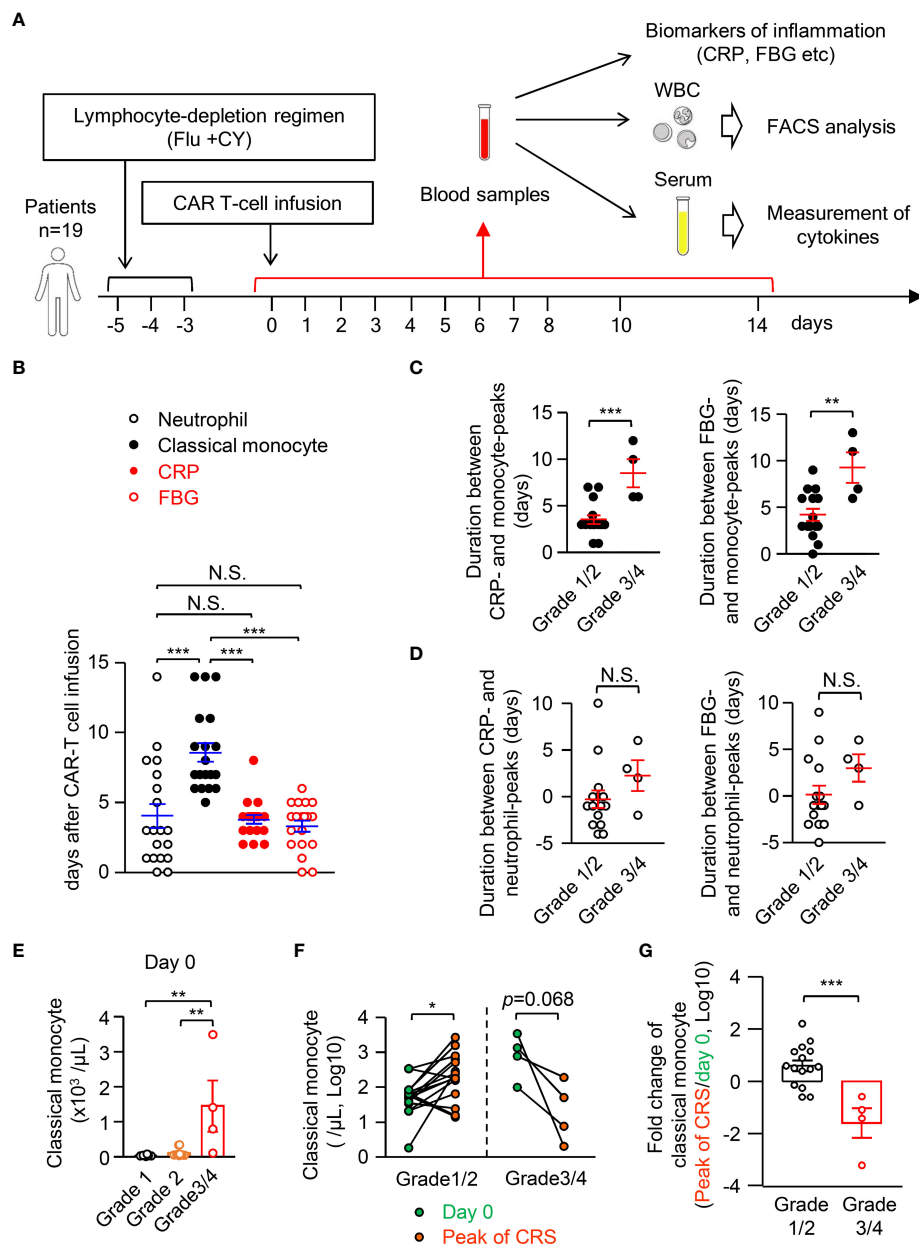


FIGURE 7

Classical monocytes disappear in the peripheral blood during human CRS. (A) Experimental strategy for monitoring inflammation biomarkers, numbers of leukocytes and levels of cytokines in blood samples of CRS patients who received CAR-T cell therapy; n=19. (B) The peak day for cell counts of neutrophils and classical monocytes, CRP and FBG in the PB of CRS patients. (C, D) Duration between CRP or FBG and classical monocytes (C) or neutrophils (D). (E) Cell count of classical monocytes in the blood of each grade of CRS at day 0. (F) Number of classical monocytes in the blood at day 0 and at the peak of CRS. (G) Fold changes of classical monocytes in the blood from day 0 to the peak of CRS are shown. * $p < 0.05$, ** $p < 0.01$, *** $p < 0.001$, N.S., not significantly different [Student's t-test (C, D, F, G) or one-way ANOVA (B, E)]. Error bars, SEM.

monocytes, i.e., *Casp3/7^{Amo}* mice, exacerbated the inflammation and increased host death due to LPS-induced sepsis (Figure 5), which suggests that the apoptosis-mediated reduction of monocytes is a novel fine-tuning mechanism to prevent excessive inflammation. In this respect, non-apoptotic cell death such as necrosis was also suggested to increase inflammation and decrease host survival. Further research will be needed to elucidate whether this tuning machinery is active in various diseases and whether its impairment leads to the onset of inflammatory diseases. In addition,

the functionally altered monocytes had a decreased ability to produce pro-inflammatory cytokines, such as TNF- α and CXCL1 (Figure 3H). In contrast, their ability to produce anti-inflammatory cytokines was not upregulated (Figure 3H), suggesting that the dysfunctional monocytes seem not to be suppressive monocyte subsets such as Ym1⁺ monocytes (14). Interestingly, monocytes that survived in the BM after LPS treatment showed a remarkable expression of G-CSF (Figure 3H). As G-CSF induces the differentiation of neutrophils and Ym1⁺ monocytes (39, 40), the

functional alteration of monocytes may affect subsequent immune responses at the later phase of inflammation. In addition, the reduced production of TNF- α and the enhanced production of G-CSF are observed in monocytes of human septic patients (41), implying that a similar functional alteration of monocytes during inflammation is widely conserved in mammals. Our findings indicated that inflammatory cytokines induce the apoptosis and functional alterations of monocyte in the periphery. With this respect, the functional alterations of monocytes, such as reduced TNF- α production, might be caused by hypoxia- or LPS-mediated upregulation of hypoxia inducible factor-1 α (HIF1 α) that reduces inflammatory cytokine production from monocytes (42, 43).

The results of this study show that “monocyte loss” is triggered in the periphery only under severe inflammation (Figures 7F, G, 4E, F; Supplementary Figures 2F, 5), which was transient and canceled as soon as the inflammation subsided both in mice and in humans (Figures 1A, 7B). On the other hand, it has been considered that a dysregulated immune response is induced in septic patients, e.g. the induction of indiscriminate apoptosis in a variety of cell types. However, we found that the susceptibility of monocytes to apoptosis is higher than that of other immune cells (Figures 2D, E, H, I; Figure 6L), which leads to the preferential removal of monocytes in a programmed manner. In contrast to the monocyte loss under excessive inflammation, monocyte tolerance is induced during mild inflammation triggered by low doses of LPS (44–46). Mechanistically, the monocyte loss was induced by pro-inflammatory cytokines independent of microbial stimuli (Figures 6G–L). Consistently, monocyte loss was also observed in patients with CAR-T cell-induced CRS (Figure 7), implying that monocyte loss is a common regulatory mechanism that limits excessive inflammation both in mice and in humans.

In another aspect, previous studies on monocyte- or monocyte-derived cell-mediated immune suppression have focused primarily on the immunological significance during the late stage of inflammation, such as sepsis, inflammatory bowel disease, and allergy (2, 14, 47, 48). Depending on the immunological context, the late stage of monocyte suppression may increase patient mortality caused by secondary infections (2, 49, 50), or it may help to terminate inflammation and promote tissue repair (14, 42, 46, 47). In contrast to these studies, we focused on the early inhibitory mechanism of hyperinflammation and newly identified that the transient reduction and dysfunction of monocytes fine-tunes the magnitude of inflammation to minimize tissue damage and to assure host survival.

The recruitment of monocytes to infected sites is often later than that of neutrophils (46, 51). We found that the more severe the inflammation, the more delayed the appearance of monocytes in the periphery, which may explain the reason for the delayed monocyte recruitment to the infected site. While previous studies with low-dose LPS treatment showed a mobilization of monocytes from the BM to peripheral tissues (26), the monocyte behavior in severe inflammatory conditions has not been fully elucidated. Supporting our conclusion, Giamarellos-Bourboulis et al. reported that septic patients with apoptosis in more than 50% of their peripheral blood monocytes have a lower mortality compared to patients with

apoptosis in less than 50% of their monocytes (52). Although their study did not prove the mechanism and causal relationship involved, it implies the apoptosis-mediated removal of monocytes with the suppression of systemic inflammation.

In this study, we used blood samples from CRS patients to elucidate whether monocyte disappearance is induced in systemic inflammatory conditions. Because CRS is triggered after CAR-T cell therapy, it is easy to monitor the progress of inflammation and cell kinetics from before the onset of inflammation. The tumor burden before CAR-T cell injection and CAR-T cell expansion is a risk factor for CRS development in cancer treatment (53, 54). However, because accurate evaluation of the tumor burden requires analysis with computed tomography (CT), magnetic resonance imaging (MRI), and/or positron emission tomography/CT (PET/CT) scanning, the identification of biomarkers that can easily predict the severity of CRS would be beneficial. Here, we demonstrate that the number of classical monocytes in the patient’s blood before CAR-T cell administration is a useful biomarker to predict the severity of CRS. The high number of classical monocytes in the periphery before CAR-T cell administration correlated with the severity of CRS, implying that monocytes are a major source of pro-inflammatory cytokines. Supporting this notion, the importance of monocytes as a source of inflammatory cytokines during CRS induced by CAR-T cell therapy was indicated in a humanized mouse model (35). Meanwhile, as the development of CRS does not correlate with the prognosis of primary disease (55), our findings further suggested that the classical monocyte counts cannot predict the outcomes of CAR-T cell therapy. In addition, temporary removal of monocytes may help control systemic inflammation, although prolonged monocyte depletion risks increased susceptibility to infection and collapse of homeostasis. Of note, we previously developed the antibody-drug conjugate (ADC) that selectively removes human monocytes and monocytic leukemia cells with minimal side effects on other hematopoietic cells by targeting monocyte progenitors (56). This ADC might also be applicable for CRS, although this is an issue for the future.

To avoid uncontrolled inflammation, the immune system is equipped with various regulatory mechanisms that function appropriately at the right time. In this study, we found the apoptotic removal and induction of dysfunctionality in monocytes at early stages of excessive inflammation (Supplementary Figure 5). Because this mechanism does not need help with adaptive immunity, it might be a primitive system that has existed since before the development of the acquired immune system. Considering this novel fine-tuning mechanism, our findings are valuable not only for extending our understanding of monocyte function but also for identifying therapeutic targets for severe inflammatory diseases.

Data availability statement

The original contributions presented in the study are included in the article/Supplementary Material. Further inquiries can be directed to the corresponding author.

Ethics statement

The studies involving humans were approved by the Institutional Review Board of the Tokyo Medical and Dental University. The studies were conducted in accordance with the local legislation and institutional requirements. The participants provided their written informed consent to participate in this study. The animal study was approved by the Institutional Animal Care Committee of the Tokyo Medical and Dental University. The study was conducted in accordance with the local legislation and institutional requirements.

Author contributions

TO: Conceptualization, Data curation, Project administration, Supervision, Validation, Writing – original draft, Writing – review & editing. MA: Data curation, Formal analysis, Investigation, Writing – review & editing. MK: Conceptualization, Data curation, Formal analysis, Funding acquisition, Investigation, Methodology, Validation, Writing – original draft, Writing – review & editing. YU: Investigation, Methodology, Resources, Writing – review & editing. TN: Investigation, Methodology, Resources, Writing – review & editing. YI: Formal analysis, Investigation, Methodology, Writing – review & editing. MY: Investigation, Methodology, Resources, Writing – review & editing.

Funding

The author(s) declare financial support was received for the research, authorship, and/or publication of this article. This work was supported by the grants from Naito Foundation (MK), the

Daiichi Sankyo Foundation of Life Science (MK), the Kanae Foundation for the Promotion of Medical Science (MK), and Multilayered Stress Diseases (JPMXP1323015483), TMDU (MK).

Acknowledgments

We thank Drs. T. Suzuki, T. Usami, H. Ishikubo and Y. Hiraoka for supporting the generation of *Casp3^{flox/flox}* and *Casp7^{-/-}* mice and T. Akashi for helping maintenance of mice.

Conflict of interest

The authors declare that the research was conducted in the absence of any commercial or financial relationships that could be construed as a potential conflict of interest.

Publisher's note

All claims expressed in this article are solely those of the authors and do not necessarily represent those of their affiliated organizations, or those of the publisher, the editors and the reviewers. Any product that may be evaluated in this article, or claim that may be made by its manufacturer, is not guaranteed or endorsed by the publisher.

Supplementary material

The Supplementary Material for this article can be found online at: <https://www.frontiersin.org/articles/10.3389/fimmu.2024.1398153/full#supplementary-material>

References

- Medzhitov R. Origin and physiological roles of inflammation. *Nature*. (2008) 454:428–35. doi: 10.1038/nature07201
- Hotchkiss RS, Moldawer LL, Opal SM, Reinhart K, Turnbull IR, Vincent JL. Sepsis and septic shock. *Nat Rev Dis Primers*. (2016) 2:16045. doi: 10.1038/nrdp.2016.45
- Rudd KE, Johnson SC, Agesa KM, Shackelford KA, Tsoi D, Kievlan DR, et al. Global, regional, and national sepsis incidence and mortality, 1990–2017: analysis for the global burden of disease study. *Lancet*. (2020) 395:200–11. doi: 10.1016/S0140-6736(19)32989-7
- Zhou F, Yu T, Du R, Fan G, Liu Y, Liu Z, et al. Clinical course and risk factors for mortality of adult inpatients with covid-19 in wuhan, China: a retrospective cohort study. *Lancet*. (2020) 395:1054–62. doi: 10.1016/S0140-6736(20)30566-3
- Medzhitov R, Janeway C Jr. Innate immunity. *N Engl J Med*. (2000) 343:338–44. doi: 10.1056/NEJM200008033430506
- Grivennikov SI, Tumanov AV, Liepinsh DJ, Kruglov AA, Marakusha BI, Shakhov AN, et al. Distinct and nonredundant *in vivo* functions of tnf produced by T cells and macrophages/neutrophils: protective and deleterious effects. *Immunity*. (2005) 22:93–104. doi: 10.1016/j.immuni.2004.11.016
- Ellman DG, Lund MC, Nissen M, Nielsen PS, Sorensen C, Lester EB, et al. Conditional ablation of myeloid tnf improves functional outcome and decreases lesion size after spinal cord injury in mice. *Cells*. (2020) 9:2407. doi: 10.3390/cells9112407
- Wolf AA, Yanez A, Barman PK, Goodridge HS. The ontogeny of monocyte subsets. *Front Immunol*. (2019) 10:1642. doi: 10.3389/fimmu.2019.01642
- van Furth R, Sluiter W. Distribution of blood monocytes between a marginating and a circulating pool. *J Exp Med*. (1986) 163:474–9. doi: 10.1084/jem.163.2.474
- Shi C, Pamer EG. Monocyte recruitment during infection and inflammation. *Nat Rev Immunol*. (2011) 11:762–74. doi: 10.1038/nri3070
- Jakubczak CV, Randolph GJ, Henson PM. Monocyte differentiation and antigen-presenting functions. *Nat Rev Immunol*. (2017) 17:349–62. doi: 10.1038/nri.2017.28
- Rivollier A, He J, Kole A, Valatas V, Kelsall BL. Inflammation switches the differentiation program of ly6chi monocytes from antiinflammatory macrophages to inflammatory dendritic cells in the colon. *J Exp Med*. (2012) 209:139–55. doi: 10.1084/jem.20101387
- Veglia F, Sanseviero E, Gabrilovich DI. Myeloid-derived suppressor cells in the era of increasing myeloid cell diversity. *Nat Rev Immunol*. (2021) 21:485–98. doi: 10.1038/s41577-020-00490-y
- Ikeda N, Asano K, Kikuchi K, Uchida Y, Ikegami H, Takagi R, et al. Emergence of immunoregulatory ym1(+)Ly6c(Hi) monocytes during recovery phase of tissue injury. *Sci Immunol*. (2018) 3:eaat0207. doi: 10.1126/sciimmunol.aat0207
- Guilliams M, Mildner A, Yona S. Developmental and functional heterogeneity of monocytes. *Immunity*. (2018) 49:595–613. doi: 10.1016/j.immuni.2018.10.005
- Serbina NV, Jia T, Hohl TM, Pamer EG. Monocyte-mediated defense against microbial pathogens. *Annu Rev Immunol*. (2008) 26:421–52. doi: 10.1146/annurev.immunol.26.021607.090326
- Cebinelli GCM, de Lima KA, Silva Castanheira FVE, Hiroki CH, Monteiro VVS, de Lima MHF, et al. Ccr2-deficient mice are protected to sepsis by the disruption of the inflammatory monocytes emigration from the bone marrow. *J Leukoc Biol*. (2021) 109:1063–70. doi: 10.1002/JLB.4MR0820-049RR

18. Ochando J, Mulder WJM, Madsen JC, Netea MG, Duivenvoorden R. Trained immunity - basic concepts and contributions to immunopathology. *Nat Rev Nephrol.* (2023) 19:23–37. doi: 10.1038/s41581-022-00633-5
19. Aida T, Chiyo K, Usami T, Ishikubo H, Imahashi R, Wada Y, et al. Cloning-free crispr/cas system facilitates functional cassette knock-in in mice. *Genome Biol.* (2015) 16:87. doi: 10.1186/s13059-015-0653-x
20. Porter D, Frey N, Wood PA, Weng Y, Grupp SA. Grading of cytokine release syndrome associated with the car T cell therapy tisagenlecleucel. *J Hematol Oncol.* (2018) 11:35. doi: 10.1186/s13045-018-0571-y
21. Nagao T, Yoshifuji K, Sadato D, Motomura Y, Saito M, Yamamoto K, et al. Establishment and characterization of a new activated B-cell-like dlbcl cell line, tmd12. *Exp Hematol.* (2022) 116:37–49. doi: 10.1016/j.exphem.2022.09.005
22. Huang H, Xia A, Sun L, Lu C, Liu Y, Zhu Z, et al. Pathogenic functions of tumor necrosis factor receptor-associated factor 6 signaling following traumatic brain injury. *Front Mol Neurosci.* (2021) 14:629910. doi: 10.3389/fnmol.2021.629910
23. Singha B, Gatla HR, Vancurova I. Transcriptional regulation of chemokine expression in ovarian cancer. *Biomolecules.* (2015) 5:223–43. doi: 10.3390/biom5010223
24. Qiao Y, He H, Jonsson P, Sinha I, Zhao C, Dahlman-Wright K. Ap-1 is a key regulator of proinflammatory cytokine tnfalpha-mediated triple-negative breast cancer progression. *J Biol Chem.* (2016) 291:5068–79. doi: 10.1074/jbc.M115.702571
25. O'Dea KP, Wilson MR, Dokpesi JO, Wakabayashi K, Tatton L, van Rooijen N, et al. Mobilization and margination of bone marrow gr-1-high monocytes during subclinical endotoxemia predisposes the lungs toward acute injury. *J Immunol.* (2009) 182:1155–66. doi: 10.4049/jimmunol.182.2.1155
26. Shi C, Jia T, Mendez-, Hohl TM, Serbina NV, Lipuma L, et al. Bone marrow mesenchymal stem and progenitor cells induce monocyte emigration in response to circulating toll-like receptor ligands. *Immunity.* (2011) 34:590–601. doi: 10.1016/j.immuni.2011.02.016
27. Kanayama M, Izumi Y, Akiyama M, Hayashi T, Atarashi K, Roers A, et al. Myeloid-like B cells boost emergency myelopoiesis through il-10 production during infection. *J Exp Med.* (2023) 220:e20221221. doi: 10.1084/jem.20221221
28. Serbina NV, Pamer EG. Monocyte emigration from bone marrow during bacterial infection requires signals mediated by chemokine receptor ccr2. *Nat Immunol.* (2006) 7:311–7. doi: 10.1038/ni1309
29. Waller K, James C, de Jong A, Blackmore L, Ma Y, Stagg A, et al. Adam17-mediated reduction in cd14(++)Cd16(+) monocytes ex vivo and reduction in intermediate monocytes with immune paresis in acute pancreatitis and acute alcoholic hepatitis. *Front Immunol.* (2019) 10:1902. doi: 10.3389/fimmu.2019.01902
30. Lemaire C, Andreau K, Souvannavong V, Adam A. Inhibition of caspase activity induces a switch from apoptosis to necrosis. *FEBS Lett.* (1998) 425:266–70. doi: 10.1016/s0014-5793(98)00252-x
31. Zhang LJ, Hao YZ, Hu CS, Ye Y, Xie QP, Thorne RF, et al. Inhibition of apoptosis facilitates necrosis induced by cisplatin in gastric cancer cells. *Anticancer Drugs.* (2008) 19:159–66. doi: 10.1097/CAD.0b013e3282f30d05
32. Leist M, Jaattela M. Four deaths and a funeral: from caspases to alternative mechanisms. *Nat Rev Mol Cell Biol.* (2001) 2:589–98. doi: 10.1038/35085008
33. Cao C, Yu M, Chai Y. Pathological alteration and therapeutic implications of sepsis-induced immune cell apoptosis. *Cell Death Dis.* (2019) 10:782. doi: 10.1038/s41419-019-2015-1
34. Karki R, Sharma BR, Tuladhar S, Williams EP, Zalduondo L, Samir P, et al. Synergism of tnf-alpha and ifn-gamma triggers inflammatory cell death, tissue damage, and mortality in sars-cov-2 infection and cytokine shock syndromes. *Cell.* (2021) 184:149–68.e17. doi: 10.1016/j.cell.2020.11.025
35. Norelli M, Camisa B, Barbiera G, Falcone L, Purevdorj A, Genua M, et al. Monocyte-derived il-1 and il-6 are differentially required for cytokine-release syndrome and neurotoxicity due to car T cells. *Nat Med.* (2018) 24:739–48. doi: 10.1038/s41591-018-0036-4
36. Vitale I, Pietrolola F, Guilbaud E, Aaronson SA, Abrams JM, Adam D, et al. Apoptotic cell death in disease-current understanding of the nccd 2023. *Cell Death Differ.* (2023) 30:1097–154. doi: 10.1038/s41418-023-01153-w
37. Baar MP, Brandt RMC, Putavet DA, Klein JDD, Derks KWJ, Bourgeois BRM, et al. Targeted apoptosis of senescent cells restores tissue homeostasis in response to chemotoxicity and aging. *Cell.* (2017) 169:132–47.e16. doi: 10.1016/j.cell.2017.02.031
38. Singh R, Letai A, Sarosiek K. Regulation of apoptosis in health and disease: the balancing act of bcl-2 family proteins. *Nat Rev Mol Cell Biol.* (2019) 20:175–93. doi: 10.1038/s41580-018-0089-8
39. Ikeda N, Kubota H, Suzuki R, Morita M, Yoshimura A, Osada Y, et al. The early neutrophil-committed progenitors aberrantly differentiate into immunoregulatory monocytes during emergency myelopoiesis. *Cell Rep.* (2023) 42:112165. doi: 10.1016/j.celrep.2023.112165
40. Roberts AW. G-csf: A key regulator of neutrophil production, but that's not all! *Growth Factors.* (2005) 23:33–41. doi: 10.1080/08977190500055836
41. Weiss M, Fischer G, Barth E, Boneberg E, Schneider EM, Georgieff M, et al. Dissociation of lps-induced monocytic ex vivo production of granulocyte colony-stimulating factor (G-csf) and tnf-alpha in patients with septic shock. *Cytokine.* (2001) 13:51–4. doi: 10.1006/cyto.2000.0796
42. Shalova IN, Lim JY, Chittethazh M, Zinkernagel AS, Beasley F, Hernandez-Jimenez E, et al. Human monocytes undergo functional re-programming during sepsis mediated by hypoxia-inducible factor-1alpha. *Immunity.* (2015) 42:484–98. doi: 10.1016/j.immuni.2015.02.001
43. Chen Q, Cui K, Zhao Z, Xu X, Liu Y, Shen Y, et al. Lps stimulation stabilizes hif-1alpha by enhancing hif-1alpha acetylation via the parp1-sirt1 and acly-tip60 pathways in macrophages. *FASEB J.* (2022) 36:e22418. doi: 10.1096/fj.202200256R
44. Kinoshita M, Miyazaki H, Nakashima H, Nakashima M, Nishikawa M, Ishikiriyama T, et al. In vivo lipopolysaccharide tolerance recruits cd11b+ Macrophages to the liver with enhanced bactericidal activity and low tumor necrosis factor-releasing capability, resulting in drastic resistance to lethal septicemia. *J Innate Immun.* (2017) 9:493–510. doi: 10.1159/000475931
45. Chen K, Geng S, Yuan R, Diao N, Upchurch Z, Li L. Super-low dose endotoxin pre-conditioning exacerbates sepsis mortality. *EBioMedicine.* (2015) 2:324–33. doi: 10.1016/j.ebiom.2015.03.001
46. Kratochil RM, Shim HB, Shim R, Lee WY, Labit E, Sinha S, et al. A monocyte-leptin-angiogenesis pathway critical for repair post-infection. *Nature.* (2022) 609:166–73. doi: 10.1038/s41586-022-05044-x
47. Egawa M, Mukai K, Yoshikawa S, Iki M, Mukaida N, Kawano Y, et al. Inflammatory monocytes recruited to allergic skin acquire an anti-inflammatory M2 phenotype via basophil-derived interleukin-4. *Immunity.* (2013) 38:570–80. doi: 10.1016/j.immuni.2012.11.014
48. Hotchkiss RS, Coopersmith CM, McDunn JE, Ferguson TA. The sepsis seesaw: tilting toward immunosuppression. *Nat Med.* (2009) 15:496–7. doi: 10.1038/nm0509-496
49. Nakamori Y, Park EJ, Shimaoka M. Immune deregulation in sepsis and septic shock: reversing immune paralysis by targeting pd-1/pd-L1 pathway. *Front Immunol.* (2020) 11:624279. doi: 10.3389/fimmu.2020.624279
50. Cao M, Wang G, Xie J. Immune dysregulation in sepsis: experiences, lessons and perspectives. *Cell Death Discovery.* (2023) 9:465. doi: 10.1038/s41420-023-01766-7
51. Serbina NV, Hohl TM, Cherny M, Pamer EG. Selective expansion of the monocytic lineage directed by bacterial infection. *J Immunol.* (2009) 183:1900–10. doi: 10.4049/jimmunol.0900612
52. Giamarellos-Bourboulis EJ, Routsis C, Plachouras D, Markaki V, Raftogiannis M, Zervakis D, et al. Early apoptosis of blood monocytes in the septic host: is it a mechanism of protection in the event of septic shock? *Crit Care.* (2006) 10:R76. doi: 10.1186/cc4921
53. Hay KA, Hanafi LA, Li D, Gust J, Liles WC, Wurfel MM, et al. Kinetics and biomarkers of severe cytokine release syndrome after cd19 chimeric antigen receptor-modified T-cell therapy. *Blood.* (2017) 130:2295–306. doi: 10.1182/blood-2017-06-793141
54. Diorio C, Shaw PA, Pequignot E, Orlenko A, Chen F, Aplenc R, et al. Diagnostic biomarkers to differentiate sepsis from cytokine release syndrome in critically ill children. *Blood Adv.* (2020) 4:5174–83. doi: 10.1182/bloodadvances.2020002592
55. Bhaskar ST, Patel VG, Porter DL, Schuster SJ, Nastoupil LJ, Perales MA, et al. Chimeric antigen receptor T-cell therapy yields similar outcomes in patients with and without cytokine release syndrome. *Blood Adv.* (2023) 7:4765–72. doi: 10.1182/bloodadvances.2022008937
56. Izumi Y, Kanayama M, Shen Z, Kai M, Kawamura S, Akiyama M, et al. An antibody-drug conjugate that selectively targets human monocyte progenitors for anti-cancer therapy. *Front Immunol.* (2021) 12:618081. doi: 10.3389/fimmu.2021.618081



OPEN ACCESS

EDITED BY

Reza Akbarzadeh,
University of Lübeck, Germany

REVIEWED BY

Chiara Agostinis,
Institute for Maternal and Child Health Burlo
Garofolo (IRCCS), Italy
József Dobó,
Hungarian Academy of Sciences (MTA),
Hungary

*CORRESPONDENCE

Carl Vahldieck
✉ carl.vahldieck@uksh.de

RECEIVED 01 May 2024

ACCEPTED 25 June 2024

PUBLISHED 11 July 2024

CITATION

Vahldieck C, Löning S, Hamacher C, Fels B,
Rudzewski B, Nickel L, Weil J, Nording H,
Baron L, Kleingarn M, Karsten CM and
Kusche-Vihrog K (2024) Dysregulated
complement activation during acute
myocardial infarction leads to endothelial
glycocalyx degradation and endothelial
dysfunction via the C5a:C5a-Receptor1 axis.
Front. Immunol. 15:1426526.
doi: 10.3389/fimmu.2024.1426526

COPYRIGHT

© 2024 Vahldieck, Löning, Hamacher, Fels,
Rudzewski, Nickel, Weil, Nording, Baron,
Kleingarn, Karsten and Kusche-Vihrog. This is
an open-access article distributed under the
terms of the [Creative Commons Attribution
License \(CC BY\)](#). The use, distribution or
reproduction in other forums is permitted,
provided the original author(s) and the
copyright owner(s) are credited and that the
original publication in this journal is cited, in
accordance with accepted academic
practice. No use, distribution or reproduction
is permitted which does not comply with
these terms.

Dysregulated complement activation during acute myocardial infarction leads to endothelial glycocalyx degradation and endothelial dysfunction via the C5a:C5a-Receptor1 axis

Carl Vahldieck^{1,2,3*}, Samuel Löning², Constantin Hamacher²,
Benedikt Fels^{2,3}, Bettina Rudzewski², Laura Nickel⁴,
Joachim Weil⁴, Henry Nording^{5,3}, Lasse Baron⁵,
Marie Kleingarn⁶, Christian Marcel Karsten⁶
and Kristina Kusche-Vihrog^{2,3}

¹Department of Anesthesiology and Intensive Care Medicine, University Medical Centre Schleswig-Holstein Campus Luebeck, Luebeck, Germany, ²Institute of Physiology, University of Luebeck, Luebeck, Germany, ³DZHK (German Research Centre for Cardiovascular Research), Partner Site Hamburg/Luebeck/Kiel, Luebeck, Germany, ⁴Medizinische Klinik II, Sana Kliniken Luebeck, Luebeck, Germany, ⁵Cardioimmunology Group, Medical Clinic II, University Heart Center Luebeck, Luebeck, Germany, ⁶Institute for Systemic Inflammation Research (ISEF), University of Luebeck, Luebeck, Germany

Introduction: Complement-mediated damage to the myocardium during acute myocardial infarction (AMI), particularly the late components of the terminal pathway (C5-convertase and C5b-9), have previously been characterized. Unfortunately, only few studies have reported a direct association between dysregulated complement activation and endothelial function. Hence, little attention has been paid to the role of the anaphylatoxin C5a. The endothelial glycocalyx (eGC) together with the cellular actin cortex provide a vasoprotective barrier against chronic vascular inflammation. Changes in their nanomechanical properties (stiffness and height) are recognized as hallmarks of endothelial dysfunction as they correlate with the bioavailability of vasoactive substances, such as nitric oxide (NO). Here, we determined how the C5a:C5aR1 axis affects the eGC and endothelial function in AMI.

Methods: Samples of fifty-five patients with ST-elevation myocardial infarction (STEMI) vs. healthy controls were analyzed in this study. eGC components and C5a levels were determined via ELISA; NO levels were quantified chemiluminescence-based. Endothelial cells were stimulated with C5a or patient sera (with/without C5a-receptor1 antagonist “PMX53”) and the nanomechanical properties of eGC quantified using the atomic force microscopy (AFM)-based nanoindentation technique. To measure actin cytoskeletal tension regulator activation (RhoA and Rac1) G-LISA assays were applied. Vascular inflammation was examined by quantifying monocyte-endothelium interaction via AFM-based single-cell-force spectroscopy.

Results: Serum concentrations of eGC components and C5a were significantly increased during STEMI. Serum and solely C5a stimulation decreased eGC height and stiffness, indicating shedding of the eGC. C5a enhanced RhoA activation, resulting in increased cortical stiffness with subsequent reduction in NO concentrations. Monocyte adhesion to the endothelium was enhanced after both C5a and stimulation with STEMI serum. eGC degradation- and RhoA-induced cortical stiffening with subsequent endothelial dysfunction were attenuated after administering PMX53.

Conclusion: This study demonstrates that dysregulated C5a activation during AMI results in eGC damage with subsequent endothelial dysfunction and reduced NO bioavailability, indicating progressively developing vascular inflammation. This could be prevented by antagonizing C5aR1, highlighting the role of the C5a:C5a-Receptor1 axis in vascular inflammation development and endothelial dysfunction in AMI, offering new therapeutic approaches for future investigations.

KEYWORDS

endothelial glycocalyx, endothelial dysfunction, complement system, C5a, C5a receptor 1, myocardial infarction, nitric oxide, atomic force microscopy

1 Introduction

During acute myocardial infarction (AMI) several innate immune pathways, including those of the complement system, are activated in the early steps of the inflammatory response to myocardial ischemia (1). There are three major pathways of complement activation: the classical, lectin, and alternative pathways. The classical pathway is initiated by the binding of C1q to immune complexes or other activating molecules like pentraxins (2). The lectin pathway is activated by recognition of carbohydrate patterns by ficolins or mannose-binding lectin (MBL) (2–4). The alternative pathway is triggered by spontaneous hydrolyzation of C3, amplifying the formation and deposition of C3b (4). All three pathways converge at the cleavage of C3 into C3a and C3b, leading to the formation of the C5 convertase (C4bC2bC3b or C3bBbC3b) that cleaves C5 into C5a and C5b (4). When C5b associates with C6 and C7, the complex becomes inserted into cell membranes and interacts with C8, inducing the binding of several units of C9 to form a lytic pore, the terminal complement complex (C5b-9n) also known as membrane attack complex (4).

Dysregulated activation of the complement system during AMI has been shown to be an important mediator of inflammatory damage and is associated with larger infarctions and poor clinical outcomes (5). C3 breakdown products and leukocyte infiltration have been demonstrated in infarcted myocardium highlighting the critical role of the complement cascade in triggering inflammation in the ischemic myocardium (6). The role of complement as a mediator of myocardial inflammation has been investigated by quantifying the products of complement activation, C3b, C4b, Bb

and C5b-9n, in patients with AMI. Although serum elevation of the early complement pathway's components like C1r, C3 and Factor B during AMI was demonstrated (7) only the late components (C5 convertase and C5b-9) of the complement pathway were correlated with necrotic mass of the myocardium and Troponin-T levels. Furthermore, C5a and C5b-9 have been shown to increased polymorphonuclear leukocytes adherence and directly induce myocardial injury (8).

Particularly, the mechanisms underlying complement-mediated injury to the myocardium mediated by the late components of the complement system's terminal pathway have previously been characterized (9–11). However, dysregulated complement activation causes not only myocardial damage, but also damage to the vascular endothelium (12, 13). Although the terminal pathway seems to play an important role in the development of endothelial damage during dysregulated complement activation, little attention has been paid to the effect of the anaphylatoxin C5a (14). Unfortunately, only few data are available so far on the mechanisms underlying C5a-induced damage to the vascular endothelium and especially the development of chronic vascular inflammation.

C5a is considered the most potent proinflammatory anaphylatoxin (5). It shows high proinflammatory activity and induces activation and polarization of lymphocytes and increased leukocyte adherence to endothelial cells (15, 16). Plasma concentrations of C5a can rise several fold under pathophysiological conditions such as AMI, causing local increases in blood flow, smooth muscle contraction, edema, cytokine storm, mast cell degranulation, and increased vascular permeability (1, 5, 13, 15, 17). The influence of the anaphylatoxin C5a on the endothelium in the context of AMI has been underestimated to

date and mechanistic knowledge of C5a-mediated changes both in endothelial cells and on the endothelial surface is limited.

During AMI the endothelium becomes an activated phenotype, resulting in a proinflammatory and prothrombotic state (18). Under healthy conditions, endothelial cells form a continuous layer along the entire vasculature, representing a crucial interface between blood and tissue. The endothelium is able to respond to external stimuli by secreting vasoactive substances and endothelium-derived relaxing factors such as nitric oxide (NO) to regulate homeostasis within the vascular system (19, 20). Healthy endothelium is covered by a negatively charged, brush-like layer: the endothelial glycocalyx (eGC). The eGC is a multifunctional layer of membrane-bound, carbohydrate-rich molecules, mostly consisting of glycoproteins and proteoglycans. Together with the underlying cellular cortex, an actin-rich layer 50–150 nm beneath the plasma membrane, the eGC forms a functional compartment that enables endothelial cells to detect and respond to external stimuli (20). Changes in the nanomechanical properties (such as stiffness) inversely correlate with endothelial NO release. Increased stiffness of the cellular actin cortex therefore reduces NO production and vice versa (20). Thus, the cellular actin cortex and the eGC can be seen as key vasoprotective players.

RhoA and its downstream effector, Rho-dependent coiled-coil kinase (ROCK), belong to the GTPase members of the Rho subfamily (21). Together, the RhoA/ROCK pathway regulates a wide array of cellular functions, including cellular polarity, motility, adhesion, proliferation, contraction, and migration (22). This signaling pathway is also known to regulate cell contraction, and permeability function in endothelial cells (22). Also, the cytoskeletal dynamics, such as changes in cell stiffness through actin polymerization/depolymerization, are regulated via the RhoA/ROCK pathway and dysregulation of this pathway has been implicated in various vascular disorders (21–23). Although reperfusion of the hypoxic myocardial tissue after AMI is critical for reoxygenation and organ salvage, it also results in myocardial ischemia and reperfusion (I/R) injury, causing further damage to the reperfused myocardial tissue (13). In fact, the vascular endothelium, or the eGC, is also impaired in the context of I/R (18). Degradation of the eGC is furthermore considered a hallmark in I/R-related endothelial dysfunction, which further impairs local microcirculation with a feed-forward loop of organ damage due to vasoconstriction, leukocyte adherence, and activation of the immune response, including the complement cascade (1, 18).

The aim of this study was to evaluate the effects of the complement anaphylatoxin C5a on the nanomechanical properties of the eGC and cellular cortex in the context of AMI. In the present study we (i) determine the importance of AMI-induced C5a elevation on mechanical changes to the endothelial cell surface using the atomic force microscopy (AFM)-based nanoindentation technique, (ii) evaluate the contribution of C5a to endothelial dysfunction and the condition of the eGC and to leukocyte-endothelium interaction, and (iii) investigate the effect of administering the C5a-Receptor-1 antagonist “PMX53” on restoring vascular nanomechanics and endothelial function.

2 Methods

2.1 Study population

Fifty-five patients with a first onset of ST-elevation myocardial infarction (STEMI) were recruited at the University of Luebeck in cooperation with the Department of Cardiology and Angiology of the Sana-Kliniken-Luebeck hospital (Germany) in accordance with the Declaration of Helsinki and approved by the Local Ethics Committee (Case: 19–310). Patients with STEMI who received a percutaneous coronary intervention (PCI) as first-line therapy during the first 120 min after STEMI was diagnosed were enrolled randomly after obtaining written informed consent. Serum samples were collected during emergency PCI (STEMI group). Fifty-five age- and sex-matched volunteers without cardiovascular comorbidities served as controls (CTR group). Serum samples from patients and controls were immediately treated according to Brandwijk et al. (24), who recommended assessing individual complement components in whole blood. Therefore, samples were kept on ice and centrifuged at 4°C within 60 min after collection. Thereafter, the samples were snap frozen and stored at -80°C. Patients in whom cardiopulmonary resuscitation was performed were excluded, as were patients who died during or after PCI. Further exclusion criteria were age below 18 years, pregnancy, or consent not given.

2.2 Enzyme-linked immunosorbent assay

Concentrations of the complement anaphylatoxin C5a and of soluble glycocalyx constituents (syndecan-1, heparan sulfate, and hyaluronan) were quantified by enzyme-linked immunosorbent assay (ELISA) (C5a: Complement C5a Human ELISA Kit; Thermo Fisher Scientific, Hamburg, Germany; catalog: BMS2088/Syndecan-1: Human CD138 ELISA kit, Diaclone Research, Besançon, France; catalog: 950.640.192/Heparan Sulfate: Human Heparan sulfate Proteoglycan (HSPG) ELISA Kit, MBS, San Diego, CA, USA; catalog: MBS2023323/Hyaluronan: Hyaluronan Quantikine ELISA Kit, R&D Systems, Minneapolis, MN, USA; catalog: DHYAL0).

2.3 Nitric oxide measurements

Concentrations of NO products [nitrites (NO_2^-) and nitrates (NO_3^-)] were determined using the chemiluminescence detector Sievers Nitric-Oxide Analyzer 280-i (NOA-280i; GE Water & Process Technologies, Analytic Instruments; Boulder, CO, USA). The assay is based on the reduction of all nitrates and nitrites into NO by vanadium(III)-chloride (VCl_3). Briefly, NO reacts with ozone (O_3) to produce nitrogen dioxide (NO_2), which is sensitively detected by its chemiluminescence.

A 100 mM NO_3^- stock solution was prepared by dissolving 84.9 mg NaNO_3 (Sigma Aldrich, Hamburg, Germany) in 10 mL deionized water. Standard dilutions (10 nM, 50 nM, 100 nM, 500 nM, 1 μM , 5

μM , 10 μM , and 100 μM NO_3^-) were prepared and injected in duplicates to create a calibration curve before the experiment.

All samples were deproteinized prior to analysis using ethanol precipitation. For this, the cell culture supernatants as well as the sera were diluted 1:3 with chilled pure ethanol (0°C). After 30 min precipitation time, the samples were centrifuged at $14000 \times g$ for 15 min and the supernatant was used for the experiment.

NO concentrations of the cell culture supernatant as well as of the STEMI and CTR sera were analyzed by injecting 50 μL duplicates of each sample into a purge vessel containing a solution of VCl_3 (50 mmol/L; Sigma-Aldrich, Hamburg, Germany; catalog: 208272) in hydrochloric acid (HCl ; 1 mol/L; Sigma-Aldrich, Hamburg, Germany; catalog: 1098214) at 95°C , continuously purged with a stream of nitrogen gas, connected to the NOA-280i. A gas bubbler between the purge vessel and the NOA-280i was filled with 15 mL of 1 M aqueous NaOH solution (Sigma-Aldrich, Hamburg, Germany; catalog: 655104) to prevent HCl vapors from entering the NOA-280i. Concentrations were calculated using the manufacturer's NO Analysis Software for Liquid (Version 3.21/Liquid, GE Water & Process Technologies, Analytic Instruments; Boulder, CO, USA).

2.4 Cell isolation and culture

Primary endothelial cells ("human umbilical vein endothelial cells"; HUVEC) were isolated as described previously in detail (25) and cultivated in Gibco Medium 199 supplemented with fetal calf serum 10% (FCS; Gibco, Carlsbad, CA, USA), penicillin/streptomycin 1% (100 U/mL, 100 mg/mL; Gibco, Carlsbad, CA, USA), large-vessel endothelial supplement 1% (Gibco, Carlsbad, CA, USA), and heparin (5000 U/mL; Biochrom, Schaffhausen, Switzerland) at 37°C , 21% O_2 and 5% CO_2 . Umbilical cords were donated by patients giving birth in the Marien-Krankenhaus Luebeck and the University Medical Centre Schleswig-Holstein Campus Luebeck (approved by Local Ethics Committee Cases: 18–325 and 2023–520_1).

EA.hy 926 endothelial cells (kindly provided by Cora-Jean S. Edgell, University of North Carolina, Chapel Hill, NC, USA) were grown in culture as described elsewhere (26). Briefly, cells were grown in 12.5 cm^2 falcon tissue culture flasks (Corning Inc., Corning, NY, USA; catalog: 353107) until they reached confluence. Cells were grown in Dulbecco's modified eagle's medium (DMEM; Thermo Fisher Scientific, Hamburg, Germany; catalog: 41966–029) supplemented with FCS (10%) and penicillin/streptomycin (100 U/mL, 100 mg/mL) at 37°C , with 21% O_2 and 5% CO_2 .

HUVEC monolayers were stimulated with the complement anaphylatoxin C5a (Merck, Darmstadt, Germany; catalog: 204902). Different concentrations of C5a (0, 1, 10, 50, and 100 ng/mL) as well as different stimulation durations (0, 30, 60, and 120 min and 24 h) were initially tested for their effect on cortical stiffness. In further experiments, HUVEC were stimulated with 50 ng/mL of C5a with or without the C5a-Receptor-1 antagonist (C5aRA) PMX53 (Sigma Aldrich, Hamburg, Germany; catalog number 533683), according to the manufacturer's instructions [concentration 1 $\mu\text{g/mL}$ (1:1000)] for 24 h. In addition, the

endothelial cells were stimulated with 10% patient (STEMI) or healthy donor (CTR) sera (instead of FCS) for 24 h either with or without C5aRA (PMX53). The concentration of C5a in the patient sera was determined by ELISA. The patient group with a concentration of C5a in the lowest quartile is hereinafter referred to as LOW and the group of patients with a concentration in the top quartile as HIGH. Differences in cortical stiffness between HIGH and LOW C5a were determined using AFM measurements.

2.5 Atomic force microscopy

The height and stiffness of the eGC and cortical stiffness in both HUVEC and mouse aortic endothelial cells were determined using the AFM-based nanoindentation technique, as described previously (25). Indentation measurements were performed on living confluent cells at 37°C in HEPES-buffered solution (standard composition in mmol/L: 140 NaCl , 5 KCl , 1 MgCl_2 , 1 CaCl_2 , 5 glucose, and 10 HEPES, pH 7.4). To determine cortical stiffness, a Nanoscope Multimode8 AFM (Veeco, Mannheim, Germany) was used. For measuring the nanomechanical properties of the eGC of HUVEC as well as for measurements of ex vivo mouse aortas, a Nanowizard4 (JPK BioAFM Business, Berlin, Germany) was employed.

Briefly, a laser beam was aligned on the back of a gold-coated triangular cantilever (Novascan Technologies, Boone, NC, USA) with a mounted spherical tip (diameter 10 μm) and a nominal spring constant of 10 pN/nm (for eGC) and 30 pN/nm (for cortical stiffness). The cantilever indents the endothelial cell surface with a loading force of 0.5 nN. The reflection of a laser beam is used to quantify the cantilever deflection. The height of the eGC can be calculated by knowing the cantilever force, the piezo displacement, and the deflection sensitivity. For each experimental condition, a total of 150–300 single cells were measured. For each single cell, 6–8 force distance curves were generated and averaged, resulting in $n = 900$ –2400 per condition. Data were collected using the Research NanoScope version 9.20 (64 bit; Bruker Nano GmbH) and calculated using the Protein Unfolding and Nano-Indentation Analysis Software (PUNIAS 3D; Version 1.0; Release 2.3; Copyright 2009).

2.6 Fluorescence staining and microscopy

Fluorescence staining and microscopy of the cortical F-actin and of components of the eGC were applied as described previously (25). Briefly, HUVEC were fixed with either 4% paraformaldehyde or 0.1% glutaraldehyde for further staining. Cortical F-actin was stained using phalloidin-tetramethylrhodamine (10 mg/mL; Sigma Aldrich) after permeabilization of the cells with 0.1% Triton X-100 (Sigma Aldrich; catalog: T8787–50ML) for 10 min. Coverslips were mounted overnight at 4°C with Dako mounting medium (Dako, Carpinteria, CA; catalog: GM30411–2). Wheat germ agglutinin (WGA; conjugate Alexa-Fluor488; Thermo Fisher, Waltham, MA) was used as overview staining for eGC components. After fixation, cells were incubated with 1:500 dilutions of WGA and mounted overnight. For immunostaining of syndecan-1 (CD138), fixed cells were incubated with the primary antibody (1:100, mouse

antihuman CD138; monoclonal antibody; Bio-Rad, Hercules, CA; catalog: MCA2459). After incubation, the coverslips were incubated with the secondary antibody (1:400, goat anti-mouse conjugate Alexa-488; Invitrogen, Carlsbad, CA; catalog: A28175) and mounted with Dako mounting medium containing Hoechst solution (1.5 mg/mL; Sigma Aldrich, Hamburg, Germany; catalog: 94403) to stain cell nuclei.

Images were rendered with a Keyence fluorescence microscope BZ9000 (Keyence Corp., Osaka, Japan; magnification x60) using the BZ Viewer/Analyzer-II (software version 2.2; Keyence Corp.). Images and stacks of WGA and phalloidin staining were analyzed for fluorescence intensity (in arbitrary units) using ImageJ software. For analyzing the amount of syndecan-1 per cell relative to control, fluorescence-dot nuclei colocalization was measured using YT Evaluation software (Version 2.1.12014; 64 bit; Synentec, Elmshorn, Germany).

2.7 Single-cell force spectroscopy and quantitative monocyte adhesion measurements

Adhesion forces between the endothelial surface and monocytes were quantified by single-cell force spectroscopy and by monocyte wash-away assays as described elsewhere (27). Human monocytes were isolated from the blood of healthy donors using the S-pluriBead Maxi Reagent Kit (pluriSelect Life Science, Leipzig, Germany; catalog number 70–50010-12) following the manufacturer's instructions.

For single-cell force spectroscopy a single human monocyte was attached to the AFM cantilever in order to measure the adhesion forces between the monocyte and HUVEC monolayers. Measurements were performed by using the Nanowizard4 CellHesion-Module (JPK BioAFM Business, Berlin, Germany). Arrow TL-2 tipless cantilevers (NanoAndMore GmbH, Wetzlar, Germany) were incubated prior to all experiments for 20 min in Corning Cell-Tak (Fisher Scientific GmbH, Schwerte, Germany; catalog: 10317081) to attach the monocyte to the cantilever. For quantifying the adhesion forces between the monocyte and the endothelial cells, the monocyte was brought into contact with the endothelial surface for 10 s with a constant set point of 0.5 V and then pulled away to obtain force-distance/adhesion curves. The maximal adhesion forces (in N) between monocyte and endothelial surface and the adhesion energy (in J) were measured and analyzed using the JPK Data processing software version 7.0.112 (Bruker Nano GmbH, Berlin, Germany).

In addition, monocyte-endothelium interaction was quantified by monocyte wash-away assays. For this, monocytes were fluorescently labeled using an Alexa Flour 488 anti-human CD14 antibody (25:1000, Biolegend, San Diego, CA, USA; catalog: 367130) and added to a confluent HUVEC monolayer for 4 h. To remove nonadherent monocytes, cells were washed carefully four times with PBS, following a standardized protocol. HUVEC and adherent monocytes were fixed with 4% paraformaldehyde and subjected to fluorescence microscopy for further analysis.

2.8 Preparation of mouse aortas/assessment of mouse aortic endothelial cell nanomechanics

Wild-type (B6.JRj), C5aR1^{-/-} (B6.129S4-C5aR1^{tm1Cge}), C5^{-/-} (B6 (Cg)Tg(Ins2-GP)zbz) and mice double deficient for C5aR1 and CXCL4 (C5aR1^{-/-}-CXCL4^{-/-}) (on C57BL/6J background) were bred and maintained in an SPF animal facility of the University of Luebeck (Case: 39.2_2020–08-20_Karsten) as described previously (28). All study animals were between 8 and 18 weeks of age and handled in accordance with the appropriate institutional and national guidelines. Both male and female mice were equally used for the experiments.

The aortas were harvested and prepared for ex vivo analysis by AFM, as described previously (29), to assess the thickness and stiffness of the eGC and cellular cortex of the mouse aorta endothelial cells using the AFM.

Briefly, aortas were harvested after sacrificing the animals and freed from the surrounding tissue. Small patches (~1mm²) of the aorta were attached on Cell-Tak-coated glass coverslips with the endothelial cells facing upwards, making them accessible for further experiments. After preparation, the ex vivo patches were cultured in minimal essential medium (Invitrogen Corp., La Jolla, CA, USA) supplemented with 10% FCS (Gibco, Carlsbad, CA, USA), 1% minimal essential medium vitamins (Invitrogen), 1% minimal essential medium nonessential amino acids (Invitrogen), and 1% penicillin/streptomycin (100 U/mL, 100 mg/mL). Integrity of the ex vivo endothelial cell monolayers derived from mouse aorta was confirmed by immunostaining of platelet endothelial cell adhesion molecule 1 (PECAM1; data not shown), and individual cells on those preparations were studied.

2.9 Small G-protein activation assays

The intracellular concentrations of GTP-bound Rac1 and RhoA GTPases were measured by using colorimetric G-LISA activity measurements (G-protein ELISA assays; Cytoskeleton, Denver, CO, USA; catalog: Rac1: BK128; RhoA: BK124). HUVEC were serum starved for 24 h and treated either with C5a or STEMI vs. CTR serum +/- C5aR1 antagonist. After processing, cell lysates were subjected to the G-LISA according to the manufacturer's instructions. The final reaction absorbance was measured using a Mitras LB940 microplate reader (Berthold Technologies, Bad Wildbad, Germany). Absorbance was detected at 490 nm. Presented data are background subtracted.

2.10 RNA extraction and quantitative real-time PCR

RNA from primary HUVEC was extracted using the innuPREP RNA Mini Kit 2.0 (IST Innu-screen GmbH, Berlin, Germany; catalog: 12183020) according to the manufacturer's protocol. cDNA of total RNA (1000 ng) was synthesized with the Go Script

Reverse Transcriptase (Promega GmbH, Walldorf, Germany; catalog: A5003) and random hexamer primers (Thermo Fisher Scientific; catalog: SO142) according to the instructions of the manufacturer.

Sequences: C5aR1 (Forward: 5'-GGCAGTGGTGGCCAGTT TCT-3'; Reverse: 5'-GGGAGGCATTTCCGCAGTGC-3'), L28 (Forward: 5'-ATGGTCGTGCGGAAGTCT-3'; Reverse: 5'-TTGTAGCGGAAGGAATTGCG-3').

L28 primers were synthesized by Invitrogen (Invitrogen, Carlsbad, CA); C5aR1 primers were synthesized by Metabion (Metabion International AG, Planegg, Germany). Quantitative real-time polymerase chain reaction (RT-PCR) was performed in the Eco48 qPCR System (PCRmax Limited Beacon Road, Staffordshire, United Kingdom) using 1 µg cDNA and the SensiMix SYBR Kit (Bioline, Luckenwalde, Germany; catalog: QT615-05) in a total volume of 12.5 µL per assay.

The cutoff point (Ct) was defined as the value when the fluorescent signal increased above the background threshold. Gene-specific mRNA expression of C5aR1 was normalized to mRNA expression of the housekeeping gene ribosomal protein L28. Relative expression values were calculated using the $2^{-\Delta\Delta CT}$ method and are presented as the relative fold change.

2.11 Wound healing assay

For wound closure experiments, EA.hy926 endothelial cell monolayers were scratched with a 200-µL sterile pipette tip and detached cells were washed away with PBS. Stimulation with C5a or STEMI vs. CTR serum +/- C5aR1 antagonist was carried out in HEPES-buffered solution. Once the scratch was made, the culture flasks were transferred into a flask heater set to 37°C.

Wound closure was analyzed with time-lapse video microscopy using an Olympus CKX53 microscope (EVIDENT Europe GmbH, Hamburg, Germany) with a 10x objective. Pictures were taken every 5 min for 24 h with a VWR VisiCam 5 (VWR International GmbH, Darmstadt, Germany) using the OPTIKA Vision Software (Version 2.13; OPTIKA S.r.l., Ponteranica, Italy). To quantify the cell migration characteristics (wound closure in %), the images were analyzed using an ImageJ (ImageJ software version 1.52a; NIH, Bethesda, MD; <https://imagej.nih.gov/ij/download.html>, last accessed 8 Feb 2024) plugin for the high-throughput image analysis of *in vitro* scratch wound healing assays developed by Suarez-Arnedo et al (30). The wound closure speed was furthermore normalized into the cell growth rate (µm/h) to render all data comparable, as the cell front velocity is independent of the initial gap width, gap creation method, gap orientation, the microscopy settings, and the objective lens' magnification. For this, the wound closure speed (surface area per time) was determined by creating a graph showing the cell-covered area per time and defining the linear part of the curve (trend line calculation). The slope of the trend line corresponds to the growth rate. To finally calculate the cell front velocity, the wound closure speed was divided by the length of the cell front (in µm). (For further information compare the ibidi Application Note 30 on Experimental Setup Optimization and Data Analysis of Wound

Healing Assays; ibidi GmbH, Gräfelfing, Germany; https://www.ibidi.com/img/cms/support/AN/AN30_Wound_Healing_Data_Analysis.pdf, last accessed Feb. 09th 2023).

2.12 Sprouting angiogenesis aortic ring assay

The sprouting angiogenesis aortic ring assay was performed as described, previously (31), with some modifications: Aortas of mice were harvested as described above and sectioned into 1 mm pieces. Matrigel (Corning) was selected for its basement membrane-like composition as embedding medium. 200 µL of Matrigel was evenly coated on 12-well plates placed on ice and polymerized by incubating in a humidified incubator at 37°C with 5% CO₂ for 30 min. Subsequently, freshly obtained aortic rings were placed at the center of each well, and an additional 300 µL of Matrigel was applied on top of the aortic ring tissue. The plates were re-incubated under the same conditions until the Matrigel was fully polymerized. The Matrigel was supplemented in its liquid state with VEGF-A (25 ng/mL, Sigma Aldrich). Following Matrigel polymerization, the aortic ring sandwich assay was incubated in 1000 µL of endothelial culture medium supplemented with 2% FCS and 1% penicillin/streptomycin. Media were replenished every 2 days throughout the assay.

To monitor sprouting in real-time, the explants were placed under a light microscope equipped with phase-contrast optics and a digital camera with a Visiscope inverted microscope (IT404, VWR, Radnor, PA, USA). Sprouting was typically observed by day 3, with maximal sprouting occurring around day 7. Sprouting was quantified using the Angiogenesis analyzer for ImageJ as described before (32).

2.13 Tube formation assay

The tube formation assay was performed, as described, previously (33). For the *in vitro* tube formation assay, MHEC-5T (6 x 10⁴ cells/well) were plated onto Matrigel-coated Angiogenesis µ-slides (ibidi, Planegg, Germany) in endothelial culture medium containing 2% FCS. Cells were co-incubated with C5a (R&D) at different concentrations. After 6h tube formation was imaged by phase-contrast microscopy. Tube Formation was analyzed using Angiogenesis analyzer for ImageJ as described before.

3 Results

3.1 C5a concentrations and eGC components are increased after myocardial infarction and alter endothelial function in STEMI patients

For forming the experimental groups, C5a concentrations were measured using ELISA in the STEMI patients' serum. The sera were further sorted by quartile according to their level of C5a concentration.

The lowest quartile as well as the top quartile were pooled to form the experimental groups LOW (mean C5a concentration: 20.43 ± 2.8 ng/mL) and HIGH (mean C5a concentration: 88.56 ± 6.9 ng/mL). Serum of healthy donors was implemented as control group (CTR; mean C5a concentration: 3.61 ± 1.1 ng/mL).

Concentrations of both C5a and the eGC components syndecan-1, heparan sulfate, and hyaluronan were significantly increased in the HIGH group compared to controls (all: $p < 0.0001$) (Figure 1A). NO bioavailability was decreased by 52% in the HIGH group compared to CTR ($p < 0.0001$).

The eGC components measured in the patients' blood correlated with the C5a concentration (Figure 1B). The C5a concentration positively correlated with syndecan-1 ($r = 0.84$; $p < 0.001$), heparan sulfate ($r = 0.53$; $p < 0.001$) and hyaluronan ($r = 0.49$; $p < 0.001$). NO concentration ($r = -0.33$; $p < 0.05$; calculated without LOW data) as well as eGC height ($r = -0.66$; $p < 0.001$) negatively correlated with C5a. Of note, C5a concentrations

correlated positively with the days until hospital discharge ($r = 0.72$; $p < 0.001$).

3.2 C5a incrementally changes the nanomechanical properties of the endothelial surface layers in a concentration-dependent manner

To quantify nanomechanic changes of the eGC and cellular cortex confluent HUVEC monolayers were treated with 10% patient or control sera and the nanomechanical properties (height and stiffness) of the endothelial surface layers (eGC and cortex) were probed by using the AFM nanoindentation technique.

Incubation with LOW serum increased the cortical stiffness by 10% compared to control-treated HUVEC (CTR vs. LOW: 0.88 ± 0.06 pN/nm vs. 1.0 ± 0.06 pN/nm; $p < 0.0001$) (Figure 2A). Treatment with

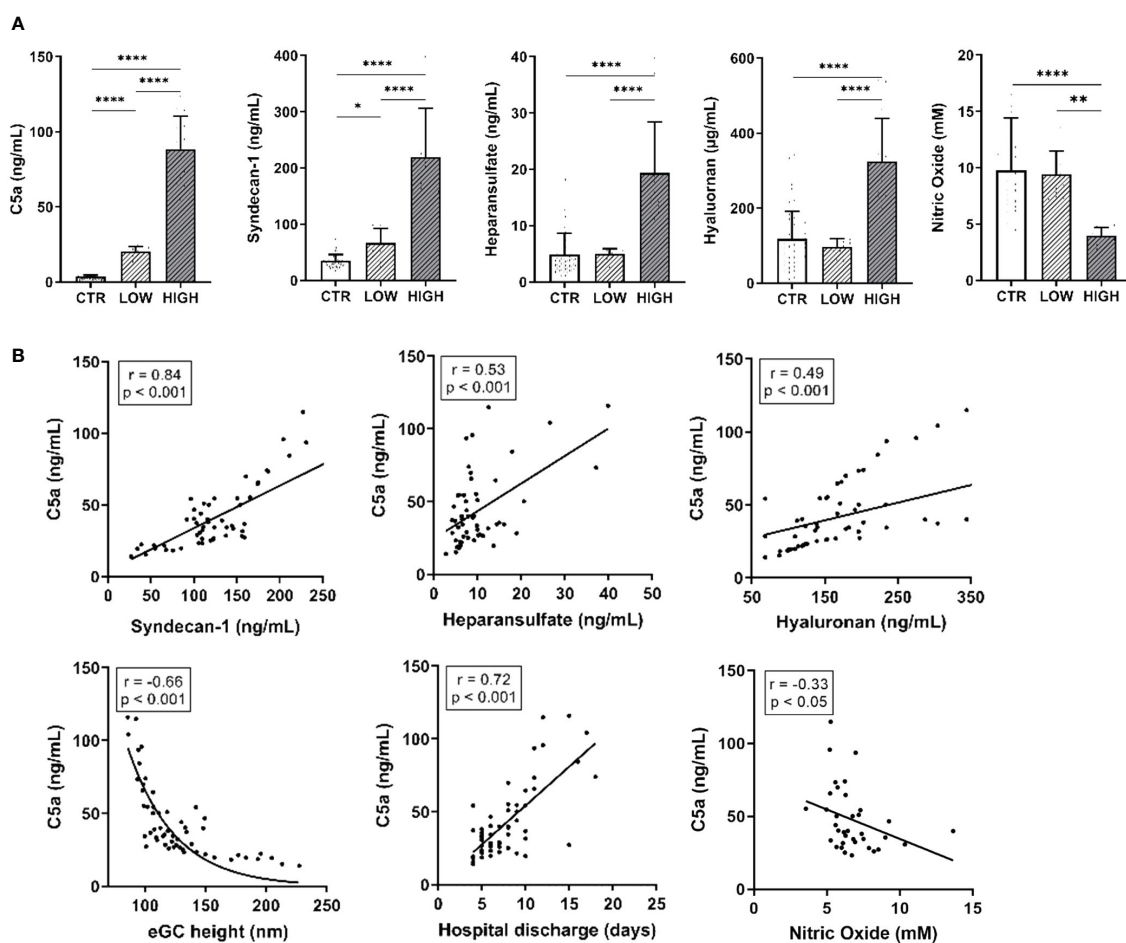


FIGURE 1

C5a Concentrations and eGC Components Are Increased After Myocardial Infarction and Alter Endothelial Function in STEMI Patients. (A) Serum levels of C5a, syndecan-1, heparan sulfate, and hyaluronan (measured by enzyme-linked immunosorbent assay, ELISA) as well as nitric oxide (NO) concentrations (measured chemiluminescence based). (B) Correlation of C5a concentrations in ST-elevation myocardial infarction (STEMI) patient sera vs. syndecan-1, heparan sulfate, and hyaluronan as well as of endothelial glycocalyx (eGC) height, days until discharge from hospital, and NO concentration (calculated without data from LOW group). Rho (r) and p-values (p) shown for correlations. Groups: LOW: STEMI patient sera of the lowest C5a concentration quartile; HIGH: STEMI patient sera of the top C5a-concentration quartile; CTR: healthy donors. p-values: **** $p < 0.0001$; ** $p < 0.01$; * $p < 0.05$.

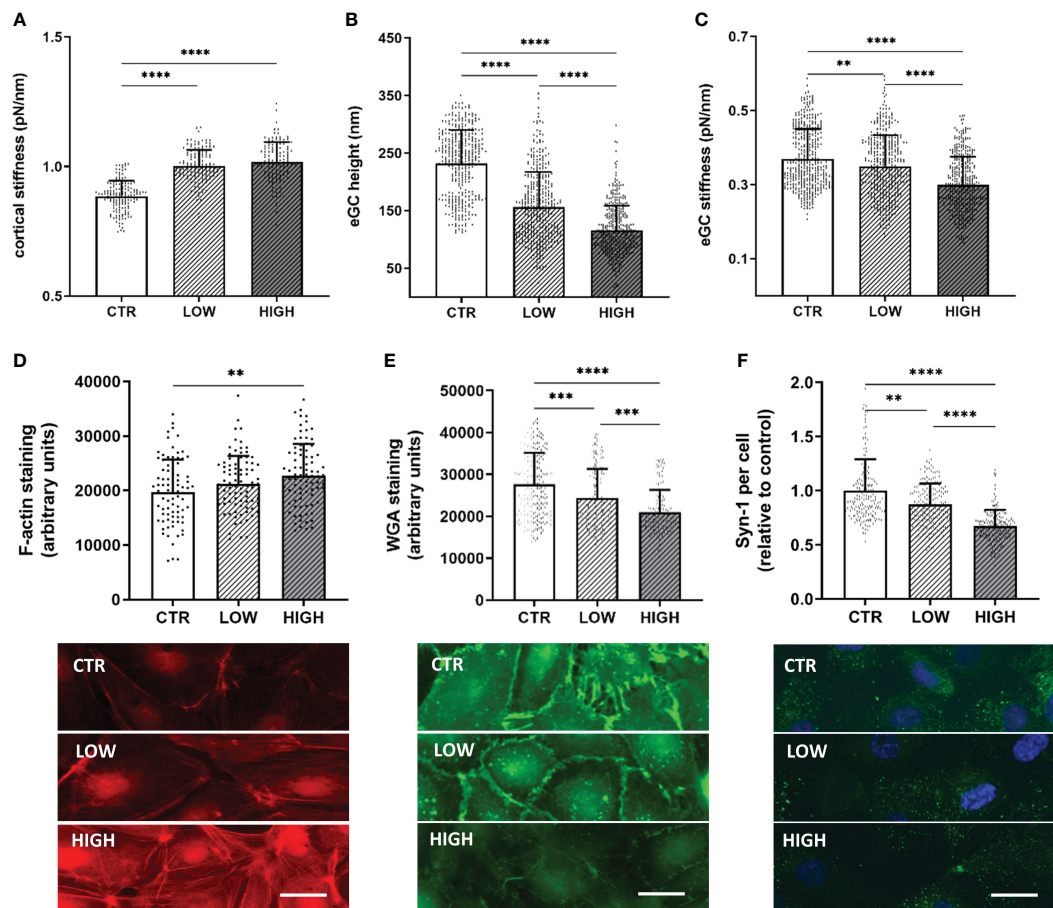


FIGURE 2

C5a Incrementally Changes the Nanomechanical Properties of the Endothelial Surface Layers in a Concentration-Dependent Manner

(A–C) Statistical analysis of atomic force microscopy (AFM) nanoindentation measurements of human umbilical vein endothelial cells (HUVEC) monolayers. Data showing mean \pm SD of (A) cortical stiffness, (B) endothelial glycocalyx (eGC) height and (C) eGC stiffness. Each dot represents a single cell measurement (8 force-distance curves per dot; N=6). (D–F) Representative fluorescence images and statistical fluorescence intensity analyses. (D) Phalloidin-tetramethylrhodamine-stained (red: F-actin) and (E) Wheat germ agglutinin (WGA)-stained (green; representing unspecific eGC components) HUVEC monolayers. Graphs showing the measured fluorescence intensity in arbitrary units. (F) Syndecan-1 antibody-stained HUVEC monolayers (green: syndecan-1; blue: cell nucleus) after stimulation. Graphs showing the amount of syndecan-1 per cell relative to the control group. (D–F: N=5; scale bars: 50 μ m). Groups: LOW: ST-elevation myocardial infarction (STEMI) patient sera of the lowest C5a concentration quartile; HIGH: STEMI patient sera of the top C5a -concentration quartile; CTR: healthy donors. p-values: ****p<0.0001; ***p<0.001; **p<0.01.

HIGH serum augmented this effect, increasing the cortical stiffness further by 12% (p<0.0001) compared to healthy controls.

eGC height was decreased by 32% (p<0.0001) after treatment with LOW serum and by 49% after HIGH serum C5a concentrations compared to controls (CTR vs. HIGH: 232.4 ± 57.7 nm vs. 115.3 ± 43.4 nm; p<0.0001) (Figure 2B). After treatment with HIGH serum, eGC damage was markedly stronger than after treatment with LOW serum (LOW overall mean 156.3 ± 60.1 nm vs. HIGH overall mean 115.3 ± 43.4 nm; p<0.0001). In addition, the eGC stiffness was impaired after serum stimulation with a decreased stiffness of 6% in the LOW (p<0.01) and 19% in the HIGH group (CTR vs. HIGH: 0.37 ± 0.08 pN/nm vs. 0.29 ± 0.07 pN/nm; p<0.0001) (Figure 2C). This combination of loss of height and reduction in stiffness of the eGC indicates shedding of the glycocalyx after stimulation with STEMI serum (20).

Results of fluorescence staining were consistent with the AFM findings. Fluorescence staining of the cortical F-actin conformed with the results of the AFM-based cortex measurements. Fluorescence intensity was increased in the LOW (7%) and the HIGH (15%; p<0.01) group compared to CTR (Figure 2D), indicating polymerization of cortical actin. eGC shedding detected by AFM could be confirmed by fluorescence staining of eGC components, as STEMI-induced eGC deterioration resulted in a reduced WGA fluorescence intensity in LOW (12%; p<0.001) and HIGH (24%; p<0.0001) serum-treated cells compared to the CTR group (Figure 2E). Additionally, the specific syndecan-1-antibody (anti-CD138) showed a reduction in syndecan-1 per cell after serum stimulation compared to CTR. Both groups, LOW (by 13%; p<0.01) and HIGH (by 33%; p<0.0001), showed significant reductions in syndecan-1 per cell compared to the control-treated HUVEC (Figure 2F).

3.3 C5a stimulation leads to cortical stiffening and eGC degradation

To evaluate the contribution of C5a on endothelial nanomechanics and condition of the eGC, different concentrations of C5a (0, 1, 10, 50, and 100 ng/mL) and different stimulation durations (0, 30, 60, and 120 min and 24 h) were applied to HUVEC monolayers. The nanomechanical properties (height and stiffness) of the cellular cortex and the eGC were quantified via AFM nanoindentation technique.

Stimulation with 50 ng/mL ($p < 0.001$) and 100 ng/mL ($p < 0.0001$) induced significant stiffening of the endothelial cortex (Figure 3A). Both concentrations were further tested in a temporal context and showed a significant increase in cortical stiffness after 24 h of stimulation (Figures 3B, C, both $p < 0.0001$). In subsequent experiments, 50 ng/mL (hereinafter referred to as C5a group) was applied, as this concentration proved to be the lowest with a significant effect on nanomechanical properties of the vascular surface.

Cortical stiffness increased by 29% after C5a stimulation compared to control conditions (CTR vs. C5a: 0.9 ± 0.06 pN/nm vs. 1.17 ± 0.12 pN/nm; $p < 0.0001$) (Figure 3D). Compared to control treatment, eGC height was diminished by 36% (CTR vs. C5a: 198.5 ± 40.0 nm vs. 124.5 ± 32.7 nm; $p < 0.001$; Figure 2E) and the eGC stiffness was reduced by 19% (CTR vs. C5a: 0.40 ± 0.07 pN/nm vs. 0.32 ± 0.05 pN/nm; $p < 0.001$; Figure 3F) after stimulation with 50 ng/mL of C5a. Both effects (Figures 3E, F) were observed after treatment with C5a, indicating eGC shedding.

The nanoindentation measurements were again confirmed by fluorescence staining of the cellular cortex and the eGC. The fluorescence signal for cortical F-actin was enhanced by 31% ($p < 0.0001$), indicating polymerization of cortical actin (Figure 3G). Unspecific staining of the eGC using WGA revealed a reduced fluorescence intensity of the C5a-treated cell surface by 19% ($p < 0.001$) (Figure 3H), which was additionally underpinned by the syndecan-1 staining showing a reduction in syndecan-1 per cell by 26% compared to controls ($p < 0.001$) (Figure 3I).

3.4 C5a-receptor-1 antagonist (PMX53) reduces impairment of the vascular surface after AMI and C5a stimulation

After observing shedding of the eGC and cortical stiffening after treatment with both patient sera and recombinant C5a, C5aRA (PMX53) was employed to investigate the influence of the C5a: C5aR1 axis on vascular surface nanomechanics and eGC integrity. To test the effect of C5aRA, two different experimental approaches were followed: i) stimulation with CTR vs. C5a (50 ng/mL) with and without C5aRA treatment; and ii) stimulation with STEMI patient serum (STEMI group: mean C5a concentration: 86.74 ± 6.5 ng/mL) vs. healthy control serum (CTR group: mean C5a concentration: 3.61 ± 1.1 ng/mL) with and without C5aRA treatment. The mean C5a concentration of the STEMI group corresponds to the mean C5a concentration of the HIGH group. The nanomechanical properties of the cellular cortex and the eGC were probed using the AFM nanoindentation technique on HUVEC monolayers.

Nanoindentation of the cellular cortex revealed increased stiffness after C5a stimulation (CTR vs. C5a: 0.85 ± 0.18 pN/nm; vs. 0.95 ± 0.17 pN/nm; $p < 0.0001$). However, treatment with C5aRA fully restored the cortex stiffness compared to CTR levels (Figure 4A). After C5a stimulation the condition of the eGC changed and height was decreased (CTR vs C5a: 172 ± 37 nm vs. 123 ± 34 nm; $p < 0.0001$) compared to controls (Figure 4B). Although treatment with C5aRA did not completely regenerate the eGC height up to control levels, there was a significant improvement in the C5a+RA group compared to the C5a group (C5a vs. C5a+RA: 122.7 ± 33.8 nm vs. 152.9 ± 30.8 nm; $p < 0.0001$). C5a-mediated shedding of the eGC led to softening of the eGC by 17% compared with CTR ($p < 0.01$) (Figure 4C) and treatment with C5aRA to full restoration of the eGC stiffness compared to controls, both indicating recovery of the eGC.

Treatment with C5aRA could reduce the STEMI-induced cortical stiffening (STEMI vs. STEMI+RA: 0.99 ± 0.2 pN/nm vs. 0.9 ± 0.2 pN/nm; $p < 0.01$) (Figure 4D). STEMI serum reduced eGC height significantly compared to controls (CTR vs. STEMI: 161 ± 29 nm vs. 138 ± 26 nm; $p < 0.0001$) (Figure 4E). This effect could not be prevented by C5aRA treatment. eGC stiffness was not affected after stimulation with the C5aR inhibitor (Figure 4F).

Treatment with C5aRA prevented the C5a-induced polymerization of cortical actin, confirming the results of AFM-based nanoindentation measurements. Simultaneously, C5aRA treatment in the context of STEMI reduced cortical F-actin (STEMI vs. STEMI+RA: $p < 0.001$) (Figure 4G).

The AFM-based detection of eGC shedding and cortical stiffening were also visualized by fluorescence staining. WGA staining revealed a reduction in eGC components after both C5a ($p < 0.0001$) and stimulation with STEMI serum ($p < 0.0001$) (Figure 4H).

Treatment with C5aRA fully restored the eGC components, reaching control levels after C5a stimulation, and the condition of the eGC was significantly improved after stimulation with STEMI serum (STEMI vs. STEMI+RA: $p < 0.05$) (Figure 4H). Consistently, syndecan-1 staining indicated a reduction in syndecan-1 per cell both after stimulation with C5a ($p < 0.0001$) and with STEMI serum ($p < 0.0001$) compared with healthy controls (Figure 3I). Fully restored syndecan-1 levels were detected after C5aRA treatment (C5a vs. C5aRA: 0.85 ± 0.2 vs. 0.93 ± 0.2 Syn-1 per cell (relative to control); $p < 0.05$) (Figure 4I). STEMI+RA stimulation resulted in a significant elevation in stainable syndecan-1 per cell (STEMI vs. STEMI+RA: 0.71 ± 0.1 vs. 0.78 ± 0.2 Syn-1 per cell (relative to control); $p < 0.05$) (Figure 4I).

Induction of C5a-Receptor-1 expression was confirmed by measuring C5a-Receptor-1 genes via quantitative PCR after stimulating HUVEC with C5a but not with STEMI serum (Figure 4J). To determine the pathway of cellular cortex stiffening, small GTPases were quantified. For this, RhoA and Rac1 were measured as key mechanotransduction players, regulating actin cytoskeletal tension using G-LISA assays. Analysis of baseline RhoA activity in confluent HUVEC monolayers revealed significantly higher RhoA activity after both C5a and stimulation with STEMI serum (both $p < 0.05$) (Figure 4K). RhoA activity was regulated to control levels in both groups after C5aRA treatment. Baseline Rac1 activity was elevated after stimulation with STEMI serum ($p < 0.05$) and reversed by C5aRA treatment (Figure 4L).

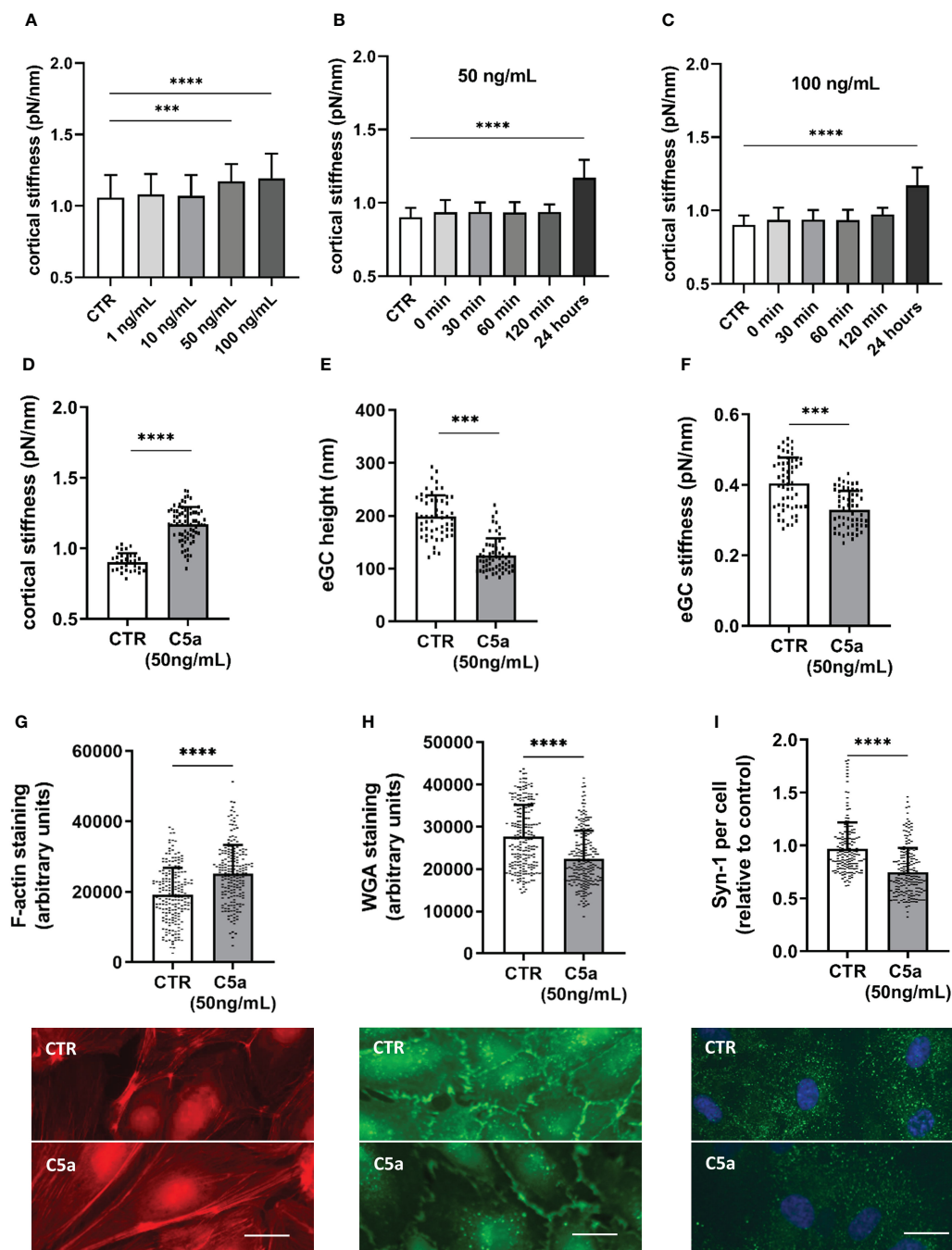


FIGURE 3

C5a stimulation leads to cortical stiffening and eGC degradation. Different concentrations of C5a as well as different stimulation durations were tested for their influence on cortical stiffness measured via atomic force microscopy (AFM) nanoindentation technique. (A) Statistical analysis of AFM measurements of human umbilical vein endothelial cells (HUVEC) monolayers. Data showing mean \pm SD of cortical stiffness after stimulation with different concentrations of C5a (0, 1, 10, 50 and 100 ng/mL; N=5). (B) Statistical analysis of AFM measurements of HUVEC monolayers showing mean \pm SD of cortical stiffness after stimulation with 50 ng/mL of C5a using different stimulation durations (0, 30, 60, and 120 min and 24 h; N=5). (C) Statistical analysis of AFM measurements of HUVEC monolayers showing mean \pm SD of cortical stiffness after stimulation with 100 ng/mL of C5a using different stimulation durations (0, 30, 60, and 120 min and 24 h; N=5). (D–F) Statistical analysis of AFM nanoindentation measurements. Data showing mean \pm SD of (D) cortical stiffness, (E) eGC height, and (F) eGC stiffness after stimulating HUVEC monolayers with 50 ng/mL of C5a for 24 h (N=5). (G–I) Representative fluorescence images and statistical fluorescence intensity analyses. (G) Phalloidin-tetramethylrhodamine-stained (red: F-actin) and (H) Wheat germ agglutinin (WGA)-stained (green; representing unspecific eGC components) HUVEC monolayers after stimulation as described. Graphs showing the measured fluorescence intensity in arbitrary units. (I) Syndecan-1 Antibody-stained HUVEC monolayers (green: syndecan-1; blue: cell nucleus) after stimulation. Graphs showing the amount of syndecan-1 per cell relative to the control group. (G–I: N=6; scale bars: 50 μ m). p-values: ****p<0.0001; ***p<0.001.

3.5 The influence of C5a and STEMI on eGC condition and cortical stiffness are attenuated in a mouse model for C5a-receptor-1-knockout

To further examine the effects of the C5a-Receptor-1 on vascular surface nanomechanics and eGC integrity ex vivo, endothelial cells derived from C5a-Receptor-1 knock-out (KO; C5aR1^{-/-}) mouse aorta were employed.

Stimulation with either C5a ($p < 0.01$) or STEMI serum ($p < 0.001$) enhanced cortical stiffness in WT mice (Figure 5A). As expected, stimulation with C5a showed no effects on the C5aR1^{-/-} mouse aortic endothelial cells, although stimulation with STEMI serum did cause cortical stiffening compared to both controls and to the C5a group (KO CTR vs. C5a vs. STEMI: 0.88 ± 0.04 pN/nm vs. 0.88 ± 0.03 pN/nm vs. 0.92 ± 0.04 pN/nm; $p < 0.001$). Cortical stiffness differed between WT and KO after simultaneous stimulations: after C5a stimulation cortical stiffness was significantly higher in WT mice than

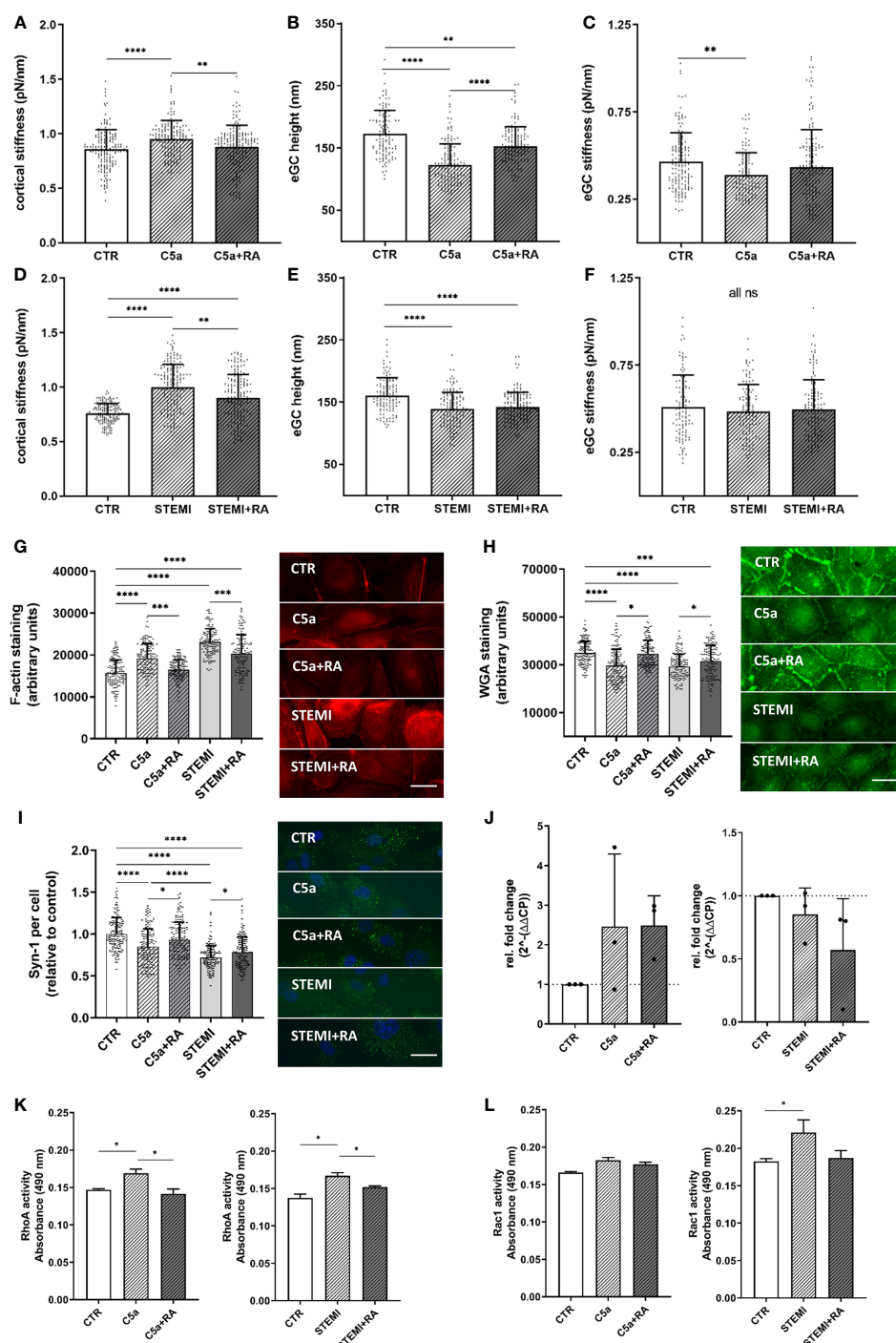


FIGURE 4 (Continued)

C5a-receptor-1 antagonist (PMX53) reduces impairment of the vascular surface after AMI and C5a stimulation. (A–C) Statistical analysis of atomic force microscopy (AFM) nanoindentation measurements of human umbilical vein endothelial cells (HUVEC) monolayers. Data showing mean \pm SD of (A) cortical stiffness, (B) endothelial glycocalyx (eGC) height, and (C) eGC stiffness of CTR, C5a, and C5a+RA groups. Each dot represents a single cell measurement (8 force-distance curves per dot; N=5) as described in detail in the methods section. (D–F) Statistical analysis of AFM nanoindentation measurements of HUVEC monolayers. Data showing mean \pm SD of (D) cortical stiffness, (E) eGC height, and (F) eGC stiffness of CTR, STEMI, and STEMI+RA groups. Each dot represents a single cell measurement (8 force-distance curves per dot; N=5) as described in detail in the methods section. (G–I) Representative fluorescence images and statistical fluorescence intensity analyses. (G) Phalloidin-tetramethylrhodamine-stained (red: F-actin) and (H) Wheat germ agglutinin (WGA)-stained (green; representing unspecific eGC components) HUVEC monolayers after stimulation as described. Graphs showing the measured fluorescence intensity in arbitrary units. (I) Syndecan-1 antibody-stained HUVEC monolayers (green: syndecan-1; blue: cell nucleus) after stimulation. Graphs showing the amount of syndecan-1 per cell relative to the control group. (G–I: N=5; scale bars: 50 μ m). (J) Expression levels of C5a-Receptor1 genes via quantitative PCR after stimulation of HUVEC. Gene-specific mRNA expression was measured using the $\Delta\Delta$ Ct method relative to expression of ribosomal protein L28 (endogenous control) and normalized to unstimulated controls (N=3). (K) Small GTPases activation analysis of RhoA from confluent HUVEC. Bar graphs show raw optical density (O.D.) measured with an absorbance wavelength of 490 nm (N=3). (L) Small GTPases activation analysis of Rac1 from confluent HUVEC after treatment. Bar graphs show raw optical density (O.D.) measured with an absorbance wavelength of 490 nm (N=3). Groups: CTR: stimulation with standard cell culture media; C5a: cell culture media + 50 ng/mL of C5a; C5a+RA: cell culture media + 50 ng/mL of C5a + C5a-Receptor antagonist (PMX53; 1:1000). Serum groups: CTR: stimulation with cell culture media + 10% Serum of healthy donors; STEMI: cell culture media + 10% serum of STEMI patients (final C5a concentration 8.7 ng/mL); STEMI+RA: cell culture media + 10% serum of STEMI patients + C5a-Receptor antagonist (PMX53; 1:1000). p-values: ****p<0.0001; ***p<0.001; **p<0.01; *p<0.05.

in C5aR1^{-/-} mice (WT C5a vs. KO C5a: 0.94 ± 0.04 pN/nm vs. 0.88 ± 0.03 pN/nm; p<0.001). C5aR1^{-/-} mice also showed less cortical stiffening after stimulation with STEMI serum compared to WT mice (WT STEMI vs. KO STEMI: 0.98 ± 0.04 pN/nm vs. 0.92 ± 0.04 pN/nm; p<0.0001) (Figure 5A).

Stimulation with C5a (p<0.05) as well as with STEMI serum (p<0.001) reduced eGC height in WT mice (Figure 5B). C5a stimulation had no impact on the eGC of C5aR1^{-/-} mice. However, stimulation with STEMI serum reduced eGC height in KO mice by 9% compared to controls (p<0.001). In direct comparison between WT and KO, eGC height was preserved in C5aR1^{-/-} mice after stimulation with C5a (WT C5a vs. KO C5a: 121.5 ± 24 nm vs. 127.2 ± 24 nm; p<0.05) as well as with STEMI serum (WT STEMI vs. KO STEMI: 115.1 ± 23 nm vs. 127.0 ± 23 nm; p<0.05) (Figure 5B).

Both C5a (p<0.001) and STEMI serum (p<0.0001) decreased eGC stiffness in WT mice (Figure 5C). C5a stimulation had no impact on eGC stiffness in C5aR1^{-/-} mice. stimulation with STEMI serum on KO aortas did decrease eGC stiffness (p<0.001). Compared to C5aR1^{-/-} mice stimulation both with C5a (WT C5a vs. KO C5a: 0.37 ± 0.05 vs. 0.46 ± 0.06 pN/nm; p<0.001) and STEMI serum (WT STEMI vs. KO STEMI: 0.36 ± 0.04 vs. 0.42 ± 0.06 pN/nm; p<0.0001) showed a higher impact on eGC stiffness in WT mice (Figure 5C).

AFM parameters were correlated within the experimental groups. eGC height was negatively associated with cortical stiffness for WT mice (r=-0.86; p<0.001). This effect was diminished in C5aR1^{-/-} mice, where no significant relationship was observed between eGC height and cortical stiffness (Figure 5D). Furthermore, eGC height was positively associated with eGC stiffness in WT mice (r=0.86; p<0.001). This correlation was much weaker in C5aR1^{-/-} mice (r=0.62; p<0.05) (Figure 5E).

In order to assess the impact of C5aR1 depletion on the potential of vessel growth, we employed the sprouting angiogenesis aortic ring assay (31). We harvested aorta sections from mice of different genotypes and found that C5aR1^{-/-} mice display reduced sprouting angiogenesis after 4, 5 and 6 days of culture compared to global C5^{-/-} and WT. Previously, we have described a C5aR1-CXCL4 axis in revascularization (34). Interestingly, C5aR1^{-/-} CXCL4^{-/-} double

deficient mice did not display this phenotype of reduced angiogenesis (Figure 5F). Thus, the C5aR1-CXCL4 axis does not seem to be the driver of the observed effect. When endothelial cells (MHEC-5T) were stimulated with C5a, on the other hand, angiogenic potential measured in the tube formation assay increased at a concentration of 200 ng/ml C5a (Figure 5G).

3.6 Endothelial function is improved after treatment with C5aRA

To investigate the impact of C5a on inflammatory processes of the vascular endothelium, we performed monocyte adhesion measurements and wound healing assays and tested the endothelial NO production. Adhesion forces between leukocytes and endothelial monolayers were measured using AFM-based single-cell force spectroscopy. Figure 6C showing exemplary force-distance curve of SCFS and Figure 6F showing exemplary picture of AFM cantilever with mounted monocyte.

Stimulation with C5a increased adhesion forces between monocytes and the HUVEC surface by 19% compared to control stimulation (CTR vs. C5a: 39.0 ± 15.0 μ N vs. 46.7 ± 16.7 μ N; p<0.001) (Figure 6A). Adhesion energy, calculated as the area under the curve (AUC) of the force-distance curves, increased after C5a stimulation by 59% (p<0.001) compared to controls (Figure 6B). This could not be prevented by administering C5aRA.

Stimulation with STEMI serum resulted in both higher adhesion forces (p<0.0001; Figure 6D) and higher adhesion energy (p<0.001; Figure 6E) compared to control conditions. However, adhesion energy was significantly decreased by 17% after C5aRA treatment (C5a vs. C5aRA: 0.19 ± 0.1 nJ vs. 0.16 ± 0.1 nJ; p<0.05) (Figure 6E). By quantifying adherent monocytes these results were confirmed. Both C5a (p<0.0001; Figure 6G) and stimulation with STEMI serum (p<0.0001; Figure 6H) enhanced the monocyte count per region of interest (ROI) compared to controls, which could not be prevented by treatment with C5aRA.

Stimulation with both C5a (CTR vs. C5a: 670 ± 102 μ M vs. 386 ± 62 μ M; p<0.01) and STEMI serum (CTR vs. C5a: 545 ± 49

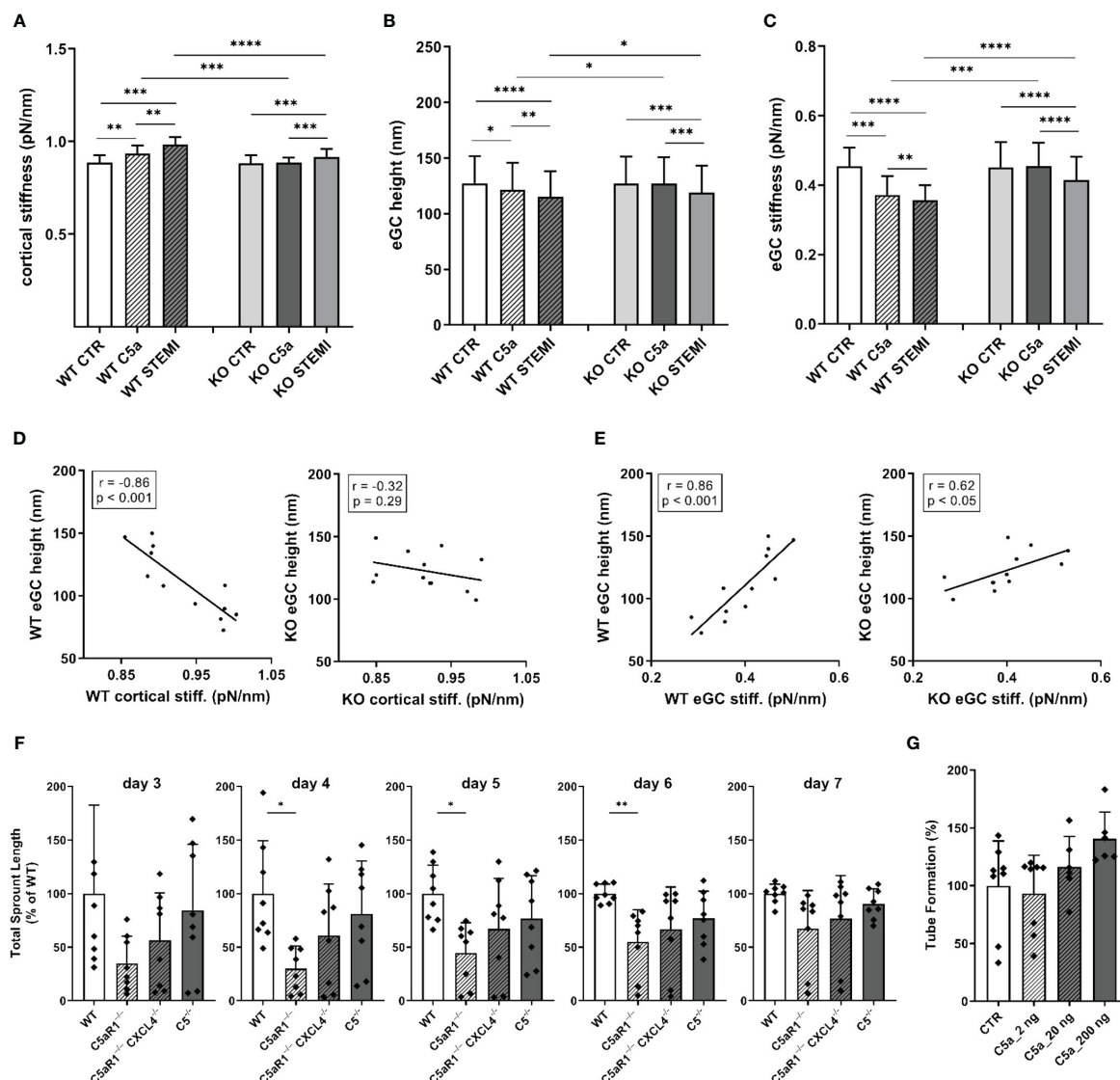


FIGURE 5

The influence of C5a and STEMI on eGC condition and cortical stiffness are attenuated in a mouse model for C5a-receptor-1-knockout.

(A–C) Statistical analysis of atomic force microscopy (AFM) nanoindentation measurements of living endothelial cells on isolated mouse aorta preparations. Aortas of wild-type (WT; N=6) and C5a-Receptor-1-knock-out (KO; C5aR1^{-/-}; N=6) mice were harvested and made available for AFM measurements as described in detail in the methods section. Groups: Preparations of WT and KO aortas were stimulated with either cell culture media (control group, CTR), cell culture media + 50 ng/mL of C5a (C5a group), or cell culture media + 10% STEMI serum (STEMI group). Data showing mean ± SD of (A) cortical stiffness, (B) eGC height, and (C) eGC stiffness of single cell measurements of living endothelial cells on isolated mouse aorta preparations (8 force-distance curves per single cell; n=50 cells per mouse; N=6 mice per group). (D) Correlation of WT endothelial glycocalyx (eGC) height vs. WT cortical stiffness and KO eGC height vs. KO cortical stiffness (CTR and stimulation with STEMI serum). (E) Correlation of WT eGC height vs. WT eGC stiffness (CTR and stimulation with STEMI serum). Rho (r) and p-values (p) shown for correlations. (F) Sprouting angiogenesis aortic ring assay of C5^{-/-} (B6(Cg)Tg(Ins2-GP)zbz) and mice double deficient for C5aR1 and CXCL4 (C5aR1^{-/-}-CXCL4^{-/-}) (on days 3, 4, 5, 6 and 7). (G) Tube formation assay of MHEC-5T cells after C5a stimulation. p-values: ****p<0.0001; ***p<0.001; **p<0.01; *p<0.05; ns, not significant.

μM vs. 361 ± 36 μM; p<0.01) resulted in reduced NO production compared to controls (Figure 6I). In both cases, treatment with C5aRA significantly improved NO production. Compared to C5a the administration of C5aRA led to a 59% higher NO concentration (p<0.05). In the STEMI group the treatment with C5aRA enhanced NO production by 40% (p<0.05) (Figure 6I).

To investigate the migration characteristics of HUVEC monolayers after C5a and stimulation with STEMI serum, wound

healing assays were performed. The endothelial growth rate (μm/h) over 24 h was significantly reduced by 63% after C5a stimulation (CTR vs. C5a: 18.8 ± 10 μm/h vs. 7.1 ± 2 μm/h; p<0.01) (Figure 6J). C5aRA enhanced the growth rate by 25% compared to C5a stimulation (p<0.05). Wound closure (%/h) was compared among all groups. Both CTR and C5a+RA groups reached 50% wound closure after 4 h. Wound closure was significantly further advanced after 3.5 h in controls compared to those in the C5a stimulation group (p<0.05).

stimulation with STEMI serum decreased the growth rate by 83% compared to controls (CTR vs. STEMI: $17.2 \pm 6 \mu\text{m/h}$ vs. $2.9 \pm .06 \mu\text{m/h}$; $p < 0.001$) (Figure 6K). In controls, 50% of wound closure was reached after 4 h whereas in the STEMI+RA group 50% closure was achieved after 9 h. The STEMI+RA group showed a nonsignificant trend towards faster growth rate compared to STEMI group by 27%. However, wound closure after 9 h was significantly further advanced in the STEMI+RA group compared to stimulation with STEMI serum ($p < 0.05$) (Figure 6K).

4 Discussion

The endothelial surface layers, endothelial cortex, and eGC are highly vulnerable to toxins and factors released during AMI, resulting in loss of their vasoprotective function (18, 20, 35). AMI-induced endothelial damage is multifactorial and complex, caused by a variety of immunologic factors present in AMI serum that are associated with cardiac mechanical stress, generalized vascular trauma, and inflammatory response (1, 35). During AMI, several innate immune pathways, including those of the

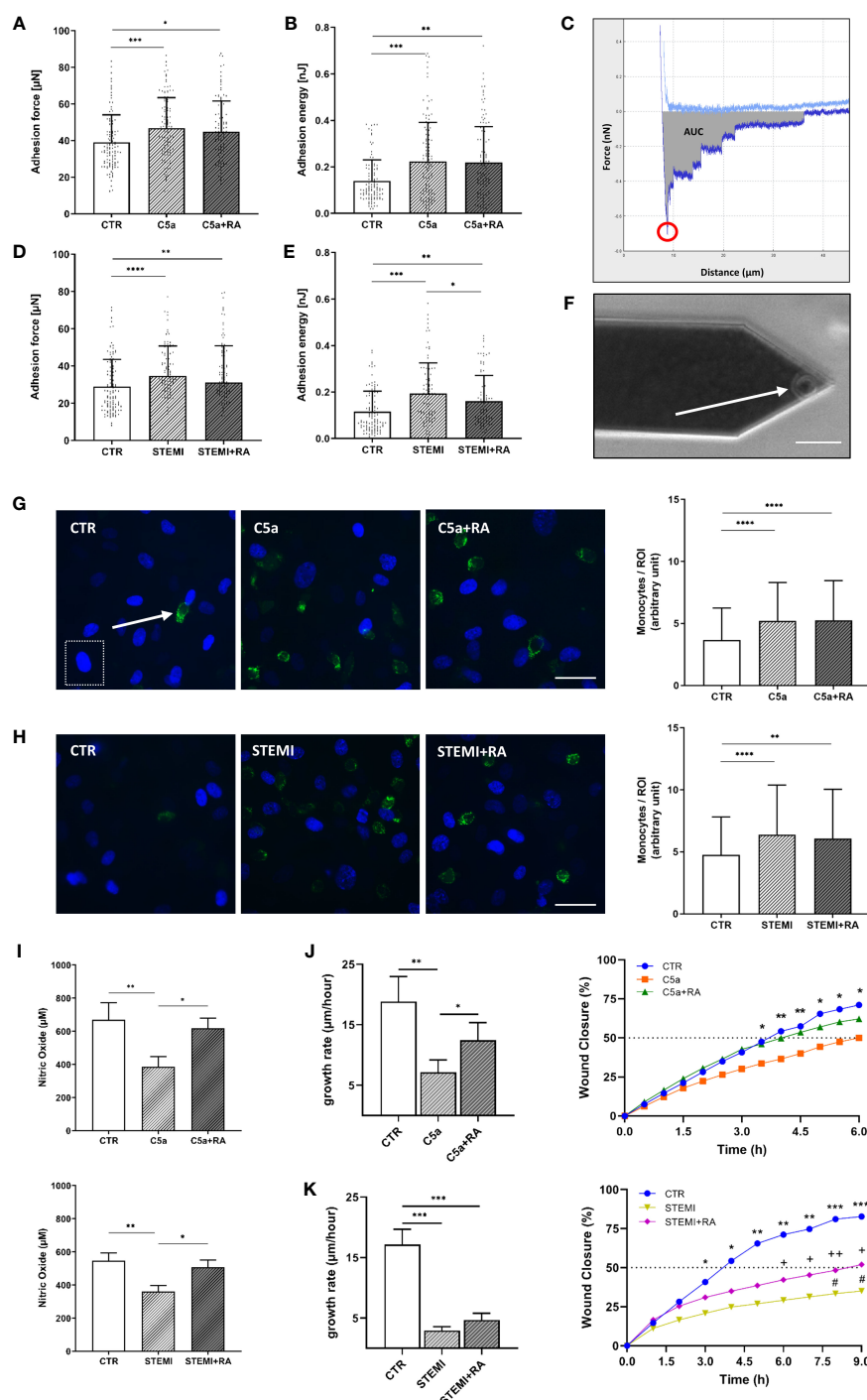


FIGURE 6 (Continued)

Endothelial function is improved after treatment with C5aRA. **(A)** Data showing mean \pm SD of monocyte adhesion forces to human umbilical vein endothelial cells (HUVEC) monolayers measured via atomic force microscopy (AFM)-based single-cell force spectroscopy (SCFS) of control (CTR), C5a, and C5a+RA groups (N=5). **(B)** Mean \pm SD of adhesion energy between monocyte and HUVEC monolayer (energy needed to separate monocyte from HUVEC) of CTR, C5a, and C5a+RA groups (N=5) measured via AFM-based SCFS. **(C)** Exemplary force-distance curve of SCFS. Red circle indicates the maximum adhesion force between monocyte and HUVEC monolayer. Gray area representing the total adhesion energy calculated as the area under the curve (AUC). **(D)** Data showing mean \pm SD of monocyte adhesion forces to HUVEC monolayers measured via AFM-based SCFS of CTR, ST-elevation myocardial infarction (STEMI), and STEMI+RA groups (N=5). **(E)** Mean \pm SD of adhesion energy between monocyte and HUVEC monolayer (energy needed to separate monocyte from HUVEC) of CTR, STEMI, and STEMI+RA groups (N=5) measured via AFM-based SCFS. **(F)** Exemplary picture of AFM cantilever with mounted monocyte (white arrow) before adhesion measurements (scale bar: 25 μ m). **(G)** Representative fluorescence images of human monocytes (green: CD14-labeled monocytes; indicated by white arrow) adhesive to HUVEC monolayer of CTR, C5a, and C5a+RA groups (blue: HUVEC nuclei; indicated by white dashed box). Statistical analysis showing mean \pm SD of adherent monocytes per region of interest (ROI) quantified via monocyte-wash-away assay with previous CD14-staining (CTR, C5a, and C5a+RA groups; N=6; scale bar: 40 μ m). **(H)** Representative fluorescence images of human monocytes (green: CD14 labeled monocytes) adhesive to HUVEC monolayer of CTR, STEMI, and STEMI+RA groups (blue: HUVEC nuclei). Statistical analysis showing mean \pm SD of adherent monocytes per region of interest (ROI) quantified via monocyte-wash-away assay with previous CD14-staining (CTR, STEMI, and STEMI+RA groups; N=6; scale bar: 40 μ m). **(I)** Statistical analysis of nitric oxide (NO) concentrations in cell culture media supernatant. NO products were measured by chemiluminescence-based via NOA-280i for CTR, C5a, and C5a+RA groups (N=3) as well as for CTR, STEMI, and STEMI+RA groups (N=3). **(J)** Statistical evaluation of wound healing assays for CTR, C5a, and C5a+RA groups (N=7). Data showing the 24-h growth rate (μ m/h) as described in the methods section as well as wound closure in % (*: CTR vs. C5a). **(K)** Statistical evaluation of wound healing assays for CTR, STEMI, and STEMI+RA groups (N=7). Data showing the 24-h growth rate (μ m/h) as described in the methods section as well as wound closure in % (*: CTR vs. STEMI; +: CTR vs. STEMI+RA; #: STEMI vs. STEMI+RA). Groups: CTR: stimulation with standard cell culture media; C5a: cell culture media + 50 ng/mL of C5a; C5a+RA: cell culture media + 50 ng/mL of C5a + C5a-Receptor antagonist (PMX53; 1:1000). Serum groups: CTR: stimulation with cell culture media + 10 % serum of healthy donors STEMI: cell culture media + 10 % serum of STEMI patients; STEMI+RA: cell culture media + 10 % serum of STEMI patients + C5a-Receptor antagonist (PMX53; 1:1000). p-values: ****p<0.0001; ***p<0.001; **p<0.01; *p<0.05; ++p<0.01; +p<0.05; #p<0.05.

complement system, are activated in the early steps of the inflammatory response to myocardial ischemia (1, 13). In this study, the effects of the complement anaphylatoxin C5a on the nanomechanical properties as well as on vascular surface function were studied in the context of AMI.

For this, serum derived from patients with a first onset of STEMI was used in an *in vitro* model to quantify the impact of elevated levels of the anaphylatoxin C5a on endothelial surface mechanics and endothelial function. Stimulation with both STEMI serum and with C5a only decreased eGC height and stiffness, indicating a C5a-mediated shedding of the eGC. In parallel, both stimulations increased cortical stiffness with a subsequent reduction in NO concentrations, enhanced monocyte adhesion to the endothelium, and decreased wound healing capacity, all indicating progressively developing endothelial dysfunction and vascular inflammation during AMI-induced C5a elevation.

Furthermore, we demonstrated that inhibiting the complement anaphylatoxin C5a using the C5aRA (PMX53) significantly reduced complement-induced vascular damage and enhanced vascular function. eGC degradation and cortical stiffening with subsequent endothelial dysfunction were both attenuated after administering C5aRA. Additionally, knock-out of the C5aR1 in mice correlated with these effects. Our findings demonstrate that the C5a:C5a-Receptor1 axis plays a central role in mediating vascular surface deterioration in the context of AMI.

During AMI, the main constituents of the eGC can be detected in patients' blood. Syndecan-1 (36), heparan sulfate (12), and hyaluronan (37) have been identified as biomarkers for eGC damage during myocardial ischemia. This also applies to our data. In addition, our data demonstrate positive correlations between eGC component levels of syndecan-1, heparan sulfate, and hyaluronan, with levels of C5a indicating a possible interaction between loss of eGC components due to complement activation. Moreover, increased serum levels of eGC components are by no

means unimportant: Jung et al. identified syndecan-1 as an independent predictor of 30-day mortality in cardiogenic shock and Wernly et al. showed that high levels of syndecan-1 are independently associated with 6-month mortality after myocardial infarction (36, 38). In the present study, mortality was not analyzed as an endpoint, but the positive correlation between elevated C5a and days until hospital discharge suggests that patients with higher C5a levels are more severely ill than patients with lower C5a levels. Indeed, correlations between enhanced complement activity and disease severity have been shown for SARS-CoV-2 infections (39), but have so far not been demonstrated in the context of AMI.

The effects between enhanced complement activity and disease severity are also reflected in the mechanical alterations of the vasculature: In the present study, the functional height of eGC was drastically reduced after incubating primary endothelial cells with sera derived from AMI patients. Intriguingly, the eGC height and stiffness incrementally decreased with rising levels of C5a (LOW vs. HIGH). In parallel, the cortical stiffness increased with rising C5a levels and was accompanied by a decrease in NO bioavailability, indicating progression of endothelial damage with progressing C5a release. There was no difference in NO availability between CTR and the LOW group, which may be due to small group size and the co-occurrence of outliers in the LOW group. Correlations between NO and C5a were therefore calculated excluding this group, although other correlations in this manuscript showed no different associations when the data of the LOW group were excluded.

The cortical stiffening accompanied by elevated levels of C5a combined with reduced NO production are most likely conferred by multiple pathways, but our data suggest an important contribution of the terminal complement pathway, especially C5a. C5a is associated with cardiovascular complications such as atherosclerosis and acute thrombosis (40). Furthermore, excessive quantities of C5a have been detected in patients with the acute

coronary syndrome, advanced atherosclerosis, and myocardial infarction and have been associated with increased cardiovascular risk in patients with advanced atherosclerosis (41).

The reduction in eGC height and stiffness (shedding) as well as stiffening of the endothelial cortex were also shown for C5a stimulation alone, demonstrating the role C5a plays in endothelial impairment during AMI. Explanations of the mechanism underlying eGC shedding and subsequent cortical stiffening are embedded in the structure of the eGC, especially syndecan-1, which functions as a backbone of the eGC formation. Syndecan-1 is composed of an ectodomain as well as a transmembrane and a cytoplasmic domain (42). The cytoplasmic domain is directly associated with the actin cytoskeletal network of the cellular cortex via linker proteins, such as syntenin and synectin, allowing mechanotransduction from the endothelial surface to intercellular cortex (42). In response, syndecan-1 initiates cytoskeletal alignment and focal adhesion formation via activation of RhoA (43). In our study, baseline RhoA activity was significantly higher after C5a stimulation – and after AMI stimulation – displaying a direct link between eGC shedding, cortical actin alignment, and C5a stimulation. At this point, the C5aR1 plays an important mechanistic role. Kaida et al. demonstrated an enhanced conversion of RhoA-GDP to RhoA-GTP dependent on the C5a-C5aR1 signal (44). Activation of RhoA regulates cell stiffness via its downstream target Rho-associated kinase (ROCK), which modulates both actin/myosin-based cytoskeletal tension and cortical actin network formation (45). Thus, binding of C5a to the C5aR1 enhances activation of ROCK via RhoA conversion, leading to endothelial stiffening which ultimately results in eGC impairment. All these effects could at least be partly prevented by administering C5aR1A (PMX53) in our study.

Despite the influence of C5a on the endothelium, we should not neglect mentioning that the effects described here are not inevitably complement-dependent, but are, in any case, complement-related. AMI-induced shedding of the eGC with subsequent impairment of endothelial function might be caused by a variety of factors present in the patients' sera which are associated with cardiac mechanical stress, generalized vascular trauma, and an inflammatory response (18). Those biomarkers and effectors of eGC degradation, are elevated and activated during AMI, including proinflammatory factors like interleukins (35), catecholamines (46), CRP (47) as well as matrix metalloproteinases (MMPs) (35). Furthermore, myocardial infarction and the following reperfusion of the occluded vessel results in a burst of free radical formation with increased generation of reactive oxygen species (ROS) (48). The increased oxidative stress and imbalanced levels of the production and accumulation of ROS not only enhances tissue damage of the myocardium, but also leads to degradation of eGC molecules (48, 49).

AMI immediately activates the sympathoadrenal system, which is associated with an excessive increase in circulating catecholamines, which, in turn, are associated with eGC damage (46). Furthermore, other immunogenic factors such as interleukins (IL) are activated during AMI. IL induce a complex network of proinflammatory cytokines via expression of integrins on leukocytes and endothelial cells. They regulate and initiate

inflammatory responses that are associated with worse myocardial function, larger infarct extent, and more severe I/R injury in AMI (35, 50). Interestingly, excessive C5a levels can direct the production of cytokines such as tumor necrosis factor α and IL-6, which both induce heparanase expression with subsequent degradation of the eGC (51, 52). This might, in part, explain the mechanisms underlying the development of endothelial dysfunction under elevated C5a conditions. C-reactive protein (CRP) is also elevated in AMI sera. CRP is an early inflammatory biomarker associated with stiffening of the endothelial cell cortex, as shown in our data (47). Moreover, CRP can trigger activation of the complement system and lead to cardiovascular complications such as atherosclerosis and acute thrombosis mediated by generating excessive C5a (5). Furthermore, AMI serum contains a variety of MMPs, a group of zinc ion-dependent proteases that degrade collagen and proteoglycans (35, 53). MMPs play a pivotal role in the development of atherosclerosis and in post-myocardial infarction cardiac remodeling as well as in the development of adverse outcomes (53, 54). C5a upregulates the expression MMP-1 and MMP-9, thus contributing to the extracellular matrix and eGC degradation (55, 56). The eGC component syndecan-1 is shed by MMP isoforms MMP-2, MMP-9, and MMP-14 (57). The up-regulated MMP-9 (58), which is even amplified by C5a (5), may be responsible for eGC impairment in AMI through cleavage of syndecan-1.

Exposure of primary endothelial cells to AMI serum significantly decreased NO bioavailability, the hallmark of endothelial dysfunction (20), indicating the presence of additional inhibitors/mechanisms suppressing NO release, which are abundant in AMI serum. In addition, stimulation with C5a alone reduced NO production. This reflects the dose-dependent influence of C5a contained in the AMI serum on NO production by uncoupling the endothelial NO synthase (eNOS) (59). Reduction in NO bioavailability was prevented by administering C5aR1A (PMX53). This clearly shows an association of the C5a:C5a-Receptor axis with NO bioavailability. Similar effects could be shown for C5a activation of pig pulmonary endothelium, which altered NOS translation with subsequent endothelial dysfunction (60).

AMI and C5a stimulation both enhanced monocyte adhesion forces quantified by single-cell force spectroscopy and in monocyte adhesion assays. By using the single-cell force spectroscopy modality adhesion forces and adhesion energy can be quantified precisely between a single monocyte and endothelial surfaces and therefore the mechanical effects of C5a or STEMI serum stimulation on cell-cell surface interactions can be measured. Our data illustrate a change from a quiescent to an activated endothelial surface, resulting in a proinflammatory and prothrombotic state. Due to its position on the endothelial surface, the eGC mediates and regulates these leukocyte-endothelium interactions (61). The eGC has been recognized as an important structure during leukocyte recruitment and adhesion (27) with a proadhesive function, thus playing a crucial role during inflammatory processes (61). A functional and intact eGC lies atop of adhesion molecules such as vascular cellular adhesion molecule-1 (VCAM-1) and intercellular adhesion-molecule-1 (ICAM-1), which are needed for leukocyte-

endothelial interaction. Unless the barrier formed by the eGC is compromised, leukocytes are ‘tip-toeing’ with their cytoskeletal protrusions on the eGC and barely reaching the adhesion molecules at the endothelial surface (27). The enhanced adhesion forces between monocytes and endothelial monolayers after C5a stimulation proves that shedding of the eGC favors the formation of bonds between binding partners on monocytes and endothelial surfaces. Furthermore, activation of RhoA/ROCK signaling, as demonstrated in the present study, was shown to contribute to lysophosphatidic acid receptor-4-induced stimulation of VCAM-1 expression (62). Thus, our findings are in line with the current state of knowledge as the interaction of C5a with endothelial cells has been demonstrated to upregulate cellular adhesion molecules (ICAM-1, VCAM-1), promoting infiltration of leukocytes to vessel walls and contributing to inflammation and atherosclerosis (5).

In the present study both, purified C5a stimulation as well as elevated levels of C5a in AMI patient’s sera, generate structural and mechanical changes on the endothelial surface, including the eGC and the cellular cortex via the C5a:C5a-Receptor1 axis. C5a activates RhoA, which accelerates endothelial stiffening via its downstream target ROCK. This causes eGC impairment, ultimately resulting in endothelial dysfunction with reduced NO bioavailability, enhanced endothelial surface activation, and decreased wound healing velocity. In parallel, a variation of other mechanistic processes is triggered by AMI, resulting in further damage to the endothelial surface and reducing vascular function. Our study confirms the important role of the C5a:C5a receptor1 axis in the development of vascular diseases and thus opens up new therapeutic approaches to improve patient health in the context of AMI. Future investigations should evaluate the role of C5a antagonism as a potential post-AMI treatment to counteract the development of endothelial dysfunction. In addition, influencing the C5a:C5a-Receptor1 axis might represent a novel approach to protect or restore the eGC in acute cardiac ischemia and prevent further development of endothelial dysfunction in the event of AMI.

Data availability statement

The raw data supporting the conclusions of this article will be made available by the authors, without undue reservation.

Ethics statement

The studies involving humans were approved by the ethics committee of the University of Luebeck (Case: 19-310). The studies were conducted in accordance with the local legislation and institutional requirements. The participants provided their written informed consent to participate in this study. The animal study was approved by Ministerium für Landwirtschaft, Energiewende, Umwelt und Ländliche Räume, Kiel, Germany (Case: 39.2_2020-08-20_Karsten). The study was conducted in accordance with the local legislation and institutional requirements.

Author contributions

CV: Conceptualization, Data curation, Formal Analysis, Investigation, Methodology, Project administration, Resources, Software, Supervision, Validation, Visualization, Writing – original draft, Writing – review & editing. SL: Formal Analysis, Investigation, Methodology, Writing – review & editing. CH: Formal Analysis, Investigation, Methodology, Writing – review & editing. BR: Investigation, Writing – review & editing, Formal Analysis, Methodology. BF: Investigation, Writing – review & editing, Supervision, Validation. LN: Data curation, Investigation, Writing – review & editing. JW: Data curation, Supervision, Writing – review & editing. LB: Investigation, Methodology, Writing – review & editing. HN: Writing – review & editing, Formal Analysis, Investigation, Methodology. MK: Writing – review & editing, Investigation, Methodology. CK: Supervision, Writing – review & editing. KK: Conceptualization, Funding acquisition, Resources, Supervision, Validation, Writing – review & editing.

Funding

The author(s) declare financial support was received for the research, authorship, and/or publication of this article. This work was supported by a research grant of the German Cardiac Society to CV and grants from the Deutsche Forschungs-Gemeinschaft (DFG) (KU1496/7-1, KU1496/7-3, INST392/1411) to KK-V.

Acknowledgments

We would like to thank all involved laboratory technicians of the University of Luebeck, as well as all involved technicians and clinicians of the Sana-Kliniken-Luebeck (at the intensive care unit and catheter laboratory) for their support of this study. The authors gratefully acknowledge Sherryll Sundell for language editing.

Conflict of interest

The authors declare that the research was conducted in the absence of any commercial or financial relationships that could be construed as a potential conflict of interest.

The handling editor declared shared affiliation with the authors SL, CH, BR, MK and CK at the time of the review.

Publisher’s note

All claims expressed in this article are solely those of the authors and do not necessarily represent those of their affiliated organizations, or those of the publisher, the editors and the reviewers. Any product that may be evaluated in this article, or claim that may be made by its manufacturer, is not guaranteed or endorsed by the publisher.

References

- Bavia L, Lidani KCF, Andrade FA, Sobrinho MIAH, Nisihara RM, de Messias-Reason IJ. Complement activation in acute myocardial infarction: An early marker of inflammation and tissue injury? *Immunol Lett.* (2018) 200:18–25. doi: 10.1016/j.imlet.2018.06.006
- Gaboriaud C, Frachet P, Thielens NM, Arlaud GJ. The human c1q globular domain: structure and recognition of non-immune self ligands. *Front Immunol.* (2011) 2:92. doi: 10.3389/fimmu.2011.00092
- Merle NS, Church SE, Fremeaux-Bacchi V, Roumenina LT. Complement system part I - molecular mechanisms of activation and regulation. *Front Immunol.* (2015) 6:262. doi: 10.3389/fimmu.2015.00262
- Ricklin D, Hajishengallis G, Yang K, Lambris JD. Complement: a key system for immune surveillance and homeostasis. *Nat Immunol.* (2010) 11:785–97. doi: 10.1038/ni.1923
- Ghosh M, Rana S. The anaphylatoxin C5a: Structure, function, signaling, physiology, disease, and therapeutics. *Int Immunopharmacol.* (2023) 118: 110081. doi: 10.1016/j.intimp.2023.110081
- Weisman HF, Bartow T, Leppo MK, Marsh HC, Carson GR, Concino MF, et al. Soluble human complement receptor type 1: *in vivo* inhibitor of complement suppressing post-ischemic myocardial inflammation and necrosis. *Science.* (1990) 249:146–51. doi: 10.1126/science.2371562
- Cubedo J, Padró T, Badimon L. Coordinated proteomic signature changes in immune response and complement proteins in acute myocardial infarction: the implication of serum amyloid P-component. *Int J Cardiol.* (2013) 168:5196–204. doi: 10.1016/j.ijcard.2013.07.181
- Altieri DC, Plescia J, Plow EF. The structural motif glycine 190-valine 202 of the fibrinogen gamma chain interacts with CD11b/CD18 integrin (alpha M beta 2, Mac-1) and promotes leukocyte adhesion. *J Biol Chem.* (1993) 268, no. 3:1847–53. doi: 10.1016/S0021-9258(18)53932-6
- Granger CB, Mahaffey KW, Weaver WD, Theroux P, Hochman JS, Filloon TG, et al. Pexelizumab, an anti-C5 complement antibody, as adjunctive therapy to primary percutaneous coronary intervention in acute myocardial infarction: the COMPLEMENT inhibition in Myocardial infarction treated with Angioplasty (COMMA) trial. *Circulation.* (2003) 108:1184–90. doi: 10.1161/01.CIR.0000087447.12918.85
- Mahaffey KW, Granger CB, Nicolau JC, Ruzyllo W, Weaver WD, Theroux P, et al. Effect of pexelizumab, an anti-C5 complement antibody, as adjunctive therapy to fibrinolysis in acute myocardial infarction: the COMPLEMENT inhibition in myocardial infarction treated with thrombolysis (COMPLY) trial. *Circulation.* (2003) 108:1176–83. doi: 10.1161/01.CIR.0000087404.53661.F8
- Vakeva AP, Agah A, Rollins SA, Matis LA, Li L, Stahl GL. Myocardial infarction and apoptosis after myocardial ischemia and reperfusion: role of the terminal complement components and inhibition by anti-C5 therapy. *Circulation.* (1998) 97:2259–67. doi: 10.1161/01.CIR.97.22.2259
- Vahldieck C, Fels B, Löning S, Nickel L, Weil J, Kusche-Vihrog K. Prolonged door-to-balloon time leads to endothelial glycocalyx damage and endothelial dysfunction in patients with ST-elevation myocardial infarction. *Biomedicines.* (2023) 11doi: 10.3390/biomedicines11112924
- Busche MN, Stahl GL. Role of the complement components C5 and C3a in a mouse model of myocardial ischemia and reperfusion injury. *Ger. Med Sci GMS E-J.* (2010) 8:Doc20. doi: 10.3205/000109
- Vogel C-W. The role of complement in myocardial infarction reperfusion injury: an underappreciated therapeutic target. *Front Cell Dev Biol.* (2020) 8:606407. doi: 10.3389/fcell.2020.606407
- Foreman KE, Vaporciyan AA, Bonish BK, Jones ML, Johnson KJ, Glovsky MM, et al. C5a-induced expression of P-selectin in endothelial cells. *J Clin Invest.* (1994) 94:1147–55. doi: 10.1172/JCI117430
- Shivshankar P, Li Y-D, Mueller-Ortiz SL, Wetsel RA. In response to complement anaphylatoxin peptides C3a and C5a, human vascular endothelial cells migrate and mediate the activation of B-cells and polarization of T-cells. *FASEB J Off Publ. Fed. Am Soc Exp Biol.* (2020) 34:7540–60. doi: 10.1096/fj.201902397R
- Marder SR, Chenoweth DE, Goldstein IM, Perez HD. Chemotactic responses of human peripheral blood monocytes to the complement-derived peptides C5a and C5a des Arg. *J Immunol Baltim. Md 1950.* (1985) 134:3325–31.
- Abassi Z, Armaly Z, Heyman SN. Glycocalyx degradation in ischemia-reperfusion injury. *Am J Pathol.* (2020) 190:752–67. doi: 10.1016/j.ajpath.2019.08.019
- Weinbaum S, Cancel LM, Fu BM, Tarbell JM. The glycocalyx and its role in vascular physiology and vascular related diseases. *Cardiovasc Eng. Technol.* (2021) 12:37–71. doi: 10.1007/s13239-020-00485-9
- Cosgun ZC, Fels B, Kusche-Vihrog K. Nanomechanics of the endothelial glycocalyx: from structure to function. *Am J Pathol.* (2020) 190:732–41. doi: 10.1016/j.ajpath.2019.07.021
- Schmandke A, Schmandke A, Strittmatter SM. ROCK and Rho: biochemistry and neuronal functions of Rho-associated protein kinases. *Neurosci Rev J Bringing Neurobiol Neurol Psychiatry.* (2007) 13:454–69. doi: 10.1177/1073858407303611
- Chi X, Wang S, Huang Y, Stamnes M, Chen J-L. Roles of rho GTPases in intracellular transport and cellular transformation. *Int J Mol Sci.* (2011) 14:7089–108. doi: 10.3390/ijms14047089
- Hossen P, Sun GY, Lee JC. Oligomeric Tau-induced oxidative damage and functional alterations in cerebral endothelial cells: Role of RhoA/ROCK signaling pathway. *Free Radic Biol Med.* (2024) 221:261–72. doi: 10.1016/j.freeradbiomed.2024.05.044
- Brandwijk RJMGE, Michels MAHM, van Rossum M, de Noijer AH, Nilsson PH, de Bruin WCC, et al. Pitfalls in complement analysis: A systematic literature review of assessing complement activation. *Front Immunol.* (2022) 13:1007102. doi: 10.3389/fimmu.2022.1007102
- Vahldieck C, Cianflone E, Fels B, Löning S, Depelmann P, Sabatino J, et al. Endothelial glycocalyx and cardiomyocyte damage is prevented by recombinant syndecan-1 in acute myocardial infarction. *Am J Pathol.* (2023) 193:474–92. doi: 10.1016/j.ajpath.2022.12.009
- Edgell CJ, McDonald CC, Graham JB. Permanent cell line expressing human factor VIII-related antigen established by hybridization. *Proc Natl Acad Sci U. S. A.* (1983) 80:3734–7. doi: 10.1073/pnas.80.12.3734
- Schierke F, Wyrwoll MJ, Wisdorf M, Niedzielski L, Maase M, Ruck T, et al. Nanomechanics of the endothelial glycocalyx contribute to Na⁺-induced vascular inflammation. *Sci Rep.* (2017) 7:46476. doi: 10.1038/srep46476
- Briukhovetska D, Ohm B, Mey FT, Aliberti J, Kleingarn M, Huber-Lang M, et al. C5aR1 activation drives early IFN- γ Production to control experimental toxoplasma gondii infection. *Front Immunol.* (2020) 11:1397. doi: 10.3389/fimmu.2020.01397
- Jeggle P, Callies C, Tarjus A, Fassot C, Fels J, Oberleithner H, et al. Epithelial sodium channel stiffens the vascular endothelium *in vitro* and in Liddle mice. *Hypertens Dallas Tex 1979.* (2013) 61:1053–9. doi: 10.1161/HYPERTENSIONAHA.111.199455
- Suarez-Arnedo A, Torres Figueroa F, Clavijo C, Arbeláez P, Cruz JC, Muñoz-Camargo C. An image J plugin for the high throughput image analysis of *in vitro* scratch wound healing assays. *PloS One.* (2020) 15:e0232565. doi: 10.1371/journal.pone.0232565
- Iqbal F, Szaraz P, Librach M, Gauthier-Fisher A, Librach CL. Angiogenic potency evaluation of cell therapy candidates by a novel application of the *in vitro* aortic ring assay. *Stem Cell Res Ther.* (2017) 8:184. doi: 10.1186/s13287-017-0631-1
- Carpentier G, Berndt S, Ferratte S, Rasband W, Cuendet M, Uzan G, et al. Angiogenesis Analyzer for ImageJ - A comparative morphometric analysis of "Endothelial Tube Formation Assay" and "Fibrin Bead Assay. *Sci Rep.* (2020) 10:11568. doi: 10.1038/s41598-020-67289-8
- Nording H, Baron L, Sauter M, Lübken A, Rawish E, Szepanowski R, et al. Platelets regulate ischemia-induced revascularization and angiogenesis by secretion of growth factor-modulating factors. *Blood Adv.* (2023) 7:6411–27. doi: 10.1182/bloodadvances.2021006891
- Nording H, Baron L, Haberthür D, Emschermann F, Mezger M, Sauter M, et al. The C5a/C5a receptor 1 axis controls tissue neovascularization through CXCL4 release from platelets. *Nat Commun.* (2021) 12:3352. doi: 10.1038/s41467-021-23499-w
- Wu Y, Pan N, An Y, Xu M, Tan L, Zhang L. Diagnostic and prognostic biomarkers for myocardial infarction. *Front Cardiovasc Med.* (2021) 7:617277. doi: 10.3389/fcvm.2020.617277
- Wernly B, Fuernau G, Masyuk M, Muessig JM, Pfeiler S, Bruno RR, et al. Syndecan-1 predicts outcome in patients with ST-segment elevation infarction independent from infarct-related myocardial injury. *Sci Rep.* (2019) 9:18367. doi: 10.1038/s41598-019-54937-x
- Savas G, Kalay N, Altin P, Dursun GK, Cetin M, Aytekin M. 'Hyaluronan as a promising biomarker for myocardial damage. *Tohoku J Exp Med.* (2019) 248:99–106. doi: 10.1620/tjem.248.99
- Jung C, Fuernau G, Muench P, Desch S, Eitel I, Schuler G, et al. Impairment of the endothelial glycocalyx in cardiogenic shock and its prognostic relevance. *Shock Augusta Ga.* (2015) 43:450–5. doi: 10.1097/SHK.0000000000000329
- Sinkovits G, Mező B, Réti M, Müller V, Iványi Z, Gál J, et al. Complement overactivation and consumption predicts in-hospital mortality in SARS-coV-2 infection. *Front Immunol.* (2021) 12:663187. doi: 10.3389/fimmu.2021.663187
- Pepys MB, Hirschfield GM. C-reactive protein: a critical update. *J Clin Invest.* (2003) 111:1805–12. doi: 10.1172/JCI18921
- Speidl WS, Exner M, Amighi J, Kastl SP, Zorn G, Maurer G, et al. Complement component C5a predicts future cardiovascular events in patients with advanced atherosclerosis. *Eur Heart J.* (2005) 26:2294–9. doi: 10.1093/eurheartj/ehi339
- Richter RP, Richter JR. Glycocalyx gone awry: pathologic cell signaling during endotheliopathy. *Am J Biomed Sci Res.* (2019) 5:118. doi: 10.34297/AJBSR
- Voyvodic PL, Min D, Liu R, Williams E, Chitalia V, Dunn AK, et al. Loss of syndecan-1 induces a pro-inflammatory phenotype in endothelial cells with a dysregulated response to atheroprotective flow. *J Biol Chem.* (2014) 289:9547–59. doi: 10.1074/jbc.M113.541573

44. Kaida T, Nitta H, Kitano Y, Yamamura K, Arima K, Izumi D, et al. C5a receptor (CD88) promotes motility and invasiveness of gastric cancer by activating RhoA. *Oncotarget*. (2016) 7:84798–809. doi: 10.18632/oncotarget.v7i51
45. Cabrera AP, Bhaskaran A, Xu J, Yang X, Scott HA, Mohideen U, et al. Senescence increases choroidal endothelial stiffness and susceptibility to complement injury: implications for choriocapillaris loss in AMD. *Invest. Ophthalmol Vis Sci*. (2016) 57:5910–8. doi: 10.1167/iops.16-19727
46. Ostrowski SR, Pedersen SH, Jensen JS, Mogelvang R, Johansson PI. Acute myocardial infarction is associated with endothelial glycocalyx and cell damage and a parallel increase in circulating catecholamines. *Crit Care Lond Engl*. (2013) 17:R32. doi: 10.1186/cc12532
47. Kusche-Vihrog K, Urbanova K, Blanqué A, Wilhelmi M, Schillers H, Kliche K, et al. C-reactive protein makes human endothelium stiff and tight. *Hypertens Dallas Tex* 1979. (2011) 57:231–7. doi: 10.1161/HYPERTENSIONAHA.110.163444
48. Zheng H, Xu Y, Liehn EA, Rusu M. Vitamin C as Scavenger of Reactive Oxygen Species during Healing after Myocardial Infarction. *Int J Mol Sci*. (2024) 25:3114. doi: 10.3390/ijms25063114
49. Agostinis C, Masat E, Bossi F, Ricci G, Menegazzi R, Lombardelli L, et al. Transcriptomics and immunological analyses reveal a pro-angiogenic and anti-inflammatory phenotype for decidual endothelial cells. *Int J Mol Sci*. (2019) 20:1604. doi: 10.3390/ijms20071604
50. Tiller C, Reindl M, Holzknacht M, Lechner I, Schwaiger J, Brenner C, et al. Association of plasma interleukin-6 with infarct size, reperfusion injury, and adverse remodelling after ST-elevation myocardial infarction. *Eur Heart J Acute Cardiovasc Care*. (2022) 11:113–23. doi: 10.1093/ehjacc/zuab110
51. Yan C, Gao H. New insights for C5a and C5a receptors in sepsis. *Front Immunol*. (2012) 3:368. doi: 10.3389/fimmu.2012.00368
52. Fels B, Acharya S, Vahldieck C, Graf T, Käding N, Rupp J, et al. Mineralocorticoid receptor-antagonism prevents COVID-19-dependent glycocalyx damage. *Pflugers Arch*. (2022) 474:1069–76. doi: 10.1007/s00424-022-02726-3
53. Myasoedova VA, Chistiakov DA, Grechko AV, Orekhov AN. Matrix metalloproteinases in pro-atherosclerotic arterial remodeling. *J Mol Cell Cardiol*. (2018) 123:159–67. doi: 10.1016/j.jmcc.2018.08.026
54. Yabluchanskiy A, Li Y, Chilton RJ, Lindsey ML. Matrix metalloproteinases: drug targets for myocardial infarction. *Curr Drug Targets*. (2013) 14:276–86. doi: 10.1016/j.jmcc.2018.08.026
55. Johnson JL, Jackson CL, Angelini GD, George SJ. Activation of matrix-degrading metalloproteinases by mast cell proteases in atherosclerotic plaques. *Arterioscler Thromb Vasc Biol*. (1998) 18:1707–15. doi: 10.1161/01.ATV.18.11.1707
56. Goligorsky MS, Sun D. Glycocalyx in endotoxemia and sepsis. *Am J Pathol*. (2020) 190:791–8. doi: 10.1016/j.ajpath.2019.06.017
57. Masola V, Zaza G, Arduini A, Onisto M, Gambaro G. Endothelial glycocalyx as a regulator of fibrotic processes. *Int J Mol Sci*. (2021) 22:2996. doi: 10.3390/ijms22062996
58. Chen Z, Yan Y, Wu J, Qi C, Liu J, Wang J. Expression level and diagnostic value of exosomal NEAT1/miR-204/MMP-9 in acute ST-segment elevation myocardial infarction. *IUBMB Life*. (2020) 72:2499–507. doi: 10.1002/iub.2376
59. Hebbel RP, Vercellotti GM. Multiple inducers of endothelial NOS (eNOS) dysfunction in sickle cell disease. *Am J Hematol*. (2021) 96:1505–17. doi: 10.1002/ajh.26308
60. Park KW, Tofukuji M, Metais C, Comunale ME, Dai HB, Simons M, et al. Attenuation of endothelium-dependent dilation of pig pulmonary arterioles after cardiopulmonary bypass is prevented by monoclonal antibody to complement C5a. *Anesth Analg*. (1999) 89:42–8. doi: 10.1097/0000539-199907000-00008
61. Marki A, Esko JD, Pries AR, Ley K. Role of the endothelial surface layer in neutrophil recruitment. *J Leukoc Biol*. (2015) 98:503–15. doi: 10.1189/jlb.3MR0115-011R
62. Eino D, Tsukada Y, Naito H, Kanemura Y, Iba T, Wakabayashi T, et al. LPA4-mediated vascular network formation increases the efficacy of anti-PD-1 therapy against brain tumors. *Cancer Res*. (2018) 78:6607–20. doi: 10.1158/0008-5472.CAN-18-0498



OPEN ACCESS

EDITED BY

Reza Akbarzadeh,
University of Lübeck, Germany

REVIEWED BY

Tomohiro Watanabe,
Kindai University Hospital, Japan
Xinhua Yu,
Research Center Borstel (LG), Germany

*CORRESPONDENCE

Runming Jin
✉ rmjin2021@126.com

RECEIVED 21 May 2024

ACCEPTED 23 July 2024

PUBLISHED 09 August 2024

CITATION

Tang H, Zhong Y, Wu Y, Huang Y, Liu Y, Chen J, Xi T, Wen Y, He T, Yang S, Liu F, Xiong R and Jin R (2024) Increased neutrophil extracellular trap formation in oligoarticular, polyarticular juvenile idiopathic arthritis and enthesitis-related arthritis: biomarkers for diagnosis and disease activity.
Front. Immunol. 15:1436193.
doi: 10.3389/fimmu.2024.1436193

COPYRIGHT

© 2024 Tang, Zhong, Wu, Huang, Liu, Chen, Xi, Wen, He, Yang, Liu, Xiong and Jin. This is an open-access article distributed under the terms of the [Creative Commons Attribution License \(CC BY\)](#). The use, distribution or reproduction in other forums is permitted, provided the original author(s) and the copyright owner(s) are credited and that the original publication in this journal is cited, in accordance with accepted academic practice. No use, distribution or reproduction is permitted which does not comply with these terms.

Increased neutrophil extracellular trap formation in oligoarticular, polyarticular juvenile idiopathic arthritis and enthesitis-related arthritis: biomarkers for diagnosis and disease activity

Hongxia Tang^{1,2}, Yucheng Zhong³, Yali Wu², Yanmei Huang⁴, Yi Liu², Jing Chen², Ting Xi², Yini Wen², Ting He², Shanshan Yang², Fan Liu², Runji Xiong¹ and Runming Jin^{1*}

¹Department of Pediatrics, Union Hospital, Tongji Medical College, Huazhong University of Science and Technology, Wuhan, China, ²Department of Rheumatology and Immunology, Wuhan Children's Hospital, Tongji Medical College, Huazhong University of Science & Technology, Wuhan, China,

³Department of Cardiovascular Surgery, Union Hospital, Tongji Medical College, Huazhong University of Science and Technology, Wuhan, Hubei, China, ⁴Department of Pathogen Biology, School of Basic Medicine, Tongji Medical College, Huazhong University of Science and Technology, Wuhan, Hubei, China

Objective: Neutrophil extracellular traps (NETs) are important factors in initiating and perpetuating inflammation. However, the role of NETs in different subtypes of juvenile idiopathic arthritis (JIA) has been rarely studied. Therefore, we aimed to explore the ability of JIA-derived neutrophils to release NETs and the effect of TNF- α (tumor necrosis factor- α) inhibitors on NET formation both *in vitro* and *in vivo*, and evaluate the associations of NET-derived products with clinical and immune-related parameters.

Methods: The ability of neutrophils to release NETs and the effect of adalimumab on NET formation was assessed via *in vitro* stimulation and inhibition studies.

Abbreviations: ANA, anti-nuclear antibody; ABST, peroxidase substrate; ANCA, anti-neutrophil cytoplasmic antibodies; AUC, the area under the curve; csDMARDS, conventional synthetic disease-modifying antirheumatic drugs; CDKs, cyclin-dependent kinases; DAMPs, damage-associated molecular patterns; DAPI, 4',6-diamidino-2-phenylindole; DPI, diphenyl iodide; Cf-DNA, cell-free DNA; FBS, fetal bovine serum; FCM, flow cytometry; GC, glucocorticoids; HLA-B27, human leukocyte antigen B27; HC, healthy control; hs-CRP, hypersensitive C-reactive protein; HRP, horseradish peroxidase; IQR, interquartile ranges; IL-17A, interleukin 17A; IgG, immunoglobulin G; JIA, juvenile idiopathic arthritis; JADAS27, Juvenile Arthritis Disease Activity Score 27; MPO, myeloperoxidase; MAPK, mitogen-activated protein kinase; ESR, erythrocyte sedimentation rate; ERA, enthesitis-related arthritis; ERK1/2, extracellular signal-regulated kinase 1/2; o-JIA, oligoarticular juvenile idiopathic arthritis; p-JIA, polyarticular JIA; PMA, phorbol-12-myristate-13-acetate; PI3K, phosphoinositide 3-kinase; RA, rheumatoid arthritis; RF, rheumatoid factor; ROC, receiver operating characteristic curve; ROS, reactive oxygen species; s-JIA, systemic juvenile idiopathic arthritis; SLE, systemic lupus erythematosus; TNF- α , tumor necrosis factor- α ; VAS, visual analog scale.

Plasma NET-derived products were detected to assess the incidence of NET formation *in vivo*. Furthermore, flow cytometry and western blotting were used to detect NET-associated signaling components in neutrophils.

Results: Compared to those derived from HCs, neutrophils derived from patients with oligoarticular-JIA, polyarticular-JIA and enthesitis-related arthritis were more prone to generate NETs spontaneously and in response to TNF- α or PMA *in vitro*. Excessive NET formation existed in peripheral circulation of JIA patients, and elevated plasma levels of NET-derived products (cell-free DNA and MPO-DNA complexes) could accurately distinguish JIA patients from HCs and were positively correlated with disease activity. Multiple linear regression analysis showed that erythrocyte sedimentation rate and TNF- α levels were independent variables and were positively correlated with cell-free DNA concentration. Notably, TNF- α inhibitors could effectively prevent NET formation both *in vitro* and *in vivo*. Moreover, the phosphorylation levels of NET-associated kinases in JIA-derived neutrophils were markedly increased.

Conclusion: Our data suggest that NETs might play pathogenic roles and may be involved in TNF- α -mediated inflammation in JIA. Circulating NET-derived products possess potential diagnostic and disease monitoring value. Furthermore, the preliminary results related to the molecular mechanisms of NET formation in JIA patients provide a theoretical basis for NET-targeted therapy.

KEYWORDS

juvenile idiopathic arthritis, neutrophils, neutrophil extracellular traps, biomarkers, tumor necrosis factor-alpha

Introduction

Juvenile idiopathic arthritis (JIA) refers to a heterogeneous group of chronic childhood arthritis of unknown etiology that persist for more than 6 weeks and occur before the age of 16 (1). The International League of Associations for Rheumatology (ILAR) identified seven subtypes of JIA according to disease manifestations within the first 6 months: oligoarticular JIA (o-JIA), rheumatoid factor negative (RF-) polyarticular JIA (p-JIA), RF-positive (RF+) p-JIA, enthesitis-related arthritis (ERA), systemic JIA (s-JIA), psoriatic arthritis and undifferentiated arthritis (1). JIA is the most common pediatric rheumatic disease with an incidence rate ranging from 1.6 to 23 cases per 100,000 people and a prevalence ranging from 3.8 to 400 cases per 100,000 people (2). JIA causes joint pain and swelling and limited range of joint motion and results in uveitis, osteopenia/osteoporosis, and growth retardation if it is not diagnosed early or treated promptly or effectively (2). However, the diagnosis of JIA relies mainly on clinical assessments and ruling out other pediatric diseases that manifest as chronic arthritis because of the lack of reliable diagnostic biomarkers. Since the development of new biological agents in the early 2000s, the outcomes of JIA in children have substantially improved (3).

However, the disease has not yet been cured, further research is needed to explore the complex immunopathological process of JIA and identify new biomarkers and therapeutic targets.

JIA is thought to be associated with genetic, epigenetic, and environmental factors, but its etiology is not fully clear (3–5). Over the years, many studies have claimed that JIA is caused primarily by dysregulation of the adaptive immune system. However, as the understanding of genetics and immunology in JIA has improved, increasing evidence has shown that the innate immune system is also involved in the pathogenesis of JIA (5–8). Specifically, neutrophils have been implicated in the disordered immune response in JIA (6, 7). It is well evidenced that abundant activated neutrophils accumulate in the synovial fluid of inflamed joints in JIA patients (9, 10). In polyarticular JIA, peripheral blood neutrophils are chronically activated even when the patient is in clinical remission (6), and activated neutrophils can form neutrophil extracellular traps (NETs) (11–13), the process of NET formation, called NETosis, was originally thought to be a process of neutrophil death distinct from apoptosis and necrosis (14–16). Notably, excessive NET formation causes an inflammatory imbalance and dysregulation of adaptive immune responses by presenting major sources of autoantigens (17, 18) and danger-

associated molecular patterns (DAMPs) (19, 20) and mediating complement and inflammasome activation (21–24). Additionally, NETs can activate T cells and autoreactive B cells, induce B-cell expansion, and promote B-cell and Th17 cell differentiation (25–28). Therefore, the role of NETs in autoimmune diseases is currently gaining increasing attention, and accumulating evidence suggests that NETs play a vital role in the initiation and perpetuation of autoimmune diseases, such as rheumatoid arthritis (RA), systemic lupus erythematosus (SLE) and anti-neutrophil cytoplasmic antibody (ANCA)-associated vasculitis (AAV) (17, 18, 20, 29). In animal models of antigen-induced arthritis, NETs contribute to articular pain and mediate joint edema, maintaining the inflammatory response (30).

JIA is not a single disease; this heterogeneity implies that different pathogenetic mechanisms underlie the various JIA subtypes. NET formation has been studied in o-JIA and p-JIA (31). In this study, NET formation was further studied in different subtypes of JIA in a larger size cohort. As such, we explored NET formation in patients with three subtypes of JIA, i.e., o-JIA, p-JIA, and ERA, respectively, and whether NET-derived products could be biomarkers for diagnosing JIA and monitoring disease activity. Furthermore, TNF- α plays a pivotal role in the pathogenesis of JIA (2, 7), and whether NETs are involved in TNF- α -mediated inflammation in JIA was investigated.

Methods

Human samples

Fifty-eight JIA patients who fulfilled the International League of Associations for Rheumatology (ILAR) criteria (1) were screened for inclusion in this study. Patients with other inflammatory or autoimmune diseases, metabolic diseases, and malignancies were excluded. Thirty healthy volunteer controls (HCs) who underwent physical examinations or elective surgery and had not received any medication for any disease were enrolled, and there was no significant difference in age and sex between HCs and patients. All participants were infection-free for at least one month and were recruited from Wuhan Children's Hospital of Tongji Medical College, Huazhong University of Technology and Science between July 2022 and August 2023. Clinical and laboratory data and blood samples were collected. Fresh neutrophils were isolated from 5 mL of EDTA-anticoagulated peripheral blood by density centrifugation using PolymorphprepTM (Axis-Shield) according to the manufacturer's protocol within 1–2 hours after collection. Contaminating erythrocytes were lysed with red blood lysis buffer (0.83% (w/v) for 4–5 min at room temperature. Trypan blue exclusion indicated that cell viability was $\geq 97\%$, and the purity of the isolated neutrophils was $\geq 90\%$ according to the forward and side of scatter plots generated from the flow cytometric analyses. Neutrophils were further analyzed by flow cytometry (Attune NxT, AFC2, Thermo Fisher) after incubation with a fluorescein isothiocyanate (FITC)-conjugated anti-CD15 antibody (BioLegend, 394705). The purified neutrophils were resuspended in phenol red-free RPMI 1640 medium supplemented with 10%

heat-inactivated fetal bovine serum (FBS) at 2.5×10^6 cells/mL. The plasma samples were aliquoted and stored at -80°C until further analysis. This study was approved by the Wuhan Children's Hospital Committee for Research Ethics and was performed following the Declaration of Helsinki. Written informed consent was obtained from all participants' parents. Because of the limited amount of peripheral blood available, not all patients were included in each experiment.

The demographic characteristics of the patients are summarized in Table 1. The Juvenile Arthritis Disease Activity Score 27 (JADAS27) includes the following four measures: physician's global assessment of disease activity, as measured on a 0–10 visual analog scale (VAS) where 0 = no activity and 10 = maximum activity; parent global assessment of well-being, as measured on a 0–10 VAS where 0 = very well and 10 = very poor; erythrocyte sedimentation rate (ESR), which was normalized to a 0 to 10 scale; and the number of joints with active disease (32, 33).

In vitro stimulation and inhibition studies

Freshly isolated neutrophils (2.5×10^5 cells, 100 μL) from JIA patients or HCs were seeded in 24-well plates on 0.001% poly-L-lysine-coated glass coverslips and incubated for 30–40 min at 37°C in 5% CO_2 . Then, the neutrophils were incubated with phorbol-12-myristate-13-acetate (PMA, 30 nM) (P1585-1MG, Sigma) for 3 hours or recombinant human TNF- α (100 ng/mL) (570102, BioLegend) for 6 hours at 37°C in 5% CO_2 . In addition, neutrophils were cultured without any stimulus for 6 hours to assess spontaneous NET formation. To visualize whether TNF- α -induced NET formation was inhibited by TNF- α antagonists, neutrophils were seeded in the same way as described above and pretreated with a humanized anti-TNF- α antibody (adalimumab, Humira, Abbvie) (4 $\mu\text{g/mL}$, equivalent to the average serum concentration in the human body) for 15 minutes prior to TNF- α stimulation. The concentrations and time points for neutrophil stimulation were determined based on the optimized protocol.

Visualizing NET formation via immunofluorescence confocal microscopy

After treatment as described above, the neutrophils were immediately fixed with 4% paraformaldehyde, rinsed three times with PBS, and blocked with 3% BSA. For immunofluorescence labeling, the neutrophils were stained using a rabbit anti-myeloperoxidase (MPO) mAb (1:800) (ab208670, Abcam) overnight at 4°C and then with an Alexa Fluor 488-conjugated goat anti-rabbit secondary antibody (A-11008; Thermo Fisher) for 1 hour at room temperature. The DNA was counterstained with 4',6-diamidino-2-phenylindole (DAPI) (C1005, Beyotime) for 5 minutes. Neutrophils and NETs were visualized using a Nikon Eclipse-Ti-S fluorescence microscope (Nikon, Tokyo, Japan). Five randomly chosen fields of each coverslip were observed, and fluorescence images of MPO and DNA were analyzed using ImageJ software (National Institutes of Health, NIH). The results

TABLE 1 Demographic, clinical, and laboratory characteristics.

Subtypes	o-JIA	p-JIA	ERA	All cases
Number (%)	29 (50%)	18 (31%)	11 (18.9%)	58 (100%)
Gender (males, %)	11 (37.93%)	4 (22.22%)	11 (100%)	26 (44.83%)
Age (mean ± SEM, y)	8.473 ± 0.7530	7.366 ± 1.151	10.68 ± 0.7825	8.548 ± 0.5524
JADA S27 (mean ± SEM)	12.27 ± 0.8272	15.11 ± 1.773	15.15 ± 1.512	13.91 ± 0.7342
RF positivity (n, %)	0 (0%)	7 (38.8%)	0 (0%)	7 (12.1%)
HLA-B27 (n, %)	0 (0%)	0 (0%)	4 (36.4%)	4 (6.9%)
ANA positivity (n, %)	13 (44.9%)	7 (38.9%)	7 (63.6%)	27 (45.55%)
active uveitis (n)	3 (10.35%)	0 (0%)	0 (0%)	3 (5.17%)
ESR (median with IQR, mm/hour)	6 (4-10)	8 (4-18)	11 (6-29.5)	7.5 (4-13)
hs-CRP (median with IQR, mg/L)	4.285 (2.035-13.63)	2.77 (1.44-31.55)	13.4 (6.105-69.95)	4.42 (1.6-16.7)
Treatment	12 (41.38%)	7(44.44%)	0 (0%)	19 (34.48%)
GCs (n, %)	1 (3.45%)	1 (5.56%)	0 (0%)	2 (5.17%)
csDMARDs (n, %)	12 (100%)	7 (100%)	0 (0%)	19 (100%)
anti-TNF-a (n, %)	10 (83.33%)	7 (100%)	0 (0%)	17 (90%)

o-JIA, oligoarticular juvenile idiopathic arthritis; p-JIA, polyarticular JIA; ERA, enthesitis-related arthritis; y, years; ANA, anti-nuclear antibodies; HLA-B27, human leukocyte antigen B27; RF, rheumatoid factor; ESR, erythrocyte sedimentation rate; hs-CRP, hypersensitive C-reactive protein; IQR, interquartile ranges; JADAS27, Juvenile Arthritis Disease Activity Score 27; GCs, glucocorticoids; csDMARDs, conventional synthetic disease-modifying antirheumatic drugs; anti-TNF-a, anti-tumor necrosis factor-alpha antibody.

are expressed as the percentage area of the microscopic field of view occupied by NETs under a 20× objective.

Since NETs are fragile and easily shed during surgery, we used SYTOX Green (Invitrogen Life Technologies, San Diego, CA, USA) to stain DNA to further visualize NET formation. The cells were fixed with 4% paraformaldehyde and rinsed 3 times with PBS. DNA was stained with 0.2 mM SYTOX Green dye for 15 min, and NETs were visualized using a Nikon Eclipse-Ti-S fluorescence microscope. A total of 5 randomly selected fields from different regions of each coverslip were imaged with a 20× objective.

Quantification of NET release via a fluorescence microplate assay

Fluorescence microscopy is laborious and time-consuming and is not suitable for the assessment of a large number of samples. Hence, a fluorescence microplate assay was used to determine the amounts of NET formation. Freshly isolated neutrophils (4×10⁴ cells per well) were cultured in 96-well black microtiter plates in RPMI 1640 medium supplemented with 10% FBS containing 0.2 μM SYTOX Green and stimulated with PMA (30 nM) or with TNF-α (100 ng/mL) for 6 hours. Neutrophils were also incubated without any stimulus for 6 hours to measure spontaneous NETosis. To quantify the inhibitory effects of adalimumab and DPI on TNF-α-induced NET formation *in vitro*, neutrophils were pretreated with adalimumab (4 μg/mL) or DPI (10 μM) (diphenyl iodide, NADPH oxidase inhibitor, Enzo Life Sciences) for 15 minutes prior to the addition of TNF-α. The samples were analyzed in triplicate. After incubation, the absorbance of each well of the 96-well black microtiter plates was measured with an EnSpire Multimode Plate

Reader (PerkinElmer, Inc) at 485 nm (excitation)/520 nm (emission). The data are expressed in relative fluorescence units (RFUs) and were calculated by subtracting the fluorescence intensity of the control cells at time 0.

Measurement of reactive oxygen species production

Neutrophils (1.5×10⁵ cells) were incubated with TNF-α (100 ng/mL) for 3 hours at 37°C or were not incubated. Then, CellROXTM Green (C10444, Invitrogen) was added to the cells, which were then incubated at 37°C for 15 minutes. Then the cells were washed with PBS to remove the unbound dye, labeled with 7-AAD (559925, BD PharmingenTM), resuspended in PBS, and subsequently detected by flow cytometer (AttuneNxt, Thermo Fisher). The fluorescence intensity of individual cells was analyzed by FlowJo software.

Western blot analysis

Neutrophils (2.5×10⁶/mL) isolated from HCs or JIA patients were either cultured in 24-well plates in the presence or absence of 100 ng/mL TNF-α (570102, BioLegend) for 3 hours at 37°C or were not cultured. Then, the cells were lysed with RIPA buffer (P0013B, Beyotime) containing a protease inhibitor cocktail (G2006, Servicebio), NaF (1 M, G2007-1, Servicebio), and Na₃VO₃ (100 mM, G2007-1, Servicebio). The cell lysates were separated by SDS-PAGE and electrotransferred onto nitrocellulose membranes (AmershamTM ProtranTM 0.2 μm NC). The following primary antibodies were used: monoclonal anti-MPO (1:1000; Abcam

ab208670), anti-GAPDH (1:1000, Cat No. CL594-60004, Proteintech), anti-phospho-PI3K (1:1000; 4292S, Cell Signaling Technology), anti-phospho-AKT (1:1000; Cell Signaling Technology, 4060 L), anti-phospho-extracellular signal-regulated kinase 1/2 (ERK1/2) (Abmart T40072) and anti-phospho-MAPK-CDK (mitogen-activated protein kinase/cyclin-dependent kinase) (1:1000; Cell Signaling Technology, 2325) antibodies. The secondary antibodies used were horseradish peroxidase (HRP)-conjugated goat anti-mouse immunoglobulin G (IgG) (1:10000) (Proteintech, SA00001-1) and HRP-conjugated goat anti-rabbit IgG (1:8000) (Proteintech, SA00001-2). The bound antibodies were detected using an enhanced chemiluminescence system.

Quantification of cell-free DNA concentrations

Cell-free DNA concentrations were quantified using a Helixyte™ Green dsDNA Quantitation Assay Kit (AAT Bioquest Catalog number: 17650). HC and JIA patient plasma samples were diluted 1:10 and incubated with Helixyte Green™ working solution for 5–10 min at room temperature away from light. Then, the fluorescence intensity was measured with an EnSpire Multimode Plate Reader (Ex/Em = 490/525 nm). The data were analyzed using serial dilutions of calf thymus DNA to generate a calibration curve.

Analysis of MPO-DNA complex levels by ELISA

A novel capture ELISA was used to quantify NET levels in JIA patients and controls by measuring the levels of the MPO-DNA complex in human plasma. The wells of 96-well plates were coated with 5 µg/mL mouse anti-human myeloperoxidase antibody (clone D02-2A1, Bio-Rad) (100 µL per well) as the capture antibody overnight at 4°C. After the wells were blocked in 1% BSA (150 µL per well) and washed 3 times with 0.05% PBST (300 µL each), 20 µL of patient plasma combined with 80 µL of incubation buffer containing a peroxidase-labeled anti-DNA mAb (Cell Death ELISA Plus, Roche; Cat. No: 11774425001) was added to each well according to the manufacturer's instructions. After three hours of incubation at RT on a shaker (300 rpm), the plates were washed with 0.05% PBST (300 µL each), and 100 µL of the peroxidase substrate (ABTS) from the kit (Cell Death Detection ELISA^{PLUS}, Roche, Cat. No: 11774425001) was added. The absorbance at a measurement wavelength of 405 nm and a reference wavelength of 490 nm was measured with a BioTek Synergy H1 microplate reader after 40 minutes of incubation at room temperature in the dark. The difference between the measured and reference absorbance was calculated as MPO-DNA complex level in the plasma of JIA patients and HCs.

Statistical analysis

Statistical analysis was performed using SPSS 18.0 statistical software or GraphPad Prism software version 8.0. Continuous

variables are presented as the means ± standard errors of the means (SEMs) or medians and interquartile ranges (IQRs). For continuous variables with normal distributions, Student's t-tests or paired-sample t tests were used to analyze differences. For nonnormally distributed data, the Mann-Whitney U test or Wilcoxon test was used for comparisons between two groups. One-way ANOVA or the Kruskal-Wallis test was used for comparisons among multiple groups. Spearman's or Pearson's rank correlation analyses were used as indicated to evaluate associations between the levels of NET components and clinical parameters, and multiple linear regression analysis was used for multivariate analysis. Receiver operating characteristic (ROC) curves were generated and the area under the curve (AUC) was analyzed to measure the sensitivity and specificity of NET-derived products for the diagnosis of JIA. *P* values less than 0.05 were considered to indicate statistical significance (**p* < 0.05, ***p* < 0.01, ****p* < 0.001, *****p* < 0.0001).

Results

Detailed demographic, clinical, and laboratory characteristics of JIA patients

Fifty-eight patients with JIA participated in the study: 29 patients with o-JIA, 18 patients with p-JIA, and 11 patients with ERA. o-JIA was the most common subtype, accounting for 50% of all JIA cases. The percentages of patients with p-JIA and ERA are also shown in Table 1. The population consisted of 32 female and 26 male children. The mean age was 8.548 ± 0.5524 y (95% CI 7.442–9.655). The mean JADAS27 was 13.91 ± 0.7342 (95% CI 12.44–15.38). The median ESR was 7.5 mm/h (IQR 4–13; range 2 and 51 mm/h). Thirty-nine patients with JIA did not receive medical treatment, nineteen patients had already undergone treatment for six months, and seventeen patients had received TNF-α inhibitor therapy. Thirty age- and sex-matched HCs were recruited as controls.

Excessive NET formation in neutrophils from patients with JIA spontaneously or in response to PMA and TNF-α *in vitro*

MPO is embedded in extracellular DNA which is the major backbone of NETs (13). NETs were identified by the colocalization of extracellular DNA and MPO, and the amounts of NETs were quantified by fluorescence microscopy and a fluorescence microplate assay (Figure 1). As shown in Figures 1A, B, the percentages of the NET-occupied area were markedly greater in JIA-derived neutrophils than in HC-derived neutrophils after no stimulation (28.75 ± 1.355% vs. 21 ± 2.236%, *p* = 0.0065), PMA stimulation (53.4 ± 2.172% vs. 40.5 ± 2.527%, *p* = 0.0021) or TNF-α stimulation (44.83 ± 2.628% vs. 34 ± 3.215%, *p* = 0.0247).

A fluorescence microplate assay was utilized to further quantify the levels of NETs in patients with different subtypes of JIA, including o-JIA, p-JIA, and ERA. Our findings showed that there

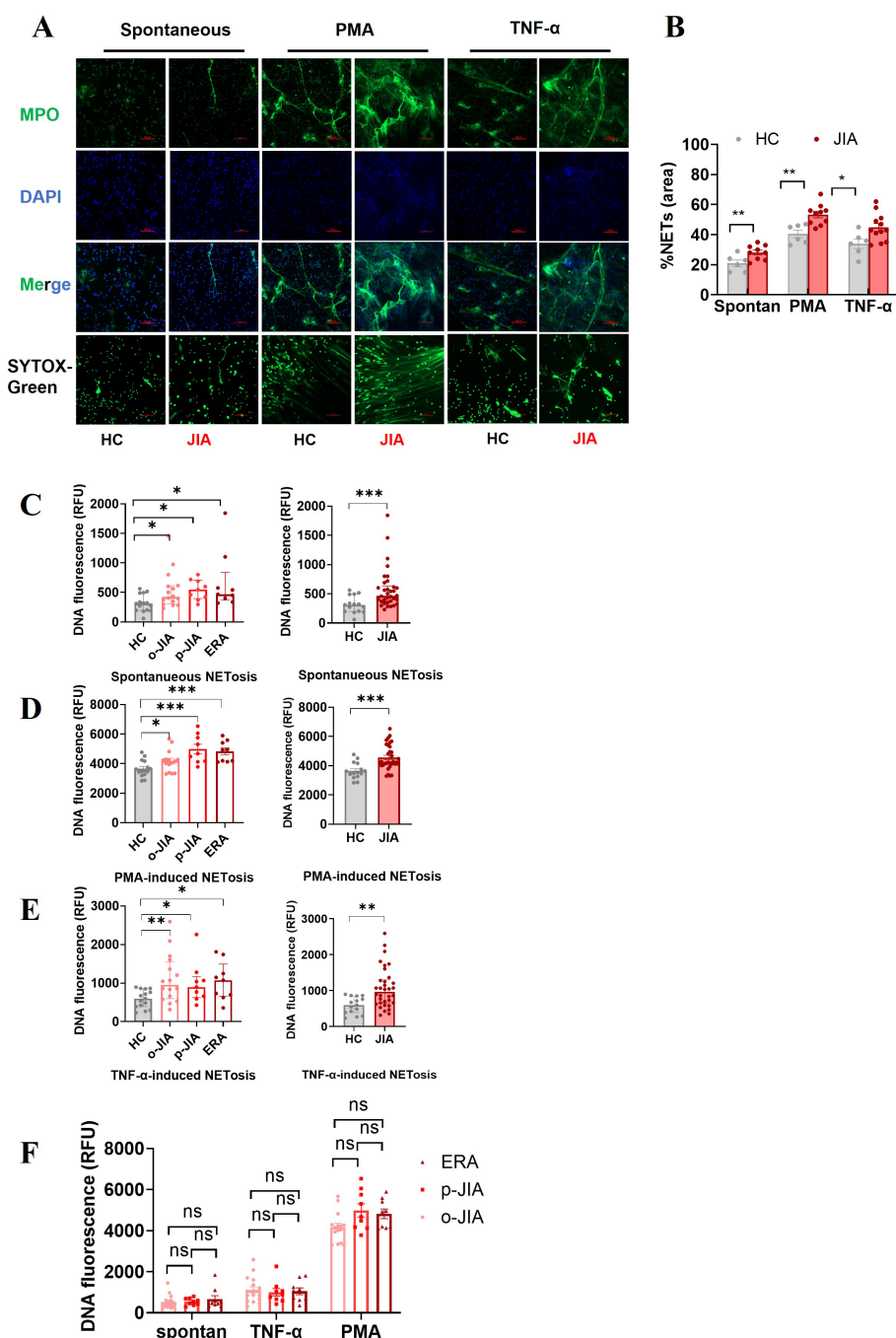


FIGURE 1

Neutrophils derived from the peripheral blood of JIA patients increase NET formation *in vitro*, either spontaneously or in response to TNF- α or PMA. (A) Representative images of NETs released by neutrophils derived from at least 10 patients with JIA and 6 HCs spontaneously or in response to PMA or TNF- α . NETs were double immunostained for extracellular DNA (DAPI; blue) and MPO (MPO antibody; green), and NETs were identified by the presence of extracellular DNA stained with SYTOX-Green. Images were captured at 20 \times magnification; the scale bars represent 100 μ m. (B) In a quantitative analysis of the above experiments, the percentages of NET-occupied areas in the total area in the JIA group were markedly higher than those in the HC group. (C–F) Quantitative assessment of NET formation in the o-JIA, p-JIA, and ERA groups by microplate assays. Neutrophils isolated from patients with o-JIA, p-JIA, and ERA and healthy controls were incubated for 6 hours under the conditions of (C) no intervention, (D) PMA (30 nM) stimulus, or (E) the addition of TNF- α (100 ng/ml). (F) The amounts of NETs were compared among the three subtypes of o-JIA, p-JIA, and ERA, respectively. The results are expressed as the fluorescence intensity of DNA in NETs. One-way ANOVA or the Kruskal–Wallis test was used to compare three or more groups. Student's independent-sample t-test was used to compare the two groups. The bar graphs show the mean \pm SEM or median with IQR. * p <0.05, ** p <0.01, *** p <0.001, ns, nonsignificant; spontan, spontaneous.

were more NETs formed by neutrophils derived from 16 o-JIA patients, 9 p-JIA patients and 9 ERA patients than from 15 HCs with no stimulation ($p = 0.0436$, $p = 0.0119$, and $p = 0.0193$, respectively; **Figure 1C**), PMA stimulation ($p = 0.0376$, $p = 0.0003$, and $p = 0.0002$, respectively; **Figure 1D**) or the addition of TNF- α ($p = 0.0059$, $p = 0.0378$, and $p = 0.0164$, respectively; **Figure 1E**). Moreover, there were significant differences in the amounts of NETs released by neutrophils after the indicated intervention between in entire cohort of JIA patients and in HCs ($p = 0.0005$, $p = 0.0004$ and $p = 0.0014$, respectively; **Figures 1C–E**), which was consistent with the results of fluorescence microscopy. Importantly, our findings revealed no significant differences in NET formation among o-JIA, p-JIA and ERA patients ($p > 0.05$, **Figure 1F**). Overall, neutrophils derived from patients with the three subtypes of JIA were more prone to release NETs in the presence or absence of TNF- α or PMA stimulation and further *in vitro* verification of TNF- α mediated NET generation was performed.

Increased plasma levels of NET-derived products in JIA patients: potential biomarkers for diagnosis and disease activity

To quantify NET formation in the peripheral blood of JIA patients, plasma levels of cf-DNA and MPO-DNA complexes, as major components of NETs, were measured, there was a marked increase in levels of cf-DNA and MPO-DNA complexes in peripheral blood of JIA patients when compared to HCs [691.4 ± 15.37 ng/mL vs. 611.2 ± 21.53 ng/mL, $p = 0.0043$; 0.1430 (IQR: 0.0952 – 0.2210) vs. 0.0797 (IQR: 0.05125 – 0.1500), $p = 0.0030$; **Figure 2A**]. Significantly, the plasma concentrations of cf-DNA in patients with o-JIA, p-JIA and ERA were significantly increased as compared to those in HCs (683.3 ± 18.73 vs. 611.2 ± 21.53 ng/mL, $p = 0.0243$; 697.9 ± 32.92 vs. 611.2 ± 21.53 ng/mL, $p = 0.0162$; 703.7 ± 38.14 vs. 611.2 ± 21.53 ng/mL, $p = 0.0401$, respectively; **Figure 2B**). Similarly, the plasma levels of MPO-DNA complex in patients with o-JIA [0.1356 (IQR: 0.0961 – 0.1806)], p-JIA [0.1295 (IQR: 0.09540 – 0.2485)] and ERA [0.1823 (IQR: 0.08975 – 0.5570)] were higher than those in HCs [0.0797 (IQR: 0.05125 – 0.1500)] ($p = 0.0163$, $p = 0.0302$ and $p = 0.0258$, respectively; **Figure 2B**), these results verified that excessive NET formation were present in peripheral blood of JIA patients. However, there were no differences in cf-DNA and MPO-DNA complex levels among the three JIA subtypes ($p > 0.05$, **Figure 2C**).

Significantly, ROC curve analysis showed that plasma levels of cf-DNA and MPO-DNA complex, as diagnostic biomarkers, could accurately distinguish JIA patients from HCs, with cut-off values of 638.4310 ng/mL and 0.0913 , respectively (**Figure 2D**). **Figure 2E** showed that the plasma concentration of cf-DNA was strongly correlated with the JADAS27 in the whole cohort of JIA patients ($r = 0.5129$, $p = 0.0002$), and in patients with o-JIA, p-JIA, and ERA ($r = 0.4573$, $p = 0.0215$; $r = 0.5005$, $p = 0.0483$; and $r = 0.7316$, $p = 0.0391$, respectively). As shown in **Figure 2F**, a significant positive correlation between MPO-DNA complex levels and disease activity (JADAS27) was identified in the whole cohort of JIA patients ($r =$

0.3399 , $p = 0.0138$) and even in o-JIA patients ($r = 0.4193$, $p = 0.0260$), and p-JIA patients ($r = 0.6434$, $p = 0.0139$), despite no significant correlation in ERA patients ($r = 0.1198$, $p = 0.7808$). Taken together, NETosis-derived products may be used to monitor disease activity, and thus predict the flares.

Associations of immune-related laboratory parameters with cell-free DNA concentrations in JIA patients

Emerging research suggests that NET remnants can interact with immune components and immune cells to modulate immune response (20). In this study, correlation studies demonstrated that the plasma concentrations of cf-DNA strongly and positively correlated with some immune-related parameters, such as the number and percentage of neutrophils and B cells, hs-CRP, ESR, and TNF- α levels, total IgG production and complement C3 and C4 levels in peripheral circulation, whereas nonsignificant correlation between IL-6 level and cf-DNA concentration was observed (**Figure 3A**). Subsequently, the 10 statistically significant variables were analyzed by multiple linear regression analysis, and the multiple linear regression equation established was statistically significant ($P < 0.05$; **Figure 3B**), only ESR and TNF- α levels were positively associated with cf-DNA concentration and were found to be independent variables, implying that TNF- α is a major inducer in triggering NET formation in JIA patients, and further verifying that cf-DNA concentration could be a biomarker for monitoring disease activity.

TNF- α inhibitors suppress TNF- α -induced NET formation both *in vitro* and *in vivo*

In vitro inhibition study showed that adalimumab (a humanized anti-TNF- α antibody) effectively suppressed TNF- α -induced NET formation, as assessed by fluorescence microscopy ($p < 0.0001$; **Figures 4A, B**). NADPH oxidase inhibitor (DPI) can almost completely inhibit PMA-induced NETosis (14, 34) which was further verified in this study ($n = 21$, $p < 0.0001$; **Figure 4C**), and was used as a positive control of effective inhibition of NETosis. Our results showed that DPI could inhibit TNF- α -induced NET formation ($n = 16$ $p = 0.0008$; **Figure 4D**), and the inhibitory effects of adalimumab and DPI on suppressing TNF- α -induced NETosis were similar ($47.57\% \pm 3.665$ vs. $49.41\% \pm 23.79$, $p = 0.7821$; **Figure 4E**). Moreover, there was no difference in the inhibitory effects of adalimumab in suppressing TNF- α -induced NETosis between JIA patients and healthy controls ($p = 0.8160$; **Figure 4F**).

Next, we examined whether TNF- α inhibitors could prevent NETosis *in vivo*. As shown in **Figure 4G** that patients with JIA had a decreased plasma concentration of cf-DNA after six months of treatment with TNF- α inhibitors (adalimumab or etanercept), along with significantly improving disease activity (reduced JADAS27) ($n = 23$, $p < 0.0001$), indicating that TNF- α inhibitors can effectively inhibit NET formation *in vivo*.

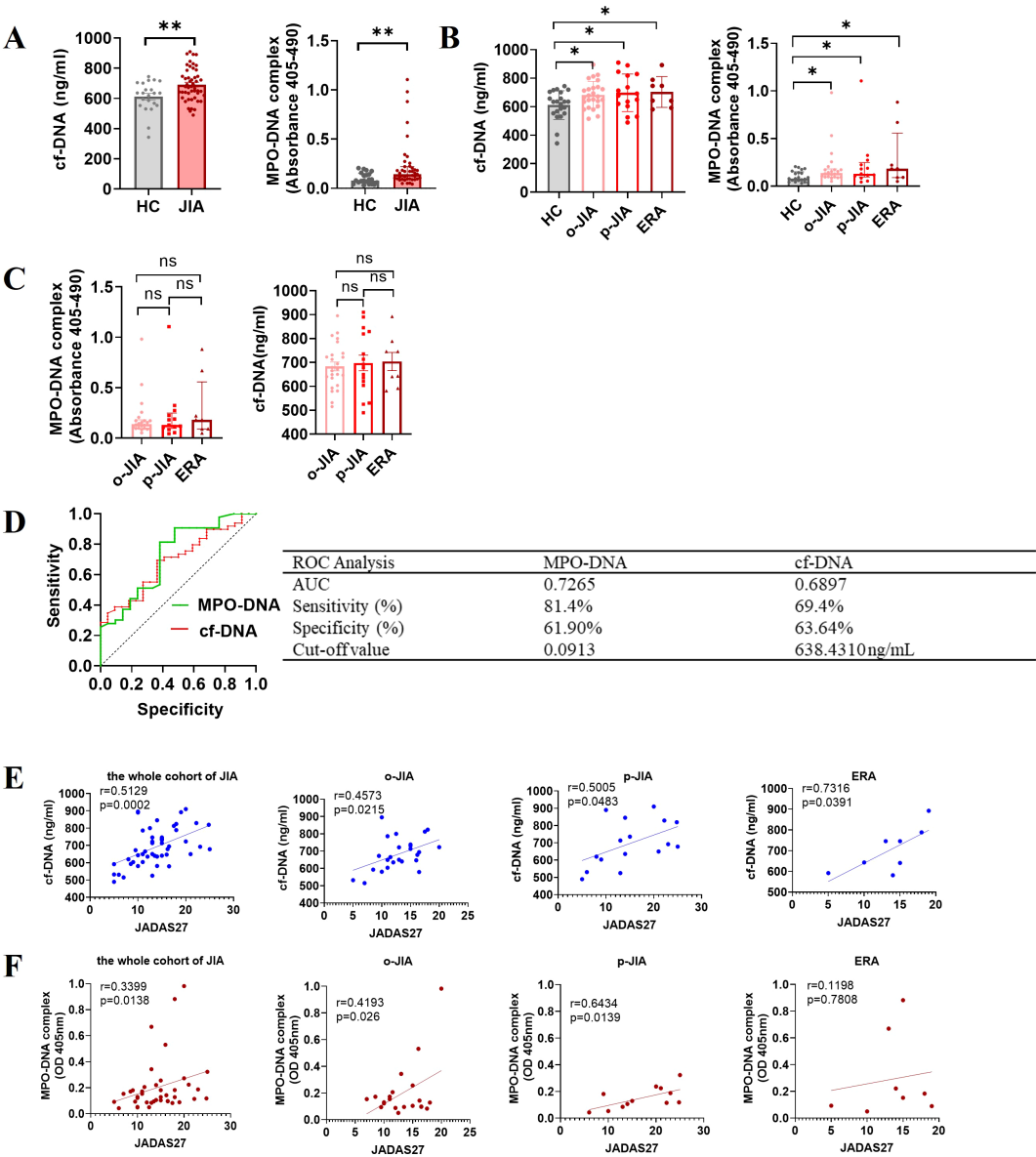


FIGURE 2
Excessive NET formation exists in the peripheral circulation of patients with JIA, with elevated NET-derived components as biomarkers for diagnosis and disease activity. **(A)** The plasma levels of NETosis-derived products, cf-DNA and MPO-DNA complexes, were compared between JIA patients and HCs. **(B)** The plasma concentrations of cf-DNA in children with o-JIA (n = 25), p-JIA (n=16) and ERA (n = 8) were higher than those in HCs (n = 22). Meanwhile, there was an increase in the plasma levels of MPO-DNA complexes in 22 o-JIA patients, 13 p-JIA patients and 8 ERA patients compared to HCs (n = 21). The bar graphs show the mean \pm SEM or the median with IQR. * $p < 0.05$, ** $p < 0.01$. **(C)** The plasma levels of cf-DNA and MPO-DNA complexes were similar among the three subtypes of JIA. ns, nonsignificant. **(D)** ROC curve analysis of cf-DNA and MPO-DNA complexes to evaluate the accuracy of these parameters as diagnostic biomarkers of disease in JIA patients (AUC = 0.6897, $p = 0.0110$; and AUC = 0.7265, $p = 0.0035$, respectively). AUC, area under the curve. **(E)** The concentrations of cf-DNA were strongly and positively associated with the JADAS27 in the whole cohort of children with JIA (n = 49) and the three JIA subtypes, i.e., o-JIA (n=25), p-JIA (n = 16), and ERA (n = 8). **(F)** A significant positive correlation between the MPO-DNA complex levels and the JADAS27 in 42 patients with JIA, 22 patients with o-JIA, and 12 patients with p-JIA, but not 8 patients with ERA. R values of Spearman or Pearson's rank correlation and p values of their null hypothesis are shown.

High expression of NET-associated signaling components in JIA-derived neutrophils

NADPH oxidase, a key enzyme in redox signaling, is a major generator of reactive oxygen species (ROS) *in vivo*. NADPH oxidase-mediated ROS generation is involved in most of the mechanisms underlying NETosis (35). TNF- α -induced NET

formation was suppressed by DPI (Figure 4E), and ROS production in neutrophils stimulated with TNF- α was significantly increased (n = 6, $p = 0.0266$; Figure 5A), indicating that NADPH oxidase-mediated ROS production was an important factor driving TNF- α -induced NET formation. To further clarify the upstream signals mediating NADPH oxidase activation, the effect of TNF- α on phosphoinositide 3-kinase (PI3K)-AKT signaling activation was examined, because this signaling pathway

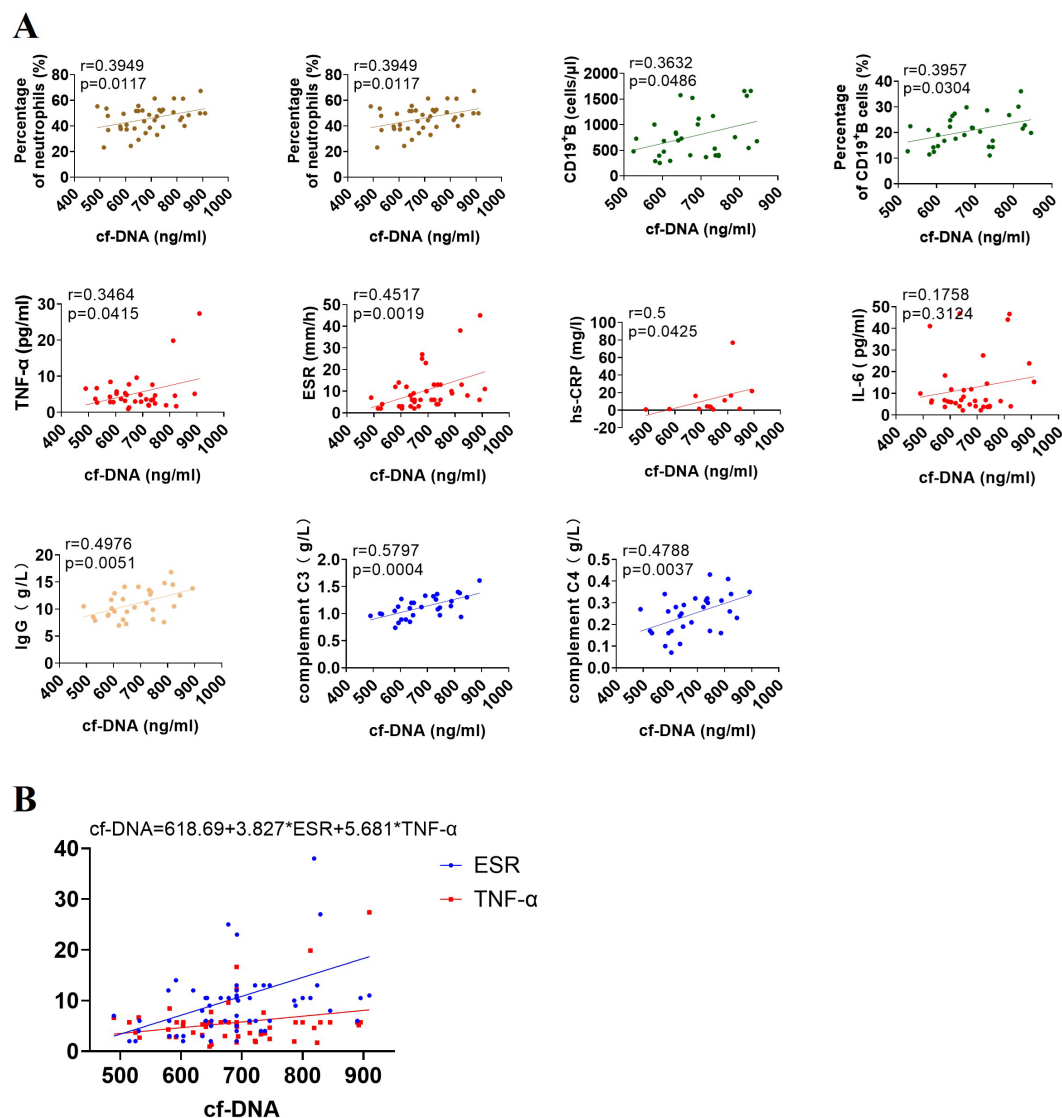


FIGURE 3

Associations of cf-DNA levels with immune-related parameters in the entire cohort of patients with JIA. (A) The concentrations of cf-DNA were strongly correlated with the number and percentage of neutrophils and CD19⁺ B cells, the expression of inflammatory markers (TNF- α , ESR, and hs-CRP), the levels of IgG, complement C3 and C4 in peripheral blood, but no correlation with IL-6 level. R values of Spearman or Pearson's rank correlation and p values of their null hypothesis are shown. (B) ESR and TNF- α are independent variables by the multiple linear regression analysis.

is involved in ROS production by NADPH oxidase (36, 37). Western blotting revealed that the levels of phosphorylated PI3K and AKT in neutrophils from JIA patients and HCs were elevated after TNF- α stimulation (Figure 6A), especially in JIA-derived neutrophils, despite nonsignificant differences between patients and HCs (Figure 6B). These results suggested that TNF- α induced NETosis through ROS- and PI3K-Akt-dependent signaling pathways.

Excessive NET formation existed in peripheral circulation of patients with o-JIA, p-JIA and ERA, so it is urgent to explore the molecular mechanisms of NETosis in JIA patients. Our findings demonstrated that basal ROS production, MPO expression, and phosphorylated PI3K and AKT levels in JIA-derived neutrophils were markedly increased compared with those in HC-derived neutrophils (Figures 5B, 6C). Previous studies have shown that the

MAPK-ERK1/2 signaling pathway is involved in NET formation through the activation of NADPH oxidase (38, 39), and NET formation is controlled by the activation of cyclin-dependent kinases 4 and 6 (CDK4/6) (40). As shown in Figure 6D, the levels of MAPK-CDKs and ERK1/2 phosphorylation were markedly higher in JIA-derived neutrophils than in HC-derived neutrophils. Overall, there might be distinct activated NETosis-associated signaling pathways in the hyperinflammatory milieu of JIA.

Discussion

Recent research has highlighted that NETs are released by neutrophils upon activation and play central roles in the initiation and perpetuation of inflammation and autoimmune responses (11),

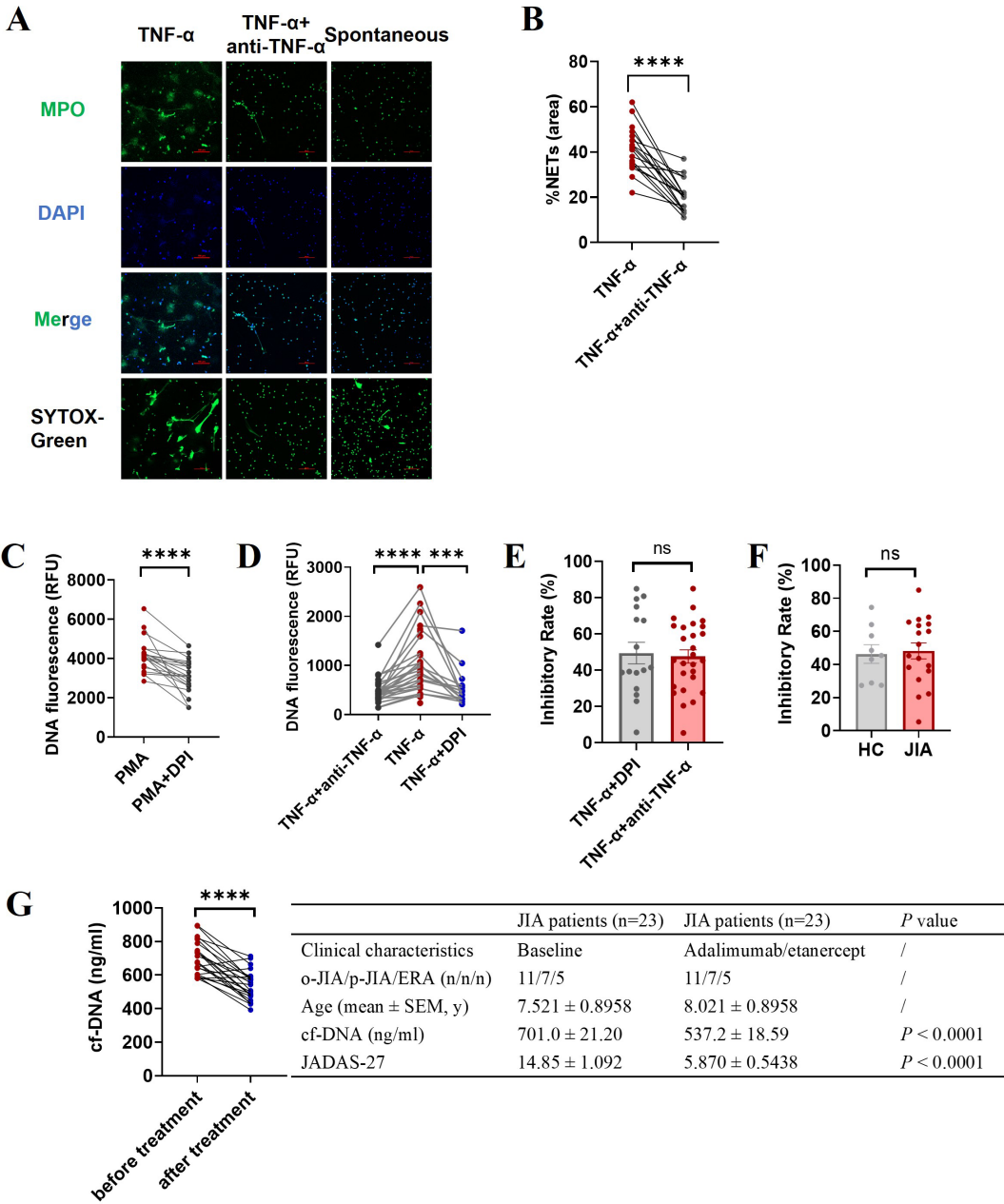


FIGURE 4
Effect of an anti-TNF- α antibody (adalimumab) on NET formation. Neutrophils isolated from JIA patients and HCs were pretreated with adalimumab (4 μ g/ml) prior to the addition of TNF- α . **(A)** Representative images of TNF- α induced NETs and minimal NET formation after adalimumab intervention. The third column is an image of spontaneous NET formation as a negative control. **(B)** The percentage of the NET-occupied area under TNF- α stimulation was significantly decreased in the presence of adalimumab ($n=18$, $41.22\% \pm 2.351$ vs. $20.39\% \pm 1.683$, $p < 0.0001$). **(C–F)** The levels of NET release were measured via microplate assays to further evidence the ability of adalimumab to inhibit NET generation. **(C)** DPI can effectively inhibit PMA-induced NETosis. **(D)** Adalimumab ($n=27$) and DPI ($n=16$) effectively inhibited TNF- α -induced NET formation ($n=27$). **(E)** Comparison of the inhibitory effects of adalimumab and DPI on TNF- α -induced NET formation. **(F)** The inhibitory rate of adalimumab in NETosis by neutrophils from JIA ($n=18$) and HCs ($n=9$) under TNF- α stimulation. **(G)** The effect of TNF- α inhibitors on cf-DNA concentration and JADAS27 in JIA patients. The data were analyzed with paired-sample *t* test or unpaired-sample *t* test. The bar graphs show the mean \pm SEM. *** $p < 0.001$, **** $p < 0.0001$, ns, nonsignificant.

and it has been verified that neutrophils are activated in JIA patients (6, 9). In this study, the capacity of neutrophils purified from patients with o-JIA, p-JIA, and ERA to generate NETs spontaneously and in response to TNF- α or PMA *in vitro* was significantly higher than that of cells derived from HCs (Figure 1). Importantly, patients with JIA had elevated plasma levels of cf-DNA and MPO-DNA complexes which were identified as NETosis-derived products compared to healthy controls (Figures 2A, B). Strangely, there was no significant difference in NET formation both *in vivo* and *ex vivo* among the three subtypes of JIA i.e., o-JIA, p-JIA, and ERA (Figures 1F, 2C). Therefore, we concluded that these activated neutrophils in JIA patients most likely contribute to the pathogenesis of JIA by releasing NETs.

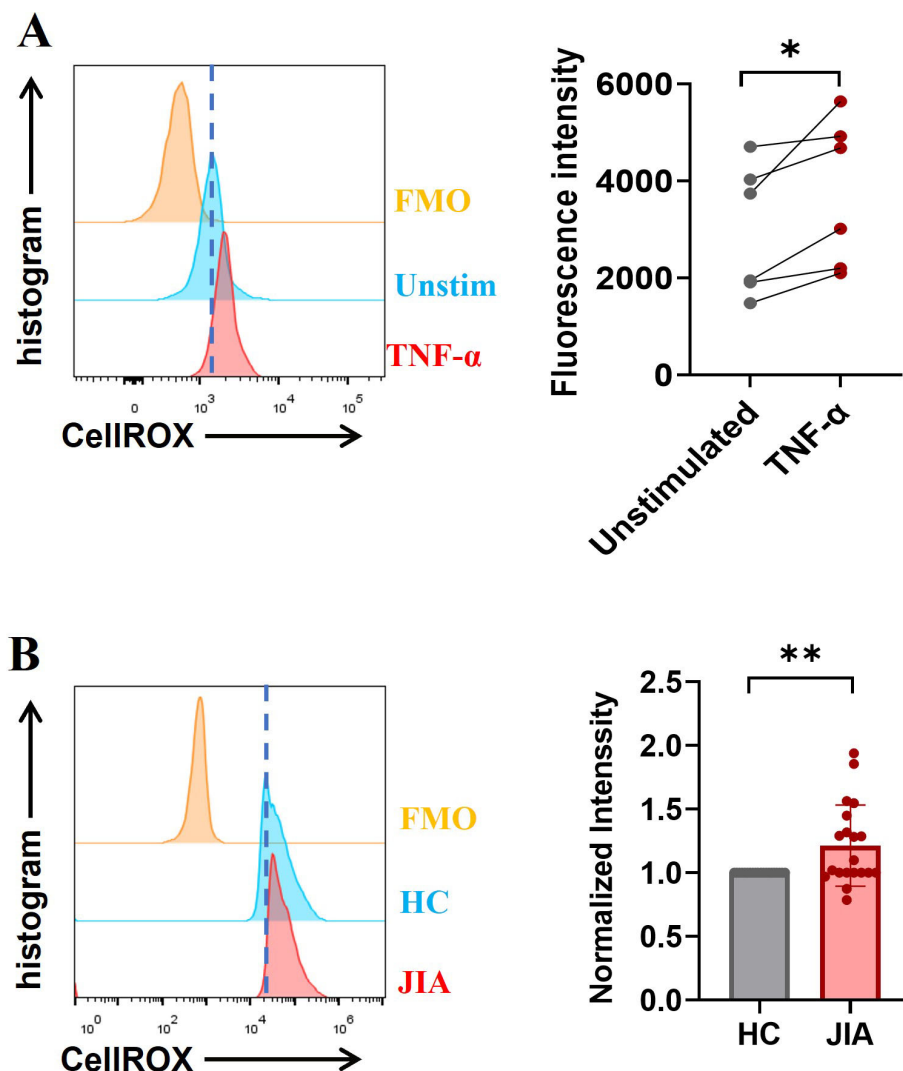


FIGURE 5

ROS levels were measured ex vivo using a FACSCalibur flow cytometer. (A) The exposure of neutrophils to TNF- α increased in the production of ROS. (B) Baseline ROS levels in neutrophils derived from JIA patients were higher than those in HC-derived neutrophils ($n = 20$; $p = 0.0074$). The paired-sample t test was used to analyze all the data. * $p < 0.05$, ** $p < 0.01$.

ROC curve analysis demonstrated that circulating levels of cf-DNA and MPO-DNA complexes could serve as potential diagnostic biomarkers for accurately distinguishing JIA patients from HCs (Figure 2D). In addition, although there was no significant correlation between the MPO-DNA complex levels and the JADAS27 in ERA patients, this was most likely due to the small sample size ($n = 8$), the plasma levels of MPO-DNA complex were associated with the JADAS27 in o-JIA and p-JIA patients (Figure 2F), and cf-DNA plasma concentrations were strongly and positively associated with the JADAS27 in patients with o-JIA, p-JIA and ERA (Figure 2E). We believed that plasma levels of NET-derived products in patients with JIA could be sufficient for monitoring disease activity, and could be used to predict disease flares. Recent research has also shown that NET formation is

increased in o-JIA patients and is correlated with the disease activity score (cJADAS10), but not in p-JIA patients (31), which are not entirely consistent with our conclusions. The main reason is likely due to their small sample size (o-JIA, $n = 4$ and p-JIA, $n = 3$). Our research not only examined a large sample size, but also investigated NET formation via *in vitro* stimulation studies and in the peripheral circulation of patients with o-JIA, p-JIA and ERA using a variety of methods, meaning that our study is more reliable than the previous data. In addition, there is rarely a study investigating NET formation in patients with JIA, we systematically explored NETosis in patients with the three subtypes of JIA i.e., o-JIA, p-JIA, and ERA, respectively.

Ayako Ohyama et al. have evidenced that there was significant CitH3 overexpression in pGIA (peptide glucose-6-phosphate

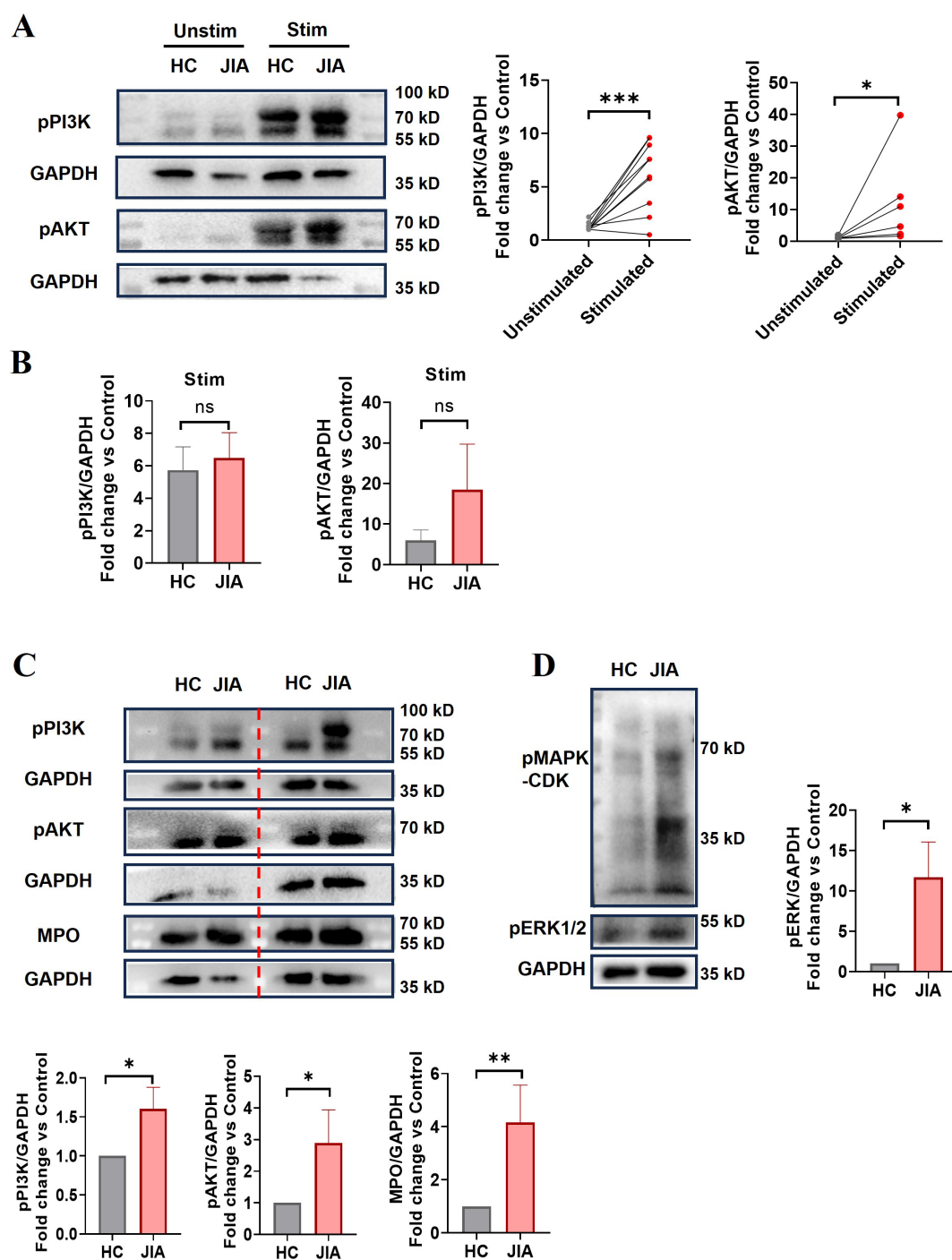


FIGURE 6

The expression levels of NET-associated signaling components. (A) The phosphorylation of PI3K and AKT in neutrophils purified from JIA patients and HCs before and after TNF- α stimulation (p-PI3K $n = 10$, $p = 0.0008$; p-AKT, $n = 6$, $p = 0.0313$). The paired-sample t test and Wilcoxon test were used to analyze the data. (B) Comparison of phosphorylated PI3K and AKT protein levels in neutrophils derived from JIA patients and HCs after TNF- α stimulation ($n = 5$, $p = 0.7340$; $n = 3$, $p = 0.3386$, respectively). (C) Phosphorylation of PI3K (15 HCs vs. 18 JIA patients, $p = 0.0222$) and AKT ($n = 10$, $p = 0.0135$) and the protein expression of MPO ($n = 15$, $p = 0.0012$) in neutrophils derived from JIA patients and HCs. (D) MAPK-CDK and ERK1/2 phosphorylation was assessed (6 HCs vs. 7 JIA patients $p = 0.0239$). (A, C, D) Representative western blots. The Mann-Whitney U test was used to compare two groups. Stim, stimulated; unstim, unstimulated. The bar graphs show the mean \pm SEM. * $p < 0.05$, ** $p < 0.01$, *** $p < 0.001$, ns, nonsignificant.

isomerase-induced arthritis) joints, and anti-IL-6 receptor antibodies could decrease neutrophilic infiltration and NETosis in the joints of pJIA (41). In addition, IL-6 inhibitors are highly effective and have been approved for use in systemic JIA (2).

However, correlation analysis revealed that cf-DNA concentration and IL-6 levels did not significantly correlate in JIA patients consisted of o-JIA, p-JIA and ERA patients, indicating IL-6 may not play a major role in o-JIA, p-JIA and ERA. Simple linear

regression of correlation studies showed that the number and percentage of neutrophils and CD19+ B cells, the levels of the systemic inflammatory markers TNF- α , hs-CRP and ESR, the serum IgG and complement C3 and C4 levels were strongly and positively correlated with cf-DNA levels (Figure 3A). However, only ESR and TNF- α levels are positively associated with cf-DNA concentration and are independent variables by multiple linear regression analysis (Figure 3B). TNF- α has been identified as a proinflammatory cytokine with a central role in arthritis, which was further proved by the clinical efficacy of the TNF- α inhibitions therapy in JIA (2). In this study, TNF- α could induce NET formation *in vitro* and the plasma concentration of cf-DNA (NETosis-derived product) was linked to the serum level of TNF- α *in vivo*, implying that TNF- α might augment inflammation by inducing NETosis in JIA patients, then lead to disease progression. ESR is a commonly objective biomarker for monitoring disease activity, and the association of cf-DNA levels with the ESR level further evidenced that cf-DNA concentration was closely associated with disease activity and could be used to monitor disease activity.

Previous work and our data confirmed that TNF- α could trigger NET formation (34) and NET-derived products in turn could act on other immune cells to secrete TNF- α (42). Therefore, there may be a vicious cycle between NETosis and TNF- α . Consequently, inhibiting NETosis in JIA patients could be useful for preventing the deleterious effects of NETs on inflammation. Anti-TNF- α biologics are effective in most JIA patients (2). However, the effect of TNF- α inhibitor therapies on NET release in JIA patients still requires further study. Recently, some research show that infliximab, a TNF- α inhibitor can inhibit NET formation and reduce disease activity in RA patients (43) and in radiographic axial spondyloarthritis patients (44). In this study, *in vitro* inhibition study showed that TNF- α -induced NET formation was substantially suppressed by adalimumab (Figures 4A, B). Furthermore, the ability of TNF- α inhibitors, including adalimumab and etanercept, to suppress NET formation significantly improved disease activity in JIA patients (Figure 4G).

Given that enhanced NET formation in the three JIA subtypes, the molecular mechanisms of NETosis in JIA patients and TNF- α -induced NETosis should be studied for NET-targeted therapy for JIA. Our study demonstrated that TNF- α -induced NET formation was markedly reduced in the presence of DPI (Figure 4D), and ROS production was increased in neutrophils following TNF- α administration (Figure 5A), suggesting that ROS generation by activated NADPH oxidases is required for TNF- α -induced NET formation. Several signaling pathways have been found to regulate the activation of NADPH oxidase, and PI3K-dependent signaling is the central pathway, and the blockade of which severely limits the activation of NADPH oxidase (37, 45), we thus examined the effect of TNF- α on PI3K-AKT-NADPH signaling activation and found TNF- α caused a dramatic increase in the phosphorylation levels of PI3K and AKT in neutrophils (Figure 6A), indicating that TNF- α -induced NETs might occur through a ROS- and PI3K-Akt

signaling-dependent pathways. Notably, NET formation in JIA patients might occur through activation of the PI3K-Akt-dependent and MAPK-ERK signaling pathways, followed by the production of ROS by NADPH oxidase and the subsequent activation of MPO, and CDKs, which was proven by increases in basal ROS production, the levels of phosphorylated PI3K and AKT, phosphorylated MAPK-CDKs and ERK1/2, and MPO expression in JIA-derived neutrophils (Figures 5B, 6C, D). Previous research has elucidated that NET formation can be initiated by various inflammatory cytokines (34) and various stimuli activate different NET-associated signaling pathways (45, 46). NETosis in JIA might occur through the activation of several signaling pathways, which might be closely associated with various stimuli. These findings may explain why NETosis is enhanced in JIA, and aid in the development of drugs that target NETs to improve the treatment of JIA. The molecular mechanism of NET formation in JIA is a preliminary study, which needs further systematic study.

In conclusion, NET formation was augmented in the three subtypes of JIA, i.e., o-JIA, p-JIA and ERA and might exert detrimental roles in JIA. Furthermore, TNF- α may be involved in the immunopathogenesis of JIA by enhancing NET formation. Importantly, NET-derived products: cf-DNA and MPO-DNA complex could be used as potential biomarkers for diagnosis and disease activity.

Data availability statement

The original contributions presented in the study are included in the article/supplementary material. Further inquiries can be directed to the corresponding author.

Ethics statement

The studies involving humans were approved by Wuhan Children's Hospital Committee for Research Ethics. The clinical trial registration number is 2023R015-E01. The studies were conducted in accordance with the local legislation and institutional requirements. Written informed consent for participation in this study was provided by the participants' legal guardians/next of kin.

Author contributions

HT: Writing – review & editing, Writing – original draft, Supervision, Resources, Methodology, Formal analysis, Conceptualization. YZ: Writing – review & editing, Project administration, Investigation. WY: Writing – original draft, Software, Formal analysis. YH: Writing – original draft, Software, Methodology. YL: Writing – original draft, Project administration,

Methodology. JC: Writing – original draft, Methodology, Data curation. TX: Writing – original draft, Methodology, Data curation. YW: Writing – original draft, Methodology, Data curation. TH: Writing – original draft, Methodology, Data curation. SY: Writing – original draft, Methodology, Data curation. FL: Writing – original draft, Data curation. RX: Writing – review & editing, Visualization, Methodology. RJ: Writing – review & editing, Validation, Resources, Project administration, Funding acquisition, Conceptualization.

Funding

The author(s) declare that no financial support was received for the research, authorship, and/or publication of this article.

References

- Petty RE, Southwood TR, Manners P, Baum J, Glass DN, Goldenberg J, et al. International League of Associations for Rheumatology classification of juvenile idiopathic arthritis: second revision, Edmonton 2001. *J Rheumatol.* (2004) 31:390–2. doi: 10.1016/j.japd.2021.05.014
- McCurdy D, Parsa MF. Updates in juvenile idiopathic arthritis. *Adv Pediatr.* (2021) 68:143–70. doi: 10.1016/j.japd.2021.05.014
- van Loosdregt J, van Wijk F, Prakken B, Vastert B. Update on research and clinical translation on specific clinical areas from biology to bedside: Unpacking the mysteries of juvenile idiopathic arthritis pathogenesis. *Best Pract Res Clin Rheumatol.* (2017) 31:460–75. doi: 10.1016/j.berh.2018.02.003
- Prakken B, Albani S, Martini A. Juvenile idiopathic arthritis. *Lancet.* (2011) 377:2138–49. doi: 10.1016/S0140-6736(11)60244-4
- Martini A, Lovell DJ, Albani S, Brunner HI, Hyrich KL, Thompson SD, et al. Juvenile idiopathic arthritis. *Nat Rev Dis Primers.* (2022) 8:5. doi: 10.1038/s41572-021-00332-8
- Jarvis JN, Petty HR, Tang Y, Frank MB, Tessier PA, Dozamorov I, et al. Evidence for chronic, peripheral activation of neutrophils in polyarticular juvenile rheumatoid arthritis. *Arthritis Res Ther.* (2006) 8:R154. doi: 10.1186/ar2048
- Sullivan KE. Inflammation in juvenile idiopathic arthritis. *Pediatr Clin North Am.* (2005) 52:335–357. doi: 10.1016/j.pcl.2005.01.002
- Macaubas C, Nguyen K, Milojevic D, Park JL, Mellins ED. Oligoarticular and polyarticular JIA: epidemiology and pathogenesis. *Nat Rev Rheumatol.* (2009) 5:616–26. doi: 10.1038/nrrheum.2009.209
- Metzemaekers M, Malengier-Devlies B, Yu K, Vandendriessche S, Yserbyt J, Matthys P, et al. Synovial fluid neutrophils from patients with juvenile idiopathic arthritis display a hyperactivated phenotype. *Arthritis Rheumatol.* (2021) 73:875–84. doi: 10.1002/art.41605
- Arve-Butler S, Schmidt T, Mossberg A, Berthold E, Gullstrand B, Bengtsson AA, et al. Synovial fluid neutrophils in oligoarticular juvenile idiopathic arthritis have an altered phenotype and impaired effector functions. *Arthritis Res Ther.* (2021) 23(1):109. doi: 10.1186/s13075-021-02483-1
- Wigerblad G, Kaplan MJ. Neutrophil extracellular traps in systemic autoimmune and autoinflammatory diseases. *Nat Rev Immunol.* (2023) 23(5):274–88. doi: 10.1038/s41577-022-00787-0
- Branzk N, Lubojemska A, Hardison SE, Wang Q, Gutierrez MG, Brown GD, et al. Neutrophils sense microbe size and selectively release neutrophil extracellular traps in response to large pathogens. *Nat Immunol.* (2014) 15:1017–25. doi: 10.1038/ni.2987
- Brinkmann V, Reichard U, Goosmann C, Fauler B, Uhlemann Y, Weiss DS, et al. Neutrophil extracellular traps kill bacteria. *Science.* (2004) 303:1532–5. doi: 10.1126/science.1092385
- Fuchs TA, Abed U, Goosmann C, Hurwitz R, Schulze I, Wahn V, et al. Novel cell death program leads to neutrophil extracellular traps. *J Cell Biol.* (2007) 176:231–41. doi: 10.1083/jcb.200606027
- Tan C, Aziz M, Wang P. The vitals of NETs. *J Leukoc Biol.* (2021) 110:797–808. doi: 10.1002/JLB.3RU0620-375R
- Jorch SK, Kubes P. An emerging role for neutrophil extracellular traps in noninfectious disease. *Nat Med.* (2017) 23:279–87. doi: 10.1038/nm.4294
- Khandpur R, Carmona-Rivera C, Vivekanandan-Giri A, Gizinski A, Yalavarthi S, Knight JS, et al. NETs are a source of citrullinated autoantigens and stimulate inflammatory responses in rheumatoid arthritis. *Sci Transl Med.* (2013) 5:178ra140. doi: 10.1126/scitranslmed.3005580

Conflict of interest

The authors declare that the research was conducted in the absence of any commercial or financial relationships that could be construed as a potential conflict of interest.

Publisher's note

All claims expressed in this article are solely those of the authors and do not necessarily represent those of their affiliated organizations, or those of the publisher, the editors and the reviewers. Any product that may be evaluated in this article, or claim that may be made by its manufacturer, is not guaranteed or endorsed by the publisher.

- Carmona-Rivera C, Kaplan MJ. Detection of SLE antigens in neutrophil extracellular traps (NETs). *Methods Mol Biol.* (2014) 1134:151–61. doi: 10.1007/978-1-4939-0326-9_11
- Denning N-L, Aziz M, Gurien SD, Wang P. DAMPs and NETs in sepsis. *Front Immunol.* (2019) 10. doi: 10.3389/fimmu.2019.02536
- Foussert E, Toes R, Desai J. Neutrophil extracellular traps (NETs) take the central stage in driving autoimmune responses. *Cells.* (2020) 9(4):915. doi: 10.3390/cells9040915
- Kahlenberg JM, Carmona-Rivera C, Smith CK, Kaplan MJ. Neutrophil extracellular trap-associated protein activation of the NLRP3 inflammasome is enhanced in lupus macrophages. *J Immunol.* (2013) 190:1217–26. doi: 10.4049/jimmunol.1202388
- de Bont CM, Boelens WC, Pruijn GJM. NETosis, complement, and coagulation: a triangular relationship. *Cell Mol Immunol.* (2018) 16:19–27. doi: 10.1038/s41423-018-0024-0
- Yipp BG, Petri B, Salina D, Jenne CN, Scott BN, Zbytniuk LD, et al. Infection-induced NETosis is a dynamic process involving neutrophil multitasking *in vivo*. *Nat Med.* (2012) 18:1386–93. doi: 10.1038/nm.2847
- Melbouci D, Haidar Ahmad A, Decker P. Neutrophil extracellular traps (NET): not only antimicrobial but also modulators of innate and adaptive immunities in inflammatory autoimmune diseases. *RMD Open.* (2023) 9(3):e003104. doi: 10.1136/rmdopen-2023-003104
- Tillack K, Breiden P, Martin R, Sospedra M. T lymphocyte priming by neutrophil extracellular traps links innate and adaptive immune responses. *J Immunol.* (2012) 188:3150–9. doi: 10.4049/jimmunol.1103414
- Gestermann N, Di Domizio J, Lande R, Demaria O, Frasca L, Feldmeyer L, et al. Netting neutrophils activate autoreactive B cells in lupus. *J Immunol.* (2018) 200:3364–71. doi: 10.4049/jimmunol.1700778
- Fang H, Shao S, Xue K, Yuan X, Qiao P, Zhang J, et al. Neutrophil extracellular traps contribute to immune dysregulation in bullous pemphigoid via inducing B-cell differentiation and antibody production. *FASEB J.* (2021) 35:e21746. doi: 10.1096/fj.202100145R
- Wilson AS, Randall KL, Pettitt JA, Ellyard JL, Blumenthal A, Enders A, et al. Neutrophil extracellular traps and their histones promote Th17 cell differentiation directly via TLR2. *Nat Commun.* (2022) 13:528. doi: 10.1038/s41467-022-28172-4
- Giaglis S, Hahn S, Hasler P. The NET outcome: are neutrophil extracellular traps of any relevance to the pathophysiology of autoimmune disorders in childhood? *Front Pediatr.* (2016) 4:97. doi: 10.3389/fped.2016.00097
- Schneider AH, Machado CC, Veras FP, Maganin AGM, de Souza FFL, Barroso LC, et al. Neutrophil extracellular traps mediate joint hyperalgesia induced by immune inflammation. *Rheumatol (Oxford).* (2021) 60:3461–73. doi: 10.1093/rheumatology/keaa794
- Heshin-Bekenstein M, Baron S, Schuler G, Shusterman A, Fidel V, Ben-Shahar Y, et al. Neutrophils extracellular traps formation may serve as a biomarker for disease activity in oligoarticular juvenile idiopathic arthritis: a pilot study. *Arthritis Res Ther.* (2023) 25(1):135. doi: 10.1186/s13075-023-03104-9
- Consolaro A, Ruperto N, Bazzo A, Pistorio A, Magni-Manzoni S, Filocamo G, et al. Development and validation of a composite disease activity score for juvenile idiopathic arthritis. *Arthritis Rheumatism.* (2009) 61:658–66. doi: 10.1002/art.24516
- Consolaro A, Giancane G, Schiappapietra B, Davi S, Calandra S, Lanni S, et al. Clinical outcome measures in juvenile idiopathic arthritis. *Pediatr Rheumatol Online J.* (2016) 14:23. doi: 10.1186/s12969-016-0085-5

34. Keshari RS, Jyoti A, Dubey M, Kothari N, Kohli M, Bogra J, et al. Cytokines induced neutrophil extracellular traps formation: implication for the inflammatory disease condition. *PLoS One*. (2012) 7:e48111. doi: 10.1371/journal.pone.0048111
35. Liu ML, Lyu X, Werth VP. Recent progress in the mechanistic understanding of NET formation in neutrophils. *FEBS J*. (2022) 289:3954–66. doi: 10.1111/febs.16036
36. Ravindran M, Khan MA, Palaniyar N. Neutrophil extracellular trap formation: physiology, pathology, and pharmacology. *Biomolecules*. (2019) 9(8):365. doi: 10.3390/biom9080365
37. Hawkins PT, Stephens LR. The role of PI3Ks in the regulation of the neutrophil NADPH oxidase. *Biochem Soc symposium*. (2007) 74:59–67. doi: 10.1042/BSS2007c06
38. Li M, Gao Y, Wang Z, Wu B, Zhang J, Xu Y, et al. Taurine inhibits Streptococcus uberis-induced NADPH oxidase-dependent neutrophil extracellular traps via TAK1/MAPK signaling pathways. *Front Immunol*. (2022) 13:927215. doi: 10.3389/fimmu.2022.927215
39. Hakkim A, Fuchs TA, Martinez NE, Hess S, Prinz H, Zychlinsky A, et al. Activation of the Raf-MEK-ERK pathway is required for neutrophil extracellular trap formation. *Nat Chem Biol*. (2010) 7:75–7. doi: 10.1038/nchembio.496
40. Amulic B, Knackstedt SL, Abu Abed U, Deigendesch N, Harbort CJ, Caffrey BE, et al. Cell-cycle proteins control production of neutrophil extracellular traps. *Dev Cell*. (2017) 43:449–462.e445. doi: 10.1016/j.devcel.2017.10.013
41. Ohya A, Osada A, Kawaguchi H, Kurata I, Nishiyama T, Iwai T, et al. Specific increase in joint neutrophil extracellular traps and its relation to interleukin 6 in autoimmune arthritis. *Int J Mol Sci*. (2021) 22(14):7633. doi: 10.3390/ijms22147633
42. Linhares-Lacerda L, Temerozo JR, Ribeiro-Alves M, Azevedo EP, Mojoli A, Nascimento MTC, et al. Neutrophil extracellular trap-enriched supernatants carry microRNAs able to modulate TNF-alpha production by macrophages. *Sci Rep*. (2020) 10:2715. doi: 10.1038/s41598-020-59486-2
43. Pérez-Sánchez C, Ruiz-Limón P, Aguirre MA, Jiménez-Gómez Y, Arias-de la Rosa I, Abalos-Aguilera MC, et al. Diagnostic potential of NETosis-derived products for disease activity, atherosclerosis and therapeutic effectiveness in Rheumatoid Arthritis patients. *J Autoimmun*. (2017) 82:31–40. doi: 10.1016/j.jaut.2017.04.007
44. Ruiz-Limon P, Ladehesa-Pineda ML, Castro-Villegas MDC, Abalos-Aguilera MDC, Lopez-Medina C, Lopez-Pedraza C, et al. Enhanced NETosis generation in radiographic axial spondyloarthritis: utility as biomarker for disease activity and anti-TNF-alpha therapy effectiveness. *J BioMed Sci*. (2020) 27:54. doi: 10.1186/s12929-020-00634-1
45. Thimmappa PY, Nair AS, Najar MA, Mohanty V, Shastry S, Prasad TSK, et al. Quantitative phosphoproteomics reveals diverse stimuli activate distinct signaling pathways during neutrophil activation. *Cell Tissue Res*. (2022) 389:241–57. doi: 10.1007/s00441-022-03636-7
46. Kenny EF, Herzig A, Kruger R, Muth A, Mondal S, Thompson PR, et al. Diverse stimuli engage different neutrophil extracellular trap pathways. *Elife*. (2017) 6:e24437. doi: 10.7554/eLife.24437



OPEN ACCESS

EDITED BY

Seng-Lai Tan,
Bicara Therapeutics, United States

REVIEWED BY

Gerson D. Keppeke,
Universidad Católica del Norte, Chile
Changrong Ge,
Karolinska Institutet (KI), Sweden

*CORRESPONDENCE

Yan Zhu
✉ zydzf2008@163.com

RECEIVED 25 May 2024

ACCEPTED 19 July 2024

PUBLISHED 16 August 2024

CITATION

Chen J, Cao Y, Xiao J, Hong Y and Zhu Y
(2024) The emerging role of neutrophil
extracellular traps in the progression of
rheumatoid arthritis.
Front. Immunol. 15:1438272.
doi: 10.3389/fimmu.2024.1438272

COPYRIGHT

© 2024 Chen, Cao, Xiao, Hong and Zhu. This is
an open-access article distributed under the
terms of the [Creative Commons Attribution
License \(CC BY\)](#). The use, distribution or
reproduction in other forums is permitted,
provided the original author(s) and the
copyright owner(s) are credited and that the
original publication in this journal is cited, in
accordance with accepted academic
practice. No use, distribution or reproduction
is permitted which does not comply with
these terms.

The emerging role of neutrophil extracellular traps in the progression of rheumatoid arthritis

Jingjing Chen¹, Yang Cao¹, Jing Xiao¹, Yujie Hong¹
and Yan Zhu^{2*}

¹The Geriatrics, Graduate School of Anhui University of Chinese Medicine, Hefei, China,

²The Geriatrics, The Second Affiliated Hospital of Anhui University of Chinese Medicine, Hefei, China

Rheumatoid arthritis (RA) is a chronic autoimmune disease with a complex etiology. Neutrophil extracellular traps (NETs) are NETWORK protein structures activated by neutrophils to induce the cleavage and release of DNA-protein complexes. Current studies have shown the critical involvement of NETs in the progression of autoimmune diseases. Neutrophils mostly gather in the inflammatory sites of patients and participate in the pathogenesis of autoimmune diseases in various ways. NETs, as the activated state of neutrophils, have attracted much attention in immune diseases. Many molecules released in NETs are targeted autoantigens in autoimmune diseases, such as histones, citrulline peptides, and myeloperoxidase. All of these suggest that NETs have a direct causal relationship between the production of autoantigens and autoimmune diseases. For RA in particular, as a disorder of the innate and adaptive immune response, the pathogenesis of RA is inseparable from the generation of RA. In this article, we investigate the emerging role of NETs in the pathogenesis of RA and suggest that NETs may be an important target for the treatment of inflammatory autoimmune diseases.

KEYWORDS

neutrophil extracellular trap, rheumatoid arthritis, autoantibody, citrullination, key role

1 Introduction

Rheumatoid arthritis (RA) is a systemic immune disorder mainly characterized by erosive joint damage involving the hands, wrists, ankles, knees, and other joints. In the early stage, the joints may become red, swollen, hot, and dysfunctional, and gradually deteriorate to stiffness and deformation in the late stage. At present, the pathogenesis of RA remains unclear, and its main pathological manifestations include immune cell infiltration, synovium hyperplasia and formation, and articular cartilage and bone destruction. Accumulating studies have been conducted regarding the molecular mechanisms of RA.

There are various breakthrough points for RA molecular mechanism research, and, among its autoantibodies, anti-citrullinated protein antibody (ACPA) is an important factor that cannot be ignored in RA disease development (1). With the increase in global life expectancy, the number of patients with RA is also rising, and the proportion of female patients is approximately three times that of male patients (2, 3). The incidence of RA is 0.5%–1%, affecting 0.2–1% of the global population. A positive family history can increase the risk of RA by approximately 3–5 times, and genetic factors cannot be ignored as a cause of RA (3). Studies have found that compared with non-RA patients, RA patients have a higher probability of suffering from multiple diseases (approximately 31–86%), a faster accumulation of comorbidity, a worse prognosis, a higher risk of disease activity, and a higher possibility of biologic agent failure. These data indicate that the clinical treatment of RA is urgent (4). Currently, disease-modifying anti-rheumatic drugs are still the first choice treatment for RA, and non-steroidal anti-inflammatory drugs and glucocorticoids have also been proven to reduce RA inflammation and pain (5). However, these drugs are also accompanied by inevitable shortcomings, such as side effects, adverse reactions, and drug resistance, and cannot really cure RA. Almost all RA patients need lifelong treatment; therefore, there is an urgent need for new treatment methods to delay the pathological process of RA and provide new therapeutic targets. Existing studies have pointed out the critical implication of neutrophils in the development of RA, and neutrophils abundantly exist in the synovial fluid and synovial tissue of RA joints (6, 7), while neutrophil extracellular traps (NETs) are important sources of citrullinated proteins and cytokines in RA and contribute to promoting the formation of ACPA. Additionally, NETs can promote the proliferation of synovial fibroblasts and produce cytokines, thus aggravating joint inflammation. Therefore, this article will explore the pathogenesis and role of NETs in RA and consider the potential and challenge of NETs as a new treatment strategy for RA, with a view to opening up new ways to prevent and treat RA.

2 Overview of NETs

2.1 The formation of NETs

Neutrophils are stimulated by phorbolate (PMA) and lipopolysaccharide (LPS). Brinkmann et al. found that the NETwork structure formed by chromatin in neutrophils had the potential of being an antibacterial barrier, and such NETwork structures containing DNA-protein were designated as NETs (8). NETs are fibrous structures released by neutrophils in response to specific stimuli. These structures are composed of neutrophil particles and decondensed chromatin coated with cytoplasmic proteins (9). NETs mainly bind neutrophil elastase (NE), myeloperoxidase (MPO), histone sphaerolysis concentrated chromatin, Caldwell protein, and defensin to capture and kill bacteria or viruses (8, 10). In the current situation regarding autoimmune diseases, a detailed proteomic analysis focusing on

the composition of specific NETs holds promise for revealing new mechanisms underlying disease onset and progression (11).

2.2 The NETosis pathway of NETs release

NETosis is a peculiar death modality of neutrophils that gives rise to the production of NETs (12), which contribute to the neutralization of invading pathogens and restoration of homeostasis. There are multiple stimuli that trigger NETosis but the mechanism by which NETosis releases NETs is not exactly the same. In spite of this, chromatin deconcentration is a necessary condition for NETosis (13). Here, we describe three pathways by which NETosis releases NETs (Table 1).

Suicidal NETosis, also known as NADPH oxidase-dependent NETs, is triggered by neutrophil receptors [such as toll-like receptor (TLR)] recognizing a variety of stimuli (such as bacteria, viruses, and fungi) and persists for a long time. Upon receiving the stimulation, calcium ions are first released from the endoplasmic reticulum (ER) into the cytoplasm, which increases the activity of protein kinase C (PKC) and induces nicotinamide adenine dinucleotide phosphate (NADPH) to form a functional complex (PHOX) through the RAF-MERK-ERK signaling pathway (14), leading to the production of reactive oxygen species (ROS) and the activation of receptor interacting protein kinase 3 (RIPK3) and mixed lineage kinase domain-like protein (MLKL). NADPH oxidase (NOX) activates PAD4, an enzyme downstream of ROS and calcium signals (15, 16). NE and MPO are released from azinotropic particles and transferred into the nucleus with the assistance of NADPH. The cleavage protein promotes chromatin decondensation, so that the decondensed chromatin containing cytoplasmic and granular components is excreted out of the cell (17), thus initiating programmed cell death (18). Relevant clinical evidence proves that suicidal NETosis requires the involvement of ROS. Neutrophils lacking sufficient ROS isolated from patients with chronic granulomatous disease fail to produce NETs under stimulation (19), and the use of NOX inhibitors can prevent the formation of NETs (20, 21) (Figure 1A).

Active NETosis, also known as non-NADPH oxidation-dependent NETs, is characterized by the fact that the nuclear membrane of neutrophils remains intact and active after the release of NETs, and neutrophils continue to migrate to bacteria, a process crucial for resisting bacterial invasion (22). NETs under this mechanism are released rapidly after exposure to *Staphylococcus aureus* through the secretion of chromatin and particles (23). Under this pathway, the formation of NETs can occur independently of the production of NADPH oxidase ROS. Specifically, PAD4 is activated in the presence of elevated levels of mitochondrial ROS and intracellular calcium (24), resulting in histone citrullination and chromatin decondensation, in which the DNA-protein complex envelopes the vesicles and releases its load outside the cell, without breaking the nuclear membrane in the process. To our knowledge, the difference between suicidal NETosis and critical NETosis lies in the dependence of the two approaches to NOX and whether the nuclear membrane is intact after chromatin release (Figure 1B).

TABLE 1 The difference between the three pathways of NETosis generation.

NETosis pathway category	Stimulating factor	Conductor receptor	Trigger key	DNA cleavage	Is the nuclear membrane intact
Suicidal NETosis	Virus, fungus, PMA	FcR	NADPH, NOX2, NE, MPO	Nuclear DNA	No
Active NETosis	Virus (<i>S. aureus</i>), fungus	TLR2/TLR4	Mitochondrial ROS, Ca ⁺ , NE, MPO	Nuclear DNA	Yes
Mitochondrial NETosis	CMS-CF/Ca5/LPS	TLR4	Mitochondrial ROS, NE, MPO	Mitochondrial DNA	NO

The third form of NETosis (mitochondrial NETosis) relies on the production of ROS, with living cells formed from mitochondrial DNA releasing NETs, instead of nuclear DNA. Mitochondrial DNA causes neutrophils to release NETs in response to granulocyte-macrophage colony-stimulating factor (GM-CSF) pre-treatment and LPS/C5a stimulation while retaining their nuclei (25, 26). Mitochondrial NETosis has also been observed in LPS-stimulated neutrophils isolated from trauma patients after orthopedic surgery (27). As reports on mitochondrial NETosis are currently limited, further studies on the mechanism of mitochondrial NETosis are needed to gain a deeper understanding (28). (Figure 1C).

2.3 Key factors triggering NETosis

Neutrophil activation is the first condition for NETosis production, and resting neutrophils under non-inflammatory conditions do not develop NETosis. Neutrophils can induce NETosis at surface pattern recognition receptors (29). In addition to the relevant receptors, NETosis can also be induced by bacterial toxins, such as ionomycin (30) and Nigericin (31). Therefore,

neutrophil activation requires the involvement of bacterial toxins or surface receptors to initiate NETosis (32). A large number of activated neutrophils and high levels of neutrophil granulocytes have also been found in the synovial and joint tissues of RA patients, which aggravate the proliferation and invasion of synovial cells activating cytokines and receptors to participate in the pathogenesis of RA (33), and relevant experiments have also yielded compelling evidence to support the activation of neutrophils and formation of NETs during the development of RA (34).

Changes in calcium concentration are also key to NETosis activation. Neutrophil activation will lead to an increase in intracellular calcium concentration, and the binding of ligand and complement receptor will trigger the ER to release stored calcium, and then open the plasma membrane calcium channel, resulting in a disturbance in the calcium ion balance. The increase of intracellular Ca²⁺ has been demonstrated to be a prerequisite for the production of NETs induced by optimal PMA (31, 35). In the context of NETosis, an increase in intracellular calcium has been observed in neutrophils induced by LPS, IL-8, and PMA, as well as by the calcium ion carriers ionomycin and A23187, leading to the formation of NETs (36). Therefore, the increase of intracellular

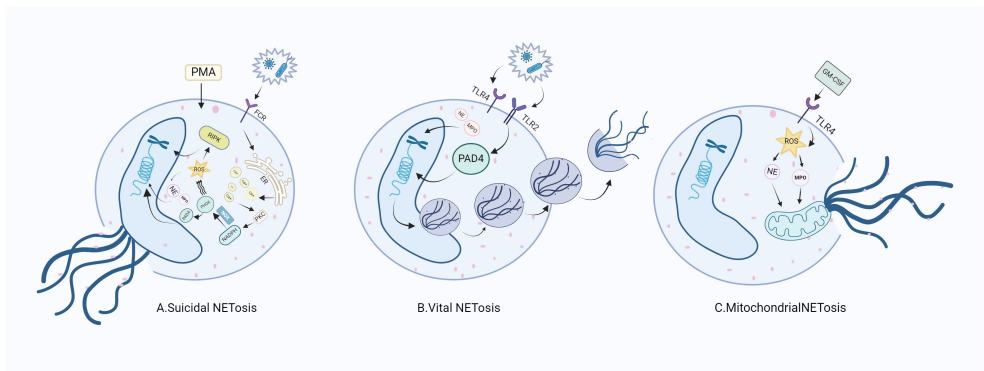


FIGURE 1 NETosis releases NETs through three different mechanisms. (A) After neutrophils are stimulated, ROS production is induced through the NADPH pathway to stimulate nuclear DNA cleavage, initiating the release of NE and MPO in neutrophils, which intensifies the direct cleavage of nuclear DNA and directly destroys the cell membrane, thus releasing NETs. (B) When stimulated, neutrophils do not depend on NADph-dependent ROS, but intracellular mitochondrial ROS can directly promote the activation of PAD4 and the release of NE and MPO, thus promoting the nuclear DNA wrapped in vesicles to release NETs. (C) Neutrophils generate NETs through the cleavage of mitochondrial DNA after stimulation. RA, rheumatoid arthritis; FcR, fragment crystallizable receptor; PMA, phorbol myristate acetate; ER, endoplasmic reticulum; PKC, protein kinase C; NADPH, nicotinamide adenine dinucleotide phosphate oxidase; NOX, nitric oxide; PIPK3: receptor interacting protein kinase 3; PAD4, peptidylarginine deiminase 4; NE, neutrophil elastase; MPO, myeloperoxidase; NETs, neutrophil extracellular traps; ROS, reactive oxygen species; TLR, toll-like receptor; GM-CSF, granulocyte macrophage colony-stimulating factor.

calcium, whether the calcium released from intracellular storage or the calcium flowing into the cell from the extracellular environment, is critical for NETosis.

PAD4, an enzyme mediated by calcium, plays a crucial role in NETosis (37). It is generally believed that PAD4 drives NETosis through citrullinated histones. PAD4 is highly expressed in neutrophils and ectopic to the nucleus in the presence of elevated cytosolic calcium concentration, and mediates the conversion of arginine residues to citrulline in the target protein (38). The internal force of PAD4 on citrullinated histones and its specific expression make it an important link mediating chromatin decondensation during NETosis (32). PAD4 itself is the target of autoantibodies and shows a high-expression profile in the synovium of RA. A positive correlation between the polymorphism of *PAD4* gene and the incidence of RA has been revealed (39, 40), which is better explained by the fact that the PAD4 inhibitor chloropyrimidine can alleviate the symptoms of collagen-induced arthritis (CIA) in mice and rats (41).

ROS production is also an important step involved in the formation of NETosis. ROS in neutrophils are mainly derived from NOX and mitochondria. Stimulating neutrophils with PMA, *S. aureus*, or group B *Streptococcus* can generate ROS within 20 min, and neutrophils with ROS scavengers can inhibit PMA-induced NETosis (20, 31). Neutrophils lacking functional NOX cannot develop NETosis under the stimulation of *S. aureus* or PMA (19). However, the exact mechanism by which NOX drives the release of NETs remains unclear (32). It has been shown that calcium ion-induced NOX-dependent NETosis is mediated by mitochondrial ROS (24). ROS are indispensable in all forms of NETosis and can promote the release of NE and MPO, thus accelerating the process of NETosis. However, its specific mechanism still needs further exploration.

3 The relationship between NETs and RA

Plenty of autoantibodies have been identified as markers of RA, including rheumatoid factor (RF) and antibodies against post-translational modified proteins [such as anti-citrullinated protein autoantibody (ACPA)] and carbamylation, which may form immune complexes within the joint and lead to the aggregation of immune cells (42). Compared with healthy individuals, RA patients present detectable activated neutrophils in the circulation, which can last for several days and accumulate in large numbers in the synovial fluid and vascular membranes of RA, leading to RA inflammation and joint destruction. The increase of neutrophils is associated with increased ROS production, elevated MPO expression, and increased citrullination mediated by PAD4 activity. Therefore, ROS, the NOX pathway, and PAD4 activity are important factors in controlling RA-inflammation-induced NETosis. High levels of ACPA and RF inducing NETosis can be detected in the serum of RA patients (43) and promote the further production of autoantigens in the form of citrullinated protein, resulting in persistent inflammation and tissue damage; abnormal NETs may exacerbate the expression of citrullinated autoantigens and immune-stimulating molecules, thereby

promoting the development of epitopes associated with RA pathogenesis. In addition, the formation of NETs promotes the recruitment of various inflammatory factors to the joint inflammation site, increasing cartilage injury and promoting the development of RA. NETs can increase the production of related pro-inflammatory factors such as IL-1 β and IL-18, further stimulating the formation of NETosis. These mechanisms contribute to inflammatory arthritis and joint destruction, thereby driving the onset of disease and the presentation of RA (44). Of course, the proper generation of NETs can activate the immunomodulatory response and alleviate the pathological process of RA by regulating T cells and dendritic cells, and NETs can also clear the apoptotic cells in joints and reduce the inflammatory response caused by these cells. We should strive to explore a balance point between optimal treatment and minimal impact and better clarify the relationship between RA and NETs. In the following article, we mainly explore the mechanism of the pathogenic effect of NETs on RA.

3.1 NETs induce the citrullination of RA

3.1.1 NETs promote the ACPA citrullination of RA

Currently, definitive diagnosis of RA depends on the detection of RF and ACPA (43), among which ACPA is recognized as one of the most important diagnostic biomarkers with high specificity and sensitivity. The specificity of ACPA is crucial for immunopathology caused by autoantibodies. Studies have shown that ACPA isolated from RA patients not only reacts with broad-spectrum citrulline peptides with different affinities but also shows heterogeneity (45). There are multiple types of structural interactions between ACPA and its citrulline antigen. ACPA interacts with citrulline and amino acid side chains and is specifically recognized or “cross-reacted” to citrulline labeled on joint proteins, showing an arthritic effect (46). Ge et al. have demonstrated that ACPA can promote proteoglycan consumption of cartilage and aggravate joint inflammation through the cross-reaction of specific ACPA with articular cartilage (47).

Citrullinated antigens on NETs play a key role in the initiation and development of autoimmunity and ACPA (48). Citrulline is derived from arginine through a post-translational modification of peptidyl arginine deiminase (PAD) and thus converted to citrulline protein (49). Exposure of citrulline protein to NETs is a key driver of autoimmunity, leading to the formation of ACPA (50). Citrulline vimentin itself is present in stimulated neutrophils or NETs, and anti-citrulline vimentin autoantibodies can induce the formation of NETs (43). At the same time, the release of NETs can further aggravate the production of ACPA, resulting in the production of inflammatory molecules such as IL-6, IL-8, chemokines, and adhesion proteins. As a result, ACPA continuously promotes neutrophils to release arginine deaminase (PADI), which can in turn modify arginine to citrulline. Thus, a vicious cycle of autoantibodies is formed (51). Moreover, it is pointed out that the exposure of citrullinated antigens by NETs to the immune system with the same citrullinated antigens and inflammatory cytokines will perpetuate NETosis (52). In addition, RA synovial cells exhibit an unusual pattern of citrullination known as cellular “hypercitrullination”. Hypercitrullination is induced by

perforin and membrane attack complex (MAC)-mediated membrane lysis pathways, which are activated in RA joints and produce ACPA (18, 53). It has also been shown that therapeutic anti-citrullinated protein autoantibody (tACPA, a therapeutic antibody that specifically recognizes citH2A and citH4) inhibits the formation of NETs in humans and mice induced by different physiological stimuli *in vivo* and *in vitro*, and that tACPA treatment prevents the release of NETs in a mouse model of CIA (54). In addition, NETs-derived NE can destroy cartilage structure and promote its citrullination, thereby increasing its immunogenicity and the production of autoantibodies and eventually leading to joint inflammation (55). Thus, NETs induce citrullination in RA patients and exacerbate RA symptoms.

3.1.2 NETs promote histone citrullination

Histone is an important component of NETs, and the histone levels in the synovial fluid of RA patients are increased compared with osteoarthritis patients. In neutrophils, PAD4-induced histone amination is a key step in NETosis, enabling the apparent release of active PDA4 into the synovial fluid of RA patients, promoting the production of autoantibodies and leading to inflammation (56). Additionally, extracellular histone plays a similar role. Owing to the inflammatory properties of NETosis and the characteristics of extracellular histone, the extracellular histone in RA synovial fluid interacts with other cells in the joint, amplifying the pro-inflammatory role of histone in RA inflammation (57). NETs that spontaneously express citrulline histone H3 (Cit-H3) have higher levels in the neutrophils of RA patients, which intensify the local

production of ACPA and accelerate the development of inflammation (58, 59). In addition, NETs directly induce STAT3 phosphorylation by interacting with TLR2 expressed on T cells through histone, which promotes the differentiation and activity of TH17 cells in the presence of Th17-cell-promoting cytokines (60), while it is known that TH17 cells can promote the of recruitment neutrophils through IL-17. Thus, histone exacerbates inflammation in RA patients by increasing the recruitment of inflammatory cells to the lesion site (Figure 2).

3.2 NETs stimulate inflammatory factors to induce synovial inflammation in RA

In RA synovium, the activation of macrophage-like synoviocytes (MLSs) underlies an important source of cytokines and proteases (61). MLSs produce several pro-inflammatory factors, including IL-6, IL-8, and tumor necrosis factor (TNF)- α , while the involvement of TNF- α and IL-6 is the core of the pathogenesis of RA. Through a series of studies in TNF-knockout mice, Kruglov et al. revealed that membrane TNF (memTNF) possesses anti-arthritic protective function and inhibits self-reactive T cells (62). TNF can also regulate the progression of arthritis by promoting the activation of Fibroblast-like synoviocytes (FLSs) and inducing autoantibodies. On the other hand, T-cell-derived TNF has been shown to play a defensive role by mobilizing the development of auto-reactive T cells (63). NETs can also directly mobilize T-cell function, induce an

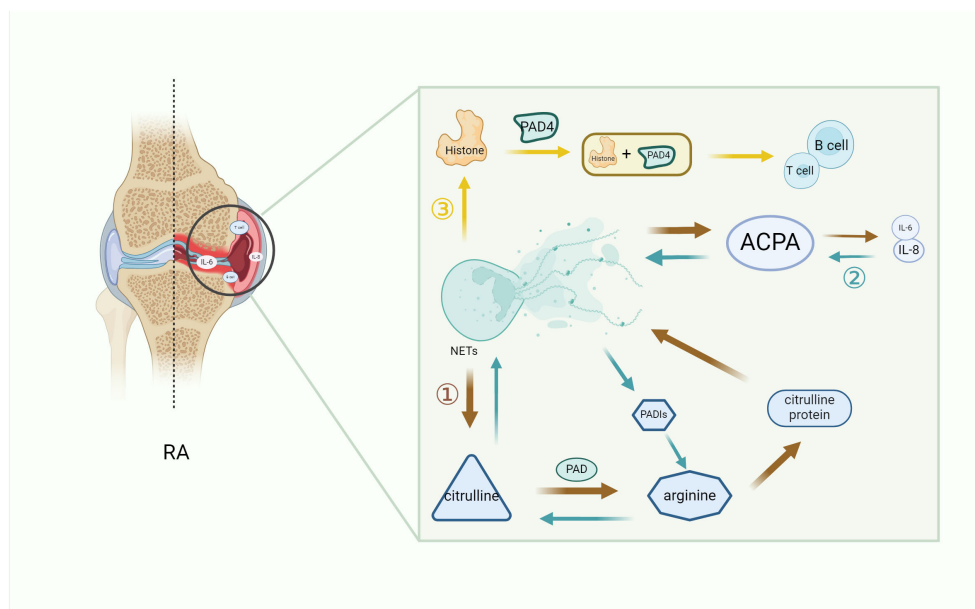


FIGURE 2

The key role of NETs in RA inflammation. NETs increase the secretion of immune cells and pro-inflammatory factors by promoting the citrullination of RA autoantibodies (1) and histones (3), while ACPA continuously promotes the formation of pro-inflammatory factors to promote citrullination (2), thus forming a vicious cycle and exacerbating the symptoms of RA. (1) Citrulline antigen in NETs is modified by PAD to form arginine, which promotes the production of citrulline protein and development of ACPA in NETs, thereby secreting pro-inflammatory factors and worsening RA. (2) The increase of pro-inflammatory factors leads to an increase in ACPA, and the reverse conversion of arginine into citrulline through PADIs leads to a vicious cycle of autoantibody formation. (3) The histones produced by NETs, which are citrullinated by PDA4, produce immune cells and aggravate RA. NETs, neutrophil extracellular trap; PADIs, arginine deiminase; IL-6, interleukin 6; IL-8, interleukin 8; B cell, B lymphocyte; T cell, T lymphocyte; PAD, peptidyl arginine deiminase; PAD4, peptidyl arginine deiminase 4; RA, rheumatoid arthritis.

increase in CD69 and CD25 expression, and lead to the activation of CD4⁺T cells, which have the potential to form inflammation and adaptive immune response (64). Studies have shown that in CD4⁺T lymphocytes of RA patients, CD28-CD4⁺T cells overexpress Bcl-2, leading to atypical clonal expansion of autoimmune T cells (65). A large number of T cells infiltrate the synovial membrane and interact with dendritic cells (DC), monocytes and macrophages to jointly mediate synovial inflammation. At the same time, the localization of NETs by synovial macrophages is inseparable from the signaling of B cells. Studies have shown that NE contained in NETs promotes the secretion of inflammatory cytokines in macrophages by activating the nuclear factor K light chain enhancer (NF- κ B) signaling pathway of B cells, and induces macrophage inflammation to aggravate RA synovial inflammation in the same way as Rab5a (66). These studies all indicate the important role of TNF- α , immune cells, and related inflammatory factors in the progression of RA. The production of NETs can promote the secretion of IL-6 (67) and TNF- α in macrophages, thus aggravating RA synovitis. At the same time, chemokines IL-8 and IL-17 contribute to the stimulation and aggregation of neutrophils to inflammatory sites. Brinkmann et al. found that IL-8 can stimulate neutrophils to produce NETs (8, 18). Ritika Khandpur et al. compared RA neutrophils with control neutrophils and found that RA neutrophils are more likely to develop NETosis after exposure to IL-17A and TNF- α (43). Interestingly, NETs have been observed to be internalized by macrophages and promote the secretion of cytokines, and the inhibition of NETs can alleviate inflammation by reducing the secretion of cytokines from macrophages (66). The production of NETs promotes the secretion of pro-inflammatory factors in MLSs, while exacerbating the distribution of inherently existing inflammatory factors in the diseased joints and exacerbating synovial inflammation.

3.3 NETs aggravate articular cartilage injury in RA

RA is characterized by persistent synovial inflammation, leading to articular cartilage and bone injury. FLSs, as the main effectors in cartilage injury (68), exhibit an aggressive phenotype and produce pathogenic inflammatory mediators, such as cytokines. Additionally, they produce mechanodegrading enzymes, especially matrix metalloproteinases and histoproteinases (69), to promote local inflammation and disease persistence (70). FLSs exhibit key immunomodulatory effects through direct interactions between secreted inflammatory cytokines and direct synovial-infiltrating immune cells (71). Specifically, the lining layer of the synovium of the joint is hyperplastic in RA, sometimes to a depth of 10–15 cells, and at the joint boundary, the lining layer may become a “pannus” tissue rich in FLSs and osteoclasts. Pannus is composed of macrophages, FLSs, dendritic cells or plasma cells, and mast cells, which mediate injury and erosion in the later stages of disease (61). Moreover, it invades adjacent articular cartilage and subchondral bone to produce inflammatory cytokines and chemokines, resulting in clinical symptoms such as swelling and pain (72).

Owing to the abundant infiltration of neutrophils in RA synovium, NETs are prone to form. The circulating neutrophils in RA patients are more likely to be stimulated by NETosis than those in healthy subjects, resulting in excessive innate and adaptive immune responses (73). NETs containing citrulline and arthrogenic peptide are internalized by FLSs via the RAGE-TLR9 endocytosis pathway, resulting in a pro-inflammatory phenotype in these cells. Once internalized, NETs promote the upregulation of MHC class II (MHCII) and load arthritogenic NET peptides into MHCII, which NETs then transport to FLS membranes where they are presented to antigen-specific T cells. This process promotes T-cell activation and B-cell response, leading to the production of ACPA and spread of inflammatory responses, eventually insulting cartilage injury (68). In short, the secretion of pro-inflammatory cytokines by FLSs exposed to extracellular traps may further increase NETosis, amplify exposure to citrulline autoantibodies, and promote the production of autoantibodies in patients, thus exacerbating cartilage injury (43). Carmona-Rivera et al. pre-incubated RA-FLSs with TLR antagonists, followed by exposure to RA-NETs, and found that the ability to internalize MPO (a molecule present in NETs) was impaired, demonstrating that FLSs internalize NETs via the RAGE-TLR9 axis and the induced pro-inflammatory features of FLSs are dependent on NETs internalization (68). Elastase in NETs can disrupt the cartilage matrix (50), and MMP8 and MMP9 have been found in RA-NETs to cause degradation of the cartilage matrix (74, 75), exacerbating cartilage injury. In addition, the immune complex formed by autoantibodies can activate macrophages to release pro-inflammatory factors, which amplify cartilage injury by releasing elastase from neutrophils (76) and trigger the occurrence of RA. NETs promote the rapid formation of osteoclasts by monocytes via the transduction of TLR4 and the NET-related protein pathway, directly affecting RA-related bone erosion (77). NETs stimulate the release of Rankl, inhibit the secretion of osteophosphorin in osteoblasts, and facilitate the formation of osteoclasts. Inhibition of NETs is a promising strategy for reducing bone erosion in patients with RA (78) (Table 2; Figure 3).

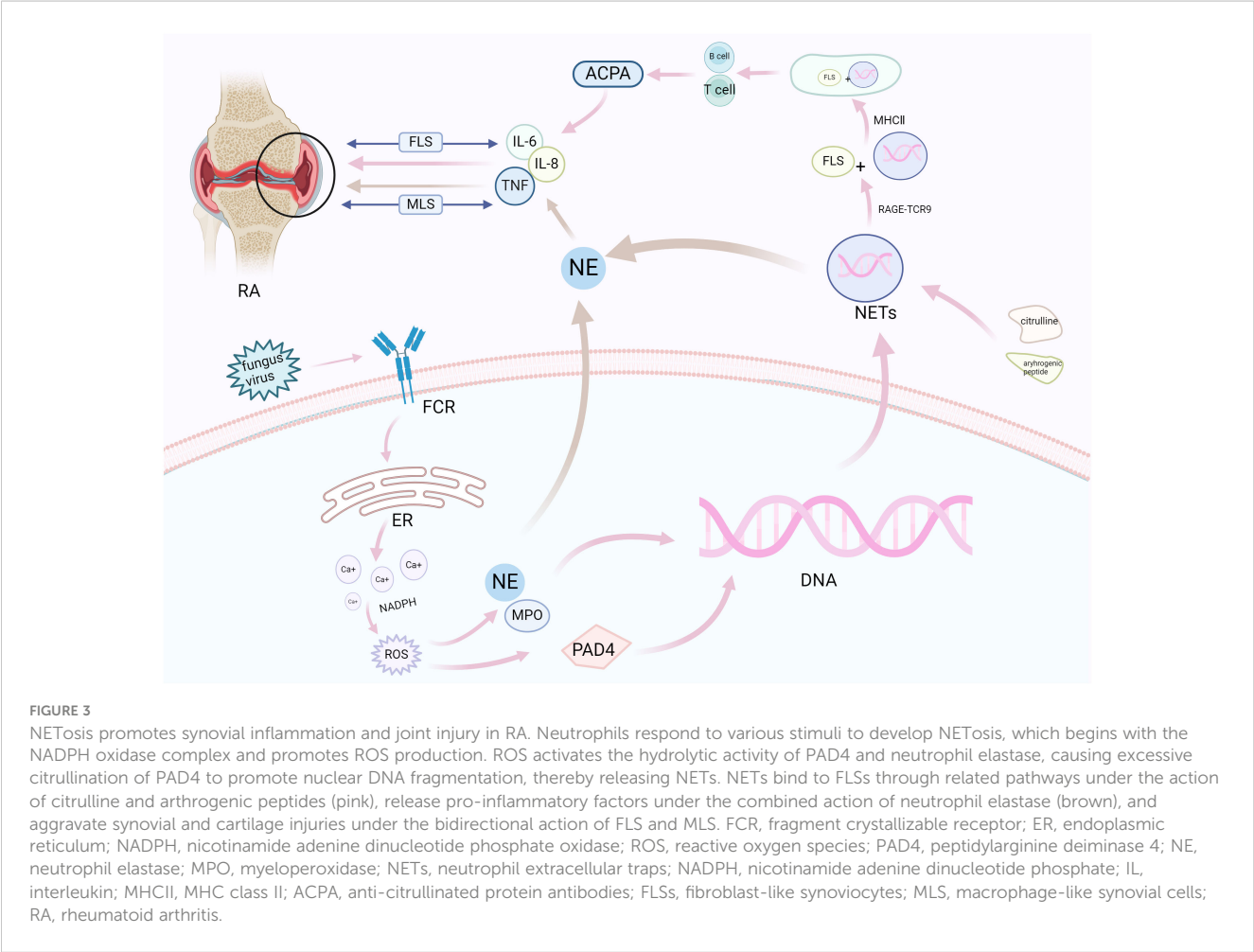
4 NETs may be the key target for controlling RA

The relevant mechanisms proposed in this study indicate that inhibition of NETs can be a key entry point for the treatment of RA. Quite a few reports have pointed out that the use of NET inhibitors can markedly mitigate joint swelling and inflammation. Alleviating the pathological process of RA by inhibiting the generation of NETs is also a hot topic at present. However, owing to the diversity and uncertainty of the pathways generating NETs in RA, there is still much room for further research on NETs. The increased level of NETs in synovial fluid may be attributed to the impaired or inhibited activity of DNA-1, and DNase can effectively eliminate NETs and inhibit the proteolytic enzyme activity of NE (79). Hence, DNase I is considered for the treatment of RA (80). In addition, the use of PAD4 inhibitors in K/BxN mouse models can effectively inhibit the formation of NETs, alleviate the degree of joint swelling,

TABLE 2 Studies on the role of NETs in RA.

The role of NETs in RA		Main findings
Citruination of RA was induced	Citruination of autoantibody (ACPA)	Increased NETs was observed in the peripheral blood and synovium of patients with RA, as were externalizing citrulline autoantibodies, which play a pathogenic role in RA (43) In CIA mouse models, the release of NETs was inhibited after tACPA treatment (54)
	Histone citruination	Citruination of histones via PAD4 promotes the production of ACPA and NETs (59) In RA risk subjects compared with controls, the results showed that NETs of citrulline protein increased, promoting ACPA production and supporting the underlying mechanism of ACPA production (58)
Stimulating inflammatory factors induced synovial inflammation of RA		IL-6 and other inflammatory factors are key factors in the pathogenesis of RA (62) Neutrophils are stimulated by IL-8 to promote the production of NETs (8) NETs are internalized by macrophages, which further produce inflammatory factors (66)
Aggravate synovial inflammation of RA		FLSs internalize NETs containing arthrogenic peptides via the RAGE-TLR9 axis, promoting inflammatory response and cartilage damage (68) MMP plays an important role in cartilage degradation. There is a need to investigate the development of Antibody (Ab)-induced arthritis in MMP-2/MMP-9 mice (75) Elastase derived from NETs was found in the peripheral blood of RA patients to magnify cartilage injury and aggravate RA inflammation (76)

and significantly reduce the fibrous structure of NETs (81). As NETs are involved in the pathological process of RA, scholars have described a monoclonal antibody (Cit-013) with a high affinity for Cit-H2 and H4, which bears significant anti-inflammatory effects and inhibits the metabolism of NETs *in vivo*. Epitope detection of RA synovium has proven the potential of Cit-013 in targeting excess citruination in RA and provided new insights into the development of antagonists for NETs in the treatment of RA (82). In addition, a large number of studies have demonstrated the feasibility of natural extracts targeting NETs to improve RA.



Quercetin inhibits neutrophil infiltration and diminishes plasma inflammatory cytokines, promotes apoptosis of activated neutrophils, and inhibits NETosis by regulating autophagy in RA mice, making it an ideal candidate in the management of RA (83). Emodin, a natural anthraquinone derivative, accelerates apoptosis but inhibits autophagy and NET formation by reducing IL-6 and TNF- α in mice with adjuvant arthritis (AA) (84). In CIA mice, polydatin (PD) reduces NET formation in myeloid neutrophils and RA patients, and treatment with PD reduces NET deposition in the ankle (85). In addition, apocynin and paeonol (APPA) can downregulate ROS levels, reduce NET formation, and inhibit TNF- α -induced cell conduction, fulfilling an anti-inflammatory role and exerting a potential therapeutic effect in RA (86). Tanshinone IIA (TIIA), by virtue of its favorable antioxidant and anti-inflammatory effects, can effectively diminish IL-6 and TNF- α levels in a mouse model of AA, reduce the formation and infiltration of NETs, and alleviate cartilage erosion of mouse ankle joint (87). *Cayratia albifolia* C.Li (CAC), as a widely used herbal medicine in autoimmune diseases, can increase anti-inflammatory activity by regulating the PI3K-Akt-mTOR signaling pathway to target NETs and macrophages, which effectively alleviates inflammatory damage in the hind paws of CIA rats and represents another effective candidate for the treatment of RA (88).

In addition, calprotectin released by NETs is identified as an inflammatory marker of RA. Calprotectin is an antimicrobial peptide mainly secreted by neutrophils, which can regulate intracellular calcium ion concentration and play an important role in immune response (89). The activation of neutrophils elevates the intracellular calcium concentration. Neutrophils release S100A8/A9 through NETosis, and the high level of S100A8/A9 found in the serum of RA patients may be caused by the disorder of NETosis (90). S100A8/A9 has been recognized as another important inflammatory marker of RA (91, 92), highlighting the exact contribution of NETosis. Calprotectin has been previously reported to increase inflammatory responses by inducing peripheral blood mononuclear cells to secrete cytokines and activating β 2 integrins of neutrophils (93). Therefore, in the diagnosis of RA, calcairein protein can be tried as a related inflammatory marker, and the development of NETs as potential biomarkers for the diagnosis and disease monitoring of RA is still an area that needs our continuous efforts. Although preclinical studies have shown that the effective inhibition of NETs is an important measure in the treatment of RA, most relevant studies remain in preclinical studies, and approved drugs targeting NETs are very scarce, such as drugs targeting PAD4 that have not been approved for human use (94). We should strive to find drugs that can specifically block NETs and explore different pathways to inhibit NETs more deeply to better promote the development of clinical therapies for RA.

5 Discussion

As the product of neutrophils, NETs exert anti-inflammatory effects and resist inflammation by acting as microorganisms that capture and kill pathogens. On the other hand, the production of

NETs under improper activation leads to tissue damage and recruits relevant pro-inflammatory factors or proteins to promote the release of inflammation, thereby amplifying joint and synovial inflammation and insulting cartilage injury in RA. Under this mechanism, the targeting of NETs has been demonstrated as an important therapeutic strategy in the management of RA. Repressing the improper activation of NETs induced by neutrophils can alleviate joint inflammation in RA. One of the anti-inflammatory mechanisms of methotrexate (MTX), a common drug used in the treatment of RA, is to reduce the production of cytokines by upregulating the level of adenosine on neutrophils, especially the inhibition of TNF- α and IL-1 β , which reduces the accumulation of white blood cells in the inflammatory site (51). Infliximab can also reduce the activation of white blood cells in the synovium of RA patients to reduce the inflammatory response (6). It is also possible to develop anti-inflammatory targets for RA based on the key factors triggering NETs. For example, the generation of ROS is an indispensable link in NETosis. Although the generation mechanism of NETs in RA has not been fully elucidated, the NOX-dependent pathway is considered the key pathway (43). By reducing the activation of NOX and maintaining the stability of mitochondrial membrane, the generation of ROS can be reduced to block lipid peroxidation, further repressing the formation of NETs and release of inflammatory factors, thus slowing down the occurrence of RA inflammation. Moreover, NE also promotes the formation of NETs. Inhibition of NE can reduce NET-mediated tissue damage and improve the efficacy of drugs to prevent the formation of NETs, without the shock caused by endotoxin (95). Although the specific mechanism and method mentioned above still need to be further explored, they can provide new ideas that may contribute to solving the global issue of RA.

From another perspective, we can also start from the pathogenesis of RA, the most striking of which is the pro-inflammatory effect generated by the interaction of cytokines induced in several ways. In addition to the induction of cytokines by NETs, the activation of other cells can also promote the release of inflammatory factors and aggravate joint inflammation. For example, macrophages can be activated by a variety of pathways, including TLR ligands, soluble proteases, cholesterol derivatives, and immune complexes. ACPA and RF act through Fc γ R1 and Fc γ R3 expressed on synovial macrophages, inducing high levels of cytokines to produce pro-inflammatory effects (96). Whether NETs co-activate inflammatory factors with other cells and their association with other cells need to be explored continuously. Further studies on the mechanism of RA cytokines can also provide a deeper understanding of the pathogenesis of RA and contribute to the development of new therapeutic targets.

Currently, cell therapy based on mesenchymal stem cells (MSCs) has become an effective treatment for autoimmune diseases, which increases the severity of arthritis in RA mouse models by inhibiting inflammatory factors and promoting the differentiation of regulatory T cells (TREGs) (97). Human gingival-derived mesenchymal stem cells (GMSCs) can inhibit the formation of NETs by inhibiting the PGE2-KA-ERK signaling pathway to improve RA (98). This method provides a new direction for NET targeting research in RA and is worthy of further study.

However, at present, the treatment of RA with NETs as the target is mostly at the research stage of animal models, e.g., PAD4 inhibitors. Although such drugs have been applied in animal and cell studies, there are still many shortcomings, and further studies are needed in the aspects of body selectivity and adverse reactions. Moreover, there is a large amount of evidence of citrullination in human RA, but in the serum transfer model, mice lacking PAD4 still show joint inflammation, indicating that citrullination of the NET component is not required in this model, and there is a great difference in the induction of NETs between mice and humans (99). Therefore, how to reduce the difference between animal models and human RA? And whether the targeted therapy of NETs in animal models can be realized in humans is still a question that we need to explore.

In this study, we mainly introduced the pathogenic role of NETs in RA, and a number of studies have shown that inhibiting the production of NETs has a good effect on alleviating the inflammatory symptoms of RA. However, some studies have shown that the use of PAD4 inhibitors in the Neonates with necrotizing enterocolitis (NEC) model characterized by bacteremia reduces the production of NETs but aggravates the inflammatory response of mice. At the same time, bacterial translocation and mortality were increased (100), and related studies found that PAD4-dependent NETs were essential for the intestinal clearance of *Citrobacter rodentium* intestinal infection, suggesting the beneficial effect of NETs (101). These conflicting results suggest that the effect of NETs on different diseases is not static, and future studies are needed to further investigate the role of NETs in RA and other diseases and explore the beneficial therapeutic effects of NETs in various diseases, including RA.

RA is a global concern, and its exact pathogenesis needs further exploration. This article briefly summarizes the production of NETs and their influence on the pathogenesis of RA, and proposes the key role of NETs in the pathogenesis of RA. To sum up, given the critical implication of NETs in RA, the targeting of NETs is a promising application in the treatment of RA. In-depth exploration of the pathogenesis of NETs in RA is expected to lead to the development of more effective treatment strategies for RA.

References

- Kurowska W, Kuca-Warnawin EH, Radzikowska A, Maslinski W. The role of anti-citrullinated protein antibodies (ACPA) in the pathogenesis of rheumatoid arthritis. *Cent Eur J Immunol*. (2017) 42:390–8. doi: 10.5114/ceji.2017.72807
- Aletaha D, Smolen JS. Diagnosis and management of rheumatoid arthritis: A review. *JAMA*. (2018) 320:1360–72. doi: 10.1001/jama.2018.13103
- Smolen JS, Aletaha D, McInnes IB. Rheumatoid arthritis. *Lancet*. (2016) 388:2023–38. doi: 10.1016/S0140-6736(16)30173-8
- Katz J, Bartels CM. Multimorbidity in rheumatoid arthritis: literature review and future directions. *Curr Rheumatol Rep*. (2024) 26:24–35. doi: 10.1007/s11926-023-01121-w
- Abbasi M, Mousavi MJ, Jamalzehi S, Alimohammadi R, Bezvan MH, Mohammadi H, et al. Strategies toward rheumatoid arthritis therapy: the old and the new. *J Cell Physiol*. (2019) 234:10018–31. doi: 10.1002/jcp.27860
- Wittkowski H, Foell D, af Klint E, Rycke LD, Keyser FD, Frosch M, et al. Effects of intra-articular corticosteroids and anti-TNF therapy on neutrophil activation in rheumatoid arthritis. *Ann Rheum Dis*. (2007) 66:1020–5. doi: 10.1136/ard.2006.061507
- Turunen S, Huhtakangas J, Nousiainen T, Valkealahti M, Melkko J, Risteli J, et al. Rheumatoid arthritis antigens homocitrulline and citrulline are generated by local myeloperoxidase and peptidyl arginine deiminases 2, 3 and 4 in rheumatoid nodule and synovial tissue. *Arthritis Res Ther*. (2016) 18:239. doi: 10.1186/s13075-016-1140-9
- Brinkmann V, Reichard U, Goosmann C, Fauler B, Uhlemann Y, Weiss DS, et al. Neutrophil extracellular traps kill bacteria. *Science*. (2004) 303:1532–5. doi: 10.1126/science.1092385
- Wang N, Ma J, Song W, Zhao C. An injectable hydrogel to disrupt neutrophil extracellular traps for treating rheumatoid arthritis. *Drug Delivery*. (2023) 30:2173332. doi: 10.1080/10717544.2023.2173332
- Chu C, Wang X, Yang C, Chen F, Shi L, Xu W, et al. Neutrophil extracellular traps drive intestinal microvascular endothelial ferroptosis by impairing Fundc1-dependent mitophagy. *Redox Biol*. (2023) 67:102906. doi: 10.1016/j.redox.2023.102906
- Foussert E, Toes R, Desai J. Neutrophil extracellular traps (NETs) take the central stage in driving autoimmune responses. *Cells*. (2020) 9:915. doi: 10.3390/cells9040915
- Steinberg BE, Grinstein S. Unconventional roles of the NADPH oxidase: signaling, ion homeostasis, and cell death. *Sci STKE*. (2007) 2007:pe11. doi: 10.1126/stke.3792007pe11
- Reis LR, Souza JD, Tomasini R, Cardoso AB, Mascio PD, Ronsein GE, et al. Citrullination of actin-ligand and nuclear structural proteins, cytoskeleton reorganization and protein redistribution across cellular fractions are early events in

Author contributions

JC: Writing – original draft. YC: Writing – review & editing. JX: Writing – review & editing. YH: Writing – review & editing. YZ: Writing – review & editing.

Funding

The author(s) declare financial support was received for the research, authorship, and/or publication of this article. This study was supported by 2023 Provincial Clinical Key Specialty Construction Project [Anhui Health Letter(2023) No.320]; Health Outstanding Talent Program [(2022)No.392]. National Natural Science Foundation of China Project: Triggering synovial hyperplasia via succinylation of sphingosine kinase 1 via glycolytic enzyme PKM2: A new mechanism of geniposide “Treating rheumatoid arthritis from toxicity and Collars”; 82374117. Provincial Department of Education (Key project): Study on the mechanism of moxibustion to improve synovitis in AA rats by inhibiting “NETs-NLRP3 inflammatome pathway”; 2023AH050858.

Conflict of interest

The authors declare that the research was conducted in the absence of any commercial or financial relationships that could be construed as a potential conflict of interest.

Publisher's note

All claims expressed in this article are solely those of the authors and do not necessarily represent those of their affiliated organizations, or those of the publisher, the editors and the reviewers. Any product that may be evaluated in this article, or claim that may be made by its manufacturer, is not guaranteed or endorsed by the publisher.

- ionomycin-induced NETosis. *Redox Biol.* (2023) 64:102784. doi: 10.1016/j.redox.2023.102784
14. He Y, Yang FY, Sun EW. Neutrophil extracellular traps in autoimmune diseases. *Chin Med J (Engl)*. (2018) 131:1513–9. doi: 10.4103/0366-6999.235122
15. Neeli I, Dwivedi N, Khan S, Radic M. Regulation of extracellular chromatin release from neutrophils. *J Innate Immun.* (2009) 1:194–201. doi: 10.1159/000206974
16. Papayannopoulos V. Neutrophil extracellular traps in immunity and disease. *Nat Rev Immunol.* (2018) 18:134–47. doi: 10.1038/nri.2017.105
17. Metzler KD, Goosmann C, Lubojemska A, Zychlinsky A, Papayannopoulos V. A myeloperoxidase-containing complex regulates neutrophil elastase release and actin dynamics during NETosis. *Cell Rep.* (2014) 8:883–96. doi: 10.1016/j.celrep.2014.06.044
18. Lee KH, Kronbichler A, Park DD, Park Y, Moon H, Kim H, et al. Neutrophil extracellular traps (NETs) in autoimmune diseases: A comprehensive review. *Autoimmun Rev.* (2017) 16:1160–73. doi: 10.1016/j.autrev.2017.09.012
19. Bianchi M, Hakkim A, Brinkmann V, Siler U, Seger RA, Zychlinsky A, et al. Restoration of NETs formation by gene therapy in CGD controls aspergillosis. *Blood.* (2009) 114:2619–22. doi: 10.1182/blood-2009-05-221606
20. Fuchs TA, Abed U, Goosmann C, Hurwitz R, Schulze I, Wahn V, et al. Novel cell death program leads to neutrophil extracellular traps. *J Cell Biol.* (2007) 176:231–41. doi: 10.1083/jcb.200606027
21. Huang SU, O'Sullivan KM. The expanding role of extracellular traps in inflammation and autoimmunity: the new players in casting dark webs. *Int J Mol Sci.* (2022) 23:3793. doi: 10.3390/ijms23073793
22. Yipp BG, Petri B, Salina D, Jenne CN, Scott B, Zbytniuk L, et al. Infection-induced NETosis is a dynamic process involving neutrophil multitasking *in vivo*. *Nat Med.* (2012) 18:1386–93. doi: 10.1038/nm.2847
23. Pilsczek FH, Salina D, Poon KK, Fahey C, Yipp BG, Sibley CD, et al. A novel mechanism of rapid nuclear neutrophil extracellular trap formation in response to *Staphylococcus aureus*. *J Immunol.* (2010) 185:7413–25. doi: 10.4049/jimmunol.1000675
24. Douda DN, Khan MA, Grasemann H, Palaniyar N. SK3 channel and mitochondrial ROS mediate NADPH oxidase-independent NETosis induced by calcium influx. *Proc Natl Acad Sci U.S.A.* (2015) 112:2817–22. doi: 10.1073/pnas.1414055112
25. Demkow U. Molecular mechanisms of neutrophil extracellular trap (NETs) degradation. *Int J Mol Sci.* (2023) 24:4896. doi: 10.3390/ijms24054896
26. Yousefi S, Mihalache C, Kozlowski E, Schmid I, Simon HU. Viable neutrophils release mitochondrial DNA to form neutrophil extracellular traps. *Cell Death Differ.* (2009) 16:1438–44. doi: 10.1038/cdd.2009.96
27. McIlroy DJ, Jarnicki AG, Au GG, Lott N, Smith DW, Hansbro PM, et al. Mitochondrial DNA neutrophil extracellular traps are formed after trauma and subsequent surgery. *J Crit Care.* (2014) 29:1131–3. doi: 10.1016/j.jccr.2014.07.013
28. Tan C, Aziz M, Wang P. The vitals of NETs. *J Leukoc Biol.* (2021) 110:797–808. doi: 10.1002/JLB.3RU0620-375R
29. Cooper PR, Palmer LJ, Chapple IL. Neutrophil extracellular traps as a new paradigm in innate immunity: friend or foe? *Periodontol 2000.* (2013) 63:165–97. doi: 10.1111/prd.12025
30. Liu C, Hermann TE. Characterization of ionomycin as a calcium ionophore. *J Biol Chem.* (1978) 253:5892–4. doi: 10.1016/S0021-9258(17)34550-7
31. Kenny EF, Herzig A, Kruger R, Muth A, Mondal S, Thompson PR, et al. Diverse stimuli engage different neutrophil extracellular trap pathways. *Elife.* (2017) 6:e24437. doi: 10.7554/eLife.24437
32. Thiam HR, Wong SL, Wagner DD, Waterman CM. Cellular mechanisms of NETosis. *Annu Rev Cell Dev Biol.* (2020) 36:191–218. doi: 10.1146/annurev-cellbio-020520-111016
33. Wright HL, Moots RJ, Edwards SW. The multifactorial role of neutrophils in rheumatoid arthritis. *Nat Rev Rheumatol.* (2014) 10:593–601. doi: 10.1038/nrrheum.2014.80
34. Wang W, Peng W, Ning X. Increased levels of neutrophil extracellular trap remnants in the serum of patients with rheumatoid arthritis. *Int J Rheum Dis.* (2018) 21:415–21. doi: 10.1111/1756-185X.13226
35. Hann J, Bueb JL, Tolle F, Brechard S. Calcium signaling and regulation of neutrophil functions: Still a long way to go. *J Leukoc Biol.* (2020) 107:285–97. doi: 10.1002/JLB.3RU0719-241R
36. de Bont CM, Koopman W, Boelens WC, Puijn GJ. Stimulus-dependent chromatin dynamics, citrullination, calcium signalling and ROS production during NETs formation. *Biochim Biophys Acta Mol Cell Res.* (2018) 1865:1621–9. doi: 10.1016/j.bbmr.2018.08.014
37. Wong SL, Wagner DD. Peptidylarginine deiminase 4: a nuclear button triggering neutrophil extracellular traps in inflammatory diseases and aging. *FASEB J.* (2018) 32:fj201800691R. doi: 10.1096/fj.201800691R
38. Rada B. Neutrophil extracellular traps. *Methods Mol Biol.* (2019) 1982:517–28. doi: 10.1007/978-1-4939-9424-3_31
39. Iwamoto T, Ikari K, Nakamura T, Kuwahara M, Toyama Y, Tomatsu T, et al. Association between PAD14 and rheumatoid arthritis: a meta-analysis. *Rheumatol (Oxford).* (2006) 45:804–7. doi: 10.1093/rheumatology/kei023
40. Barton A, Bowes J, Eyre S, Spreckley K, Hinks A, John S, et al. A functional haplotype of the PAD14 gene associated with rheumatoid arthritis in a Japanese population is not associated in a United Kingdom population. *Arthritis Rheum.* (2004) 50:1117–21. doi: 10.1002/art.20169
41. Darrah E, Giles JT, Ols ML, Bull HG, Andrade F, Rosen A, et al. Erosive rheumatoid arthritis is associated with antibodies that activate PAD4 by increasing calcium sensitivity. *Sci Transl Med.* (2013) 5:186ra65. doi: 10.1126/scitranslmed.3005370
42. van Delft M, Huizinga T. An overview of autoantibodies in rheumatoid arthritis. *J Autoimmun.* (2020) 110:102392. doi: 10.1016/j.jaut.2019.102392
43. Khandpur R, Carmona-Rivera C, Vivekanandan-Giri A, Gizinski A, Yalavarthi S, Knight JS, et al. NETs are a source of citrullinated autoantigens and stimulate inflammatory responses in rheumatoid arthritis. *Sci Transl Med.* (2013) 5:178ra40. doi: 10.1126/scitranslmed.3005580
44. Loh JT, Lam KP. Neutrophils in the pathogenesis of rheumatic diseases. *Rheumatol Immunol Res.* (2022) 3:120–7. doi: 10.2478/rir-2022-0020
45. Wu CY, Yang HY, Lai JH. Anti-citrullinated protein antibodies in patients with rheumatoid arthritis: biological effects and mechanisms of immunopathogenesis. *Int J Mol Sci.* (2020) 21:4015. doi: 10.3390/ijms21114015
46. Ge C, Holmdahl R. The structure, specificity and function of anti-citrullinated protein antibodies. *Nat Rev Rheumatol.* (2019) 15:503–8. doi: 10.1038/s41584-019-0244-4
47. Ge C, Tong D, Liang B, Lonnblom E, Schneider N, Hagert C, et al. Anti-citrullinated protein antibodies cause arthritis by cross-reactivity to joint cartilage. *JCI Insight.* (2017) 2(13):905. doi: 10.1172/jci.insight.93688
48. Wright HL, Lyon M, Chapman EA, Moots R, Edwards S. Rheumatoid arthritis synovial fluid neutrophils drive inflammation through production of chemokines, reactive oxygen species, and neutrophil extracellular traps. *Front Immunol.* (2020) 11:584116. doi: 10.3389/fimmu.2020.584116
49. Sakkas LI, Bogdanos DP, Katsiari C, Platsoucas C. Anti-citrullinated peptides as autoantigens in rheumatoid arthritis-relevance to treatment. *Autoimmun Rev.* (2014) 13:1114–20. doi: 10.1016/j.autrev.2014.08.012
50. Fresneda AM, McLaren Z, Wright HL. Neutrophils in the pathogenesis of rheumatoid arthritis and systemic lupus erythematosus: same foe different M.O. *Front Immunol.* (2021) 12:649693. doi: 10.3389/fimmu.2021.649693
51. Cecchi I, Arias DLRI, Menegatti E, Roccatello D, Collantes-Estevez E, Lopez-Pedraza C, et al. Neutrophils: Novel key players in Rheumatoid Arthritis. Current and future therapeutic targets. *Autoimmun Rev.* (2018) 17:1138–49. doi: 10.1016/j.autrev.2018.06.006
52. Barnado A, Crofford LJ, Oates JC. At the Bedside: Neutrophil extracellular traps (NETs) as targets for biomarkers and therapies in autoimmune diseases. *J Leukoc Biol.* (2016) 99:265–78. doi: 10.1189/jlb.5BT0615-234R
53. Romero V, Fert-Bober J, Nigrovic PA, Darrah E, Haque UJ, Lee AM, et al. Immune-mediated pore-forming pathways induce cellular hypercitrullination and generate citrullinated autoantigens in rheumatoid arthritis. *Sci Transl Med.* (2013) 5:209ra150. doi: 10.1126/scitranslmed.3006869
54. Chirivi R, van Rosmalen J, van der Linden M, Euler M, Schmets G, Bogatkevich E, et al. Therapeutic ACPA inhibits NETs formation: a potential therapy for neutrophil-mediated inflammatory diseases. *Cell Mol Immunol.* (2021) 18:1528–44. doi: 10.1038/s41423-020-0381-3
55. Wigerblad G, Kaplan MJ. Neutrophil extracellular traps in systemic autoimmune and autoinflammatory diseases. *Nat Rev Immunol.* (2023) 23:274–88. doi: 10.1038/s41577-022-00787-0
56. Zhao J, Jiang P, Guo S, Schrod S, He D. Apoptosis, autophagy, NETosis, necroptosis, and pyroptosis mediated programmed cell death as targets for innovative therapy in rheumatoid arthritis. *Front Immunol.* (2021) 12:809806. doi: 10.3389/fimmu.2021.809806
57. Jung J, Lee LE, Kim H, Kim JE, Jang SH, Roh JS, et al. Extracellular histones aggravate autoimmune arthritis by lytic cell death. *Front Immunol.* (2022) 13:961197. doi: 10.3389/fimmu.2022.961197
58. Okamoto Y, Devos S, Seto N, Minarchick V, Wilson T, Rothfuss HM, et al. Association of sputum neutrophil extracellular trap subsets with IgA anti-citrullinated protein antibodies in subjects at risk for rheumatoid arthritis. *Arthritis Rheumatol.* (2022) 74:38–48. doi: 10.1002/art.41948
59. Pratesi F, Dioni I, Tommasi C, Alcaro MC, Paolini I, Barbetti F, et al. Antibodies from patients with rheumatoid arthritis target citrullinated histone 4 contained in neutrophils extracellular traps. *Ann Rheum Dis.* (2014) 73:1414–22. doi: 10.1136/annrheumdis-2012-202765
60. Wilson AS, Randall KL, Pettitt JA, Ellyard JL, Blumenthal A, Enders A, et al. Neutrophil extracellular traps and their histones promote Th17 cell differentiation directly via TLR2. *Nat Commun.* (2022) 13:528. doi: 10.1038/s41467-022-28172-4
61. Jang S, Kwon EJ, Lee JJ. Rheumatoid arthritis: pathogenic roles of diverse immune cells. *Int J Mol Sci.* (2022) 23. doi: 10.3390/ijms23020905
62. Kruglov A, Drutskaya M, Schlenz D, Gorshkova E, Kurz K, Morawietz L, et al. Contrasting contributions of TNF from distinct cellular sources in arthritis. *Ann Rheum Dis.* (2020) 79:1453–9. doi: 10.1136/annrheumdis-2019-216068
63. Kondo N, Kuroda T, Kobayashi D. Cytokine NETsworks in the pathogenesis of rheumatoid arthritis. *Int J Mol Sci.* (2021) 22:10922. doi: 10.3390/ijms222010922

64. Dömer D, Walther T, Möller S, Behnen M, Laskay T. Neutrophil extracellular traps activate proinflammatory functions of human neutrophils. *Front Immunol.* (2021) 12:636954. doi: 10.3389/fimmu.2021.636954
65. Pericolini E, Alunno A, Gabrielli E, Bartoloni E, Cenci E, Chow S, et al. The microbial capsular polysaccharide galactoxylomannan inhibits IL-17A production in circulating T cells from rheumatoid arthritis patients. *PLoS One.* (2013) 8:e53336. doi: 10.1371/journal.pone.0053336
66. Ye H, Yang Q, Guo H, Wang X, Cheng L, Han B, et al. Internalisation of neutrophils extracellular traps by macrophages aggravate rheumatoid arthritis via Rab5a. *RMD Open.* (2024) 10:e003847. doi: 10.1136/rmdopen-2023-003847
67. Warnatsch A, Ioannou M, Wang Q, Papayannopoulos V. Inflammation. Neutrophil extracellular traps license macrophages for cytokine production in atherosclerosis. *Science.* (2015) 349:316–20. doi: 10.1126/science.aaa8064
68. Carmona-Rivera C, Carlucci PM, Moore E, Lingampalli N, Uchtenhagen H, James E, et al. Synovial fibroblast-neutrophil interactions promote pathogenic adaptive immunity in rheumatoid arthritis. *Sci Immunol.* (2017) 2:eag3358. doi: 10.1126/sciimmunol.aag3358
69. Bartok B, Firestein GS. Fibroblast-like synoviocytes: key effector cells in rheumatoid arthritis. *Immunol Rev.* (2010) 233:233–55. doi: 10.1111/j.0105-2896.2009.00859.x
70. Mahmoud DE, Kaabachi W, Sassi N, Tarhouni L, Rekik S, Jemali S, et al. The synovial fluid fibroblast-like synovocyte: A long-neglected piece in the puzzle of rheumatoid arthritis pathogenesis. *Front Immunol.* (2022) 13:942417. doi: 10.3389/fimmu.2022.942417
71. Xu H, Zheng SG, Fox D. Editorial: immunomodulatory functions of fibroblast-like synoviocytes in joint inflammation and destruction during rheumatoid arthritis. *Front Immunol.* (2020) 11:955. doi: 10.3389/fimmu.2020.00955
72. Turner JD, Filer A. The role of the synovial fibroblast in rheumatoid arthritis pathogenesis. *Curr Opin Rheumatol.* (2015) 27:175–82. doi: 10.1097/BOR.0000000000000148
73. Mutua V, Gershwin LJ. A review of neutrophil extracellular traps (NETs) in disease: potential anti-NETs therapeutics. *Clin Rev Allergy Immunol.* (2021) 61:194–211. doi: 10.1007/s12016-020-08804-7
74. Mathey DL, Nixon NB, Dawes PT. Association of circulating levels of MMP-8 with mortality from respiratory disease in patients with rheumatoid arthritis. *Arthritis Res Ther.* (2012) 14:R204. doi: 10.1186/ar4042
75. Itoh T, Matsuda H, Tanioka M, Kuwabara K, Itoharu S, Suzuki R, et al. The role of matrix metalloproteinase-2 and matrix metalloproteinase-9 in antibody-induced arthritis. *J Immunol.* (2002) 169:2643–7. doi: 10.4049/jimmunol.169.5.2643
76. Carmona-Rivera C, Carlucci PM, Goel RR, James E, Brooks SR, Rims C, et al. Neutrophil extracellular traps mediate articular cartilage damage and enhance cartilage component immunogenicity in rheumatoid arthritis. *JCI Insight.* (2020) 5:e139388. doi: 10.1172/jci.insight.139388
77. O'neil LJ, Oliveira CB, Wang X, Navarrete M, Barrera-Vargas A, Merayo-Chalico J, et al. Neutrophil extracellular trap-associated carbamylation and histones trigger osteoclast formation in rheumatoid arthritis. *Ann Rheum Dis.* (2023) 82:630–8. doi: 10.1136/ard-2022-223568
78. Schneider AH, Taira TM, Publio GA, Prado D, Yabuta PBD, Santos JCD, et al. Neutrophil extracellular traps mediate bone erosion in rheumatoid arthritis by enhancing RANKL-induced osteoclastogenesis. *Br J Pharmacol.* (2024) 181:429–46. doi: 10.1111/bph.16227
79. Kolaczowska E, Jenne CN, Surewaard BG, Thanabalasuriar A, Lee W, Sanz M, et al. Molecular mechanisms of NETs formation and degradation revealed by intravital imaging in the liver vasculature. *Nat Commun.* (2015) 6:6673. doi: 10.1038/ncomms7673
80. Song W, Ye J, Pan N, Tan C, Herrmann M, et al. Neutrophil extracellular traps tied to rheumatoid arthritis: points to ponder. *Front Immunol.* (2020) 11:578129. doi: 10.3389/fimmu.2020.578129
81. Zhao J, Liu Y, Shi X, Dang J, Liu Y, Li S, et al. Infusion of GMSCs relieves autoimmune arthritis by suppressing the externalization of neutrophil extracellular traps via PGE2-PKA-ERK axis. *J Adv Res.* (2023) 58:79–91. doi: 10.1016/j.jare.2023.05.001
82. van der Linden M, Kumari S, Montizaan D, Dalen S, Kip A, Foster M, et al. Anti-citrullinated histone monoclonal antibody CIT-013, a dual action therapeutic for neutrophil extracellular trap-associated autoimmune diseases. *MAbs.* (2023) 15:2281763. doi: 10.1080/19420862.2023.2281763
83. Yuan K, Zhu Q, Lu Q, Jiang H, Zhu M, Li X, et al. Quercetin alleviates rheumatoid arthritis by inhibiting neutrophil inflammatory activities. *J Nutr Biochem.* (2020) 84:108454. doi: 10.1016/j.jnutbio.2020.108454
84. Zhu M, Yuan K, Lu Q, Zhu Q, Zhang S, Li X, et al. Emodin ameliorates rheumatoid arthritis by promoting neutrophil apoptosis and inhibiting neutrophil extracellular trap formation. *Mol Immunol.* (2019) 112:188–97. doi: 10.1016/j.molimm.2019.05.010
85. Yang F, Luo X, Luo G, Zhai Z, Zhuang J, He J, et al. Inhibition of NETs formation by polydatin protects against collagen-induced arthritis. *Int Immunopharmacol.* (2019) 77:105919. doi: 10.1016/j.intimp.2019.105919
86. Cross AL, Hawkes J, Wright HL, Moots RJ, Edwards SW. APPA (apocynin and paeonol) modulates pathological aspects of human neutrophil function, without suppressing antimicrobial ability, and inhibits TNF α expression and signalling. *Inflammopharmacology.* (2020) 28:1223–35. doi: 10.1007/s10787-020-00715-5
87. Zhang S, Huang G, Yuan K, Zhu Q, Sheng H, Yu R, et al. Tanhinone IIA ameliorates chronic arthritis in mice by modulating neutrophil activities. *Clin Exp Immunol.* (2017) 190:29–39. doi: 10.1111/cei.12993
88. Wang W, Zhang ZQ, Zhang YC, Wu YQ, Yang Z, Zheng YZ, et al. Cayratia albifolia C.Li exerts anti-rheumatoid arthritis effect by inhibiting macrophage activation and neutrophil extracellular traps (NETs). *Chin Med.* (2024) 19:42. doi: 10.1186/s13020-024-00910-4
89. Bach M, Moon J, Moore R, Pan T, Nelson J, Lood C, et al. A neutrophil activation biomarker panel in prognosis and monitoring of patients with rheumatoid arthritis. *Arthritis Rheumatol.* (2020) 72:47–56. doi: 10.1002/art.41062
90. Sprengler E, Zandstra J, van Kleef ND, Goetschalckx I, Versteeg B, Aarts CE, et al. S100A8/A9 is a marker for the release of neutrophil extracellular traps and induces neutrophil activation. *Cells.* (2022) 11:236. doi: 10.3390/cells11020236
91. Inciarte-Mundo J, Frade-Sosa B, Sanmarti R. From bench to bedside: Calprotectin (S100A8/S100A9) as a biomarker in rheumatoid arthritis. *Front Immunol.* (2022) 13:1001025. doi: 10.3389/fimmu.2022.1001025
92. Abildtrup M, Kingsley GH, Scott DL. Calprotectin as a biomarker for rheumatoid arthritis: a systematic review. *J Rheumatol.* (2015) 42:760–70. doi: 10.3899/jrheum.140628
93. Ryckman C, Vandal K, Rouleau P, Talbot M, Tessier PA. Proinflammatory activities of S100: proteins S100A8, S100A9, and S100A8/A9 induce neutrophil chemotaxis and adhesion. *J Immunol.* (2003) 170:3233–42. doi: 10.4049/jimmunol.170.6.3233
94. Adrover JM, McDowell S, He XY, Quail DF, Egeblad M. NETworking with cancer: The bidirectional interplay between cancer and neutrophil extracellular traps. *Cancer Cell.* (2023) 41:505–26. doi: 10.1016/j.ccell.2023.02.001
95. Okeke EB, Louttit C, Fry C, Najafabadi AH, Han K, Nemzek J, et al. Inhibition of neutrophil elastase prevents neutrophil extracellular trap formation and rescues mice from endotoxic shock. *Biomaterials.* (2020) 238:119836. doi: 10.1016/j.biomaterials.2020.119836
96. Tardito S, Martinelli G, Soldano S, Paolino S, Pacini G, Patane M, et al. Macrophage M1/M2 polarization and rheumatoid arthritis: A systematic review. *Autoimmun Rev.* (2019) 18:102397. doi: 10.1016/j.autrev.2019.102397
97. Wang Y, Fang J, Liu B, Shao C, Shi Y. Reciprocal regulation of mesenchymal stem cells and immune responses. *Cell Stem Cell.* (2022) 29:1515–30. doi: 10.1016/j.stem.2022.10.001
98. Zhao J, Liu Y, Shi X, Dang J, Liu Y, Li S, et al. Infusion of GMSCs relieves autoimmune arthritis by suppressing the externalization of neutrophil extracellular traps via PGE2-PKA-ERK axis. *J Adv Res.* (2024) 58:79–91. doi: 10.1016/j.jare.2023.05.001
99. Apel F, Zychlinsky A, Kenny EF. The role of neutrophil extracellular traps in rheumatic diseases. *Nat Rev Rheumatol.* (2018) 14:467–75. doi: 10.1038/s41584-018-0039-z
100. Macqueen BC, Christensen RD, Yost CC, Lambert DK, Baer VL, Sheffield MJ, et al. Elevated fecal calprotectin levels during necrotizing enterocolitis are associated with activated neutrophils extruding neutrophil extracellular traps. *J Perinatol.* (2016) 36:862–9. doi: 10.1038/jp.2016.105
101. Saha P, Yeoh BS, Xiao X, Golonka RM, Singh V, Wang Y, et al. PAD4-dependent NETs generation are indispensable for intestinal clearance of *Citrobacter rodentium*. *Mucosal Immunol.* (2019) 12:761–71. doi: 10.1038/s41385-019-0139-3



OPEN ACCESS

EDITED BY

Reza Akbarzadeh,
University of Lübeck, Germany

REVIEWED BY

Maximiliano Jimenez Dalmaroni,
National University of La Plata, Argentina
Bernhard Ryffel,
Centre National de la Recherche Scientifique
(CNRS), France
Jérémie Decalf,
Genentech Inc., United States

*CORRESPONDENCE

Huimin Zhou

✉ zhm4202@163.com

RECEIVED 17 July 2024

ACCEPTED 09 September 2024

PUBLISHED 25 September 2024

CITATION

Zhu Q and Zhou H (2024) The role of cGAS-STING signaling in rheumatoid arthritis: from pathogenesis to therapeutic targets.
Front. Immunol. 15:1466023.
doi: 10.3389/fimmu.2024.1466023

COPYRIGHT

© 2024 Zhu and Zhou. This is an open-access article distributed under the terms of the [Creative Commons Attribution License \(CC BY\)](#). The use, distribution or reproduction in other forums is permitted, provided the original author(s) and the copyright owner(s) are credited and that the original publication in this journal is cited, in accordance with accepted academic practice. No use, distribution or reproduction is permitted which does not comply with these terms.

The role of cGAS-STING signaling in rheumatoid arthritis: from pathogenesis to therapeutic targets

Qiugang Zhu¹ and Huimin Zhou^{2*}

¹Department of Laboratory Medicine, Shangyu People's Hospital of Shaoxing, Shaoxing University, Shaoxing, China, ²Department of Laboratory Medicine, Wuxi Ninth People's Hospital Affiliated to Soochow University, Wuxi, China

Rheumatoid arthritis (RA) is a systemic autoimmune disease primarily characterized by erosive and symmetric polyarthritis. As a pivotal axis in the regulation of type I interferon (IFN-I) and innate immunity, the cyclic GMP-AMP synthase-stimulator of interferon genes (cGAS-STING) signaling pathway has been implicated in the pathogenesis of RA. This pathway mainly functions by regulating cell survival, pyroptosis, migration, and invasion. Therefore, understanding the sources of cell-free DNA and the mechanisms underlying the activation and regulation of cGAS-STING signaling in RA offers a promising avenue for targeted therapies. Early detection and interventions targeting the cGAS-STING signaling are important for reducing the medical burden on individuals and healthcare systems. Herein, we review the existing literature pertaining to the role of cGAS-STING signaling in RA, and discuss current applications and future directions for targeting the cGAS-STING signaling in RA treatments.

KEYWORDS

rheumatoid arthritis, cGAS, STING, signaling pathway, treatments

1 Introduction

Rheumatoid arthritis (RA) is an autoimmune disease caused by the breakdown of immune homeostasis, affecting women more frequently than men. Clinical features of RA primarily include joint swelling, pain, stiffness, weakness, deformity, and fatigue (1). Pathologically, RA is characterized by chronic inflammation of the joint synovium, formation of pannus, and infiltration of lymphocytes, macrophages, and neutrophils (2). Common treatments for RA include non-steroidal anti-inflammatory drugs (NSAIDs), synthetic disease-modifying antirheumatic drugs (DMARDs), biological DMARDs, traditional Chinese medicine, and surgical interventions (3, 4). Representative therapeutic options available for patients include celecoxib, methotrexate (MTX), glucocorticoids, tumor necrosis factor (TNF) inhibitors, IL-6R inhibitors, Janus kinases

(JAKs) inhibitors, and anti-B cell antibodies, patients may require multiple drugs with different modes of action to address the heterogeneity of RA (5). Despite these therapies, the clinical symptoms of certain patients remain unrelieved, underscoring the need for a deeper understanding of RA's pathogenic mechanisms to explore novel treatment options.

Innate immunity plays a critical role in the pathogenesis of RA, including various innate immune cells and components (6). For example, increased expression of toll-like receptors (TLRs, TLR2/3/4/7) has been reported in RA. Ligand-stimulated TLRs activate the intracellular MyD88-dependent and MyD88-independent pathway, resulting in the induction of various pro-inflammatory cytokines in RA (7). An increased interferon gene signature was observed in patients with early RA (eRA), which predicted a poor response to the initial therapies in the first 6 months after diagnosis (8). Also, there was a correlation between baseline interferon gene signature and disease activity score 28 at 6 months. Further exploration demonstrated that interferon- α played an important role in therapeutic resistance by regulating site-specific DNA methylation in B and T cells (9). Thus, dysregulated IFN-I potentially plays a role in the pathogenesis and therapeutic resistance of RA (10).

The cyclic GMP-AMP synthase-stimulator of interferon genes (cGAS-STING) signaling pathway is crucial for cells to recognize and respond to cytosolic double-stranded DNA (dsDNA), serving as a primary driver for the establishment of innate immunity through the induction of IFN-I (11). TNF- α is a pathogenic cytokine in RA, which has been demonstrated to increase DNA damage and nuclear DNA release, accompanied by reduced STING degradation (12). Thus, it is reasonable to speculate that TNF can regulate RA progression through cGAS-STING signaling. Here, we delve into the role of cGAS-STING signaling in RA from the origin of cell-free DNA (cfDNA) to the final effects. Also, the potential therapeutic applications of cGAS-STING signaling in RA treatment will be discussed, aiming to provide new insights for the future research on RA.

Abbreviations: RA, rheumatoid arthritis; IFN-I, type I interferon; cGAS, cyclic GMP-AMP synthase; STING, stimulator of interferon gene; NSAIDs, non-steroidal anti-inflammatory drugs; DMARDs, disease-modifying antirheumatic drugs; MTX, methotrexate; TNF, tumor necrosis factor; JAKs, Janus kinases; TLR, toll-like receptor; dsDNA, double-stranded DNA; cfDNA, cell free-DNA; ISGs, interferon-stimulated genes; cGAMP, cyclic GMP-AMP; ER, endoplasmic reticulum; ERGIC, ER-Golgi intermediate compartments; TBK1, TANK binding kinase 1; IRF3, interferon regulatory factor 3; NF- κ B, nuclear factor- κ B; NETs, neutrophil extracellular traps; FLSs, fibroblast-like synoviocytes; CIA, collagen-induced arthritis; CFA, complete Freund's adjuvant; CII, type II collagen; OA, osteoarthritis; FTO, fat mass and obesity-associated protein; AIA, adjuvant-induced arthritis; CMPK2, cytidine/uridine monophosphate kinase 2; MMP, matrix metalloproteinase; Pol β , polymerase β ; cNPs, cationic nanoparticles; PEG, polyethylene glycol; NiH, nanomedicine-in-hydrogel; AMDs, antimalarial drugs; HCQ, hydroxychloroquine; LEF, leflunomide; PEI-PDA, polyethyleneimine-polydopamine; TP, triptolide; ITA, itaconate.

2 An overview of the cGAS-STING signaling pathway

The cGAS-STING signaling pathway is widely distributed in immune cells, non-immune cells, tumor cells, and other tissue-derived cells (13–15). The primary function of cGAS-STING signaling is to trigger the innate immune response by inducing IFN-I production and subsequent interferon-stimulated gene (ISG) expression (16, 17). This signaling also plays roles in other cellular activities, including autophagy, pyroptosis, metabolism, and cellular senescence (18–21). Moreover, the cGAS-STING signaling can be modulated by cellular molecules, RNA virus-derived components, and post-translational modifications to maintain homeostasis under normal conditions, with its dysregulation potentially contributing to disease development (22–24).

cGAS, acts as a cytosolic DNA sensor, recognizing DNA in the cytoplasm that originates from pathogens, mitochondria, micronuclei, and dead cells (25). The activation of cGAS is triggered by its interactions with dsDNA, which is dependent on the length of DNA (>45 nucleotides) rather than the sequence (26). The availability of longer dsDNA fragments allows for the attainment of a certain signaling threshold (27, 28). Upon cGAS activation, cyclic GMP-AMP (cGAMP) is synthesized from GTP and ATP, which is responsible for eliciting the downstream signaling (29). In addition, the DNA-RNA hybrids can also induce the activation of cGAS (30). It is also noteworthy that cGAS can reside in the nucleus (31). Studies have shown that nuclear cGAS binds to nucleosomes (mainly H2A-H2B), which prevents the cGAS-DNA binding and cGAS dimerization, thereby maintaining cGAS in an inactive conformation and consequently limiting autoreactivity (32–34).

STING, initially identified before cGAS, is a 379 amino acid protein located on the endoplasmic reticulum (ER) membrane (35, 36). cGAMP binds to STING, resulting in profound conformational changes that trigger STING oligomerization. Subsequently, tetramers of STING translocate to Golgi compartments through the ER-Golgi intermediate compartments (ERGIC). STING then facilitates the recruitment of TANK binding kinase 1 (TBK1), which promotes TBK1 autophosphorylation and STING phosphorylation. This process further triggers the recruitment and phosphorylation of interferon regulatory factor 3 (IRF3). Phosphorylated IRF3 undergoes dimerization and translocates to the nucleus, initiating the expression of IFN-I. Ultimately, IFN-I induces the expression of ISGs through IFNAR. Additionally, STING also induces the activation of IKK, leading to the nuclear entry of nuclear factor- κ B (NF- κ B) and subsequent the expression of inflammatory factors (Figure 1) (16, 17). Interestingly, a previous study revealed that interferon production could be induced by membrane fusion in a STING-dependent but cGAS-independent manner (37).

cGAS-STING signaling activation and IFN-I production are involved in multiple pathological and physiological processes. During viral infections, IFN-I promotes the clearance of the virus, but it may also cause immunosuppression during chronic infections (38). However, excessive expression of IFN-I enhances the autoreactive T cell- and B cell-mediated responses, ultimately resulting in the occurrence of autoimmunity (16, 39). Although

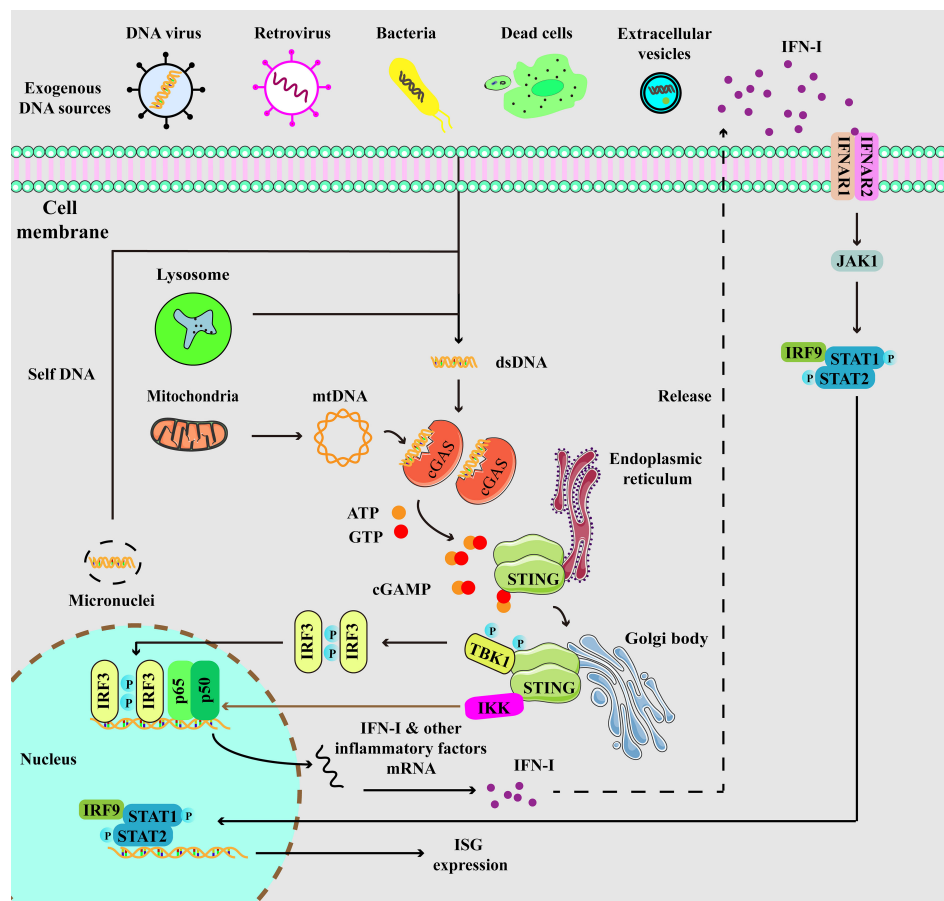


FIGURE 1

Depiction of cGAS-STING signaling. cGAS, a cytosolic DNA sensor, is able to detect cytoplasmic DNA from exogenous and endogenous sources, including DNA viruses, retrovirus, bacteria, dead cells, extracellular vesicles, micronuclei, and mitochondria. When cGAS binds to double-stranded DNA (dsDNA), it triggers the activation of its own catalytic activity, resulting in the synthesis of 2',3'-cyclic GMP-AMP (cGAMP) from ATP and GTP. cGAMP binds to STING at the endoplasmic reticulum (ER), then STING undergoes oligomerization and translocates from the ER to Golgi compartments. Then, STING is palmitoylated and serves as a platform for the recruitment of TBK1 and IKK. TBK1 phosphorylates STING, which in turn recruits IRF3 for TBK1-mediated phosphorylation. Phosphorylated IRF3 translocates to the nucleus and turns on the expression of type I interferons. Meanwhile, STING also activates IKK to facilitate NF- κ B-mediated transcription of pro-inflammatory cytokines, thereby activating inflammatory responses. Moreover, secreted IFN-I can be recognized by IFNAR, which induces the activation of JAK-STAT signaling, resulting in the expression of IFN-stimulated genes (ISGs).

other branch activations are also involved in RA, such as the cGAS-PI3K-Akt signaling pathway, this review will primarily focus on the cGAS-STING signaling pathway in the following sections (40, 41).

3 cGAS-STING signaling in the progression of RA

3.1 Elevated levels of cfDNA, cGAS, and STING in RA

There was a study that systematically reviewed the level and origin of cfDNA in RA (42). As early as 1973, cfDNA was confirmed to be elevated in the serum of RA patients (43). Later, the increased level of cfDNA was also detected in the synovial fluid. Moreover, there was an association between cfDNA levels and disease activity

(44, 45). Potential sources of cfDNA include neutrophil extracellular traps/neutrophil ETosis (NETs/NETosis), pyroptosis, and micronuclei (46–48). *In vitro*, RA synovial fluid enhanced the production of NETs by neutrophils, as evidenced by the increased levels of DNA in culture supernatants and extracellular DNA on NETs (48). A significant association between gasdermin E (GSDME) and cfDNA has been observed in RA patients, further experiments have demonstrated that NETs triggered NF- κ B/Caspase 3/GSDME-mediated pyroptosis in fibroblast-like synoviocytes (FLSs), indicating that pyroptosis is a source of cfDNA (46). Micronuclei, which also serve as a crucial source of cfDNA, have been found to be elevated in RA patients (47). This increase in micronuclei has been observed in both active and inactive RA patients, accompanied by the reduced levels of superoxide dismutase and glutathione peroxidase (49). Increased micronucleus levels were also detected in collagen-induced arthritis

(CIA) mice, a mouse model established by immunization with an emulsion of complete Freund's adjuvant (CFA) and type II collagen (CII). Notably, rituximab treatment suppressed micronucleus formation, paralleled by a decline in serum 8-hydroxydeoxyguanosine, indicating that enhanced oxidative stress might contribute to DNA damage and micronucleus formation in RA (50). Previous research found that MTX enhanced the generation of micronuclei in rat bone marrow cells (51, 52). In contrast, another study found no difference in micronucleus levels between patients who received MTX treatment and those who did not, suggesting that the generation of micronuclei was associated with RA itself (47). Collectively, both the disease itself and the pharmacological treatments have the potential to induce the formation of micronuclei in RA, thereby providing a basis for the generation of cfDNA. Consequently, the presence of cfDNA may act as the initiator for the activation of cGAS-STING signaling during RA progression.

Compared with the osteoarthritis (OA) patient-derived FLSs, the levels of cGAS mRNA and cGAS protein were higher in RA-FLSs. Moreover, overexpression of cGAS in RA-FLSs enhanced both the proliferation of these cells and the expression of pro-inflammatory factors (41). As for STING, RA patients exhibited the highest concentrations of intracellular STING when compared to those with OA, psoriatic arthritis, calcium pyrophosphate crystal-induced arthritis, and OA with calcium pyrophosphate crystals (53). Furthermore, intracellular STING positively correlated with inflammatory parameters, such as white blood cells, polymorphonuclear cells, IL-1 β , IL-8, and IL-6 (53). *Sting1*^{+/-} mice, which have a reduced expression of phosphorylated TBK1, showed a decreased severity of arthritis and improved histological changes compared to control mice (54). These findings suggest that

cfDNA-triggered cGAS-STING signaling plays a significant role in the pathogenesis of RA (Figure 2).

3.2 TNF triggers the release of mtDNA and the activation of cGAS-STING signaling in RA

TNF, a multifunctional cytokine for homeostasis and disease pathogenesis, is highly expressed in rheumatoid joint tissues (55). TNF is also the first cytokine validated as a therapeutic target for RA, and several types of TNF inhibitors have been applied in the clinical treatment (56). A previous study revealed that TNF could enhance IFN responses by activating cGAS-STING signaling, thereby supporting the joint inflammation (57). Specifically, TNF inhibited PTEN-induced kinase 1-mediated mitophagy, leading to functional alterations in mitochondria and an increase in cytoplasmic mitochondrial DNA (mtDNA) levels. Consequently, mtDNA bound to cGAS and activated the downstream signaling that mimicked the functions of macrophages from RA patients, contributing to the pathogenesis of RA (57). Additionally, TNF- α stimulation has been demonstrated to increase the expression of cGAS in FLSs, further supporting the involvement of TNF in RA progression through cGAS-STING signaling (41).

Growing evidence has indicated that obesity plays a pivotal role in multiple aspects of RA (58–60). A trend toward increased risk of RA was observed among overweight and obese women, particularly women diagnosed with RA at earlier ages (≤ 55 years) (59). Moreover, obesity has been revealed to reduce the effectiveness of TNF inhibitors, resulting in lower chances of achieving remission or low disease activity (58, 60). Increased fat mass and obesity-associated

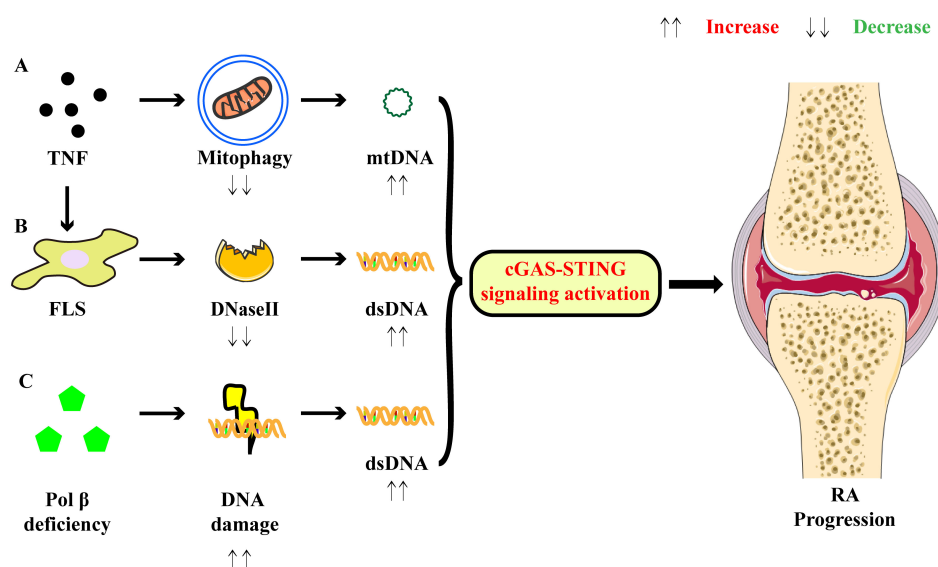


FIGURE 2

Activation of cGAS-STING signaling promotes the pathogenesis of RA. (A) TNF inhibits mitophagy and then results in increased levels of mtDNA. (B) TNF suppresses the expression of DNaseII in FLSs, leading to the accumulation of cytosolic dsDNA. (C) Pol β deficiency promotes DNA damage and dsDNA leakage, resulting in the increased levels of cytosolic dsDNA. All these contribute to the activation of cGAS-STING signaling and subsequent expression of pro-inflammatory factors, thereby supporting the joint inflammation in RA.

protein (FTO) expression has been detected in FLSs from RA patients and synovial cells from adjuvant-induced arthritis (AIA) mice (a mouse model induced by intradermal injection of CFA). The elevated expression of FTO was involved in mtDNA-mediated synovial inflammation (61). In detail, TNF- α -induced mtDNA expression was decreased when FTO was knocked down in RA-FLSs. Furthermore, FTO knockdown suppressed the activation of TNF- α -induced cGAS-STING signaling, accompanied by the decreased expression of inflammatory cytokines such as IL-6 and IL-18, subsequently alleviating AIA (61). Mechanistically, these effects elicited by FTO were dependent on cytidine/uridine monophosphate kinase 2 (CMPK2). The inhibition of CMPK2 expression following FTO reduction led to decreased mtDNA production and cGAS-STING signaling activation, thereby suppressing inflammatory cytokine expression and ameliorating arthritis (61). Therefore, TNF can contribute to the pathogenesis of RA in a cGAS-STING signaling-dependent manner by disrupting mitochondrial homeostasis, and this process can be regulated by FTO.

3.3 cGAS-STING signaling participates in the abnormal activation of FLSs

FLSs exhibit abnormal activation and proliferation in the synovium of RA patients, serving as primary effector cells responsible for mediating joint destruction and synovitis (62). *In vitro*, transfection of dsDNA upregulated the expression of IFN- α and IFN- β in RA-FLSs, suggesting that cytosolic dsDNA accumulation enhanced the IFN-I signature. Additionally, stimulation with dsDNA upregulated the production of pro-inflammatory cytokines and matrix metalloproteinase (MMP) 13 in FLSs. TNF- α -induced DNaseII reduction might be responsible for the accumulation of dsDNA in FLSs, as TNF- α stimulation decreased both the mRNA and protein levels of DNaseII (63). Mechanistically, cGAS-STING signaling was implicated in the cytosolic dsDNA-triggered responses in FLSs. Knockdown of cGAS or STING significantly suppressed the dsDNA-induced pro-inflammatory cytokines secretion (63). Additionally, another study demonstrated that dsDNA-triggered cGAS-STING signaling augmented the migratory and invasive capabilities of RA-FLSs, which were suppressed by cGAS or STING short hairpin RNA treatment (64). In this study, scientists found that activation of cGAS-STING signaling increased the levels of mitochondrial reactive oxygen species, which induced the phosphorylation of mammalian sterile 20-like kinase 1 and then activated forkhead box1, subsequently promoting FLS migration and invasion (64). Thus, cGAS-STING signaling appears to be essential for the pathogenic activities of FLSs, and this signaling represents a promising target to prevent the aberrant activation of FLSs for RA treatments.

3.4 Other factors regulate cGAS-STING signaling in RA

The cGAS-STING-NF- κ B signaling, which represents another arm of the STING signaling network, has been documented to induce macrophage pyroptosis, a process that holds significant importance in RA (65). In this study, they found that DNA

polymerase β (Pol β) regulated RA pathogenesis through STING-NF- κ B signaling-induced macrophage pyroptosis (65). In both active RA patients and CIA mice, the levels of Pol β underwent a significant downregulation, and Pol β -deficient CIA mice exhibited exacerbated disease severity. Further investigations revealed that deficiency of Pol β promoted an augmented inflammatory response and macrophage pyroptosis in CIA mice (65). This process was mechanistically linked to enhanced DNA damage and the accumulation of dsDNA, which triggered the activation of cGAS-STING signaling. Then, NF- κ B signaling was activated and NF- κ B-p65 nuclear translocation was enhanced, ultimately enhancing the expression of NLRP3, IL-1 β , and IL-18. These events contributed to macrophage pyroptosis and the progression of arthritis (65).

The role of the tumor suppressor gene p53 in RA pathogenesis has been explored in AIA rats (66). Overexpression of p53^{R211*} significantly alleviated arthritis symptoms and joint destruction in AIA rats, which were similar to those observed in MTX-treated rats. Beyond inhibiting T-cell activation and Th17 cell differentiation, the interaction between p53^{R211*} and TBK1 disrupted the formation of the trimeric TBK1-IRF3-STING complex. Thus, the phosphorylation and nuclear localization of IRF3 were inhibited, ultimately suppressing the autoimmunity and ameliorating inflammatory arthritis (66).

3.5 cGAS-STING signaling: RA onset and chronic inflammation

According to the existing literature, it seems that cGAS-STING signaling predominantly contributes to the chronic inflammation in RA. For example, there was no significant difference in the clinical scores between CIA-modeled *Sting1*^{+/-} mice and wild-type mice on days 27, 30, and 33 after the first immunization, although the clinical scores of both groups were increased. Notably, the clinical scores of *Sting1*^{+/-} mice were significantly lower than those of wild-type mice from day 36, indicating the promoting effects of STING during disease progression (54). Moreover, another study has revealed that joint injection of DNA fragments increases the arthritic score and hind paw volume in AIA rats, which may be due to the upregulation of cGAS-STING signaling (67). For disease onset, it has been demonstrated that TREX1 reduction and cfDNA accumulation can be risk factors for the onset of RA in elderly through activating the cGAS signaling cascade, and these characteristics have been observed in elderly RA patients and AIA rats. On day 12, the first symptom was observed in AIA rats injected intravenously with DNA fragments, indicating that intravenous injection of DNA promoted the disease onset (67). Although the pathogenesis is complex, targeting cfDNA and cGAS-STING signaling may open a new window for prevention and treatment strategies for RA.

4 cGAS-STING signaling: be protective in RA?

Contrary to the pathogenic effects previously mentioned, one study suggested that STING might be a “negative” regulator

in the CIA model by modulating B cell functions (68). STING-deficient mice showed disease progression comparable to wild-type mice, including incidence, arthritis scores, histopathological changes, and other inflammatory parameters such as B220⁺ cells, CD4⁺ cells, and IL-6 (68). However, STING-deficient mice exhibited elevated levels of anti-CII IgG and IgG2c after three weeks of the first immunization. Gene expression profiles suggested that the disease progression in CIA mice might not have a direct correlation with IFN. Instead, the B cell receptor emerged as a significant factor, suggesting the involvement of B cells (68). B cells from STING-deficient mice exhibited enhanced survival capabilities compared to wild-type B cells, accompanied by similar cell proliferation. Furthermore, STING activation resulted in B cell death and increased Fas expression (68). Therefore, STING played a regulatory role during the development of arthritis by modulating B cell functions, and it would be interesting to explore whether the function of B cell subtypes (such as regulatory B cells) could be regulated by cGAS-STING signaling in RA. Given the conflicting results, it is reasonable to speculate that the balance of STING signaling activation in different cells may influence the disease progression, such as in B cells and FLSs. Collectively, the role of the cGAS-STING pathway in RA suggests that further investigation is needed to clarify the underlying molecular mechanisms.

5 cGAS-STING signaling: a target for RA treatment

According to the above description, cGAS-STING signaling primarily plays a pathogenic role in RA. Increasing studies have reported the application of pharmacologic modulators targeting cGAS-STING signaling (54, 69–71) (Figure 3). As the stimulator of cGAS-STING signaling, clearance of cfDNA is promising in RA therapies. Moreover, we mainly discuss representative cGAS-STING inhibitors that have been studied in RA, and other inhibitors of cGAS-STING pathway have also been summarized in Table 1.

5.1 Scavengers of cfDNA

Cationic nanoparticles (cNPs) are composed of the diblock copolymer of poly(lactic-co-glycolic acid) (PLGA) and poly(2-(diethylamino)ethyl methacrylate) (PDMA), which have shown high DNA binding efficiency and the ability to scavenge cfDNA from RA patients (96). To decrease the risk of dissociation and toxicity, a series of silica particles grafted with PDMA (SiNP@PDMA) brush were developed. SiNP@PDMA was able to scavenge cfDNA, accompanied by the prolonged retention time in joints (97). Bioinspired nanogel composed of DNase I and a polylysine

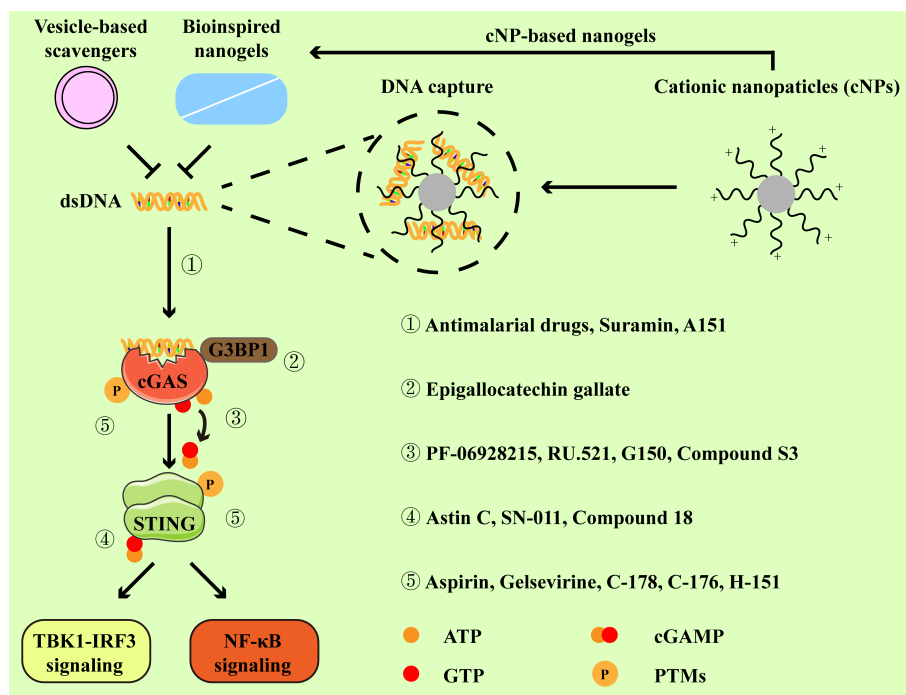


FIGURE 3

Inhibitors and their targets in the cGAS-STING pathway. Cationic nanoparticles, bioinspired nanogels, and vesicle-based scavengers serve as efficient tools to capture dsDNA, thereby preventing cGAS from activation. Representative inhibitors specifically targeting cGAS-STING pathway primarily function through the following mechanisms: ① by disrupting the interaction between cGAS and dsDNA. ② by impeding the association between GRPase-activating protein-(SH3 domain)-binding protein 1 (G3BP1, a facilitator of cGAS oligomerization) and cGAS. ③ by binding to the active site of cGAS. ④ by occupying the cyclic dinucleotide (CDN)-binding site of STING. ⑤ by suppressing the activation of cGAS-STING signaling via post-translational modifications (PTMs).

TABLE 1 Other inhibitors of cGAS-STING signaling pathway and their effects.

Modulators	Targets	Effects	Cell lines/Animal models	Applications in preclinical or clinical RA	References
PF-06928215	cGAS	binds to the active site of cGAS	Sf9 cells	–	(72)
RU.521	cGAS	binds to the active site of cGAS	RAW cells and BMDMs from AGS mice	attenuates tumor-like biologic behaviors of FLSs	(40, 73)
Compound S3	cGAS	binds to the active site of cGAS	–	–	(74)
G chemotype compounds (G150)	cGAS	binds to the active site of cGAS	THP-1 cells and primary human macrophages	–	(75)
Suramin	cGAS	displaces DNA from cGAS	THP-1 cells	reduces inflammation and repairs joint destruction in CIA rats	(76, 77)
X6	cGAS	displaces DNA from cGAS	THP-1 cells and <i>Trex</i> ^{−/−} mice	–	(78, 79)
A151	cGAS	interacts with the dsDNA-binding domain of cGAS	THP-1 cells and <i>Trex</i> ^{−/−} cells	–	(80)
Cyclopeptide inhibitors (XQ2B)	cGAS	binds to the DNA binding site of cGAS	THP-1 cells and HSV-1 infected mice	–	(81)
Aspirin	cGAS	acetylates cGAS	PBMCs from AGS patients, THP-1 cells, <i>Trex</i> ^{−/−} mice	has been used as NSAIDs	(82, 83)
CU-32, CU-76	cGAS	–	THP-1 cells	–	(84)
Astin C	STING	binds to the CDN-binding site of STING	<i>Trex</i> ^{−/−} BMDMs and <i>Trex</i> ^{−/−} mice	–	(85)
SN-011	STING	binds to the CDN-binding pocket of STING	HSV-1-infected HFFs, 293T cells, <i>Trex</i> ^{−/−} BMDMs, <i>Trex</i> ^{−/−} mice	–	(86)
Compound 18	STING	binds to the CDN-binding site of STING	–	–	(87)
C-178, C-176, H-151	STING	binds to STING palmitoylation sites	293T cells, <i>Trex</i> ^{−/−} mice	inhibits the formation and activation of osteoclasts	(88, 89)
BPK-21/5	STING	binds to STING palmitoylation sites	PBMCs	–	(90)
NO ₂ -FAs	STING	modifies STING by nitro-alkylation	RAW264.7 cells, THP-1 cells	–	(91)
Gelsevirine	STING	promotes K48-linked poly-ubiquitination of STING	Murine chondrocytes, OA mice	–	(92)
Nitisinone	STING	suppresses the cGAS-STING-NF-κB pathway	Murine chondrocytes, OA mice	–	(93)
TGP	STING	attenuates STING-IRF3 interaction	THP-1 cells and BMDMs	improves disease severity and reduces inflammation levels	(94, 95)

Sf9 cells, *Spodoptera frugiperda* cell line; BMDMs, bone marrow-derived macrophages; AGS, Aicardi-Goutières syndrome; THP-1 cells, Tohoku Hospital Pediatrics-1; *Trex*^{−/−} mice, transcription export-deficient mice; PBMCs, peripheral blood mononuclear cells; HSV-1, herpes simplex virus-1; CDN, cyclic dinucleotide; HFFs, human foreskin fibroblasts; OA, osteoarthritis; TGP, total glucosides of paeony; –, not mentioned.

dendrimer (G3K) showed potent DNA trapping abilities while retaining nearly 90% of the biological activity of DNase I, making it effective in scavenging cfDNA (98). Recently, some novel scavengers that may be used for joint injection have been explored (99, 100). cNP-pp-PEG was designed to ensure the release of cations when polyethylene glycol (PEG) was removed by MMP2, an enzyme highly expressed in inflamed joints (99). Similarly, exosomes from M2 macrophages were modified with oligolysine and MMP-cleavable PEG, allowing the release of positively charged oligolysine to effectively scavenge cfDNA

within inflamed joints (100). Although these studies have not directly explored the effects of scavengers on cGAS-STING signaling, it is possible to speculate that cGAS-STING signaling is involved in the therapeutic effects of DNA scavengers in arthritis.

5.2 Modulators of cGAS

The exploration of engineering and delivery mechanisms for modulators targeting cGAS, aimed at immunotherapy for RA, has

been conducted in recent studies (71, 101). At first, they found that cfDNA and cGAS expression in lymph nodes or spleen from CIA mice and RA patients were upregulated. As described above, cNPs could inhibit cGAS activation and pro-inflammatory responses via scavenging cfDNA. A nanomedicine-in-hydrogel (NiH) system was devised to concurrently deliver the cGAS inhibitor (RU.521) and cNPs, which could prolong the release and retention of cNPs and RU.521 in lymphoid tissues (71, 101). Loading RU.521 to cNPs resulted in a profound reduction in *ifnb*, *Nos2*, and *Tnfa* in macrophages, indicating the enhanced inhibitory effects on cGAS activation and pro-inflammatory responses (101). In CIA mice, NiH ameliorated arthritis progression and reduced arthritis severity. Moreover, NiH supported the immunosuppression in CIA mice, as indicated by the reduced production of pro-inflammatory cytokines, along with a decrease in the proportions of pro-inflammatory cells and an expansion of immunomodulatory cells (71, 101). Moreover, subcutaneous administration of NiH could also achieve the above effects, not only in lymph nodes, but also in peripheral blood (71).

Anti-malarial drugs (AMDs) are commonly applied in malaria treatment and have also shown beneficial effects on autoimmune diseases over the past decades (69, 102). According to earlier research, the majority of RA patients responded to hydroxychloroquine (HCQ) treatment, as evidenced by improvements in joint score, pain, and grip strength. Only a small part of patients experienced a flare after the initial improvement (103, 104). HCQ could suppress autoimmunity by blocking MHC II-mediated autoantigen presentation and downregulating TLR signaling, and it was observed that AMDs might also regulate the activity of cGAS (102). *In silico* studies predicted that HCQ and other AMDs interacted with cGAS-DNA complex at a site necessary for binding to cGAS and its activation by DNA, and *in vitro* experiments confirmed that quinacrine blocked the binding between dsDNA and cGAS (78). Interestingly, the interaction between quinoline- and acridine-based antimalarial drugs (QA-AMDs) and dsDNA manifested in three modes: intercalation, groove binding, and covalent binding (105). Thus, AMDs might impair DNA-stimulated cGAS activation and subsequent pro-inflammatory cytokine expression, thereby alleviating RA progression. The combination of AMDs and other therapeutic drugs for RA therapy has been explored (106, 107). Compared with the methotrexate/leflunomide (MTX/LEF) group, MTX/HCQ-treated patients had a higher level of remission rate, accompanied by a rapid remission. Remarkably, more patients treated with MTX/HCQ were able to withdraw glucocorticoid exposure than those treated with MTX/LEF (107). A novel Pluronic® F-127 nanomicelle co-loaded with HCQ and MTX exhibited therapeutic effects against murine arthritis, which efficiently suppressed the osteoclastogenesis (106). Now, there are more potent anti-inflammatory drugs and biological agents, which may limit the application of AMDs in RA treatments (3).

5.3 Modulators of STING

Recent studies have delved into compounds that modulate STING activity and their potential utilization in the treatment of RA (54, 70). C-176, a covalent small-molecule inhibitor with the ability to antagonize STING and suppress IFN-I production, has been demonstrated to attenuate the disease development and reduce the bone erosion in CIA mice. Mice treated with of C-176 displayed reduced disease scores, accompanied by the decreased level of tartrate-resistant acid phosphatase-expressing osteoclasts (88). There was a study that confirmed the efficacy of polyethyleneimine-polydopamine (PEI-PDA)@C-176 NPs in adsorbing DNA and inhibiting STING, suggesting their potential application in the treatment of RA (54). *In vitro*, PEI-PDA@C-176 NPs suppressed the phosphorylation and activation of TBK1 and IRF3, leading to a notable reduction in IFN- β , TNF- α , and IL-6 expression in human primary FLSs (54). In dsDNA-induced arthritis and CIA models, PEI-PDA@C-176 NPs effectively alleviated inflammation, which was evidenced by improved ankle swelling, reduced histological scores, and other disease indexes (54). Mechanistically, these therapeutic effects were dependent on the STING signaling pathway, because PEI-PDA@C-176 NPs only slightly reduced the clinical score in CIA-modeled *Sting1^{+/-}* mice without improvements in synovitis (54).

Triptolide (TP), the pharmacological component of the herb *Tripterygium wilfordii* Hook F (TWHF), has shown therapeutic effects in RA. Previous studies revealed that TP exerted therapeutic effects in RA by targeting RA-associated proteins (such as NF- κ B, MMP-9 and JNK), accompanied by reduced activity of FLSs and Th17 differentiation (108–110). Interestingly, a recent study has reported that TP can exerts immunomodulatory effects by regulating cGAS-STING signaling (70). FDL@TP is formed by encapsulating TP with an amphiphilic polymer (FDL) composed of folic acid and lauric acid, which has been investigated in RA treatment (70). FDL@TP exhibited the ability to specifically target joints and efficiently promoted the uptake of TP by M1 macrophages. FDL@TP reduced the expression of cGAS and STING, which further led to the reduction in TNF- α , IL-1 β , and IL-6 production (70). Importantly, FDL@TP was more effective than the same dose of TP alone in controlling inflammatory responses, also with reduced side effects (70). In recent years, nanodrugs based on TP have been developed for RA therapy, including folate-modified TP liposomes, TP nanoemulsion gel, and TP-carrying dendritic cell-derived exosomes, which are promising for localized treatment with reduced toxicity (111–113). However, their effects on cGAS-STING signaling remain to be investigated.

5.4 Other modulators of cGAS-STING signaling pathway

Additional modulators primarily target the downstream signaling of cGAS-STING signaling pathway, and some of them

have been studied in animal models. CS12192, a small molecule inhibitor of JAKs, primarily targets JAK3/1 and has inhibitory effects on TBK1. This leads to the reduced activation of IRF3 and downregulation of IFN- λ . In preclinical models of arthritis, CS12192 has been reported to ameliorate the disease severity and bone destruction, along with immunomodulatory effects such as the suppression of CD4⁺ T cell activation and reduction in pro-inflammatory cytokine production (114). Itaconate (ITA) is an endogenous metabolite from the tricarboxylic acid cycle, which has been confirmed to suppress osteoarthritis by reducing the activation of STING-dependent NF- κ B pathway. In a preclinical model of RA, ITA reduced arthritis severity and bone erosion by suppressing the proliferation and migration of FLSs. In addition, mice lacking immunoresponsive gene 1 (Irg1) failed to express endogenous ITA and showed more severe arthritis, underscoring the role of ITA in modulating inflammation (115, 116). Auranofin, a gold compound approved by U.S. Food and Drug Administration for RA treatment, has been demonstrated to act as a small-molecule inhibitor of IRF3 (117). In this study, they demonstrated that auranofin promoted the degradation of IRF3 by inducing cellular autophagy, thereby suppressing the transcriptional activities of IRF3 (117).

Although these modulators exhibit potential in inhibiting RA progression, efficacy improvement remains an important task. Moreover, considering the long course of RA, strategies to prolong the release and consumption of these inhibitors (such as the use of a hydrogel system) are important areas for future clinical research.

6 Conclusions and prospects

Hitherto, it is clear that innate immunity holds a pivotal position in the development of autoimmune diseases. In the past few years, there has been a significant increase in interest and understanding surrounding the cGAS-STING signaling, which is a main danger-sensing mechanism of innate immunity. Although there is still much to be learned in autoimmune diseases, it is promising to target cGAS-STING signaling for treatments given the abnormal activation of cGAS-STING signaling by cfDNA (16).

With the deepening of research, the significance of cGAS-STING signaling in rheumatoid arthritis has been gradually recognized. For instance, TNF has been shown to induce the release of mitochondrial DNA (mtDNA), which then activates cGAS-STING-mediated IFN responses, contributing to the progression of arthritis. This effect can be suppressed by FTO knockdown through a CMPK2-dependent manner (57, 61). In addition, dsDNA-induced cGAS-STING signaling has been shown to promote the development of arthritis through the induction of inflammatory factors in FLSs, accompanied by enhanced migration and invasion (63, 65). Notably, there was a study pointed out that deficiency of STING promoted CIA progression by enhancing B cell survival and autoantibody production (68). However, fewer studies are available to further confirm the roles of cGAS-STING signaling in the differentiation and function of B cells during RA development.

Considering the critical roles of TNF in DNaseII reduction, mtDNA release, and cGAS expression, TNF inhibitors may also inhibit the cGAS-STING signaling. For cfDNA clearance, several scavengers (such as cNPs and cNP-pp-PEG) have been developed and exhibit strong DNA-capturing abilities (96, 99). Current pharmacological modulators targeting cGAS-STING signaling mainly include NiH, PEI-PDA@C-176 NPs, and FDL@TP, and these inhibitors have been confirmed to be effective in both *in vitro* experiments and murine arthritis (54, 70, 71). Due to challenges in medicinal chemistry, one antagonist (VENT-03, targeting cGAS) has been advanced into phase I clinical trials, which aims to evaluate the safety of VENT-03 in healthy volunteers, and subsequent trial plans will target the treatment of autoimmune diseases (118). Thus, there is still a lack of evidence in treating human RA. Collectively, future explorations should pay more attention to the following fields: 1) molecular mechanisms regulating the activation of cGAS-STING signaling during RA; 2) the development of novel drugs targeting the cGAS-STING signaling pathway, with emphasis on clinical applications. These efforts may provide new insights into the therapies for RA and other autoimmune diseases.

Author contributions

QZ: Software, Writing – original draft, Writing – review & editing. HZ: Conceptualization, Investigation, Methodology, Supervision, Writing – review & editing.

Funding

The author(s) declare that no financial support was received for the research, authorship, and/or publication of this article.

Acknowledgments

The authors thank all researchers who contributed to the advancement of science.

Conflict of interest

The authors declare that the research was conducted in the absence of any commercial or financial relationships that could be construed as a potential conflict of interest.

Publisher's note

All claims expressed in this article are solely those of the authors and do not necessarily represent those of their affiliated organizations, or those of the publisher, the editors and the reviewers. Any product that may be evaluated in this article, or claim that may be made by its manufacturer, is not guaranteed or endorsed by the publisher.

References

- Lee DM, Weinblatt ME. Rheumatoid arthritis. *Lancet*. (2001) 358:903–11. doi: 10.1016/s0140-6736(01)06075-5
- McInnes IB, Schett G. The pathogenesis of rheumatoid arthritis. *New Engl J Med*. (2011) 365:2205–19. doi: 10.1056/NEJMra1004965
- Burmester GR, Pope JE. Novel treatment strategies in rheumatoid arthritis. *Lancet*. (2017) 389:2338–48. doi: 10.1016/s0140-6736(17)31491-5
- Wang X, Kong Y, Li Z. Advantages of Chinese herbal medicine in treating rheumatoid arthritis: A focus on its anti-inflammatory and anti-oxidative effects. *Front Med*. (2024) 11:1371461. doi: 10.3389/fmed.2024.1371461
- Smolen JS, Landewé RBM, Bergstra SA, Kerschbaumer A, Sepriano A, Aletaha D, et al. Eular recommendations for the management of rheumatoid arthritis with synthetic and biological disease-modifying antirheumatic drugs: 2022 update. *Ann rheum Dis*. (2023) 82:3–18. doi: 10.1136/ard-2022-223356
- Edilova MI, Akram A, Abdul-Sater AA. Innate immunity drives pathogenesis of rheumatoid arthritis. *Biomed J*. (2021) 44:172–82. doi: 10.1016/j.bj.2020.06.010
- Goh FG, Midwood KS. Intrinsic danger: activation of toll-like receptors in rheumatoid arthritis. *Rheumatol (Oxford England)*. (2012) 51:7–23. doi: 10.1093/rheumatology/ker257
- Cooles FAH, Anderson AE, Lendrem DW, Norris J, Pratt AG, Hilkens CMU, et al. The interferon gene signature is increased in patients with early treatment-naïve rheumatoid arthritis and predicts a poorer response to initial therapy. *J Allergy Clin Immunol*. (2018) 141:445–8.e4. doi: 10.1016/j.jaci.2017.08.026
- Cooles FAH, Tarn J, Lendrem DW, Naamane N, Lin CM, Millar B, et al. Interferon-A-mediated therapeutic resistance in early rheumatoid arthritis implicates epigenetic reprogramming. *Ann rheum Dis*. (2022) 81:1214–23. doi: 10.1136/annrheumdis-2022-222370
- Lin CMA, Isaacs JD, Cooles FAH. Role of ifn- α in rheumatoid arthritis. *Curr Rheumatol Rep*. (2024) 26:37–52. doi: 10.1007/s11926-023-01125-6
- Cai X, Chiu YH, Chen ZJ. The cgas-cgamp-sting pathway of cytosolic DNA sensing and signaling. *Mol Cell*. (2014) 54:289–96. doi: 10.1016/j.molcel.2014.03.040
- Yu Y, Xue X, Tang W, Su L, Zhang L, Zhang Y. Cytosolic DNA-Mediated sting-dependent inflammation contributes to the progression of psoriasis. *J Invest Dermatol*. (2022) 142:898–906.e4. doi: 10.1016/j.jid.2021.08.430
- Ni H, Zhang H, Li L, Huang H, Guo H, Zhang L, et al. T cell-intrinsic sting signaling promotes regulatory T cell induction and immunosuppression by upregulating foxp3 transcription in cervical cancer. *J Immunother Cancer*. (2022) 10:e005151. doi: 10.1136/jitc-2022-005151
- Tani T, Mathysaraja H, Campisi M, Li ZH, Haratani K, Fahey CG, et al. Trex1 inactivation unleashes cancer cell sting-interferon signaling and promotes antitumor immunity. *Cancer Discovery*. (2024) 14:752–65. doi: 10.1158/2159-8290.Cd-23-0700
- Wang H, Hu DQ, Xiao Q, Liu YB, Song J, Liang Y, et al. Defective sting expression potentiates il-13 signaling in epithelial cells in eosinophilic chronic rhinosinusitis with nasal polyps. *J Allergy Clin Immunol*. (2021) 147:1692–703. doi: 10.1016/j.jaci.2020.12.623
- Decout A, Katz JD, Venkatraman S, Ablasser A. The cgas-sting pathway as a therapeutic target in inflammatory diseases. *Nat Rev Immunol*. (2021) 21:548–69. doi: 10.1038/s41577-021-00524-z
- Hopfner KP, Hornung V. Molecular mechanisms and cellular functions of cgas-sting signalling. *Nat Rev Mol Cell Biol*. (2020) 21:501–21. doi: 10.1038/s41580-020-0244-x
- Gui X, Yang H, Li T, Tan X, Shi P, Li M, et al. Autophagy induction via sting trafficking is a primordial function of the cgas pathway. *Nature*. (2019) 567:262–6. doi: 10.1038/s41586-019-1006-9
- Bai J, Cervantes C, He S, He J, Plasko GR, Wen J, et al. Mitochondrial stress-activated cgas-sting pathway inhibits thermogenic program and contributes to overnutrition-induced obesity in mice. *Commun Biol*. (2020) 3:257. doi: 10.1038/s42003-020-0986-1
- Ding R, Li H, Liu Y, Ou W, Zhang X, Chai H, et al. Activating cgas-sting axis contributes to neuroinflammation in cvst mouse model and induces inflammasome activation and microglia pyroptosis. *J Neuroinflamm*. (2022) 19:137. doi: 10.1186/s12974-022-02511-0
- Hou Y, Wei Y, Lautrup S, Yang B, Wang Y, Cordonnier S, et al. Nad(+) supplementation reduces neuroinflammation and cell senescence in a transgenic mouse model of Alzheimer's disease via cgas-sting. *Proc Natl Acad Sci U.S.A.* (2021) 118:e2011226118. doi: 10.1073/pnas.2011226118
- Xie F, Zhu Q. The regulation of cgas-sting signaling by rna virus-derived components. *Viral J*. (2024) 21:101. doi: 10.1186/s12985-024-02359-1
- Liu J, Rui K, Peng N, Luo H, Zhu B, Zuo X, et al. The cgas-sting pathway: post-translational modifications and functional implications in diseases. *Cytokine Growth fact Rev*. (2022) 68:69–80. doi: 10.1016/j.cytogfr.2022.09.003
- Zhao J, Zhen N, Zhou Q, Lou J, Cui W, Zhang G, et al. Nets promote inflammatory injury by activating cgas-sting pathway in acute lung injury. *Int J Mol Sci*. (2023) 24:5125. doi: 10.3390/ijms24065125
- Sun L, Wu J, Du F, Chen X, Chen ZJ. Cyclic gmp-amp synthase is a cytosolic DNA sensor that activates the type I interferon pathway. *Sci (New York NY)*. (2013) 339:786–91. doi: 10.1126/science.1232458
- Luecke S, Holleufer A, Christensen MH, Jönsson KL, Boni GA, Sørensen LK, et al. Cgas is activated by DNA in a length-dependent manner. *EMBO Rep*. (2017) 18:1707–15. doi: 10.15252/embr.201744017
- Andreeva L, Hiller B, Kostrewa D, Lässig C, de Oliveira Mann CC, Jan Drexler D, et al. Cgas senses long and hmgb/tfam-bound U-turn DNA by forming protein-DNA ladders. *Nature*. (2017) 549:394–8. doi: 10.1038/nature23890
- Du M, Chen ZJ. DNA-induced liquid phase condensation of cgas activates innate immune signaling. *Sci (New York NY)*. (2018) 361:704–9. doi: 10.1126/science.aat1022
- Xie W, Patel DJ. Structure-based mechanisms of 2'3'-cgamp intercellular transport in the cgas-sting immune pathway. *Trends Immunol*. (2023) 44:450–67. doi: 10.1016/j.it.2023.04.006
- Mankan AK, Schmidt T, Chauhan D, Goldeck M, Höning K, Gaidt M, et al. Cytosolic rna: DNA hybrids activate the cgas-sting axis. *EMBO J*. (2014) 33:2937–46. doi: 10.15252/emboj.201488726
- Orzalli MH, Broekema NM, Diner BA, Hancks DC, Elde NC, Cristea IM, et al. Cgas-mediated stabilization of ifi16 promotes innate signaling during herpes simplex virus infection. *Proc Natl Acad Sci U.S.A.* (2015) 112:E1773–81. doi: 10.1073/pnas.1424637112
- Kujirai T, Zierhut C, Takizawa Y, Kim R, Negishi L, Uruma N, et al. Structural basis for the inhibition of cgas by nucleosomes. *Sci (New York NY)*. (2020) 370:455–8. doi: 10.1126/science.abd0237
- Pathare GR, Decout A, Glück S, Cavadini S, Makasheva K, Hovius R, et al. Structural mechanism of cgas inhibition by the nucleosome. *Nature*. (2020) 587:668–72. doi: 10.1038/s41586-020-2750-6
- Ugenti C, Lepelley A, Depp M, Badrock AP, Rodero MP, El-Daher MT, et al. Cgas-mediated induction of type I interferon due to inborn errors of histone pre-mrna processing. *Nat Genet*. (2020) 52:1364–72. doi: 10.1038/s41588-020-00737-3
- Sun W, Li Y, Chen L, Chen H, You F, Zhou X, et al. Eris, an endoplasmic reticulum ifn stimulator, activates innate immune signaling through dimerization. *Proc Natl Acad Sci U.S.A.* (2009) 106:8653–8. doi: 10.1073/pnas.0900850106
- Ishikawa H, Barber GN. Sting is an endoplasmic reticulum adaptor that facilitates innate immune signalling. *Nature*. (2008) 455:674–8. doi: 10.1038/nature07317
- Holm CK, Rahbek SH, Gad HH, Bak RO, Jakobsen MR, Jiang Z, et al. Influenza a virus targets a cgas-independent sting pathway that controls enveloped rna viruses. *Nat Commun*. (2016) 7:10680. doi: 10.1038/ncomms10680
- McNab F, Mayer-Barber K, Sher A, Wack A, O'Garra A. Type I interferons in infectious disease. *Nat Rev Immunol*. (2015) 15:87–103. doi: 10.1038/nri3787
- Fernandez-Ruiz R, Niewold TB. Type I interferons in autoimmunity. *J Invest Dermatol*. (2022) 142:793–803. doi: 10.1016/j.jid.2021.11.031
- Weng W, Liu Y, Hu Z, Li Z, Peng X, Wang M, et al. Macrophage extracellular traps promote tumor-like biologic behaviors of fibroblast-like synoviocytes through cgas-mediated pi3k/akt signaling pathway in patients with rheumatoid arthritis. *J Leuko Biol*. (2024) 115:116–29. doi: 10.1093/jleuko/qiad102
- Wang Y, Su GH, Zhang F, Chu JX, Wang YS. Cyclic gmp-amp synthase is required for cell proliferation and inflammatory responses in rheumatoid arthritis synoviocytes. *Mediators Inflammation*. (2015) 2015:192329. doi: 10.1155/2015/192329
- Hashimoto T, Yoshida K, Hashiramoto A, Matsui K. Cell-free DNA in rheumatoid arthritis. *Int J Mol Sci*. (2021) 22:8941. doi: 10.3390/ijms22168941
- Koffler D, Agnello V, Winchester R, Kunkel HG. The occurrence of single-stranded DNA in the serum of patients with systemic lupus erythematosus and other diseases. *J Clin Invest*. (1973) 52:198–204. doi: 10.1172/jci107165
- Leon SA, Revach M, Ehrlich GE, Adler R, Petersen V, Shapiro B. DNA in synovial fluid and the circulation of patients with arthritis. *Arthritis rheum*. (1981) 24:1142–50. doi: 10.1002/art.1780240905
- Dong C, Liu Y, Sun C, Liang H, Dai L, Shen J, et al. Identification of specific joint-inflammation cell-free DNA molecules from synovial fluids of patients with rheumatoid arthritis. *Front Immunol*. (2020) 11:662. doi: 10.3389/fimmu.2020.00662
- Mao J, Tan M, Li J, Liu C, Hao J, Zheng J, et al. Neutrophil extracellular traps induce pyroptosis of rheumatoid arthritis fibroblast-like synoviocytes via the nf-kb/caspase 3/gsdme pathway. *Inflammation*. (2024) 47:921–38. doi: 10.1007/s10753-023-01951-x
- Ramos-Remus C, Dorazco-Barragan G, Aceves-Avila FJ, Alcaraz-Lopez F, Fuentes-Ramirez F, Michel-Diaz J, et al. Genotoxicity assessment using micronuclei assay in rheumatoid arthritis patients. *Clin Exp Rheumatol*. (2002) 20:208–12.
- Wright HL, Lyon M, Chapman EA, Moots RJ, Edwards SW. Rheumatoid arthritis synovial fluid neutrophils drive inflammation through production of chemokines, reactive oxygen species, and neutrophil extracellular traps. *Front Immunol*. (2020) 11:584116. doi: 10.3389/fimmu.2020.584116

49. Karaman A, Binici DN, Melikoglu MA. Comet assay and analysis of micronucleus formation in patients with rheumatoid arthritis. *Mutat Res.* (2011) 721:1–5. doi: 10.1016/j.mrgentox.2010.11.014
50. Attia SM, Al-Hamamah MA, Alotaibi MR, Alasmari AF, Attia MSM, Ahmad SF, et al. Aneugenic and clastogenic alterations in the dba/ij mouse model of rheumatoid arthritis treated with rituximab, an anti-cd20 antibody. *Mutat Res Genet Toxicol Environ mutagen.* (2023) 888:503635. doi: 10.1016/j.mrgentox.2023.503635
51. Madhyastha S, Prabhu LV, Saralaya V, Rai R. A comparison of vitamin a and leucovorin for the prevention of methotrexate-induced micronuclei production in rat bone marrow. *Clinics (Sao Paulo Brazil).* (2008) 63:821–6. doi: 10.1590/s1807-59322008000600019
52. Shahin AA, Ismail MM, Saleh AM, Moustafa HA, Aboul-Ella AA, Gabr HM. Protective effect of folic acid on low-dose methotrexate genotoxicity. *Z fur Rheumatol.* (2001) 60:63–8. doi: 10.1007/s003930170075
53. Scanu A, Lorenzin M, Luisetto R, Galozzi P, Ortolan A, Oliviero F, et al. Identification in synovial fluid of a new potential pathogenic player in arthropathies. *Exp Biol Med (Maywood NJ).* (2022) 247:1061–6. doi: 10.1177/15353702221087966
54. Shen H, Jin L, Zheng Q, Ye Z, Cheng L, Wu Y, et al. Synergistically targeting synovium sting pathway for rheumatoid arthritis treatment. *Bioact mater.* (2023) 24:37–53. doi: 10.1016/j.bioactmat.2022.12.001
55. Noack M, Miossec P. Selected cytokine pathways in rheumatoid arthritis. *Semin Immunopathol.* (2017) 39:365–83. doi: 10.1007/s00281-017-0619-z
56. Croft M, Siegel RM. Beyond tnf: tnf superfamily cytokines as targets for the treatment of rheumatic diseases. *Nat Rev Rheumatol.* (2017) 13:217–33. doi: 10.1038/nrrheum.2017.22
57. Willemsen J, Neuhoft MT, Hoyer T, Noir E, Tessier C, Sarret S, et al. Tnf leads to mtDNA release and cgas/sting-dependent interferon responses that support inflammatory arthritis. *Cell Rep.* (2021) 37:109977. doi: 10.1016/j.celrep.2021.109977
58. Kaeley GS, MacCarter DK, Pangan AL, Wang X, Kalabic J, Ranganath VK. Clinical responses and synovial vascularity in obese rheumatoid arthritis patients treated with adalimumab and methotrexate. *J Rheumatol.* (2018) 45:1628–35. doi: 10.3899/jrheum.171232
59. Lu B, Hiraki LT, Sparks JA, Malspeis S, Chen CY, Awosogba JA, et al. Being overweight or obese and risk of developing rheumatoid arthritis among women: A prospective cohort study. *Ann rheum Dis.* (2014) 73:1914–22. doi: 10.1136/annrheumdis-2014-205459
60. Schäfer M, Meißner Y, Kekow J, Berger S, Remstedt S, Manger B, et al. Obesity reduces the real-world effectiveness of cytokine-targeted but not cell-targeted disease-modifying agents in rheumatoid arthritis. *Rheumatol (Oxford England).* (2020) 59:1916–26. doi: 10.1093/rheumatology/kez535
61. Jin L, Chen Q, Hu K, Fan D, Zhang H, Deng J, et al. The fto-cmpk2 pathway in fibroblast-like synoviocytes modulates rheumatoid arthritis synovial inflammation and cartilage homeostasis via mtDNA regulation. *Int J Biol Sci.* (2024) 20:1617–33. doi: 10.7150/ijbs.90677
62. Nygaard G, Firestein GS. Restoring synovial homeostasis in rheumatoid arthritis by targeting fibroblast-like synoviocytes. *Nat Rev Rheumatol.* (2020) 16:316–33. doi: 10.1038/s41584-020-0413-5
63. Wang J, Li R, Lin H, Qiu Q, Lao M, Zeng S, et al. Accumulation of cytosolic dsDNA contributes to fibroblast-like synoviocytes-mediated rheumatoid arthritis synovial inflammation. *Int Immunopharmacol.* (2019) 76:105791. doi: 10.1016/j.intimp.2019.105791
64. Li R, Lin W, Kuang Y, Wang J, Xu S, Shen C, et al. Cgas/sting signaling in the regulation of rheumatoid synovial aggression. *Ann Trans Med.* (2022) 10:431. doi: 10.21037/atm-21-4533
65. Gu L, Sun Y, Wu T, Chen G, Tang X, Zhao L, et al. A novel mechanism for macrophage pyroptosis in rheumatoid arthritis induced by pol B deficiency. *Cell Death Dis.* (2022) 13:583. doi: 10.1038/s41419-022-05047-6
66. Zeng Y, Ng JPL, Wang L, Xu X, Law BYK, Chen G, et al. Mutant P53(R211*) ameliorates inflammatory arthritis in aia rats via inhibition of tbk1-irf3 innate immune response. *Inflammation res: Off J Eur Histamine Res Soc.* (2023) 72:2199–219. doi: 10.1007/s00011-023-01809-w
67. Luo WD, Wang YP, Lv J, Liu Y, Qu YQ, Xu XF, et al. Age-related self-DNA accumulation may accelerate arthritis in rats and in human rheumatoid arthritis. *Nat Commun.* (2023) 14:4394. doi: 10.1038/s41467-023-40113-3
68. Tansakul M, Thim-Uam A, Saethang T, Makjaroen J, Wongprom B, Pisitkun T, et al. Deficiency of sting promotes collagen-specific antibody production and B cell survival in collagen-induced arthritis. *Front Immunol.* (2020) 11:1101. doi: 10.3389/fimmu.2020.01101
69. An J, Minie M, Sasaki T, Woodward JJ, Elkon KB. Antimalarial drugs as immune modulators: new mechanisms for old drugs. *Annu Rev Med.* (2017) 68:317–30. doi: 10.1146/annurev-med-043015-123453
70. Xu A, Yang R, Zhang M, Wang X, Di Y, Jiang B, et al. Macrophage targeted triptolide micelles capable of cgas-sting pathway inhibition for rheumatoid arthritis treatment. *J Drug Targeting.* (2022) 30:961–72. doi: 10.1080/1061186x.2022.2070173
71. Zhou S, Cheng F, Zhang Y, Su T, Zhu G. Engineering and delivery of cgas-sting immunomodulators for the immunotherapy of cancer and autoimmune diseases. *Accounts Chem Res.* (2023) 56:2933–43. doi: 10.1021/acs.accounts.3c00394
72. Hall J, Brault A, Vincent F, Weng S, Wang H, Dumlao D, et al. Discovery of pf-06928215 as a high affinity inhibitor of cgas enabled by a novel fluorescence polarization assay. *PLoS One.* (2017) 12:e0184843. doi: 10.1371/journal.pone.0184843
73. Vincent J, Adura C, Gao P, Luz A, Lama L, Asano Y, et al. Small molecule inhibition of cgas reduces interferon expression in primary macrophages from autoimmune mice. *Nat Commun.* (2017) 8:750. doi: 10.1038/s41467-017-00833-9
74. Zhao W, Xiong M, Yuan X, Li M, Sun H, Xu Y. In silico screening-based discovery of novel inhibitors of human cyclic gmp-amp synthase: A cross-validation study of molecular docking and experimental testing. *J Chem Inf model.* (2020) 60:3265–76. doi: 10.1021/acs.jcim.0c00171
75. Lama L, Adura C, Xie W, Tomita D, Kamei T, Kuryavyy V, et al. Development of human cgas-specific small-molecule inhibitors for repression of dsDNA-triggered interferon expression. *Nat Commun.* (2019) 10:2261. doi: 10.1038/s41467-019-08620-4
76. Wang M, Soreshjani MA, Mikek C, Opoku-Temeng C, Sintim HO. Suramin potently inhibits cgas synthase, cgas, in thp1 cells to modulate ifn-beta levels. *Future Med Chem.* (2018) 10:1301–17. doi: 10.4155/fmc-2017-0322
77. Sahu D, Saroha A, Roy S, Das S, Srivastava PS, Das HR. Suramin ameliorates collagen induced arthritis. *Int Immunopharmacol.* (2012) 12:288–93. doi: 10.1016/j.intimp.2011.12.003
78. An J, Woodward JJ, Sasaki T, Minie M, Elkon KB. Cutting edge: antimalarial drugs inhibit ifn- β Production through blockade of cyclic gmp-amp synthase-DNA interaction. *J Immunol (Baltimore Md: 1950).* (2015) 194:4089–93. doi: 10.4049/jimmunol.1402793
79. An J, Woodward JJ, Lai W, Minie M, Sun X, Tanaka L, et al. Inhibition of cyclic gmp-amp synthase using a novel antimalarial drug derivative in trex1-deficient mice. *Arthritis Rheumatol (Hoboken NJ).* (2018) 70:1807–19. doi: 10.1002/art.40559
80. Steinhagen F, Zillinger T, Peukert K, Fox M, Thudium M, Barchet W, et al. Suppressive oligodeoxynucleotides containing ttagg motifs inhibit cgas activation in human monocytes. *Eur J Immunol.* (2018) 48:605–11. doi: 10.1002/eji.201747338
81. Wang X, Wang Y, Cao A, Luo Q, Chen D, Zhao W, et al. Development of cyclopeptide inhibitors of cgas targeting protein-DNA interaction and phase separation. *Nat Commun.* (2023) 14:6132. doi: 10.1038/s41467-023-41892-5
82. Dai J, Huang YJ, He X, Zhao M, Wang X, Liu ZS, et al. Acetylation blocks cgas activity and inhibits self-DNA-induced autoimmunity. *Cell.* (2019) 176:1447–60 e14. doi: 10.1016/j.cell.2019.01.016
83. Gall EP. The safety of treating rheumatoid arthritis with aspirin. *Jama.* (1982) 247:63–4. doi: 10.1001/jama.1982.03320260047031
84. Padilla-Salinas R, Sun L, Anderson R, Yang X, Zhang S, Chen ZJ, et al. Discovery of small-molecule cyclic gmp-amp synthase inhibitors. *J Org Chem.* (2020) 85:1579–600. doi: 10.1021/acs.joc.9b02666
85. Li S, Hong Z, Wang Z, Li F, Mei J, Huang L, et al. The cyclopeptide astin C specifically inhibits the innate immune cdc sensor sting. *Cell Rep.* (2018) 25:3405–21.e7. doi: 10.1016/j.celrep.2018.11.097
86. Hong Z, Mei J, Li C, Bai G, Maimaiti M, Hu H, et al. Sting inhibitors target the cyclic dinucleotide binding pocket. *Proc Natl Acad Sci United States America.* (2021) 118:e2105465118. doi: 10.1073/pnas.2105465118
87. Siu T, Altman MD, Baltus GA, Childers M, Ellis JM, Gunaydin H, et al. Discovery of a novel cgamp competitive ligand of the inactive form of sting. *ACS Med Chem Lett.* (2019) 10:92–7. doi: 10.1021/acsmedchemlett.8b00466
88. Yu ZC, Fu R, Li Y, Zhao DY, Jiang H, Han D. The sting inhibitor C-176 attenuates osteoclast-related osteolytic diseases by inhibiting osteoclast differentiation. *FASEB J.* (2023) 37:e22867. doi: 10.1096/fj.202201600R
89. Haag SM, Gulen MF, Raymond L, Gibelin A, Abrami L, Decout A, et al. Targeting sting with covalent small-molecule inhibitors. *Nature.* (2018) 559:269–73. doi: 10.1038/s41586-018-0287-8
90. Vinogradova EV, Zhang X, Remillard D, Lazar DC, Suciu RM, Wang Y, et al. An activity-guided map of electrophile-cysteine interactions in primary human T cells. *Cell.* (2020) 182:1009–26.e29. doi: 10.1016/j.cell.2020.07.001
91. Hansen AL, Buchan GJ, Rühl M, Mukai K, Salvatore SR, Ogawa E, et al. Nitro-fatty acids are formed in response to virus infection and are potent inhibitors of sting palmitoylation and signaling. *Proc Natl Acad Sci United States America.* (2018) 115:E7768–e75. doi: 10.1073/pnas.1806239115
92. Feng M, Kong D, Guo H, Xing C, Lv J, Bian H, et al. Gelsevirine improves age-related and surgically induced osteoarthritis in mice by reducing sting availability and local inflammation. *Biochem Pharmacol.* (2022) 198:114975. doi: 10.1016/j.bcp.2022.114975
93. Yang T, Ma H, Lai H, Lu Y, Ni K, Hu X, et al. Nitisinone attenuates cartilage degeneration and subchondral osteoclastogenesis in osteoarthritis and concomitantly inhibits the cgas/sting/nf-kb pathway. *Eur J Pharmacol.* (2024) 965:176326. doi: 10.1016/j.ejphar.2024.176326
94. Xiu Y, Wang S, Zhang P, Li C, Wu Z, Wen J, et al. Total glucosides of paeony alleviates cgas-sting-mediated diseases by blocking the sting-irf3 interaction. *Chin J Natural Medicines.* (2024) 22:402–15. doi: 10.1016/s1875-5364(24)60572-8
95. Yang K, Zeng L, Long Z, He Q, Xiang W, Ge A, et al. Efficacy and safety of total glucosides of paeony in the treatment of 5 types of inflammatory arthritis: A systematic review and meta-analysis. *Pharmacol Res.* (2023) 195:106842. doi: 10.1016/j.phrs.2023.106842

96. Liang H, Peng B, Dong C, Liu L, Mao J, Wei S, et al. Cationic nanoparticle as an inhibitor of cell-free DNA-induced inflammation. *Nat Commun.* (2018) 9:4291. doi: 10.1038/s41467-018-06603-5
97. Liu X, Chen S, Liu L, Chen Y. Cationic brush hybrid nanoparticles scavenge cell-free DNA to enhance rheumatoid arthritis treatment. *Acta biomaterialia.* (2023) 170:215–27. doi: 10.1016/j.actbio.2023.08.032
98. Zhu H, Kong B, Che J, Zhao Y, Sun L. Bioinspired nanogels as cell-free DNA trapping and scavenging organelles for rheumatoid arthritis treatment. *Proc Natl Acad Sci U.S.A.* (2023) 120:e2303385120. doi: 10.1073/pnas.2303385120
99. Liu X, Chen S, Yan Y, Liu L, Chen Y. Nanoparticulate DNA scavenger loading methotrexate targets articular inflammation to enhance rheumatoid arthritis treatment. *Biomaterials.* (2022) 286:121594. doi: 10.1016/j.biomaterials.2022.121594
100. Wang Z, Zhang C, Meng J, Jiao Z, Bao W, Tian H, et al. A targeted exosome therapeutic confers both cfDNA scavenging and macrophage polarization for ameliorating rheumatoid arthritis. *Adv Mater (Deerfield Beach Fla).* (2023) 35:e2302503. doi: 10.1002/adma.202302503
101. Cheng F, Su T, Liu Y, Zhou S, Qi J, Guo W, et al. Targeting lymph nodes for systemic immunosuppression using cell-free-DNA-scavenging and cgas-inhibiting nanomedicine-in-hydrogel for rheumatoid arthritis immunotherapy. *Adv Sci (Weinheim Baden-Wuerttemberg Germany).* (2023) 10:e2302575. doi: 10.1002/advs.202302575
102. Schrezenmeier E, Dörner T. Mechanisms of action of hydroxychloroquine and chloroquine: implications for rheumatology. *Nat Rev Rheumatol.* (2020) 16:155–66. doi: 10.1038/s41584-020-0372-x
103. Adams EM, Yocum DE, Bell CL. Hydroxychloroquine in the treatment of rheumatoid arthritis. *Am J Med.* (1983) 75:321–6. doi: 10.1016/0002-9343(83)91211-1
104. Clark P, Casas E, Tugwell P, Medina C, Gheno C, Tenorio G, et al. Hydroxychloroquine compared with placebo in rheumatoid arthritis. *A Random Controlled Trial Ann Internal Med.* (1993) 119:1067–71. doi: 10.7326/0003-4819-119-11-199312010-00002
105. Ehsanian R, Van Waes C, Feller SM. Beyond DNA binding - a review of the potential mechanisms mediating quinacrine's therapeutic activities in parasitic infections, inflammation, and cancers. *Cell commun signal: CCS.* (2011) 9:13. doi: 10.1186/1478-811x-9-13
106. Magne TM, Helal-Neto E, Correa LB, Rebelo Alencar LM, Gemini Piperni S, Iram SH, et al. Rheumatoid arthritis treatment using hydroxychloroquine and methotrexate co-loaded nanomicelles: *in vivo* results. *Colloids surf B Biointerf.* (2021) 206:111952. doi: 10.1016/j.colsurfb.2021.111952
107. Zhang L, Chen F, Geng S, Wang X, Gu L, Lang Y, et al. Methotrexate (Mtx) plus hydroxychloroquine versus mtx plus leflunomide in patients with mtx-resistant active rheumatoid arthritis: A 2-year cohort study in real world. *J Inflammation Res.* (2020) 13:1141–50. doi: 10.2147/jir.S282249
108. Liu X, Wang Z, Qian H, Tao W, Zhang Y, Hu C, et al. Natural medicines of targeted rheumatoid arthritis and its action mechanism. *Front Immunol.* (2022) 13:945129. doi: 10.3389/fimmu.2022.945129
109. Piao X, Zhou J, Xue L. Triptolide decreases rheumatoid arthritis fibroblast-like synovioyte proliferation, invasion, inflammation and presents a therapeutic effect in collagen-induced arthritis rats via inactivating lncrna rp11-83j16.1 mediated uril and B-catenin signaling. *Int Immunopharmacol.* (2021) 99:108010. doi: 10.1016/j.intimp.2021.108010
110. Zhao Z, Huang H, Ke S, Deng B, Wang YX, Xu N, et al. Triptolide inhibits the proinflammatory potential of myeloid-derived suppressor cells via reducing arginase-1 in rheumatoid arthritis. *Int Immunopharmacol.* (2024) 127:111345. doi: 10.1016/j.intimp.2023.111345
111. Guo RB, Zhang XY, Yan DK, Yu YJ, Wang YJ, Geng HX, et al. Folate-modified triptolide liposomes target activated macrophages for safe rheumatoid arthritis therapy. *Biomater Sci.* (2022) 10:499–513. doi: 10.1039/d1bm01520f
112. Rao Q, Ma G, Li M, Wu H, Zhang Y, Zhang C, et al. Targeted delivery of triptolide by dendritic cell-derived exosomes for colitis and rheumatoid arthritis therapy in murine models. *Br J Pharmacol.* (2023) 180:330–46. doi: 10.1111/bph.15958
113. Yang M, Yang D, Han L, Fan Z, Liu J, Yuan Y. Triptolide nanoemulsion gel as a transdermal drug delivery system: preparation, pharmacokinetics, and rheumatoid arthritis evaluation. *Curr Drug delivery.* (2023). doi: 10.2174/1567201821666230808114519
114. Shan S, Zhou Y, Yu J, Yang Q, Pan D, Wang Y, et al. Therapeutic treatment of a novel selective jak3/jak1/tbk1 inhibitor, cs12192, in rat and mouse models of rheumatoid arthritis. *Int Immunopharmacol.* (2019) 77:105914. doi: 10.1016/j.intimp.2019.105914
115. Ni L, Lin Z, Hu S, Shi Y, Jiang Z, Zhao J, et al. Itaconate attenuates osteoarthritis by inhibiting sting/nf-Kb axis in chondrocytes and promoting M2 polarization in macrophages. *Biochem Pharmacol.* (2022) 198:114935. doi: 10.1016/j.bcp.2022.114935
116. Tada M, Kudo Y, Kono M, Kanda M, Takeyama S, Sakiyama K, et al. Itaconate reduces proliferation and migration of fibroblast-like synovioytes and ameliorates arthritis models. *Clin Immunol (Orlando Fla).* (2024) 264:110255. doi: 10.1016/j.jclim.2024.110255
117. Glanz A, Chakravarty S, Fan S, Chawla K, Subramanian G, Rahman T, et al. Autophagic degradation of irf3 induced by the small-molecule auranofin inhibits its transcriptional and proapoptotic activities. *J Biol Chem.* (2021) 297:101274. doi: 10.1016/j.jbc.2021.101274
118. Mullard A. Biotech step on cgas for autoimmune diseases. *Nat Rev Drug Discovery.* (2023) 22:939–41. doi: 10.1038/d41573-023-00185-8



OPEN ACCESS

EDITED BY

Kyle T. Amber,
Rush University, United States

REVIEWED BY

Jialong Chen,
Southern Medical University, China
Qi Gao,
Zhejiang Provincial People's Hospital, China

*CORRESPONDENCE

Shengnan Zhao
✉ zsn15104042205@126.com

RECEIVED 30 July 2024

ACCEPTED 15 October 2024

PUBLISHED 04 November 2024

CITATION

Shang D and Zhao S (2024) Molecular mechanisms of obesity predisposes to atopic dermatitis.
Front. Immunol. 15:1473105.
doi: 10.3389/fimmu.2024.1473105

COPYRIGHT

© 2024 Shang and Zhao. This is an open-access article distributed under the terms of the [Creative Commons Attribution License \(CC BY\)](#). The use, distribution or reproduction in other forums is permitted, provided the original author(s) and the copyright owner(s) are credited and that the original publication in this journal is cited, in accordance with accepted academic practice. No use, distribution or reproduction is permitted which does not comply with these terms.

Molecular mechanisms of obesity predisposes to atopic dermatitis

Dajin Shang¹ and Shengnan Zhao^{1,2*}

¹School of China Medical University, Shenyang, Liaoning, China, ²Department of Dermatology, The First Hospital of China Medical University, Shenyang, China

Obesity is a prevalent metabolic disease that reduces bacterial diversity, colonizes the epidermis with lipophilic bacteria, and increases intestinal pro-inflammatory species, all of which lead to impaired epithelial barriers. Adipose tissue secretes immunomodulatory molecules, such as adipokines, leptin, and adiponectin, which alters the morphology of adipocytes and macrophages as well as modulates T cell differentiation and peripheral Th2-dominated immune responses. Atopic dermatitis (AD) and obesity have similar pathological manifestations, including inflammation as well as insulin and leptin resistance. This review examines the major mechanisms between obesity and AD, which focus on the effect on skin and gut microbiota, immune responses mediated by the toll like receptor (TLR) signaling pathway, and changes in cytokine levels (TNF- α , IL-6, IL-4, and IL13). Moreover, we describe the potential effects of adipokines on AD and finally mechanisms by which PPAR- γ suppresses and regulates type 2 immunity.

KEYWORDS

atopic dermatitis, obesity, immune, adipokines, cytokines

1 Introduction

Atopic dermatitis (AD) is a chronic, recurrent, inflammatory, pruritic dermatosis with complex pathophysiology, involving disruption of the epidermal barrier, microbial dysbiosis within affected lesions, and Th2 immune responses to skin allergens (1). Impaired skin barrier function is thought to be both a cause and a consequence of AD. Severe atopic dermatitis has been linked to deficiencies in the filaggrin (FLG) protein or antimicrobial peptides (2). Increased inflammatory cell infiltration is observed in AD lesions, including T cells, dendritic cells, macrophages, mast cells, and eosinophils (3). These often precipitate increased cytokines including thymic stromal lymphopoietin (TSLP), interleukin-1 (IL-1), IL-4, IL-5, IL-6, IL-25, IL-33, and transforming growth factor- β (TGF- β), which promote inflammation and immune activation. Upregulated expression levels of IL-12, interferon- γ (IFN- γ), and granulocyte-macrophage colony-stimulating factor (GM-CSF) are detected during chronic phase (4). Additionally, Th17 and Th22 cell cytokines, such as IL13, IL-17, CCL17, tumor necrosis factor- α (TNF- α), and IL-22, promote the

formation of chronic skin lesions in AD (4). Atopic sensitization is also associated with IL9, IL33, and IL33R expression during infancy. In addition, AD could be aggravated by dysbiosis or imbalances in microbial species diversity and environmental factors including diet (5).

Obesity, a major health problem, is a result of metabolic syndrome in adipose tissue and is linked to various chronic immune disorders (6). Studies have shown that adipose expansion in early and chronic obesity activates an inflammatory program, altering the immune phenotype to a pro-inflammatory status (7). Adipose depots usually release cytokines, chemokines, and adipokines that coordinately regulate other immune cells, including eosinophils, mast cells, and macrophages in an M2-polarized or alternately activated state (7). Treatment that reduces obesity symptoms could reduce epidermal thickness and eosinophil/mast cell infiltration, along with a reduction in IgE, IL-4, IL-6, TNF- α , and AD-like lesions (8).

Currently, the association of obesity/overweight with AD is not conclusive. Studies addressing obesity in infancy or early childhood (age < 2 years) and AD have found a positive association; from childhood into adulthood; but this was not observed in other cross-sectional studies (9). It has also been shown that obesity may have a pathogenic function in AD. Obese adults are more likely to develop moderate-to-severe AD (10). Investigations have revealed that higher levels of serum IgE and cutaneous mRNA levels of TNF- α , IL-13, and IL-31 are associated with more severe AD in rat models with a higher body weight than those with lower body weight (11). Moreover, IL-5 serum level correlated with both body mass index (BMI) and waist circumference (12). Collectively, these findings indicate that obesity may predispose individuals to or exacerbate AD. The discrepancies observed here may be explained by differences in study designs, the diagnostic criteria of AD, regional differences, and by the varied definitions of overweight and obesity used across studies. Although the potential mechanisms by which obesity contributes to AD are not fully understood, several potential mechanisms should be considered.

In obese or overweight individuals, low levels of adiponectin and PPAR- γ trigger a cascade of events. First, these low levels lead to increased production of cytokines and chemokines. These signaling molecules then activate macrophages and T cells, further promoting inflammation. The resulting inflammatory state can further elevate leptin levels, which can create a vicious cycle by further suppressing adiponectin and PPAR γ (13). The leptin secreted in obese or overweight individuals can upregulate the expression levels of cytokines and chemokines, thereby increase the risk of AD. The increase in AD-related cytokines and chemokines, along with the decrease in PPAR- γ , not only induces inflammation in adipose tissue but also triggers insulin resistance and leptin resistance. This results in adipocyte hypertrophy, adipose tissue hyperplasia, and lipid accumulation, causing obesity (13). Imbalance in gut microbiota can increase an individual's susceptibility to AD by disrupting mucosal immune tolerance. This disruption can affect skin homeostasis through its influence on the signaling pathways that maintain healthy skin barrier function. However, research suggests that changes in gut microbiota alone are likely not enough to trigger the development of AD. The interaction

between specific microbial communities and the immune system, as well as other external factors such as diet, may explain the pathogenesis of AD (14).

2 Correlation between atopic dermatitis and obesity

Among the numerous research records, the results of various studies are not consistent, and the specific role of obesity in atopic dermatitis is not clear, and further exploration is needed. However, more and more evidence shows a certain correlation between atopic dermatitis and obesity. Obesity is one of the comorbidities of AD, and it has been confirmed as one of the risk factors for AD, which can also exacerbate the severity of AD. Compared to non-AD patients, AD patients have a higher probability of developing obesity, and the impact of obesity is more pronounced in the pediatric population. This implies that early-onset obesity in the childhood stage can increase the likelihood of developing AD (15). In a study of datasets in children, it was found that the prevalence of AD peaked early in the age group of 1 to 6 years, with a gradual downward trend (16). In a cohort study, AD was found to be associated with shorter stature, higher BMI, and lower weight in children during childhood. There was a clear association between AD and obesity in children before the age of 5. The association gradually weakened around the age of 5. As children grew, the association between AD and BMI was not consistent throughout childhood, further studies are needed to measure the long-term association and eliminate the impact of diet, sleep, etc. (17). Similarly, one study found that obesity was also significantly associated with the presence of AD in adults (18). Apart from age, geographical variations and gender differences may also influence the clinical presentation of AD and obesity. For instance, in North America and Asia, there is a correlation between increased prevalence of obesity and AD (19). In another study, it was found that there is a positive correlation between obesity and AD occurrence in the female population (20). The interaction between obesity and AD is mediated by various cytokines, immune mediators, and chemokines. Due to the interconnection of these two conditions, alleviating one may potentially prevent or mitigate the progression of the other disease, thereby effectively managing the conditions and enhancing individual health status (13).

3 The role of the microbiota in obesity and AD

Studies have reported a cross-talk mechanism between the skin and the gut. Dysbiosis in gut microbiota potentially disrupts microbial metabolites and pro-inflammatory factors as well as Th2 immune response, causing skin inflammation (21). Furthermore, infants with AD exhibit reduced levels of lactobacilli and bifidobacteria in their gut microbiota. There is also an increased proportion of *Escherichia coli*, *Clostridium*

difficile, and *Staphylococcus aureus* (22). Obesity reduces gut microbial diversity and beneficial microbes in the gut, including *Lactobacillus*, and *Bifidobacterium*. A high-fat and high-sugar dietary habit decreases the abundance of beneficial bacteria including bifidobacteria and lactobacilli. This dietary pattern can also induce increased gut permeability and increased expression of inflammatory markers including TNF- α (23). The abundance of lactobacilli and bifidobacteria was decreased in obese mice models, causing higher circulating levels of LPS, promoting NF- κ B pathway activation through TLR4 signaling pathway, thereby enhancing inflammatory response (24). Additionally, *Corynebacterium* colonization of the epidermis was associated with BMI. One study revealed that a high-fat diet increased skin *Corynebacterium* species and free fatty acids in mice (25). Gut microbiota analysis revealed reduced abundance of Ruminococcaceae in fecal samples of atopic eczema infants. Interestingly, the relative abundance of *Ruminococcus* was inversely related to TLR2-induced IL-6 and TNF- α in IgE-associated eczema (26). Ruminococcaceae was more abundant in the gut microbes of mice with normal weight than in obese mice (27). Moreover, the diversity of Bacteroidetes and Actinobacteria was reduced in atopic eczema infants compared to healthy controls (28). A new polysaccharide, ARS, has been shown to reverse or resist high-fat-diet-induced obesity. It appears to function by increasing the diversity of gut microbiota and optimizing the ratio of Firmicutes to Bacteroidetes (29). Topical treatments for AD, including corticosteroids, antibiotics, and calcineurin inhibitors, increase species diversity of the epidermis, including *Streptococcus*, *Cutibacterium*, and *Corynebacterium* spp (30). Functional foods that prevent obesity increase intestinal microbial diversity and beneficial bacteria (*Bifidobacterium*, *Alloprevotella*, and *Lactobacillus*) and, at the same time decrease harmful bacteria (*Staphylococcus* and *Corynebacterium* 1) (31). Research has shown that “plant-based foods” intake suppresses moderate-to-severe AD (32). *L. plantarum* LM1004 significantly improves the restoration of AD-like symptoms accompanied by decreased levels of Th2 and Th17 cell transcription factors, increased transcription factors of Treg and Th1 cells, and upregulated FLG expression (33). Gut inflammation and gut barrier leakage activate skin epithelial cells and promote the recruitment of T cells in patients with Omenn syndrome, thus exacerbating skin inflammation (34). The above findings revealed that BMI and diet influence the composition of skin microbiota and susceptibility of an individual to AD.

4 The role of the signaling pathways in obesity and AD

4.1 JAK-STAT pathway

The Janus kinase (JAK) - signal transducer and activator of transcription (STAT) pathway plays a crucial role in the immunological and physiological processes of AD and obesity. In the context of immune responses related to AD in the Th2 immune reaction, the binding of IL-4 and IL-4R stimulates the phosphorylation of JAK1 and JAK3, leading to the activation and

phosphorylation of IL-4R α and STAT6 (35). Furthermore, IL-4 and IL-13 can bind to the type II IL-4R, inducing the phosphorylation of JAK1 and TYK2, subsequently activating and phosphorylating STAT3 and STAT6. This results in the downregulation of FLG expression and impairment of skin barrier function, as well as an increase in the production of TSLP, IL-25, and IL-33 in keratinocytes (36). TSLP is a Th2 cell cytokine that can activate dendritic cells to drive Th2 cell differentiation and produce IL-4, IL-5, and IL-13 (37). Binding of the TSLPR heterodimeric receptor results in the interaction with JAK1 and JAK2, leading to phosphorylation and activation of STAT5 (38). IL-5 can also trigger the phosphorylation of JAK1 and JAK2 by binding to its corresponding receptor, resulting in the activation of STAT1, STAT3, and STAT5 (39). For Th17 immunity, the JAK-STAT pathway does not appear to be directly involved in Th17 signal transduction. However, research has shown that STAT3 is crucial for the proliferation and survival of Th17 cells (40). In Th1 immune responses, IL-12 signaling occurs through the binding of IL-12 to a heterodimeric receptor composed of IL-12R β 1 and IL-12R β 2 subunits (41). Subsequently, this interaction triggers the activation of JAK2 and TYK2, leading to the activation of STAT4-mediated signaling, and to a lesser extent, signaling mediated by STAT1, STAT3, and STAT5 (42). In skin function regulation, excessive activation of JAK1 can lead to overexpression of serine proteases in the skin, thereby impairing skin barrier function. Additionally, the STAT3 signaling molecule is a key transcription factor that regulates the differentiation of keratinocytes and maintains skin integrity (43). Secretory factors produced by adipocytes can participate in the JAK-STAT signaling pathway. In mice fed a high-fat diet, leptin secretion is associated with increased expression of STAT3 target genes. STAT3 can promote fat breakdown and inhibit fat synthesis (44). In the low-grade systemic inflammation associated with obesity, interferon-gamma (IFN- γ) secreted by CD4+ and CD8+ lymphocytes can activate STAT1 in adipocytes, leading to dysfunctional adipocyte function and insulin resistance (44). Studies have also shown that mice lacking STAT4 under high-fat diet feeding conditions can reduce adipose tissue inflammation, prevent insulin resistance, and improve glucose homeostasis (45). Additionally, STAT5 directly regulates the expression of key transcription factor PPAR γ involved in adipocyte differentiation. STAT6 in macrophages is also essential for the browning of white adipose tissue (44). Inhibiting the JAK-STAT pathway pharmacologically can lead to downregulation of interferon response, resulting in the accumulation of UCP1 and browning of adipocytes (46).

4.2 TLR pathway

TLRs recognize and bind to pathogen-associated molecular patterns (PAMPs) including peptidoglycans, lipopolysaccharides, and yeast polysaccharides, initiating a cascade of signaling events. Research has found that the TLR2-mediated immune signaling pathway is impaired in patients with AD. Blocking the TLR2 pathway inhibits pro-inflammatory cytokines (IL-6, IL-8, and IL-1 β) and promotes the expression of tight junction proteins, hence restoring the epidermal barrier in AD (47). On the other hand,

TLR4 modulates the immune balance in AD. Its activation can impair Th1 immune response, exacerbate Th2 inflammatory response, induce migration of skin dendritic cells (DCs), and promote IL-22 expression in naive CD4 T cells, resulting in incremental proliferation of keratinocytes and inflammatory infiltration (48). TLR3 expression in primary sensory neurons potentially induces itch (49). Clinical studies have shown that TLR5 and TLR9 upregulation in umbilical cord blood may significantly reduce the incidence of AD. TLR signaling pathway influences AD development. A high level of LDL-C is also a risk factor for AD. Adolescents with AD have significantly higher total cholesterol and low-density lipoprotein cholesterol (LDL-C) levels than those without AD (50). Saturated fatty acids (SFAs) and free fatty acids (FFAs) increase upon high-fat intake. SFAs can promote inflammatory signaling in macrophages via the plasma membrane (51). Moreover, an increase in SFA levels promotes the synthesis of endocannabinoids, which can cause NLRP3 inflammasome activation in macrophages of diet-induced obese mice (52). NLRP3 inflammasome activation promotes the cleavage of pro-IL-1 β and pro-IL-18, which stimulates the release of various active cytokines. IL-1 β can stimulate the production of IL-6. A previous study found that IL-6 was increased in lesion of moderate to severe AD compared to normal skin (53). Obese patients often have increased serum uric acid levels and uric acid crystals which can act as NLRP3 activators, thereby releasing pro-inflammatory cytokines (IL-1 β). Uric acid crystals can also activate the immune system by facilitating the production of reactive oxygen species (ROS) and activating the NF- κ B and MAPK pathways (54). When deposited in adipose tissue and immune cells, cholesterol crystals can also activate the NLRP3 inflammasome through similar mechanisms mentioned above (55). NLRP3 inflammasome activation promotes pro-IL-1 β and pro-IL-18 cleavage, hence releasing various active cytokines including IL-6. IL-6 is significantly upregulated in lesions of moderate to severe AD compared to normal skin (53).

5 The role of cytokines and adipokines in obesity and AD

Analysis of bodies of obese individuals has revealed the presence of metabolic abnormalities, oxidative stress, mitochondrial dysfunction, impaired immune function, and chronic low-grade inflammation (56). The infiltration of inflammatory cells into white adipose tissue (WAT) causes dysfunction of adipocytes and metabolic functions. White adipose tissue (WAT) comprises immune-regulatory cells, including M2-like adipose tissue macrophages, Tregs, Th2 cells, NK cells, and eosinophils. The quantity and phenotype of these cells vary between obese and lean individuals. Adipose secretes various cytokines, chemokines, and adipokines, which play a key role in regulating immune processes. Elevated lipid storage induce adipocyte hypertrophy, hypoxia, and cell death triggering the secretion of proinflammatory cytokines by adipocytes, including TNF- α , IL-6,

IL-8, and MCP-1 (57). For lean individuals, regulatory and immunosuppressive cells promote the clearance of dead adipose tissue, suppressing adipose tissue cell proliferation, and secreting anti-inflammatory cytokines (IL-10, IL-4, IL-13, and IL-1R α) (58).

5.1 TNF- α

TNF- α is a cytokine that plays a role in inflammation and immune responses (59). It can activate inflammatory responses, leading to the release of inflammatory cytokines and triggering inflammation. In patients with AD, TNF- α levels are typically elevated, and correlated with the severity of AD (60). High levels of TNF- α are associated with the inflammation and itching symptoms of AD. TNF- α can also promote the proliferation of skin keratinocytes and the synthesis of keratin, thereby promoting the onset of AD. The use of TNF- α inhibitors can help alleviate skin barrier dysfunction in AD patients and improve skin barrier function (61). Upregulated TNF- α in obesity activates the NF- κ B pathway via a c-Jun N-terminal kinase-dependent pathway, resulting in downregulated expression of epidermal barrier proteins, including FLG and loricrin (LOR) (62). Elevated levels of TNF- α in obese individuals may disrupt the balance between Th1 and Th2 cells. TNF- α promotes Th1 immune response by enhancing the production of pro-inflammatory cytokines such as interferon-gamma (IFN- γ) and interleukin-2 (IL-2) (63). Obesity alters skin properties, increasing surface roughness, and decreasing water content thus causing significant redness accompanied by an increase in skin blood flow. Correlation analysis revealed a significant correlation between water content and TNF- α levels in the stratum corneum (64). Moreover, obesity changes the baseline levels of serum cytokines/adipocytokines IL-6, TNF- α , and CRP/hs-CRP (65). Research has shown higher serum TNF- α levels in obese individuals than in individuals with normal weight (65). This physiological activity may be associated with the action of leptin produced during obesity (66). Leptin can augment the secretion of inflammatory cytokines including TNF- α , resulting in an inflammatory environment (67). Simultaneously, exposure to an inflammatory environment can increase leptin expression in adipose tissue, creating a feedback loop that promotes inflammation (68). TNF- α secreted by M1 pro-inflammatory adipose tissue macrophages initiates a cascade reaction by activating the NF- κ B and JNK pathways. TNF- α may stimulate the production of pro-inflammatory cytokines including IL-6, but reduce anti-inflammatory cytokine levels, including adiponectin in the inflammatory response (69). Adiponectin inhibits the TNF- α and IL-6 production in macrophages at the same time increasing levels of anti-inflammatory mediators (IL-10 and IL-1 receptor antagonist) (70, 71). Adiponectin-deficient mice exhibit an increased number of M1 macrophages in their adipose tissue, further improving cytokine production including TNF- α , IL-6, and MCP-1 (72). Additionally, TNF- α can cause the generation of reactive oxygen species (ROS) by binding to specific receptors (73).

5.2 IL-6

Research on the relationship between IL-6 levels in obesity and AD is limited. IL-6 regulates autoimmune and chronic inflammatory diseases. IL-6 signaling exerts pleiotropic effects via two primary pathways, the classical signaling and trans-signaling pathways. In the classical signaling pathway, IL-6 binds to IL-6R on the cell membrane, followed by interaction with membrane-bound gp130, hence activating JAK to initiate intracellular signaling (74). In the trans-signaling pathway, the extracellular portion of IL-6R can be proteolytically cleaved to form soluble sIL-6R. IL-6 subsequently binds to sIL-6R and continues to bind to gp130, initiating intracellular signaling (74). Activation of the classic IL-6 signaling pathway promotes macrophages polarized to M2 phenotype via upregulated IL4 response despite causing proinflammatory actions of T cells (75). Serum IL-6 levels in AD patients are significantly higher than that in healthy volunteers (76). The flg-/- mice exhibited severe clinical symptoms such as increased ear thickness and elevated IL-6 level (77). IL-6 production in adipose tissue is two to three times higher than that in subcutaneous tissue among obese individuals. IL-6 may stimulate JAK1 activation and phosphorylation, which in turn activates STAT1, STAT3, and STAT6 signaling pathways (78). IL-6 activates the STAT3 pathway of local macrophage to promote IL4Ra expression, sensitizing them to IL-4 signaling and promoting an anti-inflammatory gene expression pattern (79). Additionally, adipocytes release IL-6, promoting differentiation of Th cells, either directly or indirectly, thereby stimulating antibody production (80). IL-6/STAT3, together with TGF- β or IL-1 β and IL-23 causes the differentiation of Th17 cells, which play a pro-inflammatory role. IL-6 promotes an HFD-induced increase in FFA and leptin release from adipocytes (81). Research also reports that leptin stimulates macrophages to generate IL-6 via synergistic interaction with LPS (82).

5.3 IL-4 and IL-13

IL-4 and IL-13 negatively influence the skin barrier in AD. They downregulate FLG expression, destroy the skin structure, reduce its capacity to resist pathogens and allergens as well as weaken the capacity to maintain adequate moisture (83). IL-4 and IL-13 increase the proliferation of keratinocytes, reduce their differentiation, and prevent their full maturation (84). IL-13 also downregulates the expression of skin barrier proteins and lipids of keratinocytes by mediating MMP-9 expression. Recent studies have shown that IL-4 and IL-13 weaken skin resistance to pathogens by reducing antimicrobial peptides, hence rendering skin more susceptible to infectious organisms (85). IL-13 is also implicated in the upregulation of collagen degradation and fibrosis mediated by MMP-13, causing fibrosis, dermis thickening, and the typical lichenified lesions in AD (86). IL-4 and IL-13 also promote neurogenic itch by directly acting on pruriceptive sensory neurons (87). Th2 pathway activation mediates type 2 inflammation in AD. Th2 cells may release vital inflammatory cytokines including IL-4, IL-13, IL-5, and IL-9, recruit eosinophils

and mast cells, as well as stimulate B cell activity (82). Through their interactions with Th2 cells, M2 macrophages in white adipose tissue activate the release of Th2 cytokines, including IL-4 and IL-13 (88). A few studies have shown that obesity exerts IL-4/IL-13-associated inflammatory responses. Elsewhere, the typical Th2-dominant inflammation of AD progressed to more severe Th17-driven inflammation in obese mice. Biologic treatments inhibiting cytokines IL-4 and IL-13 treatment protects lean mice from developing AD but not obese mice (89). IL-6 secreted by inflammatory-stimulated adipocytes activates macrophages STAT3 and upregulates IL4ra expression, and increases the sensitivity of macrophages to IL-4 activation (79). Hypercholesterolemia induces strong Th2 responses to an exogenous antigen characterized by an increased induction of IL-4 and IL-10 (90).

5.4 Adipokines

Expanded fat cells themselves produce various signaling molecules through a process called autocrine signaling. These mediators have both immune system regulatory functions as well as metabolic functions, and are collectively called adipokines. For example, chemokines promote the infiltration of macrophages into white adipose tissue (WAT), while calcium-binding proteins enhance the adhesion of circulating monocytes and their recruitment as macrophages. Adipokines include pro-inflammatory ones like leptin, as well as anti-inflammatory cytokines like adiponectin. However, adiponectin levels are suppressed in both acute and chronic obesity.

5.5 Leptin

Leptin is a 16-kDa monomeric non-glycosylated protein primarily secreted by adipocytes. Circulating leptin levels are directly proportional to body fat mass (91). Leptin activates CD4⁺T lymphocytes toward Th1 phenotype and inhibits infiltration of Tregs into adipose tissue, altered immune tolerance, and inflammatory effects (92). Leptin promotes the release of IL-2 and INF- γ . IL-2 acts on IL-2R, stimulating JAK1 and JAK3 phosphorylation, further activating as well as phosphorylating STAT1, STAT3, STAT5, and STAT6. The INF- γ signaling pathway involves JAK1 and JAK2 phosphorylation, hence activating and phosphorylating STAT1 (93). The binding of leptin to LEP-R also activates the phosphoinositide 3-kinase (PI3K) and mitogen-activated protein kinase/extracellular signal-regulated kinase (MAPK/ERK) signaling cascades, as well as the JAK2-STAT signaling cascade (57). Additionally, chronic treatment of obesity with leptin promotes preadipocyte differentiation and secretion of pro-inflammatory cytokine TNF- α (94). Leptin increases TNF and IL-6 production by monocytes as well as stimulates CCL3, CCL4, and CCL5 production by macrophages via JAK2-sTAT3 pathway activation (95). Leptin also induces TNF- α expression via the JNK pathway in macrophages (96). A positive feedback mechanism is established when leptin stimulates

inflammatory mediator production, including IL-6 and TNF- α from the adipose tissue. TNF- α and IL-6 promote the expression and release of leptin.

5.6 Adiponectin

One study observation revealed a potential relationship between adiponectin and AD, i.e., obese children with asthma had higher leptin levels and lower adiponectin levels in serum than non-obese children with asthma (97). In BMDC cells, adiponectin induces DC maturation and activation, accelerating naive T cells polarized into Th1 and Th17 cells. High-fat diet-fed upregulates IFN- γ expression in adipocytes and IL-17 in CD4 T cells (98). Additional experiments have shown that adiponectin derived from adipocytes reduces T lymphocytes, thus producing IFN- γ and IL-17 (99). Adiponectin-deficient mice had higher TNF α levels in the blood. Adiponectin abrogated LPS-stimulated production of TNF- α in macrophages and suppressed TLR-mediated NF- κ B activation in mouse macrophages (100). In this context, adiponectin may exert anti-inflammatory mechanisms in AD. However, additional studies are necessary to comprehensively understand this mechanism.

5.7 Resistin

Resistin, named as a result of inducing insulin resistance, is a 12.5-kDa cysteine-rich peptide, produced by macrophages and peripheral monocytes. Nevertheless, the potential role of resistance in AD is unclear. Studies revealed that blood content of resistin increases in AD boys unlike in healthy children (101). Besides, resistin upregulates pro-inflammatory cytokines including TNF- α , IL-1 β , IL-6, and IL-12 via NF- κ B signaling pathway activation (102). However, other findings contradict previous results. Studies also discovered a decrease of resistin in AD patients, with an inverse correlation between blood resistin quantity and SCORAD score (103, 104). Notably, resistin weakens the atopic immune response by suppressing dendritic cell function (92). Thus, lower levels of resistin are thought to be associated with increased severity of AD symptoms in adults. Nonetheless, additional studies are necessary to define and validate the role of resistin in AD.

5.8 Fatty acid binding protein

Fatty acid binding protein (FABP) regulates fatty acid uptake, transport, and metabolism. Epidermal-FABP (FABP5), an extensively studied member of the FABP family, has been reported to be positively correlated with adiposity, glucose metabolism, and lipolysis parameters and linked to the development of AD (105, 106). Mass spectrometry of AD skin revealed that FABP5 is highly expressed in both acute and chronic AD lesions (107). Elsewhere, it was demonstrated that FABP5 promoted TNF- α -induced NF- κ B signaling by forming a complex with valosin-containing protein (VCP) in keratinocytes (108).

Another study provided evidence supporting a Th17-related mechanism in AD, involving FABP5. Knockdown of FABP5 in HaCaT cells resulted in a significant reduction of the expression of Th17-inducing cytokines, including IL-6 and TGF- β (109). In HFD-induced obese mice models, FABP5 expression in skin macrophages promoted saturated FA-induced IL-1 β production and instigated chronic inflammatory skin lesions (110). Indeed, adipose-FABP (FABP4) and FABP5 regulate different signaling pathways in macrophages. Although FABP5 expression activates the STAT1/2/IFN β , LTA4/LTB4, RAR/CD11c, or NLRP3/IL-1 β pathways, FABP4 mainly stimulates NF κ B/IL-6, COX2/PGE2, CER/cell death, or LXR/SCD1 in macrophages (111).

5.9 Zinc- α 2-glycoprotein

Zinc- α 2-glycoprotein (ZAG), a 43-kDa protein produced by adipocytes and keratinocytes in the skin plays a role in lipolysis in adipocytes (112). In sera and skin of AD patients, it was reported that the expression of ZAG was consistently reduced. ZAG regulated FLG and TSLP expression in normal human epidermal keratinocytes (NHEKs) and repaired abnormalities in the skin barrier under AD conditions (113). Furthermore, topical ZAG treatment decreased levels of IL-4, IL-17a, Ifng and levels of serum total IgE, and restored ADAM17 and Notch1 signaling in AD-induced mice (113).

5.10 Visfatin

Visfatin, a novel adipocytokine, has been linked to chronic inflammatory diseases. A study suggested a connection between visfatin and both adult-onset AD and classical AD in adults during the chronic phase of the disease. The study also found a significant correlation between visfatin levels and eosinophil counts in AD patients (114). Visfatin induced pro-inflammatory effects by dose-dependently up-regulating IL-1 β , IL-1Ra, IL-6, IL-10, and TNF- μ in human monocytes (115). Moreover, it stimulated the production of chemokines such as CXCL8, CXCL10, and CCL20 in human keratinocytes (116). However, the serum concentration of visfatin in AD children was significantly reduced compared to that of healthy subjects (101), which differs from finding of other studies. This is likely due to differences in the underlying mechanism of child AD and adult AD. Some studies have shown that patients with adult-onset AD have significantly higher serum visfatin levels than those who had developed the skin lesions in childhood (113).

5.11 Lipocalin-2

Lipocalin-2 (LCN2) is associated with various obesity-related disorders, such as Type 2 diabetes and non-alcoholic fatty liver disease (117). It circulates in the body in two main forms: a single molecule (25 kDa monomer) and a double molecule (46 kDa homodimer). Notably, LCN2 can block the breakdown of MMP-9, an enzyme involved in tissue remodeling (118). Interestingly,

research suggests LCN2 may also play a role in AD. A study using a mouse model of AD found upregulated levels of LCN2 in spinal astrocytes, which are cells that support nerve function in the spinal cord. This finding suggests a potential link between LCN2 and itch sensation at the spinal level in AD (119). Furthermore, the LCN2 gene has binding sites for several inflammatory signaling molecules, including NF- κ B, STAT1, STAT3, and C/EBP (120).

6 PPAR- γ and AD

Peroxisome proliferator-activated receptor-gamma (PPAR- γ) is a critical transcription factor involved in adipogenesis. PPAR- γ plays an important role in regulating adipocyte differentiation and lipid metabolism, hence providing positive feedback regulation of adipogenesis. Accumulating evidence indicates that PPAR- γ regulates type 2 immune response (121).

PPAR- γ agonists reduce neutrophil MPO activity in response to LPS and induce neutrophil apoptosis in a dose-dependent manner (122). PPAR- γ activation also impairs the functional capacity of eosinophils, hence reducing antibody-dependent cellular cytotoxicity (ADCC), CD69 expression induced by IL-5, and release of eosinophil-derived neurotoxin (EDN) (123). Mast cell activation mediated by IgE plays a significant role in AD, which is

also suppressed by activated PPAR- γ (124). PPAR- γ is a key factor mediating M2 phenotype associated with type 2 cytokine activation (such as IL-4 and IL-13). PPAR- γ prevents the uptake of lipids by ILC2s, IL-33 signaling activation, and reduces the severity of airway inflammation (125). Mice treated with PPAR- γ agonists showed reduced levels of cytokines IL-4, IL-5, and IL-13 (126), whereas mice without PPAR- γ mice revealed enhanced release of epithelial-derived alarm proteins including IL-25, IL-33, and TSLP as well as NF- κ B activation (127). However, the effect of PPAR- γ deletion on IL-4 expression was unclear (128). Activated PPAR- γ reduces the expression of pro-inflammatory cytokines including TNF- α , IFN- γ , and IL-2 as well as promotes the activity of suppressive Treg cells (129).

Experimental evidence indicates that PPAR- γ in epithelial cell Treg cells is activated by TCR signaling in an IRF4-dependent manner. PPAR- γ binds to IRF4 and modulates IL-33 receptor (IL-33R) expression on Treg cells (130). The role of PPAR- γ in other TH cell subsets has also been proposed. IL-9 expression in the skin positively correlates with the severity of chronic atopic dermatitis (cAD) and acute contact dermatitis reactions (aACD) (131). TH9 cells can be perceived as a highly differentiated subset of TH2 cells that can simultaneously promote the levels of IL-5, IL-13, and IL-9 (128). IL-9 is preferentially downregulated among the TH2 cytokines upon inhibition of PPAR- γ expression (132). The

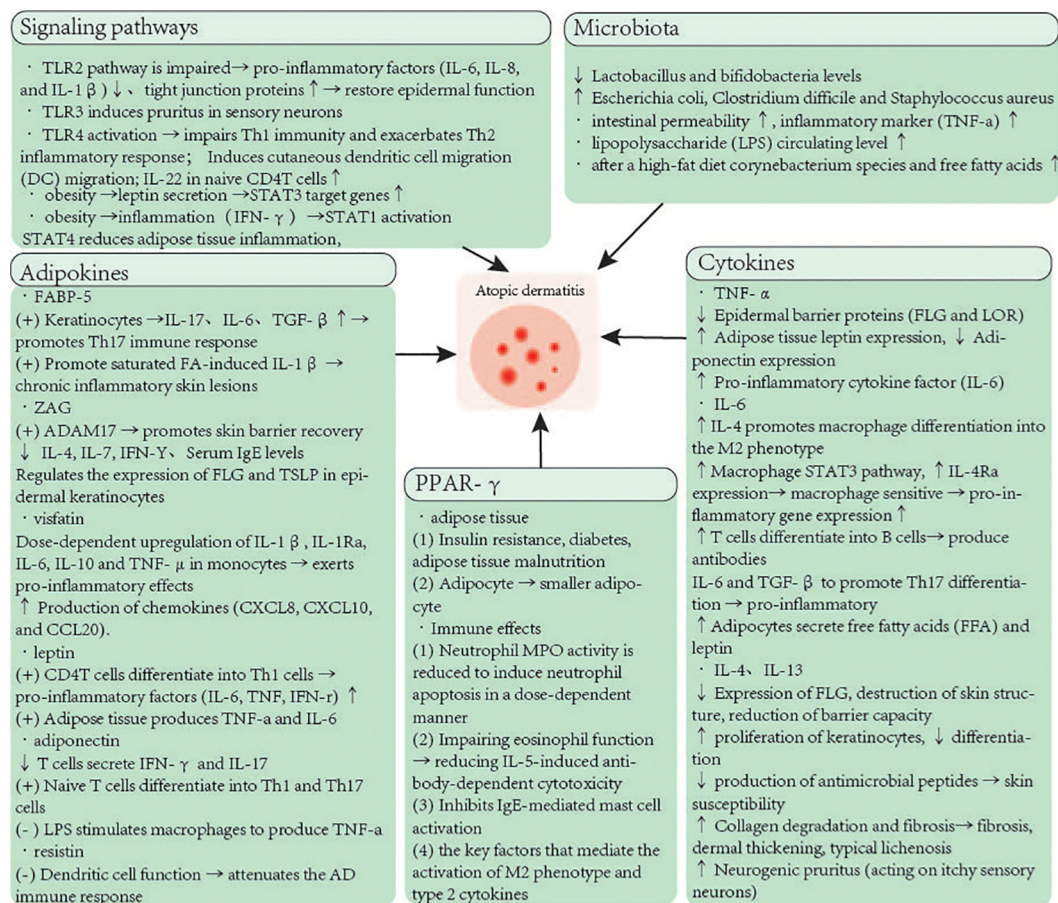


FIGURE 1

The molecular mechanisms of obesity predisposes to AD.

relationship between TH9 immune response and AD is poorly understood. However, cytokine secretion including IL-5 and IL-13 by TH9 cells implies a potential relationship with AD.

7 Conclusion

Current clinical research and scientific studies suggest that overweight or obesity are considered primary factors leading to the pathogenesis of inflammatory skin diseases. Our review covers multiple important aspects. Under the influence of initial inflammatory factors, obese individuals experience a complex interplay of various pro-inflammatory and anti-inflammatory signals within their bodies. Inflamed adipocytes locally and systemically secrete pro-inflammatory cytokines, a process that damages both adipose tissue itself and skin functions. Another key factor in obesity involves the gut microbiota, which plays a role in energy homeostasis, circulatory system, and immune response. The increase in skin lipids following obesity can lead to dysbiosis of the microbial ecosystem, resulting in colonization by lipophilic bacteria. Concurrently, obesity also alters the pathological changes of inflammatory diseases, shifting the classical Th2-type immune response to a more severe Th17-type immune response through the action of adipokines, thereby affecting keratinocyte differentiation, epithelial barrier permeability, and antimicrobial peptide production. Simultaneously, maintaining balance in the gut microbiota and probiotics play a complex role in preventing atopic dermatitis (AD), including inhibition of inflammation, alteration of microbial diversity, and enhancement of skin barrier function. These contents provide more thinking and inspiration about AD, and will have a positive impact on the field of AD (Figure 1).

More data is needed to understand how weight and BMI affect the effectiveness of AD therapy. Reducing weight and managing obesity might decrease inflammatory mediators and cytokines from

adipose tissue, thereby improving the inflammatory state and alleviating AD symptoms. As such, besides targeting skin lesions in the treatment of AD, the management and intervention of obesity should also be emphasized to comprehensively contain disease progression.

Author contributions

DS: Writing – original draft, Data curation. SZ: Writing – review & editing, Investigation, Funding acquisition.

Funding

The author(s) declare financial support was received for the research, authorship, and/or publication of this article. The Foundation of Liaoning Provincial Department of Science and Technology (2023JH2/20200029).

Conflict of interest

The authors declare that the research was conducted in the absence of any commercial or financial relationships that could be construed as a potential conflict of interest.

Publisher's note

All claims expressed in this article are solely those of the authors and do not necessarily represent those of their affiliated organizations, or those of the publisher, the editors and the reviewers. Any product that may be evaluated in this article, or claim that may be made by its manufacturer, is not guaranteed or endorsed by the publisher.

References

- David Boothe W, Tarbox JA, Tarbox MB. Atopic dermatitis: pathophysiology. *Adv Exp Med Biol.* (2017) 1027:21–37. doi: 10.1007/978-3-319-64804-0_3
- Peng W, Novak N. Pathogenesis of atopic dermatitis. *Clin Exp Allergy.* (2015) 45:566–74. doi: 10.1111/cea.2015.45.issue-3
- Hamilton JD, Suarez-Farinas M, Dhingra N, Cardinale I, Li X, Kostic A, et al. Dupilumab improves the molecular signature in skin of patients with moderate-to-severe atopic dermatitis. *J Allergy Clin Immunol.* (2014) 134:1293–300. doi: 10.1016/j.jaci.2014.10.013
- Sugaya M. The role of th17-related cytokines in atopic dermatitis. *Int J Mol Sci.* (2020) 21. doi: 10.3390/ijms21041314
- McAleer JP. Obesity and the microbiome in atopic dermatitis: Therapeutic implications for PPAR-gamma agonists. *Front Allergy.* (2023) 4:1167800. doi: 10.3389/falgy.2023.1167800
- Duan Y, Gong K, Xu S, Zhang F, Meng X, Han J. Regulation of cholesterol homeostasis in health and diseases: from mechanisms to targeted therapeutics. *Signal Transduct Target Ther.* (2022) 7:265. doi: 10.1038/s41392-022-01125-5
- Ellulu MS, Patimah I, Khaza'ai H, Rahmat A, Abed Y. Obesity and inflammation: the linking mechanism and the complications. *Arch Med Sci.* (2017) 13:851–63. doi: 10.5114/aoms.2016.58928
- Park J, Youn DH, Kang J, Ahn KS, Kwak HJ, Um JY. Taeumjowi-tang, a traditional Korean sasang remedy, improves obesity-atopic dermatitis comorbidity by regulating hypoxia-inducible factor 1 alpha. *Front Pharmacol.* (2019) 10:1458. doi: 10.3389/fphar.2019.01458
- Ali Z, Suppli Ulrik C, Agner T, Thomsen SF. Is atopic dermatitis associated with obesity? A systematic review of observational studies. *J Eur Acad Dermatol Venereol.* (2018) 32:1246–55. doi: 10.1111/jdv.2018.32.issue-8
- Kok WL, Yew YW, Thng TG. Comorbidities associated with severity of atopic dermatitis in young adult males: A national cohort study. *Acta Derm Venereol.* (2019) 99:652–6. doi: 10.2340/00015555-3175
- Jeong KY, Lee J, Li C, Han T, Lee SB, Lee H, et al. Juvenile obesity aggravates disease severity in a rat model of atopic dermatitis. *Allergy Asthma Immunol Res.* (2015) 7:69–75. doi: 10.4168/aaair.2015.7.1.69
- Salem AM. Th1/Th2 cytokines profile in overweight/obese young adults and their correlation with airways inflammation. *J Taibah Univ Med Sci.* (2022) 17:38–44. doi: 10.1016/j.jtumed.2021.09.006
- Yang S, Zhu T, Wakefield JS, Mauro TM, Elias PM, Man MQ. Link between obesity and atopic dermatitis: Does obesity predispose to atopic dermatitis, or vice versa? *Exp Dermatol.* (2023) 32:975–85. doi: 10.1111/exd.14801
- Mahmud MR, Akter S, Tamanna SK, Mazumder L, Esti IZ, Banerjee S, et al. Impact of gut microbiome on skin health: gut-skin axis observed through the lenses of therapeutics and skin diseases. *Gut Microbes.* (2022) 14:2096995. doi: 10.1080/19490976.2022.2096995

15. Zhang S, Zhang B, Liu Y, Li L. Adipokines in atopic dermatitis: the link between obesity and atopic dermatitis. *Lipids Health Dis.* (2024) 23:26. doi: 10.1186/s12944-024-02009-z
16. Augustin M, Radtke MA, Glaeske G, Reich K, Christophers E, Schaefer I, et al. Epidemiology and comorbidity in children with psoriasis and atopic eczema. *Dermatology.* (2015) 231:35–40. doi: 10.1159/000381913
17. Nicholas MN, Keown-Stoneman CDG, Maguire JL, Drucker AM. Association between atopic dermatitis and height, body mass index, and weight in children. *JAMA Dermatol.* (2022) 158:26–32. doi: 10.1001/jamadermatol.2021.4529
18. Luo X, Xiang J, Dong X, Cai F, Suo J, Wang Z, et al. Association between obesity and atopic disorders in Chinese adults: an individually matched case-control study. *BMC Public Health.* (2013) 13:12. doi: 10.1186/1471-2458-13-12
19. Zhang A, Silverberg JL. Association of atopic dermatitis with being overweight and obese: a systematic review and metaanalysis. *J Am Acad Dermatol.* (2015) 72:606–616.e604. doi: 10.1016/j.jaad.2014.12.013
20. Lee JH, Han KD, Jung HM, Youn YH, Lee JY, Park YG, et al. Association between obesity, abdominal obesity, and adiposity and the prevalence of atopic dermatitis in young Korean adults: the Korea national health and nutrition examination survey 2008–2010. *Allergy Asthma Immunol Res.* (2016) 8:107–14. doi: 10.4168/aaair.2016.8.2.107
21. Kim JE, Kim HS. Microbiome of the skin and gut in atopic dermatitis (AD): understanding the pathophysiology and finding novel management strategies. *J Clin Med.* (2019) 8. doi: 10.3390/jcm8040444
22. Zachariassen LF, Krych L, Engkilde K, Nielsen DS, Kot W, Hansen CH, et al. Sensitivity to oxazolone induced dermatitis is transferable with gut microbiota in mice. *Sci Rep.* (2017) 7:44385. doi: 10.1038/srep44385
23. Cuevas-Sierra A, Ramos-Lopez O, Riezu-Boj JJ, Milagro FI, Martinez JA. Diet, gut microbiota, and obesity: links with host genetics and epigenetics and potential applications. *Adv Nutr.* (2019) 10:S17–30. doi: 10.1093/advances/nmy078
24. Schoeler M, Caesar R. Dietary lipids, gut microbiota and lipid metabolism. *Rev Endocr Metab Disord.* (2019) 20:461–72. doi: 10.1007/s11554-019-09512-0
25. Moestrup KS, Chen Y, Schepeler T, Schweiger PJ, Jensen KB. Dietary control of skin lipid composition and microbiome. *J Invest Dermatol.* (2018) 138:1225–8. doi: 10.1016/j.jid.2017.12.005
26. West CE, Ryden P, Lundin D, Engstrand L, Tulic MK, Prescott SL. Gut microbiome and innate immune response patterns in IgE-associated eczema. *Clin Exp Allergy.* (2015) 45:1419–29. doi: 10.1111/cea.2015.45.issue-9
27. Feng J, Ma H, Huang Y, Li J, Li W. Ruminococcaceae_UCG-013 promotes obesity resistance in mice. *Biomedicine.* (2022) 10. doi: 10.3390/biomedicine10123272
28. Hu C, van Meel ER, Medina-Gomez C, Kraaij R, Barroso M, Kieft-de Jong J, et al. A population-based study on associations of stool microbiota with atopic diseases in school-age children. *J Allergy Clin Immunol.* (2021) 148:612–20. doi: 10.1016/j.jaci.2021.04.001
29. Liu Z, Ma C, Gao H, Huang X, Zhang Y, Liu C, et al. A polysaccharide from *Salvia miltiorrhiza* radix inhibits weight gain of mice with high-fat diet by modulating intestinal bacteria. *J Sci Food Agric.* (2024) 104:479–87. doi: 10.1002/jsfa.v104.1
30. Kong HH, Oh J, Deming C, Conlan S, Grice EA, Beatson MA, et al. Temporal shifts in the skin microbiome associated with disease flares and treatment in children with atopic dermatitis. *Genome Res.* (2012) 22:850–9. doi: 10.1101/gr.130129.111
31. Ni J, Shangguang Y, Jiang L, He C, Ma Y, Xiong H. Pomelo peel dietary fiber ameliorates alterations in obesity-related features and gut microbiota dysbiosis in mice fed on a high-fat diet. *Food Chem X.* (2023) 20:100993. doi: 10.1016/j.fochx.2023.100993
32. Lim JJ, Reginald K, Say YH, Liu MH, Chew FT. A dietary pattern of frequent plant-based foods intake reduced the associated risks for atopic dermatitis exacerbation: Insights from the Singapore/Malaysia cross-sectional genetics epidemiology cohort. *BMC Public Health.* (2023) 23:1818. doi: 10.1186/s12889-023-16736-y
33. Kim IS, Lee SH, Kwon YM, Adhikari B, Kim JA, Yu DY, et al. Oral Administration of beta-Glucan and *Lactobacillus plantarum* Alleviates Atopic Dermatitis-Like Symptoms. *J Microbiol Biotechnol.* (2019) 29:1693–706. doi: 10.4014/jmb.1907.07011
34. Rigoni R, Fontana E, Dobbs K, Marrella V, Taverniti V, Maina V, et al. Cutaneous barrier leakage and gut inflammation drive skin disease in Omenn syndrome. *J Allergy Clin Immunol.* (2020) 146:1165–1179 e1111. doi: 10.1016/j.jaci.2020.04.005
35. Miyazaki T, Kawahara A, Fujii H, Nakagawa Y, Minami Y, Liu ZJ, et al. Functional activation of Jak1 and Jak3 by selective association with IL-2 receptor subunits. *Science.* (1994) 266:1045–7. doi: 10.1126/science.7973659
36. Furue M. Regulation of Skin Barrier Function via Competition between AHR Axis versus IL-13/IL-4–JAK–STAT6/STAT3 Axis: Pathogenic and Therapeutic Implications in Atopic Dermatitis. *J Clin Med.* (2020) 9. doi: 10.3390/jcm9113741
37. Shi Z, Jiang W, Wang M, Wang X, Li X, Chen X, et al. Inhibition of JAK/STAT pathway restrains TSLP-activated dendritic cells mediated inflammatory T helper type 2 cell response in allergic rhinitis. *Mol Cell Biochem.* (2017) 430:161–9. doi: 10.1007/s11010-017-2963-7
38. Pandey A, Ozaki K, Baumann H, Levin SD, Puel A, Farr AG, et al. Cloning of a receptor subunit required for signaling by thymic stromal lymphopoietin. *Nat Immunol.* (2000) 1:59–64. doi: 10.1038/76923
39. Gandhi NA, Bennett BL, Graham NM, Pirozzi G, Stahl N, Yancopoulos GD. Targeting key proximal drivers of type 2 inflammation in disease. *Nat Rev Drug Discovery.* (2016) 15:35–50. doi: 10.1038/nrd4624
40. Durant L, Watford WT, Ramos HL, Laurence A, Vahedi G, Wei L, et al. Diverse targets of the transcription factor STAT3 contribute to T cell pathogenicity and homeostasis. *Immunity.* (2010) 32:605–15. doi: 10.1016/j.immuni.2010.05.003
41. Bastian D, Wu Y, Betts BC, Yu XZ. The IL-12 cytokine and receptor family in graft-vs.-host disease. *Front Immunol.* (2019) 10:988. doi: 10.3389/fimmu.2019.00988
42. Gotthardt D, Trifunopoulos J, Sexl V, Putz EM. JAK/STAT cytokine signaling at the crossroad of NK cell development and maturation. *Front Immunol.* (2019) 10:2590. doi: 10.3389/fimmu.2019.02590
43. Yasuda T, Fukada T, Nishida K, Nakayama M, Matsuda M, Miura I, et al. Hyperactivation of JAK1 tyrosine kinase induces stepwise, progressive pruritic dermatitis. *J Clin Invest.* (2016) 126:2064–76. doi: 10.1172/JCI82887
44. Gurzov EN, Stanley WJ, Pappas EG, Thomas HE, Gough DJ. The JAK/STAT pathway in infection. *FEBS J.* (2016) 283:3002–15. doi: 10.1111/febs.2016.283.issue-16
45. Dobrian AD, Galkina EV, Ma Q, Hatcher M, Aye SM, Butcher MJ, et al. STAT4 deficiency reduces obesity-induced insulin resistance and adipose tissue inflammation. *Diabetes.* (2013) 62:4109–21. doi: 10.2337/db12-1275
46. Moisan A, Lee YK, Zhang JD, Hudak CS, Meyer CA, Prummer M, et al. White-to-brown metabolic conversion of human adipocytes by JAK inhibition. *Nat Cell Biol.* (2015) 17:57–67. doi: 10.1038/ncb3075
47. Fang Z, Li L, Zhang H, Zhao J, Lu W, Chen W. Gut microbiota, probiotics, and their interactions in prevention and treatment of atopic dermatitis: A review. *Front Immunol.* (2021) 12:720393. doi: 10.3389/fimmu.2021.720393
48. Yoon J, Leyva-Castillo JM, Wang G, Galand C, Oyoshi MK, Kumar L, et al. IL-23 induced in keratinocytes by endogenous TLR4 ligands polarizes dendritic cells to drive IL-22 responses to skin immunization. *J Exp Med.* (2016) 213:2147–66. doi: 10.1084/jem.20150376
49. Jang YH, Choi JK, Jin M, Choi YA, Ryoo ZY, Lee HS, et al. House Dust Mite Increases pro-Th2 Cytokines IL-25 and IL-33 via the Activation of TLR1/6 Signaling. *J Invest Dermatol.* (2017) 137:2354–61. doi: 10.1016/j.jid.2017.03.042
50. Seong MK, Shin M. Low-density lipoprotein cholesterol is associated with atopic dermatitis in Korean adolescents. *Int Arch Allergy Immunol.* (2023) 184:1230–6. doi: 10.1159/000533401
51. Curley S, Gall J, Byrne R, Yvan-Charvet L, McGillicuddy FC. Metabolic inflammation in obesity-at the crossroads between fatty acid and cholesterol metabolism. *Mol Nutr Food Res.* (2021) 65:e1900482. doi: 10.1002/mnfr.201900482
52. Gora IM, Ciechanowska A, Ladyzynski P. NLRP3 inflammasome at the interface of inflammation, endothelial dysfunction, and type 2 diabetes. *Cells.* (2021) 10. doi: 10.3390/cells10020314
53. Guttman-Yassky E, Diaz A, Pavel AB, Fernandes M, Lefferdink R, Erickson T, et al. Use of tape strips to detect immune and barrier abnormalities in the skin of children with early-onset atopic dermatitis. *JAMA Dermatol.* (2019) 155:1358–70. doi: 10.1001/jamadermatol.2019.2983
54. Eleftheriadis T, Pissas G, Antoniadis G, Makri P, Liakopoulos V, Stefanidis I. Urate crystals induce NLRP3 inflammasome-dependent IL-1 β secretion and proliferation in isolated primary human T-cells. *Hippokratia.* (2015) 19:41–6.
55. Haneklaus M, O'Neill LA. NLRP3 at the interface of metabolism and inflammation. *Immunol Rev.* (2015) 265:53–62. doi: 10.1111/imr.2015.265.issue-1
56. Perez LM, Pareja-Galeano H, Sanchis-Gomar F, Emanuele E, Lucia A, Galvez BG. 'Adipaging': ageing and obesity share biological hallmarks related to a dysfunctional adipose tissue. *J Physiol.* (2016) 594:3187–207. doi: 10.1111/imr.12285
57. Francisco V, Pino J, Gonzalez-Gay MA, Mera A, Lago F, Gomez R, et al. Adipokines and inflammation: is it a question of weight? *Br J Pharmacol.* (2018) 175:1569–79. doi: 10.1111/bph.14181
58. Taylor EB. The complex role of adipokines in obesity, inflammation, and autoimmunity. *Clin Sci (Lond).* (2021) 135:731–52. doi: 10.1042/CS20200895
59. Jang DI, Lee AH, Shin HY, Song HR, Park JH, Kang TB, et al. The role of tumor necrosis factor alpha (TNF-alpha) in autoimmune disease and current TNF-alpha inhibitors in therapeutics. *Int J Mol Sci.* (2021) 22. doi: 10.3390/ijms22052719
60. Chan TC, Sanyal RD, Pavel AB, Glickman J, Zheng X, Xu H, et al. Atopic dermatitis in Chinese patients shows T(H)2/T(H)17 skewing with psoriasisiform features. *J Allergy Clin Immunol.* (2018) 142:1013–7. doi: 10.1016/j.jaci.2018.06.016
61. Ogai K, Matsumoto M, Aoki M, Minematsu T, Kitamura K, Kobayashi M, et al. Increased level of tumour necrosis factor-alpha (TNF-alpha) on the skin of Japanese obese males: measured by quantitative skin blotting. *Int J Cosmet Sci.* (2016) 38:462–9. doi: 10.1111/ics.2016.38.issue-5
62. Kim BE, Kim J, Goleva E, Berdyshev E, Lee J, Vang KA, et al. Particulate matter causes skin barrier dysfunction. *JCI Insight.* (2021) 6. doi: 10.1172/jci.insight.145185
63. Webster JD, Vucic D. The balance of TNF mediated pathways regulates inflammatory cell death signaling in healthy and diseased tissues. *Front Cell Dev Biol.* (2020) 8:365. doi: 10.3389/fcell.2020.00365
64. Mori S, Shiraishi A, Epplen K, Butcher D, Murase D, Yasuda Y, et al. Characterization of skin function associated with obesity and specific correlation to local/systemic parameters in American women. *Lipids Health Dis.* (2017) 16:214. doi: 10.1186/s12944-017-0608-1

65. Zhang Y, Jia R, Zhang Y, Sun X, Mei Y, Zou R, et al. Effect of non-surgical periodontal treatment on cytokines/adipocytokines levels among periodontitis patients with or without obesity: a systematic review and meta-analysis. *BMC Oral Health*. (2023) 23:717. doi: 10.1186/s12903-023-03383-3
66. Divella R, Daniele A, DE Luca R, Mazzocca A, Ruggieri E, Savino E, et al. Synergism of adipocytokine profile and ADIPOQ/TNF-alpha polymorphisms in NAFLD-associated metS predict colorectal liver metastases outgrowth. *Cancer Genomics Proteomics*. (2019) 16:519–30. doi: 10.21873/cgp.20154
67. Evans AC, Papachristou GI, Whitcomb DC. Obesity and the risk of severe acute pancreatitis. *Minerva Gastroenterol Dietol*. (2010) 56:169–79.
68. Sobis J, Kunert L, Rykaczewska-Czerwinska M, Swietochowska E, Gorczyca P. The effect of aripiprazole on leptin levels of patients with chronic schizophrenia and a comparison of leptin, acute phase protein, and cytokine levels with regard to body mass and body composition indexes. *Endokrynol Pol*. (2022) 73:35–42. doi: 10.5603/EP.a2021.0110
69. Lu Y, Van Bever HP, Lim TK, Kuan WS, Goh DY, Mahadevan M, et al. Obesity, asthma prevalence and IL-4: Roles of inflammatory cytokines, adiponectin and neuropeptide Y. *Pediatr Allergy Immunol*. (2015) 26:530–6. doi: 10.1111/pai.2015.26.issue-6
70. Yokota T, Oritani K, Takahashi I, Ishikawa J, Matsuyama A, Ouchi N, et al. Adiponectin, a new member of the family of soluble defense collagens, negatively regulates the growth of myelomonocytic progenitors and the functions of macrophages. *Blood*. (2000) 96:1723–32. doi: 10.1182/blood.V96.5.1723
71. Wolf AM, Wolf D, Rumpold H, Enrich B, Tilg H. Adiponectin induces the anti-inflammatory cytokines IL-10 and IL-1RA in human leukocytes. *Biochem Biophys Res Commun*. (2004) 323:630–5. doi: 10.1016/j.bbrc.2004.08.145
72. Wang J, Polaki V, Chen S, Bihl JC. Exercise improves endothelial function associated with alleviated inflammation and oxidative stress of perivascular adipose tissue in type 2 diabetic mice. *Oxid Med Cell Longev*. (2020) 2020:8830537. doi: 10.1155/2020/8830537
73. Bastard JP, Maachi M, Lagathu C, Kim MJ, Caron M, Vidal H, et al. Recent advances in the relationship between obesity, inflammation, and insulin resistance. *Eur Cytokine Netw*. (2006) 17:4–12.
74. Huang S, Wang H, Zheng H, Li W, Shi J, Shen C, et al. Association between IL-6 polymorphisms and Atopic Dermatitis in Chinese Han children. *Front Pediatr*. (2023) 11:1156659. doi: 10.3389/fped.2023.1156659
75. Wueest S, Konrad D. The controversial role of IL-6 in adipose tissue on obesity-induced dysregulation of glucose metabolism. *Am J Physiol Endocrinol Metab*. (2020) 319:E607–13. doi: 10.1152/ajpendo.00306.2020
76. Zheng HY, Zhao L, Li CX, Li SH. Correlation between serum IL-16 and atopic dermatitis. *Genet Mol Res*. (2016) 15. doi: 10.4238/gmr.15016556
77. Xiao C, Sun Z, Gao J, Bai Y, Zhang C, Pang B, et al. Enhanced phenotype of calcipotriol-induced atopic dermatitis in filaggrin-deficient mice. *FASEB J*. (2021) 35: e21574. doi: 10.1096/fj.202002709R
78. Huang IH, Chung WH, Wu PC, Chen CB. JAK-STAT signaling pathway in the pathogenesis of atopic dermatitis: An updated review. *Front Immunol*. (2022) 13:1068260. doi: 10.3389/fimmu.2022.1068260
79. Luan D, Dadpey B, Zaid J, Bridge-Corner PE, DeLuca JH, Xia W, et al. Adipocyte-secreted IL-6 sensitizes macrophages to IL-4 signaling. *Diabetes*. (2023) 72:367–74. doi: 10.2337/db22-0444
80. Jones SA, Jenkins BJ. Recent insights into targeting the IL-6 cytokine family in inflammatory diseases and cancer. *Nat Rev Immunol*. (2018) 18:773–89. doi: 10.1038/s41577-018-0066-7
81. Wueest S, Konrad D. The role of adipocyte-specific IL-6-type cytokine signaling in FFA and leptin release. *Adipocyte*. (2018) 7:226–8. doi: 10.1080/21623945.2018.1493901
82. Paddenberg E, Osterloh H, Jantsch J, Nogueira A, Proff P, Kirschneck C, et al. Impact of leptin on the expression profile of macrophages during mechanical strain. *In Vitro. Int J Mol Sci*. (2022) 23. doi: 10.3390/ijms231810727
83. Akdis CA, Arkwright PD, Bruggen MC, Busse W, Gadina M, Guttman-Yassky E, et al. Type 2 immunity in the skin and lungs. *Allergy*. (2020) 75:1582–605. doi: 10.1111/all.14318
84. Morioka C, Komaki M, Taki A, Honda I, Yokoyama N, Iwasaki K, et al. Neuroprotective effects of human umbilical cord-derived mesenchymal stem cells on periventricular leukomalacia-like brain injury in neonatal rats. *Inflammation Regener*. (2017) 37:1. doi: 10.1186/s41232-016-0032-3
85. Chiriccozzi A, Maurelli M, Peris K, Girolomoni G. Targeting IL-4 for the treatment of atopic dermatitis. *Immunotargets Ther*. (2020) 9:151–6. doi: 10.2147/ITT.S260370
86. Bieber T. Interleukin-13: Targeting an underestimated cytokine in atopic dermatitis. *Allergy*. (2020) 75:54–62. doi: 10.1111/all.13954
87. Schmelz M. Itch processing in the skin. *Front Med (Lausanne)*. (2019) 6:167. doi: 10.3389/fmed.2019.00167
88. Villarroya F, Cereijo R, Gavalda-Navarro A, Villarroya J, Giral M. Inflammation of brown/beige adipose tissues in obesity and metabolic disease. *J Intern Med*. (2018) 284:492–504. doi: 10.1111/joim.2018.284.issue-5
89. Bapat SP, Whitty C, Mowery CT, Liang Y, Yoo A, Jiang Z, et al. Obesity alters pathology and treatment response in inflammatory disease. *Nature*. (2022) 604:337–42. doi: 10.1038/s41586-022-04536-0
90. Robertson AK, Zhou X, Strandvik B, Hansson GK. Severe hypercholesterolaemia leads to strong Th2 responses to an exogenous antigen. *Scand J Immunol*. (2004) 59:285–93. doi: 10.1111/j.0300-9475.2004.01403.x
91. Obradovic M, Sudar-Milovanovic E, Soskic S, Essack M, Arya S, Stewart AJ, et al. Leptin and obesity: role and clinical implication. *Front Endocrinol (Lausanne)*. (2021) 12:585887. doi: 10.3389/fendo.2021.585887
92. Jaworek AK, Szepietowski JC, Szafraniec K, Jaworek M, Halubiec P, Wojas-Pelc A, et al. Adipokines as biomarkers of atopic dermatitis in adults. *J Clin Med*. (2020) 9. doi: 10.3390/jcm9092858
93. Choi JH, Park BH, Kim HG, Hwang YP, Han EH, Jin SW, et al. Inhibitory effect of Psidium guajava water extract in the development of 2,4-dinitrochlorobenzene-induced atopic dermatitis in NC/Nga mice. *Food Chem Toxicol*. (2012) 50:2923–9. doi: 10.1016/j.fct.2012.04.044
94. Palhinha L, Liechocki S, Hottz ED, Pereira J, de Almeida CJ, Moraes-Vieira PMM, et al. Leptin induces proadipogenic and proinflammatory signaling in adipocytes. *Front Endocrinol (Lausanne)*. (2019) 10:841. doi: 10.3389/fendo.2019.00841
95. Kiguchi N, Maeda T, Kobayashi Y, Fukazawa Y, Kishioka S. Leptin enhances CC-chemokine ligand expression in cultured murine macrophage. *Biochem Biophys Res Commun*. (2009) 384(3):311–5. doi: 10.1016/j.bbrc
96. Lee SM, Choi HJ, Oh CH, Oh JW, Han JS. Leptin increases TNF-alpha expression and production through phospholipase D1 in Raw 264.7 cells. *PLoS One*. (2014) 9:e102373. doi: 10.1371/journal.pone.0102373
97. Yuksel H, Sogut A, Yilmaz O, Onur E, Dinc G. Role of adipokines and hormones of obesity in childhood asthma. *Allergy Asthma Immunol Res*. (2012) 4:98–103. doi: 10.4168/aa.2012.4.2.98
98. Surendar J, Frohberger SJ, Karunakaran I, Schmitt V, Stamminger W, Neumann AL, et al. Adiponectin limits IFN-gamma and IL-17 producing CD4 T cells in obesity by restraining cell intrinsic glycolysis. *Front Immunol*. (2019) 10:2555. doi: 10.3389/fimmu.2019.02555
99. Tsang JY, Li D, Ho D, Peng J, Xu A, Lamb J, et al. Novel immunomodulatory effects of adiponectin on dendritic cell functions. *Int Immunopharmacol*. (2011) 11:604–9. doi: 10.1016/j.intimp.2010.11.009
100. Szabo CE, Ilies RF, Aioanei CS, Catana A, Cret V, Serban RS, et al. The role of adiponectin, TNF-alpha and glutathione in the pathogenesis and evolution of type 1 diabetes. *Diabetes Metab Syndr Obes*. (2019) 12:2303–8. doi: 10.2147/DMSO.S220133
101. Machura E, Szczepanska M, Ziora K, Ziora D, Swietochowska E, Barc-Czarnecka M, et al. Evaluation of adipokines: apelin, visfatin, and resistin in children with atopic dermatitis. *Mediators Inflammation*. (2013) 2013:760691. doi: 10.1155/2013/760691
102. Pine GM, Batugedara HM, Nair MG. Here, there and everywhere: Resistin-like molecules in infection, inflammation, and metabolic disorders. *Cytokine*. (2018) 110:442–51. doi: 10.1016/j.cyt.2018.05.014
103. Banihani SA, Abu-Alia KF, Khabour OF, Alzoubi KH. Association between resistin gene polymorphisms and atopic dermatitis. *Biomolecules*. (2018) 8. doi: 10.3390/biom8020017
104. Farag AGA, Hammam MA, Khaled HN, Soliman S, Tayel NR, El-Shamendy AA, et al. Resistin adipokine in atopic dermatitis patients: A clinical, biochemical, and genetic study. *J Cosmet Dermatol*. (2020) 19:2929–35. doi: 10.1111/jocd.v19.11
105. Li B, Hao J, Zeng J, Sauter ER. SnapShot: FABP functions. *Cell*. (2020) 182:1066–1066.e1061. doi: 10.1016/j.cell.2020.07.027
106. Yu L, Li L. Potential biomarkers of atopic dermatitis. *Front Med (Lausanne)*. (2022) 9:1028694. doi: 10.3389/fmed.2022.1028694
107. Broccardo CJ, Mahaffey SB, Strand M, Reisdorff NA, Leung DY. Peeling off the layers: skin taping and a novel proteomics approach to study atopic dermatitis. *J Allergy Clin Immunol*. (2009) 124:1113–1115 e1111–1111. doi: 10.1016/j.jaci.2009.07.057
108. Hao J, Yu J, Yorek MS, Yu CL, Pope RM, Chimenti MS, et al. Keratinocyte FABP5-VCP complex mediates recruitment of neutrophils in psoriasis. *Cell Rep*. (2023) 42:113449. doi: 10.1016/j.celrep.2023.113449
109. Lee J, Kim B, Chu H, Zhang K, Kim H, Kim JH, et al. FABP5 as a possible biomarker in atopic march: FABP5-induced Th17 polarization, both in mouse model and human samples. *EBioMedicine*. (2020) 58:102879. doi: 10.1016/j.ebiom.2020.102879
110. Zhang Y, Li Q, Rao E, Sun Y, Grossmann ME, Morris RJ, et al. Epidermal Fatty Acid binding protein promotes skin inflammation induced by high-fat diet. *Immunity*. (2015) 42:953–64. doi: 10.1016/j.immuni.2015.04.016
111. Hao J, Yan F, Zhang Y, Triplett A, Zhang Y, Schultz DA, et al. Expression of adipocyte/macrophage fatty acid-binding protein in tumor-associated macrophages promotes breast cancer progression. *Cancer Res*. (2018) 78:2343–55. doi: 10.1158/0008-5472.CAN-17-2465
112. Banaszak M, Gorna I, Przyslawski J. Zinc and the innovative zinc-alpha2-glycoprotein adipokine play an important role in lipid metabolism: A critical review. *Nutrients*. (2021) 13. doi: 10.3390/nut13062023

113. Noh JY, Shin JU, Kim JH, Kim SH, Kim BM, Kim YH, et al. ZAG regulates the skin barrier and immunity in atopic dermatitis. *J Invest Dermatol.* (2019) 139:1648–1657.e1647. doi: 10.1016/j.jid.2019.01.023
114. Suga H, Sugaya M, Miyagaki T, Kawaguchi M, Morimura S, Kai H, et al. Serum visfatin levels in patients with atopic dermatitis and cutaneous T-cell lymphoma. *Eur J Dermatol.* (2013) 23:629–35. doi: 10.1684/ejd.2013.2107
115. Moschen AR, Kaser A, Enrich B, Mosheimer B, Theurl M, Niederegger H, et al. Visfatin, an adipocytokine with proinflammatory and immunomodulating properties. *J Immunol.* (2007) 178:1748–58. doi: 10.4049/jimmunol.178.3.1748
116. Kanda N, Hau CS, Tada Y, Tatsuta A, Sato S, Watanabe S. Visfatin enhances CXCL8, CXCL10, and CCL20 production in human keratinocytes. *Endocrinology.* (2011) 152:3155–64. doi: 10.1210/en.2010-1481
117. Moschen AR, Adolph TE, Gerner RR, Wieser V, Tilg H. Lipocalin-2: A master mediator of intestinal and metabolic inflammation. *Trends Endocrinol Metab.* (2017) 28:388–97. doi: 10.1016/j.tem.2017.01.003
118. Villalvilla A, Garcia-Martin A, Largo R, Gualillo O, Herrero-Beaumont G, Gomez R. The adipokine lipocalin-2 in the context of the osteoarthritic osteochondral junction. *Sci Rep.* (2016) 6:29243. doi: 10.1038/srep29243
119. Shiratori-Hayashi M, Koga K, Tozaki-Saitoh H, Kohro Y, Toyonaga H, Yamaguchi C, et al. STAT3-dependent reactive astrogliosis in the spinal dorsal horn underlies chronic itch. *Nat Med.* (2015) 21:927–31. doi: 10.1038/nm.3912
120. Guo H, Jin D, Chen X. Lipocalin 2 is a regulator of macrophage polarization and NF-kappaB/STAT3 pathway activation. *Mol Endocrinol.* (2014) 28:1616–28. doi: 10.1210/me.2014-1092
121. Saltiel AR, Olefsky JM. Inflammatory mechanisms linking obesity and metabolic disease. *J Clin Invest.* (2017) 127:1–4. doi: 10.1172/JCI92035
122. Croasdell A, Duffney PF, Kim N, Lacy SH, Sime PJ, Phipps RP. PPARgamma and the innate immune system mediate the resolution of inflammation. *PPAR Res.* (2015) 2015:549691. doi: 10.1155/2015/549691
123. Matsuwaki Y, Ueki S, Adachi T, Oyamada H, Kamada Y, Yamaguchi K, et al. The synthetic PPARgamma agonist troglitazone inhibits IL-5-induced CD69 upregulation and eosinophil-derived neurotoxin release from eosinophils. *Pharmacology.* (2005) 74:169–73. doi: 10.1159/000085034
124. Nagata K, Kasakura K, Miura R, Yashiro T, Nishiyama C. Suppressive role of PPARgamma in the IgE-dependent activation of mast cells. *Int Immunol.* (2020) 32:143–50. doi: 10.1093/intimm/dxz069
125. Karagiannis F, Masouleh SK, Wunderling K, Surendar J, Schmitt V, Kazakov A, et al. Lipid-droplet formation drives pathogenic group 2 innate lymphoid cells in airway inflammation. *Immunity.* (2020) 52:885. doi: 10.1016/j.immuni.2020.04.021
126. Vieira Braga FA, Kar G, Berg M, Carpaij OA, Polanski K, Simon LM, et al. A cellular census of human lungs identifies novel cell states in health and in asthma. *Nat Med.* (2019) 25:1153–63. doi: 10.1038/s41591-019-0468-5
127. Henriksson J, Chen X, Gomes T, Ullah U, Meyer KB, Miragaia R, et al. Genome-wide CRISPR screens in T helper cells reveal pervasive crosstalk between activation and differentiation. *Cell.* (2019) 176:882–896.e818. doi: 10.1016/j.cell.2018.11.044
128. Micosse C, von Meyenn L, Steck O, Kipfer E, Adam C, Simillion C, et al. Human "T(H)9" cells are a subpopulation of PPAR-gamma(+) T(H)2 cells. *Sci Immunol.* (2019) 4. doi: 10.1126/sciimmunol.aat5943
129. Stark JM, Coquet JM, Tibbitt CA. The role of PPAR-gamma in allergic disease. *Curr Allergy Asthma Rep.* (2021) 21:45. doi: 10.1007/s11882-021-01022-x
130. Kolodin D, van Panhuys N, Li C, Magnuson AM, Cipolletta D, Miller CM, et al. Antigen- and cytokine-driven accumulation of regulatory T cells in visceral adipose tissue of lean mice. *Cell Metab.* (2015) 21:543–57. doi: 10.1016/j.cmet.2015.03.005
131. Renert-Yuval Y, Del Duca E, Pavel AB, Fang M, Lefferdink R, Wu J, et al. The molecular features of normal and atopic dermatitis skin in infants, children, adolescents, and adults. *J Allergy Clin Immunol.* (2021) 148:148–63. doi: 10.1016/j.jaci.2021.01.001
132. Bertschi NL, Steck O, Luther F, Bazzini C, von Meyenn L, Scharli S, et al. PPAR-gamma regulates the effector function of human T helper 9 cells by promoting glycolysis. *Nat Commun.* (2023) 14:2471. doi: 10.1038/s41467-023-38233-x



OPEN ACCESS

EDITED BY

Reza Akbarzadeh,
University of Lübeck, Germany

REVIEWED BY

Antje Mueller,
University of Lübeck, Germany
Yael Alippe,
Washington University in St. Louis,
United States

*CORRESPONDENCE

Ping Li
✉ graceli008@sohu.com

[†]These authors have contributed equally to this work

RECEIVED 16 June 2024

ACCEPTED 15 November 2024

PUBLISHED 11 December 2024

CITATION

Sun R, Chu J and Li P (2024) Inflammasomes and idiopathic inflammatory myopathies.
Front. Immunol. 15:1449969.
doi: 10.3389/fimmu.2024.1449969

COPYRIGHT

© 2024 Sun, Chu and Li. This is an open-access article distributed under the terms of the [Creative Commons Attribution License \(CC BY\)](#). The use, distribution or reproduction in other forums is permitted, provided the original author(s) and the copyright owner(s) are credited and that the original publication in this journal is cited, in accordance with accepted academic practice. No use, distribution or reproduction is permitted which does not comply with these terms.

Inflammasomes and idiopathic inflammatory myopathies

Rui Sun^{1†}, Jiyan Chu^{1,2†} and Ping Li^{1*}

¹Department of Rheumatology, General Hospital of Northern Theater Command, Shenyang, Liaoning, China, ²Graduate School, Dalian Medical University, Dalian, Liaoning, China

Idiopathic inflammatory myopathies (IIM) are a group of systemic autoimmune diseases characterized by muscle weakness and elevated serum creatine kinase levels. Recent research has highlighted the role of the innate immune system, particularly inflammasomes, in the pathogenesis of IIM. This review focuses on the role of inflammasomes, specifically NLRP3 and AIM2, and their associated proteins in the development of IIM. We discuss the molecular mechanisms of pyroptosis, a programmed cell death pathway that triggers inflammation, and its association with IIM. The NLRP3 inflammasome, in particular, has been implicated in muscle fiber necrosis and the subsequent release of damage-associated molecular patterns (DAMPs), leading to inflammation. We also explore the potential therapeutic implications of targeting the NLRP3 inflammasome with inhibitors such as glyburide and MCC950, which have shown promise in reducing inflammation and improving muscle function in preclinical models. Additionally, we discuss the role of caspases, particularly caspase-1, in the canonical pyroptotic pathway associated with IIM. The understanding of these mechanisms offers new avenues for therapeutic intervention and a better comprehension of IIM pathophysiology.

KEYWORDS

idiopathic inflammatory myopathy, inflammasome, pyroptosis, NLR family pyrin domain containing 3 (NLRP3), absent in melanoma 2 (AIM2), caspase, gasdermin D (GSDMD)

Background

Idiopathic inflammatory myopathies (IIMs) are a rare and diverse group of systemic autoimmune diseases, with an incidence ranging from 1 to 11 cases per million individuals (1, 2). The disease primarily presents with muscle weakness and pain in the proximal limbs, often accompanied by elevated serum creatine kinase levels. It can also affect various other organs, including the heart, lungs, skin, and digestive tract. The most common subtypes of IIM include dermatomyositis (DM), polymyositis (PM), inclusion body myositis (IBM), immune-mediated necrotizing myopathy (IMNM), and overlap myositis (3). In recent years, the identification of myositis-specific antibodies (MSAs) and myositis-associated antibodies (MAAs) has significantly improved the diagnosis and treatment of IIM (4, 5). At the same time, research suggests that abnormal activation of the innate immune system strongly influences the onset and progression of IIM (6, 7).

Pyroptosis is a lytic form of programmed cell death distinct from apoptosis and increasingly recognized for its critical role in the host's innate immune response. Pyroptosis can occur in various cell types, including immune cells like macrophages, monocytes, and dendritic cells, as well as non-immune cells such as intestinal epithelial cells, stromal cells, hepatocytes, and myocytes (8–10). While controlled pyroptotic activity is crucial for maintaining cellular homeostasis and exerting protective functions, excessive cell death and delayed clearance of dead cells and their fragments may lead to the release of self-antigens, damage-associated molecular patterns (DAMPs), and pro-inflammatory cytokines, exaggerating immune and inflammatory responses and promoting disease development (11–14).

Pyroptosis at glance

Our understanding of pyroptosis began in 1986 when Friedlander first observed cell death and cell content leakage in murine macrophages induced by anthrax lethal toxin (15), and this pivotal moment laid the foundation for the discovery of a new type of cell death pathway. In 1992, an enzyme initially known as ICE (interleukin-1 β converting enzyme) and later identified as inflammatory caspase was found to process pro-interleukin-1 β (IL-1 β) into its mature form, highlighting the role of caspases in inflammation (16, 17). That same year, Zychlinsky and colleagues erroneously identified pyroptosis as apoptosis in human macrophages infected by *Shigella flexneri* (18). However, the true nature of this cell death process began to emerge in 1996, with reports indicating that the invasion plasmid antigen B (ipaB) of *Shigella flexneri* activated caspase-1, suggesting a distinct mechanism of cell death from apoptosis (19). In 2001, Cookson and Brennan first proposed the term “pyroptosis.” The term is derived from Greek, where “pyro” means fire or fever, and “ptosis” means falling. Pyroptosis is a pro-inflammatory programmed cell death characterized by pore formation, membrane rupture, and leakage of cellular contents (7, 11, 20). The introduction of this term was a crucial step in distinguishing pyroptosis from non-inflammatory apoptosis.

In 2002, the inflammasome was identified as a multiprotein complex capable of activating pro-inflammatory caspases and pro-IL-1 β (21). This groundbreaking discovery linked the molecular mechanism of inflammation with cell death pathways. For a long time, pyroptosis was considered to be mediated by caspase-1. In 2011, Kayagaki and colleagues discovered that caspase-11 could induce death in mouse macrophages. This process is similar to caspase-1-mediated pyroptosis and is therefore termed “non-canonical pyroptotic pathway” (22). In 2014, Shi J and colleagues revealed that human caspase-4 and caspase-5 have the same function (23).

In 2015, gasdermin D (GSDMD) was identified as the crucial executor of pyroptosis, a milestone discovery after being cleaved by caspase-1 or caspase-4/5/11 (24). This, along with the subsequent definition of pyroptosis as gasdermin-mediated programmed cell death (25, 26), has fundamentally changed our understanding of cell death mechanisms (Table 1). In 2017, Shao's research group

found that chemotherapeutic drugs can induce pyroptosis by triggering caspase-3-mediated cleavage of GSDME (29). The following year, it was discovered that caspase-8 also cleaves GSDMD, thereby initiating pyroptosis during *Yersinia* infection (30, 31). In 2020, it was found that pyroptosis can also be induced independently of caspase, significantly changing our understanding of this process. Granzyme A (GZMA) secreted by cytotoxic T lymphocytes and natural killer (NK) cells cross-domain cleaves GSDMB specifically, activating GSDMB-dependent pyroptosis in malignant cells (32). Similarly, granzyme B (GZMB) from these immune cells can also initiate GSDME-dependent apoptotic cell death in tumor cells through caspase-3-mediated cleavage of GSDME (33).

The journey through the history of pyroptosis has been marked by significant discoveries that have deepened our understanding of cell death and its role in immune responses (Figure 1). As research continues, the intricate mechanisms and regulatory pathways of pyroptosis will likely reveal further insights into the complex interplay between cell death and inflammation. In particular, recent studies have identified the contribution of inflammasomes to the pathogenesis of immune-related myopathies (IIM), and this article aims to summarize the research findings on this topic.

Inflammasomes

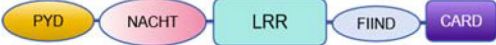




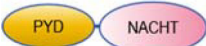





The inflammasome is a complex composed of multiple proteins, formed in response to immune signals from pathogen-associated molecular patterns (PAMPs) and damage-associated molecular patterns (DAMPs), playing a key role in coordinating host immune responses (27). The inflammasome sensor complex is composed of two receptor families: the nucleotide-binding oligomerization domain-like receptors (NLRs), including NLRP1, NLRP3, NLRP6, NLRP7, NLRC4, NLRP10 and NLRP12, and the PYHIN family containing the HIN domain, including AIM2 and pyrin (28) (Table 1).

Currently, most research on inflammasomes converged on infection and cancer fields. Due to the rare nature of the disease, research on idiopathic inflammatory myopathies (IIMs) is relatively limited, mainly converged on NLRP3 and AIM2. Exploring pyroptosis mechanisms in IIMs remains an underdeveloped area, with many knowledge gaps needing to be filled. Here, we review the latest progress of inflammasomes in patients with IIMs.

The role of NLRP3 inflammasome in IIMs

NLRP3 inflammasome is a multiprotein complex that plays a crucial role in the innate immune response. Due to its involvement in various inflammatory diseases, including idiopathic inflammatory myopathies (IIM), this inflammasome has been extensively studied (34). NLRP3 is expressed in monocytes, neutrophils, dendritic cells, lymphocytes, epithelial cells, and muscle cells. It consists of the NLRP3 protein, the adaptor protein ASC, and pro-caspase-1. The NLRP3 protein is a

TABLE 1 Classification, domains, and common activators of inflammasome component protein (27, 28).

Classification	Sensor protein	Effector domain	Common activators
NLRs family	NLRP1		anthracis lethal toxin, DPP8/9 inhibitors tegument protein ORF45
	NLRP3		ATP, ion flux (K+ efflux), particulate matter, ROS, pathogen-associated RNA, bacterial and fungal toxins, and component
	NLRC4		Gram-negative bacteria and flagellin, the type III or IV secretion system proteins
	NLRP6		Gram-positive, bacteria-derived lipoteichoic acid, LPS, viral infections
	NLRP7		mycoplasma and Gram-positive bacterial infections
	NLRP10		phospholipase C activator 3m3-FBS
	NLRP12		Yersinia pestis infection
PYHIN family	AIM2		cytosolic dsDNA of viral, bacterial, or host origin
	Pyrin		RhoA inhibiting microbial toxins
ASC protein			
Pro-caspase			

115 kDa cytosolic protein, containing three domains: the C-terminal leucine-rich repeat (LRR) domain that senses danger signals, the nucleotide-binding and oligomerization domain (NACHT) with ATPase activity, and the N-terminal PYD domain that interacts with ASC (34). The structure of the NLRP3 inflammasome has been described as ring-shaped, with a curved LRR and a globular NACHT domain. Under normal physiological conditions, the interaction between the NACHT and LRR domains keeps NLRP3 in a self-inhibited state. However, cellular stress factors, whether pathogen-associated molecular patterns (PAMPs) or damage-associated molecular patterns (DAMPs), can disrupt this balance (34, 35). Upon activation, NLRP3 undergoes conformational changes, leading to self-cleavage to form P20 and P10 subunits. The NACHT domain plays a critical role in ATP binding and hydrolysis. The P20 subunit contains the LRR domain, while the P10 subunit contains the NACHT and PYD domains. This cleavage and subsequent interaction between the PYD domain of NLRP3 and ASC are key steps in assembling the inflammasome complex, resulting in the recruitment and activation of pro-caspase-1. Once activated, caspase-1 processes the pro-forms of IL-1 β and IL-18, leading to their maturation and secretion, thereby propagating the inflammatory response.

NLRP3 inflammasome is associated with various diseases, including metabolic syndrome such as obesity, type 2 diabetes

(T2D) (36), and gout (37), neurodegenerative diseases such as Alzheimer’s disease (AD) (38) and multiple sclerosis (MS) (39), inflammatory bowel diseases (IBD) such as Crohn’s disease and ulcerative colitis (40, 41), cardiovascular diseases (42), autoimmune conditions like systemic lupus erythematosus (SLE) (43–45) and rheumatoid arthritis (RA) (46), various cancers (47), and infections including viral, bacterial, and fungal pathogens (11). The role of NLRP3 inflammasome in these diseases highlights its importance in immune responses and inflammation. NLRP3 inflammasome is also involved in the pathogenesis of idiopathic inflammatory myopathy through multiple mechanisms.

Canonical pathway

Canonical activation involves two steps. The initial priming step is promoted by pattern recognition receptors such as Toll-like receptors and cytokine receptors (e.g., IL-1R, TNFR) on the membrane, triggering NF- κ B nuclear translocation, thereby enhancing the expression of NLRP3 and pro-IL-1 β at the transcription and translation levels (48). Recently, many studies have provided strong evidence indicating that the priming step is not limited to transcriptional upregulation, post-translational modifications (PTMs) of NLRP3 protein, such as ubiquitination

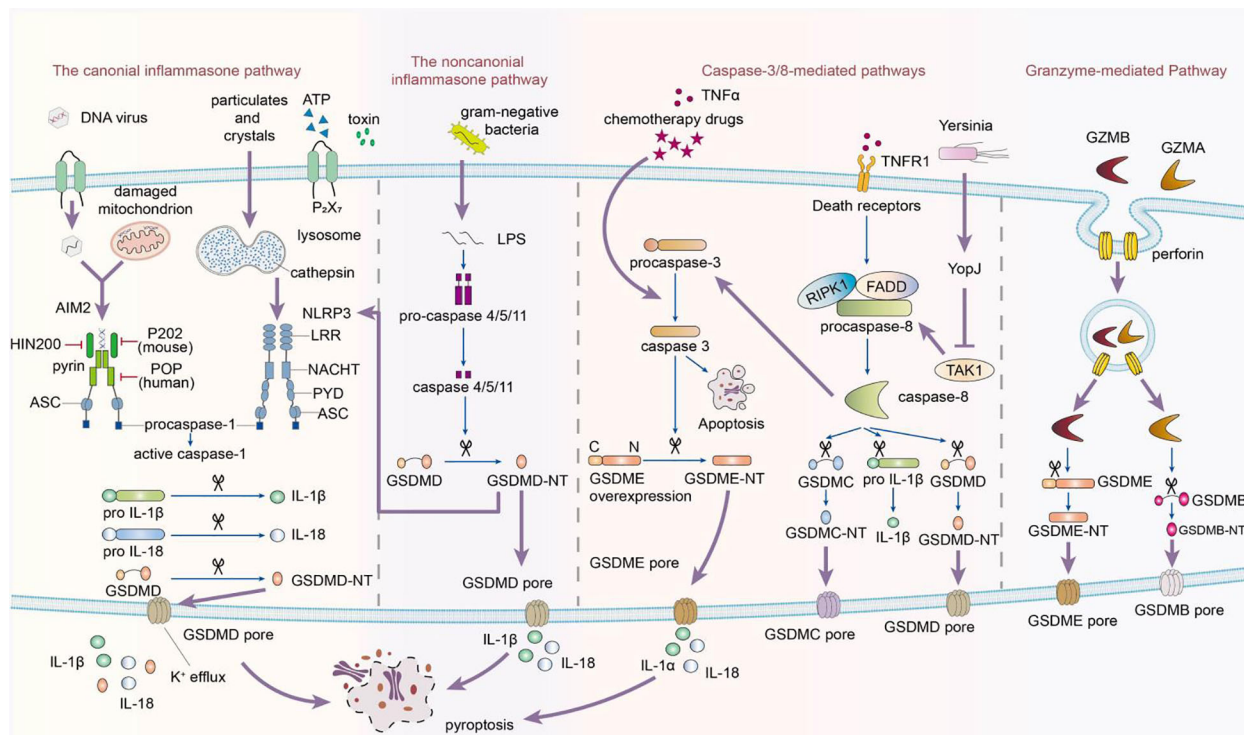


FIGURE 1

This image depicts the activation of the inflammasome, which follows a biphasic signaling pattern. The process begins with a priming signal initiated by pattern recognition receptors. There are four recognized pathways in signal activation. The canonical pathway depends on Caspase-1, while the noncanonical signaling cascade relies on Caspase-4/5/11. Caspase-1, -4, -5, and -11 selectively cleave GSDMD, releasing its N-terminal fragments to form transmembrane pores in the cytoplasmic lipid bilayer, leading to pyroptosis. Additionally, Caspase-3 can induce pyroptosis in incomplete pathways by cleaving GSDME when cells highly express GSDME in response to tumor necrosis factor- α (TNF- α). Conversely, in cells with negative or low GSDME expression, Caspase-3 triggers apoptosis. In the caspase-8-mediated pathway, inhibiting TAK1 induces the activation of caspase-8, which cleaves GSDMD, resulting in pyroptosis. In the granzyme-mediated pathway, CAR T cells rapidly activate caspase-3 in target cells by releasing GZMB, which then activates GSDME, causing extensive pyroptosis. Additionally, GZMA and GZMB in cytotoxic lymphocytes enter target cells through perforin and induce pyroptosis. GZMA hydrolyzes GSDMB, and GZMB directly activates GSDME.

and phosphorylation, also play a critical role in the activation of the NLRP3 inflammasome (49–51). The next step is the activation step, where secondary signals can be induced by various stimuli, including microbial invasion, exotoxins, extracellular ATP, crystals, and double-stranded DNA, leading to oligomerization of the NLRP3 inflammasome and activation of caspase-1 (52–63). Once activated, caspase-1 is responsible for the proteolytic cleavage of pro-inflammatory cytokines IL-1 β and IL-18, converting them into their mature biologically active forms. Increasing evidence emphasizes the importance of NLRP3 inflammasome activation, caspase-1 activation, and IL-1 β release in the development of autoimmune diseases such as systemic lupus erythematosus, multiple sclerosis, and ulcerative colitis (39–41, 43–45).

Recent research has revealed the significance of NLRP3 inflammasome signaling cascade in idiopathic inflammatory myopathies. Yin Xi's research group reported that compared to healthy controls, patients with polymyositis (PM) and dermatomyositis (DM) showed elevated levels of NLRP3, IL-1 β , and IL-18 mRNA in muscle fiber tissues, as well as increased expression of NLRP3 and caspase-1 p20 protein subunit (64). The

study indicates that in DM/PM patients, the high expression of NLRP3 inflammasomes in muscle tissues activates caspase-1 expression, leading to upregulation of IL-1 β and IL-18 levels, enhancing cellular immunity. There was no significant difference in the expression levels of NLRP3 and caspase-1 between DM and PM patients, possibly due to NLRP3 inflammasomes being involved in local muscle inflammation in DM/PM, with the released IL-1 β /IL-18 possibly exacerbating disease progression (64). The activation of NLRP3 inflammasomes in DM/PM is attributed to muscle fiber necrosis, releasing high mobility group box-1, ATP, and hyaluronic acid as damage-associated molecular patterns, which may serve as activators of NLRP3 inflammasomes (63, 65). Additionally, Xia P and colleagues assessed the role of NLRP3 inflammasomes in PM using an experimental rat model and C2C12 myoblast cells (66). They observed a significant upregulation of NLRP3, caspase-1, and IL-1 β in affected muscles, and treatment with NLRP3 inflammasome inhibitor MCC950 or NLRP3-specific siRNA reduced inflammation and improved muscle function, highlighting the importance of the NLRP3/caspase-1/IL-1 β Canonical pathway in PM.

Non-canonical pathway

The non-Canonical activation of NLRP3 inflammasome occurs in one step, bypassing the induction phase. In a mouse model of experimental autoimmune myositis (EAM), researchers observed elevated levels of NLRP3, caspase-4, caspase-5, caspase-11, pannexin-1, ATP-activated P2X7 receptor (P2X7R), and GSDMD mRNA and protein in muscle tissue, accompanied by increased serum concentrations of IL-1 β and IL-18 (67). Lipopolysaccharide (LPS) from gram-negative bacteria activates caspase-4/5/11, promoting the release of ATP through the pannexin-1 channel. This ATP subsequently activates the P2X7R channel, leading to potassium (K⁺) efflux. These signals trigger NLRP3 inflammasome, resulting in the secretion of IL-1 β and IL-18 and the induction of pyroptosis (23). This process disrupts the ion balance of the cell membrane, leading to membrane rupture, release of intracellular inflammatory contents, and initiation of an inflammatory response. ATP and K⁺ also act as secondary messengers to activate NLRP3 inflammasome, enhancing the production of inflammatory factors, and potentially exacerbating pyroptosis, inflammation, and muscle damage.

Glyburide is a sulfonylurea antidiabetic drug known to block ATP-sensitive potassium channels on pancreatic β cells (68). Previous studies have shown that in conditions such as renal impairment (69), sepsis-induced myocardial injury (70), and asthma (71), glyburide reduces inflammation by inhibiting NLRP3 activation and decreasing levels of inflammatory mediators such as IL-1 β and IL-18 (72). Following glyburide intervention, expression of NLRP3, IL-1 β , and IL-18 in skeletal muscle tissues of experimental autoimmune myocarditis (EAM) mice is reduced, muscle strength is improved, and scabs form at sites of muscle rupture and abscess (67). These results suggest that the NLRP3 inflammasome-mediated IL-1 β /IL-18 pathway plays a role in the pathogenesis of idiopathic inflammatory myopathy, and glyburide inhibiting this pathway leads to reduced secretion of inflammatory factors, alleviation of inflammation, and improvement in muscle strength. Glyburide may become a novel targeted therapeutic drug for controlling or treating IIMs (67).

Bright blue G (BBG), also referred to as Coomassie blue, is a potent antagonist of P2X7R (67). Studies have shown that intravenous injection of BBG can improve recovery in mice with spinal cord injury and reduce local inflammation (73). BBG can also significantly reduce cardiac fibrosis by lowering the expression levels of NLRP3, IL-1 β , and caspase-1 (74). Following BBG intervention, the levels of P2X7R, NLRP3, and IL-1 β proteins, as well as P2X7R mRNA in the muscles of EAM mice, decreased, while IL-18 levels remained unchanged. In addition, new hair growth appeared in the alopecia area compared to before the intervention, and muscle strength increased. Previously ruptured and suppurative ulcers began to scab over, and new granulation tissue appeared (67). This indicates that P2X7R may play a role in the development of IIM through the NLRP3 inflammasome/IL-1 β pathway. BBG inhibits the P2X7R-mediated NLRP3/IL-1 β pathway, reduces inflammation, and gradually restores function.

In summary, glyburide and BBG are promising therapeutic agents for the treatment of IIMs. However, these findings are based solely on experiments in animals, further research is needed to confirm their efficacy and safety in clinical settings.

Interactions of NLRP3 inflammasome with other pathways

Metabolic pathway

The rapidly developing field of immunometabolism delves deep into the intricate interplay between metabolic reprogramming and immune system function, providing new insights into immune responses in health and disease (75). Cellular metabolism involves six major pathways: glycolysis, tricarboxylic acid (TCA) cycle, fatty acid oxidation, fatty acid synthesis, amino acid metabolism, and pentose phosphate pathway (76). Glycolysis converts glucose to pyruvate and generates adenosine triphosphate (ATP). Under normal oxygen conditions, pyruvate enters the TCA cycle and undergoes oxidative phosphorylation, while under low oxygen conditions, it is converted to lactate (77).

Skeletal muscle is a key component in glucose uptake, containing numerous energy-sensing molecules that respond to changes in energy homeostasis in pathological conditions (78). Intrinsic immune receptors on muscle cells and immune cells, such as Toll-like receptors and nucleotide-binding oligomerization domain-like receptors, can influence muscle metabolism through intercellular communication (79–81). Mass spectrometry and bioinformatics studies have shown disturbances in various glycolytic processes, NLRP3 inflammasomes, and programmed cell death pathways in muscle tissues of patients with DM/PM (82). Upregulation of pyruvate kinase M2 (PKM2) was observed in muscle fibers of DM/PM patients and was positively correlated with the expression levels of NLRP3 inflammasomes (82).

In addition, a protein related to pyroptosis is elevated in DM/PM muscle tissues, with a more pronounced effect in PM. In myositis patients expressing anti-signal recognition particle autoantibodies, levels of PKM2 in muscle tissue and interleukin-1 β (IL-1 β) in plasma are high, indicating a link between metabolic imbalance and immune activation. The PKM2 inhibitor shikonin has been found to reduce the activation of NLRP3 inflammasomes in muscle fibers stimulated by IFN γ , reducing pyroptotic cell death, underscoring the role of NLRP3 inflammasomes in the pathogenesis of IIM (82).

Neutrophil extracellular traps pathway

In recent years, research has revealed that neutrophil dysregulation is a driving factor behind IIMs (83, 84). NETs serve as biomarkers for disease activity and are crucial in the pathogenesis of IIMs (85, 86). When stimulated, neutrophils form a DNA-based protein network, including histones, myeloperoxidase (MPO),

neutrophil elastase, antimicrobial peptide LL-37, matrix metalloproteinase 9 (MMP9), and other granular proteins, which eliminate pathogens (87, 88). This process is known as NETosis (89–92). NETs undeniably enhance host defenses by capturing pathogens. However, excessive activation and insufficient degradation of NETs can worsen inflammation, and tissue damage, and cause autoimmune diseases like IIMs (86, 93, 94). NETosis releases nuclear contents into the extracellular space, akin to damage-associated molecular patterns (DAMPs). In autoimmune diseases such as IIM, excessive NET formation leads to tissue damage and disease progression. In IIM-ILD, NETs can harm pulmonary vascular endothelial cells, increasing vascular permeability and causing edema (95). By promoting lung fibroblast proliferation and differentiation into myofibroblasts, NETs contribute to pulmonary fibrosis via the TLR9-miR-7-Smad2 pathway (96). NETs can activate the NLRP3 inflammasome, resulting in the release of IL-1 β and other pro-inflammatory cytokines, amplifying the inflammatory response in IIM (97). Experimental autoimmune myositis (EAM) mouse models have provided insights into NETs' role in IIM-ILD (98). These models show increased NET formation following immunization with skeletal muscle homogenate and pertussis toxin (PTX) (98), with NET presence in the lungs correlating with ILD severity, indicating a pathogenic role for NETs.

Given NETs' role in IIM-ILD, targeting their formation or degradation could offer new therapeutic strategies. Small molecules or biologics that inhibit NET release by neutrophils might reduce tissue damage and inflammation in IIM (99, 100). Enhancing DNase I activity or other enzymes degrading NETs could mitigate excessive NET formation effects (101). Targeting the NLRP3 inflammasome or other downstream pathways activated by NETs might provide additional therapeutic benefits (102–104). Further research is required to fully understand NETs' contribution to IIM pathogenesis and develop targeted therapies for managing IIM-ILD. Future studies should investigate specific NET components, genetic factors influencing NET formation, and novel therapeutic agents that modulate NET-associated pathways.

Autophagy and endoplasmic reticulum stress pathways

NLRP3 inflammasome can interact with other cellular pathways, such as autophagy and endoplasmic reticulum (ER) stress, which can be particularly relevant in muscle cells under metabolic stress (105–107). The dysregulation of these pathways can lead to the accumulation of damaged organelles and protein aggregates, which can activate the NLRP3 inflammasome (107).

Inclusion body myositis (IBM) is a complex muscle disease characterized by progressive muscle weakness and atrophy, significantly impacting the quality of life of affected individuals. The pathogenesis of IBM is not fully understood, but it has been recognized that both inflammatory and degenerative mechanisms play a role in the onset and progression of the disease. In IBM, NLRP3 inflammasome is upregulated, and its activation is associated with the accumulation of characteristic protein

aggregates (107). These aggregates include β -amyloid proteins, tau proteins, and others found in neurodegenerative diseases, suggesting a potential common pathological mechanism (108).

Autophagy is the cellular process responsible for degrading and recycling damaged proteins and organelles. Dysfunction of autophagy is associated with IBM as it may lead to the accumulation of protein aggregates and promote muscle fiber degeneration. The NLRP3 inflammasome can be activated by dysfunctional autophagy activity and reactive oxygen species (ROS) that play a significant role in IBM pathophysiology. Therefore, there is a reciprocal relationship between autophagy and activation of the NLRP3 inflammasome, and they can mutually influence each other (109).

Endoplasmic reticulum(ER) stress is another key factor in the pathogenesis of IBM. The ER is responsible for protein folding and modifications. When its function is impaired, it may lead to the accumulation of misfolded proteins, which can aggregate. NLRP3 inflammasome can be activated by ER stress. Conversely, activation of NLRP3 inflammasome may further impair ER function, forming a vicious cycle, and exacerbating muscle fiber damage and inflammation (108).

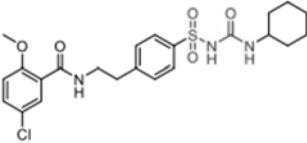
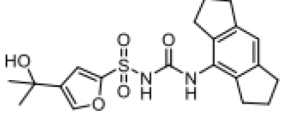
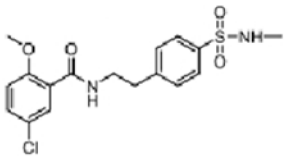
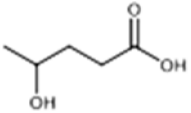
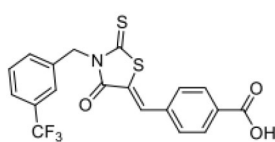
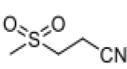
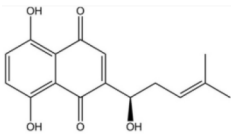
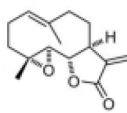
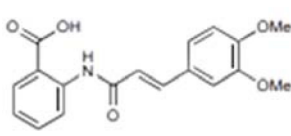
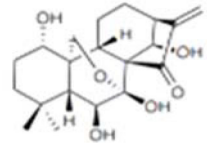
The upregulation of NLRP3 in IBM is associated with inflammatory cytokines and ubiquitin (a marker of protein degradation) levels (109). This indicates that the complex interactions between NLRP3 inflammasome, autophagy, and ER stress may be key driving factors in the pathogenesis of IBM. However, further studies are needed to elucidate the exact roles of these pathways in the pathogenesis of IBM. Understanding the complex interactions between NLRP3 inflammasome, autophagy, and ER stress may provide new insights for therapies for IBM and other muscle diseases characterized by protein aggregation and inflammation.

NLRP3 inhibitors

In DM, PM, IBM, and anti-synthetase syndrome, the NLRP3 inflammasome has been shown to play a central role. Targeting the NLRP3 inflammasome may bring new hope for the treatment of IIM. Several types of NLRP3 inhibitors have been identified, including Glyburide, synthetic small molecules such as MCC950, JC124, BHB, CY-09, and OLT1177, natural products such as Shikonin, Parthenolide, Tranilast, and Oridonin (Table 2). These inhibitors have shown high efficiency and specificity in inhibiting NLRP3 activation, providing valuable tools for studying the pathogenesis of diseases (123–125). Pharmacological modulation of NLRP3 inflammasomes has been explored in preclinical models of diseases such as atherosclerosis (126), gout (127), and inflammatory bowel disease (128), providing promising evidence of the potential of NLRP3 inhibitors in the treatment of inflammatory diseases.

Glyburide is a sulfonylurea antidiabetic drug that can block the ATP-sensitive K⁺ channels on pancreatic β -cells (129). Recent studies have reported its potential anti-inflammatory effects, which can inhibit the expression of NLRP3 inflammasome (129). Following glyburide intervention, the expression levels of NLRP3, IL-1 β , and IL-18 in mice decreased, muscle strength improved, and ulcers and purulent sites

TABLE 2 Structure, target, and mechanism of potential inhibitors of NLRP3 inflammasome.

Agent	Structure	Target	Potential mechanism	References
Gyburide		NLRP3 (indirectly)	Inhibits ATP-sensitive K ⁺ channels; Downstream of P2X7 resulting in inhibition of ASO aggregation.	(110)
MCC950		NLRP3	Alkylates the cysteines in the ATPase domain of NLRP3, inhibits NLRP3 ATPase activity.	(111, 112)
JC124		NLRP3?	Blocks the expression of NLRP3, ASC, caspase-1, pro-IL-1 β , TNF α and iNOS.	(113, 114)
β -hydroxybutyrate (BHB)		NLRP3 (indirectly)	Covalent modification of the catalytic cysteine residue in the active site caspase-1 resulting in caspase-1 blocking and resulting of pro-IL-1 β /18.	(115)
CY-09		NLRP3	Blocks the ATPase domain of NLRP3 resulting in inhibition of canonical and non-canonical NLRP3 inflammasome activation.	(116)
OLT1177		NLRP3	Inhibits NLRP3 ATPase activity, and blocks NLRP3 inflammasome activation.	(117)
Shikonin		NLRP3 (indirectly)	inhibiting the activation of PKM2	(118)
Parthenolide		NLRP1, NLRP3	Suppresses IL-1 β /18 release.	(119, 120)
Tranilast		NLRP3 (indirectly)	Inhibits NLRP3 ATPase activity by cysteine modification, blocks NLRP3 inflammasome activation.	(121)
Oridonin		NLRP3	Inhibits NLRP3 ATPase activity, blocks NLRP3 inflammasome activation. Binds to cysteine of NLRP3 to abolish NLRP3-NEK7 interaction, blocks NLRP3 inflammasome activation.	(122)

began to scab (68). These findings suggest that the NLRP3 inflammasome-mediated IL-1 β /IL-18 pathway is related to the pathogenesis of IIMs. The hypoglycemic side effects of glyburide limit its widespread use, therefore, the development of glyburide analogs is expected to become a new targeted drug for controlling or treating IIM.

MCC950 is a sulfonamide derivative and a selective inhibitor of NLRP3, specifically inhibiting the activation of NLRP3 without affecting AIM2, NLRC4, or NLRP1 inflammasomes, with no risk of hypoglycemia (123, 130). Previous reports have indicated that MCC950 can block the processing of IL-1 β by caspase-1 (123, 130),

and subsequent studies have suggested its potential to simultaneously inhibit both canonical and non-canonical NLRP3 inflammasome activation and IL-1 β production by blocking ASC aggregation (123, 130). In the context of IIM, MCC950 has been shown to reduce the overexpression of MHC-I in C2C12 cells co-cultured under LPS/ATP challenge (67). *In vitro* experiments, pretreatment with MCC950 effectively inhibited NLRP3 inflammasome and pyroptosis activation in human pulmonary microvascular endothelial cells (HPMECs) stimulated by NETs (110). *In vivo*, inhibition of NLRP3 inflammasome by MCC950 reduced the expression of NLRP3, IL-1 β , and MHC-I in muscle tissues of PM model rats, alleviating the severity of muscle inflammation and the levels of CRP, CK, and LDH in serum (65). MCC950 effectively inhibited the activation of NLRP3 inflammasomes in lung microvascular endothelial cells (PMECs) in a mouse model of experimental autoimmune myositis (110). The anti-inflammatory and anti-pyroptotic effects of MCC950 have also been confirmed in Duchenne muscular dystrophy muscle specimens.

Shikonin is a traditional Chinese medicine isolated from *Lithospermum erythrorhizon*, a plant of the *Lithospermum* genus, and has anti-cancer and anti-inflammatory properties (111). As a PKM2 inhibitor, Shikonin can prevent muscle cell pyroptosis by indirectly inhibiting the activation of the NLRP3 inflammasome (82, 111), potentially providing therapeutic benefits in idiopathic inflammatory myopathies.

Some other NLRP3 inhibitors have been studied for other metabolic and autoimmune diseases, but have not been tested in the context of IIM. JC124 is an innovative sulfonamide analogue that has been shown to provide significant anti-inflammatory benefits in the context of traumatic brain injury (112), acute myocardial infarction, and Alzheimer's disease (131). The compound demonstrates its efficacy by significantly downregulating the expression of key inflammatory mediators [including NLRP3, ASC, caspase-1, pro-IL-1 β , TNF α , and inducible nitric oxide synthase (iNOS)], all of which are critical steps in the inflammatory cascade. Beta-hydroxybutyrate (BHB) is a ketone body that supports mammalian cell metabolism during energy deficiency, serving as an alternative source of ATP and exerting its antioxidant effects, with neuroprotective properties (118). In 2015, Youm et al. reported that BHB can inhibit the activation of the NLRP3 inflammasome without affecting the activation of NLRC4, AIM2, or the non-Canonical caspase-11 inflammasome, and inhibits NLRP3 inflammasome by preventing K⁺ efflux, reducing ASC aggregation, and speck formation (118). CY-09 is a small molecule compound specifically developed to inhibit the assembly and activation of the NLRP3 inflammasome by binding to the ATP binding site of the NLRP3 NACHT domain, suppressing NLRP3 ATPase activity (113). It has shown excellent therapeutic effects *in vivo* in CAPS and T2D mouse models. OLT1177 is a β -sulfonyl nitrile identified as a drug candidate for the treatment of osteoarthritis and acute gouty arthritis (114). It inhibits the activity of NLRP3 ATPase, blocking the activation of the NLRP3 inflammasome, with no effect on the NLRC4 and AIM2 inflammasomes (114). It has potential in the treatment of NLRP3-related diseases. Parthenolide is a sesquiterpene lactone derived from the plant *Tanacetum parthenium*. It reduces NLRP3 ATPase and caspase-1 activity by inhibiting NF- κ B (115, 116). Tranilast, a tryptophan metabolite analogue, inhibits NLRP3 ATPase activity

through cysteine modification and blocks the activation of NLRP3 inflammasome (117). Oridonin, a bioactive diterpenoid, mainly derived from the herbal plant *Rabdosia rubescens*, eliminates the interaction between NLRP3 and NEK7 by binding to the cysteine of NLRP3, thus blocking the activation of NLRP3 inflammasome (119).

It is looking forward to more research to elucidate the therapeutic potential of these inhibitors in IIM.

AIM2 inflammasome in IIM

The absence of melanoma 2 (AIM2), a member of the AIM-like receptor (ALR) family, plays a critical role in the intracellular DNA innate immune response. It is a 39 kDa protein composed of 344 amino acids, and the encoding gene AIM2 is located in the q22 region of human chromosome 1 (120, 121). Cloned in 1997 as a tumor suppressor, AIM2 gained attention only in 2009. It is characterized by an N-terminal pyrin domain (PYD) and a C-terminal HIN-200 domain, also known as the PYHIN domain, which is crucial for recognizing double-stranded DNA (dsDNA) (122, 132). Upon dsDNA recognition, AIM2 initiates the assembly of ASC, leading to the proteolytic activation of pro-caspase-1. This activation is essential for the AIM2 inflammasome complex, with significant implications for regulating inflammatory responses (133–136). AIM2's sensitivity to dsDNA is highly dependent on the length and sequence of DNA, with the optimal response occurring between 80 and 200 base pairs (137).

In addition to tissue damage caused by various infections, radiation, systemic lupus erythematosus, and rheumatoid arthritis (138–140), AIM2 also plays an important role in the progression of myositis (141). Loell et al. demonstrated through transcriptome microarray technology and immunoblotting that immunosuppressive therapy can downregulate the expression of AIM2 and caspase-1 in skeletal muscle samples from patients with DM and PM, suggesting that this may be a potential therapeutic strategy to reduce inflammation in IIM patients. The balance between the anti-inflammatory effects and the negative impact on muscle remodeling must be considered (141).

Interactions of AIM2 inflammasome with other pathways

cGAS-STING pathway

The activity of AIM2 is regulated by its interaction with other innate immune sensors and cellular homeostasis. It interacts with the cGAS-STING pathway, which triggers type I interferon responses in response to cytoplasmic dsDNA. While the cGAS-STING signaling pathway can promote the initial activation of AIM2 inflammasomes, the AIM2 inflammasomes can also inhibit the cGAS-STING signaling pathway through the disruption of intracellular potassium levels caused by caspase-1-mediated cleavage of cGAS and GSDMD pore formation (142). Baatarjav et al. found that AIM2 deficiency leads to macrophage accumulation and impaired renal function recovery, and further

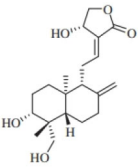
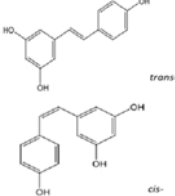
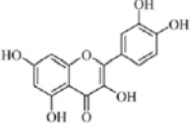
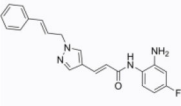
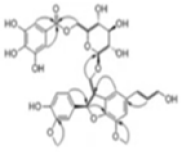
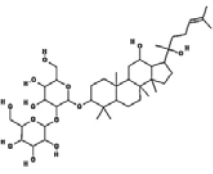
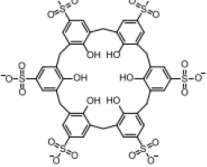
studies revealed that AIM2 deficiency exacerbates inflammation through the STING-TBK1-IRF3/NF- κ B signaling pathway, even in the absence of IL-1 β mobilization (143).

AIM2 interaction with NLRP3

Multiple reports indicate that these two inflammasomes are essential in many inflammatory responses, including bacterial infections, malaria parasite infections, and STING agonist stimulation (144–146). AIM2 is also involved in a

form of mixed cell death pathway called PANoptosis, which simultaneously activates pyroptosis, programmed cell death, and necrotic cell death, where AIM2 has been reported to form a complex with pyrin and ZBP1 to execute this form of inflammatory cell death (147). Furthermore, changes in cellular metabolism also affect AIM2 responses. For example, excess cholesterol can trigger the release of mitochondrial DNA (mtDNA) and the activation of AIM2 (148). There are reports indicating that upregulation of the glycolytic enzyme pyruvate kinase M2 subtype in macrophages initiates the response of AIM2 and NLRP3 inflammasomes (149).

TABLE 3 Structure, target, and mechanism of potential inhibitors of AIM2 inflammasome.

Agent	Structure	Target(s)	Potential mechanism	References
andrographolide		AIM2 inflammasome activation	preventing AIM2 translocation to the nucleus	(144, 150)
EFLA 945 (resveratrol)		AIM2 inflammasome	restrict the AIM2 inflammasome activation through preventing DNA entry	(151)
Quercetin		NLRP3 inflammasomes, AIM2 inflammasomes direct inhibitor	Phosphorylate ASC and inhibit pro-caspase-1 recruitment	(152, 153)
RGFP966		AIM2 inflammasomes	selectively inhibit histone deacetylase 3, modulates the acetylation and phosphorylation of STAT1 to suppress AIM2,	(154)
Cornus officinalis Seed Extract		AIM2 inflammasomes	inhibited the cleavage of caspase-1, the translocation and speck formation of ASC,inhibit AIM2 speck formation	(155)
Ginsenoside		NLRP3 inflammasome AIM2 inflammasome (predominant)	Attenuate IL-1 β secretion as well as pathogen clearance ,inhibit AIM2 inflammasome activation.	(156)
4-sulfonic Calixarenes		cGAS,TLR9, AIM2 inflammasomes (direct inhibitor)	Bind completelyto the DNA binding inflammasomes site through exposed sulfonic acid group to suppress AIM2 inflammasomes formation	(157)

AIM2 inhibitors

In the process of searching for AIM2 inflammasome inhibitors, various natural products have shown potential (Table 3). The diterpene lactone andrographolide from *Andrographis paniculata* has been suggested to inhibit the activation of the AIM2 inflammasome by preventing AIM2 translocation to the nucleus (158), significantly improving radiation-induced lung injury and alleviating the progression of radiation pneumonitis and lung fibrosis (141). Extracts from *Cornus officinalis* and *Panax ginseng*, known as ginsenosides, have been shown to inhibit the secretion of IL-1 β and IL-18 induced by AIM2 inflammasome activation, as well as the aggregation of ASC and cleavage of Gasdermin D (159, 160). EFLA945 is a water-soluble extract from *Vitis amurensis* leaves containing resveratrol and paeoniflorin 3-O-glucoside, which may inhibit AIM2-dependent IL-1 β secretion associated with the pathogenesis of psoriasis (150). Quercetin, a flavonoid with anti-inflammatory properties, has been shown to downregulate the expression of AIM2 and pro-caspase-1 in keratinocytes stimulated by IFN- γ and poly(dA:dT), thereby inhibiting the JAK2/STAT1 pathway and reducing inflammation caused by inflammatory skin diseases (155, 156).

A group of compounds also showed inhibitory effects on the AIM2 inflammasome, demonstrating their therapeutic potential (Table 3). RGFP966 is a selective inhibitor of histone deacetylase 3 that inhibits AIM2 by regulating the acetylation and phosphorylation of STAT1, thereby alleviating ischemic brain injury (151). 4-sulfonated macrocyclic compounds bind to the

DNA-binding inflammasome site, inhibiting the formation of the AIM2 inflammasome through exposed sulfonate groups (152). Synthetic oligonucleotides, super ODNs containing the TTAGGG sequence, can compete with dsDNA to bind to the HIN200 domain of AIM2, thereby inhibiting the activation of the AIM2 inflammasome (153). POP3 can directly bind to the PYD domain of AIM2, prevent interaction with ASC, and inhibit the secretion of IL-1 β (154).

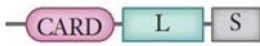
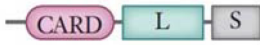

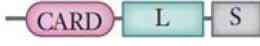


Inhibitors targeting AIM2 have shown great potential in treating autoimmune diseases. Future research is expected to explore the role of AIM2 in the pathogenesis of IIMs, and the mechanism of action, efficacy, and safety of AIM2 inhibitors.

Caspases

Caspases are a family of endopeptidases that specifically cleave their substrates at aspartic or glutamic acid residues, playing a pivotal role in the regulation of cellular processes (157). In mammalian cells, this family encompasses at least 14 distinct members (161–163). They are broadly classified into two functional groups: apoptotic caspases and inflammatory caspases, as detailed in Table 4.

Apoptotic caspases are instrumental in initiating and executing apoptosis, a tightly regulated process that typically does not trigger an immune response (164). These caspases can be further divided into initiator and effector caspases based on their roles in the apoptotic pathway (164–166). Initiator caspases, such as caspase-

TABLE 4 Classification, Structure and Function of Caspases (164–166).

Classification		Caspase	Structure	Function
inflammatory caspase	initiator caspase	caspase-1		It can cleave a variety of substrates, including pro-IL-1 β , pro-IL-18, and GSDMD.
		caspase-4h/5h/11m		They can cleave GSDMD into N-GSDMD, but can not cleave pro-IL-1 β /pro-IL-18. Nevertheless, they can facilitate the maturation and secretion of IL-1 β /IL-18 through the NLRP3/caspase-1 pathway.
		caspase-12		undefined.
		caspase-13(bovine)		unknown
Apoptotic Caspase	initiator caspase	caspase-2		Its function is described to be cell-cycle related.
		caspase-8\10		To initiate apoptosis via activating the executioner caspases-3, -6, and -7.
		caspase-9		
	effector caspases	caspase-3		They are responsible for the characteristic morphological changes of apoptosis.
		caspase-6\7		
undefined		caspase-14		It is linked to cell differentiation.

m, murine and h, human.

2, -8, -9, and -10, act as proteolytic signal amplifiers, responsible for activating the downstream effector caspases. Effector caspases, including caspase-3, -6, and -7, are tasked with cleaving a variety of cellular proteins at specific sites, thereby facilitating the progression of apoptosis.

In contrast, inflammatory caspases, which include caspase-1, -4, -5, and -11. Research has indicated that Caspase-1 plays a critical role in orchestrating the canonical pyroptotic cascade, while Caspase-4 and -5 in humans, along with Caspase-11 in murine models, govern the noncanonical pyroptotic pathway (163, 165). The roles of caspase-12, -13, and -14 are less defined and are subjects of ongoing research (161, 163). Interestingly, Caspase-3 is primarily associated with apoptosis, but recent studies have suggested that influenced by TNF or various chemotherapeutic agents, GSDME may induce a transition from apoptotic to pyroptotic cellular death through Caspase-3 modulation (29).

Caspase-1 in IIM

In IIM, the caspase-1-mediated canonical pathway has been identified as a crucial element in the pathogenesis. Caspase-1 is a key enzyme responsible for protein hydrolysis in the pyroptosis pathway. In the cytoplasm, pro-caspase-1 exists initially in an inactive state. Upon stimulation by various factors, it is activated from its inactive pro-form pro-caspase-1 to an active state by the inflammasome complex, leading to its self-cleavage into p20 and p10 subunits, forming an active p20/p10 heterodimeric enzyme. Activated caspase-1 converts pro-interleukins, such as pro-IL-1 β and pro-IL-18, into their active forms IL-1 β and IL-18, enhancing the inflammatory response, cleaving GSDM D into N-terminal and C-terminal fragments, thus leading to pyroptosis (166). This activation is crucial for regulating cell death and inflammatory responses, emphasizing its role in IIM (167).

In DM/PM patients, studies have shown that caspase-1 is mainly located in the muscle fiber sarcolemma and is associated with sites of tissue regeneration (167). The distribution of active

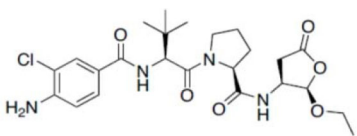
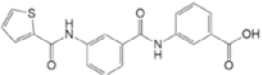
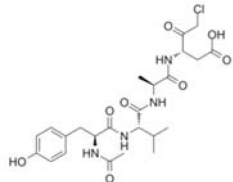
caspase-1 is similar to IL-1 β , with increased levels of caspase-1 mRNA and caspase-1 p20 protein (64, 82). Experimental autoimmune myositis (EAM) mouse models also show a significant increase in the expression of caspase-1 mRNA and proteins, including pro-caspase-1 and its cleaved form caspase-1 p20, compared to control groups (64). These findings suggest that caspase-1 is involved in the activation of proIL-1 β and plays a role in cell proliferation.

Death cells may serve as a repository of self-antigens, triggering systemic autoimmunity in susceptible individuals. Anti-PM/Scl autoantibodies are common in patients with overlap myositis and scleroderma, targeting the exosome subunit PM/Scl-75. Schilders demonstrated that cleavage of PM/Scl-75 was inhibited by caspase inhibitors, with caspase-1 being the most effective, followed by caspase-8, while inhibition by caspase-3 and -7 was weaker (168). Cleavage occurs at Asp369 at the C-terminal, with the N-terminal fragment still attached to the exosome (168). Follicular T helper (TFH) cells participate in B cell differentiation and autoantibody production. In anti-MDA5 positive IIM patients, there is a significant increase in active caspase-1 on TFH cells, suggesting a role for caspase-1 on TFH cells in the pathogenesis of anti-MDA5 positive IIM and potentially serving as a disease biomarker for this patient subgroup (169).

Caspase-1 inhibitors

Comprehensive research has highlighted the key role of caspase-1 in the pathophysiology of IIM (64, 66, 82, 108, 141, 167–169), indicating its potential as a biomarker of disease activity and therapeutic target (Table 5). The discovery of small PYD or CARD-only proteins (POPs and COPs) has introduced new regulatory mechanisms. Devi S et al. demonstrated that COPs can regulate the activation of inflammasomes by altering CARD-CARD interactions, thereby reducing the activation of NLRP3 inflammasomes and disease progression (173). Zhou Y et al. showed the therapeutic potential of extracellular vesicles containing

TABLE 5 Structure, target, and mechanism of potential inhibitors of caspase-1.

Agent	Structure	Target	Potential mechanism	References
VX-765		Caspase-1	Suppresses interleukin-1 β levels and inhibits Th17 responses and germinal center reactions.	(170)
CZL80		Caspase-1	It is a structure-matching compound with a strong affinity to the active sites of caspase-1.	(171)
AC-YVAD-CMK		selective caspase-1 inhibitor	decrease the expression of NLRP1 inflammasome, and relieve the release of IL-1 β and IL-18 induced by NLRP1 inflammasome.	(172)

a caspase-1 inhibitor (EVs-VX-765) derived from dendritic cells, which significantly suppressed levels of interleukin-1 β and inhibited Th17 responses and follicular reactions. This approach holds promise in the treatment of myasthenia gravis and other autoimmune diseases, including IIM (174). CZL80 is a compound with a strong affinity for the active site of caspase-1 (175). AC-YVAD-CMK is a selective caspase-1 inhibitor that reduces the expression of NLRP1 inflammasomes and alleviates the release of IL-1 β and IL-18 induced by NLRP1 inflammasomes (176) (Table 6).

Human caspase-4, -5, or mouse caspase-11 in IIM

Human caspase-4 and -5, as well as their murine homolog caspase-11, are critical cysteine proteases in immune responses, particularly in inflammasome complexes activation (170–172, 181). These enzymes are crucial for sensing cytoplasmic lipopolysaccharide (LPS) from Gram-negative bacteria, which is a major trigger of inflammation. Caspase-4/5/11 is activated by binding to LPS through its caspase recruitment domain (CARD), leading to its aggregation and self-cleavage, forming noncanonical inflammasomes. This process operates without additional adapter proteins or cofactors, making caspase-4/5/11 sensors and effectors in immune responses (23). Once activated, these caspases initiate proteolytic processing of the ubiquitin-1 transmembrane channel, promoting ATP release and subsequent activation of the P2X7 receptor channel. They also cleave GSDMD to form membrane pores, triggering pyroptosis, a programmed cell death that facilitates the release of inflammatory cytokines such as interleukin-1 β (IL-1 β) and IL-18, crucial for

defending against bacterial infections. Notably, caspase-4/5/11 does not process pro-IL-1 β into its mature form (22, 182); instead, it induces cell death through GSDMD cleavage, and the release of IL-1 β depends on subsequent caspase-1 activation (183, 184). Elevated caspase-4, caspase-5, GSDMD, NLRP3, ubiquitin-1, and purinergic receptor P2X7 were observed in the muscles of DM and PM patients. The positive correlation between muscular tissue pathology scores and these protein markers suggests a direct link between muscle pathology and their expression (185). In mice, the activation of caspase-11 is driven by type I interferons (IFNs), and its activation is weakened in the absence of type I IFN signaling during bacterial infection (186–188). This response is crucial for caspase-11 to interact with its ligands, as IFN-induced GTPases disrupt pathogen-containing vacuoles, allowing caspase-11 to detect cytosolic LPS (120). Human guanylate-binding protein-1 (hGBP1) assists caspase-4 in detecting LPS through a “detergent-like” mechanism, exposing lipid A in the outer membrane of Gram-negative bacteria (189–191). Another pathway for cytosolic LPS entry involves host proteins, with HMGB1-bound LPS mediating caspase-11 activation (189). Caspase-11 promotes potassium efflux through GSDMD cleavage and pore formation, leading to the activation of NLRP3 and the release of IL-1 β . Apart from detecting LPS, noncanonical caspases also possess pattern recognition receptor (PRR) activity; for instance, caspase-11 can bind oxidized phospholipids (oxPAPC) derived from dying cells as damage-associated molecular patterns (DAMPs) to trigger IL-1 β release and pyroptosis (192). However, other studies have shown that oxPAPC binds caspase-4 and caspase-11 to inhibit the

TABLE 6 Characteristics of gasdermin family members (177–180).

Protein	Chromosome	Normal human tissue expression	Activation mechanism	Biological function
sGSDMA	17q21.1 (H), 11D (M)	Gut epithelium, skin, mammary gland, and kidney	Streptococcus pyogenes (SpeB virulence factor)	It is associated with mitochondrial homeostasis. Gasdermin A gene mutation can cause alopecia, asthma, local cutaneous sclerosis, and inflammatory bowel disease.
GSDMB	17q21 (H)	Esophagus and gastrointestinal epithelium, respiratory system, liver, colon, and lymphocytes	Caspase 1; granzyme A; caspase-3, -6 and -7 <i>in vitro</i>	It is associated with pyroptosis and anti-tumor immunity. Gasdermin B mutation can cause breast cancer and asthma
GSDMC	8q24.21 (H), 15D1 (M)	Stomach, small intestine, cecum and colon epithelium, airway epithelium, skin, spleen, vagina, and bladder	Caspase 8	GSDMC/caspase-8 mediates a non-canonical pyroptosis pathway in cancer cells, causing tumor necrosis.
GSDMD	8q24.3 (H), 15D3 (M)	Immune cells, liver, gut epithelium, kidney	Caspases 1, 4 and 5 (h); caspases 1 and 11 (m); caspase 8; cathepsin G; neutrophil elastase	It is associated with pyroptosis which is crucial for maintaining immune homeostasis, host defense against infections and various inflammation, such T2DM, cryopyrin-associated periodic syndromes, sepsis and autoinflammatory (25, 41–43).
GSDME (DFNA5)	7p15.3 (H), 6B2.3 (M)	Placenta, heart, brain and kidney	Caspases 3, 7, and 8; granzyme B	It is associated with hearing impairment, cancer, and autoimmune disease.
PJVK (DFNB59)	2q31.2 (H), 2C3 (M)	Auditory system, including neurons, hair cells, supporting cells, and spiral ganglion cells in the inner ear	Unknown	It is associated with hearing impairment in humans and mice.

m, murine and h, human.

activation of noncanonical inflammasomes (193). These conflicting results may stem from differences in specific oxPAPC moieties, which require further investigation (194).

Understanding the roles of caspase-4, caspase-5, and caspase-11 in myositis and other inflammatory conditions is crucial for the development of targeted therapies. Modulating their activities may help reduce inflammation and muscle damage, or enhance pathogen clearance, providing potential therapeutic options for inflammatory muscle diseases.

Gasdermins

Gasdermin (GSDM) is the executor of pyroptosis. GSDM was initially discovered in the gastrointestinal tract and skin, hence the name (“gas-dermin”). GSDMs are a functionally diverse family of proteins, including GSDMA, GSDMB, GSDMC, GSDMD, GSDME (or DFNA5), and PJVK (DFNB59), which are expressed in multiple cell types and tissues (195) (Table 5). GSDM is the core of pyroptotic execution, mediating the formation of membrane pores and leading to cell lysis (196). Except for PJVK (DFNB59), whose function remains unclear, these proteins all contain an N-terminal domain with the intrinsic ability to form necrotic pores and a C-terminal domain that regulates cell death inhibition through interactions within the molecule (23, 177, 197). Protein proteolytic cleavage occurs at the junction between the N-terminal and C-terminal domains of GSDM, releasing the C-terminal domain, thereby promoting translocation of the N-terminal domain of GSDM to

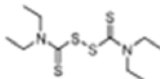
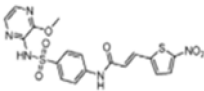
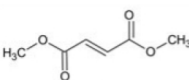
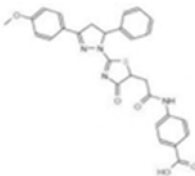
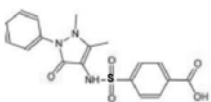
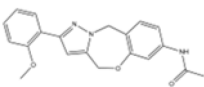
the cell membrane, where it aggregates to form pores (23, 177, 197). The N-terminal fragments of GSDMs have a high affinity for phosphatidylinositol phosphates located in the inner leaflet of the plasma membrane and a lower affinity for phosphatidylserine (178). Additionally, GSDMs can also target cardiolipin primarily found in mitochondrial and bacterial membranes (196).

GSDMD and GSDME in IIM

GSDMD is the most extensively studied member of the GSDM family, located in the 8q24 region of chromosome 8. This protein is widely distributed in various tissues and immune cells. Both human and mouse GSDMD consist of a 31kDa NT pore-forming domain and a 22kDa CT inhibitory domain, connected by a domain containing a cleavage site. This connector is cleaved by Canonical caspase-1 or non-Canonical caspase-4/5/11 upon activation of various inflammasomes, leading to the separation of GSDMD-NT and GSDMD-CT. GSDMD-NT is inserted into membranes and polymerizes to form pores, releasing cytokines (179, 180, 198). GSDMD, as a key executor of pyroptosis, plays a crucial role in the development and progression of various inflammatory diseases, autoimmune diseases, and many other systemic diseases (199).

Recent studies have found that the expression levels of Caspase-4, Caspase-5, Caspase-11, and GSDMD proteins in the skeletal muscle tissue of the EAM group were higher than those in the control group. Additionally, the mRNA expression levels of Caspase-11 and GSDMD in the EAM group were higher than

TABLE 7 Structure and mechanism of potential inhibitors of GSDMD inflammasome.

Agent	Structure	Potential mechanism	References
Disulfiram (DSF)		Modifying Cys191 of GSDMD and inhibiting the oligomerization of GSDMD-NT	(204)
Necrosulfonamide (NSA)		Binding directly to Cys191 of GSDMD and inhibiting the oligomerization of GSDMD-NT	(205)
Dimethyl fumarate (DMF)		Succinating Cys191 of GSDMD, blocking caspase-GSDMD interactions and inhibiting the oligomerization of GSDMD-NT	(206)
C202-2729		Binding directly to GSDMD-NT and inhibiting the oligomerization of GSDMD-NT	(207)
GI-Y1		Target Arg7 residue of GSDMD-N, inhibit GSDMD-mediated lipid-binding, pore formation and mitochondrial binding	(208)
LDC7559		Inhibit the cleavage of GSDMD in neutrophil cell death pathway (NETosis)	(209)

those in the control group. Furthermore, the levels of serum IL-18 and IL-1 β detected in mice in the EAM group were higher than those in the control group, suggesting that the non-Canonical mediated activation of the GSDMD inflammatory necrosis pathway may be related to the pathogenesis of IIM (67).

Interstitial lung involvement is a prominent feature of IIM-ILD, and endothelial injury may play a key role in the leakage. In the experimental autoimmune myositis (EAM) model in mice, the expression of downstream joint protein ASC, activated Caspase-1 fragment, pyroptosis protein GSDMD, and the related inflammation factor IL-1 β significantly increased in pulmonary microvascular endothelial cells (PMECs), and this was also observed after *in vitro* stimulation with NETs, suggesting that NETs-induced pyroptosis occurs through the canonical pyroptosis pathway (110).

GSDME, historically known as DFNA5, is associated with hereditary hearing loss (198). It is activated by cleavage of Caspase-3, promoting the transition from apoptotic pathway to pyroptosis. The activation of GSDME is related to the mitochondrial apoptotic pathway, and when cells with high GSDME expression undergo chemotherapy, apoptosis may transition to pyroptosis (29, 200). Liu et al. found GSDME and Caspase-3 in the muscle tissue immunohistochemical staining of DM patients, providing preliminary evidence for the association between GSDME-dependent pyroptosis and muscle bundle atrophy (201).

GSDMD inhibitors

Given that GSDMD is a crucial protein in executing pyroptosis and is associated with inflammation signaling, activation of various inflammatory bodies, and the release of downstream inflammatory cytokines, inhibiting its activation is thought to be an effective approach to managing related inflammatory conditions. In recent years, several small synthetic molecular inhibitors have been found to inhibit GSDMD-mediated pyroptosis through different mechanisms (202, 203) (Table 7).

Disulfiram (DSF), a drug for treating alcohol addiction, covalently modifies human/mouse Cys191/Cys192 in GSDMD and inhibits the oligomerization of GSDMD-NT (204). Necrosulfonamide (NSA) is a small molecule that directly binds to Cys191 of GSDMD, preventing the aggregation of GSDMD-NT, especially blocking MLKL, to inhibit plasma membrane rupture and reduce cell death (205). Dimethyl fumarate (DMF) is known for its anti-inflammatory and immune-modulating properties, and studies have found its effectiveness in treating diseases such as multiple sclerosis (MS) and psoriasis. Although the exact mechanism is unclear, research has shown that DMF modifies Cys191 of GSDMD and inhibits the polymerization of GSDMD-NT (206). Furthermore, DMF is marketed under the brand name Tecfidera for psoriasis management. NSA exhibits significant therapeutic benefits in various diseases. C202-2729 is a small molecule known for its strong anti-inflammatory effects. Its efficacy has been demonstrated in mouse models of endotoxin shock and experimental autoimmune encephalomyelitis (EAE), indicating its potential in treating inflammatory diseases (207). The mechanism of action of C202-2729 involves the direct binding of the N-terminus of GSDMD

to inhibit GSDMD activation, thereby preventing the translocation of the N-terminal GSDMD fragment to the cell membrane, inhibiting pore formation, and the release of mature IL-1 β , which is a key pro-inflammatory cytokine (207). In 2023, a new GSDMD inhibitor, GI-Y1, was discovered through virtual and pharmacological screening. GI-Y1 inhibits GSDMD-mediated lipid binding, pore formation, and mitochondrial binding by targeting the Arg7 residue of GSDMD-N in cardiac muscle cells, suggesting its potential cardioprotective effects against myocardial ischemia/reperfusion injury (208). LDC7559 is an inhibitor of neutrophil extracellular traps, which binds to GSDMD and inhibits NETosis. Mechanistically, LDC7559 can neutralize the toxicity of GSDMD-N in humans and mice, showing a direct inhibitory effect on GSDMD activity (209).

In conclusion, these findings underscore the key roles of GSDMD and GSDME in the pathogenesis of pyroptosis, closely associated with the occurrence and progression of DM and PM. Inhibitors of GSDMD may present novel therapeutic opportunities for the management of IIM. The potential to modulate GSDMD proteins offers a hopeful avenue for the development of treatment strategies aimed at alleviating the burden of IIM by interrupting the pyroptosis cascade reaction.

Conclusion and prospects

The pathogenesis of IIM is complex, involving the interplay of immune dysregulation, inflammation, and cellular stress. Pyroptosis has emerged as a key pathological process in IIM, with NLRP3 and AIM2 inflammasomes, caspases, and gasdermin proteins playing central roles, which may offer new therapeutic strategies for IIM. Future directions in IIM research should include detailed explorations into the molecular mechanisms underlying pyroptosis, the development of targeted therapies towards the pyroptotic pathway, and evaluation of the efficacy and safety of these interventions in clinical trials. Understanding the interactions between inflammasome-mediated pyroptosis and other pathways, such as NETs, autophagy, and endoplasmic reticulum stress, may reveal additional therapeutic targets. The potential of immune metabolic pathways in regulating pyroptosis also warrants exploration. Ultimately, a deeper understanding of inflammasomes in IIM may lead to more effective treatment approaches and improved patient outcomes.

Author contributions

RS: Funding acquisition, Writing – original draft, Conceptualization. JC: Writing – original draft. PL: Supervision, Writing – review & editing, Conceptualization, Visualization.

Funding

The author(s) declare financial support was received for the research, authorship, and/or publication of this article. This study was supported by Natural Science Foundation of Liaoning Province

(2019-MS-350); General Hospital of Northern Theater Command Applied Basic Project (2021-HL-059).

Conflict of interest

The authors declare that the research was conducted in the absence of any commercial or financial relationships that could be construed as a potential conflict of interest.

References

1. Tan JA, Roberts-Thomson PJ, Blumbergs P, Hakendorf P, Cox SR, Limaye V. Incidence and prevalence of idiopathic inflammatory myopathies in South Australia: a 30-year epidemiologic study of histology-proven cases. *Int J Rheum Dis.* (2013) 16:331–38. doi: 10.1111/j.1756-185X.2011.01669.x
2. Dobloug C, Garen T, Bitter H, Stjärne J, Stenseth G, Grøve L, et al. Prevalence and clinical characteristics of adult polymyositis and dermatomyositis; data from a large and unselected Norwegian cohort. *Ann Rheum.* (2015) 74:1551–56. doi: 10.1136/annrheumdis-2013-205127
3. Lundberg IE, de Visser M, Werth VP. Classification of myositis. *Nat Rev Rheumatol.* (2018) 14:269–78. doi: 10.1038/nrrheum.2018.41
4. McHugh NJ, Tansley SL. Autoantibodies in myositis. *Nat Rev Rheumatol.* (2018) 14:290–302. doi: 10.1038/nrrheum.2018.56
5. Pestronk A, Choksi R. Pathology features of immune and inflammatory myopathies, including a polymyositis pattern, relate strongly to serum autoantibodies. *J Neuropathol Exp Neurol.* (2021) 80:812–20. doi: 10.1093/jnen/nlab071
6. Shi J, Tang M, Zhou S, Xu D, Zhao J, Wu C, et al. Programmed cell death pathways in the pathogenesis of idiopathic inflammatory myopathies. *Front Immunol.* (2021) 12:783616. doi: 10.3389/fimmu.2021.783616
7. Hornung T, Wenzel J. Innate immune-response mechanisms in dermatomyositis: an update on pathogenesis, diagnosis and treatment. *Drugs.* (2014) 74:981–98. doi: 10.1007/s40265-014-0240-6
8. Taabazuing CY, Okondo MC, Bachovchin DA. Pyroptosis and apoptosis pathways engage in bidirectional crosstalk in monocytes and macrophages. *Cell Chem Biol.* (2017) 24:507–14.e4. doi: 10.1016/j.chembiol.2017.03.009
9. Jia C, Zhang J, Chen H, Zhuge Y, Chen H, Qian F, et al. Endothelial cell pyroptosis plays an important role in Kawasaki disease via HMGB1/RAGE/cathepsin B signaling pathway and NLRP3 inflammasome activation. *Cell Death Dis.* (2019) 10:778. doi: 10.1038/s41419-019-2021-3
10. Shi H, Gao Y, Dong Z, Yang J, Gao R, Li X, et al. GSDMD-mediated cardiomyocyte pyroptosis promotes myocardial I/R injury. *Circ Res.* (2021) 129:383–96. doi: 10.1161/CIRCRESAHA.120.318629
11. Man SM, Karki R, Kanneganti TD. Molecular mechanisms and functions of pyroptosis, inflammatory caspases, and inflammasomes in infectious diseases. *Immunol Rev.* (2017) 277:61–75. doi: 10.1111/imr.12534
12. Evavold CL, Ruan J, Tan Y, Xia S, Wu H, Kagan JC. The pore-forming protein gasdermin D regulates interleukin-1 secretion from living macrophages. *Immunity.* (2018) 48:35–44.e6. doi: 10.1016/j.immuni.2017.11.013
13. Vanden Berghe T, Linkermann A, Joann-Lanhouet S, Walczak H, Vandenabeele P. Regulated necrosis: the expanding network of non-apoptotic cell death pathways. *Nat Rev Mol Cell Biol.* (2014) 15:135–47. doi: 10.1038/nrm3737
14. Tang D, Kang R, Berghe TV, Vandenabeele P, Kroemer G. The molecular machinery of regulated cell death. *Cell Res.* (2019) 29:347–64. doi: 10.1038/s41422-019-0164-5
15. Friedlander AM. Macrophages are sensitive to anthrax lethal toxin through an acid-dependent process. *J Biol Chem.* (1986) 261:7123–6. doi: 10.1016/S0021-9258(17)38364-3
16. Cerretti DP, Kozlosky CJ, Mosley B, Nelson N, Van Ness K, Greenstreet TA, et al. Molecular cloning of the interleukin-1 beta converting enzyme. *Science.* (1992) 256:97–100. doi: 10.1126/science.1373520
17. Thornberry NA, Bull HG, Calaycay JR, Chapman KT, Howard AD, Kostura MJ, et al. A novel heterodimeric cysteine protease is required for interleukin-1 beta processing in monocytes. *Nature.* (1992) 356:768–74. doi: 10.1038/356768a0
18. Zychlinsky A, Prevost MC, Sansonetti PJ. Shigella flexneri induces apoptosis in infected macrophages. *Nature.* (1992) 358:167–9. doi: 10.1038/358167a0
19. Chen Y, Smith MR, Thirumalai K, Zychlinsky A. A bacterial invasin induces macrophage apoptosis by binding directly to ICE. *EMBO J.* (1996) 15:3853–60. doi: 10.1002/j.1460-2075.1996.tb00759.x
20. Cookson BT, Brennan MA. Pro-inflammatory programmed cell death. *Trends Microbiol.* (2001) 9:113–14. doi: 10.1016/s0966-842x(00)01936-3
21. Martinon F, Burns K, Tschopp J. The inflammasome: a molecular platform triggering activation of inflammatory caspases and processing of proIL-beta. *Mol Cell.* (2002) 10:417–26. doi: 10.1016/s1097-2765(02)00599-3
22. Kayagaki N, Warming S, Lamkanfi M, Vande Walle L, Louie S, Dong J, et al. Non-canonical inflammasome activation targets caspase-11. *Nature.* (2011) 479:117–21. doi: 10.1038/nature10558
23. Shi J, Zhao Y, Wang Y, Gao W, Ding J, Li P, et al. Inflammatory caspases are innate immune receptors for intracellular LPS. *Nature.* (2014) 514:187–92. doi: 10.1038/nature13683
24. Shi J, Zhao Y, Wang K, Shi X, Wang Y, Huang H, et al. Cleavage of GSDMD by inflammatory caspases determines pyroptotic cell death. *Nature.* (2015) 526:660e5. doi: 10.1038/nature15514
25. Broz P, Pelegrin P, Shao F. The gasdermins, a protein family executing cell death and inflammation. *Nat Rev Immunol.* (2020) 20:143–57. doi: 10.1038/s41577-019-0228-2
26. Shi J, Gao W, Shao F. Pyroptosis: gasdermin-mediated programmed necrotic cell death. *Trends Biochem Sci.* (2017) 42:245–54. doi: 10.1016/j.tibs.2016.10.004
27. Liu Z, Wang C, Lin C. Pyroptosis as a double-edged sword: The pathogenic and therapeutic roles in inflammatory diseases and cancers. *Life Sci.* (2023) 318:121498. doi: 10.1016/j.lfs.2023.121498
28. Evavold C, Kagan J. How inflammasomes inform adaptive immunity. *J Mol Biol.* (2018) 430:217–37. doi: 10.1016/j.jmb.2017.09.019
29. Wang Y, Gao W, Shi X, Ding J, Liu W, He H, et al. Chemotherapy drugs induce pyroptosis through caspase-3 cleavage of a gasdermin. *Nature.* (2017) 547:99–103. doi: 10.1038/nature22393
30. Sarhan J, Liu BC, Muendlein HI, Li P, Nilson R, Tang AY, et al. Caspase-8 induces cleavage of gasdermin D to elicit pyroptosis during yersinia infection. *Proc Natl Acad Sci USA.* (2018) 115:E10888–97. doi: 10.1073/pnas.1809548115
31. Orning P, Weng D, Starheim K, Ratner D, Best Z, Lee B, et al. Pathogen blockade of TAK1 triggers caspase-8-dependent cleavage of gasdermin D and cell death. *Science.* (2018) 362:1064–9. doi: 10.1126/science.aau2818
32. Zhou Z, He H, Wang K, Shi X, Wang Y, Su Y, et al. Granzyme A from cytotoxic lymphocytes cleaves GSDMB to trigger pyroptosis in target cells. *Science.* (2020) 368: eaaz7548. doi: 10.1126/science.aaz7548
33. Zhang Z, Zhang Y, Xia S, Kong Q, Li S, Liu X, et al. Gasdermin E suppresses tumour growth by activating anti-tumour immunity. *Nature.* (2020) 579:415–20. doi: 10.1038/s41586-020-2071-9
34. Fu J, Wu H. Structural mechanisms of NLRP3 inflammasome assembly and activation. *Annu Rev Immunol.* (2023) 41:301–16. doi: 10.1146/annurev-immunol-081022-021207
35. Dick MS, Sborgi L, Rühl S, Hiller S, Broz P. ASC filament formation serves as a signal amplification mechanism for inflammasomes. *Nat Commun.* (2016) 7:11929. doi: 10.1038/ncomms11929
36. Sharma BR, Kanneganti TD. NLRP3 inflammasome in cancer and metabolic diseases. *Nat Immunol.* (2021) 22:550–9. doi: 10.1038/s41590-021-00886-5
37. Liu YR, Wang JQ, Li J. Role of NLRP3 in the pathogenesis and treatment of gout arthritis. *Front Immunol.* (2023) 14:1137822. doi: 10.3389/fimmu.2023.1137822
38. Heneka MT, Kummer MP, Stutz A, Delekate A, Schwartz S, Vieira-Saecker A, et al. NLRP3 is activated in Alzheimer's disease and contributes to pathology in APP/PS1 mice. *Nature.* (2013) 493:674–8. doi: 10.1038/nature11729
39. Cui Y, Yu H, Bu Z, Wen L, Yan L, Feng J. Focus on the role of the NLRP3 inflammasome in multiple sclerosis: pathogenesis, diagnosis, and therapeutics. *Front Mol Neurosci.* (2022) 15:894298. doi: 10.3389/fnmol.2022.894298
40. Zhen Y, Zhang H. NLRP3 inflammasome and inflammatory bowel disease. *Front Immunol.* (2019) 10:276. doi: 10.3389/fimmu.2019.00276
41. Guo W, Liu W, Jin B, Geng J, Li J, Ding H, et al. Asiatic acid ameliorates dextran sulfate sodium-induced murine experimental colitis via suppressing mitochondria-

Publisher's note

All claims expressed in this article are solely those of the authors and do not necessarily represent those of their affiliated organizations, or those of the publisher, the editors and the reviewers. Any product that may be evaluated in this article, or claim that may be made by its manufacturer, is not guaranteed or endorsed by the publisher.

mediated NLRP3 inflammasome activation. *Int Immunopharmacol.* (2015) 24:232–8. doi: 10.1016/j.intimp.2014.12.009

42. Zheng Y, Xu L, Dong N, Li F. NLRP3 inflammasome: The rising star in cardiovascular diseases. *Front Cardiovasc Med.* (2022) 9:927061. doi: 10.3389/fcvm.2022.927061

43. Yang Q, Yu C, Yang Z, Wei Q, Mu K, Zhang Y, et al. Deregulated NLRP3 and NLRP1 inflammasomes and their correlations with disease activity in systemic lupus erythematosus. *J Rheumatol.* (2014) 41:444–52. doi: 10.3899/jrheum.130310

44. Ehteshami N, Zare Rafie M, Esmaeilzadeh E, Dehany M, Davar S, Mosallaei M, et al. Three functional variants in the NLRP3 gene are associated with susceptibility and clinical characteristics of systemic lupus erythematosus. *Lupus.* (2021) 30:1273–82. doi: 10.1177/09612033211014273

45. Ummerino D. Lupus nephritis: NLRP3 inflammasome ignites podocyte dysfunction. *Nat Rev Rheumatol.* (2017) 13:451. doi: 10.1038/nrrheum.2017.97

46. Yin H, Liu N, Sigdel KR, Duan L. Role of NLRP3 inflammasome in rheumatoid arthritis. *Front Immunol.* (2022) 13:931690. doi: 10.3389/fimmu.2022.931690

47. Tengesdal IW, Dinarello CA, Marchetti C. NLRP3 and cancer: Pathogenesis and therapeutic opportunities. *Pharmacol Ther.* (2023) 251:108545. doi: 10.1016/j.pharmthera.2023.108545

48. Bauernfeind FG, Horvath G, Stutz A, Alnemri ES, MacDonald K, Speert D, et al. Cutting edge: NF-kappaB activating pattern recognition and cytokine receptors license NLRP3 inflammasome activation by regulating NLRP3 expression. *Immunity.* (2009) 13:787–91. doi: 10.1016/j.immunity.0901363

49. Yang J, Liu Z, Xiao TS. Post-translational regulation of inflammasomes. *Cell Mol Immunol.* (2017) 14:65–79. doi: 10.1038/cmi.2016.29

50. Shim DW, Lee KH. Posttranslational regulation of the NLR family pyrin domain-containing 3 inflammasome. *Front Immunol.* (2018) 9:1054. doi: 10.3389/fimmu.2018.01054

51. O'Keefe ME, Dubyak GR, Abbott DW. Post-translational control of NLRP3 inflammasome signaling. *J Biol Chem.* (2024) 300:107386. doi: 10.1016/j.jbc.2024.107386

52. Chui AJ, Okondo MC, Rao SD, Gai K, Griswold AR, Johnson DC, et al. N-terminal degradation activates the NLRP1B inflammasome. *Science.* (2019) 364:82–5. doi: 10.1126/science.aau1208

53. Sandstrom A, Mitchell PS, Goers L, Mu EW, Lesser CF, Vance RE. Functional degradation: A mechanism of NLRP1 inflammasome activation by diverse pathogen enzymes. *Science.* (2019) 364:eau1330. doi: 10.1126/science.aau1330

54. Xu H, Shi J, Gao H, Liu Y, Yang Z, Shao F, et al. The N-end rule ubiquitin ligase UBR2 mediates NLRP1B inflammasome activation by anthrax lethal toxin. *EMBO J.* (2019) 38:e101996. doi: 10.15252/embj.2019101996

55. Hollingsworth LR, Sharif H, Griswold AR, Fontana P, Mintseris J, Dagbay KB, et al. DPP9 sequesters the C terminus of NLRP1 to repress inflammasome activation. *Nature.* (2021) 592:778–83. doi: 10.1038/s41586-021-03350-4

56. Zhong FL, Robinson K, Teo DET, Tan KY, Lim C, Harapas CR, et al. Human DPP9 Represses NLRP1 Inflammasome and Protects against Autoinflammatory Diseases via Both Peptidase Activity and FIIND Domain Binding. *J Biol Chem.* (2018) 293:18864–78. doi: 10.1074/jbc.RA118.004350

57. Huang M, Zhang X, Toh GA, Gong Q, Wang J, Han Z, et al. Structural and biochemical mechanisms of NLRP1 inhibition by DPP9. *Nature.* (2021) 592:773–7. doi: 10.1038/s41586-021-03320-w

58. Martinon F, Pétrilli V, Mayor A, Tardivel A, Tschopp J. Gout-associated uric acid crystals activate the NALP3 inflammasome. *Nature.* (2006) 440:237–41. doi: 10.1038/nature04516

59. Mariathasan S, Weiss DS, Newton K, McBride J, O'Rourke K, Roose-Girma M, et al. Cryopyrin activates the inflammasome in response to toxins and ATP. *Nature.* (2006) 440:228–32. doi: 10.1038/nature04515

60. Muñoz-Planillo R, Kuffa P, Martínez-Colón G, Smith BL, Rajendiran TM, Núñez G. K⁺ Efflux is the common trigger of NLRP3 inflammasome activation by bacterial toxins and particulate matter. *Immunity.* (2013) 38:1142–53. doi: 10.1016/j.immuni.2013.05.016

61. Eigenbrod T, Dalpke AH. Bacterial RNA: an underestimated stimulus for innate immune responses. *J Immunol.* (2015) 195:411–8. doi: 10.4049/jimmunol.1500530

62. Skeldon A, Saleh M. The inflammasomes: molecular effectors of host resistance against bacterial, viral, parasitic, and fungal infections. *Front Microbiol.* (2011) 2:15. doi: 10.3389/fmicb.2011.00015

63. Wang Y, Viollet B, Terkeltaub R, Liu-Bryan R. AMP-activated protein kinase suppresses urate crystal-induced inflammation and transduces colchicine effects in macrophages. *Ann Rheumatol Dis.* (2016) 75:286–94. doi: 10.1136/annrheumdis-2014-206074

64. Yin X, Han GC, Jiang XW, Shi Q, Pu CQ. Increased expression of the NOD-like receptor family, pyrin domain containing 3 inflammasomes in dermatomyositis, and polymyositis is a potential contributor to their pathogenesis. *Chin Med J.* (2016) 129:1047–1052. doi: 10.4103/0366-6999.180528

65. Jha S, Srivastava SY, Brickey WJ, Iocca H, Toews A, Morrison JP, et al. The inflammasome sensor, NLRP3, regulates CNS inflammation and demyelination via caspase-1 and interleukin-18. *J Neurosci.* (2010) 30:15811–20. doi: 10.1523/JNEUROSCI.4088-10.2010

66. Xia P, Shao YQ, Yu CC, Xie Y, Zhou ZJ. NLRP3 inflammasome up-regulates major histocompatibility complex class I expression and promotes inflammatory infiltration in polymyositis. *BMC Immunol.* (2022) 23:39. doi: 10.1186/s12865-022-00515-2

67. Ma M, Chai K, Deng R. Study of the correlation between the noncanonical pathway of pyroptosis and idiopathic inflammatory myopathy. *Int Immunopharmacol.* (2021) 98:107810. doi: 10.1016/j.intimp.2021.107810

68. Ashcroft FM. ATP-sensitive potassium channelopathies: focus on insulin secretion. *J Clin Invest.* (2005) 115:2047–58. doi: 10.1172/JCI25495

69. Haque S, Lan X, Wen H, Lederman R, Chawla A, Attia M, et al. HIV promotes NLRP3 inflammasome complex activation in murine HIV-associated nephropathy. *Am J Pathol.* (2016) 186:347–58. doi: 10.1016/j.ajpath.2015.10.002

70. Marchetti C, Chojnacki J, Toldo S, Mezzaroma E, Tranchida N, Rose SW, et al. A novel pharmacologic inhibitor of the NLRP3 inflammasome limits myocardial injury after ischemia-reperfusion in the mouse. *J Cardiovasc Pharmacol.* (2014) 63:316–22. doi: 10.1097/FJC.0000000000000053

71. Li R, Wang J, Li R, Zhu F, Xu W, Zha G, et al. ATP/P2X7-NLRP3 axis of dendritic cells participates in the regulation of airway inflammation and hyper-responsiveness in asthma by mediating HMGB1 expression and secretion. *Exp Cell Res.* (2018) 366:1–15. doi: 10.1016/j.yexcr.2018.03.002

72. Lamkanfi M, Mueller JL, Vitari AC, Misaghi S, Fedorova A, Deshayes K, et al. Glyburide inhibits the Cryopyrin/Nalp3 inflammasome. *J Cell Biol.* (2009) 187:61–70. doi: 10.1083/jcb.200903124

73. Peng W, Cotrina ML, Han X, Yu H, Bekar L, Blum L, et al. Systemic administration of an antagonist of the ATP-sensitive receptor P2X7 improves recovery after spinal cord injury. *Proc Natl Acad Sci USA.* (2009) 106:12489–93. doi: 10.1073/pnas.0902531106

74. Zhou J, Tian G, Quan Y, Li J, Wang X, Wu W, et al. Inhibition of P2X7 purinergic receptor ameliorates cardiac fibrosis by suppressing NLRP3/IL-1 β Pathway. *Oxid Med Cell Longev.* (2020) 2020:7956274. doi: 10.1155/2020/7956274

75. Mathis D, Shoelson SE. Immunometabolism: an emerging frontier. *Nat Rev Immunol.* (2011) 11:81–3. doi: 10.1038/nri2922

76. O'Neill LA, Kishton RJ, Rathmell J. A guide to immunometabolism for immunologists. *Nat Rev Immunol.* (2016) 16:553–65. doi: 10.1038/nri.2016.70

77. Maher TM. Aerobic glycolysis and the Warburg effect. An unexplored realm in the search for fibrosis therapies? *Am J Respir Crit Care Med.* (2015) 192:1407–9. doi: 10.1164/rccm.201508-1699ED

78. Freyssen D. Energy sensing and regulation of gene expression in skeletal muscle. *J Appl Physiol.* (2007) 102:529–40. doi: 10.1152/japplphysiol.01126.2005

79. Pilon NJ, Krook A. Innate immune receptors in skeletal muscle metabolism. *Exp Cell Res.* (2017) 360:47–54. doi: 10.1016/j.yexcr.2017.02.035

80. DeFronzo RA, Tripathy D. Skeletal muscle insulin resistance is the primary defect in type 2 diabetes. *Diabetes Care.* (2009) 32:S157–63. doi: 10.2337/dc09-S302

81. Pilon NJ, Bilan PJ, Fink LN, Klip A. Cross-talk between skeletal muscle and immune cells: muscle-derived mediators and metabolic implications. *Am J Physiol Endocrinol Metab.* (2013) 304:E453–65. doi: 10.1152/ajpendo.00553.2012

82. Liu D, Xiao Y, Zhou B, Gao S, Li L, Zhao L, et al. PKM2-dependent glycolysis promotes skeletal muscle cell pyroptosis by activating the NLRP3 inflammasome in dermatomyositis/polymyositis. *Rheumatol (Oxford England).* (2021) 60:2177–89. doi: 10.1093/rheumatology/keaa473

83. Seto N, Torres-Ruiz JJ, Carmona-Rivera C, Pinal-Fernandez I, Pak K, Purmalek MM, et al. Neutrophil dysregulation is pathogenic in idiopathic inflammatory myopathies. *JCI Insight.* (2020) 5:e134189. doi: 10.1172/jci.insight.134189

84. Liu L, Wang J, Zhang P, Sun W, Zhu X, Sun X, et al. Promising neutrophil-associated biomarkers in lung diseases of patients with antisynthetase syndrome and dermatomyositis. *J Immunol Res.* (2022) 2022:1886083. doi: 10.1155/2022/1886083

85. Torres-Ruiz J, Carrillo-Vazquez DA, Leal-Alanis A, Zentella-Dehesa A, TapiaRodriguez M, Maravillas-Montero JL, et al. Low-density granulocytes and neutrophil extracellular traps as biomarkers of disease activity in adult inflammatory myopathies. *J Clin Rheumatol.* (2022) 28:e480–7. doi: 10.1097/RHU.0000000000001772

86. Wigerblad G, Kaplan MJ. Neutrophil extracellular traps in systemic autoimmune and autoinflammatory diseases. *Nat Rev Immunol.* (2022) 23:274–88. doi: 10.1038/s41577-022-00787-0

87. Kolaczowska E, Kubes P. Neutrophil recruitment and function in health and inflammation. *Nat Rev Immunol.* (2013) 13:159–75. doi: 10.1038/nri3399

88. Liew PX, Kubes P. The neutrophil's role during health and disease. *Physiol Rev.* (2019) 99:1223–48. doi: 10.1152/physrev.00012.2018

89. Brinkmann V, Reichard U, Goosmann C, Fauler B, Uhlemann Y, Weiss DS, et al. Neutrophil extracellular traps kill bacteria. *Science.* (2004) 303:1532–5. doi: 10.1126/science.1092385

90. Yipp BG, Petri B, Salina D, Jenne CN, Scott BN, Zbytniuk LD, et al. Infection-induced NETosis is a dynamic process involving neutrophil multitasking. *vivo Nat Med.* (2012) 18:1386–93. doi: 10.1038/nm.2847

91. Yipp BG, Kubes P. NETosis: how vital is it? *Blood.* (2013) 122:2784–94. doi: 10.1182/blood-2013-04-457671

92. Manfredi AA, Ramirez GA, Rovere-Querini P, Maugeri N. The neutrophil's choice: phagocytosis vs make neutrophil extracellular traps. *Front Immunol.* (2018) 9:288. doi: 10.3389/fimmu.2018.00288

93. Duvvuri B, Pachman LM, Morgan G, Khojah AM, Klein-Gitelman M, Curran ML, et al. Neutrophil extracellular traps in tissue and periphery in juvenile dermatomyositis. *Arthritis Rheumatol.* (2020) 72:348–58. doi: 10.1002/art.41078
94. Opinc AH, Makowska JS. Antisynthetase syndrome - much more than just a myopathy. *Semin Arthritis Rheumatol.* (2021) 51:72–83. doi: 10.1016/j.semarthrit.2020.09.020
95. Zhang Y, Yan B, Liu Y. Neutrophil extracellular traps-induced endothelial cell damage in the pathogenesis of dermatomyositis-associated interstitial lung disease. *Zhonghua Nei Ke Za Zhi.* (2017) 56:650–4. doi: 10.3760/cma.j.issn.0578-1426.2017.09.006
96. Zhang S, Jia X, Zhang Q, Zhang L, Yang J, Hu C, et al. Neutrophil extracellular traps activate lung fibroblast to induce polymyositis-related interstitial lung diseases via TLR9-miR-7-Smad2 pathway. *J Cell Mol Med.* (2020) 24:1658–69. doi: 10.1111/jcmm.14858
97. Munzer P, Negro R, Fukui S, di Meglio L, Aymonnier K, Chu L, et al. NLRP3 inflammasome assembly in neutrophils is supported by PAD4 and promotes NETosis under sterile conditions. *Front Immunol.* (2021) 12:683803. doi: 10.3389/fimmu.2021.683803
98. Bai L, Zhu J, Ma W, Li F, Zhao P, Zhang S. Neutrophil extracellular traps are involved in the occurrence of interstitial lung disease in a murine experimental autoimmune myositis model. *Clin Exp Immunol.* (2024) 215:126–36. doi: 10.1093/cei/uxad104
99. Li X, Xiao S, Filipczak N, Yalamarty SSK, Shang H, Zhang J, et al. Role and therapeutic targeting strategies of neutrophil extracellular traps in inflammation. *Int J Nanomed.* (2023) 18:5265–87. doi: 10.2147/IJN.S418259
100. Ravindran M, Khan MA, Palaniyar N. Neutrophil extracellular trap formation: physiology, pathology, and pharmacology. *Biomolecules.* (2019) 9:365. doi: 10.3390/biom9080365
101. Filipczak N, Li X, Saawant GR, Yalamarty SSK, Luther E, Torchilin VP. Antibody-modified DNase I micelles specifically recognize the neutrophil extracellular traps (NETs) and promote their degradation. *J Control Release.* (2023) 354:109–19. doi: 10.1016/j.jconrel.2022.12.062
102. Yang S, Feng Y, Chen L, Wang Z, Chen J, Ni Q, et al. Disulfiram accelerates diabetic foot ulcer healing by blocking NET formation via suppressing the NLRP3/Caspase-1/GSDMD pathway. *Transl Res.* (2023) 254:115–27. doi: 10.1016/j.trsl.2022.10.008
103. Kumar R, Patil G, Dayal S. NLRP3-induced NETosis: A potential therapeutic target for ischemic thrombotic diseases? *Cells.* (2023) 12:2709. doi: 10.3390/cells12232709
104. Wang M, Zhao H, Zhao H, Huo C, Yuan Y, Zhu Y. Moxibustion-mediated alleviation of synovitis in rats with rheumatoid arthritis through the regulation of NLRP3 inflammasome by modulating neutrophil extracellular traps. *Heliyon.* (2023) 10:e23633. doi: 10.1016/j.heliyon.2023.e23633
105. Pang Q, Wang P, Pan Y, Dong X, Zhou T, Song X, et al. Irisin protects against vascular calcification by activating autophagy and inhibiting NLRP3-mediated vascular smooth muscle cell pyroptosis in chronic kidney disease. *Cell Death Dis.* (2022) 13:283. doi: 10.1038/s41419-022-04735-7
106. Wu M, Li H, He J, Liang J, Liu Y, Zhang W. RIM72 Alleviates Muscle Inflammation in mdx Mice via Promoting Mitophagy-Mediated NLRP3 Inflammasome Inactivation. *Oxid Med Cell Longev.* (2023) 2023:8408574. doi: 10.1155/2023/8408574
107. Snedden AM, Kellett K, Lilleker JB, Hooper NM, Chinoy H. The role of protein aggregation in the pathogenesis of inclusion body myositis. *Clin Exp Rheumatol.* (2022) 40:414–24. doi: 10.55563/clinexprheumatol/pp050
108. Kummer K, Bertram I, Zechel S, Hoffmann DB, Schmidt J. Inflammasome in skeletal muscle: NLRP3 is an inflammatory cell stress component in inclusion body myositis. *Int J Mol Sci.* (2023) 24:10675. doi: 10.3390/ijms241310675
109. Naddaf E, Nguyen TKO, Watzlawik JO, Gao H, Hou X, Fiesel FC, et al. NLRP3 inflammasome activation and altered mitophagy are key pathways in inclusion body myositis. *medRxiv.* (2024) 1624308845. doi: 10.1101/2024.06.15.24308845
110. Zhao P, Zhu J, Bai L, Ma W, Li F, Zhang C, et al. Neutrophil extracellular traps induce pyroptosis of pulmonary microvascular endothelial cells by activating the NLRP3 inflammasome. *Clin Exp Immunol.* (2024) 217:89–98. doi: 10.1093/cei/uxae028
111. Guo C, He J, Song X, Tan L, Wang M, Jiang P, et al. Pharmacological properties and derivatives of shikonin-A review in recent years. *Pharmacol Res.* (2019) 149:104463. doi: 10.1016/j.phrs.2019.104463
112. Kuwar R, Rolfe A, Di L, Xu H, He L, Jiang Y, et al. A novel small molecular NLRP3 inflammasome inhibitor alleviates neuroinflammatory response following traumatic brain injury. *J Neuroinflamm.* (2019) 16:81. doi: 10.1186/s12974-019-1471-y
113. Jiang H, He H, Chen Y, Huang W, Cheng J, Ye J, et al. Identification of a selective and direct NLRP3 inhibitor to treat inflammatory disorders. *J Exp Med.* (2017) 214:3219–38. doi: 10.1084/jem.20171419
114. Marchetti C, Swartzwelter B, Gamboni F, Neff CP, Richter K, Azam T, et al. OLT1177, a β -sulfonyl nitrile compound, safe in humans, inhibits the NLRP3 inflammasome and reverses the metabolic cost of inflammation. *Proc Natl Acad Sci USA.* (2018) 115:E1530–9. doi: 10.1073/pnas.1716095115
115. Juliana C, Fernandes-Alnemri T, Wu J, Datta P, Solorzano L, Yu J-W, et al. Anti-inflammatory compounds parthenolide and Bay 11-7082 are direct inhibitors of the inflammasome. *J Biol Chem.* (2010) 285:9792–802. doi: 10.1074/jbc.M109.082305
116. Saadane A, Masters S, Didonato J, Li J, Berger M. Parthenolide inhibits IkB Kinase, NF- κ B activation, and inflammatory response in cystic fibrosis cells and mice. *Am J Respir Cell Mol Biol.* (2007) 36:728–36. doi: 10.1165/rcmb.2006-0323OC
117. Huang Y, Jiang H, Chen Y, Wang X, Yang Y, Tao J, et al. Tranilast directly targets NLRP3 to treat inflammasome-driven diseases. *EMBO Mol Med.* (2018) 10:e8689. doi: 10.15252/emmm.201708689
118. Youm YH, Nguyen KY, Grant RW, Goldberg EL, Bodogai M, Kim D, et al. The ketone metabolite β -hydroxybutyrate blocks NLRP3 inflammasome-mediated inflammatory disease. *Nat Med.* (2015) 21:263–9. doi: 10.1038/nm.3804
119. He H, Jiang H, Chen Y, Ye J, Wang A, Wang C, et al. Oridonin is a covalent NLRP3 inhibitor with strong anti-inflammasome activity. *Nat Commun.* (2018) 9:2550. doi: 10.1038/s41467-018-04947-6
120. Kumari P, Russo AJ, Shivcharan S, Rathinam VA. AIM2 in health and disease: Inflammasome and beyond. *Immunol Rev.* (2020) 297:83–95. doi: 10.1111/immr.12903
121. Fernandes-Alnemri T, Yu JW, Datta P, Wu J, Alnemri ES. AIM2 activates the inflammasome and cell death in response to cytoplasmic DNA. *Nature.* (2009) 458:509–13. doi: 10.1038/nature07710
122. Hornung V, Ablasser A, Charrel-Dennis M, Bauernfeind F, Horvath G, Caffrey DR, et al. AIM2 recognizes cytosolic dsDNA and forms a caspase-1-activating inflammasome with ASC. *Nature.* (2009) 458:514–8. doi: 10.1038/nature07725
123. Coll RC, Robertson AA, Chae JJ, Higgins SC, Muñoz-Planillo R, Innes MC, et al. A small-molecule inhibitor of the NLRP3 inflammasome for the treatment of inflammatory diseases. *Nat Med.* (2015) 21:248–55. doi: 10.1038/nm.3806
124. Zahid A, Li B, Kombe AJK, Jin T, Tao J. Pharmacological inhibitors of the NLRP3 inflammasome. *Front Immunol.* (2019) 10:2538. doi: 10.3389/fimmu.2019.02538
125. Zhan X, Li Q, Xu G, Xiao X, Bai Z. The mechanism of NLRP3 inflammasome activation and its pharmacological inhibitors. *Front Immunol.* (2023) 13:1109938. doi: 10.3389/fimmu.2022.1109938
126. Zeng W, Wu D, Sun Y, Suo Y, Yu Q, Zeng M, et al. The selective NLRP3 inhibitor MCC950 hinders atherosclerosis development by attenuating inflammation and pyroptosis in macrophages. *Sci Rep.* (2021) 11:19305. doi: 10.1038/s41598-021-98437-3
127. Tian Y, He X, Li R, Wu Y, Ren Q, Hou Y. Recent advances in the treatment of gout with NLRP3 inflammasome inhibitors. *Bioorg Med Chem.* (2024) 112:117874. doi: 10.1016/j.bmc.2024.117874
128. Zhang J, Zeng S, Wang P, Chen Y, Zeng C. NLRP3: A promising therapeutic target for inflammatory bowel disease. *Curr Drug Targets.* (2023) 24:1106–16. doi: 10.2174/0113894501255960231101105113
129. Perregaux DG, McNiff P, Liberte R, Hawryluk N, Peurano H, Stam E, et al. Identification and characterization of a novel class of interleukin1 post-translational processing inhibitors. *J Pharmacol Exp Ther.* (2001) 299:187–97.
130. Coll RC, Hill JR, Day CJ, Zamosnikova A, Boucher D, Massey NL, et al. MCC950 directly targets the NLRP3 ATP-hydrolysis motif for inflammasome inhibition. *Nat Chem Biol.* (2019) 15:556–9. doi: 10.1038/s41589-019-0277-7
131. Fulp J, He L, Toldo S, Jiang Y, Boice A, Guo C, et al. Structural insights of benzenesulfonamide analogues as NLRP3 inflammasome inhibitors: design, synthesis, and biological characterization. *J Med Chem.* (2018) 61:5412–23. doi: 10.1021/acs.jmedchem.8b00733
132. Lugrin J, Martinon F. The AIM2 inflammasome: sensor of pathogens and cellular perturbations. *Immunol Rev.* (2018) 281:99–114. doi: 10.1111/immr.12618
133. Yagarajah T, Ong KC, Perera D, Wong KT. AIM2 inflammasome-mediated pyroptosis in enterovirus A71-infected neuronal cells restricts viral replication. *Sci Rep.* (2017) 7:5845. doi: 10.1038/s41598-017-05589-2
134. Hu B, Jin C, Li HB, Tong J, Ouyang X, Cetinbas NM, et al. The DNA-sensing AIM2 inflammasome controls radiation-induced cell death and tissue injury. *Science.* (2016) 354:765–8. doi: 10.1126/science.aaf7532
135. Lian Q, Xu J, Yan S, Huang M, Ding H, Sun X, et al. Chemotherapy-induced intestinal inflammatory Responses are Mediated by Exosome Secretion of Double-Strand DNA via AIM2 Inflammasome Activation. *Cell Res.* (2017) 27:784–800. doi: 10.1038/cr.2017.54
136. Jin T, Perry A, Jiang J, Smith P, Curry JA, Unterholzner L, et al. Structures of the HIN domain: DNA complexes reveal ligand binding and activation mechanisms of the AIM2 inflammasome and IFI16 receptor. *Immunity.* (2012) 36:561–71. doi: 10.1016/j.immuni.2012.02.014
137. Matyszcwski M, Morrone SR, Sohn J. Digital signaling network drives the assembly of the AIM2-ASC inflammasome. *Proc Natl Acad Sci USA.* (2018) 115:E1963–72. doi: 10.1073/pnas.1712860115
138. Uresti-Rivera EE, García-Hernández MH. AIM2-inflammasome role in systemic lupus erythematosus and rheumatoid arthritis. *Autoimmunity.* (2022) 55:443–54. doi: 10.1080/08916934.2022.2103802
139. Chou WC, Guo Z, Guo H, Chen L, Zhang G, Liang K, et al. AIM2 in regulatory T cells restrains autoimmune diseases. *Nature.* (2021) 591:300–5. doi: 10.1038/s41586-021-03231-w
140. Gao J, Peng S, Shan XN, Deng G, Shen L, Sun J, et al. Inhibition of AIM2 inflammasome-mediated pyroptosis by Andrographolide contributes to the

amelioration of radiation-induced lung inflammation and fibrosis. *Cell Death disease*. (2019) 10:957. doi: 10.1038/s41419-019-2195-8

141. Loell I, Raouf J, Chen YW, Wang K, Zhang D, Xu W, et al. Effects on muscle tissue remodeling and lipid metabolism in muscle tissue from adult patients with polymyositis or dermatomyositis treated with immunosuppressive agents. *Arthritis Res Ther*. (2016) 18:136. doi: 10.1186/s13075-016-1033-y
142. Banerjee I, Behl B, Mendonca M, Shrivastava G, Russo AJ, Menoret A, et al. Gasdermin D restrains type I interferon response to cytosolic DNA by disrupting ionic homeostasis. *Immunity*. (2018) 49:413–26.e5. doi: 10.1016/j.immuni.2018.07.006
143. Baatarjav C, Komada T, Karasawa T, Yamada N, Sampilvanjil A, Matsumura T, et al. dsDNA-induced AIM2 pyroptosis halts aberrant inflammation during rhabdomyolysis-induced acute kidney injury. *Cell Death Differ*. (2022) 29:2487–502. doi: 10.1038/s41418-022-01033-9
144. Marim FM, Franco MMC, Gomes MTR, Miraglia MC, Giambartolomei GH, Oliveira SC. The role of NLRP3 and AIM2 in inflammasome activation during *Brucella abortus* infection. *Semin Immunopathol*. (2017) 39:215–23. doi: 10.1007/s00281-016-0581-1
145. Kalantari P, DeOliveira RB, Chan J, Corbett Y, Rathinam V, Stutz A, et al. Dual engagement of the NLRP3 and AIM2 inflammasomes by plasmodium-derived hemozoin and DNA during malaria. *Cell Rep*. (2014) 6:196–210. doi: 10.1016/j.celrep.2013.12.014
146. Messaoud-Nacer Y, Culerier E, Rose S, Maillat I, Rouxel N, Briault S, et al. STING agonist diABZI induces PANoptosis and DNA mediated acute respiratory distress syndrome (ARDS). *Cell Death Dis*. (2022) 13:269. doi: 10.1038/s41419-022-04664-5
147. Oh S, Lee J, Oh J, Yu G, Ryu H, Kim D, et al. Integrated NLRP3, AIM2, NLR4, PIRIN inflammasome activation and assembly drive PANoptosis. *Cell Mol Immunol*. (2023) 20:1513–26. doi: 10.1038/s41423-023-01107-9
148. Dang EV, McDonald JG, Russell DW, Cyster JG. Oxysterol restraint of cholesterol synthesis prevents AIM2 inflammasome activation. *Cell*. (2017) 171:1057–71.e11. doi: 10.1016/j.cell.2017.09.029
149. Xie M, Yu Y, Kang R, Zhu S, Yang L, Zeng L, et al. PKM2-dependent glycolysis promotes NLRP3 and AIM2 inflammasome activation. *Nat Commun*. (2016) 7:13280. doi: 10.1038/ncomms13280
150. Chung IC, Yuan SN, OuYang CN, Hu SI, Lin HC, Huang KY, et al. EFLA 945 restricts AIM2 inflammasome activation by preventing DNA entry for psoriasis treatment. *Cytokine*. (2020) 127:154951. doi: 10.1016/j.cyto.2019.154951
151. Zhang MJ, Zhao QC, Xia MX, Chen J, Chen YT, Cao X, et al. The HDAC3 inhibitor RGFP966 ameliorated ischemic brain damage by downregulating the AIM2 inflammasome. *FASEB J*. (2020) 34:648–62. doi: 10.1096/fj.20190394RRR
152. Green JP, El-Sharkawy LY, Roth S, Zhu, Cao J, Leach AG, et al. Discovery of an inhibitor of DNA-driven inflammation that preferentially targets the AIM2 inflammasome. *iScience*. (2023) 26:106758. doi: 10.1016/j.isci.2023.106758
153. Kaminski JJ, Schattgen SA, Tzeng TC, Bode C, Klinman DM, Fitzgerald KA, et al. Synthetic oligodeoxynucleotides containing suppressive TTAGGG motifs inhibit AIM2 inflammasome activation. *J Immunol*. (2013) 191:3876–83. doi: 10.4049/jimmunol.1300530
154. Panchanathan R, Ramalingam V, Liu H, Choubey D. Human prostate epithelial cells activate the AIM2 inflammasome upon cellular senescence: role of POP3 protein in aging-related prostatic inflammation. *Life (Basel)*. (2021) 11:366. doi: 10.3390/life11040366
155. Domiciano TP, Wakita D, Jones HD, Crother TR, Verri WA Jr, Arditi M, et al. Quercetin inhibits inflammasome activation by interfering with ASC oligomerization and prevents interleukin-1 mediated mouse vasculitis. *Sci Rep*. (2017) 7:41539. doi: 10.1038/srep41539
156. Lee KM, Kang JH, Yun M, Lee SB. Quercetin inhibits the poly(dA:dT)-induced secretion of IL-18 via down-regulation of the expressions of AIM2 and pro-caspase-1 by inhibiting the JAK2/STAT1 pathway in IFN-gamma-primed human keratinocytes. *Biochem Biophys Res Commun*. (2018) 503:116–22. doi: 10.1016/j.bbrc.2018.05.191
157. Ruan J. Structural insight of gasdermin family driving pyroptotic cell death. *Adv Exp Med Biol*. (2019) 1172:189–205. doi: 10.1007/978-981-13-9367-9_9
158. Zeng B, Wei A, Zhou Q, Yuan M, Lei K, Liu Y, et al. Andrographolide: A review of its pharmacology, pharmacokinetics, toxicity and clinical trials and pharmaceutical researches. *Phytother Res*. (2022) 36:336–64. doi: 10.1002/ptr.7324
159. Lee SB, Kang JH, Sim EJ, Jung YR, Kim JH, Hillman PF, et al. Cornus officinalis seed extract inhibits AIM2-inflammasome activation and attenuates imiquimod-induced psoriasis-like skin inflammation. *Int J Mol Sci*. (2023) 24:5653. doi: 10.3390/ijms24065653
160. Kim J, Ahn H, Han BC, Lee SH, Cho YW, Kim CH, et al. Korean red ginseng extracts inhibit NLRP3 and AIM2 inflammasome activation. *Immunol Lett*. (2014) 158:143–50. doi: 10.1016/j.imlet.2013.12.017
161. Van Opdenbosch N, Lamkanfi M. Caspases in cell death, inflammation, and disease. *Immunity*. (2019) 50:1352–64. doi: 10.1016/j.immuni.2019.05.020
162. Ramirez MLG, Salvesen GS. A primer on caspase mechanisms. *Semin Cell Dev Biol*. (2018) 82:79–85. doi: 10.1016/j.semcdb.2018.01.002
163. Kesavardhana S, Malireddi RKS, Kanneganti TD. Caspases in cell death, inflammation, and pyroptosis. *Annu Rev Immunol*. (2020) 38:567–95. doi: 10.1146/annurev-immunol-073119-095439
164. Alnemri ES, Livingston DJ, Nicholson DW, Salvesen G, Thornberry NA, Wong WW, et al. Human ICE/CED-3 protease nomenclature. *Cell*. (1996) 87:171. doi: 10.1016/s0092-8674(00)81334-3
165. Man SM, Kanneganti TD. Converging roles of caspases in inflammasome activation, cell death and innate immunity. *Nat Rev Immunol*. (2016) 16:7–21. doi: 10.1038/nri.2015.7
166. Cao D, Xi R, Li H, Zhang Z, Shi X, Li S, et al. Discovery of a covalent inhibitor of pro-caspase-1 zymogen blocking NLRP3 inflammasome activation and pyroptosis. *J Med Chem*. (2024) 67:15873–91. doi: 10.1021/acs.jmedchem.4c01558
167. Mackiewicz Z, Hukkanen M, Povilenaite D, Sukura A, Fonseca JE, Virtanen I, et al. Dual effects of caspase-1, interleukin-1 β , tumor necrosis factor- α , and nerve growth factor receptor in inflammatory myopathies. *Clin Exp Rheumatol*. (2003) 21:41–8.
168. Schilders G, Rajmakers R, Malmegrim KC, Vande Walle L, Saelens X, Vree Egberts W, et al. Caspase-mediated cleavage of the exosome subunit PM/Scf-75 during apoptosis. *Arthritis Res Ther*. (2007) 9:R12. doi: 10.1186/ar2119
169. Zhou M, Li M, Guo C, Wang S, Li X, Zhao S, et al. Circulating TFH cells is correlated with disease activity in anti-MDA5 antibody positive idiopathic inflammatory myopathies. *Clin Exp Rheumatol*. (2021) 39:804–10. doi: 10.55563/clinexpheumatol/gfqlcz
170. Faucheu C, Blanchet AM, Collard-Dutilleul V, Lalanne JL, Diu-Hercend A. Identification of a cysteine protease closely related to interleukin-1 β -converting enzyme. *Eur J Biochem*. (1996) 236:207–13. doi: 10.1111/j.1432-1033.1996.t01-1-00207.x
171. Munday NA, Vaillancourt JP, Ali A, Casano FJ, Miller DK, Molineaux SM, et al. Molecular cloning and pro-apoptotic activity of ICEReII and ICEReIII, members of the ICE/CED-3 family of cysteine proteases. *J Biol Chem*. (1995) 270:15870–6. doi: 10.1074/jbc.270.26.15870
172. Kamens J, Paskind M, Hugunin M, Talanian RV, Allen H, Banach D, et al. Identification and characterization of ICH-2, a novel member of the interleukin1 β -converting enzyme family of cysteine proteases. *J Biol Chem*. (1995) 270:15250–6. doi: 10.1074/jbc.270.25.15250
173. Xevi S, Indramohan M, Jäger E, Carriere J, Chu LH, Almeida L, et al. CARD-only proteins regulate *in vivo* inflammasome responses and ameliorate gout. *Cell Rep*. (2023) 42:112265. doi: 10.1016/j.celrep.2023.112265
174. Zhou Y, Du T, Yang CL, Li T, Li XL, Liu W, et al. Extracellular vesicles encapsulated with caspase-1 inhibitor ameliorate experimental autoimmune myasthenia gravis by targeting macrophages. *J Control Release*. (2023) 364:458–72. doi: 10.1016/j.jconrel.2023.11.006
175. Tang YS, Feng B, Wang Y, Sun H, You Y, Yu J, et al. Structure-based discovery of CZL80, a caspase-1 inhibitor with therapeutic potential for febrile seizures and later enhanced epileptogenic susceptibility. *Br J Pharmacol*. (2020) 177:3519–34. doi: 10.1111/bph.15076
176. Yang M, Fang JT, Zhang NS, Qin L, Zhuang YY, Wang WW, et al. Caspase-1 inhibitor AC-YVAD-CMK inhibits pyroptosis and ameliorates acute kidney injury in a model of sepsis. *BioMed Res Int*. (2021) 2021:6636621. doi: 10.1155/2021/6636621
177. He WT, Wan H, Hu L, Chen P, Wang X, Huang Z, et al. Gasdermin D is an executor of pyroptosis and required for interleukin-1 β secretion. *Cell Res*. (2015) 25:1285–98. doi: 10.1038/cr.2015.139
178. Liu X, Zhang Z, Ruan J, Pan Y, Magupalli VG, Wu H, et al. Inflammasome-activated gasdermin D causes pyroptosis by forming membrane pores. *Nature*. (2016) 535:153–8. doi: 10.1038/nature18629
179. Qiu S, Liu J, Xing F. [amp]]squo;Hints in the killer protein gasdermin D: unveiling the secrets of gasdermins driving cell death. *Cell Death Differ*. (2017) 24:588–96. doi: 10.1038/cdd.2017.24
180. Fischer FA, Chen KW, Bezbarad JS. Posttranslational and therapeutic control of gasdermin-mediated pyroptosis and inflammation. *Front Immunol*. (2021) 12:661162. doi: 10.3389/fimmu.2021.661162
181. Kang SJ, Wang S, Hara H, Peterson EP, Namura S, Amin-Hanjani S, et al. Dual role of caspase-11 in mediating activation of caspase-1 and caspase-3 under pathological conditions. *J Cell Biol*. (2000) 149:613–22. doi: 10.1083/jcb.149.3.613
182. Ramirez MLG, Poreba M, Snipas SJ, Grobocz K, Drag M, Salvesen GS. Extensive peptide and natural protein substrate screens reveal that mouse caspase-11 has much narrower substrate specificity than caspase-1. *J Biol Chem*. (2018) 293:7058–67. doi: 10.1074/jbc.RA117.001329
183. Lee BL, Stowe IB, Gupta A, Kornfeld OS, Roose-Girma M, Anderson K, et al. Caspase-11 auto-proteolysis is crucial for noncanonical inflammasome activation. *J Exp Med*. (2018) 215:2279–88. doi: 10.1084/jem.20180589
184. Rühl S, Broz P. Caspase-11 activates a canonical NLRP3 inflammasome by promoting K⁺ efflux. *Eur J Immunol*. (2015) 45:2927–36. doi: 10.1002/eji.201545772
185. Deng R, Chai KX, Ma M. Expression and significance of ROS mediated by NADPH oxidases in skeletal muscle tissues of an animal model of idiopathic inflammatory myopathy. *Med J West China*. (2022) 34:1102–1108. doi: 10.3969/j.issn.1672-3511.2022.08.003
186. Schauvliege R, Vanrobaeys J, Schotte P, Beyaert R. Caspase-11 gene expression in response to lipopolysaccharide and interferon- γ requires nuclear factor- κ B and signal transducer and activator of transcription (STAT) 1. *J Biol Chem*. (2002) 277:41624–30. doi: 10.1074/jbc.M207852200

187. Yen JH, Ganea D. Interferon γ induces mature dendritic cell apoptosis through caspase-11/caspase-3 activation. *Blood*. (2009) 114:1344–54. doi: 10.1182/blood-2008-12-196592
188. Rathinam VAK, Vanaja SK, Waggoner L, Sokolovska A, Becker C, Stuart LM, et al. TRIF licenses caspase-11-dependent NLRP3 inflammasome activation by Gram-negative bacteria. *Cell*. (2012) 150:606–19. doi: 10.1016/j.cell.2012.07.007
189. Deng M, Tang Y, Li W, Wang X, Zhang R, Zhang X, et al. The endotoxin delivery protein HMGB1 mediates caspase-11-dependent lethality in sepsis. *Immunity*. (2018) 49:740–53.e7. doi: 10.1016/j.immuni.2018.08.016
190. Kutsch M, Sistemic L, Lesser CF, Goldberg MB, Herrmann C, Coers J. Direct binding of polymeric GBP1 to LPS disrupts bacterial cell envelope functions. *EMBO J*. (2020) 39:e104926. doi: 10.15252/embj.2020104926
191. Wandel MP, Kim BH, Park ES, Boyle KB, Nayak K, Lagrange B, et al. Guanylate-binding proteins convert cytosolic bacteria into caspase-4 signaling platforms. *Nat Immunol*. (2020) 21:880–91. doi: 10.1038/s41590-020-0697-2
192. Zanoni I, Tan Y, Di Gioia MD, Broggi A, Ruan J, Shi J, et al. An endogenous caspase-11 ligand elicits interleukin-1 release from living dendritic cells. *Science*. (2016) 352:1232–6. doi: 10.1126/science.aaf3036
193. Chu LH, Indramohan M, Ratsimandresy RA, Gangopadhyay A, Morris EP, Monack DM, et al. The oxidized phospholipid oxPAPC protects from septic shock by targeting the non-canonical inflammasome in macrophages. *Nat Commun*. (2018) 9:996. doi: 10.1038/s41467-018-03409-3
194. Vladyskovskaya E, Ozhegov E, Hoetker JD, Xie Z, Ahmed Y, Suttles J, et al. Reductive metabolism increases the proinflammatory activity of aldehyde phospholipids. *J Lipid Res*. (2011) 52:2209–25. doi: 10.1194/jlr.M013854
195. Zheng Z, Deng W, Lou X, Bai Y, Wang J, Zeng H, et al. Gasdermins: pore-forming activities and beyond. *Acta Biochim Biophys Sin (Shanghai)*. (2020) 52:467–74. doi: 10.1093/abbs/gmaa016
196. Ding J, Wang K, Liu W, She Y, Sun Q, Shi J, et al. Pore-forming activity and structural autoinhibition of the gasdermin family. *Nature*. (2016) 535:111–6. doi: 10.1038/nature18590
197. Kayagaki N, Stowe IB, Lee BL, O'Rourke K, Anderson K, Warming S, et al. Caspase-11 cleaves gasdermin D for non-canonical inflammasome signalling. *Nature*. (2015) 526:666–71. doi: 10.1038/nature15541
198. Kahlenberg JM, Carmona-Rivera C, Smith CK, Kaplan MJ. Neutrophil extracellular trap-associated protein activation of the NLRP3 inflammasome is enhanced in lupus macrophages. *J Immunol*. (2013) 190:1217–26. doi: 10.4049/jimmunol.1202388
199. Van Laer L, Huizing EH, Verstreken M, van Zuijlen D, Wauters JG, Bossuyt PJ, et al. Nonsyndromic hearing impairment is associated with a mutation in DFNA5. *Nat Genet*. (1998) 20:194–7. doi: 10.1038/2503
200. Rogers C, Fernandes-Alnemri T, Mayes L, Alnemri D, Cingolani G, Alnemri ES. Cleavage of DFNA5 by caspase-3 during apoptosis mediates progression to secondary necrotic/pyroptotic cell death. *Nat Commun*. (2017) 8:14128. doi: 10.1038/ncomms14128
201. Liu M, Li L, Dai T, Hou Y, Li W, Zhao Y, et al. Gasdermin E-dependent mitochondrial pyroptotic pathway in dermatomyositis: A possible mechanism of perifascicular atrophy. *J Neuropathol Exp Neurol*. (2020) 79:551–61. doi: 10.1093/jnen/nlaa023
202. Zhu C, Xu S, Jiang R, Yu Y, Bian J, Zou Z. The gasdermin family: emerging therapeutic targets in diseases. *Signal Transduct Target Ther*. (2024) 9:87. doi: 10.1038/s41392-024-01801-8
203. Cheng CK, Yi M, Wang L, Huang Y. Role of gasdermin D in inflammatory diseases: from mechanism to therapeutics. *Front Immunol*. (2024) 15:1456244. doi: 10.3389/fimmu.2024.1456244
204. Hu JJ, Liu X, Xia S, Zhang Z, Zhang Y, Zhao J, et al. FDA-approved disulfiram inhibits pyroptosis by blocking gasdermin D pore formation. *Nat Immunol*. (2020) 21:736–45. doi: 10.1038/s41590-020-0669-6
205. Yang W, Tao K, Wang Y, Huang Y, Duan C, Wang T, et al. Necrosulfonamide ameliorates intestinal inflammation via inhibiting GSDMD-mediated pyroptosis and MLKL-mediated necroptosis. *Biochem Pharmacol*. (2022) 206:115338. doi: 10.1016/j.bcp.2022.115338
206. Saidu NEB, Kaviani N, Leroy K, Jacob C, Nicco C, Batteux F, et al. Dimethyl fumarate, a two-edged drug: Current status and future directions. *Med Res Rev*. (2019) 39:1923–52. doi: 10.1002/med.21567
207. Cao R, Li Z, Wu C, Ji S, Li Y, Cao X, et al. Identification of a small molecule with strong anti-inflammatory activity in experimental autoimmune encephalomyelitis and sepsis through blocking gasdermin D activation. *J Immunol*. (2022) 209:820–8
208. Zhong L, Han J, Fan X, Huang Z, Su L, Cai X, et al. Novel GSDMD inhibitor GI Y1 protects heart against pyroptosis and ischemia/reperfusion injury by blocking pyroptotic pore formation. *Basic Res Cardiol*. (2023) 118:40. doi: 10.1007/s00395-02301010-4
209. Amara N, Cooper MP, Voronkova MA, Webb BA, Lynch EM, Kollman JM, et al. Selective activation of PFKFB3 suppresses the phagocytic oxidative burst. *Cell*. (2021) 184:4480–94.e15. doi: 10.1016/j.cell.2021.07.004



OPEN ACCESS

EDITED BY

Tamas Nemeth,
Semmelweis University, Hungary

REVIEWED BY

Julien Subburayalu,
Technical University Dresden, Germany
Maria Ntinopoulou,
University of Ioannina, Greece

*CORRESPONDENCE

Kathrin Kalies

✉ kathrin.kalies@uni-luebeck.de

RECEIVED 10 September 2024

ACCEPTED 04 December 2024

PUBLISHED 22 January 2025

CITATION

Raudszus L, Bahreini F, Allan S, Kalies K-U,
Caldwell CC and Kalies K (2025)
Nanoparticles containing intracellular
proteins modulate neutrophil functional
and phenotypic heterogeneity.
Front. Immunol. 15:1494400.
doi: 10.3389/fimmu.2024.1494400

COPYRIGHT

© 2025 Raudszus, Bahreini, Allan, Kalies,
Caldwell and Kalies. This is an open-access
article distributed under the terms of the
[Creative Commons Attribution License \(CC BY\)](https://creativecommons.org/licenses/by/4.0/).
The use, distribution or reproduction in other
forums is permitted, provided the original
author(s) and the copyright owner(s) are
credited and that the original publication in
this journal is cited, in accordance with
accepted academic practice. No use,
distribution or reproduction is permitted
which does not comply with these terms.

Nanoparticles containing intracellular proteins modulate neutrophil functional and phenotypic heterogeneity

Leonore Raudszus¹, Farbod Bahreini¹, Susanne Allan²,
Kai-Uwe Kalies², Charles C. Caldwell³ and Kathrin Kalies^{1*}

¹Institute of Anatomy, University of Luebeck, Luebeck, Germany, ²Institute of Biology, University of Luebeck, Luebeck, Germany, ³Department of Surgery, College of Medicine, University of Cincinnati, Cincinnati, OH, United States

Neutrophils are rapidly recruited to sites of infection, injury, or to immune complexes. Upon arrival, they initiate degranulation, release reactive oxygen species (ROS), and/or nuclear extracellular traps (NETs) to eliminate invading microorganisms, clear debris, or remove abnormal immunoglobulins. While these processes ideally trigger healing and a return to balance, overshooting neutrophil function can lead to life-threatening infections such as sepsis or persistent inflammation observed in various autoimmune diseases. However, recent evidence highlights a phenotypic and functional heterogeneity of neutrophils that extends well beyond their traditional - potentially harmful - role as first responders. For example, neutrophils regulate ongoing inflammation by modulating macrophage function through efferocytosis, T cell responses by antigen presentation and the release of cytokines. The factors that induce neutrophil differentiation into activating or regulatory phenotypes remain poorly defined. Here, we hypothesize that intracellular components that have been released into the extracellular space could contribute to the phenotypic heterogeneity of neutrophils. To find out, we used nanoparticles composed of intracellular proteins (cell-derived nanoparticles, CDNPs) and analyzed their effects on cultured murine bone marrow neutrophils (BMN). We observed that CDNPs activate BMN transiently with an increase in the expression of CD11b without triggering classical effector functions. Additionally, CDNPs induce the secretion of IL-10, shift PMA-induced cell death toward apoptosis, and increase the expression of CD80. Mechanistically, our findings indicate that 26% of BMNs ingest CDNPs. These BMNs preferentially express CD54+, fail to migrate toward CXCL12, exhibit diminished responses to LPS, and undergo apoptosis. These data identify CDNPs as biomaterials that modulate neutrophil behavior by fine-tuning the expression of CD11b and CD80.

KEYWORDS

neutrophils, heterogeneity, intracellular content, cell-derived nanoparticles, damage-associated molecular pattern, resolution

Introduction

Neutrophils are among the first cells to infiltrate sites of infection or injury, as well as locations where immune complexes are deposited in autoimmune diseases. They are capable of inducing robust responses, which can potentially cause collateral tissue damage (1). Conventionally, neutrophils have been described as short-lived cells with a defined set of effector functions such as phagocytosis, degranulation, ROS release, formation of NETs, and the secretion of specific cytokines. However, recent studies have uncovered unexpected phenotypic heterogeneity and functional plasticity in neutrophils, suggesting that these cells can significantly influence the duration, severity, and outcome of subsequent immune responses (2). Thus, neutrophils may either exacerbate ongoing tissue-damaging inflammation or promote regulatory, resolving, and tissue-repairing processes (3, 4). The factors that regulate this neutrophilic heterogeneity are poorly defined. Their identification will be important to develop new therapeutic approaches.

This study explores the hypothesis that the differentiation of neutrophils into either activating or regulatory phenotypes may be influenced by proteins that are typically localized intracellularly but are released during accidental cell injury. The presence of such intracellular proteins in the extracellular space has traditionally been associated with the initiation of inflammation, even in the absence of pathogens. These intracellular components are termed “Danger-” or “Damage-Associated Molecular Patterns” (DAMPs) because they are recognized by Pattern Recognition Receptors, thereby activating innate immune cells and inducing inflammation (5, 6). Typical examples include HMGB1, histones, S100 proteins, and heat shock proteins, which have been studied extensively *in vitro* and *in vivo*, where each protein was introduced individually for investigation (7, 8). However, the complexity of *in vivo* scenarios is far greater, involving a diverse array of intracellular proteins, such as cytoskeletal elements, chaperones, and enzymes, as well as combinations of these proteins with nucleic acids and lipids, released either individually or as complexes. Currently, there is no data available on the impact of these protein mixtures on neutrophils. To address this, we employed CDNPs, which predominantly consist of intracellular proteins and are structured as nanoparticles ranging from 100 to 200 nm in size. The primary proteins present in CDNPs include Annexins (ANXA1-5), HSP60, actin, galectin, and vimentin, among others, as well as small amounts of nucleic acids (9, 10).

According to our current understanding of how intracellular contents influence innate immune cells, CDNPs would be categorized as DAMPs. However, previous studies have shown that CDNPs exert regulating capacities. Thus, CDNPs accelerate and improve the healing of antibody-induced skin wounds in the

mouse model for the skin blistering disease epidermolysis bullosa acquisita (9). CDNPs also showed promise in critical medical situations such as sepsis, as observed in the murine cecal ligation and puncture model, where they positively influenced the host response (10).

In this study, we assessed the effects of CDNPs on various neutrophil functions, including phagocytosis, ROS release, NETosis, cytokine secretion, apoptosis, migration, and the expression of phenotypic markers such as CD11b, CD80, CD86, MHCII, and CD54 in cultures of murine bone marrow cells (BMC). We found that CDNPs did not activate traditional effector functions; however, a transient increase in CD11b, upregulation of CD80 expression and apoptosis were observed, indicating that intracellular content indeed seems to regulate inflammatory processes by modulating the phenotype of neutrophils. Further research is needed to decipher and better understand the effects of intracellular content on the heterogeneity of neutrophil subsets.

Materials and methods

Mice/bone marrow cells

For all experiments, BMC were isolated from inbred C57BL/6J mice aged 8–12 weeks. Mice were anesthetized with CO₂ and killed by cervical dislocation. Tibiae and femora were flushed with HBSS (Thermo Fisher Scientific, USA). For each experiment, the bone marrow of two mice was combined. The BMC were flushed through a cell strainer, pelleted, and red blood cells were lysed with Ammonium-Chloride-Potassium buffer. Then, the BMC were resuspended in RPMI 1640 (Lonza, Switzerland), supplemented with 5% FBS, 1 x Non-essential amino acids, 1 mM Sodium Pyruvate, 100 U/ml Penicillin/100 µg/ml Streptomycin, 7.5 mg/L Gentamycin, 5.25 µg/L 2-mercaptoethanol, 2 mM L-Glutamine (all Thermo Fisher Scientific, USA), 20 mM Hepes Sodium Salt (Sigma Aldrich (Germany)). Cells were counted and adjusted to 2 x 10⁶ cells/mL. 10⁶ BMC in 0.5 mL medium were used per sample unless indicated otherwise. All murine experiments were approved by the Institutional Animal Care and Use Committee of the University of Cincinnati (protocol no. 10-05-10-01). The approval date was June 26, 2018. Detailed materials are provided in the STAR*Method format in the supplement.

CDNP isolation and preparation

CDNPs were isolated from the murine fibroblast cell line MC3T3E1 (Deutsche Sammlung von Mikroorganismen und Zellkulturen, Braunschweig, Germany). The fibroblasts were disrupted by ultrasound, and the fragments were pelleted at 5000 g for 30 min. The supernatant was ultracentrifuged at 50000 g for 150 min to pellet the particles. To dissolve the remaining membranes, chloroform (C. Roth GmbH & Co. KG, Germany) was added at a final concentration of 5% for 15 seconds. Phase separation was achieved by centrifugation at 9000 g for 15 min. In the supernatant remained the CDNPs. To ensure a consistent quality of the protein

Abbreviations: ARDS, acute respiratory distress syndrome; BMC, bone marrow cells; BMN, bone marrow neutrophils; CDNPs, Cell-derived Nanoparticles; CFSE, Carboxyfluorescein succinimidyl ester; DAMPs, Damage-Associated Molecular Patterns; FVS, Fixable Viability Stain; MFI, Mean Fluorescence Intensity; NETs, nuclear extracellular traps; PMA, Phorbol 12-myristate 13-acetate; ROS, reactive oxygen species.

pattern, each CDNP preparation was analyzed by SDS Page Gels (pre-cast 4-12% Bis-Tris Midi Protein Gels, ThermoFisher Scientific, USA). To compensate for batch variations, several CDNP preparations were combined into pools. Endotoxin was removed by treatment with 1% Triton X-114 (Sigma Aldrich, Germany) as described in (11). PBS that was used for control samples was also treated with Triton X-114. Endotoxin levels were measured with a Limulus Amebocyte assay using the commercially available PierceTM Chromogenic Endotoxin Quant Kit (Thermo Fisher Scientific, USA) according to the manufacturer's instructions. 0.1 EU/mL was used as a lower limit for endotoxin contamination.

CFSE-labeling of CDNPs

The CDNPs were labeled with Carboxyfluorescein succinimidyl ester (CFSE) as previously described (10). The CDNP suspension was incubated with 10 μ M CFSE (Becton Dickinson, USA) per 100 μ g/mL CDNPs at 37°C for 20 min. Excessive CFSE was captured by adding a medium containing 10% fetal bovine serum (Thermo Fisher Scientific, USA) and incubation for 10 min. The PBS control sample was treated the same way.

Intracellular and surface labeling of cells using flow cytometry

For intracellular and surface labeling of cells, the samples were centrifuged and treated with Fc-receptor blocking buffer (containing anti-mouse CD16/32 antibody and 5% rat serum (Thermo Fisher Scientific, USA)) for 10 min, followed by incubation with antibodies for 20 min. BMC were washed and analyzed with the Attune[®] NxTTM Acoustic Focusing Cytometer (Thermo Fisher Scientific, USA) or the LSR II Flow Cytometer (Becton Dickinson, USA). The following fluorescent-labeled antibodies were used: Anti-Histone H3 (citrulline R2 + R8 + R17) Primary Antibody (Polyclonal), FITC Anti-Myeloperoxidase antibody (clone: 2D4) (both from Abcam, UK); APC anti-mouse CD86 Antibody (clone: GL-1), APC-Cy7 anti-mouse CD86 Antibody (clone: GL-1), Brilliant Violet 605TM anti-mouse/human CD11b Antibody (clone: M1/70), Pacific BlueTM anti-mouse I-Ab Antibody (MHC II) (clone: AF6-120.1), Pacific BlueTM anti-mouse Ly-6G Antibody (clone: 1A8), PE anti-mouse CD80 Antibody (clone: 16-10A1), PerCP/Cy5.5 anti-mouse Ly-6G Antibody (clone: 1A8), APC anti-mouse Ly-6G Antibody (clone: 1A8), Brilliant Violet 421TM anti-mouse/human CD11b Antibody (clone: M1/70) (all from BioLegend, USA); Anti-mouse CD16/32 Antibody (clone: 93) (from BioLegend, USA or Thermo Fisher Scientific, USA); APC Hamster Anti-Mouse CD54 (clone: 3E2), APC Rat Anti-CD11b (clone: M1/70), APC-Cy7 Rat Anti-CD11b (clone: M1/70), FITC Hamster Anti-Mouse CD54 (clone: 3E2), Fixable Viability Stain 570, PE Hamster Anti-Mouse CD54 (clone: 3E2), PE Rat Anti-Mouse Ly-6G (clone: 1A8) (all from Becton Dickinson, USA), PE CD11b Monoclonal Antibody (clone: M1/70), Fixable

Viability Dye eFluor 780; Alexa Fluor 700 Goat anti-Rabbit IgG (H +L) Cross-Adsorbed Secondary Antibody [all from Thermo Fisher Scientific (USA)].

Functional assays

Unless indicated otherwise, the cells were always pretreated with 10 μ g/mL CDNPs for 45 min before further stimulation or direct analysis. For some experiments, the cells were stimulated with 100 ng/mL LPS (Lipopolysaccharides from *Escherichia coli* O111: B4, Sigma Aldrich, Germany) for 24 hours at 37°C between preincubation and further stimulation or direct analysis.

Chemotaxis

BMC were isolated and pretreated as described above, transferred to 5 mL tubes and counted; 10⁶ cells were added to the top well insert of a Transwell[®] plate (Corning, USA). The bottom well contained 100 ng/mL Recombinant Mouse CXCL12 (SDF-1 α) (BioLegend, USA). After 3 hours of incubation at 37°C, non-migrated cells from the top well insert and migrated cells from the bottom well were transferred to 5 mL tubes, respectively, pelleted, and counted before flow cytometry analysis. The percentage of neutrophils in the top and bottom wells, respectively, was determined, and the percentage of migrated neutrophils was calculated.

Phagocytosis

E. coli (K-12 strain, BioParticlesTM, Alexa FluorTM 488 conjugate, Thermo Fisher Scientific, USA) were prepared according to the manufacturer's instructions. The particles conjugated to a fluorescent dye and opsonized with *E. coli*-specific polyclonal IgG antibodies (*E. coli* Opsonizing Reagent, Thermo Fisher Scientific, USA) were incubated with pretreated BMC for 15 min at 37°C in a water bath. The cells were fixed by adding 500 μ L of 1% paraformaldehyde (Thermo Fisher Scientific, USA) washed and stained for flow cytometry. Ly6G+/CD11b+ granulocytes emitting a fluorescence around 520 nm were considered as neutrophils that had phagocytosed *E. coli* particles. To discriminate internalized *E. coli* BioParticlesTM from those bound to the cell surface, the samples were reanalyzed after quenching extracellular fluorescence with trypan blue (Sigma Aldrich, Germany) (final concentration 0.43 mg/mL; **Supplementary Figure 1**). Additionally, a second phagocytosis assay was performed using pHrodoTM dye, which emits fluorescence only in the acidic milieu inside the phagolysosome. The *E. coli* particles (pHrodoTM Red *E. coli* BioparticlesTM conjugate, Thermo Fisher Scientific, USA) were prepared according to the manufacturer's instructions. The opsonized and conjugated particles were incubated with

pretreated BMC (for 60 min at 37°C). Then, the cells were fixed with 1% PFA for 5 min, washed, and stained with antibodies as described above. Ly6G+/CD11b+ granulocytes emitting a fluorescence around 585 nm were considered as neutrophils that had phagocytosed particles.

ROS release

BMC were isolated and pretreated as described above. The cells were loaded with 2 μ M Dihydrorhodamine 123 (DHR 123) (Sigma Aldrich, Germany) for 10 min. The cells were put on ice to stop the reaction and washed twice before antibody staining. The cells were kept on ice during the whole staining procedure. Ly6G+/CD11b+ granulocytes were analyzed for their green fluorescence (Mean Fluorescence Intensity, MFI of DHR 123).

NETosis assay

BMC were isolated and pretreated as described. They were then exposed to 100 ng/mL Phorbol 12-myristate 13-acetate (PMA, Sigma Aldrich, Germany) for 3 hours at 37°C. After washing and fixing in 1% PFA for 5 min, the cells were resuspended in blocking buffer and stained with a primary H3 antibody for 30 min at room temperature. Following another wash, cells were incubated with Alexa Fluor 700-conjugated antibodies against H3, FITC-conjugated anti-MPO antibodies, surface markers Ly6G, and CD11b for 30 min, then analyzed by flow cytometry. Ly6G+/CD11b+/H3+/MPO+ cells were identified as NETosing cells.

Apoptosis assay

BMC were isolated and pretreated as described above. The cells were stimulated with 100 ng/mL PMA (Sigma Aldrich, Germany) for 3 hours at 37°C. The cells were pelleted, washed, and first stained with anti-Ly6G and anti-CD11b antibodies. Then, the cells were stained with a Fixable Viability Stain (FVS) according to the manufacturer's instructions. Then, active caspase 3 was stained according to the manufacturer's instructions (FITC Active Caspase-3 Apoptosis Kit, Becton Dickinson, USA). Cells were identified as follows: viable (FVS-/casp3-), apoptotic (FVS+/casp3+), necrotic (FVS+/casp3-) cells.

IL-10 and TNF- α release

BMC were isolated and pretreated as described above and stimulated with 100 ng/mL LPS for 24 hours at 37°C. The supernatants were analyzed for IL-10 and TNF- α levels using a Cytometric Bead Array Kit (Mouse Inflammation Kit, Becton Dickinson) according to the manufacturer's instructions.

Statistical analysis

Data were analyzed using GraphPad Prism Version 5.03 (GraphPad Software Inc., USA). Linear regressions for standard curves were fit with Microsoft Excel 365 (Microsoft, USA). Data in scatter or bar plots are expressed as mean \pm standard deviation (SD). Non-parametric tests (Mann-Whitney and Kruskal-Wallis test) were used for experiments with one factor. Experiments with two factors were compared with one- or two-way ANOVA with Dunn's or Bonferroni posttests. To account for multiple comparisons, as is the case in chemotaxis and phagocytosis assays, we report the adjusted significance level when one dataset was compared to multiple others (12). We considered test results with a p-value < 0.05 statistically significant. Statistical analysis focused on the differences between PBS- and CDNP-treated BMN. Figure 5 compares CDNP⁻ and CDNP⁺ BMN. All significant and nonsignificant changes are shown in the figure's graphs. We used OpenAI's ChatGPT (version as of December 2024) for its assistance in language editing.

Results

Bone marrow neutrophils recognize CDNPs but exhibit only transient activation

CD11b, an established early activation marker for neutrophils, has been shown to have increased expression in response to CDNPs during ongoing inflammation in sepsis (10). To find out whether CDNPs would impact CD11b expression under steady-state conditions, we cultured BMC from naïve C57BL/6 mice and exposed them to CDNPs for 45 min, 3 hours, and 24 hours. Neutrophils were identified by their expression of CD11b and Ly6G (referred to as BMN, Figure 1A). The results depicted in Figure 1B reveal that even though CD11b is constitutively expressed on BMN, CDNPs increase its expression rapidly 45 min after starting the culture. This augmented CD11b expression persisted for 3 hours but ceased after 24 hours. Notably, both groups exhibited a transient decrease in CD11b expression after 3 hours of culturing. This phenomenon resolved after 24 hours of culture and might be attributed to the adaptation process to the culture flasks. To mimic inflammatory conditions LPS was added to the cultures for 24 hours after a 45 min preincubation period with either CDNPs or vehicle. A 3.5-fold increased expression of CD11b was found in the control group, which was lowered significantly by the presence of CDNPs (Figure 1C). Finally, we determined whether CDNPs would affect the viability of BMN during the 3 hours and 24 hours culture period. BMN were stained with Fixable Viability Stain (FVS) and caspase 3 to assess the percentage of viable and apoptotic cells. The percentage of apoptotic cells increased by 8.5% in the PBS group and slightly higher (9%) in the CDNP group within 24 hours but was not significantly different between the two groups (Figures 1D, E). In summary, the initial upregulation of CD11b expression indicates that BMN recognize CDNPs. This recognition leads to a transient activation and is followed by a diminished responsiveness to LPS at later time points without compromising the cell viability.

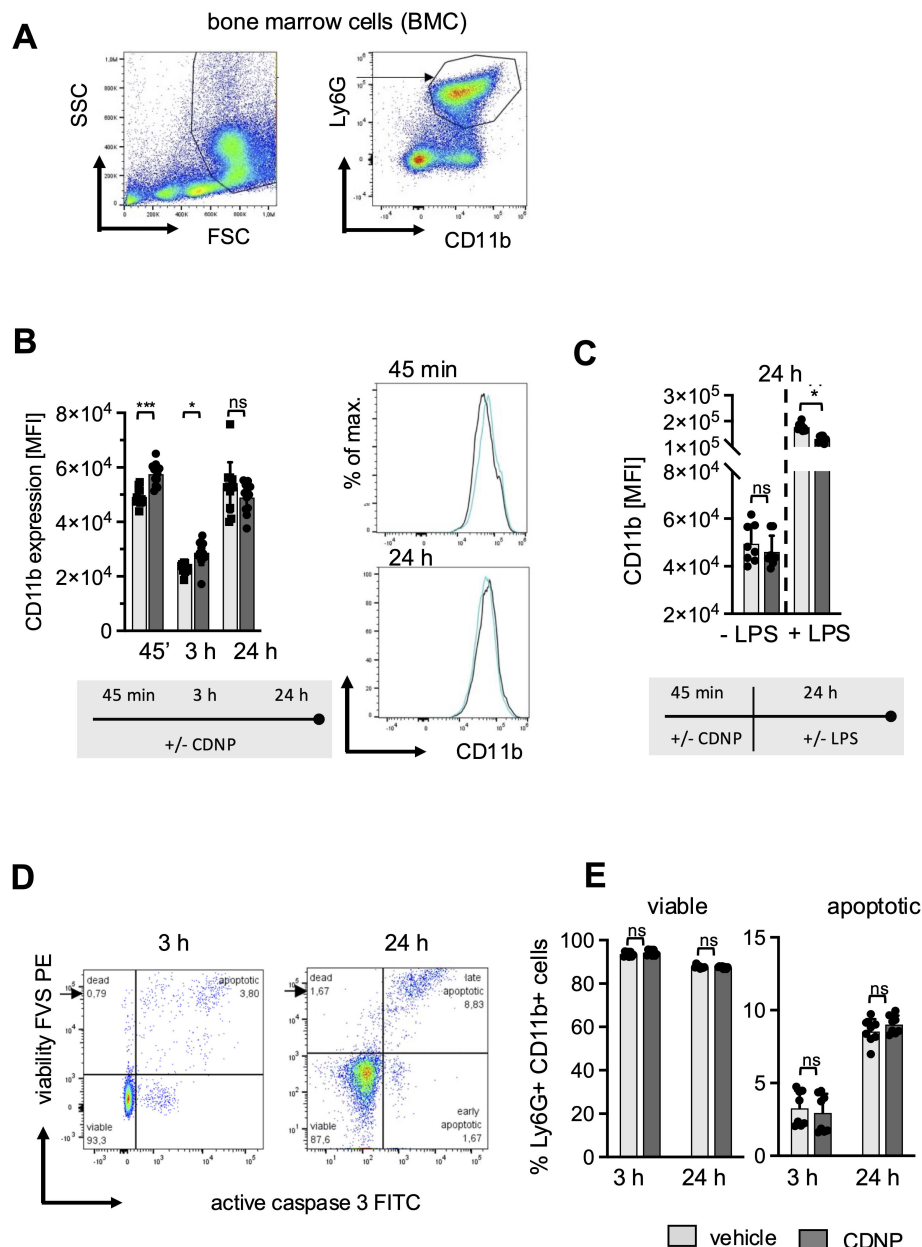


FIGURE 1

CDNPs activate Ly6G+CD11b+ BMN rapidly and transiently without affecting cell viability. BMC from C57BL/6 mice were incubated with 10 μ g/mL CDNPs and analyzed at indicated time points. **(A)** BMN were identified as Ly6G+CD11b+ cells by flow cytometry as depicted. **(B)** The MFI of CD11b in BMN was measured 45 min, 3 hours, or 24 hours after incubation with CDNPs. Representative histograms are shown for 45 min and 24 hours (right). **(C)** The MFI of CD11b was measured in BMN after preincubation with 10 μ g/mL CDNPs for 45 min following addition of 100 ng/mL LPS and culture for 24 hours. **(D)** The percentage of viable and apoptotic Ly6G+CD11b+ BMN was determined by staining with Fixable Viability Stain (FVS) and an anti-active caspase-3 antibody, 3 hours and 24 hours after incubation. A representative dot plot is shown (viable: FVS-Casp3⁻; apoptotic: FVS-Casp3⁺). **(E)** Data obtained in **(D)** are expressed as mean \pm SD. Data from 2 independent experiments with $n = 8-12$ (2 \times 4-6 pseudo-replicates) are expressed as mean \pm SD. Significance was determined with two-way ANOVA and Bonferroni post-tests. * $p < 0.05$, *** $p < 0.001$. Bars: PBS (pale gray), CDNP (dark gray). The incubation periods are illustrated below the graphs.

CDNPs do not induce classical effector functions in BMN but stimulate the secretion of IL-10

The biphasic behavior of CD11b expression on BMN upon exposure to CDNPs raises the question of whether CDNPs promote further inflammatory responses in neutrophils.

Considering the particulate structure and intracellular content of CDNPs, one would anticipate that CDNPs act as DAMPs and trigger antimicrobial effector functions. To explore this further, phagocytosis, ROS release, and cytokine expression were assessed in BMN subjected to a 45-minute preincubation with CDNPs. The impact of CDNPs on phagocytosis was evaluated using two complementary assays. The first method assessed the direct

uptake of fluorescently labeled *E. coli* (Alexa 488) by neutrophils, providing a straightforward measure of phagocytic activity. In this assay, approximately 24% of BMN internalized *E. coli* within 15 minutes. In CDNP-treated cells, this uptake slightly decreased to 22%, though the difference was not statistically significant (Figure 2A; Supplementary Figure 1). To confirm that the

observed uptake reflected true internalization rather than surface binding, the second assay used pHrodoTM-labeled *E. coli*. This dye fluoresces only upon entry into the endosomal compartment, allowing a more specific assessment of bacterial ingestion. In this method, LPS was added. Over extended incubation periods (45 min and 24 hours), the percentage of

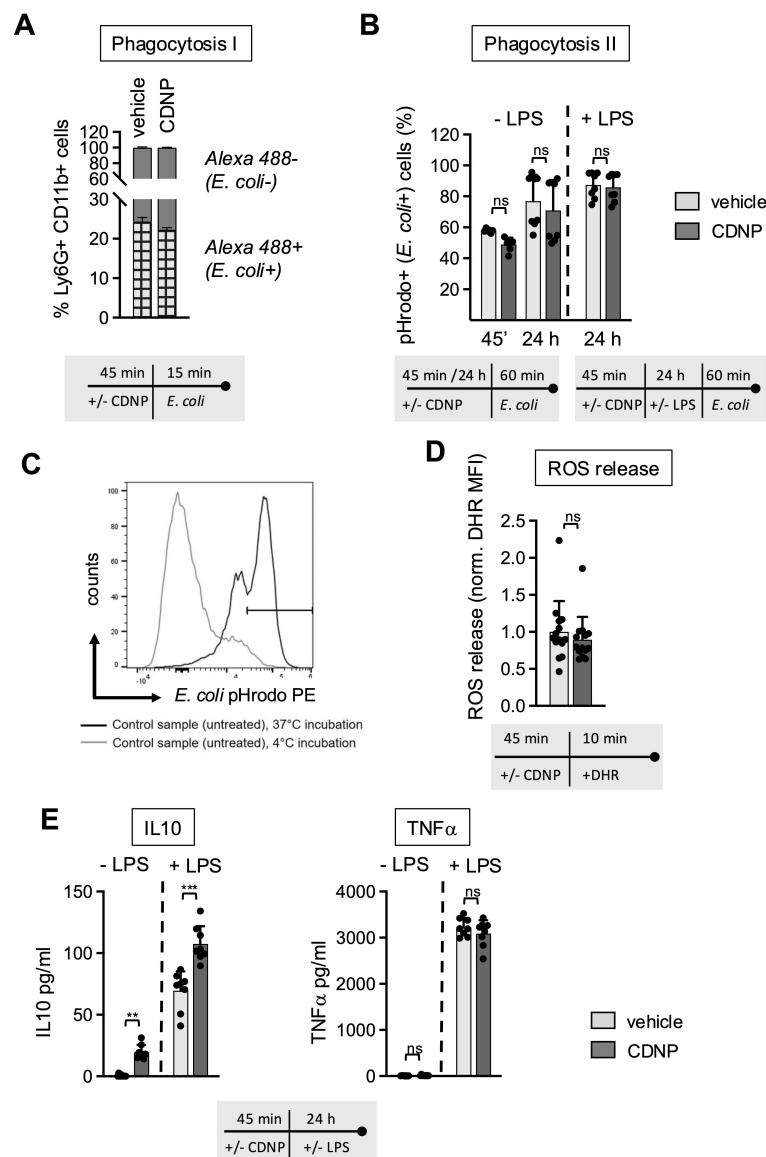


FIGURE 2

CDNPs do not induce antimicrobial effector functions; instead, they support the secretion of IL-10. (A–E) BMC from C57BL/6 mice were preincubated with 10 µg/mL CDNPs for 45 min and subsequently treated as described. (A) Opsonized, Alexa Fluor 488-positive *E. coli* particles were added to CDNP-preincubated BMC and incubated for an additional 15 min. The percentage of Ly6G+CD11b+Alexa Fluor 488+ BMN (checked bar) was determined using flow cytometry before and after treatment with trypan blue (Supplementary Figure 1). (B) To exclude surface-bound *E. coli* from analysis, CDNP-preincubated BMC were exposed directly to pHrodoTM Red *E. coli* BioparticlesTM conjugates for 60 min without LPS (left bars) or cultured for an additional 24 hours with addition of 100 ng/mL LPS before exposure to pHrodoTM Red *E. coli* BioparticlesTM conjugates for 60 min (right). The percentage of Ly6G+CD11b+pHrodo+ (587 nm) BMN was determined by flow cytometry. (C) A representative plot for incubation at 37°C and 4°C is shown. (D) Intracellular ROS release in Ly6G+CD11b+BMN was measured by staining CDNP-preincubated cells with DHR 123 for 10 min at 37°C. The MFI of DHR 123 was measured using flow cytometry. (E) BMC were incubated with 10 µg/mL CDNPs for 45 min and cultured without further stimulation or with 100 ng/mL LPS for 24 hours. IL-10 and TNF-α were analyzed in the supernatant using a Cytometric Bead Array. Data are expressed as mean ± SD, pooled data from 2 independent experiments with n = 8 (2 × 4 pseudo-replicates) per group. Data in (D) were pooled from 3 independent experiments with n=14 (2 × 4 and 1 × 6). Significance was determined with a two-way-ANOVA. ** p < 0.01 *** p < 0.001, adjusted significance level α(k=2) = 0.025. Bars: PBS (pale gray), CDNP (dark gray). The incubation periods are illustrated below the graphs. ns means not significant.

BMN that internalized pHrodoTM-labeled *E. coli* increased from roughly 50% to 80%. Notably, no differences were observed between CDNP-treated and control cells, even after 24 hours of LPS exposure (Figures 2B, C). To assess whether CDNPs induce the production of reactive oxygen species, we compared the levels of oxidized Dihydrorhodamine by measuring the intracellular Mean Fluorescence Intensity (MFI). Interestingly, no effect on ROS release was found in CDNPs-treated BMN (Figure 2D). Next, we assessed the secretion of the anti-inflammatory cytokine IL-10 and the pro-inflammatory cytokine TNF- α . As shown in Figure 2E, CDNP treatment alone stimulated the secretion of IL-10 while not affecting TNF- α levels. This pattern became more pronounced upon stimulation with LPS. A marked elevation of IL-10 secretion was found in the CDNP-treated BMC, whereas TNF- α levels remained unchanged when compared to the control group. These findings, together with the data on phagocytosis and ROS release, suggest that CDNPs do not activate BMN. Instead, CDNPs rather enhance the regulatory activities of BMN.

CDNPs shift the PMA-induced cell death toward apoptosis

Next, we investigated whether CDNPs would impact the mode of cell death in BMN and introduced PMA to the cultures. PMA is known to induce the release of NETs while simultaneously initiating the process of neutrophil death (13, 14). BMN were preincubated for 45 min with CDNPs and cultured for an additional 3 hours with or without the addition of PMA. As shown in Figure 3, PMA induced the release of NETs in approximately 60% of the BMN, as judged by Histone 3 (H3) and Myeloperoxidase (MPO) positivity. CDNPs alone did not induce NETs and did not influence the PMA-induced NET release (Figure 3A). To differentiate between necrotic and apoptotic BMN, a live-dead staining (FVS) and caspase 3 staining for the detection of necrotic cells and apoptotic cells, respectively, were used (Figure 3B). As depicted in Figure 3C, PMA activation induced cell death in approximately 37% of the cells. Significantly more dead BMN (51%) were found in the CDNP-treated group. However, upon comparing the incidence of apoptotic and necrotic BMN, it becomes obvious that the presence of CDNPs shifted the cell death toward apoptosis (Figure 3C).

CDNPs enhance the antigen-presenting capacity of BMN by increasing the expression of CD80

After having established that the CDNP-induced early increase in CD11b expression on BMN is not followed by a full-scale activation but rather by a transition to a less responsive phenotype, the question arises whether other surface molecules, especially those involved in more regulatory functions, would be modulated by exposure to CDNPs. We chose CD80, CD86, and MHCII as markers for antigen presentation and the adhesion molecule CD54 (ICAM-1), primarily expressed on activated and aged neutrophils, and monitored their expression for 45 min,

3 hours, and 24 hours (4, 15–17). As shown in Figure 4, CD80, constitutively expressed on all BMN (18, 19), exhibited a 2.5-fold increase in expression after 45 min of culture with CDNPs compared to the control group. Exposure to CDNPs not only accelerated but also augmented CD80 expression during the complete culture period (Figure 4A). In contrast, CDNPs did not markedly affect MHC II, CD86, or CD54 expression at any time point. All three markers increased over time in the control and CDNP-treated groups from approximately 5% after 45 min to 20% after 24 hours (Figures 4B–D; Supplementary Figure 2). A slight yet significant reduction of CD54 expressing BMN was observed in the CDNP-treated group (Figure 4D). CD54 is known for its role in mediating adhesion during the transmigration of endothelial cells (17, 20). To investigate whether the emergence of these 20% aged CD54+ BMN would affect the migratory behavior, we conducted transmigration assays. Because CD54 expression correlates with the chemokine receptor CXCR4 we exposed BMN to CXCL12, a ligand for CXCR4 (21, 22). Following a 45-min incubation with CDNPs or vehicle, BMN were either directly exposed to CXCL12 for 3 hours or cultured for an additional 24 hours with or without LPS, then exposed to CXCL12 for 3 hours (Figure 4E). No significant changes could be observed. Regardless of the culture duration, 40–67% of the BMN migrated towards CXCL12, with LPS addition showing no impact. Notably, although not statistically significant, the number of migrating BMN increased slightly and CDNP-treated groups tended to migrate to a lesser extent than the controls after 24 hours of culture, irrespective of the presence of LPS. In summary, CDNPs selectively upregulated CD80 in synergy with aging while leaving other antigen presenting markers unaffected.

CDNPs are specifically ingested by CD54+ neutrophils that do not migrate towards CXCL12

Previous reports have indicated that CD54 expression on neutrophils correlates not only with aging but also with increased phagocytic activity (16, 17). To investigate whether this also applies to the ingestion of CDNPs, we labeled CDNPs with CFSE prior to preincubation with BMC for 45 min. The cells were then cultured for an additional 24 hours, with or without LPS stimulation, and CD54 expression was assessed on CDNP⁺ and CDNP[−] BMN. Overall, approximately 26% of BMN ingested CDNPs, indicated by CFSE positivity (CDNP⁺ BMN), a situation that did not increase with the addition of LPS (Figure 5A). Interestingly, 60% of this CDNP⁺ BMN population expressed CD54, while none of the CDNP[−] BMN did. Upon LPS addition, the CD54+ phenotype was induced in almost 90% of the CDNP[−] BMN, increasing to nearly 100% in the CDNP⁺ BMN population (Figure 5B). CDNPs were apparently preferentially ingested by CD54+ BMN. We also investigated whether CDNP⁺ BMN and CDNP[−] BMN differed in their migratory capacity. Remarkably, CDNP⁺ BMN completely failed to migrate in response to CXCL12 (Figure 5C). Further phenotypical analysis revealed that 50–60% of the CDNP⁺ BMN expressed CD86 and MHCII, respectively, which were not found in

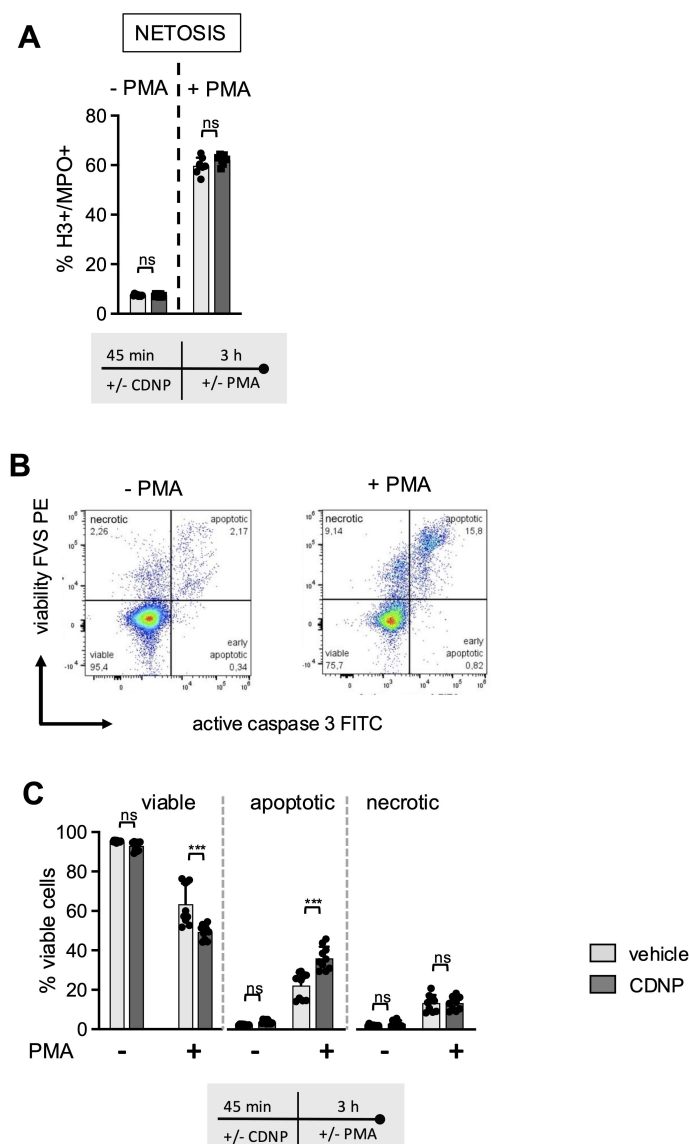


FIGURE 3

CDNPs shift PMA induced cell death in Ly6G+CD11b+BMN towards apoptosis. (A–C) BMC from C57BL/6 mice were preincubated with 10 µg/mL CDNPs for 45 min and subsequently stimulated with 100ng/mL PMA for 3 hours. (A) NET formation was identified by staining with fluorescently labeled antibodies against H3 and MPO (H3+/MPO+) in Ly6G+CD11b+ BMN. (B) A representative dot plot of vehicle-treated BMN is shown. Cell death rates within the Ly6G+CD11b+ cell population were determined by flow cytometry using FVS and active caspase 3 (casp3) (viable: FVS-casp3-; apoptotic: FVS+casp3+; necrotic: FVS+casp3-). (C) Data obtained in (B) are expressed as mean ± SD, pooled data from 2 independent experiments with n = 10 (2 x 5 pseudo-replicates) per group. Significance was determined with a two-way ANOVA with Bonferroni posttests. *** p < 0.001. In (A) for the PMA treated group n = 7–8 (2 x 3–4 pseudo-replicates) are shown. One pair of values was excluded in the PMA treated group because the CDNP-treated sample had apparently not been stimulated with PMA. Bars: PBS (pale gray), CDNP (dark gray). The incubation periods are illustrated below the graphs. ns means not significant.

the CDNP⁺ BMN population. Unlike the effect on CD54 expression, LPS did not affect CD86 and MHCII expression (Figure 5D). This situation was different for CD80, which was significantly higher (4.6-fold) expressed in the CDNP⁺ BMN without activation. LPS stimulation increased CD80 expression levels in both CDNP⁺ and CDNP⁻ BMN (Figure 5E). Next, we assessed the expression levels of the activation marker CD11b in CDNP⁺ and CDNP⁻ BMN. In contrast to the increased expression of CD54, as well as CD80, CD86, and MHCII, there was no difference in CD11b expression between CDNP⁺ and CDNP⁻ BMN (Figure 5F). Moreover, the

expression of CD11b decreased in the CDNP⁺ BMN upon LPS stimulation. These data demonstrate that CDNPs are selectively ingested by a distinct subset of BMN that exhibits an aged phenotype (CD54+), possesses antigen-presenting features (MHCII+, CD86+), and lacks the ability to migrate in response to CXCL12. Additionally, the expression of CD80 was increased in CDNP⁺ BMN without further stimulation, while the LPS-induced upregulation of CD11b was impaired in CDNP⁺ BMN. Finally, considering the shift towards apoptosis observed in PMA-induced cell death and the complete lack of migration towards CXCL12, we

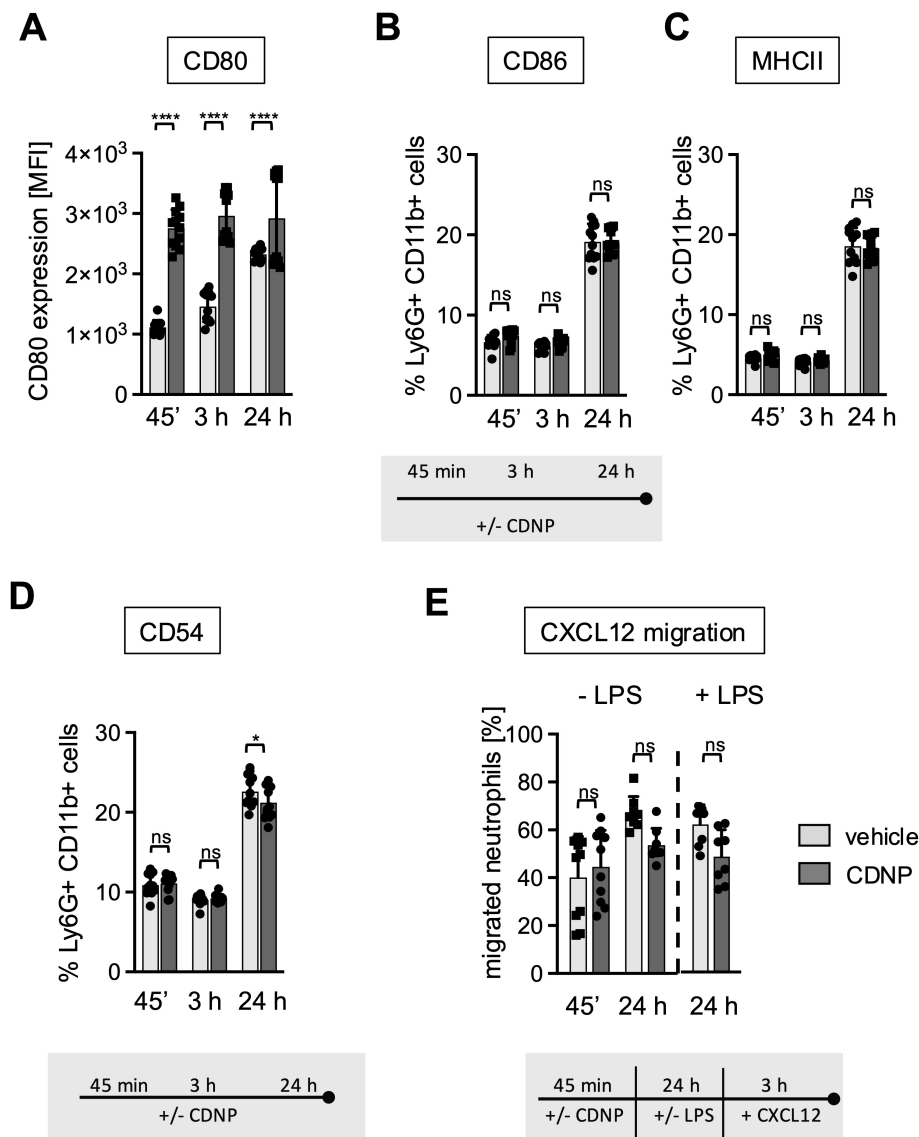


FIGURE 4

20% of BMN mature to a CD86⁺/MHCII⁺/CD54⁺ subset during culture. (A–D) BMC from C57BL/6 mice were incubated with 10 µg/mL CDNPs for 45 min, 3 hours or 24 hours. (A) The MFI of CD80 expression and (B–D) The percentage of MHCII, CD86 and CD54 expressing BMN was determined by flow cytometric analysis. Representative histograms for CD80, CD86, MHCII, and CD54 are shown in [Supplementary Figure 2](#). (E) Following exposure to CDNPs for 45 min and subsequent culture for 24 hours with or without 100 ng/mL LPS, BMC were stimulated with 100 ng/mL of CXCL12 for 3 h in transwell plates. The percentage of migrated BMN was calculated by flow cytometry. Data are expressed as mean ± SD, pooled data from 2 independent experiments with n = 8–12 (2 × 4–6 pseudo-replicates) per group. Significance was determined with a two-way ANOVA with Bonferroni post-tests. * p < 0.05, **** p < 0.0001, adjusted significance level α (k=2) = 0.025. Bars: PBS (pale gray), CDNP (dark gray). The incubation periods are illustrated between the graphs. ns means not significant.

hypothesized that CDNP⁺ BMN might exhibit a higher rate of apoptosis compared to their CDNP⁻ BMN counterparts. Indeed, analysis of active caspase 3 reveals that 76% of the CDNP⁺ BMN undergo apoptosis within 24 hours in culture, which is not found in the CDNP⁻ BMN ([Figures 6A, B](#)).

In summary, contrary to the current view that intracellular contents act as DAMPs that trigger sterile inflammation, our data indicate that when intracellular content in the form of CDNPs are released into the extracellular space and recognized by innate immune cells, they can induce also anti-inflammatory effects. The recognition of CDNPs by BMN induces a rapid but transient

activation, followed by the development of a regulatory and/or apoptotic phenotype. Importantly, this CDNP-induced modulation of BMN reduces further activation by LPS.

Discussion

Based on previous findings that CDNPs play a regulatory role in inflammation, notably in an autoimmune mouse model for local wound healing and in the systemic CLP model, a condition of severe systemic immune dysregulation, we hypothesized they would have a

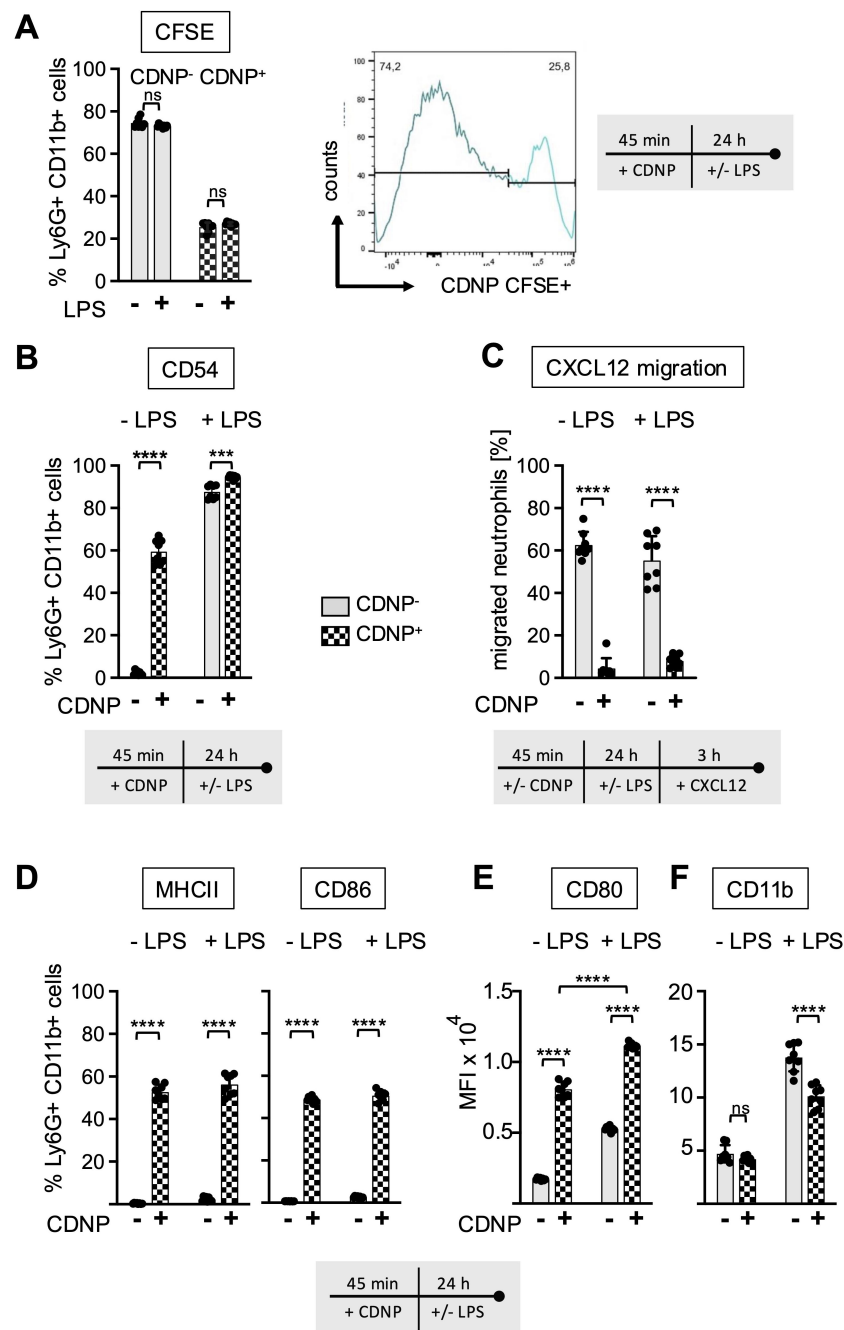


FIGURE 5

CDNPs are internalized by 26% of BMN and modulate their expression of CD80 and CD11b. BMC from C57BL/6 mice were preincubated with 10 µg/mL CFSE-labeled CDNPs for 45 min and subsequently cultured with or without LPS for 24 hours (A) The percentage of the CFSE-labeled subset among the Ly6G+CD11b+ BMN was determined by flow cytometry. To establish that CFSE-labeled CDNPs were internalized rather than surface-bound, samples were analyzed before and after treatment with trypan blue in initial experiments (Supplementary Figure 3). (B) The percentage of CD54 expressing cells in CFSE- (CDNP-) and CFSE+ (CDNP+) BMN is shown. (C) Following exposure to CDNPs for 45 min and subsequent culture for 24 h with or without 100ng/mL LPS, BMC were stimulated with 100 ng/mL of CXCL12 for 3 h in transwell plates. The percentage of migrated CDNP- and CDNP+ BMN was calculated by flow cytometry. (D) The percentage of CD86 and MHCII expressing cells in CDNP- and CDNP+ BMN is shown. Representative histograms for CD80, CD86, MHCII and CD54 are shown in Supplementary Figure 4. (E, F) The MFI of CD11b (E) and CD80 (F) was assessed in CDNP- and CDNP+ BMN. Data are presented as mean \pm SD, pooled data from 2 independent experiments with $n = 8-12$ (2 \times 4-6 pseudo-replicates) per group. Significance was determined with a two-way with Bonferroni posttests. *** $p < 0.001$; **** $p < 0.0001$. Bars: CDNP- BMN (pale gray), CDNP+ BMN (patterned). The incubation periods are illustrated below the graphs. Supplementary Figure 3 provides additional information on the quenching of surface-bound CFSE. The incubation periods are illustrated below the graphs or in (A) on the right side. ns means not significant.

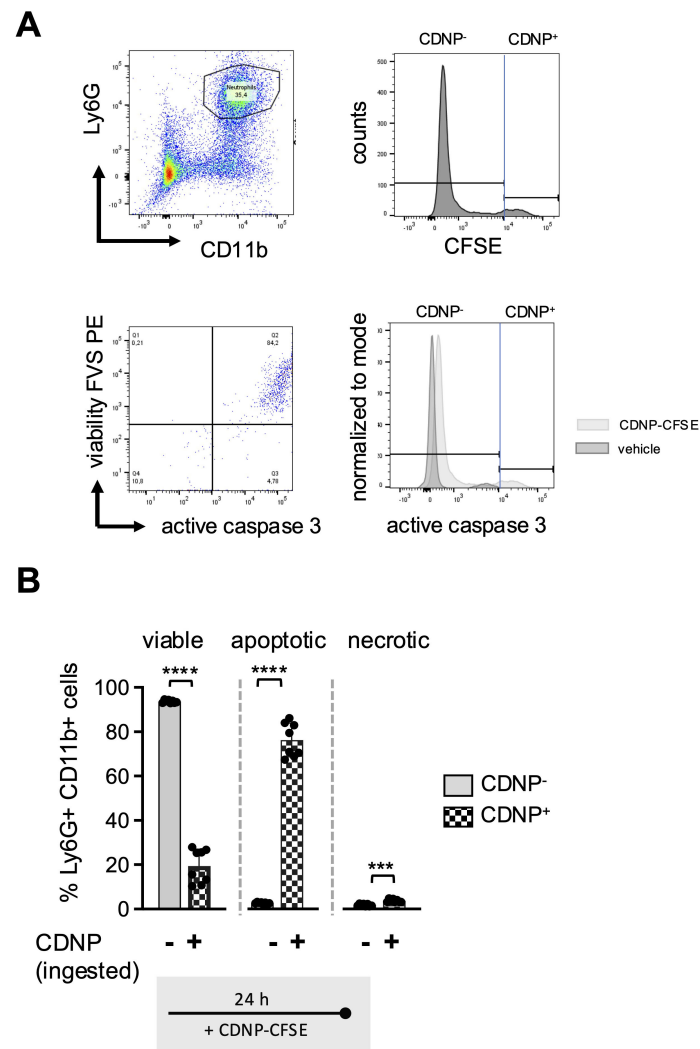


FIGURE 6

80% of the CDNP+BMN become apoptotic. BMC from C57BL/6 mice were preincubated with 10 μ g/mL CFSE-labeled CDNPs for 45 min and subsequently cultured for 24 hours. The percentage of the CFSE-labeled subset among the Ly6G⁺CD11b⁺ BMN was determined by flow cytometry. To establish that CFSE-labeled CDNPs were internalized rather than surface-bound, samples were analyzed before and after treatment with trypan blue in initial experiments (Supplementary Figure 3). (A) Dot plot and histograms show a representative example of the percentage of the CFSE-labeled BMN subset within the Ly6G⁺CD11b⁺ BMNs (upper panel), as well as the distribution of viable, apoptotic, and necrotic BMNs within the CDNP⁻ and CDNP⁺ Ly6G⁺CD11b⁺ cell population, identified by staining with FVS and an active caspase-3 antibody. Viable cells were defined as FVS⁻Casp3⁻, apoptotic cells as FVS⁺Casp3⁺, and necrotic cells as FVS⁺Casp3⁻ (lower panel). (B) The percentage of viable apoptotic and necrotic cells in CFSE⁻ (CDNP⁻) and CFSE⁺ (CDNP⁺) BMN is shown. Data are presented as mean \pm SD, pooled data from 2 independent experiments with n = 8–12 (2 \times 4–6 pseudo-replicates) per group. Significance was determined with a Kruskal-Wallis test. *** p < 0.001; **** p < 0.0001. Bars: CDNP⁻ BMN (pale gray), CDNP⁺ BMN (patterned).

similar regulatory impact on the function of neutrophils (9, 10). Neutrophils are the main driver cells in both clinical settings (23–25), but the impact of CDNPs on neutrophils under steady state conditions has not been investigated in detail. To find out, we used freshly isolated BMC from healthy mice and cultured them directly without further purification to prevent any kind of pre-activation (26). The exposure of these cultured BMC to CDNPs revealed three major findings: CDNPs (i) induce a transient upregulation and downregulation of CD11b without triggering effector functions; (ii) promote regulatory functions such as secretion of IL-10, a shift toward apoptosis, and upregulation of the antigen-presenting

molecule CD80; and (iii) are predominantly ingested by CD54+ non-migrating BMN cells, which undergo apoptosis within 24 hours.

Our first results reveal that CDNPs are readily recognized by resting BMN in culture, as evidenced by the upregulation of CD11b within 45 min, which persisted for 3 hours before ceasing after 24 hours (Figure 1B). CD11b, the α -chain of the β 2-integrin Mac-1, on the surface of neutrophils, is primarily associated with neutrophil adhesion and migration into tissues. It is also linked with degranulation of secretory vesicles, phagocytosis, and superoxide production (27–29). Despite a slight but statistically insignificant decrease in migration, no significant impact on these classical

effector functions was observed in the CDNP-treated groups (Figures 2A–D, 3A, 4E). It is plausible that the transient increase in CD11b expression results from the activation of danger-sensing receptors that recognize CDNPs as DAMPs. However, this signaling seems insufficient to induce full activation. Interestingly, the addition of LPS to the culture medium suppressed CD11b expression, suggesting that additional stimulation is not the key to triggering effector functions via CDNPs. Instead, CDNPs may shift BMN from an activated state to a hyporesponsive state of tolerance (Figure 1C). This indicates that it is not the absence of supplementary signals needed for full activation, but rather that CDNPs potentially induce a state of tolerance in BMN. Another explanation could be the shedding of surface markers due to CDNP-induced apoptosis. However, this seems unlikely, as CDNP⁺ BMN undergoing apoptosis express specific surface markers that are not found on the CDNP[−] BMN population (Figures 5B, D, E).

Secondly, corresponding with the lack of effector functions in the CDNP-treated groups, we observed a significant increase in IL-10 secretion in the BMC (Figure 2E) and a proapoptotic effect during the PMA-induced cell death (Figure 3C). The secretion of both cytokines was elevated upon exposure to LPS. This increase of IL10 expression following LPS exposure might be explained by the involvement of type I interferons (30). The elevated expression of IL10 in response to CDNP supports the notion that CDNPs induce not only a hyporesponsive but rather a regulatory phenotype of neutrophils that contributes to the resolution of ongoing inflammation. The concept that extracellularly appearing endogenous proteins can have resolving capacities has been previously reported. For instance, it has been reported that HSP27, S100 proteins, or vimentin (31–34) induce IL-10, and annexin A1 has proapoptotic effects (35). MALDI-TOF analysis revealed that CDNPs contain plentiful proteins, including those mentioned above as potential initiators of resolution. These proteins include annexins, S100 proteins, heat shock proteins, calreticulin, and HMGB1 (10) (Data not shown). The question arises whether these individual intracellular proteins would have similar effects when compared to multicomponent particles such as CDNPs. Notably, the most abundant proteins in CDNPs are the members of the Annexin family. Therefore, we specifically investigated whether Annexin A1 and Annexin A5 could individually induce some of the observed CDNP-induced effects on BMN. Culturing BMN with recombinantly produced Annexin A1 and Annexin A5 showed no effect on CD11b expression (Supplementary Figure 5), or ROS release (Data not shown). Thus, despite their previously reported anti-inflammatory activities (35–37), Annexin A1 and A5 do not mimic the role of CDNPs in cultured BMN. These data support our hypothesis that intracellular content released upon inflammation or injury will exert its activity rather as multicomponent particles instead of individually soluble molecules. Furthermore, we found that CDNPs affected the antigen-presenting markers CD80, CD86, and MHC II unexpectedly: they selectively upregulated CD80 (Figure 4A). Specifically, CDNP-treated neutrophils expressed higher levels of CD80 at early and late time points (Figure 4A). In contrast, CD86 and MHC II showed a different expression

pattern: the initially low percentages of positive BMN increased after 24 hours of incubation, regardless of CDNP treatment (Figures 4B–D). The differing time points of CD80 and CD86 expression are particularly surprising because both molecules are typically upregulated on mature antigen-presenting cells to promote the T cell priming (38). However, distinct expression patterns of CD80 and CD86 have been reported, with CD80 notably associated with immunosuppressive effects (18, 19, 39). Consistent with this sequential expression, one study suggests that CD80 is the initial ligand responsible for maintaining aspects of immune tolerance through interactions with CTLA-4. The subsequent upregulation of CD86 follows as a result of inflammatory stimuli and can override this inhibition, leading to the T cell activation (40). Further research should explore the potential of CDNPs to modulate the interaction between neutrophils and T cells.

Our third finding reveals that CDNPs are selectively ingested by CD54⁺ BMN (Figure 5B) and that these CDNP⁺ BMN, in particular, are more prone to undergo apoptosis while simultaneously expressing antigen-presenting markers (Figures 5, 6). The expression of the adhesion molecule CD54 on neutrophils is primarily associated with their ability to perform reverse transendothelial migration from tissues into the circulation and potentially back to the bone marrow. Our data indicates that CDNP⁺ BMN do not respond to the chemotactic stimulus CXCL12, even though 60% of CDNP⁺ BMN express CD54 under normal conditions, and 90–100% express CD54 following LPS stimulation (Figures 5B, C). This lack of migration might be due to the apoptotic phenotype of CDNP⁺ BMN. Furthermore, recent studies have demonstrated that CD54 is associated with phagocytic activity in human and murine neutrophils (17). This raises the question of whether phagocytosis of CDNPs upregulates CD54 or if CD54⁺ BMN preferentially ingest CDNPs. Resolving this question is challenging. On one hand, CD54 expression increases in 20% of BMN over time, with significantly lower expression observed in the CDNP-treated group (Figure 4D). On the other hand, CD54 expression is restricted to CDNP⁺ BMN and is strongly upregulated upon LPS stimulation (Figure 5B). To further investigate the effect of phagocytosis on CD54 expression, we compared the MFI of CD54 on BMN after ingestion of pHrodo-labeled *E. coli* particles and incubation with CDNPs, LPS, or both (see experimental setup in Figure 2B). Interestingly, uptake of *E. coli* particles alone did not affect CD54 expression (Supplementary Figure 6). However, LPS stimulation independently increased CD54 expression on BMN, irrespective of *E. coli* particle exposure. These findings indicate that phagocytosis alone does not enhance CD54 expression, suggesting that BMN may already express CD54 prior to CDNP ingestion (Figure 5B). Further studies are needed to explore this hypothesis in greater depth. Regarding the effect of CDNPs on CD54 expression, we observed notable variability and no significant changes. Pre-incubation with CDNPs for 45 minutes prior to LPS exposure tended to reduce CD54 expression in both pHrodo[−] (*E. coli*[−]) and pHrodo⁺ (*E. coli*⁺) BMN, though the reduction was not statistically significant. However, it eliminated the significance between unstimulated and LPS-stimulated pHrodo[−] (*E. coli*[−]) and pHrodo⁺ (*E. coli*⁺) BMN.

These findings suggest that CDNPs might contribute to the modulation of CD54 expression in a context-dependent manner, primarily in BMN that have internalized CDNPs. In addition to its role in phagocytosis, CD54 may also facilitate interactions with T cells during priming by promoting binding to T cells (41, 42). Consistent with the enhanced CD54 expression observed in approximately 20% of BMN after 24 h of culturing, similar trends were noted for CD86 and MHCII (Figures 4B–D). The acquisition of antigen-presenting markers and the loss of chemotactic responses in a fraction of neutrophils over time have been previously reported (43). Given the apoptotic phenotype of most of the CDNP⁺ BMN, the question arises: What occurs within a natural microenvironment? Do CDNP⁺ BMN interact directly with T cells before undergoing apoptosis, or are they first phagocytosed by tissue macrophages, which then go on to interact with T cells? Both possibilities are feasible. For example, it has been reported that neutrophils and T cells may encounter each other at sites of inflammation, where they might actively interact (42). One may speculate that upon ingestion, CDNPs are processed, and their proteins are presented as peptides in MHC II to T cells. Another possibility is that neutrophils that ingest intracellular proteins in form of CDNPs become apoptotic and are subsequently phagocytosed by tissue macrophages, which then develop a regulatory phenotype (3, 44). The effects of CDNPs on CD4 T cell differentiation have been demonstrated in murine wound healing and *Leishmania major* infection models, showing a systemic shift from Th1 to Th2 responses (9). However, while it is unlikely, it cannot be ruled out that neutrophils may play a role in antigen presentation. To investigate this further *in vitro*, macrophages, T cells and an inflammatory environment will be required, as the activation of CD4 T cells necessitates co-stimulation or the presence of an adjuvant (41, 42, 45). *In vitro* assays may be limited by the challenge of aligning the optimal timing and microenvironment for all cell types involved. Further, *in vivo* experiments will be needed to investigate whether and how CDNP⁺ neutrophils affect antigen presentation to CD4 T cells. Therefore, the activation and differentiation of CD4 T cells should be assessed by examining the expression of PD-1, Tox, IRF4, and CD44 (46), as well as the emergence of regulatory T cells. Additionally, it would be interesting to analyze the expression of MHC I on CDNP⁺ neutrophils and its potential effects on CD8 T cells. One of the most suitable *in vivo* models for studying neutrophil function and potential interactions with T cells is the acute respiratory distress syndrome (ARDS), in which a high number of neutrophils accumulate locally in the pulmonary microcirculation (46). In contrast to the CLP sepsis model, which affects the entire peritoneum, the LPS-induced ARDS mouse model allows for a focus on specific tissue niches, such as areas beneath and above the airway epithelium (47). LPS and CDNPs could be injected intratracheally. Additionally, B cell responses might also be influenced by CDNP exposure, given their role as antigen-presenting cells, with or without T cell help. Our lab previously demonstrated that the injection of CDNPs in the *Leishmania major* model shifted *Leishmania major*-specific IgG subclasses from IgG2 to IgG1 (9).

In summary, our data indicate that neutrophil stimulation does not necessarily lead to their complete activation. Instead, it progresses through a multistep process that can be modulated at specific stages. Recent evidence suggests that the tissue microenvironment, particularly specific tissue niches, drives neutrophil heterogeneity and functionality (2). It is plausible that during insults such as infection, immune complex deposition, or tissue injury that provoke neutrophil immigration, each neutrophil is exposed to a distinct tissue microenvironment. Some neutrophils may bind directly to pathogens, immune complexes, or freshly released cell debris via their pattern recognition receptors or Fc gamma receptors, leading to full-scale activation. Other neutrophils might ingest released intracellular content or cell debris that have been modified by exposure to ROS or derive from the release of NETs and develop into a regulatory phenotype. Our data show that CDNPs modulate the expression of surface markers and induce apoptosis in neutrophils. As the response progresses, these modified neutrophils may become predominant, contributing to the resolution of inflammation, potentially by undergoing apoptosis and regulating tissue macrophages through efferocytosis (44, 46). This scenario aligns with prior findings suggesting that extracellular appearing intracellular proteins can serve as both DAMPs and SAMPs (solution-associated molecular patterns), initially triggering an injury-induced response followed by the restoration of homeostasis (48). It has been suggested that neutrophils have the capacity to de-prime back to a basal state after initial priming and may even undergo cycles of priming and de-priming (46). One could speculate that CDNPs might be one of the potential factors supporting this de-priming process before they undergo apoptosis. Given that neutrophils undergo significant changes in cell shape during priming, it will be interesting to investigate the role of CDNPs in the early priming process. One possible approach would be to study the expression of aquaporins (AQP), specifically of AQP9, a molecule typically involved in the regulation of cell size. Assessing the expression of AQP9 could provide new insights (49). Moreover, future studies should aim to precisely define the components within CDNPs that mediate the effects during inflammation and determine whether individual proteins or combinations of several proteins are more effective. Several reports indicate that the therapeutic effects of individual DAMPs, such as HSP10 and HMGB1, were not confirmed in preclinical and early clinical trials (48, 50, 51). This outcome might differ for CDNPs, as they more accurately reflect the *in vivo* situation by consisting of multiple components.

One of the main limitations of this study is that BMN might be immature and not fully functional because they have not yet been released into the bloodstream. To determine whether mature neutrophils recognize CDNPs, we injected CDNPs nine times into the peritoneum of healthy mice. Two hours before harvesting the peritoneal cells, labeled CDNPs were injected. Despite high variability in the percentage of neutrophils migrating into the peritoneum (Supplementary Figure 7), we observed that approximately 22% of the neutrophils took up CDNPs and increased CD11b expression *in vivo* (Supplementary Figures 7A–D), consistent with the *in vitro* data. These results demonstrate that CDNPs interact with mature neutrophils *in vivo* under steady-state conditions, just as they do with the BMN cultures. Additionally, we

previously showed that CDNPs are taken up by neutrophils in the CLP model of sepsis, which improved the disease course by lowering IL-6 levels (10). Furthermore, under inflammatory conditions, such as sepsis, the involvement of immature neutrophils, rather than mature ones, is often observed (52). Another limitation of this study is that we did not investigate the potential underlying mechanisms. For example, to better understand how CDNPs affect apoptosis during the PMA-induced cell death (Figure 3), PMA could be replaced by Ionomycin. Ionomycin, a Ca^{2+} ionophore, induces NETosis and cell death more directly and rapidly compared to PMA, which activates protein kinase C in a slower and more sustained process.

Furthermore, unraveling the steps of CDPN-induced apoptosis following ingestion will be crucial to understand their role in potential therapeutic application. It can be speculated that CDNPs, particularly after uptake, interact with the autophagy process. In this context, the specific nature of the proteins present in CDNPs may not play a significant role (53, 54). However, these experiments were designed as a pilot study to provide preliminary insights into the modulatory effects of CDNPs on neutrophils, highlighting the need for further investigation in future studies. Recently, it has been proposed that dying cells do not release intracellular content randomly but in a concerted manner to fine-tune the immune response (55). Based on this hypothesis, CDNPs could be one of these factors, specifically composed to initiate the resolution of inflammation. The structural organization of intracellular molecules in these particles could target multiple signaling pathways in neutrophils (and potentially other immune cells) simultaneously, thereby eliciting a balanced immune response that favors resolution. Further studies will be needed to define how the release of CDNPs shapes local interactions within tissue niches and coordinates neutrophil fate.

Data availability statement

The raw data supporting the conclusions of this article will be made available by the authors, without undue reservation.

Ethics statement

All murine experiments were approved by the Institutional Animal Care and Use Committee of the University of Cincinnati (protocol no. 10-05-10-01) or the Ministry of Energy, Agriculture, the Environment, Nature and Digitalization of Schleswig-Holstein (Ministerium für Energiewende, Landwirtschaft, Umwelt, Natur und Digitalisierung Schleswig-Holstein) (protocol no. 1_2018-8-31_Kalies) and executed by certified personnel.

Author contributions

LR: Data curation, Investigation, Methodology, Visualization, Writing – original draft, Writing – review & editing. FB: Data

curation, Investigation, Methodology, Visualization, Writing – review & editing. CCC: Methodology, Resources, Conceptualization, Supervision, Funding acquisition, Writing – review & editing. KK: Methodology, Resources, Conceptualization, Supervision, Funding acquisition, Writing – original draft, Writing – review & editing. SA: Methodology, Resources, Writing – review & editing. KuK: Methodology, Resources, Writing – review & editing.

Funding

The author(s) declare financial support was received for the research, authorship, and/or publication of this article. This study was funded by the German Research Foundation (DFG) within the framework the graduate schools IRTG1911 and the RTG2633. We acknowledge financial support by the Land Schleswig-Holstein within the funding program Open Access Publikationsfonds.

Acknowledgments

We thank Holly Goetzmann for her technical assistance. We thank OpenAI's ChatGPT (version as of December 2024) for its assistance in language editing.

Conflict of interest

KK and KUK are part-time scientific consultants for Varicula Biotech GmbH. KUK is also a shareholder in Varicula Biotech GmbH. The preparation process of CDNPs has been filed as a provisional patent application by Varicula Biotech GmbH in Germany (P37052DE). KK is listed as an inventor. The study design, interpretation of data, and the final form of the manuscript were not influenced by Varicula Biotech GmbH.

The remaining authors declare that the research was conducted in the absence of any commercial or financial relationships that could be construed as a potential conflict of interest.

Publisher's note

All claims expressed in this article are solely those of the authors and do not necessarily represent those of their affiliated organizations, or those of the publisher, the editors and the reviewers. Any product that may be evaluated in this article, or claim that may be made by its manufacturer, is not guaranteed or endorsed by the publisher.

Supplementary material

The Supplementary Material for this article can be found online at: <https://www.frontiersin.org/articles/10.3389/fimmu.2024.1494400/full#supplementary-material>

References

- Siwicki M, Kubes P. Neutrophils in host defense, healing, and hypersensitivity: Dynamic cells within a dynamic host. *J Allergy Clin Immunol.* (2023) 151:634–55. doi: 10.1016/j.jaci.2022.12.004
- Silvestre-Roig C, Fridlender ZG, Glogauer M, Scapini P. Neutrophil diversity in health and disease. *Trends Immunol.* (2019) 40:565–83. doi: 10.1016/j.it.2019.04.012
- Korns D, Frasn SC, Fernandez-Boyanapalli R, Henson PM, Bratton DL. Modulation of macrophage efferocytosis in inflammation. *Front Immunol.* (2011) 2:57. doi: 10.3389/fimmu.2011.00057
- Li Y, Wang W, Yang F, Xu Y, Feng C, Zhao Y. The regulatory roles of neutrophils in adaptive immunity. *Cell Commun Signal.* (2019) 17:147–58. doi: 10.1186/s12964-019-0471-y
- Matzinger P. Tolerance, danger, and the extended family. *Annu Rev Immunol.* (1994) 12:991–1045. doi: 10.1146/annurev.iy.12.040194.005015
- Zindel J, Kubes P. DAMPs, PAMPs, and LAMPs in immunity and sterile inflammation. *Annu Rev Pathol.* (2020) 15:493–518. doi: 10.1146/annurev-pathmechdis-012419-032847
- Chen L, Zhao Y, Lai D, Zhang P, Yang Y, Li Y, et al. Neutrophil extracellular traps promote macrophage pyroptosis in sepsis. *Cell Death Dis.* (2018) 9:597. doi: 10.1038/s41419-018-0538-5
- Gong T, Liu L, Jiang W, Zhou R. DAMP-sensing receptors in sterile inflammation and inflammatory diseases. *Nat Rev Immunol.* (2020) 20:95–112. doi: 10.1038/s41577-019-0215-7
- Kunz N, Hauenschild E, Maass S, Kalies KU, Klinger M, Barra M, et al. Nanoparticles prepared from porcine cells support the healing of cutaneous inflammation in mice and wound re-epithelialization in human skin. *Exp Dermatol.* (2017) 26:1199–206. doi: 10.1111/exd.13450
- Kunz N, Xia BT, Kalies KU, Klinger M, Gemoll T, Habermann JK, et al. Cell-derived nanoparticles are endogenous modulators of sepsis with therapeutic potential. *Shock.* (2017) 48:346–54. doi: 10.1097/shk.0000000000000855
- Liu S TR, McClure S, Styba G, Shi Q, Jackowski G. Removal of endotoxin from recombinant protein preparations. *Clin Biochem.* (1997) 30:455–63. doi: 10.1016/S0009-9120(97)00049-0
- Sedgwick P. Multiple hypothesis testing and Bonferroni's correction. *BMJ.* (2014) 349:g6284. doi: 10.1136/bmj.g6284
- Damascena HL, Silveira WAA, Castro MS, Fontes W. Neutrophil activated by the famous and potent PMA (Phorbol myristate acetate). *Cells.* (2022) 11. doi: 10.3390/cells11182889
- Remijnsen Q, Vanden Berghe T, Wirawan E, Asselbergh B, Parthoens E, De Rycke R, et al. Neutrophil extracellular trap cell death requires both autophagy and superoxide generation. *Cell Res.* (2011) 21:290–304. doi: 10.1038/cr.2010.150
- Hampton HR, Bailey J, Tomura M, Brink R, Chtanova T. Microbe-dependent lymphatic migration of neutrophils modulates lymphocyte proliferation in lymph nodes. *Nat Commun.* (2015) 6:7139. doi: 10.1038/ncomms8139
- Uhl B, Vadlau Y, Zuchtriegel G, Nekolla K, Sharaf K, Gaertner F, et al. Aged neutrophils contribute to the first line of defense in the acute inflammatory response. *Blood.* (2016) 128:2327–37. doi: 10.1182/blood-2016-05-718999
- Vignarajah M, Wood AJT, Nemes E, Subburayalu J, Herre J, Nourshargh S, et al. Regulation of ICAM-1 in human neutrophils. *J Leukoc Biol.* (2024) 116:901–8. doi: 10.1093/jleuko/qiae090
- Mencacci A, Montagnoli C, Bacci A, Cenci E, Pizzurra L, Spreca A, et al. CD80 +Gr-1+ myeloid cells inhibit development of antifungal Th1 immunity in mice with candidiasis. *J Immunol.* (2002) 169:3180–90. doi: 10.4049/jimmunol.169.6.3180
- Windhagen A, Maniak S, Gebert A, Ferger I, Wurster U, Heidenreich F. Human polymorphonuclear neutrophils express a B7-1-like molecule. *J Leukoc Biol.* (1999) 66:945–52. doi: 10.1002/jlb.66.6.945
- Hubbard AK, Rothlein R. Intercellular adhesion molecule-1 (ICAM-1) expression and cell signaling cascades. *Free Radic Biol Med.* (2000) 28:1379–86. doi: 10.1016/s0891-5849(00)00223-9
- Capucetti A, Albano F, Bonecchi R. Multiple roles for chemokines in neutrophil biology. *Front Immunol.* (2020) 11:1259. doi: 10.3389/fimmu.2020.01259
- Wang J, Hossain M, Thanabalasuriar A, Gunzer M, Meininger C, Kubes P. Visualizing the function and fate of neutrophils in sterile injury and repair. *Science.* (2017) 358:111–6. doi: 10.1126/science.aam9690
- Ramoni D, Tirandi A, Montecucco F, Liberale L. Sepsis in elderly patients: the role of neutrophils in pathophysiology and therapy. *Intern Emerg Med.* (2024). doi: 10.1007/s11739-023-03515-1
- Salzer CE, Bergmann CB, Hotchkiss RS, Crisologo PA, Caldwell CC. Functional characterization of neutrophils allows source control evaluation in a murine sepsis model. *J Surg Res.* (2022) 274:94–101. doi: 10.1016/j.jss.2021.12.037
- Sitaru C, Kromminga A, Hashimoto T, Brocker EB, Zillikens D. Autoantibodies to type VII collagen mediate Fcγma-dependent neutrophil activation and induce dermal-epidermal separation in cryosections of human skin. *Am J Pathol.* (2002) 161:301–11. doi: 10.1016/s0002-9440(10)61482-x
- Sounbuli K, Alekseeva LA, Markov OV, Mironova NL. A comparative study of different protocols for isolation of murine neutrophils from bone marrow and spleen. *Int J Mol Sci.* (2023) 24. doi: 10.3390/ijms242417273
- Ledderose C, Hashiguchi N, Valsami EA, Rusu C, Junger WG. Optimized flow cytometry assays to monitor neutrophil activation in human and mouse whole blood samples. *J Immunol Methods.* (2023) 512:113403. doi: 10.1016/j.jim.2022.113403
- Othman A, Sekheri M, Filep JG. Roles of neutrophil granule proteins in orchestrating inflammation and immunity. *FEBS J.* (2022) 289:3932–53. doi: 10.1111/febs.15803
- Weirich E, Rabin RL, Maldonado Y, Benitz W, Modler S, Herzenberg LA, et al. Neutrophil CD11b expression as a diagnostic marker for early-onset neonatal infection. *J Pediatr.* (1998) 132:445–51. doi: 10.1016/s0022-3476(98)70018-6
- Ernst O, Glucksam-Galnoy Y, Bhatta B, Athamna M, Ben-Dror I, Glick Y, et al. Exclusive temporal stimulation of IL-10 expression in LPS-stimulated mouse macrophages by cAMP inducers and type I interferons. *Front Immunol.* (2019) 10:1788. doi: 10.3389/fimmu.2019.01788
- Austermann J, Roth J, Barczyk-Kahlert K. The good and the bad: monocytes' and macrophages' Diverse functions in inflammation. *Cells.* (2022) 11. doi: 10.3390/cells11121979
- De AK, Kodys KM, Yeh BS, Miller-Graziano C. Exaggerated human monocyte IL-10 concomitant to minimal TNF-α induction by heat-shock protein 27 (Hsp27) suggests Hsp27 is primarily an antiinflammatory stimulus. *J Immunol.* (2000) 165:3951–8. doi: 10.4049/jimmunol.165.7.3951
- Venereau E, Ceriotti C, Bianchi ME. DAMPs from cell death to new life. *Front Immunol.* (2015) 6:422. doi: 10.3389/fimmu.2015.00422
- Yu MB, Guerra J, Firek A, Langridge WHR. Extracellular vimentin modulates human dendritic cell activation. *Mol Immunol.* (2018) 104:37–46. doi: 10.1016/j.molimm.2018.09.017
- Sugimoto MA, Vago JP, Teixeira MM, Sousa LP. Annexin A1 and the resolution of inflammation: modulation of neutrophil recruitment, apoptosis, and clearance. *J Immunol Res.* (2016) 2016:8239258. doi: 10.1155/2016/8239258
- Vago JP, Nogueira CR, Tavares LP, Soriani FM, Lopes F, Russo RC, et al. Annexin A1 modulates natural and glucocorticoid-induced resolution of inflammation by enhancing neutrophil apoptosis. *J Leukoc Biol.* (2012) 92:249–58. doi: 10.1189/jlb.0112008
- Munoz LE, Frey B, Pausch F, Baum W, Mueller RB, Brachvogel B, et al. The role of annexin A5 in the modulation of the immune response against dying and dead cells. *Curr Med Chem.* (2007) 14:271–7. doi: 10.2174/092986707779941131
- Wang S, Chen L. Co-signaling molecules of the B7-CD28 family in positive and negative regulation of T lymphocyte responses. *Microbes Infect.* (2004) 6:759–66. doi: 10.1016/j.micinf.2004.03.007
- Nolan A, Kobayashi H, Naveed B, Kelly A, Hoshino Y, Hoshino S, et al. Differential role for CD80 and CD86 in the regulation of the innate immune response in murine polymicrobial sepsis. *PloS One.* (2009) 4:e6600. doi: 10.1371/journal.pone.0006600
- Sansom DM, Manzotti CN, Zheng Y. What's the difference between CD80 and CD86? *Trends Immunol.* (2003) 24:314–9. doi: 10.1016/s1471-4906(03)00111-x
- Abi Abdallah DS, Egan CE, Butcher BA, Denkers EY. Mouse neutrophils are professional antigen-presenting cells programmed to instruct Th1 and Th17 T-cell differentiation. *Int Immunol.* (2011) 23:317–26. doi: 10.1093/intimm/dxr007
- Minns D, Smith KJ, Hardisty G, Rossi AG, Gwyer Findlay E. The outcome of neutrophil-T cell contact differs depending on activation status of both cell types. *Front Immunol.* (2021) 12:633486. doi: 10.3389/fimmu.2021.633486
- Iking-Konert C, Cseko C, Wagner C, Stegmaier S, Andrassy K, Hansch GM. Transdifferentiation of polymorphonuclear neutrophils: acquisition of CD83 and other functional characteristics of dendritic cells. *J Mol Med (Berl).* (2001) 79:464–74. doi: 10.1007/s001090100237
- Doran AC, Yurdagul A Jr., Tabas I. Efferocytosis in health and disease. *Nat Rev Immunol.* (2020) 20:254–67. doi: 10.1038/s41577-019-0240-6
- Yang CW, Strong BS, Miller MJ, Unanue ER. Neutrophils influence the level of antigen presentation during the immune response to protein antigens in adjuvants. *J Immunol.* (2010) 185:2927–34. doi: 10.4049/jimmunol.1001289
- Vassallo A, Wood AJ, Subburayalu J, Summers C, Chilvers ER. The counter-intuitive role of the neutrophil in the acute respiratory distress syndrome. *Br Med Bull.* (2019) 131:43–55. doi: 10.1093/bmb/ldz024
- Grommes J, Soehnlein O. Contribution of neutrophils to acute lung injury. *Mol Med.* (2011) 17:293–307. doi: 10.2119/molmed.2010.00138
- Land WG. Use of DAMPs and SAMPs as therapeutic targets or therapeutics: A note of caution. *Mol Diagn Ther.* (2020) 24:251–62. doi: 10.1007/s40291-020-00460-z
- Bashant KR, Vassallo A, Herold C, Berner R, Menschner L, Subburayalu J, et al. Real-time deformability cytometry reveals sequential contraction and expansion during neutrophil priming. *J Leukoc Biol.* (2019) 105:1143–53. doi: 10.1002/jlb.MA0718-295RR

50. Roh JS, Sohn DH. Damage-associated molecular patterns in inflammatory diseases. *Immune Netw.* (2018) 18:e27. doi: 10.4110/in.2018.18.e27
51. Shields AM, Panayi GS, Corrigan VM. Resolution-associated molecular patterns (RAMP): RAMPs defending immunological homeostasis? *Clin Exp Immunol.* (2011) 165:292–300. doi: 10.1111/j.1365-2249.2011.04433.x
52. Jarczak D, Kluge S, Nierhaus A. Sepsis-pathophysiology and therapeutic concepts. *Front Med (Lausanne).* (2021) 8:628302. doi: 10.3389/fmed.2021.628302
53. Germic N, Frangez Z, Yousefi S, Simon HU. Regulation of the innate immune system by autophagy: neutrophils, eosinophils, mast cells, NK cells. *Cell Death Differ.* (2019) 26:703–14. doi: 10.1038/s41418-019-0295-8
54. Germic N, Frangez Z, Yousefi S, Simon HU. Regulation of the innate immune system by autophagy: monocytes, macrophages, dendritic cells and antigen presentation. *Cell Death Differ.* (2019) 26:715–27. doi: 10.1038/s41418-019-0297-6
55. Mazlo A, Tang Y, Jenei V, Brauman J, Yousef H, Bacsi A, et al. Resolution potential of necrotic cell death pathways. *Int J Mol Sci.* (2022) 24. doi: 10.3390/ijms24010016



OPEN ACCESS

EDITED BY

Reza Akbarzadeh,
University of Lübeck, Germany

REVIEWED BY

Akihiko Murata,
Tottori University, Japan
Hiroaki Harada,
Mitsui Memorial Hospital, Japan

*CORRESPONDENCE

Roland Csépanyi-Kömi
✉ csepanyi-komi.roland@semmelweis.hu

RECEIVED 11 October 2024

ACCEPTED 10 February 2025

PUBLISHED 26 February 2025

CITATION

Czárán D, Sasvári P, Lőrincz K, Ella K, Gellén V
and Csépanyi-Kömi R (2025) ARHGAP25: a
novel player in the Pathomechanism of
allergic contact hypersensitivity.
Front. Immunol. 16:1509713.
doi: 10.3389/fimmu.2025.1509713

COPYRIGHT

© 2025 Czárán, Sasvári, Lőrincz, Ella, Gellén
and Csépanyi-Kömi. This is an open-access
article distributed under the terms of the
[Creative Commons Attribution License \(CC BY\)](#).
The use, distribution or reproduction in other
forums is permitted, provided the original
author(s) and the copyright owner(s) are
credited and that the original publication in
this journal is cited, in accordance with
accepted academic practice. No use,
distribution or reproduction is permitted
which does not comply with these terms.

ARHGAP25: a novel player in the Pathomechanism of allergic contact hypersensitivity

Domonkos Czárán¹, Péter Sasvári¹, Kende Lőrincz²,
Krisztina Ella¹, Virág Gellén¹ and Roland Csépanyi-Kömi^{1*}

¹Semmelweis University, Department of Physiology, Budapest, Hungary, ²Semmelweis University, Department of Dermatology, Venereology and Dermatocology, Budapest, Hungary

Objective: Contact hypersensitivity (CHS), or allergic contact dermatitis (ACD), is an inflammatory skin disorder characterized by an exaggerated allergic reaction to specific haptens. During this delayed-type allergic reaction, the first contact with the allergen initiates the sensitization phase, forming memory T cells. Upon repeated contact with the hapten, the elicitation phase develops, activating mostly macrophages, cytotoxic T cells, and neutrophilic granulocytes. Our group previously demonstrated that the leukocyte-specific GTPase-activating protein ARHGAP25 regulates phagocyte effector functions and is crucial in the pathomechanism of autoantibody-induced arthritis. Here, we investigate its role in the pathogenesis of the more complex inflammatory process of contact hypersensitivity.

Methods: For sensitization, the abdomens of wild-type and ARHGAP25 deficient (KO) mice on a C57BL/6 background, as well as bone marrow chimeric mice, were coated with 3% TNCB (2-chloro-1,3,5-trinitrobenzene) or acetone in the control group. After five days, ears were treated with 1% TNCB for elicitation. Swelling of the ears caused by edema formation was evaluated by measuring the ear thickness. Afterward, ears were harvested, and histological analysis, investigation of leukocyte infiltration, cytokine production, and changes in relevant signaling pathways were carried out. ARHGAP25 expression at the mRNA and protein levels was measured using murine ear and human skin samples.

Results: ARHGAP25 expression increased in human patients suffering from contact dermatitis and in contact hypersensitivity induced in mice. Our data suggest that ARHGAP25 expression is infinitesimal in keratinocytes. In the CHS mouse model, the absence of ARHGAP25 mitigated the severity of inflammation in a leukocyte-dependent manner by reducing the infiltration of phagocytes and cytotoxic T cells. ARHGAP25 altered cytokine composition in the sensitization and elicitation phase of the disease. However, this protein did not affect T cell homing and activation in the sensitization phase.

Conclusion: Our findings suggest that ARHGAP25 is essential in developing contact hypersensitivity by modulating the cytokine environment and leukocyte infiltration. Based on these findings, we propose ARHGAP25 as a promising candidate for future therapeutic approaches and a potential ACD biomarker.

KEYWORDS

ARHGAP25, contact hypersensitivity, allergic contact dermatitis, TNCB, GTPase activating protein (GAP)

1 Introduction

Allergic contact dermatitis (ACD) is a common skin disease that affects approximately 15% of the population worldwide, thus having a substantial socio-economic impact (1). The pathomechanism of ACD is associated with inflammation and is classified as a type IV delayed-type hypersensitivity reaction. Its development can be divided into two distinct phases: In the sensitization phase, the first contact with the allergens, the so-called haptens, results in a pro-inflammatory environment in the skin, in which activation of the innate and adaptive immune cells occurs. Langerhans cells in the epidermis or langerin-dermal dendritic cells in the dermis take up the allergen and present them to naive T cells, creating a memory T cell population (2–4). Although it was demonstrated that neutrophils are also required for the sensitization phase, the underlying mechanism is not yet fully understood (5). The second contact with the allergen initiates the elicitation phase, causing the proliferation and infiltration of these memory T cells (especially CD8+ cells), which in turn produce different cytokines (e.g., IFN γ and IL-1 β) recruiting and activating other leukocyte types such as macrophages and neutrophilic granulocytes into the dermis and the epidermis. Even though mainly these leukocytes are responsible for the tissue damage, mast cells, NK cells, and $\gamma\delta$ T cells are also recruited to the lesion sites (6, 7). Keratinocytes, crucial non-hematopoietic players in the sensitization and elicitation phase, produce different types of cytokines, taking part in the activation of T cells (8). They contribute to creating a pro-inflammatory milieu but are also targeted by cytotoxic T cells (9).

Recently, we reported that ARHGAP25 is an essential regulatory component of developing autoantibody-induced arthritis (10). This GTPase-activating protein turns off RAC monomeric GTPase-mediated signaling by accelerating its GTPase activity (11, 12). This way, ARHGAP25 regulates phagocyte effector functions such as migration, phagocytosis, and superoxide production (13–15). Although this protein was initially considered leukocyte-specific, its importance has also been described in many tumor cell types even though the expression level of ARHGAP25 in non-hematopoietic cells is usually very low (13, 16–20). Surprisingly, ARHGAP25 expression in fibroblast-like synoviocytes was detected in amounts similar to what is expected in neutrophils (10). In the absence of ARHGAP25, the joint operation of fibroblast-like synoviocytes, macrophages, and neutrophils alters the cytokine environment in the synovium,

leading to the reduced infiltration of phagocytes, which results in mitigated inflammation and tissue damage (10).

These findings lead us to investigate ARHGAP25's role in an immunological model with a complex interplay between leukocytes and non-hematopoietic cells to challenge our current views on ARHGAP25's leukocyte-selective roles in immune responses. Contact hypersensitivity (CHS) involves orchestrated interactions between T cells, leukocytes of the innate immune system, and keratinocytes (6, 7). It was reported that keratinocyte-specific deletion of RAC resulted in normal epidermis development and hair follicle loss. Furthermore, RAC1-null keratinocytes are sensitized to leukocyte-derived IFN- γ , which causes their altered differentiation (44). RAC1 was also shown to regulate tight junction barrier function, motility, and cell cycle progression in these cells (45, 46). Furthermore, we observed that ACD or CHS increased ARHGAP25 gene expression in humans and mice, supporting the importance of ARHGAP25 in the pathomechanism of these diseases.

Thus, we investigated the role of ARHGAP25 in the well-characterized contact hypersensitivity mouse model induced by 2-chloro-1,3,5-trinitrobenzene (TNCB) (21–23). The first administration of TNCB on the abdominal skin sensitizes the mice via a T cell-dependent manner, while the second challenge on the ear skin elicits contact hypersensitivity (24).

In the present study, we show that total or leukocyte-specific absence of ARHGAP25 reduces ear swelling upon TNCB challenge and suppresses the infiltration of phagocytes and T cells into the inflamed ear tissue. The lack of ARHGAP25 alters the cytokine milieu formed by the sensitization and the elicitation with the allergen.

Our data suggest that ARHGAP25 is involved in developing and causing allergic contact dermatitis by regulating leukocytes, mainly cytotoxic T cells and macrophages. The elevated gene expression observed in human patients confirms the protein's importance in the disease and even raises the possibility that it could be used as a biomarker for ACD.

2 Methods

2.1 Human skin tissue sample collection

For research purposes, skin samples were taken from patients diagnosed with dermatitis after informed consent (Table 1).

TABLE 1 Clinical information of patients included in the study.

	Patient 1.	Patient 2.	Patient 3.
Age (years)	76	52	71
Sex	Female	Female	Male
Medical history	Symptoms of necrobiosis lipiodica, topical neomycin treatment and subsequent disseminated contact dermatitis development	Atopic dermatitis treated with a fragrance containing cream and subsequent symptoms of disseminated contact dermatitis	Treatment of suspected scabies with a benzyl benzoate preparation and due to this, disseminated contact dermatitis development
Biopsy site	Right lower extremity	Right retroauricular region	Right scapular region
Histology	Spongiotic dermatitis, lymphocyte exocytosis, mixed infiltrate with lymphocytes and eosinophils	Spongiotic dermatitis, lymphocyte exocytosis, mixed infiltrate with lymphocytes and eosinophils	Spongiotic dermatitis, lymphocyte exocytosis, mixed infiltrate with lymphocytes and eosinophils
Serology	Normal IgE level (<100 NE/L)	Elevated IgE level 572 NE/L (<100 NE/L), specific IgE against Birch, Mountain, Hazel pollens, and aspergillus	Elevated IgE level 1688 NE/L (<100 NE/L), no specific IgE

Symptomatic and asymptomatic sampling areas were selected and biopsied by a dermatologist. Prior to sampling, the selected skin area was properly disinfected and anesthetized with lidocaine infiltration. A biopsy punch (diameter of the circular blade: 5 mm) was used to excise the skin samples. After hemostasis, the defect was primarily closed with a simple knotted suture. Immediately after excision, the tissue sample was placed on dry ice in sterile Eppendorf tubes for further processing. The studies involving humans were approved by the Committee of Science and Research Ethics of the Medical Research Council (ETT TUKEB) and approved by the Department of Health Administration of the National Public Health Center of Hungary (Ethical approval number: IV/1707-6/2020/EKU).

2.2 Experimental animals

Age-matched male, wild-type, and Arhgap25 knock-out mice on a C57BL/6 background were used for the experiments. Animals were bred in a conventional animal facility at Semmelweis University in individually sterile ventilated cages (Tecniplast, Buguggiate, Italy) and moved to the conventional (MD) room two weeks before experiments. All measurements conducted using experimental mice followed the EU Directive 2010/63/EU for animal experiments and were approved by the Animal Experimentation Review Board of Semmelweis University and the Government Office for Pest County, Hungary (Ethical approval numbers: PE/EA/1967-7/2017, PE/EA/00284-7/2021, BA/73/00070-2/2020).

To generate Arhgap25^{-/-} bone marrow chimeric mice, WT recipient animals carrying the CD45.1 allele on C57BL/6 genetic background were lethally irradiated with 11 Gy from a ¹³⁷Cs source using a GSM D1 irradiator as described previously (25). Afterward, unfractionated bone marrow cells from femurs and tibias of ARHGAP25^{-/-} donor mice (carrying the CD45.2 allele) were injected into the retro-orbital plexus of recipient animals. The repopulation of the hematopoietic compartment by donor cells was confirmed four weeks after the transplantation. To this end, peripheral blood was drawn and labeled for Ly6G and CD45.1 or

CD45.2, and samples were analyzed using a flow cytometer (CytoFLEX, BeckmanCoulter). The ratio of donor-derived cells among neutrophils was calculated, and only mice with over 95% of the cells of donor origin were used in our experiments.

2.3 Induction of allergic contact hypersensitivity

The shaved skin on the abdomen of animals was coated with 3% (m/v) 2-chloro-1,3,5-trinitrobenzene (TNCB, Sigma Aldrich) dissolved in acetone (Molar Chemicals), this initiates the sensitization phase of the allergic reaction. Control mice received vehicle (acetone) treatment only at this point, therefore, no sensitization was initiated. After five days, the animals were anesthetized with isoflurane (Baxter), and ear thickness was measured using a microcaliper (Kroeplin) by an observer blinded to the experimental setup. Then, both the previously TNCB-treated and control animals were treated topically on the ears with 1% (m/v) TNCB. Since in the case of control animals, this was the first encounter with the allergen, the sensitization phase begins in them at this point. In the case of the other treatment group, this is the second encounter with TNCB, therefore, the elicitation phase of the allergic reaction is initiated in them. After 24 hours, ear thickness was measured again, animals were sacrificed, and the ears were harvested for further experiments.

2.4 Epidermis isolation of mouse ears

One day after the TNCB challenge, mice were sacrificed, the ears were coated with betadine for 5 minutes, washed with distilled water, removed, rewashed, and incubated for 5 minutes in 70% ethanol. Afterward, the ears were washed with distilled water three times and incubated in a 5 mg/ml Dispase II (Sigma Aldrich) enzyme cocktail dissolved in DMEM culture medium (Lonza) for 24 hours at 4°C. Subsequently, the ears' epidermis was peeled off with two forceps, cleaned off the remaining connective tissue in distilled water, and snap-frozen in liquid nitrogen for further analysis.

2.5 Gene expression analysis

Human tissue samples and mouse ear samples were isolated, immediately frozen in liquid nitrogen, and then ground. Samples were lysed using TRI ReagentTM (Invitrogen) and stored at -80°C until RNA preparation. Total RNA was extracted according to the manufacturer's protocol. cDNA was synthesized using iScriptTM gDNA Clear cDNA Synthesis Kit (Bio-Rad) following the manufacturer's instructions. Relative expression levels of mouse *Arhgap25* and human *ARHGAP25* were measured using a LightCycler[®] 480 system (Roche) with TaqMan hydrolysis probes (see Table 2). mouse *Rplp0* and human *RPLP0* were used as the reference genes. The second derivative maximum method was applied for data analysis using LightCycler[®] Relative Quantification Software (version 1.5.0.39, Roche).

2.6 Histology

Excised ears were fixed using 4% paraformaldehyde (Sigma-Aldrich), treated with xylol (Lach:ner), dehydrated in ethanol, and embedded in paraffin using a Leica EG1150H embedding station. Sections were prepared (8 µm) and stained with hematoxylin and eosin (Leica). Representative images were captured on a Nikon fluorescent microscope with a 20x objective.

2.7 Measurement of different leukocyte types in the blood and ears of mice

Twenty-four hours after TNCB treatment of the ears of the animals, 20 µl of blood was collected from the tail of each mouse in phosphate-buffered saline (PBS) containing 5% FBS (Capricorn Scientific) and 0.5% heparin (Teva). These blood samples were divided into two parts of equal volumes: in one whole leukocyte number (with CD45-FITC), myeloid cells (with CD11b-eFluor450), neutrophil granulocytes (with

Ly6G-PerCP-Cy5.5) and macrophages (with F4/80-PE), in the other part, leukocytes (CD45-FITC), T cells (CD3-eFluor450) helper T cells (CD4-PerCP-Cy5.5) and cytotoxic T cells (CD8-PE) were labeled (all antibodies were purchased from ThermoFisher Scientific). After washing with PBS, samples were measured with a Cytoflex cytometer (Beckman Coulter), and the number of different leukocytes in 1 µl blood was determined using a multi-step gating strategy (Supplementary Figure S1). Parallely, the removed ears were cut into small pieces, and the connective tissue was digested with 200 µg/mL Liberase enzyme cocktail (Roche) in Hank's Balanced Salt Solution (HBSS, Cytia) supplemented with 200 mM HEPES (Sigma-Aldrich), leaving the cells intact. Afterward, the samples were filtered with a cell strainer (70 µm pore size, Sigma-Aldrich), centrifuged, and supernatants were saved for cytokine measurements. The sedimented fraction was resuspended in PBS containing 5% FBS, divided into two equal volumes, stained for different leukocyte subtypes, and measured by flow cytometry as described above.

2.8 Cytokine measurements

The amount of IL-1β and MIP-2 in the ears was determined by sandwich ELISA kits (R&D systems) from the supernatants of the digested ear samples (see above), according to the instructions provided by the manufacturer. A broad picture of the cytokine profile in the different experimental groups was assessed from pooled samples (from 9 mice per group) using a Mouse Cytokine Array kit (R&D systems) following the protocol provided by the company.

2.9 In vitro migration assay

Untreated WT and ARHGAP25-deficient mice were sacrificed, their femur and tibia were excised, and bone marrow was washed out. Afterward, polymorphonuclear neutrophils (PMN) were isolated using percoll gradient centrifugation as described

TABLE 2 Primer and probe sequences for gene expression analysis.

gene		sequence
mouse <i>Rplp0</i>	forward	5'-CTCGCTTTCTGGAGGGTGTGTC-3'
	reverse	5'-AGTCTCCACAGACAATGCCA-3'
	probe	5'FAM-TGCCTCGGTGCCCACTCCA-TAMRA3'
mouse <i>Arhgap25</i>	forward	5'-CCTCCTTTGACAGGGACACA-3'
	reverse	5'-CTTTGCCTCATCTGCGTTCA-3'
	probe	5'FAM- ACCTCCGAGACCTGCCAGAGCC -TAMRA3'
human <i>RPLP0</i>	forward	5'-TCGTCTTTAAACCCTGCGTG-3'
	reverse	5'-TGTCTGCTCCCAATGAAAC-3'
	probe	5'FAM- CCCTGTCTCCCTGGGCATCAC-TAMRA3'
human <i>ARHGAP25</i>	forward	5'-TGGCTACTGTGATTGGTGTG-3'
	reverse	5'-GGGTATATCCTTGGACTTGGG-3'
	probe	5'FAM-CGAAGACCCTGCCGTGATCATGAG-TAMRA3'

previously (26). Transwell inserts (3 µm pore size polycarbonate membrane; Corning) and wells of 24-well tissue culture plates were precoated with 10% FBS and washed with HBSS. For stimulus, saved supernatants of the ear lysate of the different treatment groups of WT and KO animals were used. Supernatants were centrifuged at 12000 RPM for 10 minutes to remove cellular debris, pooled (9 samples per experimental group), and diluted 2-fold with HBSS. Wells were filled with 1 ml of these supernatants, then inserts were placed inside, and were filled with 2×10^5 neutrophils in 200 µl HBSS. After one-hour incubation at 37°C, plates were spun, inserts were removed, and the number of neutrophils that transmigrated into the wells was determined using an acid phosphatase assay (27, 28).

2.10 Measurements of T cell numbers and activation from lymph nodes

Five days after treatment of the shaved abdominal skin of animals with either TNCB or acetone, mice were sacrificed, and the inguinal and axillary lymph nodes were harvested. The lymph nodes were mechanically fragmented in PBS and filtered through cell strainers with 70 µm pore size. Total cell numbers for each mouse were counted in a Bürker chamber, then 200 µl of the samples were stained for 1 hour at 4°C with the following specific fluorophore-conjugated antibodies: CD3-eF450, CD4-PerCP-Cy5.5, CD8-PE, CD69-APC, CD25-FITC (ThermoFisher Scientific). Single-stained and unstained samples were also prepared for compensation. Afterward, samples were centrifuged, washed 3 times with PBS, and measured with flow cytometry. During evaluation, the number of different T cell types (helper and cytotoxic) in all four lymph nodes and the ratios of activated T cells (CD25 and CD69 positive cells) within the T cell subtypes were determined.

2.11 Retroorbital transfer of lymph node-derived cells

Using the remaining lymph node-derived cell samples (see above), 5 million cells were taken out, centrifuged, resuspended in

alpha-MEM medium (Capricorn Scientific), and injected into the retroorbital plexus of recipient mice. Our three experimental groups were WT recipient mice receiving cells derived from WT lymph nodes (WT→; WT), *Arhgap25*^{-/-} recipient mice receiving cells from WT lymph nodes (WT→; *Arhgap25*^{-/-}), and WT recipient mice receiving cells derived from *Arhgap25*^{-/-} lymph nodes (*Arhgap25*^{-/-}→; WT). In each group, we used lymph nodes from mice sensitized with TNCB on the abdomen. After one hour of the cell transfer, the ear thickness of the recipient animals was measured with a micro caliper, and ears were painted with TNCB as described previously. Twenty-four hours later, ear thickness was measured again, and in each case, ear thickness increase was calculated.

2.12 Western blot analysis

Harvested mouse ears, epidermis of ears, or human skin samples were snap-frozen and ground up in liquid nitrogen. They were then lysed in the following solution: 30 mM Na-HEPES, 100 mM NaCl, 1% [w/v] Triton-X-100, 20 mM NaF, 1 mM Na-EGTA, 1 mM Na-EDTA, 100 mM benzamidine, 1% [w/v] aprotinin, 1% [w/v] protease inhibitor cocktail, 1% [w/v] phosphatase inhibitor cocktail, and 1% [w/v] phenylmethylsulfonyl fluoride (pH 7.5), on ice for 10 minutes. The protein concentration of the samples was determined according to Bradford. Subsequently, they were incubated for 5 minutes at 95°C with 4x reducing buffer, and 40 µg of each sample was separated on 4-15% polyacrylamide gradient gels (Bio-Rad). Following separation, the proteins were blotted onto nitrocellulose membranes (Bio-Rad), blocked with EveryBlot Blocking Buffer (Bio-Rad), and incubated with the specified primary antibodies (Table 3) overnight at 4°C. After this, the bound primary antibodies were labeled with a horseradish peroxidase-conjugated secondary antibody specific to rabbit IgG (GE Healthcare). After the development of X-ray films (Fujifilm), the membranes were stripped (if necessary) with 2% Sodium dodecyl sulfate (SDS, Sigma-Aldrich) and 0.7% 2-mercaptoethanol (Serva) in PBS at 55°C for 20 minutes, and GAPDH was identified as a loading control (Cell Signaling, 1:5000 dilution). Densitometry was conducted using ImageJ software (ver. 1.53o), and the data was normalized to GAPDH for total protein and to total-MAPK for phospho-MAPK signals.

TABLE 3 Antibodies used for Western blot analysis.

Specificity	Dilution	Manufacturer	Catalog number	RRID
Total-p38 MAPK	1:1000	Cell Signaling	9212S	AB_330713
Total-NF-κB p65	1:1000	Cell Signaling	8242S	AB_10859369
Total-E-cadherin	1:1000	Cell Signaling	#3195	AB_2291471
Total-I-κB	1:1000	Cell Signaling	4812S	AB_10694416
Total-β-catenin	1:500	Cell Signaling	#8480	AB_11127855
Phospho-p38 MAPK	1:1000	Cell Signaling	4511S	AB_2139682
GAPDH	1:5000	Cell Signaling	14C10	AB_561053
ARHGAP25	1:5000	ImmunoGenes	–	–
rabbit IgG (secondary)	1:5000	GE Healthcare	RPN4301	AB_2650489

2.13 Statistical analysis

All data were analyzed and plotted using GraphPad Prism 10.0.1 Software. Comparison of experimental groups was carried out by two-way ANOVA with Tukey's multiple comparison tests or when there were only two groups (in the case of ARHGAP25 expression experiments) unpaired t-test. All *p* values <0.05 were considered statistically significant.

3 Results

3.1 ARHGAP25 is overexpressed in human allergic contact dermatitis and in TNCB-induced contact hypersensitivity in mice

It was reported that gene expression of ARHGAP25 can be altered in different types of tumor cells (16–18, 29). We also demonstrated that in terminally differentiated neutrophilic granulocytes, stimulation decreases ARHGAP25 expression (12). However, it is unknown whether complex inflammatory conditions affect ARHGAP25's expression. Thus, we decided to compare ARHGAP25 expression in skin samples affected by ACD to that of healthy skin areas in self-controlled RT-qPCR and WB experiments. We observed a remarkable elevation of ARHGAP25 mRNA and protein levels in skin areas showing symptoms of ACD compared to the healthy control skin samples collected from the same patients (Figures 1A, C, D). The clinical information of patients is indicated in Table 1. Next, we decided to use the TNCB-induced contact hypersensitivity model to mimic human ACD in mice. For this, WT animals were treated with either 3% TNCB or, in the case of controls, only the solvent on the abdomen. Five days later, ears were painted with 1% TNCB in both groups, as detailed in the Methods section. RT-qPCR measurements revealed that the *Arhgap25* mRNA and protein levels were increased significantly upon the second exposure to TNCB in the total ear lysates (Figures 1B, C, E). According to this, we decided that this murine model is suitable for our experiments, which aim to investigate the role of ARHGAP25 in contact hypersensitivity. Since ARHGAP25 is highly expressed in leukocytes, but lately it was discovered, that certain other cell types express it as well (10, 16, 17, 30), we decided to also measure the expression of this protein in the epidermis of murine ear samples. RT-qPCR and WB experiments revealed no detectable ARHGAP25 in the mouse ear epidermis, neither in the RNA, nor in the protein level, and even the second treatment with the allergen did not increase its expression (Figures 1B, C, E). This suggests that keratinocytes do not express ARHGAP25, and the detected signals in human skin, and murine total ear samples is due to the infiltrated leukocytes.

3.2 Lacking ARHGAP25 results in decreased ear swelling after repeated TNCB treatment

To investigate the role of ARHGAP25 in the complex inflammatory process of contact hypersensitivity, allergic reaction

was induced in WT, and ARHGAP25 knock-out mice as described previously. One day after the elicitation with TNCB on the ears, histological analysis revealed substantial leukocyte accumulation in WT ears, which was reduced in the case of ARHGAP25 KO animals (Figure 2A). Prior to ear treatment, there was no difference in ear thickness between the two genotypes (Figures 2A, B). Even after sensitization, measuring and calculating ear thickening revealed no significant difference between WT and KO animals (Figures 2A, C, D). However, the second administration of TNCB resulted in a remarkable increase in ear thickening in WT animals, which was significantly lower in KO animals (Figures 2A, C, D). We also generated bone marrow chimeric mice to investigate whether only cells with hematopoietic origin are responsible for the observed difference. These animals carry ARHGAP25 knock-out leukocytes on a WT background (*Arhgap25*^{-/-}→WT) or, in the case of the control chimeric mice, WT leukocytes on a WT background (WT→WT). Interestingly, similar results were obtained as in the case of regular KO and WT mice. Before the treatment of the ears with the allergen, no difference in ear thickness was detected (Figure 2E), and sensitization did not cause any difference between WT and KO chimeras either. After elicitation, however, ear thickening increased in both groups but to a significantly lesser degree in KO chimeric mice (Figures 2F, G).

Our results indicate that ARHGAP25 plays a significant role in developing the disease and acts through mostly the hematopoietic cells.

3.3 After the second exposure to the contact allergen, the infiltration of phagocytes and T cells is reduced in the ears of *Arhgap25*^{-/-} mice

Next, we measured leucocyte counts from ear tissue and blood to determine whether the observed reduction in inflammatory ear swelling in the case of ARHGAP25-deficient animals is associated with altered leukocyte recruitment. To this end, blood was collected 24 hours after treating the ears with TNCB. Mice were sacrificed, ears were removed, connective tissue was lysed, and cells were labeled with specific antibodies. Flow cytometry analysis revealed that repeated treatment of the WT mice with the allergen caused a significant increase in the number of CD45+ leukocytes, CD45+CD11b+ double-positive myeloid phagocytes, CD45+CD11b+Ly6G+ neutrophils, and CD45+CD11b+F4/80+ macrophages compared to only sensitized animals (Figures 3A–D). In the case of the *Arhgap25*^{-/-} mice, the cell counts did not differ from WT after sensitization; however, the second TNCB treatment failed to induce a significant increase in the number of any of these leukocyte types (Figures 3A–D).

Moreover, the number of CD45+ leukocytes, myeloid cells, and macrophages was significantly reduced in the ear tissue of *Arhgap25*^{-/-} mice after elicitation, compared to elicited WT animals (Figures 3A, B, D). Analysis of the peripheral blood revealed that the number of WT myeloid cells and neutrophils decreased significantly upon the second TNCB challenge compared to those WT mice, which encountered the allergen only once. This reduction was not present in KO animals (Figures 3E–G). Interestingly, the absence of

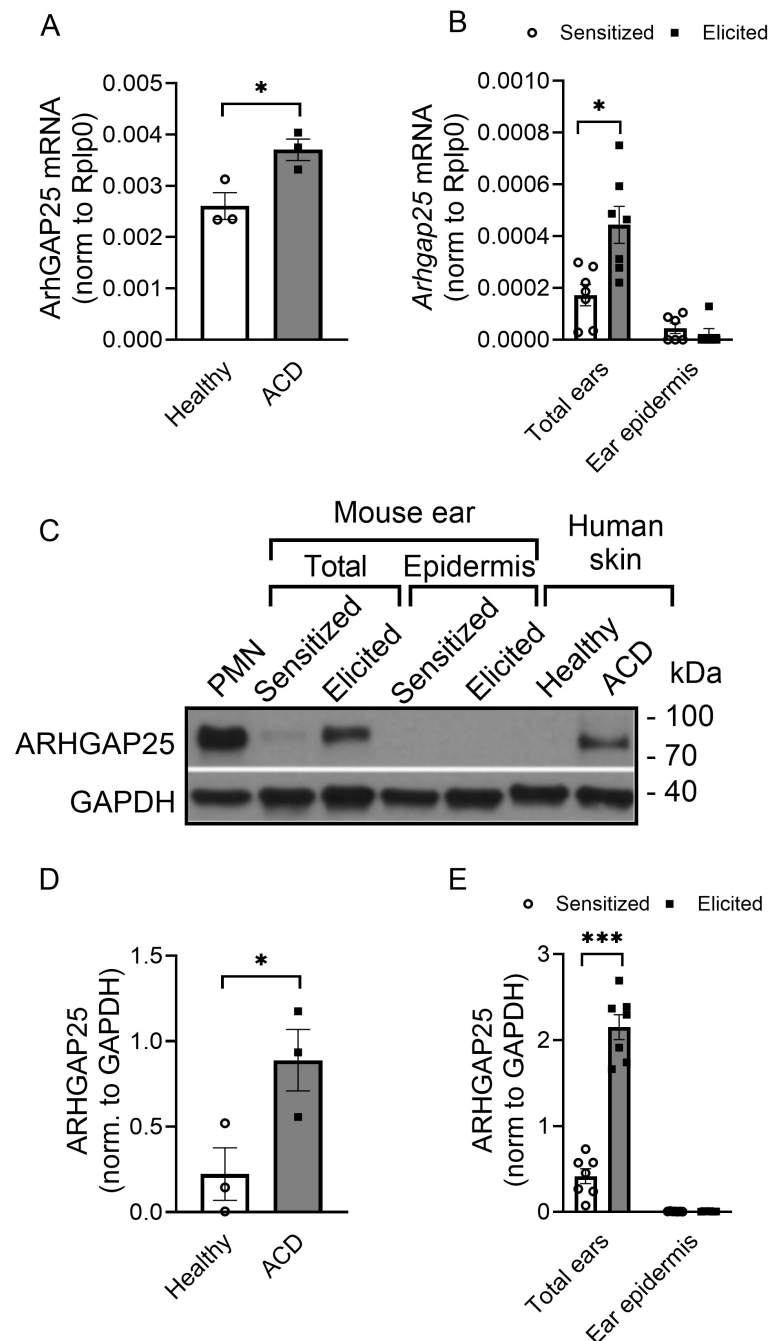


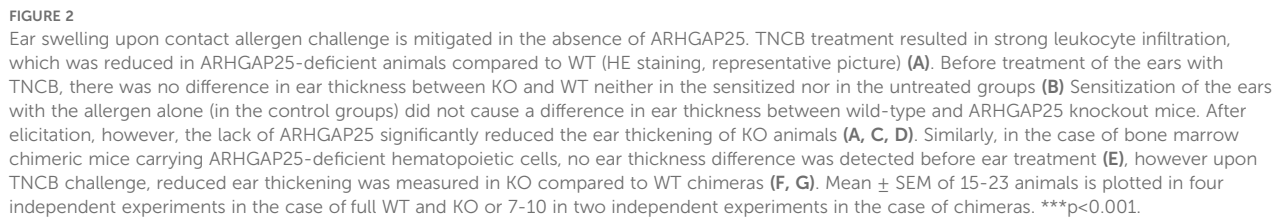
FIGURE 1

The expression level of ARHGAP25 is elevated in contact hypersensitivity. ARHGAP25 mRNA and protein expression was measured from snap-frozen and lysed human skin samples, mouse ears, and the epidermis of mouse ears. In the qRT-PCR experiments, Rplp0 mRNA was used as a reference gene for normalization. GAPDH proteins were used as a loading control for Western blot experiments. In the case of human samples, skin with allergic contact dermatitis (ACD) had significantly elevated mRNA (A) and protein expression of ARHGAP25, compared to healthy skin tissues (C, D). Similarly, in the total ear lysates of mice, allergen treatment resulted in remarkable overexpression both on the mRNA (B) and the protein level (C, E). On the other hand, neither the mRNA of ARHGAP25 nor the protein itself could be detected in the epidermis of control or allergic mouse ears, suggesting that keratinocytes are not expressing this gene (B, C, D). Mean \pm SEM of 7 mice and 3 human samples per group are plotted, * $p < 0.05$, *** $p < 0.001$. PMN, Polymorphonuclear neutrophils; ACD, Allergic contact dermatitis.

ARHGAP25 decreased the number of leukocytes, myeloid cells, and neutrophils in sensitized animals compared to sensitized WT mice (Figures 3E–G), which might be the result of ARHGAP25's intrinsic effect on leukocyte distribution or its potential role in the sensitization phase too.

At the same time, the number of monocytes did not differ between the WT and KO, either after sensitization or elicitation (Figure 3H).

Helper and cytotoxic T cells are critical players of ACD; thus, we also investigated the number of these cells in the ears and blood. Our



increased these cell counts in the WT but not in *Arhgap25*^{-/-} mice. As a result, the difference between elicited WT and KO animals' T cells and cytotoxic T cell numbers was significant (Figures 4A–C). Similarly, the CD45+CD3+ T cell count was decreased in the blood of

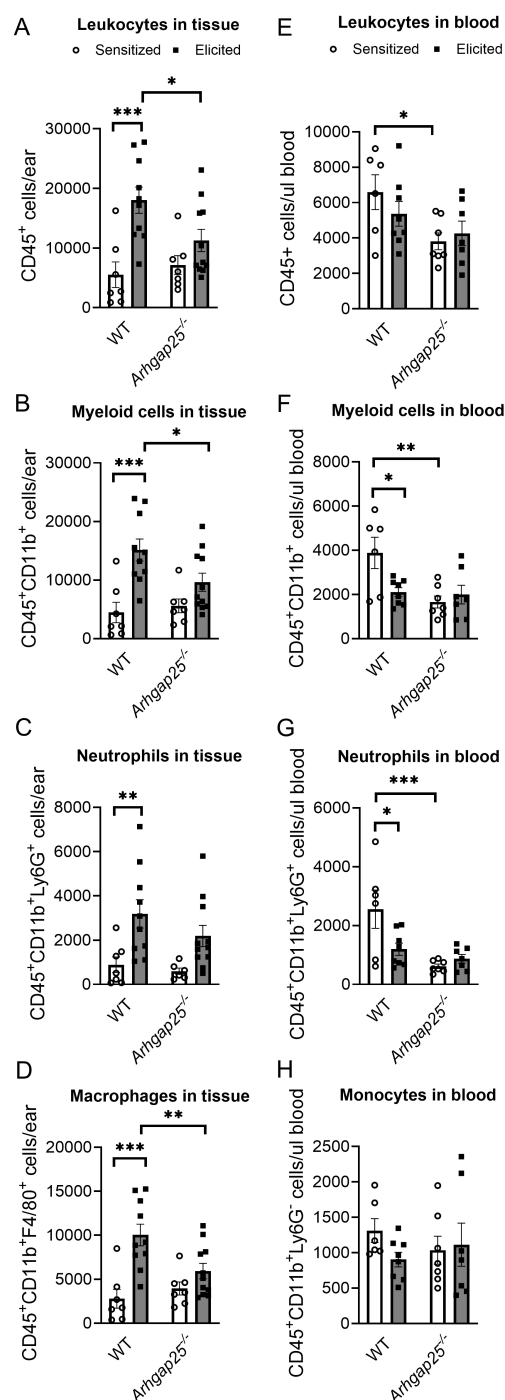


FIGURE 3

Lacking ARHGAP25 decreased phagocyte recruitment into the inflamed ears. After the TNCB treatment of ears, blood was collected from the tails of wild type and ARHGAP25 knockout mice, ears were digested with Liberase enzyme cocktail, and the numbers of different leukocyte types were determined by flow cytometry, using a multi-step gating strategy. According to our results, in the inflamed ears, leukocytes (A) and, in particular, phagocytes of the myeloid lineage (B), mostly macrophages (D), were significantly lower in KO mice compared to WT after second antigen exposure, while neutrophil numbers only slightly decreased (C). In the blood of control animals, the absence of ARHGAP25 resulted in reduced numbers of leukocytes (E), myeloid phagocytes (F), and, most notably, neutrophils compared to WT (G). In contrast, monocyte numbers were not affected (H). Mean \pm SEM of 6–11 mice per group in three independent experiments are plotted. * $p < 0.05$, ** $p < 0.01$, *** $p < 0.001$.

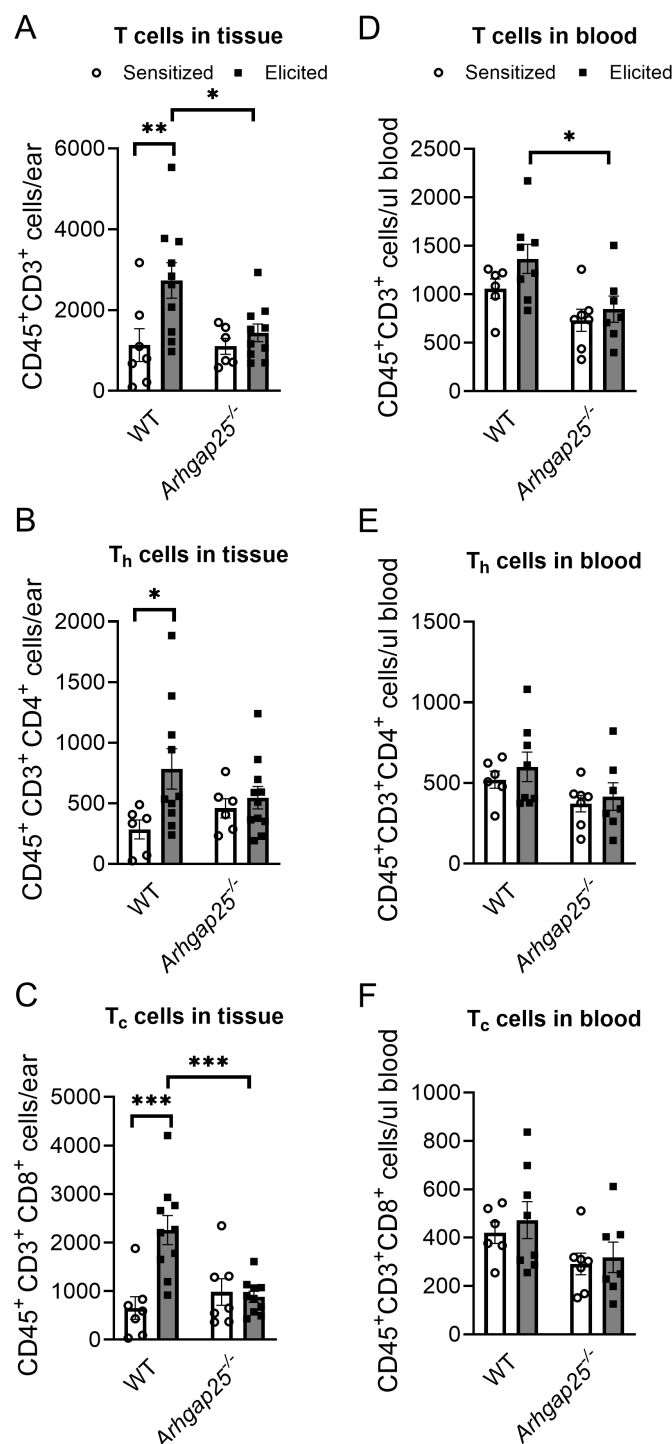


FIGURE 4

Cytotoxic T-cell infiltration was reduced in ARHGAP25 deficient animals after allergen challenge. Similarly, as in the case of myeloid phagocytes, numbers of different subpopulations of T cells were measured in the blood and the ears of animals after TNCB treatment. In the elicited ears, total T cell recruitment was reduced, cytotoxic T cell numbers decreased (A, C), while helper T cell numbers were unaffected (B). On the other hand, total T cell numbers were reduced in the blood of animals treated with TNCB twice (D), but helper and cytotoxic T cells did not show any alterations between the two genotypes (E, F). Mean \pm SEM of 6–11 mice per group in three independent experiments are plotted. * $p < 0.05$, ** $p < 0.01$, *** $p < 0.001$.

the *Arhgap25*^{-/-} mice after elicitation compared to WT (Figure 4D). On the other hand, the number of T cells did not differ in the sensitized animals, just as the number of helper or cytotoxic T cells did not differ, neither in the sensitized nor the elicited animals

(Figures 4D–F). These data suggest that ARHGAP25 primarily affects the infiltration of effector leukocytes in the elicitation phase of the disease, and the protein is less involved in leukocyte recruitment during sensitization.

3.4 In the absence of ARHGAP25, cytokine composition in the allergen-treated ears is altered

Since the difference in leukocyte infiltration in the case of KO animals could be either the reason or the consequence of an altered cytokine profile, cytokine array and ELISA measurements were conducted. Supernatants of digested ear samples were pooled (9 per experimental group) and used on a mouse cytokine array (Figures 5A, B). Densitometric analysis of the array revealed that sICAM-1, C5/C5a, IL-1 α , and TIMP-1 were present at a high level in both the sensitized and elicited mice, independently from the genotype. IL-1ra and CCL2 also showed high expression in sensitized animals, but their signal was further increased upon the second exposure to the allergen (Figures 5A–C). Expression of most CC and CXC chemokines was low in the sensitized mice, and the second treatment with the allergen increased their level, but to a much higher degree in the WT than in the KO animals. KC (CXCL1) level was in the intermediate range in WT after sensitization, whereas *Arhgap25*^{−/−} mice showed lower signals. However, the second allergen challenge increased expression to a similar level in both genotypes. In contrast, the SDF-1 (CXCL12) level decreased in the WT upon the second treatment with the allergen, while it increased slightly in the knock-out. M-CSF expression was in the medium range in the WT before and also after the second treatment with TNCB, whereas it showed lower expression in the KO, in both treatment groups. Interestingly, IFN- γ , IL-17, IL-7, IL-27, and IL-4 signals were decreased in the WT upon elicitation but remained at low levels in the KO in both groups, suggesting an altered cytokine milieu not only in the elicitation, but also in the sensitization phase (Figures 5A–C).

Next, we measured the exact concentrations of IL-1 β and MIP-2 (CXCL2), which were proven to be influenced by ARHGAP25 in inflammatory conditions (10). The second encounter with the allergen significantly increased the concentration of IL-1 β both in WT and KO. However, its amount in the KO mice was considerably lower than in the WT (Figure 5D). MIP-2 showed a similar picture; however, we did not observe a significant decrease in the KO compared to the WT after the second encounter with the allergen. It also should be noted that the elicitation did not cause a substantial increase in MIP-2 concentration in the case of KO (Figure 5E).

A transwell migration assay was conducted to connect the difference observed in leukocyte infiltration to the altered cytokine composition in the absence of ARHGAP25. With this assay, we could test whether altered cytokine milieu affects neutrophil migration *in vitro*. Bone marrow-derived neutrophils were isolated, and their transmigrating capability toward the cytokine containing pooled, cell-free supernatants obtained from digested ear samples of sensitized or elicited WT and KO mice was measured (9 per experimental group). When we compared the individual effects of each supernatant, we did not observe any difference in the migration of WT and KO neutrophils. However, the supernatant collected from elicited WT animals significantly

increased the migration of both WT and KO cells compared to the supernatant of only sensitized WT mice.

Interestingly, the supernatant obtained from the ears of elicited KO mice could not enhance the migration of either WT or KO neutrophils compared to the supernatant of sensitized KO mice. Moreover, transmigration of both WT and ARHGAP25 deficient neutrophils was significantly decreased towards the supernatant of elicited KO, compared to that of elicited WT (Figure 5F).

3.5 T cell counts and activation are not affected by ARHGAP25 in the draining lymph nodes after sensitization

Since T lymphocytes, especially helper T cells, play a key role in the development of CHS, and the expression of specific cytokines is already altered during sensitization, it is crucial to clarify whether these results could be caused by altered activation or infiltration of ARHGAP25-deficient T cells. Thus, we harvested the inguinal and axillary lymph nodes of sensitized WT and *Arhgap25*^{−/−} mice. Flow cytometric analysis of the lymph node-derived cells revealed that sensitization with TNCB on the abdominal skin significantly increased the total cell number. The helper (CD3⁺CD4⁺) and cytotoxic (CD3⁺CD8⁺) T cell counts in the lymph nodes were also increased in both genotypes; however, the differences were statistically insignificant (Figures 6A, B, Supplementary Figure S2).

We were also curious whether the activation state of T cells could be altered in ARHGAP25-deficient animals after sensitization. Using flow cytometry, we measured the expression of CD25, as the alpha subunit of the IL-2 receptor is a late activation marker of lymphocytes and regulatory T cells, and the expression of the transmembrane C-type lectin protein CD69, an early activation marker of T cells (31). We found that the ratio of CD25 expressing CD4⁺ helper T cells was significantly increased upon sensitization, while the ratio of CD69 expressing cells was considerably higher within both sensitized CD4⁺ helper and CD8⁺ cytotoxic T cells than the unsensitized control. However, we could not detect significant differences between WT and KO cells (Figures 6C–F).

These data suggest that, in the absence of ARHGAP25, neither the number of T cells nor the activation state differs from WT after sensitization in the draining lymph nodes.

Next, we investigated whether the activated, lymph node-derived cells deficient in ARHGAP25 could reduce the severity of CHS on a WT background. Thus, we obtained cells from the inguinal and axillary lymph nodes of sensitized WT and *Arhgap25*^{−/−} mice and transferred them into resting recipient WT and KO animals (as a sensitization step). After the cell transfer, the ears of the recipient mice were treated with TNCB as elicitation with the allergen, and ear thickness was measured as previously. Surprisingly, we found that ear thickening was reduced significantly only in KO-recipient animals receiving WT lymph node cells (WT \rightarrow *Arhgap25*^{−/−}). Ear thickening after transferring KO lymph node cells into WT mice (*Arhgap25*^{−/−} \rightarrow WT) did not differ from the wt cell receiving wt recipient (WT \rightarrow WT) (Figure 6G).

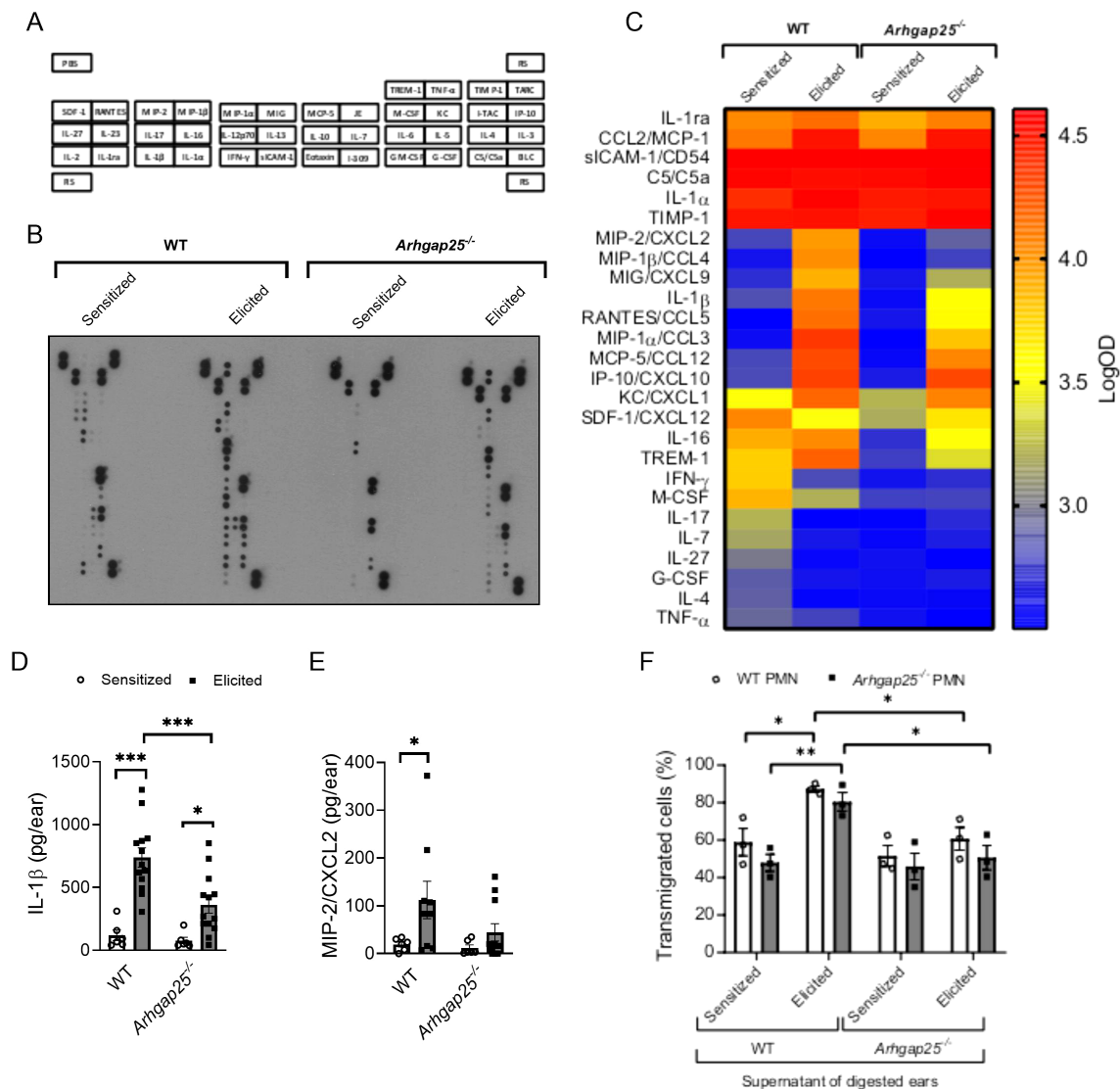


FIGURE 5

In the absence of ARHGAP25, allergen treatment reduced cytokine production and altered cytokine profile. Pooled samples of the digested ears' supernatant were used on a cytokine array to detect possible alterations of cytokine profile in the case of ARHGAP25 deficient mice. The map of cytokines immobilized on the membranes in duplicates is shown (A). Representative picture of an x-ray film developed from the array (B). Heat map of integrated pixel density in Logarithmic scale of different cytokines of the array in the experimental groups (C). The concentration of IL-1β and MIP-2 was determined from the supernatants with sandwich ELISA. After TNCB treatment significantly lower IL-1β amount was measured in KO ears compared to WT (D), but only a decreased tendency of MIP-2 amount was measured in the ARHGAP25 deficient ears (E). Transwell assay was conducted using bone marrow-derived neutrophils and pooled, cell-free supernatants of digested ear samples. Both WT and ARHGAP25 KO neutrophils transmigrated to a significantly higher degree when the supernatant of WT elicited ears was added as a stimulus, compared to when the supernatant of WT sensitized ears. Similarly, higher transmigration of both genotypes was measured in the direction of WT elicited supernatant samples compared to KO elicited ones (F). Cytokine array and transwell was measured using pooled samples of 9 animals per experimental group. Mean ± SEM of 6–13 mice per group are plotted in case of the ELISA measurements, and 3 mice per genotype in the case of transwell assay *p<0.05, **p<0.01, ***p<0.001. PMN, Polymorphonuclear neutrophils.

These data suggest that ARHGAP25 is rather involved in the elicitation phase of CHS than in the sensitization phase. Furthermore, it is likely that altered T cell functions, such as reduced activation, are not responsible for the milder inflammation observed in the absence of ARHGAP25 but rather the altered cytokine environment is. Of course, it cannot be ruled out that KO T cells also participate in forming the altered cytokine environment. However, a detailed investigation of the role of ARHGAP25 in T cells is beyond the scope of this project and will be the subject of another publication.

3.6 ARHGAP25 affects β-catenin-signaling in the sensitization phase of contact hypersensitivity

Next, we set out to investigate the possibly altered signaling pathways by ARHGAP25, which could result in the previously described changes in allergic inflammation. Western blot experiments targeting β-catenin, E-cadherin, p38 MAPK, NF-κB, and I-κB were conducted from whole ear tissue lysates (Figure 7A). Densitometric analysis revealed that the second challenge with the

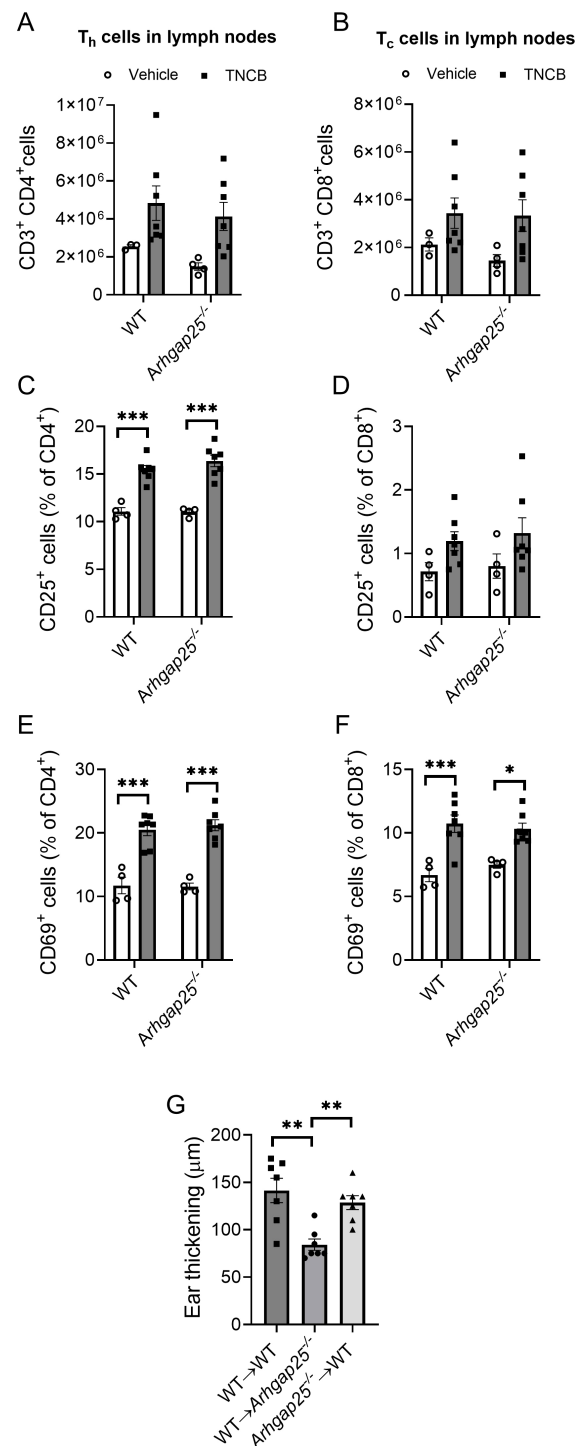


FIGURE 6

The absence of ARHGAP25 did not affect T cell count and activation in the lymph nodes during sensitization. Inguinal and axillary lymph nodes of mice were excised five days after abdominal allergen or vehicle treatment. After homogenization, the obtained cells were labeled for different T cell-specific (CD3, CD4, and CD8) and T cell activation markers (CD25 and CD69). Flow cytometry revealed that allergen treatment increased the number of T helper cells (A) and cytotoxic T cells in the lymph nodes (B) independently of the genotype. The ratio of activated, CD25-positive T helper cells significantly increased in the allergen-treated animals compared to vehicle-treated ones, but there was no difference between KO and WT in this regard either (C). In the case of cytotoxic T cells, a similar increase was detectable, although it was not significant (D). Activation was measured through CD69 positivity as well, which significantly increased in both helper (E) and cytotoxic T cells (F) and was also independent of the genotype. Five million cells derived from lymph nodes of TNCB-treated mice were injected retroorbitally into recipient animals, and the increase in ear thickness was measured after 24 hours. In the case of ARHGAP25 deficient mice receiving WT lymph node-derived cells, ear thickening was significantly lower than WT cells receiving WT and KO cells receiving WT animals (G). Mean \pm SEM of 3–7 mice per group in two independent experiments are plotted. * $p < 0.05$, ** $p < 0.01$, *** $p < 0.001$.

allergen significantly reduced β -catenin expression in WT and KO. We found that sensitization alone also resulted in a significant decrease of β -catenin level in the KO compared to WT (Figure 7B). However, neither the second challenge with TNCB nor the genotype affected the expression of E-cadherin, total p38MAPK, phospho/total p38MAPK, or I- κ B (Figure 7B). Although, based on our previous results, we expected that ARHGAP25 would influence NF- κ B signaling, we only managed to observe small, non-significant changes: After the second exposure to the allergen, NF- κ B expression is reduced slightly in KO mice compared to WT (Figure 7B).

4 Discussion

An in silico analysis in 2004 discovered ARHGAP25 as a new member of the ARHGAP gene family (32). These proteins encoded

by ARHGAP genes regulate the monomeric (or so-called “small”) G proteins of the Rho family. Our research group was the first to clone the full-length ARHGAP25 protein and proved that its GTPase activating effect is specific to RAC, a prominent member of the Rho family (13). In silico data mining, Northern blot, and Western blot experiments revealed that ARHGAP25 is present in all the major leukocyte types. As a phagocyte physiology research group, we investigated its role only in neutrophilic granulocytes. Later, a publication described the regulatory effect of ARHGAP25 on B cells (33), but there is still no data about its role in other immune cells, such as dendritic cells or T lymphocytes.

Meanwhile, more and more publications report ARHGAP25 as an essential regulator of migration and metastasis of tumor cells with non-hematopoietic origin (16–20, 29, 30, 34, 35). Surprisingly, our recent study revealed that, besides leukocytes, ARHGAP25 is highly expressed in fibroblast-like synoviocytes and may be involved in their regulation during the development of serum-

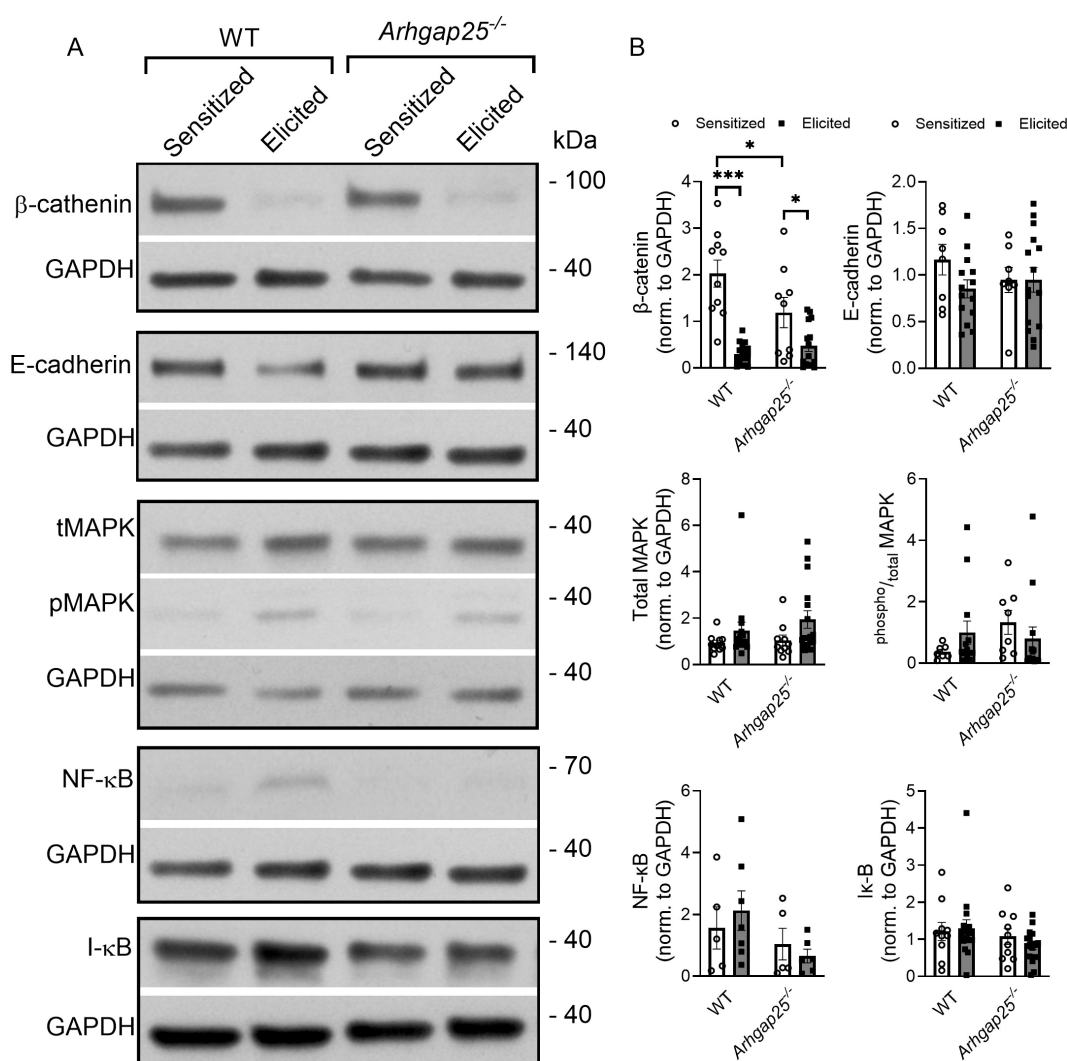


FIGURE 7

Investigation of the signaling pathways likely affected by ARHGAP25 in allergic dermatitis. Twenty-four hours after treating ears with TNCB, ears were removed, snap-frozen in liquid nitrogen, lysed, and western blot analysis of different signaling proteins was conducted. Representative western blots for the β -catenin, E-cadherin, p38MAPK, NF- κ B, and I- κ B are shown (A). Densitometric evaluation of the Western blots (B). Mean \pm SEM of 5–16 mice per group are plotted. *p < 0.05; ***p < 0.001.

transfer arthritis (10). Interestingly, examining skin samples of human patients suffering from allergic contact dermatitis also showed significantly increased expression of ARHGAP25 at the mRNA and protein levels.

These results prompted us to investigate the role of ARHGAP25 in a more complex inflammatory disease model in which neutrophils and macrophages participate together with dendritic cells, mast cells, T cells, and with non-hematopoietic keratinocytes. For this purpose, we chose the 2-chloro-1,3,5-trinitrobenzene (TNCB)-induced contact hypersensitivity mouse model, a well-known and widely used model of human allergic contact dermatitis. The first TNCB treatment sensitizes the animals, and the second encounter with the allergen triggers the inflammatory disease. Consistent with the human results, we observed increased ARHGAP25 expression in the ear tissue samples of TNCB-treated mice (21–23).

Investigating the severity of inflammation, the first TNCB treatment did not result in any significant difference in the thickening of the ears between WT and ARHGAP25-deficient mice. However, the second encounter with the allergen markedly enhanced the ear thickening, a characteristic disease symptom resulting from intense leukocyte infiltration and edema formation. However, this was significantly less pronounced in KO. Repeating the experiments with bone-marrow chimeric mice, in which only the cells with hematopoietic origin are ARHGAP25 knock-out (or WT in the control), and the non-hematopoietic cells are WT, we found similar differences as in the case of the complete knock-out vs WT. This strongly suggests that ARHGAP25 participates in the development of CHS by regulating leukocyte functions and does not directly affect the non-hematopoietic cells, such as keratinocytes. This was further confirmed by our investigations, where we ruled out the presence of ARHGAP25 in the ear epidermis, even after the elicitation phase.

As we described earlier, lacking ARHGAP25 enhances the migration capability, especially the extravasation of leukocytes (10, 14). Based on this, we would expect an increased leukocyte infiltration in the inflamed ears of KO mice. However, similarly to the serum-transfer arthritis model (10), the absence of ARHGAP25 suppressed immune cell infiltration upon the second exposure of TNCB. This difference was especially obvious in the case of macrophages and cytotoxic T cells, perhaps the most important cell types in the elicitation phase of the disease. These results prompted us to investigate the cytokine milieu in the inflamed ears. With the limitations of the cytokine array in mind (being a semi-quantitative method measured from pooled samples), we observed that most of the CC and CXC chemokines' levels increased as a response to the second contact with the allergen, and this increase was less pronounced in KO.

In contrast, most interleukins showed a different profile. While they decreased after the second encounter with TNCB in the WT groups, the initial elevation after the sensitization was absent in the case of the KO. These data, supplemented with the quantitative analysis of IL-1 β and MIP-2 expression providing similar results, suggest that ARHGAP25 regulates the cytokine environment in inflammatory conditions both in the sensitization and the elicitation phase of CHS. *In vitro* transwell assay supported these

findings since supernatants obtained from the ear lysate of elicited KO mice could not increase the migration of either WT or KO neutrophils, whereas supernatants collected from digested ears of elicited WT mice resulted in a similar increase in the migration of both WT and KO cells. These data suggest that not the cell-autonomous migration but the cytokine milieu is affected by the lack of ARHGAP25; therefore, this is the likely reason behind the observed difference in the leukocyte recruitment to the inflamed tissue.

Helper T cells are the key players in the sensitization phase of CHS, while cytotoxic T cells are essential effectors of the elicitation phase. The first contact with TNCB resulted in elevated cell counts and increased T cell activation in the inguinal and axillary lymph nodes, proving a successful sensitization. However, lacking ARHGAP25 did not cause any alteration compared to WT. We successfully initiated sensitization in resting recipient animals by transferring lymph node-derived cells from sensitized mice. However, the second encounter with TNCB decreased ear thickening only if KO recipients received WT lymph node-derived cells, compared to when WT animals received WT lymph node cells. Conversely, in WT recipients which received KO cells, no difference was observed. These results confirmed our hypothesis that ARHGAP25 plays a more significant role in elicitation than sensitization and suggest that the T cell homing and activation in the draining lymph nodes after sensitization is not affected by ARHGAP25.

To reveal the molecular mechanisms behind the altered cytokine composition in the absence of ARHGAP25, β -catenin, E-cadherin, MAPK, NF- κ B, and I κ B were investigated at the protein level in the allergen-treated ears. KEGG analysis suggested that these candidates are likely involved in processes characteristic of CHS (data not shown). In addition, it was reported that overexpression of a dominant negative RAC mutant in HeLa cells ultimately inhibits TNF-induced NF- κ B activation (36). Ximei Wu et al. described that RAC1 activation is necessary for the nuclear accumulation of β -catenin (37). RAC is also involved in the β 1 integrin-mediated activation of p38 MAPK (38). Finally, Braga et al. showed that in keratinocytes, RAC is necessary to redistribute E-cadherin to cell borders (39). Based on these findings, the possible role of ARHGAP25 through RAC also arises. Interestingly, we found significant differences only in the case of the β -catenin. Its level was significantly decreased after the second exposure to the allergen, both in WT and KO. However, the absence of ARHGAP25 significantly decreased its level after the first encounter with TNCB. These findings are consistent with the results of Jaewoong et al., who described that β -catenin is involved in regulating inflammatory cytokine release upon house dust allergen and showed that its silencing reduces NF- κ B activity (40). Our study could not detect any significant differences in the NF- κ B protein level; only a downward trend was observed in favor of the KO after the second challenge with TNCB. In our recent paper we identified two new candidates as molecular interactors of ARHGAP25: Syk and 14-3-3 (41) which have been reported to regulate β -catenin (42, 43). Although ARHGAP25 seems to participate predominantly in the elicitation phase, our data indicates that ARHGAP25 regulates the expression of certain cytokines even during sensitization which

suggest that ARHGAP25 may take part in the establishment of an initial pro-inflammatory environment as well, probably through the β -catenin pathway. This may further enhance the inflammatory response during elicitation.

Our study has several limitations that should be considered. While the TNCB-induced mouse model is a well-established tool for studying allergic contact dermatitis (ACD), it does not fully replicate human disease. Additionally, using TNCB as an allergen may not represent the diversity of allergens encountered in human ACD. Our focus on ARHGAP25 provides valuable insights, but it needs to capture the broader complexity of ACD pathogenesis, including interactions with other genes, signaling pathways, and immune cells. The molecular mechanisms underlying ARHGAP25's role also require further clarification. In human studies, the sample size and potential variability related to, e.g., environmental factors could influence the results. Despite this, we can conclude that ARHGAP25 is necessary to develop contact hypersensitivity. This GTPase-activating protein regulates allergic skin inflammation by modulating the cytokine milieu and, through this, leukocyte infiltration. In addition to being a significant player in inflammatory processes and thus may be a therapeutic target, the increase in its expression observed in human patients suffering from ACD suggests that ARHGAP25 might even be used as a biomarker. However, the clinical relevance of ARHGAP25 in human ACD remains to be validated, requiring further translational research.

Data availability statement

The raw data supporting the conclusions of this article will be made available by the authors, without undue reservation.

Ethics statement

The studies involving humans were approved by Committee of Science and Research Ethics of the Medical Research Council (ETT TUKÉB) and approved by the Department of Health Administration of the National Public Health Center of Hungary (Ethical approval number: IV/1707-6/2020/EKU). The studies were conducted in accordance with the local legislation and institutional requirements. The participants provided their written informed consent to participate in this study. The animal study was approved by Animal Experimentation Review Board of Semmelweis University and the Government Office for Pest County, Hungary (Ethical approval numbers: PE/EA/1967-7/2017, PE/EA/00284-7/2021, BA/73/00070-2/2020). The study was conducted in accordance with the local legislation and institutional requirements.

Author contributions

DC: Formal analysis, Investigation, Writing – original draft, Writing – review & editing. PS: Formal analysis, Investigation, Writing – review & editing. KL: Investigation, Methodology,

Writing – review & editing. KE: Formal analysis, Funding acquisition, Investigation, Writing – review & editing. VG: Formal analysis, Investigation, Writing – review & editing. RC-K: Conceptualization, Funding acquisition, Supervision, Writing – original draft, Writing – review & editing.

Funding

The author(s) declare that financial support was received for the research, authorship, and/or publication of this article. This research was funded by research grant No. FK_18 128376 to R. Cs-K., TKP2021-EGA-24 and TKP2021-EGA-25 from the National Research Development and Innovation Office, Hungary. The project also received funding from the János Bolyai Research Scholarship of the Hungarian Academy of Sciences to R. Cs-K. and K. E. The SE250+ Excellence PhD Scholarship supported D. Cz. and P. S. (EFOP-3.6.3-VEKOP-16-2017-00009).

Acknowledgments

The authors thank Regina Tóth-Kun and Bianka Farkas for their expert technical assistance. We also thank Éva Wisniewski for the valuable advice regarding murine epidermis isolation.

Conflict of interest

The authors declare that the research was conducted in the absence of any commercial or financial relationships that could be construed as a potential conflict of interest.

Generative AI statement

The author(s) declare that no Generative AI was used in the creation of this manuscript.

Publisher's note

All claims expressed in this article are solely those of the authors and do not necessarily represent those of their affiliated organizations, or those of the publisher, the editors and the reviewers. Any product that may be evaluated in this article, or claim that may be made by its manufacturer, is not guaranteed or endorsed by the publisher.

Supplementary material

The Supplementary Material for this article can be found online at: <https://www.frontiersin.org/articles/10.3389/fimmu.2025.1509713/full#supplementary-material>

References

- Alfonso JH, Bauer A, Bensefa-Colas L, Boman A, Bubas M, Constandt L, et al. Minimum standards on prevention, diagnosis and treatment of occupational and work-related skin diseases in Europe - position paper of the COST Action StanDerm (TD 1206). *J Eur Acad Dermatol Venereol.* (2017) 31 Suppl 4:31–43. doi: 10.1111/jdv.14316
- Shabgah AG, Fattahi E, Shahneh FZ. Interleukin-17 in human inflammatory diseases. *Postepy Dermatol Alergol.* (2014) 31:256–61. doi: 10.5114/pdia.2014.40954
- Silvestre MC, Sato MN, Reis V. Innate immunity and effector and regulatory mechanisms involved in allergic contact dermatitis. *Bras Dermatol.* (2018) 93:242–50. doi: 10.1590/abd1806-4841.20186340
- Silvestre MC, Reis V. Evaluation of the profile of inflammatory cytokines, through immunohistochemistry, in the skin of patients with allergic contact dermatitis to nickel in the acute and chronic phases. *Bras Dermatol.* (2018) 93:829–35. doi: 10.1590/abd1806-4841.20187126
- Weber FC, Nemeth T, Csepregi JZ, Dudeck A, Roers A, Ozsvari B, et al. Neutrophils are required for both the sensitization and elicitation phase of contact hypersensitivity. *J Exp Med.* (2015) 212:15–22. doi: 10.1084/jem.20130062
- Scheinman PL, Vocanson M, Thyssen JP, Johansen JD, Nixon RL, Dear K, et al. Contact dermatitis. *Nat Rev Dis Primers.* (2021) 7:38. doi: 10.1038/s41572-021-00271-4
- Azeem M, Kader H, Kerstan A, Hetta HF, Serfling E, Goebeler M, et al. Intricate relationship between adaptive and innate immune system in allergic contact dermatitis. *Yale J Biol Med.* (2020) 93:699–709.
- Gober MD, Gaspari AA. Allergic contact dermatitis. *Curr Dir Autoimmun.* (2008) 10:1–26. doi: 10.1159/000131410
- Smith HR, Basketter DA, McFadden JP. Irritant dermatitis, irritancy and its role in allergic contact dermatitis. *Clin Exp Dermatol.* (2002) 27:138–46. doi: 10.1046/j.1365-2230.2002.00997.x
- Czaran D, Sasvari P, Horvath AI, Ella K, Sudy AR, Borbely E, et al. Lacking ARHGAP25 mitigates the symptoms of autoantibody-induced arthritis in mice. *Front Immunol.* (2023) 14:1182278. doi: 10.3389/fimmu.2023.1182278
- Ligeti E, Welti S, Scheffzek K. Inhibition and termination of physiological responses by GTPase activating proteins. *Physiol Rev.* (2012) 92:237–72. doi: 10.1152/physrev.00045.2010
- Csepányi-Komi R, Pasztor M, Bartos B, Ligeti E. The neglected terminators: Rho family GAPs in neutrophils. *Eur J Clin Invest.* (2018) 48 Suppl 2:e12993. doi: 10.1111/eci.12993
- Csepányi-Komi R, Sirokmany G, Geiszt M, Ligeti E. ARHGAP25, a novel Rac GTPase-activating protein, regulates phagocytosis in human neutrophilic granulocytes. *Blood.* (2012) 119:573–82. doi: 10.1182/blood-2010-12-324053
- Csepányi-Komi R, Wisniewski E, Bartos B, Levai P, Nemeth T, Balazs B, et al. Rac GTPase activating protein ARHGAP25 regulates leukocyte transendothelial migration in mice. *J Immunol.* (2016) 197:2807–15. doi: 10.4049/jimmunol.1502342
- Lorincz AM, Szarvas G, Smith SM, Ligeti E. Role of Rac GTPase activating proteins in regulation of NADPH oxidase in human neutrophils. *Free Radic Biol Med.* (2014) 68:65–71. doi: 10.1016/j.freeradbiomed.2013.12.001
- Tao L, Zhu Y, Gu Y, Zheng J, Yang J. ARHGAP25: A negative regulator of colorectal cancer (CRC) metastasis via the Wnt/beta-catenin pathway. *Eur J Pharmacol.* (2019) 858:172476. doi: 10.1016/j.ejphar.2019.172476
- Xu K, Liu B, Ma Y. The tumor suppressive roles of ARHGAP25 in lung cancer cells. *Oncotargets Ther.* (2019) 12:6699–710. doi: 10.2147/OTT.S207540
- Shi F, Wu J, Jia Q, Li K, Li W, Shi Y, et al. Relationship between the expression of ARHGAP25 and RhoA in non-small cell lung cancer and vasculogenic mimicry. *BMC Pulm Med.* (2022) 22:377. doi: 10.1186/s12890-022-02179-5
- Han S, Jin X, Hu T, Chi F. ARHGAP25 suppresses the development of breast cancer by an ARHGAP25/Wnt/ASCL2 feedback loop. *Carcinogenesis.* (2023) 44:369–82. doi: 10.1093/carcin/bgad042
- Huang WK, Chen Y, Su H, Chen TY, Gao J, Liu Y, et al. ARHGAP25 inhibits pancreatic adenocarcinoma growth by suppressing glycolysis via AKT/mTOR pathway. *Int J Biol Sci.* (2021) 17:1808–20. doi: 10.7150/ijbs.55919
- Harada D, Takada C, Tsukumo Y, Takaba K, Manabe H. Analyses of a mouse model of the dermatitis caused by 2,4,6-trinitro-1-chlorobenzene (TNCB)-repeated application. *J Dermatol Sci.* (2005) 37:159–67. doi: 10.1016/j.jdermsci.2004.11.007
- Honda T, Egawa G, Grabbe S, Kabashima K. Update of immune events in the murine contact hypersensitivity model: toward the understanding of allergic contact dermatitis. *J Invest Dermatol.* (2013) 133:303–15. doi: 10.1038/jid.2012.284
- Shiohara T, Hayakawa J, Mizukawa Y. Animal models for atopic dermatitis: are they relevant to human disease? *J Dermatol Sci.* (2004) 36:1–9. doi: 10.1016/j.jdermsci.2004.02.013
- Zemelka-Wiacek M, Majewska-Szczepanik M, Gajdanowicz P, Szczepanik M. Contact hypersensitivity as a murine model of allergic contact dermatitis. *J Vis Exp.* (2023) 19(191). doi: 10.3791/6525
- Kovacs M, Nemeth T, Jakus Z, Sitaru C, Simon E, Futosi K, et al. The Src family kinases Hck, Fgr, and Lyn are critical for the generation of the *in vivo* inflammatory environment without a direct role in leukocyte recruitment. *J Exp Med.* (2014) 211:1993–2011. doi: 10.1084/jem.20132496
- Mocsai A, Ligeti E, Lowell CA, Berton G. Adhesion-dependent degranulation of neutrophils requires the Src family kinases Fgr and Hck. *J Immunol.* (1999) 162:1120–6. doi: 10.4049/jimmunol.162.2.1120
- Yang TT, Sinai P, Kain SR. An acid phosphatase assay for quantifying the growth of adherent and nonadherent cells. *Anal Biochem.* (1996) 241:103–8. doi: 10.1006/abio.1996.0383
- Nemeth T, Futosi K, Sitaru C, Ruland J, Mocsai A. Neutrophil-specific deletion of the CARD9 gene expression regulator suppresses autoantibody-induced inflammation *in vivo*. *Nat Commun.* (2016) 7:11004. doi: 10.1038/ncomms11004
- Zhang Y, Lin Y, Zhu Y, Zhang X, Tao L, Yang M. ARHGAP25 expression in colorectal cancer as a biomarker associated with favorable prognosis. *Mol Clin Oncol.* (2022) 16:84. doi: 10.3892/mco.2022.2517
- Liu X, Zhang S, Wang D, Lv K, Wang Y, Peng L. The expression and clinical significance of ARHGAP25 in osteosarcoma based on bioinformatics analysis. *Sci Rep.* (2024) 14:18720. doi: 10.1038/s41598-024-68318-6
- Adamczyk M, Bartosinska J, Raczkiewicz D, Kowal M, Surdacka A, Krasowska D, et al. The expression of activation markers CD25 and CD69 increases during biologic treatment of psoriasis. *J Clin Med.* (2023) 12(20):6573. doi: 10.3390/jcm12206573
- Katoh M, Katoh M. Identification and characterization of ARHGAP24 and ARHGAP25 genes in silico. *Int J Mol Med.* (2004) 14:333–8. doi: 10.3892/ijmm.14.2.333
- Lindner SE, Egelston CA, Huard SM, Lee PP, Wang LD. Arhgap25 deficiency leads to decreased numbers of peripheral blood B cells and defective germinal center reactions. *Immunohorizons.* (2020) 4:274–81. doi: 10.4049/immunohorizons.2000021
- Thuault S, Comunale F, Hasna J, Fortier M, Planchon D, Elarouci N, et al. The RhoE/ROCK/ARHGAP25 signaling pathway controls cell invasion by inhibition of Rac activity. *Mol Biol Cell.* (2016) 27:2653–61. doi: 10.1091/mbc.e16-01-0041
- Tao L, Gu Y, Zheng J, Yang J, Zhu Y. Weichang'an suppressed migration and invasion of HCT116 cells by inhibiting Wnt/beta-catenin pathway while upregulating ARHGAP25. *Biotechnol Appl Biochem.* (2019) 66:787–93. doi: 10.1002/bab.v66.5
- Williams LM, Lali F, Willetts K, Balague C, Godessart N, Brennan F, et al. Rac mediates TNF-induced cytokine production via modulation of NF-kappaB. *Mol Immunol.* (2008) 45:2446–54. doi: 10.1016/j.molimm.2007.12.011
- Wu X, Tu X, Joeng KS, Hilton MJ, Williams DA, Long F. Rac1 activation controls nuclear localization of beta-catenin during canonical Wnt signaling. *Cell.* (2008) 133:340–53. doi: 10.1016/j.cell.2008.01.052
- Mainiero F, Soriani A, Strippoli R, Jacobelli J, Gismondi A, Piccoli M, et al. RAC1/P38 MAPK signaling pathway controls beta1 integrin-induced interleukin-8 production in human natural killer cells. *Immunity.* (2000) 12:7–16. doi: 10.1016/S1074-7613(00)80154-5
- Braga VM, Del Maschio A, Machesky L, Dejana E. Regulation of cadherin function by Rho and Rac: modulation by junction maturation and cellular context. *Mol Biol Cell.* (1999) 10:9–22. doi: 10.1091/mbc.10.1.9
- Jang J, Ha JH, Kim SM, Kim W, Kim K, Chung SI, et al. beta-catenin mediates the inflammatory cytokine expression induced by the Der p 1 house dust mite allergen. *Mol Med Rep.* (2014) 9:633–8. doi: 10.3892/mmr.2013.1852
- Sasvari P, Pettko-Szandtner A, Wisniewski E, Csepányi-Komi R. Neutrophil-specific interactome of ARHGAP25 reveals novel partners and regulatory insights. *Sci Rep.* (2024) 14:20106. doi: 10.1038/s41598-024-71002-4
- Zhen J, Jiao K, Yang K, Wu M, Zhou Q, Yang B, et al. The 14-3-3eta/GSK-3beta/beta-catenin complex regulates EndMT induced by 27-hydroxycholesterol in HUVECs and promotes the migration of breast cancer cells. *Cell Biol Toxicol.* (2021) 37:515–29. doi: 10.1007/s10565-020-09564-y
- Zheng H, Jia L, Liu CC, Rong Z, Zhong L, Yang L, et al. TREM2 promotes microglial survival by activating wnt/beta-catenin pathway. *J Neurosci.* (2017) 37:1772–84. doi: 10.1523/JNEUROSCI.2459-16.2017
- Pedersen E, Wang Z, Stanley A, Peyrollier K, Rösner LM, Werfel T, et al. RAC1 in keratinocytes regulates crosstalk to immune cells by Arp2/3-dependent control of STAT1. *J Cell Sci.* (2012) 125(Pt 22):5379–90. doi: 10.1242/jcs.107011
- Trujillo-Paez JV, Peng G, Le Thanh Nguyen H, Nakamura M, Umehara Y, Yue H, et al. Calcitriol modulates epidermal tight junction barrier function in human keratinocytes. *J Dermatol Sci.* (2024) 114(1):13–23. doi: 10.1016/j.jdermsci.2024.02.001
- Hirata H, Dobrokhotov O, Sokabe M. Coordination between cell motility and cell cycle progression in keratinocyte sheets via cell-cell adhesion and Rac1. *iScience.* (2020) 23(11):101729. doi: 10.1016/j.isci.2020.101729



OPEN ACCESS

EDITED BY
Kyle T. Amber,
Rush University, United States

REVIEWED BY
Li Zhou,
Wuhan University, China
Ming-Lin Liu,
University of Pennsylvania, United States
Sawa Kostin,
Brandenburg Medical School Theodor
Fontane, Germany

*CORRESPONDENCE
Rui Qiang
✉ 2247283120@qq.com
Wenliang Lyu
✉ lwwenliang@sohu.com
Jiuchong Wang
✉ wangjiuchong@sohu.com;

†These authors have contributed equally to this work

RECEIVED 10 October 2024
ACCEPTED 17 February 2025
PUBLISHED 05 March 2025

CITATION
Li Y, Cao Z, Liu J, Qiang R, Wang J and Lyu W
(2025) Current perspectives and trends of
neutrophil extracellular traps in organ fibrosis:
a bibliometric and visualization study.
Front. Immunol. 16:1508909.
doi: 10.3389/fimmu.2025.1508909

COPYRIGHT
© 2025 Li, Cao, Liu, Qiang, Wang and Lyu. This
is an open-access article distributed under the
terms of the [Creative Commons Attribution
License \(CC BY\)](#). The use, distribution or
reproduction in other forums is permitted,
provided the original author(s) and the
copyright owner(s) are credited and that the
original publication in this journal is cited, in
accordance with accepted academic
practice. No use, distribution or reproduction
is permitted which does not comply with
these terms.

Current perspectives and trends of neutrophil extracellular traps in organ fibrosis: a bibliometric and visualization study

Yanbo Li^{1†}, Zhengmin Cao^{1†}, Jing Liu^{1†}, Rui Qiang^{2*},
Jiuchong Wang^{1*} and Wenliang Lyu^{1*}

¹Department of Infectious Diseases, Guang'anmen Hospital, China Academy of Traditional Chinese Medicine, Beijing, China, ²Department of Oncology, Beijing Hospital of Traditional Chinese Medicine Shunyi Hospital, Beijing, China

New insights into the role of immune responses in the fibrosis process provide valuable considerations for the treatment of organ fibrotic diseases. Neutrophil extracellular traps (NETs) represent a novel understanding of neutrophil functions, and their involvement in organ fibrotic diseases has garnered widespread attention in recent years. This study aims to conduct a bibliometric analysis and literature review focusing on the mechanisms by which NETs participate in fibrotic diseases. Specifically, we utilized a bibliometric dataset that includes 220 papers published in 139 journals, originating from 425 organizations across 39 countries, with a total citation count of 12,301. Keyword co-occurrence analysis indicates that the research focus on the mechanisms of NETs in organ fibrosis is likely to center on NETosis, immune responses, immune thrombosis, inflammation, and tissue damage associated with NET formation. In conclusion, our findings underscore the current status and emerging trends in NET research related to organ fibrosis, offering novel insights into the mechanisms by which NETs contribute to the pathogenesis of fibrotic diseases, as well as potential therapeutic strategies.

KEYWORDS

bibliometrics, visualization, neutrophil extracellular traps, organ fibrosis, neutrophil, immune response

1 Introduction

Fibrosis is a disease characterized by the excessive deposition of extracellular matrix and the destruction of normal parenchymal structures, leading to organ dysfunction (1). Fibrosis can affect various organs and systems throughout the body, including the lungs, liver, heart, kidneys, and skin, resulting in a significant disease burden. Epidemiological data indicate that the annual incidence of major fibrosis-related diseases is approximately 4,968 cases per 100,000 population (2). The pathological process of fibrosis involves dynamic interactions among various cell types. When tissue damage occurs, locally released chemokines attract

immune cell populations from the circulation to the site of injury, including neutrophils, monocytes, and macrophages. These immune cells produce and release a multitude of pro-inflammatory and pro-fibrotic factors, stimulating the activation and abnormal proliferation of fibroblast (3, 4).

Neutrophils are the most abundant type of effector cells and granulocytes within the immune system (5). Once activated, neutrophils can release NETs through a special way of programmed cell death, which is called NETosis (6). Recent studies have elucidated the intricate mechanisms underlying NETosis (7). The primary structural component of NETs is nuclear DNA, and chromatin condensation is an essential prerequisite for its extrusion into the extracellular space. A key event in NETosis is the condensation of chromatin, a process mediated by PAD4-induced histone citrullination (8). The nuclear membrane serves as the initial physical barrier to chromatin release. The rupture of this membrane is facilitated by phosphorylation events, including PKC α -mediated phosphorylation of lamin B (9) and CDK4/6-mediated phosphorylation of lamin A/C (10). The plasma membrane represents the second physical barrier to NET release. Its rupture is primarily associated with the disintegration of the cortical cytoskeleton, including the degradation of actin filaments, microtubules, and peripheral vimentin cytoskeleton (11). Additionally, the actin cytoskeleton is regulated by Rho kinase, which plays a role in the early nuclear translocation of PKC α and CDK4/ (12).

Recent studies have highlighted a significant link between NETs and various organ fibroses, including pulmonary and myocardial fibrosis. NETs contribute to tissue damage through mechanisms such as immune thrombosis, sterile inflammation, and immune dysregulation, driving the progression of fibrotic diseases (13, 14). However, a comprehensive, evidence-based analysis focusing on the current state of research and future directions in the context of NETs and fibrosis remains lacking. This study aims to fill this gap by providing an overview of the latest research trends. Using bibliometric and visual analysis of Web of Science (WOS) publications from 2010 to 2023, we identify key research areas, including NETosis, NET-mediated immune cell crosstalk, NET-induced fibroblast activation and cytotoxicity, and NET-driven immune thrombosis. By synthesizing existing knowledge, this study offers a comprehensive, evidence-based resource for advancing research in the field of NETs and fibrotic diseases.

2 Method

2.1 Data search and retrieval strategy

Literature from Web of Science Core Collection database between January 1, 2010 to September 31, 2023 was downloaded for this study. See search strategy in the Supplementary Information. To ensure accurate interpretation of the results, only article and review in English were included.

2.2 Data process and visualization

To visualize collaborations between countries, institutions, and authors, as well as to analyze co-citations and keyword co-occurrences, VOSviewer version 1.6.16 was used. A burst detection analysis of keywords was conducted using CiteSpace version 6.2.R6. In addition, Scimago Graphica provided visualization support for the analysis. To eliminate redundant entries, synonymous expressions were manually standardized. For instance, “liver fibrosis” and “hepatic fibrosis” were merged.

3 Result

3.1 Annual publications and citation

The study contains 220 papers from 39 countries, 425 organizations, published in 139 journals, and 12301 quotes. **Figure 1** shows the annual number of publications and citation frequency for the period 2010 to 2024. In general, the number of annual publications has increased steadily and quickly. The involvement of NETs in the etiology of fibrotic disorders was not studied before 2010. The number of articles increased slowly between 2010 and 2018, and the research was still in its infancy. The rate of publications started to pick up speed after 2018. In addition, omitting data for 2024 due to incomplete data, there is significant increase in annual postings to over 30 in 2021, 2022, 2023. We hypothesize that this may be related to the increased heat in the NETs research field (15).

3.2 Distribution of countries/regions

Currently, a total of 39 different countries/regions have published studies on NETs in relation to fibrotic diseases, as shown in **Figure 2**. Papers in related fields have been published mainly in North American, Asian, and European countries. **Figure 2B** shows the number of publications in these countries/regions. The United States had the most publications (31.81%, 70), followed by China (20.90%, 46) and Germany (11.82%, 26). **Table 1** shows the top 10 countries/regions. **Figure 2C** shows that in our analysis of global collaborations using the VOS observer, we found that the main links between countries/regions were concentrated between North America and Europe and America, and between North America and East Asia.

3.3 Contributions of institutions

CiteSpace generates a network visualization map of institutional collaboration. The paper on NETs in the study of fibrotic diseases includes contributions from 425 institutions. The United States and China have a large number of institutions engaged in scientific

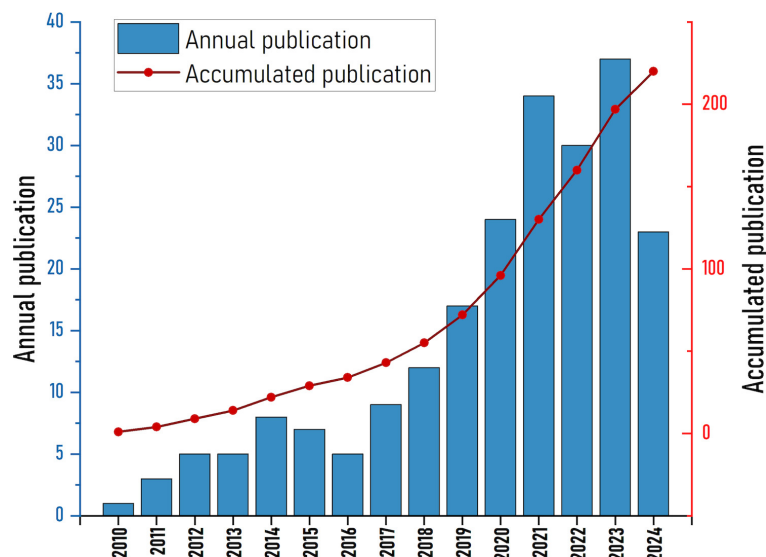


FIGURE 1
Global publication output on NETs in fibrosis diseases from 2010 to 2024.

research. Most of the articles were published by the University of Lisbon, Harvard University, University of Georgia and Democritus University of Thrace from the United States, Sweden and Greece. The VOS viewer presents inter-agency collaboration, as shown in Figure 3. It is found that the University of Lisbon has the highest total connection, but its cooperation with other institutions is limited; Chinese scientific research institutions, represented by Nanjing Medical University and Chinese Academy of Science, and Harvard Medical School formed a green group, suggesting wider cooperation and exchanges.

3.4 Journals and co-cited journals

A total of 139 journals have published articles in the field of NETs and fibrotic diseases. Table 2 lists the 10 journals with the largest number of publications. The journal with the most published papers is *Frontiers in Immunology* (N=17), followed by *International Journal of Molecular Sciences* (N=10) and *Plos One* (N=6). The top three cited journals are *Frontiers in Immunology* (N=569), *Journal of Immunology* (N=480) and *Plos One* (N=427). Among the top 10 magazines, there are 3 journals in JCR Q1 and 7 journals in JCR Q2, and the IF value of 8 journals exceeds 5 points, among which the journal with the highest IF value is *Autoimmunity Reviews* (IF=8.3).

Table 3. Top 10 journals in terms of citations. *Frontiers in Immunology* (569 co-citations) was the most cited magazine, followed by *Journal of Immunology* (480 co-citations) and *Plos One* (427 co-citations). Among the top 10 journals, the journal with the highest impact factor is *Nature Medicine* (IF=89.8), followed by *Science* (IF=83.4) and *Blood* (IF=22.8).

Figure 4 shows dual-map overlay of journals in which research was published. The cited journals were displayed on the right side of

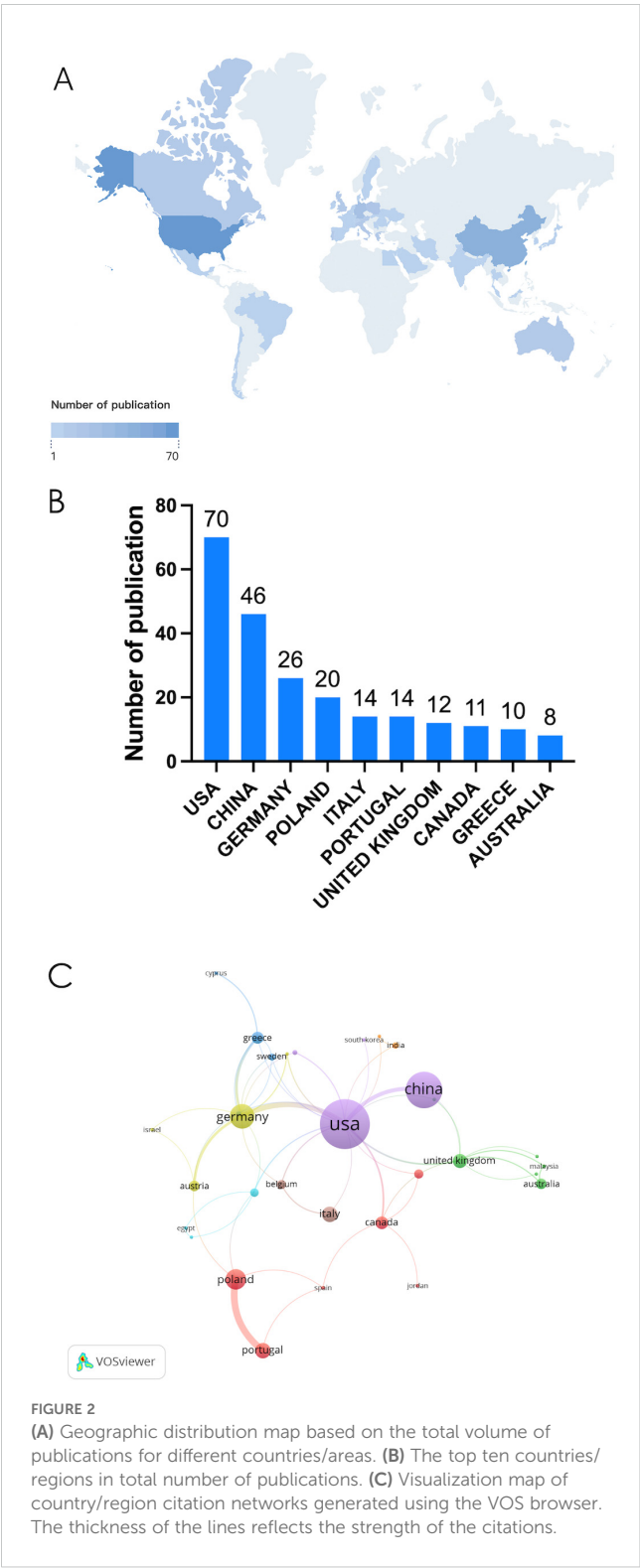
the map, and the citing journals were on the left. Reference paths are shown in different colors. The width of the pathway is related to the frequency of being cited. Currently there are 2 main citation pathways, which means that articles published in *Biology/Molecular/Genetics* journals are usually cited by studies published in *Molecular/Biology/Immunology* and *Medicine/Medical/Clinical* journals.

3.5 Authors

A total of 1574 authors were identified as contributors to the field during the literature search. Table 4 summarizes the top 10 authors by the number of publications. Rebordao Maria Rosa and Ferreira-dias Graca have the most publications, with 13 and 12 papers respectively, indicating their leading achievements in the field. The author cooperation network diagram constructed by VOSviewer shows that there is a strong cooperation relationship between high-yield authors and research teams in the field (Figure 5). The thicker the line between the authors, the more they have published together. Rebordao Maria Rosa and Ferreira-dias Graca are leading researchers in this field, and their cooperation network is the most extensive and influential.

3.6 References with citation bursts

Figure 6 shows the 25 most frequently cited documents. The earliest citation burst occurred in 2007, and the latest in 2021. Among these references, "Cystic Fibrosis Sputum DNA Has NETosis Characteristics and Neutrophil Extracellular Trap Release Is Regulated by Macrophage Migration-Inhibitory Factor" by Markryan Dwyer et al. had the highest burst strength (strength 6.74).



3.7 Keywords analysis of research hotspots

Using CiteSpace and VOSviewer for keyword co-occurrence, timeline, clustering, and burst analysis helps understand the research hotspots, frontiers, and trends in this field. According to VOSviewer statistics, there are 1250 keywords across 220 articles. If these keywords had similar means, they were merged. Through the

TABLE 1 Top 10 countries / regions with the highest number of publications.

rank	country	documents	citations	total link strength
1	USA	70	3033	42
2	CHINA	46	898	9
3	GERMANY	26	1572	30
4	POLAND	20	380	17
5	ITALY	14	260	3
6	PORTUGAL	14	165	15
7	UNITED KINGDOM	12	474	12
8	CANADA	11	860	7
9	GREECE	10	712	10
10	AUSTRALIA	8	239	4

analysis of keywords, we can understand the current situation of NETs in the field of fibrotic diseases.

We employed CiteSpace and VOSviewer to analyze keyword co-occurrence in NETs-related fibrosis research (Figure 7A). The identified research hotspots can be broadly categorized into three main areas. The first group, represented in red, focuses on the pathological mechanisms of NETs in immune thrombosis, including thrombosis, deep vein thrombosis, contributing factors, COVID-19, and rheumatoid arthritis. The second group, denoted in green, emphasizes the immune response and fibrosis promoted by NETs, covering terms such as apoptosis, collagen, inflammation, and macrophages. The third group, shown in blue, highlights fibrotic diseases associated with NETs, including airway inflammation, cystic fibrosis, *Pseudomonas aeruginosa*, and lung disease. Furthermore, our co-occurrence analysis revealed keywords such as “chromatin decompaction,” “NET formation,” and “nuclear membrane rupture,” which are critical to the key steps of nuclear DNA extrusion, extracellular release, and NET formation. Although these terms do not form an independent cluster, they represent important findings that deepen our understanding of NETosis, which is also a prominent research focus within the NETs field.

Figure 7B shows the visualization of keyword time overlap. The earliest key is displayed in purple and blue; The latest keywords are displayed in orange and red. The results showed that the early research on NETs and fibrotic diseases mainly focused on airway inflammation, *pseudomonas-aeruginosa*, disease, release, etc. At this stage, the research mainly focused on proving the accumulation of NETs in tissues in cystic fibrosis, pulmonary fibrosis and other disease models. The latest research mainly focuses on net formation, apoptosis, collagen, injection, etc., suggesting that the recent research focuses on the mechanism that the accumulation of noose NETs aggravates or promotes the fibrosis process. The above analysis results are helpful for researchers to speculate on the future development direction of this field.

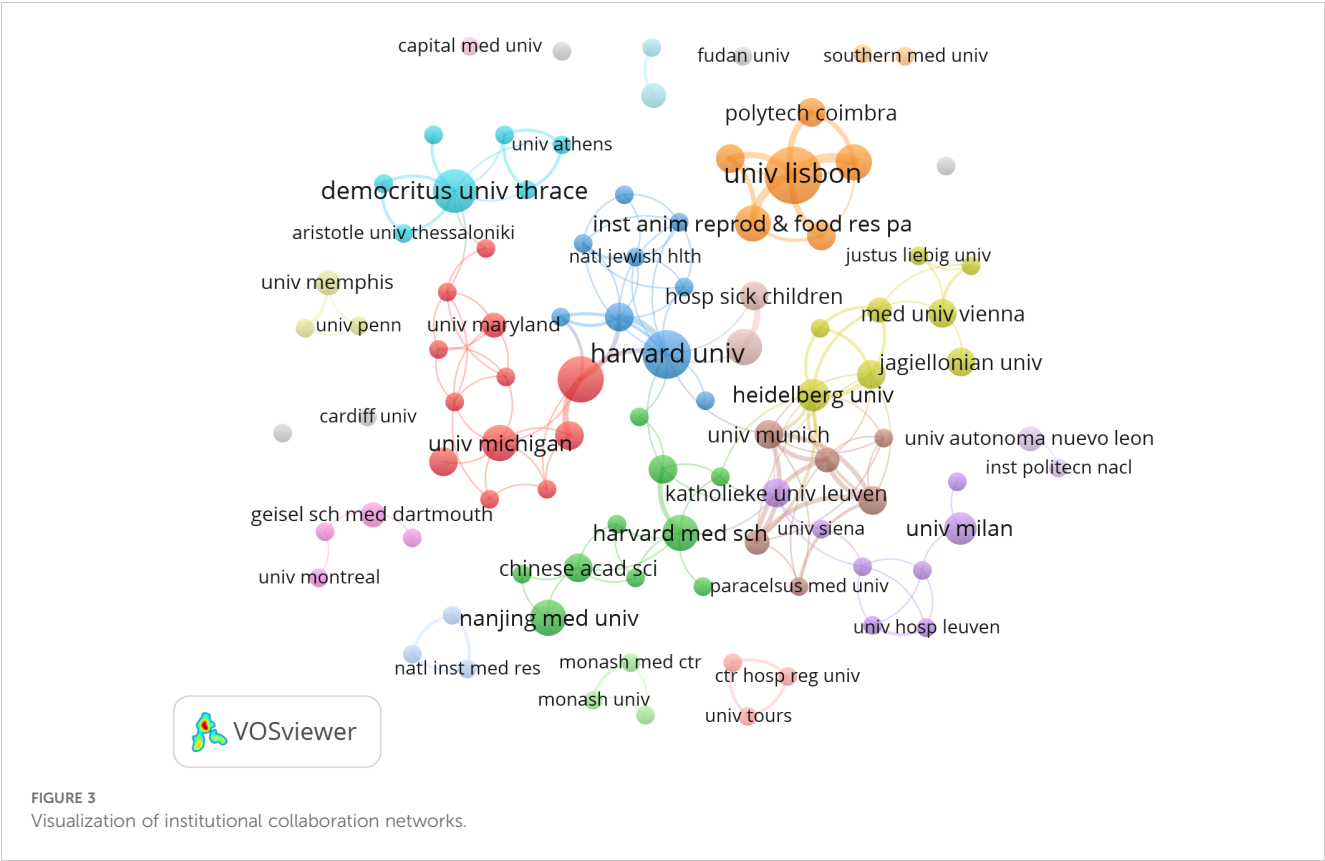


Figure 7C presents a keyword time overlap visualization. Keywords from earlier studies are depicted in purple and blue, while those from more recent research are shown in orange and red. The results indicate that early studies on NETs and fibrotic diseases predominantly focused on airway inflammation, *Pseudomonas aeruginosa*, and the pathogenesis and release of NETs. During this period, research primarily concentrated on the accumulation of NETs in tissue in disease models, such as cystic fibrosis and pulmonary fibrosis. In contrast, more recent studies have shifted toward topics like chromatin

decompaction, NET formation, macrophages, and apoptosis, suggesting a focus on uncovering novel mechanisms of NETosis and its role in promoting fibrosis. These findings provide valuable insights for researchers in predicting future trends in this field.

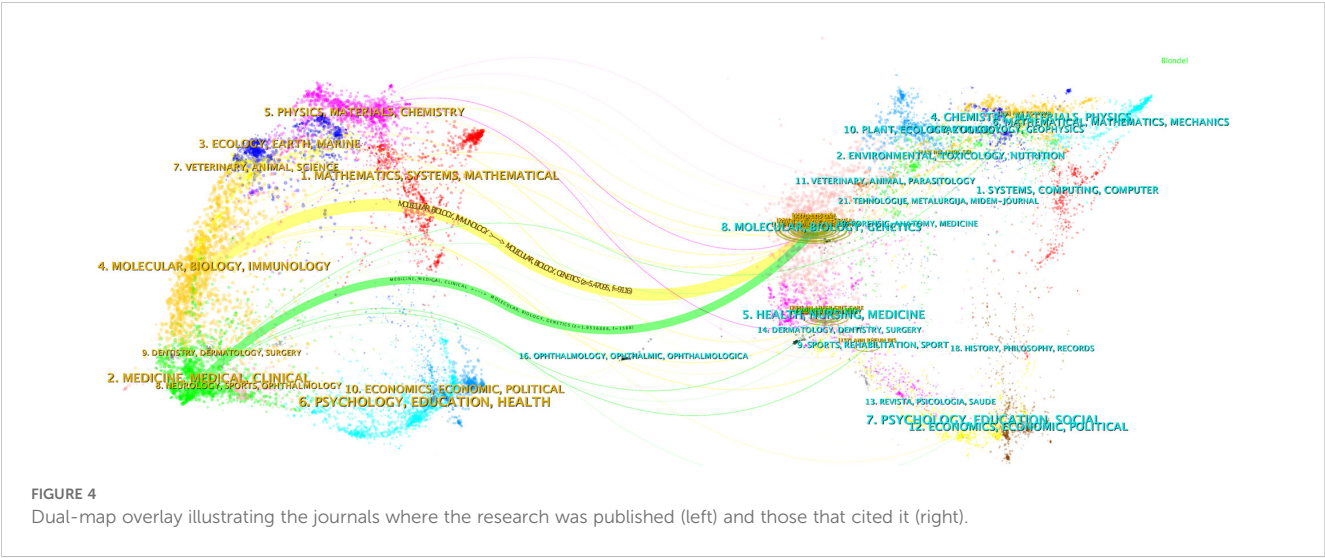
Figure 7C shows the top 25 keywords of the strongest reference burst. It is worth noting that the citation outbreak of some keywords, such as pulmonary fibrosis (2020–2024), dam (2022–2024) and immunity (2022–2024), lasted until 2024, which means that related research fields are still widely concerned today.

TABLE 2 Top 10 journals with the highest number of publications.

Rank	Journal	Count	IF	JCR
1	Frontiers in Immunology	17	5.7	Q1
2	International Journal of Molecular Sciences	10	5.6	Q2
3	Plos One	6	3.7	Q2
4	Journal of Clinical Medicine	5	4.6	Q2
5	American Journal of Respiratory Cell and Molecular Biology	4	5.8	Q2
6	Autoimmunity Reviews	4	8.3	Q1
7	Biomedicines	4	5.2	Q2
8	Biomolecules	4	5.2	Q2
9	Frontiers in Pharmacology	4	5.4	Q2
10	JCI Insight	4	8.6	Q1

TABLE 3 Top 10 most cited journals.

Rank	Co-cited journal	Citations	IF	JCR
1	Frontiers in Immunology	569	5.7	Q1
2	Journal of Immunology	480	4.9	Q2
3	Plos One	427	3.9	Q2
4	Blood	418	22.8	Q1
5	Nature Medicine	328	89.8	Q1
6	Science	295	83.4	Q1
7	American Journal Of Respiratory And Critical Care Medicine	284	20	Q1
8	PNAS	280	11.2	Q1
9	Journal of Clinical Investigation	258	13.3	Q1
10	Journal of Experimental Medicine	225	13.9	Q1



4 Discussion

4.1 Global trends on NETs in fibrosis diseases

As far as we know, this is the first bibliometrics study on NETs and fibrotic diseases. Our results reveal significant findings, research interests and frontiers in this particular area. Figure 1 shows the global growth trend of NETs publications in the field of fibrotic diseases from 2010 to 2024. In the last five years, the literature on NETs and fibrotic diseases has increased rapidly. The exponential growth of literature on neutrophil extracellular traps (NETs) and organ fibrosis since 2010 can be attributed to three interconnected factors: 1) seminal studies have established NETs as pivotal mediators of fibrotic progression across multiple organ systems, including the lung, liver, and kidney. Key discoveries have catalyzed interdisciplinary investigations into their pathophysiological roles; 2) cutting-edge methodologies have revolutionized NETs research. Innovations in single-cell sequencing, multiplex immunofluorescence imaging, and mouse models of fibrosis have made the spatiotemporal

dynamics of NETs precise characterization of NETs; 3) strategic initiatives by major funding bodies have prioritized fibrotic disease mechanisms. Therefore, we assume that although the research on NETs and fibrotic diseases is still in its infancy, this field will continue to grow in the next few years.

According to the distribution of countries/regions (Figure 2), the United States is the countries with the largest proportion of published documents in this field. Correspondingly, Harvard University and University of Georgia in the United States are also in an important position in the institutional cooperation network. Despite the increasing volume of Chinese publications, the limited frequency of international collaborations in Chinese-led research may hinder its visibility and reduce editorial confidence, thereby restricting the ability of Chinese institutions to publish in high-impact international journals. Furthermore, many studies from China have primarily focused on validating established NET-fibrosis pathways in disease models, rather than introducing novel mechanisms, which may diminish their appeal to top-tier journals. Additionally, Chinese researchers often face language and presentation challenges as non-native English speakers, which can further impede the dissemination of their work. We argue that addressing these barriers will significantly enhance the global influence of Chinese institutions in this field.

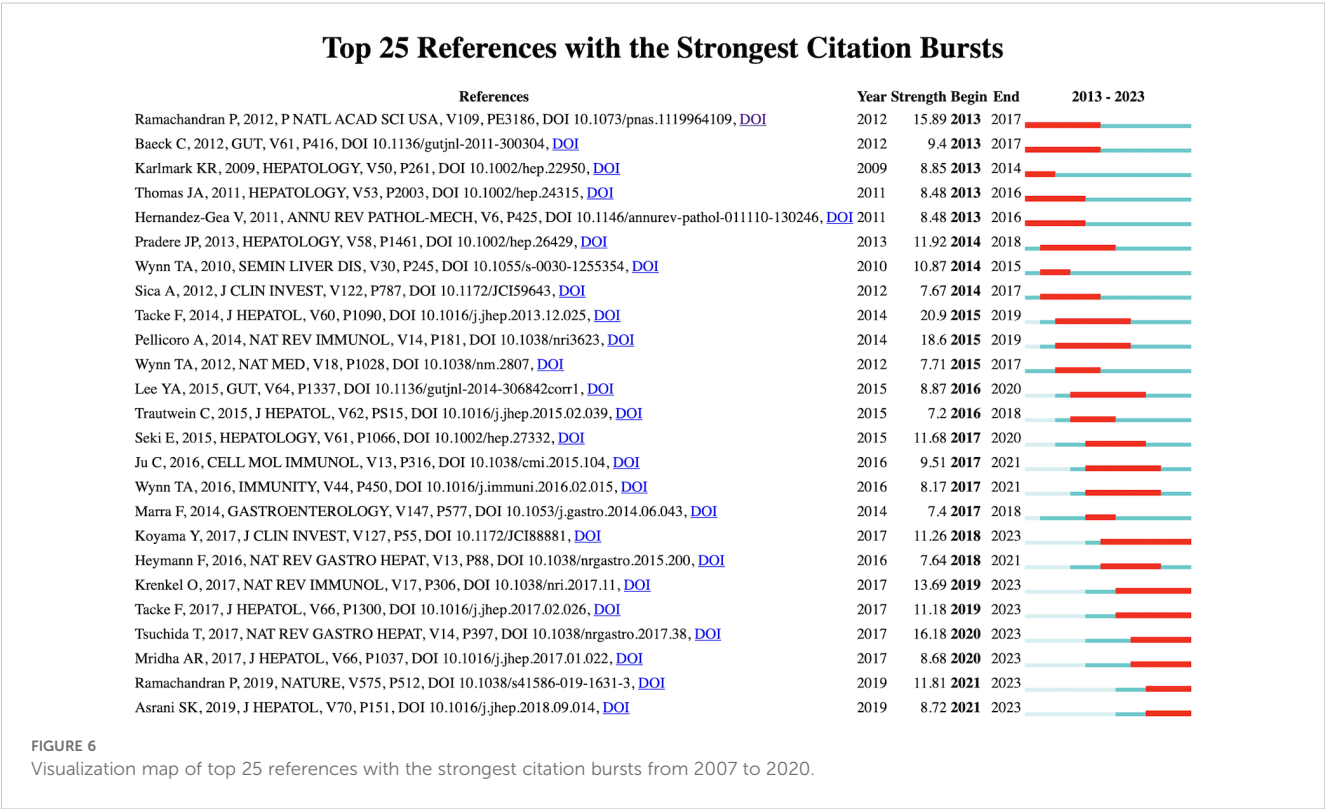
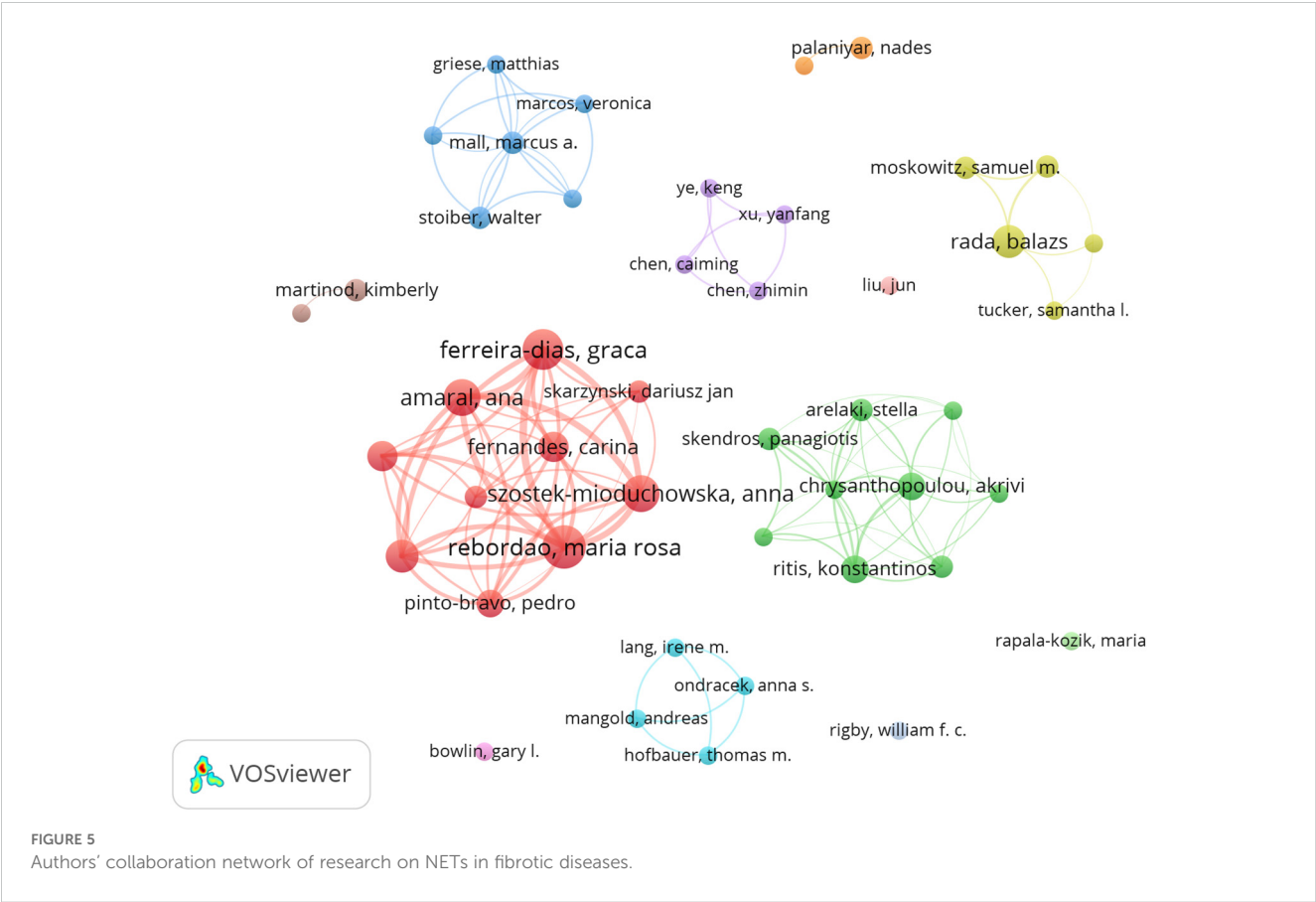
Among the journals shown in Table 2, Frontiers in Immunology, International Journal of Molecular Sciences and Plos One may be the leading journals in the field of fibrotic diseases in NETs, especially the molecular, biological and genetic related sections. In addition, among the top ten authors, Rebordao Maria Rosa and her team have published the most papers and played a major role in this field.

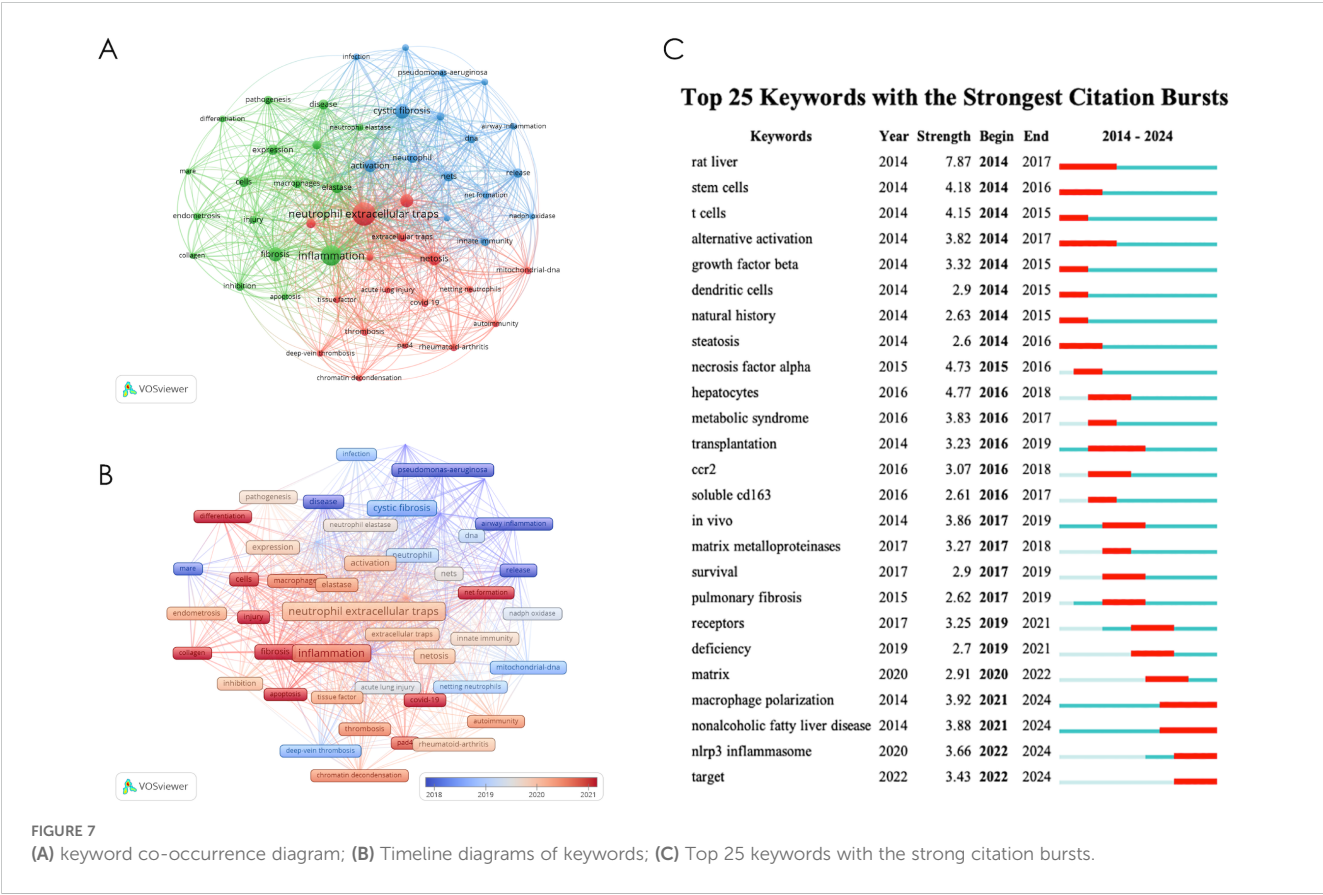
4.2 Hotspots and emerging frontiers in NETs in fibrosis diseases

The reference of citation explosion (Figure 6) shows the widely cited literature in this field, shows the work that scientists are interested in at different stages, and may partially highlight the

TABLE 4 Authors in the top 10 publications.

Rank	Authors	Count
1	Rebordao Maria Rosa	13
2	Ferreira-dias Graca	12
3	Amaral Ana	10
4	Szostek-mioduchowska Anna	10
5	Lukasik Karolina	8
6	Rada Balazs	8
7	Fernandes Carina	7
8	Skarzynski Dariusz J.	7
9	Chrysanthopoulou Akrivi	6
10	Pinto-bravo Pedro	6





changes and trends of research in this field. Most of the early references on outbreak are related to the mechanism of NETs formation and release (16, 17). In 2010, Veronica Marcos et al. first reported that NETs are rich in the airway fluid of cystic fiber patients and mouse models (18). Although the manuscript was withdrawn one year after its publication, this article still attracted the attention of the industry in a short time and was cited 159 times. The role of NETs in the pathological process of cystic fibrosis has been continuously focused on in the subsequent citation outbreak literature (19–21). With the deepening of research, the effects of NETs-derived components such as Neutrophil elastase and Histones have been discovered (22). The review published by Samir Rahman et al. in *Front Immunol* in 2014 summarized the new understanding of NETs in cystic fibrosis (23). After that, the direction of citing outbreak literature gradually diversified, and diseases such as aging-related organ fibrosis (24), COVID-19-related pulmonary fibrosis (25), hepatic fibrosis and systemic sclerosis are gradually gaining attention, and research is progressively deepening to explore the pathological mechanism.

The strongest citation trends associated with specific keywords can serve as predictors for the future trajectory of network research in the field of fibrotic diseases. The results of the keyword co-occurrence analysis highlighted key terms such as “NETosis mechanism,” “immune response,” “fibrosis,” “tissue damage,” and “immune thrombosis.” In the subsequent sections, we will provide a

detailed overview of the latest research findings related to these topics.

4.2.1 The key mechanism of NETosis

Chromatin decondensation or dissolution is considered a prerequisite for NET formation. PAD4-mediated histone citrullination has been identified as a key driver of this process (8). PAD4 facilitates chromatin decondensation by disrupting the tight interaction of histone H1, which is involved in chromatin compaction (26). Recent studies have expanded the role of citrullination beyond histones, including its impact on proteins associated with nuclear and chromatin structures, such as LMNB1, LBR, VIM, and actin filament-related proteins. These findings add a layer of complexity to our understanding of PAD4’s role in NETosis (27). Additionally, histone acetylation contributes to chromatin decondensation by neutralizing positive charges, weakening chromatin’s overall structure and enabling the binding of various proteins that trigger transcriptional programs. These genome-wide transcriptional events are essential for chromatin depolymerization (28). Furthermore, neutrophil elastase (NE) has been recognized as a critical factor in chromatin depolymerization (29). NE translocates from cytoplasmic granules to the nucleus via yet-to-be-identified mechanisms, where it promotes chromatin decondensation by cleaving histones (30). Under the synergistic effect of the above mechanisms, the thick chromatin is decondensed

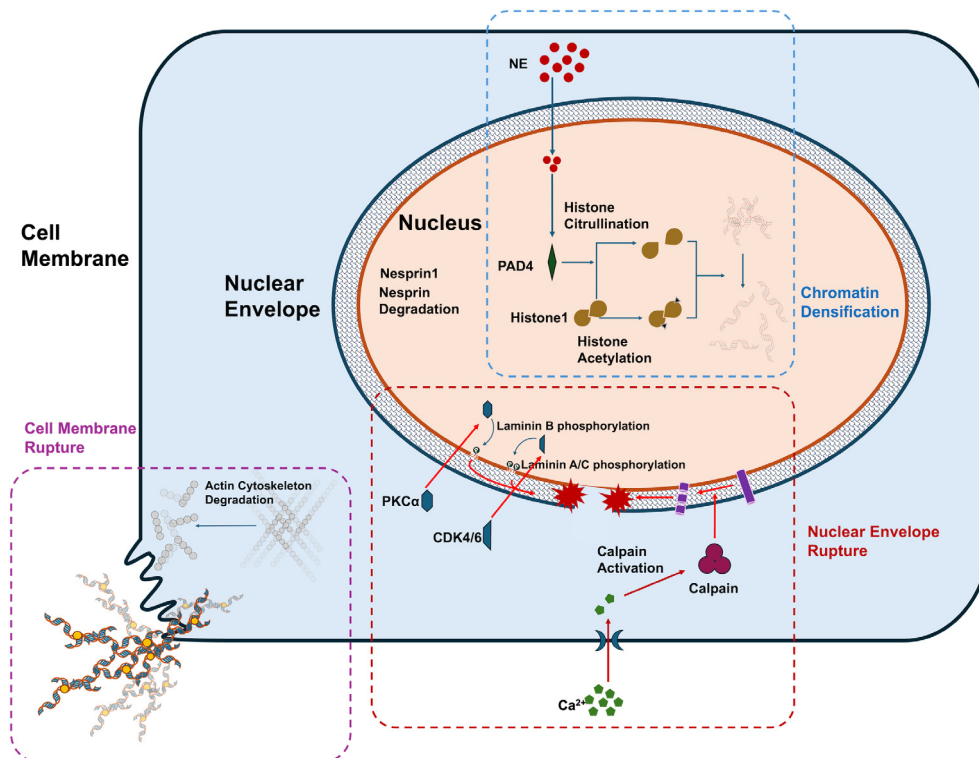


FIGURE 8
The key mechanism of NETosis.

and dissolved, making it possible for it to be released into the extracellular.

It is widely believed that the nuclear envelope represents the first physical barrier that must be breached for NETs release. The nuclear envelope consists of the outer and inner nuclear membranes and the nuclear lamina, which provides structural support. The nuclear lamina is composed of A-type and B-type lamins (31). Recent studies have reported new findings regarding lamin degradation and nuclear envelope rupture. During NETosis, PKC α , which is localized in the cytoplasm of resting neutrophils, translocates to the nucleus. Activated PKC α phosphorylates lamin B, facilitating nuclear envelope rupture. Pharmacological inhibition of PKC α has been shown to suppress NET formation *in vitro* (9). CDK4/6 has also been found to phosphorylate lamin A/C, contributing to nuclear envelope rupture. The use of CDK4/6 inhibitors (abemaciclib/LY2835219) effectively inhibits NET formation in human neutrophils (10). In addition to kinases, calpain-mediated proteolysis also plays a role in nuclear envelope rupture. Recent evidence suggests that Ca²⁺ influx leads to sustained elevation of cytosolic and nuclear Ca²⁺ levels, which activate calpain, causing degradation of the actin cytoskeleton and nuclear nesprin-1. The structural disruption of nesprin-1 leads to the disappearance of nuclear envelope morphology. Calpain inhibitors have been shown to suppress NET formation through this mechanism (32).

The second physical barrier released by NETs is the plasma membrane. The cortical actin cytoskeleton beneath the plasma membrane plays a crucial role in maintaining cell membrane

stability. The rapid disintegration of the cortical actin cytoskeleton is a key event in the extrusion of NETs during the later stages of NET formation. Following stimulation, neutrophils from both mice and humans exhibit rapid breakdown of the actin cytoskeleton, leading to the shedding of membrane microbubbles, disintegration and remodeling of microtubules and intermediate filaments, and blistering of the plasma membrane (11). Additionally, NET formation can directly induce plasma membrane rupture through pyroptosis-related inflammatory factors. Gasdermin E (GSDMD), a pore-forming protein implicated in apoptosis and plasma membrane rupture, translocates to the plasma membrane where it forms pores (33). Recent studies have highlighted the role of GSDMD in NET formation. During NET formation, GSDMD is hydrolyzed and activated, which enhances membrane permeability and facilitates NET extrusion (34). Pharmacological inhibition of GSDMD has been shown to suppress NET release, and interestingly, neutrophil elastase (NE) may also participate in GSDMD activation (35). These findings provide new insights into the mechanisms by which NE contributes to NET formation. The above NETosis mechanism is shown in Figure 8.

4.2.2 NETs-immune cell crosstalk

The inflammatory response characterized by the infiltration of immune cells such as neutrophils, macrophages, and monocytes is considered a key culprit in the development of organ fibrosis. The intricate relationships among these cells have been a focal point of

interest and challenge. NETs, as products of neutrophils, contain various pro-inflammatory mediators such as cytokines and chemokines, providing a pathway for crosstalk between neutrophils and other immune cells, including macrophages and monocytes, thereby exerting a broad impact on the immune mechanisms underlying fibrotic diseases.

Current understanding of the crosstalk between NETs and macrophages is the most advanced. On one hand, NETs are involved in the phenotypic transformation of macrophages. NETs were found to promote the conversion of macrophages to myofibroblast-like phenotypes via the TGF- β 1/Smad3 signaling pathway in a renal fibrosis model (36). Myofibroblasts are the primary cell type responsible for collagen deposition during the fibrotic disease process and play a significant role in tissue repair and pathological fibrosis. In a model of myocardial infarction, free DNA from NETs can enhance the proliferation of Mer tyrosine kinase/Major Histocompatibility Complex II macrophages (Mertk-MHC-IIo-int) through the Toll-like receptor 9 pathway (37). Mertk-MHC-IIo-int is a pro-inflammatory macrophage type that promotes extracellular matrix degradation and phagocytosis of cellular debris. This finding suggests that NETs may play a beneficial role in ventricular remodeling by inducing specific immune responses in macrophages. The contradictory evidence may relate to the high plasticity and functional diversity of macrophages in chronic inflammation and tissue injury.

On the other hand, NETs facilitate macrophage infiltration and the subsequent release of pro-inflammatory cytokines from macrophages. In a heart failure with preserved ejection fraction (HFpEF) model, NETs were associated with macrophage infiltration and inflammatory responses; the breakdown of NETs by DNase 1 significantly reduced macrophage numbers in cardiac tissue and decreased IL-10 expression in macrophage (38). Additionally, NETs can elevate α -SMA levels in macrophage (39), a mechanism that plays an important role in renal fibrosis induced by hyperuricemia. In a mouse model of pulmonary fibrosis, NETs were found to antagonize the production of the anti-fibrotic cytokine IL-27 in macrophages, exacerbating tissue remodeling and fibrosis (40).

Recent findings also shed light on the crosstalk between NETs and monocytes. In a mouse model of MASH disease, NETs induced the production of pro-inflammatory factors such as IL-1 β and TNF- α in monocytes, triggering the recruitment of monocyte-derived macrophages and the activation of senescent cells, with the NLRP3 signaling pathway potentially involved in this process (41).

4.2.3 Fibrosis and tissue damage

Fibroblasts are key effector cells in the process of organ fibrosis, and NETs can influence their activation and proliferation through various mechanisms. NETs have been shown to target classical signaling pathways, such as TGF- β (42) and NLRP3 (41), promoting fibroblast activation, as evidenced by increased expression levels of biomarkers such as vimentin, α -SMA, and COL1A1. Additionally, NETs selectively impact the metabolic reprogramming of fibroblasts during the activation of hepatic stellate cells (HSCs) in liver fibrosis. HSCs co-cultured with NETs exhibit elevated oxygen consumption rates (OCR) and extracellular acidification rates (ECAR), indicating increased mitochondrial respiration and aerobic glycolysis. Further studies have demonstrated that the metabolic regulatory effects of

NETs on HSCs are dependent on the arachidonic acid pathway, particularly involving cyclooxygenase-2 (COX-2) and Prostaglandin E2 (PGE2) (43).

Moreover, NETs can promote the epithelial-mesenchymal transition (EMT) in lung epithelial cells, inducing the expression of α -SMA, Snail, and Twist, while simultaneously decreasing E-cadherin expression, thereby facilitating lung fibrosis (44). The role of NETs in driving EMT in lung epithelial cells has also been demonstrated in critically ill patients with COVID-19. Studies have shown that lung tissues from critically ill COVID-19 patients exhibit high expression of both epithelial and mesenchymal markers. In an *in vitro* model, it was confirmed that the EMT expression pattern induced by SARS-CoV-2 correlates with NETosis (25). These findings suggest that NETs play a crucial role in the pathogenesis of COVID-19-associated pulmonary fibrosis.

The cytotoxic effects of NETs can also impact parenchymal cells, leading to a series of pathological changes. NETs can reduce the resistance of bronchial and airway epithelial cells, increasing the paracellular flux of macromolecules, which induces apoptosis in airway cells. Furthermore, exposure to NETs has been found to cleave E-cadherin protein (45), processes that collectively contribute to the disruption of epithelial barrier function. Emerging evidence suggests that neutrophil extracellular trap formation (NETosis) is implicated in the pathogenesis of advanced heart failure. Histopathological analyses have demonstrated significant NETosis deposition accompanied by substantial neutrophil infiltration within myocardial tissue from end-stage heart failure patient (46). Mechanistically, this neutrophil-derived inflammatory response may drive the pathological progression from compensated to decompensated cardiac hypertrophy through dual mechanisms: 1) Sustained release of pro-inflammatory mediators that potentiate myocardial fibrogenesis, and 2) Direct cytotoxic effects causing cardiomyocyte death and extracellular matrix remodeling (47).

Research on the components of NETs further elucidates its profibrotic and tissue-damaging effects. Studies indicate that NETs contain antimicrobial proteins and histones, which exhibit high biological toxicity and are involved in inflammatory responses, epithelial-mesenchymal transition (EMT), and epithelial injury. Several reviews have summarized the pathological processes of NET components in pulmonary fibrosis (48–50). Among these, NE has been the subject of considerable research. NE is implicated in neutrophil-mediated airway inflammation and can also stimulate excessive mucus secretion in models of cystic fibrosis (51), damaging the defensive functions of epithelial cells (52). Furthermore, NETs contain bioactive inflammatory cytokines such as IL-17, which promote fibroblast differentiation. Co-culturing lung fibroblasts with IL-17-rich NETs *in vitro* results in a fibrotic phenotype characterized by increased CCN2 expression, enhanced migration and healing abilities, and elevated collagen release (53).

4.2.4 Immune thrombus

NETs have been found to play a significant role in promoting a hypercoagulable state and thrombosis in patients with fibrosis, with coagulation imbalance considered one of the important reasons for the progression of fibrotic diseases, often associated with severe clinical manifestations (54, 55). The pro-thrombotic effects of NETs are

complex; on one hand, they serve as activators of thrombosis, while on the other hand, they act as scaffolds that influence the stability of thrombi. The mechanisms by which NETs stimulate thrombus formation may be related to the expression of tissue factor (TF) and IL-17A by NETs. Studies have shown that NETs extracted from the peripheral blood of patients with active systemic lupus erythematosus can express active TF and IL-17A, inducing thrombin production that activates the coagulation mechanism and promotes HSC activation (14). NETosis and the immunothrombosis induced by NETs play critical roles in COVID-19-related conditions such as pulmonary fibrosis and nonalcoholic steatohepatitis (NASH) (56). SARS-CoV-2 infection triggers complement activation accompanied by both neutrophil TF expression and NETs carrying active TF production, increasing its procoagulant activity (57). SARS-CoV-2 has been implicated in a range of lung diseases, including pulmonary nodules. Activated neutrophils have been detected in the lung tissues of patients with pulmonary nodules, accompanied by the formation of NETs (58). These findings suggest that NETs may play a role in the sequelae of COVID-19, however, further studies are required to substantiate this association.

Additionally, key components of NETs, such as free DNA, also exhibit pro-coagulant properties. Upon entering the plasma, free DNA binds to factor XII (FXII), triggering the production of thrombin. Furthermore, NETs serve as direct mediators of thrombosis (59). As complex extracellular structures, NETs provide a scaffold for the aggregation of platelets and fibrin. Pathological examination of alveolar tissues from patients who succumbed to severe COVID-19 revealed that NETs are important constituents of microvascular and macrovascular thrombi (60). When microvascular thrombosis occurs, it triggers a cascade of inflammatory responses, involving immune cells and fibroblasts. This amplifies the inflammatory response, further exacerbating ECM deposition, which may be one of the mechanisms by which NETs promote the formation of immune thrombus and contribute to fibrosis (61). These findings collectively suggest that NETs represent reliable and promising therapeutic targets for COVID-19-related lung diseases. Current research on therapeutic strategies has primarily focused on the direct degradation of NETs and the inhibition of key pathways involved in NETosis, with DNase I and PAD4 inhibitors serving as key examples. The pharmacological effects of these strategies are mainly centered on anti-inflammatory and antithrombotic therapies. Among these, recombinant human DNase (rhDNase) is an FDA-approved drug that promotes the degradation of NETs by catalyzing the hydrolysis of extracellular DNA. Administration of rhDNase has been shown to reduce the inflammatory response, decrease platelet activation, and improve local blood flow in mouse models of acute respiratory distress syndrome (ARDS) (62).

5 Summary and outlook

This study combines bibliometric analysis with a review of the research hotspots related to the pathological mechanisms by which NETs participate in fibrotic diseases, offering certain advantages over previous studies that relied solely on bibliometric analysis or narrative reviews. To our knowledge, this is the first bibliometric

study focusing on the relationship between NETs and fibrotic diseases. It is important to note that the bibliometric analysis is limited to literature retrieved from the WoS, which may result in an incomplete collection of relevant studies. Consequently, the discussions presented in this paper have certain limitations.

Although our findings indicate a rapid increase in the literature concerning NETs in the context of fibrosis, several significant challenges and unresolved issues remain. First, the intricate mechanisms underlying NETosis are still not fully elucidated. For instance, the initial triggers of NETosis remain unclear, as does the sequence of events, such as whether chromatin condensation occurs prior to or simultaneously with the rupture of the nuclear membrane. Addressing these questions will provide a more comprehensive understanding of this complex process and potentially inform the development of targeted therapeutic strategies aimed at NETs to prevent fibrotic diseases. Second, the crosstalk between neural networks and immune cells represents a highly complex process with numerous unresolved questions. Specifically, it remains uncertain whether NETs interact with lymphocytes, and the precise mechanisms by which immune cell crosstalk promotes fibrosis are yet to be determined. Furthermore, the role of NET components in the promotion of fibrosis is still unclear, with most studies focusing on pulmonary fibrosis models. The involvement of enzymes such as neutrophil elastase (NE) and myeloperoxidase (MPO) in myocardial and liver fibrosis remains poorly understood. Future research should aim to clarify the specific mechanisms by which NETs contribute to fibrotic diseases, including their interactions with a broader spectrum of immune cells, the pathways through which NETs activate fibroblasts, and the potential cytotoxic effects of NETs themselves. Based on our findings, these areas represent critical directions for future investigation.

Data availability statement

The original contributions presented in the study are included in the article/supplementary material, further inquiries can be directed to the corresponding author/s.

Author contributions

YL: Writing – original draft, Writing – review & editing. ZC: Writing – original draft, Writing – review & editing. JL: Writing – original draft, Writing – review & editing. RQ: Supervision, Writing – original draft. WL: Supervision, Writing – review & editing. JW: Writing – review & editing, Supervision, Validation.

Funding

The author(s) declare that financial support was received for the research, authorship, and/or publication of this article. This work was supported by Beijing Traditional Chinese Medicine Hospital

Shunyi Hospital Level Project (SYYJ-202402) and Young Elite Scientists Sponsorship Program by CAST (2023QNRC001).

Acknowledgments

We are grateful to the Yingke Qianxin team for helping us to search the literature.

Conflict of interest

The authors declare that the research was conducted in the absence of any commercial or financial relationships that could be construed as a potential conflict of interest.

References

- Zhao M, Wang L, Wang M, Zhou S, Lu Y, Cui H, et al. Targeting fibrosis, mechanisms and clinical trials. *Signal Transduct Target Ther.* (2022) 7:206. doi: 10.1038/s41392-022-01070-3
- Zhao X, Kwan JYY, Yip K, Liu PP, Liu F-F. Targeting metabolic dysregulation for fibrosis therapy. *Nat Rev Drug Discovery.* (2020) 19:57–75. doi: 10.1038/s41573-019-0040-5
- Hao M, Han X, Yao Z, Zhang H, Zhao M, Peng M, et al. The pathogenesis of organ fibrosis: Focus on necroptosis. *Br J Pharmacol.* (2023) 180:2862–79. doi: 10.1111/bph.v180.22
- Pakshir P, Hinz B. The big five in fibrosis: Macrophages, myofibroblasts, matrix, mechanics, and miscommunication. *Matrix Biol.* (2018) 68–69:81–93. doi: 10.1016/j.matbio.2018.01.019
- Tu H, Ren H, Jiang J, Shao C, Shi Y, Li P. Dying to defend: neutrophil death pathways and their implications in immunity. *Adv Sci (Weinh).* (2024) 11:e2306457. doi: 10.1002/advs.202306457
- Liu M-L, Lyu X, Werth VP. Recent progress in the mechanistic understanding of NET formation in neutrophils. *FEBS J.* (2022) 289:3954–66. doi: 10.1111/febs.v289.14
- Singh J, Boettcher M, Dölling M, Heuer A, Hohberger B, Leppkes M, et al. Moonlighting chromatin: when DNA escapes nuclear control. *Cell Death Differ.* (2023) 30:861–75. doi: 10.1038/s41418-023-01124-1
- Wang Y, Li M, Stadler S, Correll S, Li P, Wang D, et al. Histone hypercitrullination mediates chromatin decondensation and neutrophil extracellular trap formation. *J Cell Biol.* (2009) 184:205–13. doi: 10.1083/jcb.200806072
- Li Y, Li M, Weigel B, Mall M, Werth VP, Liu M-L. Nuclear envelope rupture and NET formation is driven by PKC α -mediated lamin B disassembly. *EMBO Rep.* (2020) 21:e48779. doi: 10.15252/embr.201948779
- Amulic B, Knackstedt SL, Abu Abed U, Deigendesch N, Harbort CJ, Caffrey BE, et al. Cell-cycle proteins control production of neutrophil extracellular traps. *Dev Cell.* (2017) 43(4):449–62.e5. doi: 10.1016/j.devcel.2017.10.013
- Thiam HR, Wong SL, Qiu R, Kittisopikul M, Vahabikashi A, Goldman AE, et al. NETosis proceeds by cytoskeleton and endomembrane disassembly and PAD4-mediated chromatin decondensation and nuclear envelope rupture. *Proc Natl Acad Sci U S A.* (2020) 117:7326–37. doi: 10.1073/pnas.1909546117
- Li M, Lyu X, Liao J, Werth VP, Liu M-L. Rho Kinase regulates neutrophil NET formation that is involved in UVB-induced skin inflammation. *Theranostics.* (2022) 12:2133–49. doi: 10.7150/thno.66457
- He L, Liu R, Yue H, Zhang X, Pan X, Sun Y, et al. Interaction between neutrophil extracellular traps and cardiomyocytes contributes to atrial fibrillation progression. *Signal Transduct Target Ther.* (2023) 8:279. doi: 10.1038/s41392-023-01497-2
- Frangou E, Chrysanthopoulou A, Mitsios A, Kambas K, Arelaki S, Angelidou I, et al. REDD1/autophagy pathway promotes thromboinflammation and fibrosis in human systemic lupus erythematosus (SLE) through NETs decorated with tissue factor (TF) and interleukin-17A (IL-17A). *Ann Rheum Dis.* (2019) 78:238–48. doi: 10.1136/annrheumdis-2018-213181
- Wan Y, Shen J, Ouyang J, Dong P, Hong Y, Liang L, et al. Bibliometric and visual analysis of neutrophil extracellular traps from 2004 to 2022. *Front Immunol.* (2022) 13:1025861. doi: 10.3389/fimmu.2022.1025861
- Fuchs TA, Abed U, Goosmann C, Hurwitz R, Schulze I, Wahn V, et al. Novel cell death program leads to neutrophil extracellular traps. *J Cell Biol.* (2007) 176:231–41. doi: 10.1083/jcb.200606027
- Papayannopoulos V, Metzler KD, Hakkim A, Zychlinsky A. Neutrophil elastase and myeloperoxidase regulate the formation of neutrophil extracellular traps. *J Cell Biol.* (2010) 191:677–91. doi: 10.1083/jcb.201006052
- Marcos V, Zhou Z, Yildirim AO, Bohla A, Hector A, Vitkov L, et al. CXCR2 mediates NADPH oxidase-independent neutrophil extracellular trap formation in cystic fibrosis airway inflammation. *Nat Med.* (2010) 16:1018–23. doi: 10.1038/nm.2209
- Young RL, Malcolm KC, Kret JE, Caceres SM, Poch KR, Nichols DP, et al. Neutrophil extracellular trap (NET)-mediated killing of *Pseudomonas aeruginosa*: evidence of acquired resistance within the CF airway, independent of CFTR. *PLoS One.* (2011) 6:e23637. doi: 10.1371/journal.pone.0023637
- Manzenreiter R, Kienberger F, Marcos V, Schilcher K, Krautgartner WD, Obermayer A, et al. Ultrastructural characterization of cystic fibrosis sputum using atomic force and scanning electron microscopy. *J Cyst Fibros.* (2012) 11:84–92. doi: 10.1016/j.jcf.2011.09.008
- Dubois AV, Gauthier A, Br  a D, Varaigne F, Diot P, Gauthier F, et al. Influence of DNA on the activities and inhibition of neutrophil serine proteases in cystic fibrosis sputum. *Am J Respir Cell Mol Biol.* (2012) 47:80–6. doi: 10.1165/rcmb.2011-0380OC
- Saffarzadeh M, Juenemann C, Queisser MA, Lochnit G, Barreto G, Galuska SP, et al. Neutrophil extracellular traps directly induce epithelial and endothelial cell death: a predominant role of histones. *PLoS One.* (2012) 7:e32366. doi: 10.1371/journal.pone.0032366
- Rahman S, Gadjeva M. Does NETosis contribute to the bacterial pathoadaptation in cystic fibrosis? *Front Immunol.* (2014) 5:378. doi: 10.3389/fimmu.2014.00378
- Martindon K, Witsch T, Erpenbeck L, Savchenko A, Hayashi H, Cherpokova D, et al. Peptidylarginine deiminase 4 promotes age-related organ fibrosis. *J Exp Med.* (2017) 214:439–58. doi: 10.1084/jem.20160530
- Pandolfi L, Bozzini S, Frangipane V, Percivalle E, De Luigi A, Violatto MB, et al. Neutrophil extracellular traps induce the epithelial-mesenchymal transition: implications in post-COVID-19 fibrosis. *Front Immunol.* (2021) 12:663303. doi: 10.3389/fimmu.2021.663303
- Christophorou MA, Castelo-Branco G, Halley-Stott RP, Oliveira CS, Loos R, Radzishewska A, et al. Citrullination regulates pluripotency and histone H1 binding to chromatin. *Nature.* (2014) 507:104–8. doi: 10.1038/nature12942
- Reis LR, Souza Junior DR, Tomasin R, Bruni-Cardoso A, Di Mascio P, Ronsein GE. Citrullination of actin-ligand and nuclear structural proteins, cytoskeleton reorganization and protein redistribution across cellular fractions are early events in ionomycin-induced NETosis. *Redox Biol.* (2023) 64:102784. doi: 10.1016/j.redox.2023.102784
- Hamam HJ, Khan MA, Palaniyar N. Histone acetylation promotes neutrophil extracellular trap formation. *Biomolecules.* (2019) 9. doi: 10.3390/biom910032
- Tokuhiro T, Ishikawa A, Sato H, Takita S, Yoshikawa A, Anzai R, et al. Oxidized phospholipids and neutrophil elastase coordinately play critical roles in NET formation. *Front Cell Dev Biol.* (2021) 9:718586. doi: 10.3389/fcell.2021.718586
- Metzler KD, Goosmann C, Lubojemska A, Zychlinsky A, Papayannopoulos V. A myeloperoxidase-containing complex regulates neutrophil elastase release and actin dynamics during NETosis. *Cell Rep.* (2014) 8:883–96. doi: 10.1016/j.celrep.2014.06.044
- Goldberg MW, Huttenlauch I, Hutchison CJ, Stick R. Filaments made from A- and B-type lamins differ in structure and organization. *J Cell Sci.* (2008) 121:215–25. doi: 10.1242/jcs.022020

Generative AI statement

The author(s) declare that no Generative AI was used in the creation of this manuscript.

Publisher's note

All claims expressed in this article are solely those of the authors and do not necessarily represent those of their affiliated organizations, or those of the publisher, the editors and the reviewers. Any product that may be evaluated in this article, or claim that may be made by its manufacturer, is not guaranteed or endorsed by the publisher.

32. Singh J, Zlatar L, Muñoz-Becerra M, Lochnit G, Herrmann I, Pfister F, et al. Calpain-1 weakens the nuclear envelope and promotes the release of neutrophil extracellular traps. *Cell Commun Signal.* (2024) 22:435. doi: 10.1186/s12964-024-01785-6
33. Lieberman J, Wu H, Kagan JC. Gasdermin D activity in inflammation and host defense. *Sci Immunol.* (2019) 4(39):eaav1447. doi: 10.1126/sciimmunol.aav1447
34. Sollberger G, Choidas A, Burn GL, Habenberger P, Di Lucrezia R, Kordes S, et al. Gasdermin D plays a vital role in the generation of neutrophil extracellular traps. *Sci Immunol.* (2018) 3(26):eaar6689. doi: 10.1126/sciimmunol.aar6689
35. Silva CMS, Wanderley CWS, Veras FP, Sonego F, Nascimento DC, Gonçalves AV, et al. Gasdermin D inhibition prevents multiple organ dysfunction during sepsis by blocking NET formation. *Blood.* (2021) 138:2702–13. doi: 10.1182/blood.2021011525
36. Wang Y, Li Y, Chen Z, Yuan Y, Su Q, Ye K, et al. GSDMD-dependent neutrophil extracellular traps promote macrophage-to-myofibroblast transition and renal fibrosis in obstructive nephropathy. *Cell Death Dis.* (2022) 13:693. doi: 10.1038/s41419-022-05138-4
37. Wei X, Zou S, Xie Z, Wang Z, Huang N, Cen Z, et al. EDIL3 deficiency ameliorates adverse cardiac remodeling by neutrophil extracellular traps (NET)-mediated macrophage polarization. *Cardiovasc Res.* (2022) 118:2179–95. doi: 10.1093/cvr/cvab269
38. Zhang X-L, Wang T-Y, Chen Z, Wang H-W, Yin Y, Wang L, et al. HMGB1-promoted neutrophil extracellular traps contribute to cardiac diastolic dysfunction in mice. *J Am Heart Assoc.* (2022) 11:e023800. doi: 10.1161/JAHA.121.023800
39. Wu F, Chen C, Lin G, Wu C, Xie J, Lin K, et al. Caspase-11/GSDMD contributes to the progression of hyperuricemic nephropathy by promoting NETs formation. *Cell Mol Life Sci.* (2024) 81:114. doi: 10.1007/s00018-024-05136-z
40. Riehl DR, Sharma A, Roewe J, Murke J, Ruppert C, Eming SA, et al. Externalized histones fuel pulmonary fibrosis via a platelet-macrophage circuit of TGFβ1 and IL-27. *Proc Natl Acad Sci U S A.* (2023) 120:e2215421120. doi: 10.1073/pnas.2215421120
41. Babuta M, Morel C, de Carvalho Ribeiro M, Calenda C, Ortega-Ribera M, Thevkar Nagesh P, et al. Neutrophil extracellular traps activate hepatic stellate cells and monocytes via NLRP3 sensing in alcohol-induced acceleration of MASH fibrosis. *Gut.* (2024) 73(11):1854–69. doi: 10.1136/gutjnl-2023-331447
42. He L, Liu R, Yue H, Zhu G, Fu L, Chen H, et al. NETs promote pathogenic cardiac fibrosis and participate in ventricular aneurysm formation after ischemia injury through the facilitation of perivascular fibrosis. *Biochem Biophys Res Commun.* (2021) 583:154–61. doi: 10.1016/j.bbrc.2021.10.068
43. Xia Y, Wang Y, Xiong Q, He J, Wang H, Islam M, et al. Neutrophil extracellular traps promote MASH fibrosis by metabolic reprogramming of HSC. *Hepatology.* (2024) 81(3):947–61. doi: 10.1097/HEP.0000000000000762
44. Lin H, Liu J, Li N, Zhang B, Nguyen VD, Yao P, et al. NETosis promotes chronic inflammation and fibrosis in systemic lupus erythematosus and COVID-19. *Clin Immunol.* (2023) 254:109687. doi: 10.1016/j.clim.2023.109687
45. Hudock KM, Collins MS, Imbrogno MA, Kramer EL, Brewington JJ, Ziady A, et al. Alpha-1 antitrypsin limits neutrophil extracellular trap disruption of airway epithelial barrier function. *Front Immunol.* (2022) 13:1023553. doi: 10.3389/fimmu.2022.1023553
46. Kostin S, Richter M, Krizanic F, Sasko B, Kelesidis T, Pagonas N. NETosis is an important component of chronic myocardial inflammation in patients with heart failure. *Circ Heart Fail.* (2025) 18:e012231. doi: 10.1161/CIRCHEARTFAILURE.124.012231
47. Hein S, Arnon E, Kostin S, Schönburg M, Elsässer A, Polyakova V, et al. Progression from compensated hypertrophy to failure in the pressure-overloaded human heart: structural deterioration and compensatory mechanisms. *Circulation.* (2003) 107:984–91. doi: 10.1161/01.CIR.0000051865.66123.B7
48. Yan S, Li M, Liu B, Ma Z, Yang Q. Neutrophil extracellular traps and pulmonary fibrosis: an update. *J Inflammation (Lond).* (2023) 20:2. doi: 10.1186/s12950-023-00329-y
49. Keir HR, Chalmers JD. Neutrophil extracellular traps in chronic lung disease: implications for pathogenesis and therapy. *Eur Respir Rev.* (2022) 31(163):210241. doi: 10.1183/16000617.0241-2021
50. Law SM, Gray RD. Neutrophil extracellular traps and the dysfunctional innate immune response of cystic fibrosis lung disease: a review. *J Inflammation (Lond).* (2017) 14:29. doi: 10.1186/s12950-017-0176-1
51. Gehrig S, Duerr J, Weitnauer M, Wagner CJ, Graeber SY, Schatterny J, et al. Lack of neutrophil elastase reduces inflammation, mucus hypersecretion, and emphysema, but not mucus obstruction, in mice with cystic fibrosis-like lung disease. *Am J Respir Crit Care Med.* (2014) 189:1082–92. doi: 10.1164/rccm.201311-1932OC
52. Jiang D, Wenzel SE, Wu Q, Bowler RP, Schnell C, Chu HW. Human neutrophil elastase degrades SPLUNC1 and impairs airway epithelial defense against bacteria. *PLoS One.* (2013) 8:e64689. doi: 10.1371/journal.pone.0064689
53. Ntinopoulou M, Cassimos D, Roupakia E, Kolettas E, Panopoulou M, Mantadakis E, et al. [amp][iota;nterleukin-17A-enriched neutrophil extracellular traps promote immunofibrotic aspects of childhood asthma exacerbation. *Biomedicine.* (2023) 11(8):2104. doi: 10.3390/biomedicine11082104
54. Arcanjo A, Logullo J, Menezes CCB, de Souza Carvalho Giangiarulo TC, Dos Reis MC, de Castro GMM, et al. The emerging role of neutrophil extracellular traps in severe acute respiratory syndrome coronavirus 2 (COVID-19). *Sci Rep.* (2020) 10:19630. doi: 10.1038/s41598-020-76781-0
55. Prével R, Dupont A, Labrousse-Colomer S, Garcia G, Dewitte A, Rauch A, et al. Plasma markers of neutrophil extracellular trap are linked to survival but not to pulmonary embolism in COVID-19-related ARDS patients. *Front Immunol.* (2022) 13:851497. doi: 10.3389/fimmu.2022.851497
56. Du J, Zhang J, Chen X, Zhang S, Zhang C, Liu H, et al. Neutrophil extracellular traps induced by pro-inflammatory cytokines enhance procoagulant activity in NASH patients. *Clin Res Hepatol Gastroenterol.* (2022) 46:101697. doi: 10.1016/j.clinre.2021.101697
57. Skendros P, Mitsios A, Chrysanthopoulou A, Mastellos DC, Metallidis S, Rafailidis P, et al. Complement and tissue factor-enriched neutrophil extracellular traps are key drivers in COVID-19 immunothrombosis. *J Clin Invest.* (2020) 130:6151–7. doi: 10.1172/JCI141374
58. Kanda R, Nakano K, Nawata A, Iwata S, Nakayama S, Tanaka Y. Remission of granulomatosis with polyangiitis only after resection of a pulmonary nodule. *Intern Med.* (2022) 61:2803–8. doi: 10.2169/internalmedicine.8447-21
59. Liu X, Arfman T, Wichapong K, Reutelingsperger CPM, Voorberg J, Nicolaes GAF. PAD4 takes charge during neutrophil activation: Impact of PAD4 mediated NET formation on immune-mediated disease. *J Thromb Haemost.* (2021) 19:1607–17. doi: 10.1111/jth.15313
60. Sonzogni A, Previtali G, Seghezzi M, Grazia Alessio M, Gianatti A, Licini L, et al. Liver histopathology in severe COVID 19 respiratory failure is suggestive of vascular alterations. *Liver Int.* (2020) 40:2110–6. doi: 10.1111/liv.14601
61. Airola C, Pallozzi M, Cerrito L, Santopaolo F, Stella L, Gasbarrini A, et al. Microvascular thrombosis and liver fibrosis progression: mechanisms and clinical applications. *Cells.* (2023) 12(13):1712. doi: 10.3390/cells12131712
62. Jarrahi A, Khodadadi H, Moore NS, Lu Y, Awad ME, Salles EL, et al. Recombinant human DNase-I improves acute respiratory distress syndrome via neutrophil extracellular trap degradation. *J Thromb Haemost.* (2023) 21:2473–84. doi: 10.1016/j.jtha.2023.04.044



OPEN ACCESS

EDITED BY

Reza Akbarzadeh,
University of Lübeck, Germany

REVIEWED BY

Xianyu Li,
China Academy of Chinese Medical Sciences,
China
Michael Adu Gyamfi,
Charité University Medicine Berlin, Germany

*CORRESPONDENCE

Felix I. L. Clanchy

✉ felix.clanchy@kennedy.ox.ac.uk

RECEIVED 21 July 2024

ACCEPTED 17 March 2025

PUBLISHED 30 April 2025

CITATION

Borghese F, Williams RO and Clanchy FIL
(2025) IRAK3 is upregulated in rheumatoid
arthritis synovium and delays the onset of
experimental arthritis.
Front. Immunol. 16:1468341.
doi: 10.3389/fimmu.2025.1468341

COPYRIGHT

© 2025 Borghese, Williams and Clanchy. This is
an open-access article distributed under the
terms of the [Creative Commons Attribution
License \(CC BY\)](#). The use, distribution or
reproduction in other forums is permitted,
provided the original author(s) and the
copyright owner(s) are credited and that the
original publication in this journal is cited, in
accordance with accepted academic
practice. No use, distribution or reproduction
is permitted which does not comply with
these terms.

IRAK3 is upregulated in rheumatoid arthritis synovium and delays the onset of experimental arthritis

Federica Borghese¹, Richard O. Williams¹
and Felix I. L. Clanchy^{1,2*}

¹Kennedy Institute of Rheumatology, University of Oxford, Oxford, United Kingdom, ²Botnar Institute for Musculoskeletal Sciences, Nuffield Department of Orthopaedics, Rheumatology and Musculoskeletal Sciences, University of Oxford, Oxford, United Kingdom

Tumour necrosis factor (TNF) is a potent inducer of endotoxin tolerance-associated molecules, such as interleukin-1 receptor-associated kinase 3 (IRAK3), and also a therapeutic target in inflammatory autoimmune diseases, as it upregulates the production of inflammatory mediators. The role of IRAK3 was assessed in rheumatoid arthritis (RA), a disease which is amenable to TNF blockade. As a variant of IRAK3 lacks the death domain required for its canonical role, isoform expression was determined in different inflammatory milieu by immunoblotting. RA synovial explant expression of IRAK3 was measured by qPCR. The expression of the larger, “classical” IRAK3 isoform predominated in macrophages treated with various stimuli. The expression of IRAK3 was higher in RA synovium compared to osteoarthritis synovium. Using collagen-induced arthritis, a murine model of RA, the immunomodulatory role of IRAK3 was investigated with wild-type (WT) and IRAK3-deficient mice expressing the MHC-II A^g allele. Disease progression was significantly accelerated in IRAK3^{-/-} mice. In addition, the circulating levels of IL-1 β were greater, and there were fewer Tregs both before and after the onset of disease. Inflammatory gene expression was higher in the arthritic paws of IRAK3^{-/-} mice. This study demonstrates that IRAK3 deficiency accelerates the progression of arthritis and increases molecular markers of disease severity.”

KEYWORDS

arthritis, inflammation, IRAK3, macrophages, cytokines

Introduction

Rheumatoid arthritis (RA) is a chronic inflammatory disease that primarily affects the joints and, without adequate treatment, results in progressive destruction. It is more frequent in women than men, and its prevalence is 0.5%–1% in developed countries (1). Although the cause of RA is not fully elucidated, genetic and environmental factors are associated with susceptibility to the disease.

The efficacy of tumour necrosis factor (TNF) blockade in combination with methotrexate for the treatment of RA indicates a central role for TNF in disease progression. However, TNF has both pro-inflammatory and immunomodulatory actions, and several studies have demonstrated that TNF blockade can prevent endotoxin tolerance (ET), due in part to a reduction in interleukin-1 receptor-associated kinase 3 (IRAK3) expression (2). IRAK3 (also known as IRAK-M) is a member of the IRAK family, together with IRAK1, 2 and 4, and is expressed predominantly in macrophage (M ϕ)-lineage cells (3). By preventing signaling via MyD88, IRAK3 is a pivotal inhibitor of the Toll-like receptor (TLR) and IL-1 β /IL-18 signaling pathways. The IRAK proteins have several structural similarities such as a death domain, kinase/pseudo-kinase domain, and, excepting IRAK4, a TRAF6 binding domain (4, 5). As a common denominator of the IRAK proteins, the death domain facilitates intermolecular binding between IRAKs (6). Lacking kinase activity, IRAK3 inhibits the MyD88 pathway by associating with IRAK4 via their respective death domains, thereby altering the normal assembly of the MyD88–IRAK4–IRAK1 signaling complex (4). Finer mapping of the functional structures of IRAK3 has revealed putative key amino acids necessary for its activity (7, 8). An isoform of IRAK3 lacks most of the death domain, and its function is largely unknown, but mutations and deletions in this region can reduce the inhibition of inflammatory mediator secretion in M ϕ -lineage cells, suggesting that it is unable to perform the canonical inhibitory function of the classical variant (6).

Several studies have indicated a role for IRAK3 in reducing or delaying inflammatory disease. For example, the accelerated development of asthma is associated with variants of *IRAK3* in multiple studies, the first of which identified several potentially pathogenic mutations in the protein-coding region (9–11); *IRAK3* is also a key gene biomarker in the peripheral blood of childhood asthma patients with exacerbation of disease activity (12). *IRAK3* suppresses a murine model of systemic lupus erythematosus (SLE) (13), but a trend towards the association of genetic variants of *IRAK3* was not statistically significant in a study of a European SLE population (14). A deficiency of *IRAK3* in an atherosclerosis murine model led to an exacerbation of disease activity (15). *IRAK3* is one of eight core genes associated with osteoarthritis (OA) in patients with metabolic syndrome (16). In circulating monocytes, the expression of *IRAK3* was higher in RA patients with low/moderate disease activity compared to high disease activity (17). In RA fibroblast-like synoviocytes, the expression of *IRAK3* (and other IRAK family members) is increased by TLR ligands (18). *IRAK3* can also contribute to the development of disease. *IRAK3* is upregulated in IgG4-related disease manifesting in salivary gland inflammation with M2 M ϕ -associated fibrosis (19); fibrosis was also promoted by *IRAK3* in a bleomycin-induced lung injury model (20). *IRAK3* has been demonstrated to promote some forms of cancer (21–23).

The cytokines IL-1 β and TNF are highly expressed within the inflamed RA joint and, by binding to their respective receptors, cause inflammatory signaling, including the NF- κ B signaling pathway (24, 25). Inflammation-driven tissue remodeling also releases Damage-associated molecular patterns (DAMPs), which

triggers TLR signaling (26). In the OA joint, inflammation is driven by the IL-1 β and mechano-sensitive signaling pathways rather than the significant leucocyte infiltrate and synovial hyperplasia observed in RA (27). TNF induces the expression of regulatory signaling proteins such as *IRAK3*; in time, *IRAK3* attenuates signaling via TLR/IL-1 β , including the NF- κ B pathway.

This study's purpose was to investigate *IRAK3*-associated mechanisms in the context of a chronic inflammatory disease for which anti-TNF is efficacious (28), as its expression has been shown to be dependent on TNF *in vitro* (2). The expression of *IRAK3* was determined in human M ϕ given a range of stimuli and in human RA synovial explants. *IRAK3* has two main isoforms, and it was established that M ϕ predominantly express the longer, classical isoform of *IRAK3* in M ϕ given a range of stimuli; *IRAK3* expression was higher in RA synovium compared to OA synovium. To investigate the systemic effects of *IRAK3*, collagen-induced arthritis (CIA) was induced in mice lacking this gene. The development of arthritis was accelerated and characterized by increased circulating levels of IL-1 β and reduced IL-5. While regulatory T cells (Tregs) were reduced in the lymph nodes (LNs) of *IRAK3*^{−/−} during CIA, there was an increased T-cell gene expression profile in *IRAK3*^{−/−} arthritic joints, compared to wild-type (WT) joints.

Materials and methods

Irak3 KO mice

Mice lacking *IRAK3* (B6.129S1-*IRAK3*^{tm1Flv/J}) with a C57BL/6 background, were kindly provided by Hans-Joachim Anders courtesy of Koichi Kobayashi and Richard Flavell; the genetic modification introduces a stop mutation resulting in a significantly truncated mutant transcript (29). Knockout (KO) status was screened using the following primers: forward primer 5'-CGTTCATAACACACCTCTCTGC-3'; reverse primer 5'-TTCTATCGCCTTCTTGACGAGTTC-3'. WT status was determined using the following primers: forward primer 5'-GCCAGAAGAATACATCAGACAGGG-3'; reverse primer 5'-TGTTTCGGGTCATCCAGCAC-3'. C57BL/6 *IRAK3*^{−/−} mice (which express the MHC-II allele A^b) were crossed with the congenic C57BL/6N^q mice (expressing the MHC-II allele A^q) to increase susceptibility to arthritis (30); C57BL/6N^q mice were generously provided by Johan Bäcklund (Karolinska Institute). Mice were crossed to create heterogeneous breeding pairs, which were further crossed and their progeny screened for H2^q homozygotic mice that were homozygous for a lack of *Irak3*; see [Supplementary Table 1](#) for primers. All mice were housed in pathogen-free conditions with *ad libitum* food and water at the Kennedy Institute of Rheumatology (KIR). All procedures were conducted in accordance with UK Home Office regulations and guidelines.

Collagen-induced arthritis

Male C57BL/6N^q *IRAK3*^{−/−} and C57BL/6N^q WT mice were immunized with bovine type II collagen in complete Freund's

adjuvant as previously described (31). After mice developed clinical arthritis, the disease severity in the paws was scored as follows: 0, normal; 1, slight swelling and/or erythema; 2, clear swelling; and 3, pronounced edematous swelling/ankylosis. Clinical parameters were measured for 10 days after disease onset in each animal, and then animals were euthanized; blood plasma, spleens, inguinal lymph nodes, and paws were harvested. For pre-onset studies, tissue harvests took place 14 days after immunization.

Phenotyping cell subsets by flow cytometry

To analyze Th lymphocyte subsets, cells from the spleen and LN were isolated as previously described (28). Leucocytes were directly stained with viability dye (Zombie NIR Fixable Viability dye, BioLegend, San Diego, CA, USA), and antibodies for CD4 (RM4-5, BioLegend) and CD25 (PC61, BioLegend); then fix/permeabilized and stained intra-cellularly for FoxP3 (236A/E7, eBioscience, San Diego, CA, USA), Gata3 (TWAJ, eBioscience), ROR γ t (Q31-378, BD Biosciences, San Jose, CA, USA), Tbet (4BD10, BioLegend), and Helios (22F6, BioLegend); and analyzed using the FACSDIVA software (BD Biosciences) and FlowJo (TreeStar). To quantify T-cell subsets, live cells were gated into Tregs (CD4⁺CD25⁺FoxP3⁺), natural Tregs (CD4⁺CD25⁺FoxP3⁺Helios⁺), Th2 (CD4⁺Gata⁺), Th1 (CD4⁺Tbet⁺), and Th17 (CD4⁺ROR γ t⁺) cells.

Murine plasma biomarkers

Blood was collected via cardiac puncture into microcentrifuge tubes containing heparin. Samples were then centrifuged at 13,000 rpm for 10 minutes at 4°C. Plasma was then stored at -80°C until the measurement of anti-collagen responses as previously described (32). Inflammatory mediators in murine plasma were measured using the Mouse TH1/TH2 9-Plex Ultra-Sensitive Kit (MesoScale Discovery, Rockville, MD, USA; catalogue number K15013C-1) according to the manufacturer's instructions.

Gene expression in murine tissue

Paws were snap-frozen in liquid nitrogen and processed as previously described (31). Briefly, tissue was pulverized with the BioPulverizerTM (BioSpec, Bartlesville, OK, USA). Paw powder was then homogenized in 500 μ L of TRIzol reagent (Invitrogen, Carlsbad, CA, USA) using the Sample Grinding Kit (GE Healthcare, Chicago, IL, USA). Chloroform (100 μ L) was added to the tube, and the lysate was mixed and then centrifuged to separate the mixture into a lower phenol phase and upper aqueous separated by an interphase. The aqueous phase of the phenol/chloroform extraction was mixed with an equal volume of ethanol and then added to an RNA extraction column (miRNeasy Mini Kit, Qiagen, Valencia, CA, USA), and mRNA extraction was completed according to the manufacturer's instructions.

cDNA was reverse transcribed from 500 ng of RNA using a High Capacity cDNA Reverse Transcription Kit (Applied Biosystems, Foster City, CA, USA), according to the manufacturer's protocol. The expression of target genes was determined using TaqMan assays (Thermo Fisher Scientific, Waltham, MA, USA) and qPCR master mix (Taqyon Low ROX Probe 2x dTTP blue, Eurogentec, Seraing, Belgium) and was expressed relative to *Gapdh* gene expression using the $\Delta\Delta$ CT approximation method; see [Supplementary Table 2](#) for TaqMan assays. Murine M ϕ from mice lacking either *Tnfrsf1a* or *Tnfrsf1b* were derived from bone marrow as previously described (33) and stimulated for up to 12 hours with Lipopolysaccharide (LPS) (10 ng/mL) before being processed for RNA extraction, reverse transcription, and qPCR.

Human IRAK3 isoforms

“Classical” full-length IRAK3 (producing NP_009130.2) and “alternative” death domain-truncated IRAK3 (producing NP_001135995.1) were cloned by traditional molecular biology techniques and transfected into HEK293 cells using Lipofectamine 2000 (Thermo Fisher Scientific). After 24 hours, cells were lysed for extraction using the Proteome Profiler Human NF κ B Pathway Array kit (R&D Systems, Minneapolis, MN, USA). Human monocyte-derived M ϕ (MDM) were derived from monocytes and stimulated as previously described (33). Briefly, MDM were differentiated from monocytes for 5 days in 10% foetal bovine serum supplemented Roswell Park Memorial Institute 1640 medium (FBS RPMI) (10⁷ cells/10 mL/10-cm dish) supplemented with 50 ng/mL macrophage-colony stimulating factor (M-CSF) (PeproTech, Cranbury, NJ, USA); MDM were re-plated into 12-well plates, rested overnight, and then stimulated with medium alone, LPS (10 ng/mL, Merck, Darmstadt, Germany), LPS + IFN γ (10 ng/mL + 10 ng/mL, Merck/PeproTech), TNF (50 ng/mL, PeproTech), granulocyte macrophage-colony stimulating factor (GM-CSF) (50 ng/mL, PeproTech), IL-4 (50 ng/mL, PeproTech), or TGF- β 1 (100 ng/mL, PeproTech) for 20 hours; protein and RNA were extracted using an Isolate II RNA/DNA/Protein kit (Bioline, Luckenwalde, Germany). Protein concentration was determined (PierceTM BCA Protein Assay Kit, Thermo Fisher Scientific), and 4 μ g of protein was boiled in Laemmli buffer (Alfa Aesar), run on a polyacrylamide gel (NuPAGETM 4%–12% Bis-Tris Mini Protein Gels, Thermo Fisher Scientific), and then transferred to a nitrocellulose membrane for immunoblotting. IRAK3 was detected using the antibody clone SAB3500193 (Merck) or AF6264 (R&D Systems) according to the manufacturer's instructions; β -actin was detected using AC-74 (Merck).

Synovial explants from RA and OA patients were processed as previously described (34). Briefly, synovial membrane tissue was obtained from RA and OA patients' joints, dissected from the surrounding tissues, and digested *in vitro* with Liberase TL (Merck) and DNaseI (Merck) diluted in RPMI. After incubation at 37°C for 1–2 hours, the digestion was halted by the addition of RPMI containing 10% FBS, and the digestion passed through a cell

strainer and washed, and erythrocyte lysis was performed. The cells were then washed and pelleted for RNA extraction and reverse transcription. Gene expression was measured by standard curve qPCR using a linearized plasmid containing the “classical” *IRAK3* isoform and housekeeping gene (*HPRT1*); tissues were collected in compliance with approval from the Riverside Research Ethics Committee. The gene expression of *IRAK3* in MDM was determined by $\Delta\Delta CT$ approximation.

Statistical analyses

Data were analyzed using Excel (Microsoft Ltd.), Prism (GraphPad Software Ltd.), and MultiExperiment Viewer (TM4 software). Student's t-test or one-way ANOVA with *post-hoc* analysis was used to test statistical significance. A p-value <0.05 was considered statistically significant.

Results

The larger, “classical” *IRAK3* isoform predominates in M ϕ

We and others have demonstrated the differential expression of splice variants with different functional properties in inflammatory conditions (33, 35). Although most research has focused on the larger variant of *IRAK3*, which has the full-length death domain necessary for associating with the Myddosome complex (6), we demonstrated that two commercially available antibodies were able to detect both isoforms (Figures 1A–C) before determining whether mature M ϕ primed with different inflammatory stimuli (including TNF) expressed different proportions of each isoform. Only the larger isoform was observed in human MDM primed with different stimuli (Figure 1D, see Supplementary Figure 1 for quantification). As previously observed (2), the expression of *IRAK3* is induced by TNF (Figures 1E, F); however, murine M ϕ from *Tnfrsf1*^{−/−} mice had significantly reduced the expression of *IRAK3* compared to WT or *Tnfrsf2*^{−/−} mice (Figure 1G). In synovial explants from OA and RA patients, the expression of *IRAK3* was measured by standard curve qPCR; *IRAK3* was found to be higher in RA patient samples (Figure 1H).

Creation of an *IRAK3*^{−/−} mouse susceptible to CIA

As *IRAK3* variants have an association with accelerated and exacerbated disease activity in humans, we bred a transgenic *Irak3*^{−/−} mouse onto a background suitable for CIA in order to determine how the lack of this gene altered experimental disease. The murine MHC-II A^q molecule has a high degree of similarity to HLA-DRB1*0101 and *0401, which confer susceptibility to human RA (30). Most

genetically modified mouse strains have a C57BL/6 (H2^b) background, which is resistant to the development of autoreactive T-cell responses to type II collagen in CIA. Hence, it has been proposed that C57BL/6N^q mice (expressing A^q) serve as an international standard in studies of T cell-driven immunopathology (30). We crossed *IRAK3*^{−/−} mice onto C57BL/6N^q mice after developing a PCR method for genotyping H2^b and H2^a mice; this necessitated the sequencing of relevant genomic regions of each strain (Supplementary Figure 2A) and a comparison of genotyping by flow cytometry and PCR (Supplementary Figures 2B–D, 3). The *IRAK3*^{−/−} N^q mice were used for CIA, with disease induction being performed as previously described (33). As shown in Figure 2A, the progression of the disease in *IRAK3*^{−/−} N^q mice was significantly more rapid, with the average time to arthritis onset being 26 versus 38 days in the WT group (Figures 2A, B). Disease activity was similar, although there was a trend towards increased severity in *IRAK3*^{−/−} mice, as indicated by greater paw swelling at later time-points (Figures 2C–E); this was consistent with significantly higher levels of IL-1 β and lower levels of IL-5 detected in the plasma of *IRAK3*^{−/−} N^q mice (Figure 3A).

Accelerated arthritis in *IRAK3*^{−/−} mice is associated with reduced peripheral Tregs

To further investigate the differences in kinetics and severity of disease between WT and KO mice, an analysis of auto-antibodies and Th lymphocyte subsets was performed to assess systemic changes between strains. Anti-collagen auto-antibodies were measured in the plasma of arthritic animals to determine humoral responses and infer cytokines present in proximity to auto-reactive B cells; IgG1 and IgG2a anti-collagen antibodies were measured to determine class switching. Surprisingly, while the level of IgG1 antibodies was virtually the same in both strains, the EC₅₀ for a serial dilution analysis was higher for IgG2a antibodies in the *IRAK3*^{−/−} group, indicating lower titers for this Ig class (Figure 3B).

In spleens and lymph nodes, no difference between the two strains was found for Th1 and Th17 cell activity; however, the proportion of Tregs was reduced in *IRAK3*^{−/−} spleens and lymph nodes; Th2 cells were reduced in spleens (Figures 3C, D). The ratio of Treg:Th17 cells was also significantly reduced in spleens (Figure 3D) and nominally lower in LN (Figure 3C). These data were consistent with mean fluorescence intensity of FoxP3 staining in FoxP3⁺ cells that was almost threefold higher in WT versus KO lymph nodes (2,914.50 \pm 298.9 vs. 1,159.9 \pm 114.9, $p = 1.6 \times 10^{-6}$) and spleens (3,015.4 \pm 332.3 vs. 1,081.9 \pm 96.9, $p = 7.4 \times 10^{-7}$) (data not shown). As disease progression was accelerated in *IRAK3*^{−/−} mice, we measured the proportions of T-cell subsets (Supplementary Figures 4A, B) and anti-collagen antibody titers in the pre-onset period (Supplementary Figure 4C); a similar reduction in Tregs was observed in *IRAK3*^{−/−} mice, but anti-collagen antibody titers were lower and not dissimilar between strains at this time. In the spleens of naïve *IRAK3*^{−/−} mice, there were minor increases in CD4⁺ cells co-expressing Tbet, Gata3, or

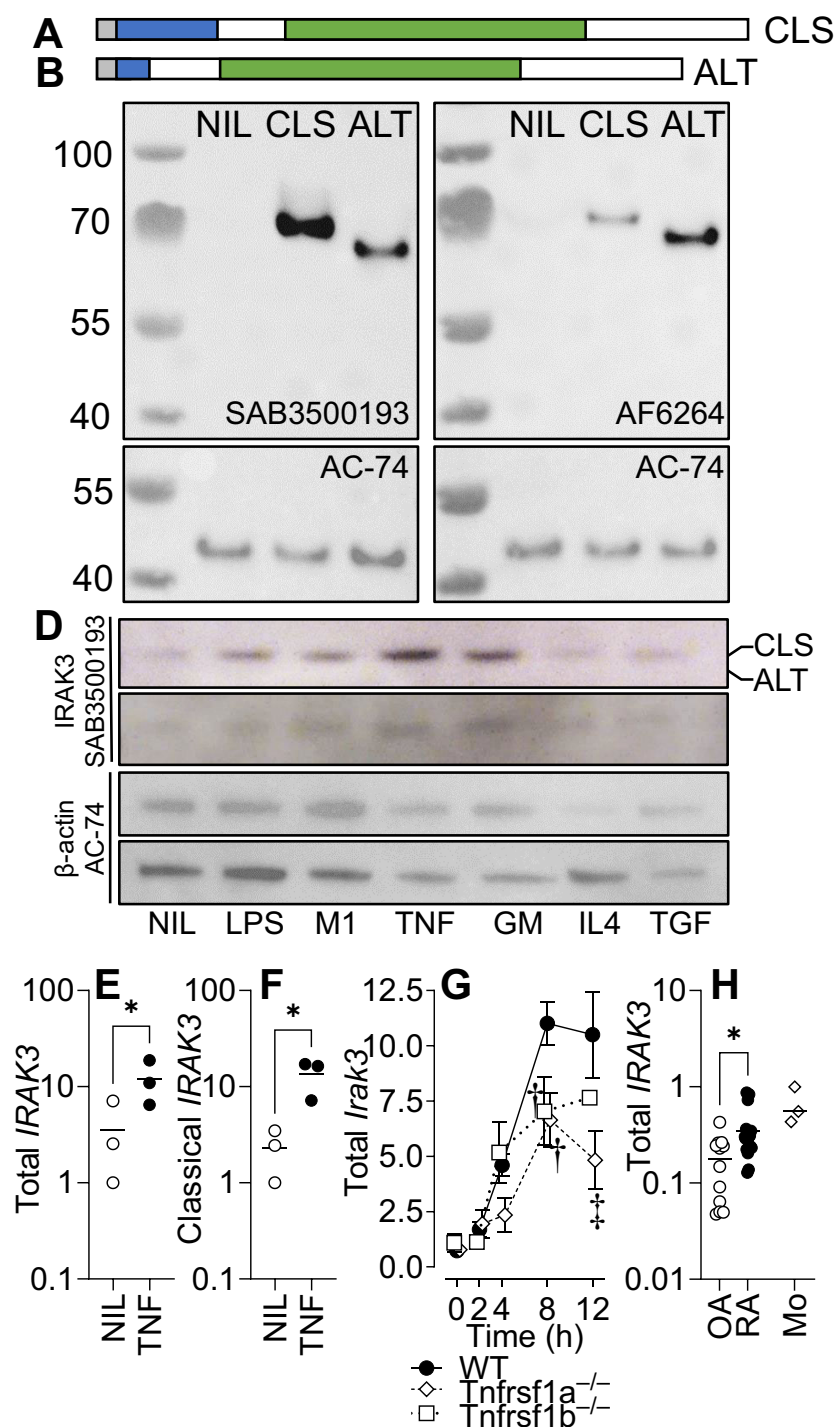


FIGURE 1

IRAK3 isoform expression in primed macrophages. IRAK3 N-terminal to death domain (DD) (a.a. 1–14) is shaded grey, DD (15–104) is shaded blue, and pseudokinase domain (a.a. 171–446) is shaded green. (A) “Classical” full-length (CLS; NP_009130.2 a.a. 1–596). (B) “Alternative” IRAK-3 (ALT; NP_009130.2 a.a. 1–44, 105–596 of CLS) that lacks most of the DD. (C) Western blotting for IRAK3 in HEK293 cells (NIL) or HEK293 cells overexpressing classical or alternative IRAK3 blotted with two antibodies for IRAK3. (D) IRAK3 expression in monocyte-derived Mφ, unstimulated (NIL) or stimulated for 20 h with LPS, LPS/IFN γ (M1), TNF, GM-CSF (GM), IL-4, or TGF- β 1 (TGF); representative blots of two donors stained for IRAK3 (SAB3500193) and β -actin (AC-74). Gene expression of (E) both *IRAK3* isoforms and (F) the classical *IRAK3* isoform in TNF-stimulated human Mφ. (G) Gene expression of *Irak3* in LPS-stimulated (10 ng/mL) murine bone marrow-derived Mφ from wild-type or transgenic mice lacking either *Tnfrsf1a* or *Tnfrsf1b*; ANOVA for each respective knockout (KO) vs. wild type (WT), $\dagger p < 0.01$, $\ddagger p < 0.001$, $n = 3$ –5 experiments. (H) Total *IRAK3* gene expression in osteoarthritis (OA) and rheumatoid arthritis (RA) synovial explants and normal healthy monocytes (Mo), $n = 12$ OA, 19 RA, and 3 Mo. For (E, F, H) * $p < 0.05$, Student's t-test.

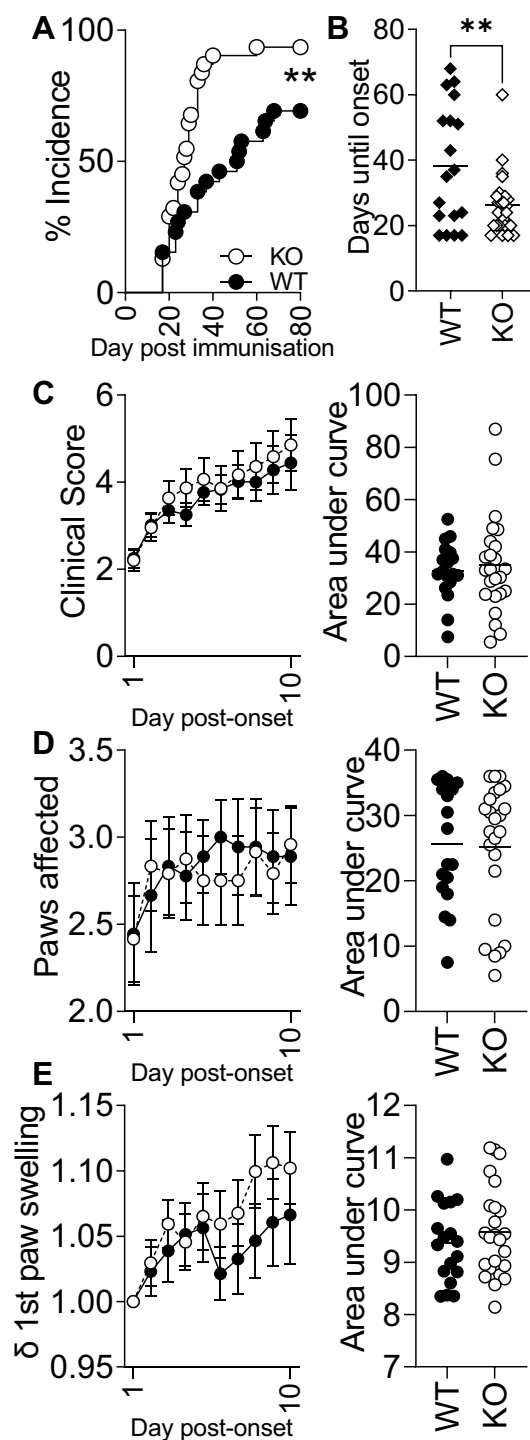


FIGURE 2

Experimental arthritis onset is accelerated and more efficient in IRAK3^{-/-} mice. (A) IRAK3^{-/-} mice [Knockout (KO)] develop arthritis significantly earlier than wild type (WT) (Mantel–Cox test), taking on average half the time to develop symptoms (B); ** $p < 0.01$, Student's t-test. (C) Global clinical score, (D) the paws affected for each mouse, and (E) change in swelling in the individual first affected paw relative to day 0 were assessed daily during the post-onset 10-day observational period. Data are combined from two independent experiments with a total of 18 (WT) and 24 (KO) mice per group; values are mean \pm SEM.

ROR γ t (Supplementary Figures 4D, E). These data indicate significant systemic differences, particularly in regard to T helper subsets, between the strains in the course of experimental arthritis.

IRAK3^{-/-} joints have higher T cell-associated gene expression

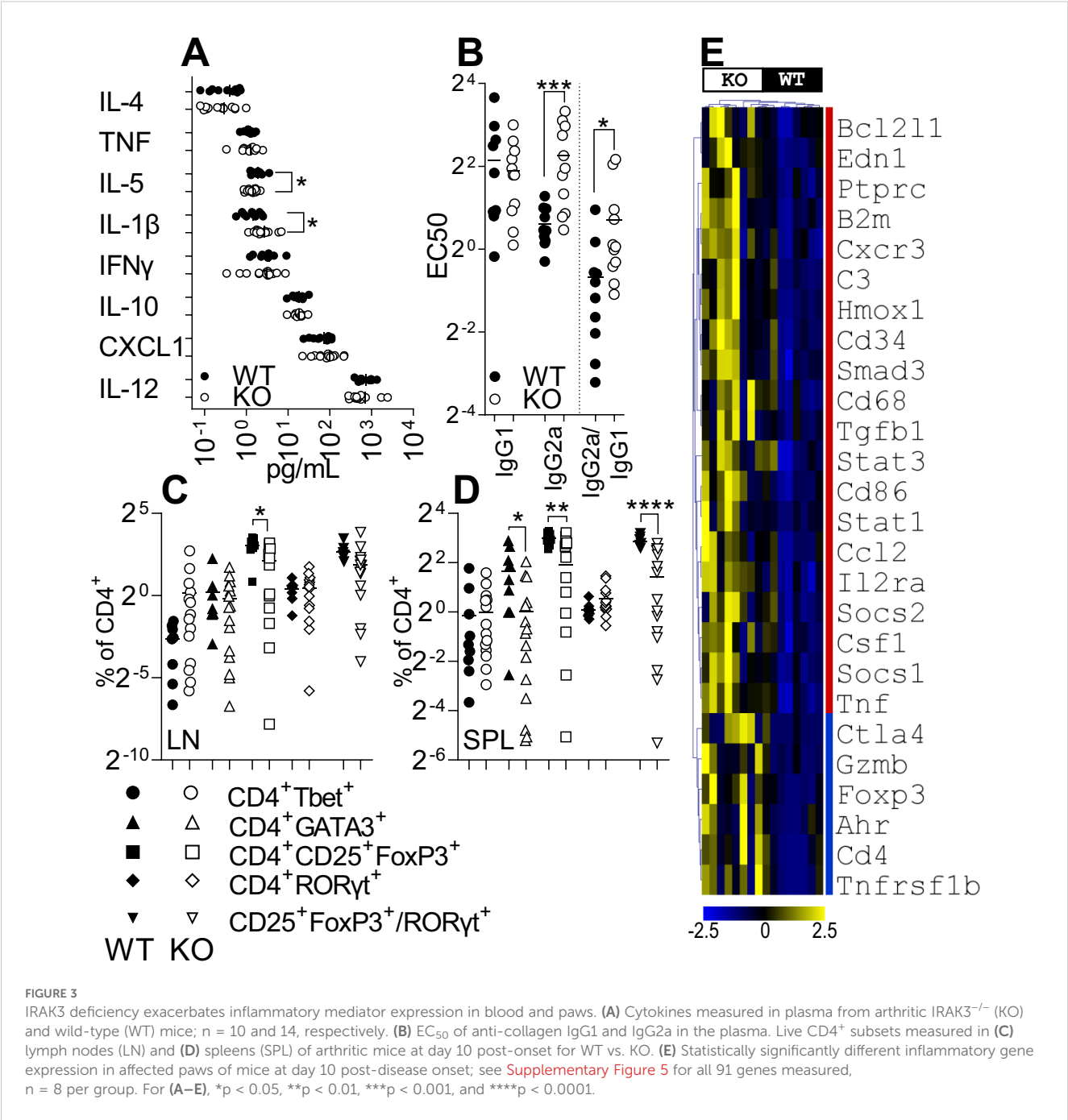
As there were systemic differences between strains, we then compared gene expression localized to the affected joints to determine in finer detail the differences beyond the nominal differences in paw swelling.

Despite IRAK3^{-/-} and WT mouse joints showing relatively minor clinical differences in CIA, a clear difference between the groups was observed when a panel of genes specific for the Th17 and Treg subpopulations was measured (Figure 3E, Supplementary Figure 5). IRAK3^{-/-} CIA paws expressed higher levels of *Cd3e* and *Cd4*, suggesting increased numbers of CD4⁺ lymphocytes in the paws of IRAK3^{-/-} mice compared with WT mice. Concomitantly, IRAK3^{-/-} paws expressed higher levels of *Stat3* and *Ahr*, two markers associated with the differentiation of Th17 cells, and significantly higher levels of *FoxP3*, *Il2ra*, *Ctla4*, and *Tnfrsf1b*, which are expressed by Tregs; higher levels of *Il12b*, *Ilb*, *Il6*, and *Il17* were also measured, although the difference did not reach statistical significance. *Tnf* and *Tgfb1* gene expression levels were also significantly higher in the IRAK3^{-/-} group.

Discussion

IRAK3 expression and disease status

The influence of IRAK3 on the response to therapy has been observed in RA, in which an IRAK3 polymorphism has been shown to be predictive of response to anti-TNF (36). IRAK3 dysregulation is also associated with accelerated and exacerbated asthma (9) and infectious diseases (37), and increased IRAK3 expression in peripheral blood leucocytes is associated with reduced disease activity in RA (17). Animal models using IRAK3 knockout mice have confirmed its role in inhibiting inflammatory responses, but few studies have compared IRAK3 isoforms (6, 38); the disruption of the death domain has been demonstrated to prevent the immunomodulatory activity of IRAK3 (6). We and others have previously demonstrated relatively high levels of inflammatory gene expression (including TNF, which induces IRAK3) in affected joints in arthritis (31). As blocking TNF *in vitro* has been shown to prevent the induction of IRAK3 (2), this study investigated the role of IRAK3 in an animal model of RA, a disease which is amenable to TNF blockade. We began by determining the isoforms of IRAK3 present in mature M ϕ exposed to different inflammatory stimuli. As it lacks most of the death domain, the capacity of the alternative isoform to attenuate TLR/IL-1 β signaling is likely to be reduced; however other putative actions, such as guanylate cyclase activity, may still be intact (7). We observed that only the longer classical form of IRAK3 was expressed at the protein level.



IRAK3 and disease activity

A deficit of Tregs or Treg activity is a feature of the failure of tolerance in autoimmune disease in multiple disease models (39–41). Changes to cell composition in spleens and lymph nodes of IRAK3^{-/-} animals, as has been observed previously (22), may have contributed to reduced antibody class switching. While FoxP3 is a phenotype-defining transcription factor for Tregs, the two main sub-types, natural and inducible, were reduced. Most relevant to the current study is the observation that IRAK3 reduces the severity of disease in experimental autoimmune encephalomyelitis (EAE) by Lui B et al. (38); in that study, IRAK3 deficiency accelerated disease progression and increased the ratio of Th17 to Tregs, which we also observed during arthritis.

Reduced CD3⁺FoxP3⁺ T cells were also observed in the spleens of IRAK3-deficient mice in a colorectal cancer model (22). An increase of CD4⁺GATA⁺ lymphocytes was measured in the spleens of WT mice, which also had increased plasma levels of IL-5, which is secreted by GATA3⁺ Th2 lymphocytes (42).

A panel of inflammatory genes was assessed for the IRAK3^{-/-} and WT CIA paws. There was a significant difference in the production of pro-inflammatory mediators in the paws of the IRAK3^{-/-} group. In particular, pro-inflammatory cytokine genes such as *Tnf*, *Il12b*, *Il1b*, *Il6*, and *Il17* were all expressed at higher levels in the IRAK3^{-/-} mice, although the difference was not always statistically significant; the expression of *Tgfb1* and *Il10* was also increased. When genes specific for different T-cell subsets were assessed in arthritic paws, an increased

expression of both Th17 and Treg markers was observed. IRAK3^{-/-} arthritic paws expressed higher levels of pan-lymphocytic markers *Cd3* and *Cd4*. *Smad3* and *Foxp3*, which are Treg-associated transcription factors, were higher in IRAK3^{-/-} paws as were *Stat3* and *Il23r*, which are more specific for the Th17 subset. Interestingly, *Ctla4* appeared to be expressed in the IRAK3^{-/-} joints at higher levels. CTLA-4 binding to the B7 family members blocks the co-stimulatory signal represented by CD28-B7; this mechanism is used by nTregs to control T-cell activity and as such is suggested to represent a marker for nTregs. Based on these data, we could hypothesize that Th17 and Tregs are increased in the IRAK3^{-/-} paws. The perturbation of T helper subsets in LN and spleen, and increased T cell-associated gene expression in paws, is suggestive of differences in the mobilization and trafficking of T-cell subsets in the absence of IRAK3.

Fewer significant differences were measured in pre-onset lymph nodes and spleens; however, there were a reduced number of FoxP3⁺Helios⁺ cells in IRAK3^{-/-} LN and spleens, and a lower ratio of Tregs to RORγ⁺ lymphocytes in spleens. This indicates a cellular re-distribution of Th sub-populations between different compartments during the pre- and post-onset periods, although an indirect effect of prolonged and exacerbated inflammation on T-cell FoxP3 expression cannot be discounted. The paws as the primary site of the inflammation would contain more pathological cells, such as Th17, and this phenotype may have been stabilized by the higher levels of IL-6 and TGF-β1.

Conclusions

A limitation of this study is the moderately different expression profile of IRAK3 between humans and mice. While humans tend to express IRAK3 mainly in Mφ-lineage cells, murine expression is somewhat broader and includes other myeloid cells and epithelial cells. Regardless, the association of accelerated development in some forms of human disease and IRAK3 variants is supportive of the immunosuppressive role of IRAK3. Replicating the effect of IRAK3 by therapeutically targeting IRAK4 has been pursued via the development of IRAK4 inhibitors (43) for the treatment of inflammatory disease. In conclusion, we measured dampened and delayed inflammation in a murine model of arthritis in IRAK3-replete mice, as evidenced by reduced IL-1β and higher IL-5 levels in the plasma and more Tregs in draining lymph nodes and spleens; higher immune cell infiltration was suggested by the gene expression profiles in the affected joints of IRAK3^{-/-} mice. This observation is consistent with the known immunomodulatory role of IRAK3 and is similar to the associated changes to disease progression observed in other contexts. The reduced prevalence of Tregs is likely to be a causative factor as part of a wider perturbation in lymphocyte mobilization and phenotypic distribution.

Data availability statement

Sequences in **Supplementary Figure 2** have been deposited in GenBank and have the Accession numbers PV441886 (Ab) and

PV441887 (Aq). The raw data supporting the conclusions of this article will be made available by the authors, without undue reservation.

Ethics statement

Human tissues were collected in compliance with approval from the Riverside Research Ethics Committee (06/Q0605/8; NRES Committee). The studies were conducted in accordance with the local legislation and institutional requirements. The participants provided their written informed consent to participate in this study. All animal procedures were conducted in accordance with UK Home Office regulations and guidelines. The study was conducted in accordance with the local legislation and institutional requirements.

Author contributions

FB: Conceptualization, Formal analysis, Investigation, Resources, Validation, Visualization, Writing – original draft, Writing – review & editing. RW: Conceptualization, Funding acquisition, Project administration, Supervision, Writing – original draft, Writing – review & editing. FC: Conceptualization, Investigation, Project administration, Supervision, Visualization, Writing – original draft, Writing – review & editing.

Funding

The author(s) declare that financial support was received for the research and/or publication of this article. This research was supported in part by a Biotechnology and Biological Sciences Research Council (BBSRC) Collaborative Awards in Science and Engineering (CASE) studentship (BB/J013137/1) in collaboration with UCB Celltech (FB/ROW) and Cancer Research UK (CRUK) Oxford Centre (CRUKDF 0318-FC) (FC).

Acknowledgments

We would like to acknowledge the animal house staff for their excellent care of animals and the use of the KIR flow cytometry facility. We thank Johan Bäcklund for the kind gift of mice that were used to create IRAK3^{-/-} NQ mice.

Conflict of interest

The authors declare that the research was conducted in the absence of any commercial or financial relationships that could be construed as a potential conflict of interest.

Publisher's note

All claims expressed in this article are solely those of the authors and do not necessarily represent those of their affiliated organizations, or those of the publisher, the editors and the reviewers. Any product that may be evaluated in this article, or claim that may be made by its manufacturer, is not guaranteed or endorsed by the publisher.

Supplementary material

The Supplementary Material for this article can be found online at: <https://www.frontiersin.org/articles/10.3389/fimmu.2025.1468341/full#supplementary-material>

SUPPLEMENTARY TABLE 1

Genotyping primers Primers 1-8 were used for genotyping A^a and A^b mice. Primers 9 and 10 were used to clone the sequence in [Supplementary Figure 2A](#).

SUPPLEMENTARY TABLE 2

Taqman qPCR assays Taqman qPCR assays and associated genes used for the measurement of gene expression in murine arthritic paws.

SUPPLEMENTARY FIGURE 1

Quantification of IRAK3 protein expression in human Mφ Relative band intensity for IRAK3 and β-actin was measured using ImageJ and expressed relative to the unstimulated control. Values are mean+SEM, n=2.

SUPPLEMENTARY FIGURE 2

Determination of I-A^b and I-A^a alleles by PCR. (A) Genomic sequence comparing A^a and A^b alleles of H2-Ab1 (NM_207105.3), exon 3 to 5. Yellow highlighting

indicates exons. Asterisks indicate identical sequence between alleles. Underlined text indicates primer binding sites for PCRs in (C). (B) Phenotyping of A^a and A^b alleles by flow cytometry by gating on (i) peripheral blood monocytes in erythrocyte-lysed leucocytes from (ii) A^a mice, (iii) heterozygous A^{a/b} mice or (iv) A^b mice. (C) Genotyping PCRs for (i, ii) A^a mice, (iii, iv) heterozygous A^{a/b} mice or (v, vi) A^b mice. (D) Samples from (C) were tested using two primer pairs per reaction. Primer combinations (and PCR product length in bp) for (C(i-vi)): L-R 1&5 (561), 1&7(617), 3&5(457), 3&7(513), 2&6(551), 2&8(608), 4&6(454), 4&8(511). Primers for (D): 1, 4, 6 & 7. See [Supplementary Table 1](#) for primer details. Thermocycler conditions were as follows: 96°C 120 sec, (96°C 30 sec, 63°C 30 sec, 72°C 20 sec) × 35 cycles, 72°C 120 sec. PCR reactions were run on a 1.5% agarose gel alongside Hyperladder 1kb Plus (Bioline, BIO-33068).

SUPPLEMENTARY FIGURE 3

Generation and genotyping of IRAK3^{-/-}H2q mice. Representative genotyping of (A) WT and heterogeneous (IRAK3^{+/-}) mice and (B, C) IRAK3^{-/-} mice bearing H2q, H2b/q and H2b haplotypes.

SUPPLEMENTARY FIGURE 4

IRAK3 deficiency reduces CD4⁺RORγt⁺ and CD4⁺Foxp3⁺ cells prior to disease onset The percentages of subsets of CD4⁺ lymphocytes, defined by the expression of the transcription factors Tbet, Gata3, FoxP3, Rorγt, and Helios in (A) the lymph nodes (LN) and (B) spleens (SPL) of pre-onset IRAK3^{-/-} and WT mice (n=5 and 8, respectively). (C) Plasma from pre-onset mice was assayed for anti-collagen IgG1 and IgG2a antibodies; values are mean ± SEM n=6-7/group. Percentages of subsets of CD4⁺ lymphocytes in (D) LN and (E) SPL from unimmunized, naïve mice; * p<0.05, ** p<0.01, **** p<0.0001, Student's t-test.

SUPPLEMENTARY FIGURE 5

Inflammatory gene expression is increased in affected paws of IRAK3^{-/-} mice. Gene expression of immune-related genes in the affected paws of mice 10 days post disease onset relative to *Gapdh* using the ΔΔCT method; * p<0.05, ** p<0.01, *** p<0.001, Student's t-test, n=8/group.

References

- McInnes IB, Schett G. The pathogenesis of rheumatoid arthritis. *N Engl J Med*. (2011) 365:2205–19. doi: 10.1056/NEJMra1004965
- del Fresno C, Gómez-García L, Caveda L, Escoll P, Arnalich F, Zamora R, et al. Nitric oxide activates the expression of IRAK-M via the release of TNF-α in human monocytes. *Nitric Oxide*. (2004) 10:213–20. doi: 10.1016/j.niox.2004.04.007
- Wesche H, Gao X, Li X, Kirschning CJ, Stark GR, Cao Z. IRAK-M is a novel member of the Pelle/interleukin-1 receptor-associated kinase (IRAK) family. *J Biol Chem*. (1999) 274:19403–10. doi: 10.1074/jbc.274.27.19403
- Lange SM, Nelen MI, Cohen P, Kulathu Y. Dimeric structure of the pseudokinase IRAK3 suggests an allosteric mechanism for negative regulation. *Structure*. (2021) 29:238–51.e4. doi: 10.1016/j.str.2020.11.004
- Pereira M, Gazzinelli RT. Regulation of innate immune signaling by IRAK proteins. *Front Immunol*. (2023) 14:1133354. doi: 10.3389/fimmu.2023.1133354
- Du J, Nicolaes GA, Kruijswijk D, Versloot M, van der Poll T, van 't Veer C. The structure function of the death domain of human IRAK-M. *Cell Commun Signal*. (2014) 12:77. doi: 10.1186/s12964-014-0077-3
- Turek I, Nguyen TH, Galea C, Abad I, Freihat L, Manallack DT, et al. Mutations in the vicinity of the IRAK3 guanylate cyclase center impact its subcellular localization and ability to modulate inflammatory signaling in immortalized cell lines. *Int J Mol Sci*. (2023) 24. doi: 10.3390/ijms24108572
- Gürkan B, Poelman H, Pereverzeva L, Kruijswijk D, de Vos AF, Groenen AG, et al. The IRAK-M death domain: a tale of three surfaces. *Front Mol Biosci*. (2023) 10:1265455. doi: 10.3389/fmolb.2023.1265455
- Balaci L, Spada MC, Olla N, Sole G, Loddo L, Anedda F, et al. IRAK-M is involved in the pathogenesis of early-onset persistent asthma. *Am J Hum Genet*. (2007) 80:1103–14. doi: 10.1086/518259
- Liu Y, Zhang M, Lou L, Li L, Zhang Y, Chen W, et al. IRAK-M associates with susceptibility to adult-onset asthma and promotes chronic airway inflammation. *J Immunol (Baltimore Md: 1950)*. (2019) 202:899–911. doi: 10.4049/jimmunol.1800712
- Pino-Yanes M, Sánchez-Machín I, Cumplido J, Figueroa J, Torres-Galván MJ, González R, et al. IL-1 receptor-associated kinase 3 gene (IRAK3) variants associate with asthma in a replication study in the Spanish population. *J Allergy Clin Immunol*. (2012) 129:573–5. doi: 10.1016/j.jaci.2011.10.001
- Wei W, Huang J, Ma Y, Ma X, Fang L, Fang W, et al. IL-1 signaling pathway molecules as key markers in childhood asthma. *Pediatr Allergy Immunol*. (2021) 32:305–13. doi: 10.1111/pai.13388
- Lech M, Kantner C, Kulkarni OP, Ryu M, Vlasova E, Heesemann J, et al. Interleukin-1 receptor-associated kinase-M suppresses systemic lupus erythematosus. *Ann rheumatic diseases*. (2011) 70:2207–17. doi: 10.1136/ard.2011.155515
- Sánchez E, García-Bermúdez M, Jiménez-Alonso J, de Ramón E, Sánchez-Román J, Ortego-Centeno N, et al. Association study of IRAK-M and SIGIRR genes with SLE in a large European-descent population. *Lupus*. (2012) 21:1166–71. doi: 10.1177/0961203312449494
- Geng S, Chen K, Yuan R, Peng L, Maitra U, Diaio N, et al. The persistence of low-grade inflammatory monocytes contributes to aggravated atherosclerosis. *Nat Commun*. (2016) 7:13436. doi: 10.1038/ncomms13436
- Li J, Wang G, Xv X, Li Z, Shen Y, Zhang C, et al. Identification of immune-associated genes in diagnosing osteoarthritis with metabolic syndrome by integrated bioinformatics analysis and machine learning. *Front Immunol*. (2023) 14:1134412. doi: 10.3389/fimmu.2023.1134412
- Gomes da Silva IIF, Barbosa AD, Souto FO, Maia MMD, Crovella S, Souza PRE, et al. MYD88, IRAK3 and Rheumatoid Arthritis pathogenesis: Analysis of differential gene expression in CD14 + monocytes and the inflammatory cytokine levels. *Immunobiology*. (2021) 226:152152. doi: 10.1016/j.imbio.2021.152152
- Cho ML, Ju JH, Kim HR, Oh HJ, Kang CM, Jhun JY, et al. Toll-like receptor 2 ligand mediates the upregulation of angiogenic factor, vascular endothelial growth factor and interleukin-8/CXCL8 in human rheumatoid synovial fibroblasts. *Immunol Lett*. (2007) 108:121–8. doi: 10.1016/j.imlet.2006.11.005
- Chinju A, Moriyama M, Kakizoe-Ishiguro N, Chen H, Miyahara Y, Haque A, et al. CD163+ M2 macrophages promote fibrosis in IgG4-related disease via toll-like receptor 7/interleukin-1 receptor-associated kinase 4/NF-κB signaling. *Arthritis Rheumatol*. (2022) 74:892–901. doi: 10.1002/art.42043
- Ballinger MN, Newstead MW, Zeng X, Bhan U, Mo XM, Kunkel SL, et al. IRAK-M promotes alternative macrophage activation and fibroproliferation in bleomycin-induced lung injury. *J Immunol (Baltimore Md: 1950)*. (2015) 194:1894–904. doi: 10.4049/jimmunol.1402377

21. Tunalı G, Rúbies Bedós M, Nagarajan D, Fridh P, Papakyriacou I, Mao Y. IL-1 receptor-associated kinase-3 acts as an immune checkpoint in myeloid cells to limit cancer immunotherapy. *J Clin Invest.* (2023) 133. doi: 10.1172/JCI161084
22. Zhang Y, Diao N, Lee CK, Chu HW, Bai L, Li L. Neutrophils deficient in innate suppressor IRAK-M enhances anti-tumor immune responses. *Mol Ther.* (2020) 28:89–99. doi: 10.1016/j.yimthe.2019.09.019
23. Niveditha D, Sharma H, Majumder S, Mukherjee S, Chowdhury R, Chowdhury S. Transcriptomic analysis associated with reversal of cisplatin sensitivity in drug resistant osteosarcoma cells after a drug holiday. *BMC Cancer.* (2019) 19:1045. doi: 10.1186/s12885-019-6300-2
24. Williams RO, Marinova-Mutafchieva L, Feldmann M, Maini RN. Evaluation of TNF-alpha and IL-1 blockade in collagen-induced arthritis and comparison with combined anti-TNF-alpha/anti-CD4 therapy. *J Immunol (Baltimore Md: 1950).* (2000) 165:7240–5. doi: 10.4049/jimmunol.165.12.7240
25. Tak PP, Firestein GS. NF-kappaB: a key role in inflammatory diseases. *J Clin Invest.* (2001) 107:7–11. doi: 10.1172/JCI11830
26. Unterberger S, Davies KA, Rambhatla SB, Sacre S. Contribution of toll-like receptors and the NLRP3 inflammasome in rheumatoid arthritis pathophysiology. *Immunotargets Ther.* (2021) 10:285–98. doi: 10.2147/ITT.S288547
27. Vincent TL. Mechanoflamination in osteoarthritis pathogenesis. *Semin Arthritis Rheum.* (2019) 49:S36–s8. doi: 10.1016/j.semarthrit.2019.09.018
28. Clanchy FIL, Williams RO. Ibuprofen inhibits chemokine expression in rheumatoid arthritis synovial fibroblasts and exhibits immunomodulatory activity in experimental arthritis. *Arthritis Rheumatol.* (2019) 71:703–11. doi: 10.1002/art.2019.71.issue-5
29. Kobayashi K, Hernandez LD, Galán JE, Janeway CA Jr., Medzhitov R, Flavell RA. IRAK-M is a negative regulator of Toll-like receptor signaling. *Cell.* (2002) 110:191–202. doi: 10.1016/S0092-8674(02)00827-9
30. Backlund J, Li C, Jansson E, Carlsen S, Merky P, Nandakumar KS, et al. C57BL/6 mice need MHC class II Aq to develop collagen-induced arthritis dependent on autoreactive T cells. *Ann rheumatic diseases.* (2013) 72:1225–32. doi: 10.1136/annrheumdis-2012-202055
31. Clanchy FIL, Borghese F, Bystrom J, Balog A, Penn H, Hull DN, et al. TLR expression profiles are a function of disease status in rheumatoid arthritis and experimental arthritis. *J Autoimmun.* (2021) 118:102597. doi: 10.1016/j.jaut.2021.102597
32. Campbell IK, Rich MJ, Bischof RJ, Dunn AR, Grail D, Hamilton JA. Protection from collagen-induced arthritis in granulocyte-macrophage colony-stimulating factor-deficient mice. *J Immunol (Baltimore Md: 1950).* (1998) 161:3639–44. doi: 10.4049/jimmunol.161.7.3639
33. Clanchy FIL, Borghese F, Bystrom J, Balog A, Penn H, Taylor PC, et al. Disease status in human and experimental arthritis, and response to TNF blockade, is associated with MHC class II invariant chain (CD74) isoform expression. *J Autoimmun.* (2022) 128:102810. doi: 10.1016/j.jaut.2022.102810
34. Piccinini AM, Williams L, McCann FE, Midwood KS. Investigating the role of toll-like receptors in models of arthritis. *Methods Mol Biol (Clifton NJ).* (2016) 1390:351–81. doi: 10.1007/978-1-4939-3335-8_22
35. Ren P, Lu L, Cai S, Chen J, Lin W, Han F. Alternative splicing: A new cause and potential therapeutic target in autoimmune disease. *Front Immunol.* (2021) 12:713540. doi: 10.3389/fimmu.2021.713540
36. Sode J, Vogel U, Bank S, Andersen PS, Hetland ML, Loch H, et al. Confirmation of an IRAK3 polymorphism as a genetic marker predicting response to anti-TNF treatment in rheumatoid arthritis. *Pharmacogenomics J.* (2018) 18:81–6. doi: 10.1038/tpj.2016.66
37. Al-Qahtani AA, Lyroni K, Aznaourova M, Tseliou M, Al-Anazi MR, Al-Ahdal MN, et al. Middle east respiratory syndrome corona virus spike glycoprotein suppresses macrophage responses via DPP4-mediated induction of IRAK-M and PPARγ. *Oncotarget.* (2017) 8:9053–66. doi: 10.18632/oncotarget.14754
38. Liu B, Gu Y, Pei S, Peng Y, Chen J, Pham LV, et al. Interleukin-1 receptor associated kinase (IRAK)-M -mediated type 2 microglia polarization ameliorates the severity of experimental autoimmune encephalomyelitis (EAE). *J Autoimmun.* (2019) 102:77–88. doi: 10.1016/j.jaut.2019.04.020
39. Rajendeeran A, Tenbrock K. Regulatory T cell function in autoimmune disease. *J Transl Autoimmun.* (2021) 4:100130. doi: 10.1016/j.jtauto.2021.100130
40. Schlöder J, Shahneh F, Schneider FJ, Wieschendorf B. Boosting regulatory T cell function for the treatment of autoimmune diseases - That's only half the battle! *Front Immunol.* (2022) 13:973813. doi: 10.3389/fimmu.2022.973813
41. Huang YS, Tseng WY, Clanchy FIL, Topping LM, Ogbechi J, McNamee K, et al. Pharmacological modulation of T cell immunity results in long-term remission of autoimmune arthritis. *Proc Natl Acad Sci United States America.* (2021) 118. doi: 10.1073/pnas.2100939118
42. Stark JM, Tibbitt CA, Coquet JM. The metabolic requirements of th2 cell differentiation. *Front Immunol.* (2019) 10:2318. doi: 10.3389/fimmu.2019.02318
43. Wang Z, Wesche H, Stevens T, Walker N, Yeh WC. IRAK-4 inhibitors for inflammation. *Curr Top Med Chem.* (2009) 9:724–37. doi: 10.2174/156802609789044407



OPEN ACCESS

EDITED BY

Kyle T. Amber,
Rush University, United States

REVIEWED BY

Krisztina Ella,
Semmelweis University, Hungary
Kyeorda Kemp,
Oakland University, United States

*CORRESPONDENCE

Takashi Tanaka
✉ takashi.tanaka@riken.jp

†PRESENT ADDRESS

Akiko Sugimoto-Ishige,
Laboratory for Infectious Diseases and
Immunology, RIKEN Center for Integrative
Medical Sciences, Yokohama, Kanagawa,
Japan
Aya Jodo,
Laboratory for Metabolic Networks, RIKEN
Center for Integrative Medical Sciences,
Yokohama, Kanagawa, Japan
Takashi Tanaka,
Laboratory for Developmental Genetics,
RIKEN Center for Integrative Medical
Sciences, Yokohama, Kanagawa, Japan

RECEIVED 07 November 2024

ACCEPTED 28 April 2025

PUBLISHED 03 June 2025

CITATION

Sugimoto-Ishige A, Jodo A and Tanaka T
(2025) Fbxo16 mediates degradation of
NF- κ B p65 subunit and inhibits inflammatory
response in dendritic cells.
Front. Immunol. 16:1524110.
doi: 10.3389/fimmu.2025.1524110

COPYRIGHT

© 2025 Sugimoto-Ishige, Jodo and Tanaka.
This is an open-access article distributed under
the terms of the [Creative Commons Attribution
License \(CC BY\)](#). The use, distribution or
reproduction in other forums is permitted,
provided the original author(s) and the
copyright owner(s) are credited and that the
original publication in this journal is cited, in
accordance with accepted academic
practice. No use, distribution or reproduction
is permitted which does not comply with
these terms.

Fbxo16 mediates degradation of NF- κ B p65 subunit and inhibits inflammatory response in dendritic cells

Akiko Sugimoto-Ishige[†], Aya Jodo[†] and Takashi Tanaka^{*†}

Laboratory for Inflammatory Regulation, RIKEN Center for Integrative Medical Sciences, Yokohama, Kanagawa, Japan

Activation of transcription factor NF- κ B is tightly regulated by negative regulatory systems that prevent excessive inflammation leading to autoimmune diseases. We previously demonstrated that PDLIM2, a PDZ-LIM domain-containing nuclear protein, functions as a ubiquitin E3 ligase that targets the p65 subunit of NF- κ B and STAT3/STAT4 transcription factors for proteasomal degradation, thus terminating immune responses in dendritic cells and CD4⁺T cells, respectively. In this study, we have demonstrated that PDLIM2 forms a ubiquitin ligase complex with Cullin 1, a scaffold protein, providing a platform consisting of complex and Skp1, an adaptor protein. Moreover, by screening using siRNA for F-box-containing proteins, we have identified Fbxo16 as a substrate-recognition receptor for p65 in this complex. Fbxo16 bound to p65 and promoted its polyubiquitination and degradation, thereby suppressing NF- κ B transactivation. Consistently, Fbxo16 deficiency in dendritic cells resulted in a larger amount of nuclear p65 and thus enhanced production of proinflammatory cytokines. On the other hand, Fbxo16 could not promote the degradation of STAT3 or STAT4, and Fbxo16 deficiency did not affect STAT3- and STAT4-mediated immune responses of CD4⁺T cells. These results delineate a role of Fbxo16, as a substrate receptor for p65 in a PDLIM2-containing ubiquitin ligase complex, in negatively regulating NF- κ B-mediated inflammatory responses in dendritic cells.

KEYWORDS

F-box protein, NF- κ B, ubiquitin E3 ligase, inflammation, PDLIM2

1 Introduction

Dendritic cells detect invading pathogens by their sensors, such as Toll-like receptors (TLR). TLR stimulation activates dendritic cells to induce inflammatory responses through the activation of the nuclear factor κ B (NF- κ B) transcription factor. In unstimulated cells, the p65/p50 heterodimer of NF- κ B is associated with I κ B α and sequestered in the cytoplasm. TLR signaling results in proteasomal degradation of I κ B α . NF- κ B p65/p50 then enters the nucleus and induces the expressions of various inflammation-related genes,

such as interleukin-6 (IL-6) and IL-12 (1). IL-6 and IL-12 then activate signal transducer and activator of transcription 4 (STAT4) and STAT3 in naïve T-helper (Th) cells and direct the differentiation of these cells into distinct Th subsets, Th1 and Th17 cells, respectively. Th1 and Th17 cells produce effector cytokines, such as IFN- γ and IL-17 respectively and fight against different types of microbial pathogens (2). On the other hand, these immune responses should be tightly regulated by negative regulatory systems to prevent excessive inflammation leading to the onset of autoimmune diseases or allergic diseases (3, 4). Notably, genome-wide association studies (GWAS) have demonstrated that variants of negative regulators of these signaling pathways, including A20, CYLD and IRAK-M, are associated with human immune disorders, including inflammatory bowel diseases, rheumatoid arthritis, and asthma (5–7).

PDLIM2 (also designated as SLIM or mystique), that belongs to a LIM protein family, is a nuclear protein containing both PDZ (designated after the first-identified three proteins; PSD-95, Dig and ZO-1) and LIM (designated after the first-identified three proteins; Lin-11, Isl-1 and Mec-3) domains (8–10). We have previously demonstrated that the LIM domain possesses ubiquitin E3 ligase activity (9) and PDLIM2 functions as a nuclear ubiquitin E3 ligase for the p65 subunit of NF- κ B in dendritic cells (11). PDLIM2 not only promotes polyubiquitination of p65 through its LIM domain, but also shuttles p65 to the intranuclear compartments, PML (promyelocytic leukemia protein) nuclear bodies, where p65 is finally degraded by the proteasome, thereby negatively regulating NF- κ B activity. Consistently, PDLIM2 deficiency resulted in enhanced production of proinflammatory cytokines in dendritic cells. In addition, PDLIM2 also promotes polyubiquitination and degradation of STAT4 and STAT3 transcription factors in CD4⁺T cells and inhibits the differentiation of naïve T cells into Th1 and Th17 cells (9, 12). Thus, PDLIM2 negatively regulates immune responses in both innate and acquired immunity, preventing autoimmune diseases (13).

We have recently focused on the analysis of how PDLIM2-mediated NF- κ B p65 degradation in the nucleus is controlled in dendritic cells. We have previously demonstrated that the chaperone protein HSP70 binds to PDLIM2 in the nucleus and promotes the shuttling of NF- κ B to the proteasome together with the proteasome-associated protein BAG-1 (14). We have further shown that PDLIM7, another LIM protein, forms heterodimer with PDLIM2 and promotes its K63-linked ubiquitination and then facilitate the transport of the NF- κ B-PDLIM2 complex to the proteasome together with the ubiquitin-recognizing protein p62/Sqstm1 (15). However, the detailed molecular mechanisms of how PDLIM2 recognizes and polyubiquitinates target proteins remain unclear.

LIM domain is structurally related to the RING (really interesting new gene) finger domain, that has ubiquitin E3 ligase activity (16). Both LIM domain and RING finger domains consist of eight conserved cysteines (Cys) or histidine (His) residues, so the LIM domain might be a subtype of RING finger domain (17). To date, over 600 RING finger proteins are identified as ubiquitin E3

ligases. RING-type ubiquitin ligases are mainly classified into two types, which are monomer-type and multi-subunit complex-type (18). The multi-subunit complex-type ubiquitin E3 ligase is composed of one core scaffold protein Cullin, providing a platform of the complex, thus this complex is called the Cullin-Ring ubiquitin ligase complex (CRL) (19, 20). Cullin has seven family members, including Cullin 1, 2, 3, 4A, 4B, 5 and 7. One end of each Cullin protein binds to a substrate-recognizing receptor directly or through an adaptor protein. For example, Cullin 3 directly binds to BTB domain-containing substrate receptors, whereas Cullin 1 associates with various substrate receptor F-box proteins through an adaptor Skp1. The other end of Cullin binds to RING finger protein, an E2 enzyme-recruiting subunit, which facilitates ubiquitin transfer onto the substrate bound to the substrate receptor (21, 22). In this study, we have demonstrated that PDLIM2 forms a functional ubiquitin E3 ligase complex CRL1 with Cullin 1 and Skp1 together with Fbxo16 as a substrate-recognition component. Fbxo16 recognizes p65 and promotes its polyubiquitination and degradation cooperatively with PDLIM2, thereby suppressing p65-mediated NF- κ B transactivation. In contrast, Fbxo16 did not polyubiquitinate and promote the degradation of STAT4 or STAT3, other substrates of PDLIM2 for ubiquitin-dependent degradation (9, 12). Consistently, Fbxo16 deficiency in dendritic cells resulted in augmented production of p65-mediated proinflammatory cytokines, whereas STAT4 and STAT3-mediated Th1 and Th17 differentiation of CD4⁺T cells were not affected by Fbxo16 deficiency. These results demonstrated that Fbxo16 is a p65-recognizing component in the PDLIM2-containing ubiquitin E3 ligase complex and inhibits NF- κ B-dependent inflammatory responses in dendritic cells.

2 Materials and methods

2.1 Expression plasmids

For the c-Myc-tagged Fbxo16, the complementary DNA (cDNA) of mouse *Fbxo16* (GeneBank accession: NM_001114088) was amplified by KOD-Plus-Neo DNA polymerase (TOYOBO) and subcloned into pCMV-Myc (Clontech). For the c-Myc-tagged Δ F-box mutant of Fbxo16 (Δ F), the coding region between amino acids 92–129 was deleted from the full-length c-Myc-Fbxo16 plasmid by mutagenesis with In-Fusion cloning using primers; 5'-CTACCAAGATGCTCAAGTGCCTGCGC-3' and 5'-TGAGCATCTTGGTAGTAAAATCCAG-3'. The c-Myc-tagged PDLIM2, Flag-tagged p65 and Flag-p65-IRES-Venus were previously described (9, 11). For the HA-tagged PDLIM2, a HA-tag plus the coding sequence of murine *Pdlim2* (GeneBank accession: NM_145978) was inserted into pCMV-Myc (Clontech), as a result, the c-Myc-tag was replaced with the HA-tag. For the Flag-tagged PDLIM2, mouse *Pdlim2* was subcloned into pCMV-DYKDDDDK (Clontech). Expression plasmids for Flag-tagged murine p50 (#20018), murine TRAF6 (#21624), murine MyD88 (#13093) and human IKK β (#23298) were purchased from Addgene. The pRL-Null renilla construct (#E2271) was purchased

from Promega. The ELAM-1 luciferase reporter construct was provided by D. Golenbock (23).

2.2 Reagents and antibodies

Lipopolysaccharide (LPS; from *Salmonella typhimurium*; L-2262) was purchased from Sigma-Aldrich/Merck. CpG oligonucleotides (ODN 1668, #tlrl-1668) were purchased from InvivoGen. MG132 (#474791) was purchased from Calbiochem/Merck. Murine GM-CSF (#415-ML) was purchased from R&D Systems. Human ligand for the receptor tyrosine kinase Flt3 (Flt3L) (#300-19) was purchased from Peprotech. Anti-DYKDDDDK (NU01102) antibody, that corresponds to an anti-Flag antibody, was purchased from Nacalai USA. Anti-p65 (sc-372), p50 (sc-7178), I κ B α (sc-371) and PKC (sc-10800) antibodies were from Santa Cruz Biotechnology. Anti-LSD1 (#2184), cdc37 (#3604), Histone H3 (#4499) Lamin B1 (#12586) and Skp1 (#12248) antibodies were from Cell Signaling Technology. Anti-HSP90 (#13171-1-AP) and Cullin 7 (#13738-1-AP) antibodies were from Proteintech. Anti-Cullin 1 (ab75817), Cullin 2 (ab166917) and Cullin 3 (ab75851) antibodies were from Abcam. Anti- γ -actin (#016-27821) antibody were purchased from FUJIFILM Wako Pure Chemicals. HRP-conjugated anti-c-Myc antibody (M047-7), anti-c-Myc antibody-conjugated agarose (M047-8), anti-HA antibody (M180-3), and DDDDK-tagged Protein PURIFICATION GEL (#3328R) (used for immunoprecipitation of Flag-tagged proteins) were purchased from MBL. Anti-ubiquitin antibody (clone FK-2; BML-PW8810) was from Enzo Life Sciences. As a secondary antibody, HRP-goat anti-rabbit IgG (#111-035-003) was purchased from Jackson ImmunoResearch and HRP-conjugated sheep anti-mouse IgG (NA931) was purchased from GE Healthcare.

2.3 Cell culture, transfection, and reporter assay

Mouse embryonic fibroblasts (MEFs) were prepared as previously described (15). GM-CSF-differentiated bone marrow cells (GM-CSF-BMCs), Flt3L-differentiated bone marrow-derived dendritic cells (BMDC), macrophages, CD4⁺T, CD8⁺T and CD19⁺B cells were prepared as previously described (15). Human embryonic kidney (HEK) 293T cells, MEFs, GM-CSF-BMCs and BMDC were cultured in DMEM supplemented with 10% FCS. CD4⁺T cells were cultured in RPMI1640 supplemented with 10% FCS.

Effectene transfection reagents (QIAGEN) was used for transient transfection. For the reporter assay with the Dual Luciferase Reporter System (Promega), MEFs and HEK293T cells were transfected with the ELAM-1 luciferase and pRL-Null renilla reporter constructs and analyzed as previously described (15). Luciferase activity of the ELAM-1 luciferase reporter was normalized to the renilla luciferase activity and represented as fold-change to the control.

2.4 Subcellular fractionation, immunoprecipitation, and ubiquitination assay

All lysis buffers contained a protease inhibitor (Roche). Cytoplasmic, nuclear soluble and insoluble fractions were extracted as previously described (11). Anti-cdc37 (cytoplasm), anti-LSD1 (nuclear soluble fraction), and anti-Lamin B or Histone H3 (nuclear insoluble fraction) were used for checking the purity of the fractionation. For co-immunoprecipitation between Skp1 and PDLIM2 or Fbxo16, cells were lysed in 50 mM Tris pH 8.0, 0.5% NP-40, 5 mM EDTA, 50 mM NaCl, 50 mM sodium fluoride. For other co-immunoprecipitation experiments, cells were lysed in RIPA buffer (25 mM Tris pH 8.0, 150 mM NaCl, 1% NP-40, 1% sodium deoxycholate, 0.1% SDS). Whole cell extracts were then incubated with anti-c-Myc agarose or DDDDK-tagged Protein PURIFICATION GEL (MBL) overnight and washed four times with lysis buffer and analyzed by immunoblot analysis as previously described (15). For ubiquitination assay, His-tagged proteins were purified from whole cell lysates with His60 Nickel Superflow Resin (TAKARA BIO INC.) as previously described (24) and analyzed by immunoblot analysis.

2.5 Immunofluorescence staining

HEK293T cells, cultured on poly-L-lysine-coated slides, were transfected with Flag-p65-IRES-Venus without or with wild-type or Δ F mutant of Fbxo16, and analyzed by immunofluorescence staining as previously described (11).

2.6 Knockdown experiments with siRNA

HEK293T cells were first transfected with siRNA by Lipofectamine RNAiMAX (Thermo Fisher Scientific Inc.), then transfected with indicated plasmids and lysed with RIPA buffer and subjected to immunoprecipitation or immunoblot analysis. GM-CSF-BMCs were transfected with siRNA by the Neon Transfection System (Invitrogen) and analyzed as previously described (15). The siRNAs for 39 human Fbxo proteins (Supplementary Table 1), 10 murine Fbxo proteins (Supplementary Table 3) and control siRNA (12935–300) were selected from Stealth Select RNAi predesigned siRNAs (Thermo Fisher Scientific Inc.) and purchased.

2.7 Real-time PCR analysis

The synthesis of cDNA and the quantitative real-time PCR analyses were performed as previously described (15). To analyze the expression of proinflammatory cytokines in GM-CSF-BMCs, we used Taqman Fast Advanced Master Mix and probes for mouse *Il-6* (Mm00446190), *Il-12b* (Mm00434174), *Il-1 β* (Mm00434228), *Cxcl2* (Mm00436450), *Cxcl10* (Mm00445235), *Csf3*

(Mm00438334) and 18S rRNA (4319413E) from the TaqMan Gene Expression Assay (Applied Biosystems/Thermo Fisher Scientific). To analyze the expression of human and murine FBXO proteins, we used Fast SYBR Green Master Mix (Applied Biosystems/Thermo Fisher Scientific), and the primer pairs shown in [Supplementary Tables 2 ; Supplementary Table 4](#) (Thermo Fisher Scientific Inc.). The cycle threshold (Ct) value of each gene expression was normalized to that of 18S rRNA and the fold-change to the control was calculated by the $\Delta\Delta C_t$ method.

2.8 Generation of *Fbxo16*-deficient mice

The murine genomic *Fbxo16* allele was knocked out using the Alt-R CRISPR-Cas9 system (IDT) with the target sequence, TTTTACTACCAAGCTTCCAA(GGG). The crRNA containing this target sequence and tracrRNA were synthesized by IDT, mixed with Cas9 protein forming an RNP complex, and microinjected into pronuclei of C57BL/6J embryos. Mice were screened by PCR and sequencing analysis to determine the mutated region. The mutant line, in which deletion of a part of exon IV and intron IV in genomic DNA introduces a premature termination codon at the beginning of exon V, was selected for further study. This mutation deleted almost the entire region of the F-box domain, which is essential for Fbxo16 activity ([Supplementary Figure 1](#)). The mice with this deletion were crossed with wild-type C57BL/6J mice, that were purchased from CREA Japan, Inc, to generate heterozygous mice, and homozygotes were obtained by crossing of heterozygotes. The sequences of primer sets used for genotyping were as follows. Forward: 5'-GACTCTCTGTGTTCCCTGTTTCCTC-3' and Reverse: 5'-AGGTGGCAATGCTGTCTACTGAG-3'. Mice were kept under specific pathogen free conditions and used for the experiments between 4 and 5 weeks of age. All experiments were approved by the Institutional Animal Care and Use Committee (IACUC) of RIKEN Yokohama Branch and performed in accordance with the committee's guidelines.

2.9 T-helper cell differentiation experiments

CD4⁺ T cells were purified from spleen by MACS and cultured with plate-bound anti-CD3 (0.1 μ g/ml) plus soluble anti-CD28 (1 μ g/ml) for 3 days under Th1 and Th17 subset skewing conditions as follows; IL-12 (1 ng/ml) for Th1; TGF- β (0.5 ng/ml) plus IL-6 (10 ng/ml) for Th17, and then restimulated with plate-bound anti-CD3 (1 μ g/ml) for 20 h and the production of IFN- γ and IL-17A in the supernatants was measured by ELISA (BD Biosciences).

2.10 Statistical Analyses

The student's t test was used for all the statistical analysis. Data are represented as the mean values \pm the standard deviation of the mean (SD).

3 Results

3.1 PDLIM2 bound to Cullin 1 and Skp1 forming a ubiquitin E3 ligase complex

During our initial study using mass-spectrometry-based proteomic screening for proteins coimmunoprecipitated with PDLIM2, we found that Skp1 is one of the PDLIM2-interacting proteins. Since Skp1 is an adaptor protein in the Cullin 1 and Cullin 7-containing Cullin-RING-ligase complexes (CRL1 and CRL7, respectively) (19), we predicted that PDLIM2 could form a complex with Cullin 1 and/or Cullin 7 plus Skp1 to function as a ubiquitin E3 ligase. We first clarified the subcellular localization of Cullin 1 and Cullin 7 in dendritic cells (BMDC) and mouse embryonic fibroblasts (MEFs) by immunoblot analysis ([Figure 1A](#)). The ratios of nuclear/cytoplasmic expression of Cullin 1 or Cullin 7 in each blot were calculated using densitometric analysis ([Supplementary Figure 2](#)). Cullin 1 was found in both the cytoplasm and nucleus in dendritic cells and MEFs. On the other hand, Cullin 7 expression was detected only in the cytoplasm in MEFs and was not detected in dendritic cells. The purity of the cytoplasmic and nuclear fractions was demonstrated by anti-PKC and LSD1 antibodies, respectively. These data suggest that Cullin 1, but not Cullin 7, could contribute to the PDLIM2-dependent degradation of nuclear p65 in dendritic cells. We therefore focused on Cullin 1 for the following studies.

We then determined if PDLIM2 can bind to Cullin 1. HEK293T cells, transfected with Flag-tagged PDLIM2, were immunoprecipitated with an anti-Flag antibody and then immunoblotted with anti-Cullin 1 and also anti-Cullin 2 and Cullin 3 as controls. Although PDLIM2 could bind to all the Cullin proteins we tested ([Figure 1B](#)), we demonstrated that PDLIM2 more strongly associated with Cullin 1 compared to Cullin 2 and Cullin 3 by densitometric analysis of the coimmunoprecipitated amount of each Cullin relative to the total amount of input ([Figure 1C](#)). Moreover, consistent with our previous study described above, PDLIM2 could also bind to Skp1 in this assay ([Figure 1D](#)). We previously demonstrated that PDLIM2 polyubiquitinated p65 and then transported p65 to the insoluble nuclear compartments, where p65 was degraded by the proteasome (11). To examine the effect of Cullin 1 and Skp1 on p65 degradation by PDLIM2, we knocked down Cullin 1 or Skp1 in HEK293T cells transfected with p65 without or with PDLIM2 and examined the levels of soluble and insoluble nuclear p65 protein. Knockdown of either Cullin 1 or Skp1 resulted in the increase of p65, mostly in the insoluble nuclear fraction, where p65 is degraded ([Figure 1E](#)), suggesting that both Cullin 1 and Skp1 are required for p65 degradation by PDLIM2. Moreover, the binding between PDLIM2 and p65 was impaired by the specific knockdown of either Cullin 1 or Skp1 ([Figure 1F](#), [Supplementary Figure 3](#)). These data demonstrate that PDLIM2 can bind to Cullin 1 and Skp1 forming a CRL1 complex to function as a ubiquitin E3 ligase mediating p65 degradation.

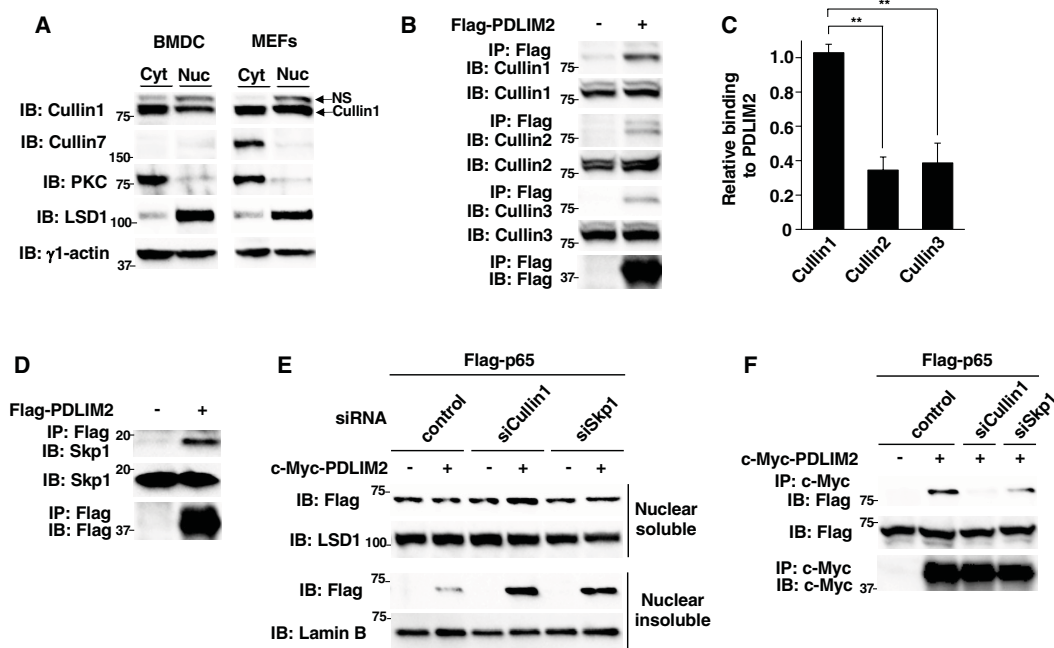


FIGURE 1

PDLIM2 bound to Cullin 1 and Skp1 forming a ubiquitin E3 ligase complex. (A) Expression of Cullin 1 and Cullin 7 in cytoplasmic and nuclear extracts of dendritic cells (BMDC) and fibroblasts (MEFs). The purity of the fractions of cytoplasmic and nuclear extracts was checked with anti-PKC and anti-LSD1 antibodies, respectively. NS, Non-specific band. (B) Interaction of PDLIM2 and Cullins in whole cell lysates of HEK293T cells, transfected with Flag-PDLIM2, then immunoprecipitated (IP) with anti-Flag, and immunoblotted (IB) with anti-Cullin 1, Cullin 2 or Cullin 3. (C) Densitometric analysis of the coimmunoprecipitated amount of each Cullin protein relative to the total amount of input. Shown are the mean \pm SD. ** $P < 0.01$. (D) Interaction of PDLIM2 and Skp1 in whole cell lysates of HEK293T cells, transfected with Flag-PDLIM2, then immunoprecipitated with anti-Flag, and immunoblotted with anti-Skp1. (E) Effect of Cullin 1 or Skp1 deficiency on PDLIM2-mediated p65 degradation in soluble and insoluble nuclear extracts of HEK293T cells, first transfected with control siRNA or siRNA against Cullin 1 or Skp1, then transfected with Flag-p65 without or with c-Myc-PDLIM2 and analyzed by immunoblot with anti-Flag antibody. (F) Effect of Cullin 1 or Skp1 deficiency on the interaction of PDLIM2 and p65 in HEK293T cells, first transfected with control siRNA or siRNA against Cullin 1 or Skp1 and then transfected with Flag-p65 without or with c-Myc-PDLIM2. Whole cell lysates were immunoprecipitated with anti-c-Myc and immunoblotted with anti-Flag. Data are representative of three (A–F) independent experiments.

3.2 Fbxo16 is a substrate-recognizing component in the PDLIM2-containing ubiquitin E3 ligase complex

In the PDLIM2-containing CRL1 complex, PDLIM2 is thought to be an E2-recruiting subunit and the substrate receptor should be some F-box protein (17–19). This idea prompted us to identify the F-box protein that functions as a substrate receptor for p65 and promotes its degradation in the nucleus. More than sixty F-box proteins have been identified thus far in humans and mice. These F-box proteins are classified into three classes depending on their domain structure in the molecule, namely the FBXW family (containing the F-box and a WD40 domain), the FBXL family (containing the F-box and a Leu-rich repeat) and the FBXO family which has only the F-box domain (21, 22). To date, the functions of these F-box proteins have been intensively studied mainly in cell cycle regulation and tumorigenesis. In contrast, the roles of F-box proteins in immune regulation remain unclear. Since the FBXO family is the largest subfamily of F-box proteins, we focused on it in our attempt to identify the FBXO protein involved in the binding to p65 in the PDLIM2-containing CRL1 complex.

For the first screening, we used a co-immunoprecipitation assay with PDLIM2 and p65. We transfected HEK293T cells with Flag-p65 and c-Myc-PDLIM2 in the absence or presence of siRNA against 39 Fbxo proteins (Supplementary Table 1), immunoprecipitated them with an anti-c-Myc beads, and immunoblotted with anti-Flag to determine if siRNA targeting any of these Fbxo proteins could disrupt the binding between p65 and PDLIM2. Among the Fbxo proteins, knockdown of 10 FBXO family members, including Fbxo2, 7, 9, 10, 15, 16, 22, 41, 47 and 48, impaired the association of PDLIM2 with p65 (Figure 2A). Note that Fbxo18 knockdown did not inhibit this interaction. For the second more stringent screening, we tested if knockdown of any of these ten candidate FBXO proteins interferes with PDLIM2-dependent p65 degradation. We transfected HEK293T cells with Flag-p65 and c-Myc-PDLIM2 in the absence or presence of siRNA specific to these ten FBXO proteins and measured p65 protein levels in the soluble nuclear fraction. The reduction of mRNA encoding each FBXO protein in cells transfected with each FBXO protein-specific siRNA was confirmed by real-time PCR analysis (Supplementary Figure 4) using the primers shown in Supplementary Table 2. PDLIM2 overexpression markedly

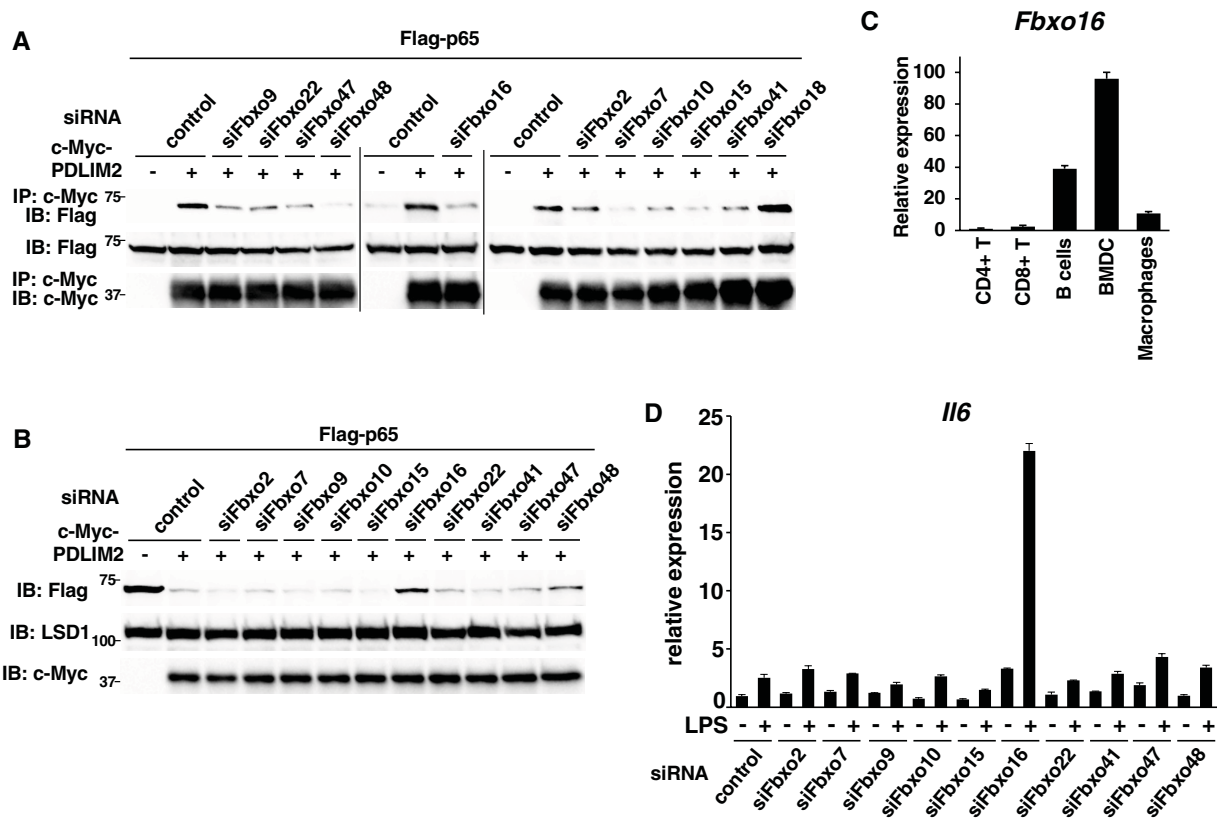


FIGURE 2

Fbxo16 is a substrate-recognizing component in the PDLIM2-containing ubiquitin E3 ligase complex. (A) Effect of deficiency of Fbxo proteins on the interaction of PDLIM2 and p65 in HEK293T cells, first transfected with control siRNA or siRNA-specific to Fbxo9, 22, 47, 48, 16, 2, 7, 10, 15, 41 or 18 and then transfected with Flag-p65 without or with c-Myc-PDLIM2. Whole cell lysates were immunoprecipitated with anti-c-Myc and immunoblotted with anti-Flag. (B) HEK293T cells first transfected without or with siRNA-specific to Fbxo2, 7, 9, 10, 15, 16, 22, 41, 47 or 48, then transfected with plasmids encoding Flag-p65 without or with c-Myc-PDLIM2. The soluble nuclear extracts were analyzed by anti-Flag antibody. (C) Real-time PCR analysis of Fbxo16 expression in immune cells, including CD4⁺T, CD8⁺T, CD19⁺B cells, BMDC and macrophages. (D) Effect of deficiency of Fbxo proteins on IL-6 expression in GM-CSF-BMCs transfected with control siRNA or siRNA against Fbxo2, 7, 9, 10, 15, 16, 22, 41, 47 or 48, left untreated or stimulated with LPS (0.1 ng/ml) for 5 h, and analyzed by real-time PCR. Data are representative of three (A), five (B), three (C; means \pm SD) or four (D; means \pm SD) independent experiments.

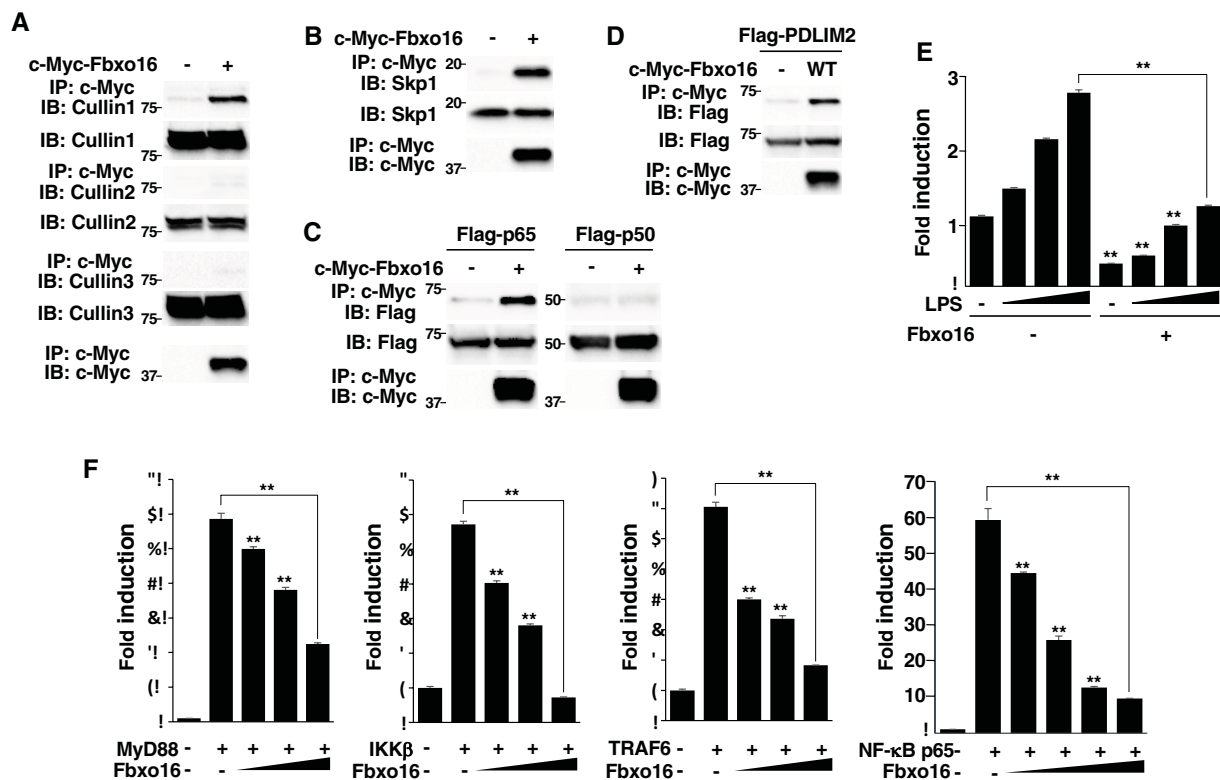
decreased p65 protein in this fraction, whereas only Fbxo16 knockdown clearly reverted the PDLIM2-dependent decrease in p65 protein levels (Figure 2B), suggesting that Fbxo16 is most likely to be the substrate-recognizing subunit in the PDLIM2-containing CRL1 complex.

We then examined the expression of Fbxo16 in immune cells and found that it is expressed at highest levels in dendritic cells (BMDC) but at very low levels in CD4⁺ and CD8⁺ T cells (Figure 2C). We have previously shown that PDLIM2 negatively regulates TLR-mediated p65-activation in dendritic cells, so that PDLIM2-deficient dendritic cells have enhanced TLR-mediated inflammatory cytokine production (11). For the final screening, we have therefore examined if knockdown of any of the ten candidate FBXO proteins in dendritic cells augmented LPS-induced IL-6 expression. We transfected GM-CSF-differentiated bone marrow cells (GM-CSF-BMCs) with siRNA specific to the candidate FBXO proteins (Supplementary Table 3), stimulated cells with LPS and examined IL-6 expression by real-time PCR analysis. The efficiency of knockdown by each FBXO protein was determined by real-time PCR analysis (Supplementary Figure 5) using specific

primers shown in Supplementary Table 4. We could detect a striking augmentation of LPS-induced IL-6 expression only in Fbxo16 knockdown dendritic cells compared to control cells (Figure 2D). Taking these data together, we speculated that Fbxo16 is the best candidate for the substrate-recognizing receptor for p65 in the PDLIM2-containing CRL1 complex.

3.3 Fbxo16 forms a CRL1 complex, binds to p65 and negatively regulates NF- κ B signaling

To demonstrate that Fbxo16 is a substrate p65-recognizing subunit in the PDLIM2-containing CRL1 complex, we first examined the association of Fbxo16 with the other components in the complex. HEK293T cells were transfected with c-Myc-Fbxo16, immunoprecipitated with anti-c-Myc beads, and immunoblotted with antibodies against Cullin 1, Cullin 2, Cullin 3 and Skp1. We demonstrated that Fbxo16 binds to Cullin1 and Skp1, but not Cullin2 or Cullin3 (Figures 3A, B), which is



compatible with the general feature of F-box proteins that forms a CRL1 complex through Skp1. We then tested if Fbxo16 interacted with p65 and found that Fbxo16 could bind to p65, but not to p50, component of NF-κB (Figure 3C). Moreover, we have also shown by a co-immunoprecipitation assay that Fbxo16 binds to PDLIM2 (Figure 3D). These data demonstrated that Fbxo16 can physically interact with all the components in PDLIM2-containing CRL1 complex.

Since PDLIM2 inhibits TLR-mediated NF-κB activation (11), we next tested the effect of Fbxo16 on TLR-mediated, NF-κB-induced transactivation in a luciferase assay. MEFs were transfected with the ELAM-1 luciferase reporter that can be driven by NF-κB, and then stimulated with LPS for 5 hr. LPS stimulation increased luciferase activity, while coexpression of Fbxo16 markedly inhibited transactivation of the LPS-induced luciferase reporter (Figure 3E). In contrast to the nuclear localization of PDLIM2, Fbxo16 is localized in both the cytoplasm and the nucleus (<https://www.proteinatlas.org/>), suggesting that Fbxo16 might target upstream cytoplasmic signaling molecules in addition to p65. To

rule out this possibility, we cotransfected HEK293T cells with p65 or upstream cytoplasmic signaling molecules MyD88, TRAF6, or IKKβ to activate the ELAM-1 luciferase reporter, without or with Fbxo16, and examined if Fbxo16 could affect gene activation driven by these molecules. Fbxo16 inhibited MyD88-, TRAF6-, IKKβ-, and p65-mediated NF-κB activation to almost the same extent (Figure 3F). These data suggest that Fbxo16 acts on p65, the most downstream molecule, to inhibit NF-κB signaling.

3.4 Fbxo16 mediates the polyubiquitination and degradation of p65 through its F-box domain

Since PDLIM2 promoted polyubiquitination of p65 and following its degradation by proteasome (11), we investigated if Fbxo16 also polyubiquitinate p65 and found that Fbxo16 could promote polyubiquitination of p65 in a dose-dependent manner (Figure 4A). To assess the activity of Fbxo16 to degrade p65, we next

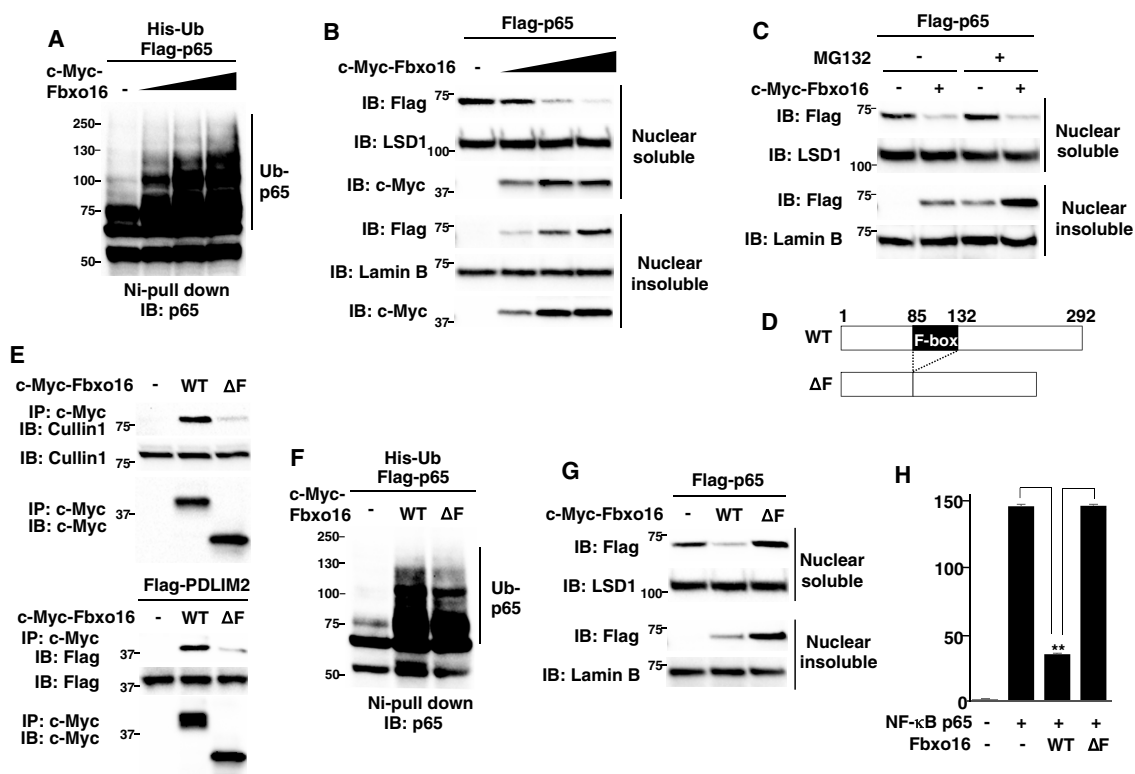


FIGURE 4

Fbxo16 mediates the polyubiquitination and degradation of p65 through its F-box domain. (A) Ubiquitination assay of p65 in HEK293T cells transfected with His-ubiquitin (His-Ub), p65 and increasing amounts (wedge) of Fbxo16. The purified ubiquitinated proteins were analyzed by immunoblot with anti-p65. (B) Effect of Fbxo16 on soluble and insoluble nuclear p65 in HEK293T cells transfected with Flag-p65 and increasing amounts (wedge) of c-Myc-Fbxo16, analyzed by immunoblot with anti-Flag antibody. (C) Effect of proteasome inhibitor on PDLIM2-mediated p65 degradation in soluble and insoluble nuclear extracts of HEK293T cells, transfected with Flag-p65 without or with c-Myc-Fbxo16, then left untreated or treated for 4 h with MG132 (10 μM) and analyzed by immunoblot with anti-Flag antibody. (D) The structure of the wild-type Fbxo16 protein and Fbxo16 mutant lacking the F-box domain (ΔF). (E) Effect of the deletion of F-box domain on the interaction of Fbxo16 and Cullin 1 (top) or PDLIM2 (bottom) in HEK293T cells, transfected without or with c-Myc-wild-type or ΔF Fbxo16, immunoprecipitated with anti-c-Myc and immunoblotted with anti-Cullin 1 antibody (top), or transfected with Flag-PDLIM2 along with or without c-Myc-wild-type or ΔF Fbxo16, immunoprecipitated with anti-c-Myc and immunoblotted with anti-Flag antibody (bottom). (F) Ubiquitination assay of p65 in HEK293T cells cotransfected with His-ubiquitin, p65 along without or with wild-type or ΔF Fbxo16. The purified ubiquitinated proteins were analyzed by immunoblot with anti-p65. (G) Effect of the deletion of F-box domain on Fbxo16-mediated p65 degradation in soluble and insoluble nuclear extracts of HEK293T cells transfected with Flag-p65, along without or with wild-type or ΔF Fbxo16 and analyzed by immunoblot with anti-Flag antibody. (H) Luciferase assay in HEK293T cells transfected with ELAM-1 luciferase reporter, pRL-Null renilla constructs and Flag-p65 without or with wild-type or ΔF Fbxo16. Data are representative of three (A–C, E–G) or three (H; means ± SD, **P<0.01) independent experiments.

transfected HEK293T cells with Flag-p65 together without or with c-Myc-Fbxo16 and examined the p65 protein in soluble and insoluble nuclear fractions. The p65 protein expression was decreased in the soluble nuclear fraction but increased in the insoluble nuclear fraction by coexpression of Fbxo16 (Figure 4B). MG132, a proteasome inhibitor, treatment led to the increase of p65 in the insoluble, but not soluble, nuclear fraction (Figure 4C), suggesting that Fbxo16, possibly together with PDLIM2, promotes the transport of p65 to the insoluble nuclear fraction and following proteasomal degradation of p65 in this compartment. To clarify the role of the F-box domain, which is responsible for the binding to Skp1 in the CRL1 complex, we generated a Fbxo16 mutant lacking the F-box domain; ΔF (Figure 4D). This mutant was impaired to bind to either Cullin1 or PDLIM2 and to polyubiquitinate p65 (Figures 4E, F), indicating that CRL1 complex formation was almost completely disrupted by deletion of the F-box domain. We then transfected HEK293T cells with Flag-p65 together without or with wild-type or ΔF Fbxo16 and examined

the p65 protein level in soluble and insoluble nuclear fractions. As with the experiments in Figure 4B, wild-type Fbxo16 reduced p65 in the soluble nuclear fraction, whereas Fbxo16-ΔF could not decrease p65 in this fraction, possibly because the transport of p65 from soluble to insoluble fractions was almost completely impaired by this mutation (Figure 4G). Moreover, Fbxo16 ΔF transfectants resulted in much more accumulation of insoluble p65 than wild-type transfectants. This can be due to reduced p65 degradation in the insoluble fraction as a consequent of impaired p65 polyubiquitination in Fbxo16-ΔF transfectants. Consistently, the activity of Fbxo16-ΔF to inhibit NF-κB activation in the luciferase assay was completely impaired (Figure 4H). These data indicated that Fbxo16, and possibly CRL complex formation itself, is essential for both intranuclear transport of p65 to the insoluble fraction and following p65 degradation in this fraction.

To visualize the effect of Fbxo16 on p65 degradation in the nucleus, we next used a plasmid that bicistronically expresses both Flag-tagged p65 and Venus proteins (Flag-p65-IRES-Venus) and

transfected it into HEK293T cells without or with the Fbxo16 expression plasmid. Cells were then examined by indirect immunofluorescence using confocal microscopy. The percentage of Flag⁺•Venus⁺ or Flag⁻•Venus⁺ cells per total Venus⁺ cells was calculated to assess the effects of Fbxo16 on nuclear p65. Overexpressed p65 exhibited homogeneous nuclear distribution (Figure 5A, left column). On the other hand, Fbxo16 coexpression led to the loss of nuclear p65 staining (Figure 5A, right column). In control cells, 96.8 ± 1.0% of Venus-expressing cells also expressed Flag-p65, whereas only 22.8 ± 4.2% of Venus-expressing cells expressed Flag-p65 in Fbxo16 transfectant. Notably, cells with coexpression of Fbxo16-ΔF restored the Flag-p65 expression up to 79.5 ± 2.2% due to impaired ubiquitination-dependent degradation of p65 (Figure 5B).

3.5 NF-κB-mediated inflammatory responses were enhanced in Fbxo16 deficient dendritic cells

We next investigate the role of Fbxo16 in the regulation of TLR-mediated NF-κB activation. We knocked down Fbxo16 in GM-CSF-differentiated bone marrow cells (GM-CSF-BMCs) by siRNA, stimulated them with LPS, and analyzed the effect of Fbxo16 deficiency on LPS-induced proinflammatory cytokine gene expression. The expression of IL-6, IL12, IL-1β, CXCL-2, CXCL-10, and G-CSF (Csf3) was significantly upregulated in LPS-stimulated Fbxo16 knockdown cells compared to LPS-stimulated control cells at all time points we tested (Figure 6A). We then examined the effect of Fbxo16 knockdown on LPS-induced p65 activation by immunoblot. The amounts of p65 protein in the

nuclear soluble and nuclear insoluble, but not cytoplasmic, fractions were increased in LPS-stimulated Fbxo16 knockdown cells compared to LPS-stimulated control cells (Figure 6B). The increased nuclear p65 level by Fbxo16 knockdown was quantified using densitometric analysis (Supplementary Figure 6). It is of note that the LPS-induced degradation of IκBα, leading to the nuclear translocation of p65, was normal in Fbxo16 knock down cells, indicating that the increased nuclear p65 by Fbxo16 knockdown was due to impaired p65 degradation in the nucleus. These data suggest that Fbxo16 promotes the degradation of nuclear, but not cytoplasmic, p65 protein and negatively regulates NF-κB-mediated inflammatory responses. We next examined the synergistic effects of Fbxo16 and PDLIM2 on LPS-induced IL-6 expression. We knocked down Fbxo16 and/or PDLIM2 in GM-CSF-BMCs at a suboptimal condition, in which lower amount of siFbxo16 and/or siPDLIM2 was transfected compared to Figure 6A. and examined the expression of IL-6 by real-time PCR analysis. Double knockdown of Fbxo16 and PDLIM2 resulted in augmented production of IL-6 compared to control cells or cells knocked down either Fbxo16 or PDLIM2 (Figure 6C). We also examined the synergistic effect of Fbxo16 and PDLIM2 on p65 degradation in the nucleus. We transfected HEK293T cells with Flag-p65 along with c-Myc-Fbxo16 and/or HA-PDLIM2 in a suboptimal condition, in which lower amounts of Fbxo16 and PDLIM2 were transfected compared to Figures 2B, 4C. Overexpression of either Fbxo16 or PDLIM2 barely reduced p65 levels in the soluble nuclear fraction, whereas the coexpression of Fbxo16 plus PDLIM2 markedly decreased p65 protein. (Figure 6D). To further confirm the role of Fbxo16 in PDLIM2-mediated degradation p65 protein, we transfected HEK293T cells with Flag-p65 together without or with c-Myc-Fbxo16 and examined the p65 protein level in soluble

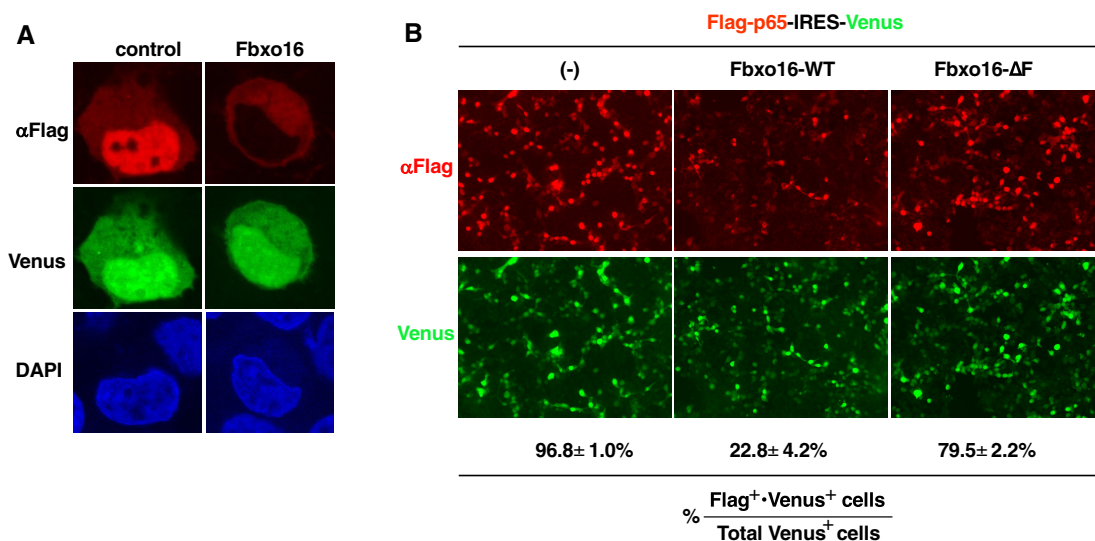


FIGURE 5

Confocal microscopy of F-box-dependent p65 degradation by Fbxo16 (A) Immunofluorescence staining of HEK293T cells transfected with the Flag-p65-IRES-Venus construct without or with c-Myc-Fbxo16 plasmid. Anti-Flag staining (top); Venus expression (middle). The nucleus was stained with DAPI (bottom) (B) Immunofluorescence staining of HEK293T cells transfected with the Flag-p65-IRES-Venus construct without or with c-Myc-wild-type or ΔF Fbxo16 plasmid. Anti-Flag staining (top); Venus expression (bottom). The percentage of Flag⁺•Venus⁺ cells per total Venus⁺ cells was shown. Data are representative of three (A, B) independent experiments.

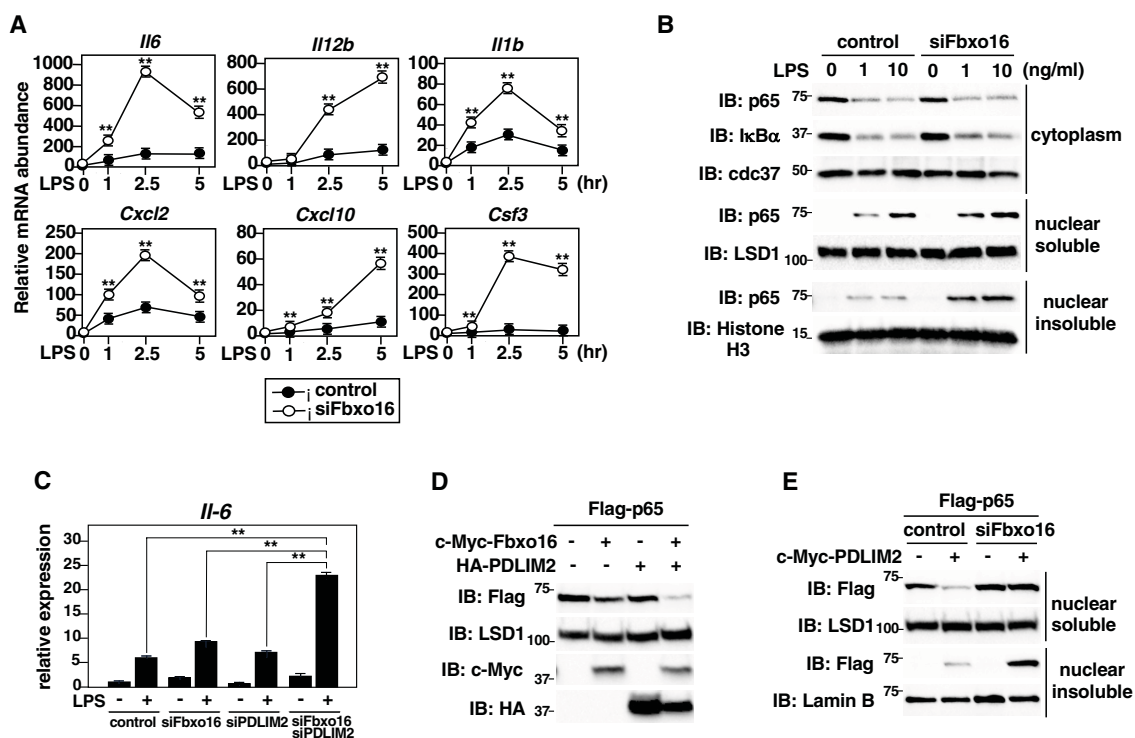


FIGURE 6

NF- κ B-mediated inflammatory responses were enhanced in Fbxo16 deficient dendritic cells. (A) Expression of proinflammatory cytokine genes in GM-CSF-BMCs transfected with control siRNA or Fbxo16 against siRNA, stimulated with LPS (0.1 ng/ml) for 1, 2.5 and 5 hr, and analyzed by real-time PCR. (B) Effect of Fbxo16 deficiency on cytoplasmic and soluble and insoluble nuclear p65 in GM-CSF-BMCs transfected with control siRNA or Fbxo16 against siRNA, then stimulated with 0, 1, or 10 ng/ml of LPS for 1 h and analyzed with indicated antibodies. (C) Effect of Fbxo16 and/or PDLIM2 deficiency on IL-6 expression in GM-CSF-BMCs transfected with control siRNA or siRNA against Fbxo16 and/or PDLIM2, then stimulated with 0 (-) or 0.1 (+) ng/ml of LPS for 2 h and analyzed by real-time PCR. (D) Synergistic effect of Fbxo16 and PDLIM2 expression on soluble nuclear p65 in HEK293T cells transfected with Flag-p65, together with c-Myc-tagged Fbxo16 and/or HA-tagged PDLIM2 in the indicated combination and analyzed by immunoblot with anti-Flag antibody. (E) Effect of Fbxo16 deficiency on soluble and insoluble nuclear p65 in HEK293T cells first transfected with control siRNA or siRNA against Fbxo16, transfected with Flag-p65 without or with c-Myc-PDLIM2 and analyzed by immunoblot with anti-Flag antibody. Data are representative of four (A; means \pm SD, ** P <0.01), three (B), three (C; means \pm SD, ** P <0.01) or three (D, E) independent experiments.

and insoluble nuclear fractions in the absence or presence of siRNA against Fbxo16. Fbxo16 knockdown completely restored the PDLIM2-mediated decrease of soluble nuclear p65 to the original level and led to the accumulation of insoluble nuclear p65 protein (Figure 6E). Taking these data together, we concluded that Fbxo16 and PDLIM2 form a complex and synergistically promotes the intranuclear transport of p65 to the insoluble fraction and its degradation in this compartment, thereby suppressing inflammatory responses.

3.6 Fbxo16 does not promote polyubiquitination and degradation of STAT3/4

We next examined the substrate specificity of Fbxo16. Since PDLIM2 binds to and promote polyubiquitination and degradation of STAT3/4 as well as p65 (9, 12), we first tested if Fbxo16 knockdown affected the ability of PDLIM2 to bind to STAT3/4. We transfected HEK293T cells with Flag-tagged STAT3 or STAT4 and c-Myc-tagged PDLIM2 in the absence or presence of siRNA

against Fbxo16, immunoprecipitated with an anti-c-Myc beads, and immunoblotted with anti-Flag or anti-STAT4 antibody. In contrast to the impaired interaction between p65 and PDLIM2 in Fbxo16 knockdown cells (Figure 2A), Fbxo16 knockdown did not interfere with the binding of PDLIM2 to either STAT3 or STAT4 (Figure 7A, Supplementary Figure 7). We next examined if PDLIM2 promoted polyubiquitination and degradation of STAT3/4. As shown in Figure 7B, Fbxo16 did not lead to the ubiquitination of either STAT3 or STAT4. Moreover, overexpression of PDLIM2, but not Fbxo16, promoted degradation of STAT3 and STAT4, although p65 could be degraded by either Fbxo16 or PDLIM2 (Figure 7C).

3.7 Enhanced p65-mediated inflammatory responses, but normal Th1 and Th17 differentiation in Fbxo16-deficient mice

Finally, to investigate the *in vivo* roles of Fbxo16, we generated Fbxo16-deficient mice by the CRISPR-Cas9 system (Supplementary Figure 1). Since the antibodies that can sufficiently detect endogenous Fbxo16 protein are not available, we analyzed

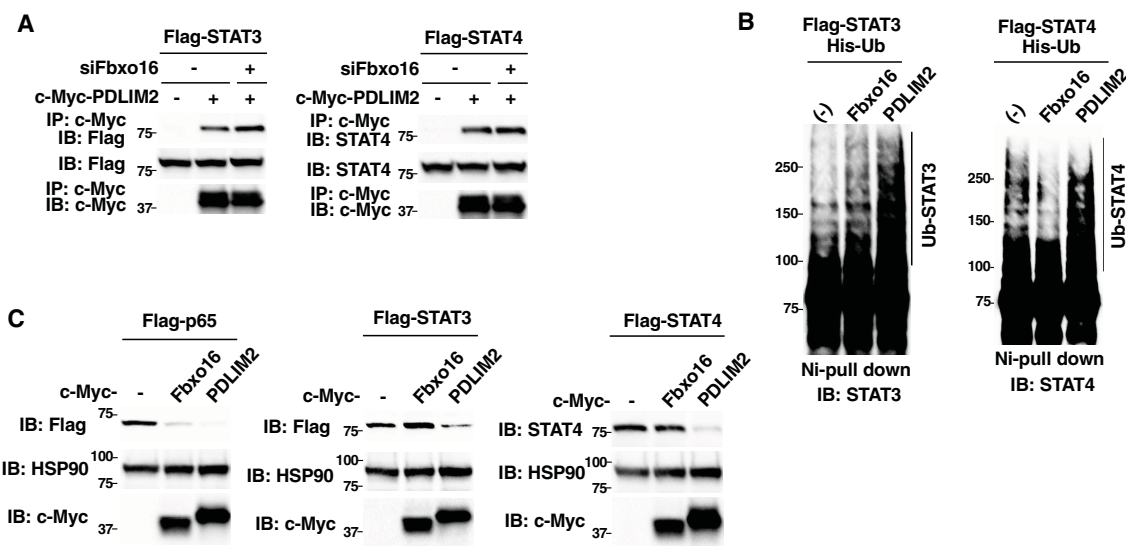


FIGURE 7

Fbxo16 does not promote polyubiquitination and degradation of STAT3/4. (A) Effect of Fbxo16 deficiency on the interaction of PDLIM2 and STAT3 (left) or STAT4 (right) in HEK293T cells, transfected Flag-STAT3 (left) or Flag-STAT4 (right) together without or with c-Myc-PDLIM2, then immunoprecipitated with anti-c-Myc and immunoblotted with anti-Flag (left) or anti-STAT4 (right). (B) Ubiquitination assay of STAT3/4 in 293T cells transfected with His-Ub, Flag-STAT3 (left) or Flag-STAT4 (right) without or with c-Myc Fbxo16 or PDLIM2. The purified ubiquitinated proteins by Ni-NTA beads were analyzed with anti-STAT3 (left) or anti-STAT4 (right) antibodies, respectively. (C) Effect of Fbxo16 or PDLIM2 expression on the degradation of p65 (left), STAT3 (middle) or STAT4 (right) in whole cell lysates of HEK293T cells transfected with Flag-p65 (left), STAT3 (middle) or STAT4 (right) along without or with c-Myc-Fbxo16 or PDLIM2 and analyzed with anti-Flag (left and middle) or anti-STAT4 (right) antibodies. Data are representative of three (A–C) independent experiments.

expression of Fbxo16 mRNA in *Fbxo16*^{-/-} GM-CSF-BMCs and spleen cells by real-time PCR. Compared to *Fbxo16*^{+/+} cells, Fbxo16 mRNA expression was reduced in both *Fbxo16*^{-/-} GM-CSF-BMCs and spleen cells (Figure 8A), which might be ascribed to nonsense-mediated mRNA decay due to the newly generated premature termination codon just after the deleted region (25). Moreover, even if truncated Fbxo16 protein could be expressed at a very low level, it would not be functional because almost the entire region of the F-box domain, which is essential for Fbxo16 activity (Figures 4E–H), is missing due to the CRISPR-Cas9-mediated deletion. We then examined the LPS-induced production of proinflammatory cytokine by *Fbxo16*^{-/-} GM-CSF-BMCs. The LPS-stimulated GM-CSF-BMCs from *Fbxo16*^{-/-} mice produced two- to threefold more IL-6 and IL-12 than the LPS-stimulated *Fbxo16*^{+/+} cells (Figure 8B). We next examined the differentiation of CD4⁺T cells into Th1 and Th17 cells driven by the IL-12-mediated STAT4 or IL-6-mediated STAT3 activation of transcription factors, respectively, and found that both Th1 and Th17 cell differentiation were unaffected in the *Fbxo16*^{-/-} CD4⁺T cells (Figure 8C), suggesting that Fbxo16 specifically regulate p65-dependent NF-κB-signaling in GM-CSF-BMCs, but not STAT3/4-mediated T-helper cell differentiation in CD4⁺T cells. Taking these data together, we propose the model that Fbxo16 functions as a substrate-recognizing receptor for p65 in the PDLIM2-containing CRL1 complex, thereby mediating the degradation of p65 in dendritic cells but does not act as substrate receptor for STAT3/4 in CD4⁺T cells (Figure 8D).

4 Discussion

NF-κB activation is essential for in dendritic cells to induce inflammatory responses and initiate T cell-mediated acquired immune responses. On the other hand, excessive and persistent activation of NF-κB may lead to autoimmune and allergic diseases. Notably, activated NF-κB is detected at the regions of inflammation in these diseases (3). The NF-κB activation should therefore be strictly controlled by negative regulatory systems. Recently, the molecular mechanisms negatively regulating NF-κB signaling have been intensively studied (26, 27). Many factors that suppress various signal transduction molecules, from the receptor on the cell surface to the promoter on the DNA, have already been identified. The ubiquitin-dependent degradation of p65 subunit of NF-κB is one of the most efficient mechanism terminating NF-κB signaling. So far, several ubiquitin E3 ligases for p65 have been reported, including SOCS1 (suppressor of cytokine signaling 1) (28), COMMD1 (COMM domain containing 1) (29), PPARγ (peroxisome proliferator-activated receptor-γ) (30), ING4 (inhibitor of growth protein 4) (31), MKRN2 (makorin ring finger protein 2) (32), RNF182 (RING finger protein 182) (33), RBCK1 (RanBP2-type and C3HC4-type zinc finger-containing 1) (34), TRIM7 (tripartite motif-containing 7) (35) and LRSAM1 (leucine-rich and sterile alpha motif containing 1) (36). PPARγ, TRIM7, LRSAM1, RBCK1 and RNF182 have RING finger domain, whereas ING4 contains a PHD domain, a subtype of the RING domain. Notably, SOCS1 and COMMD1 form a CRL2 complex

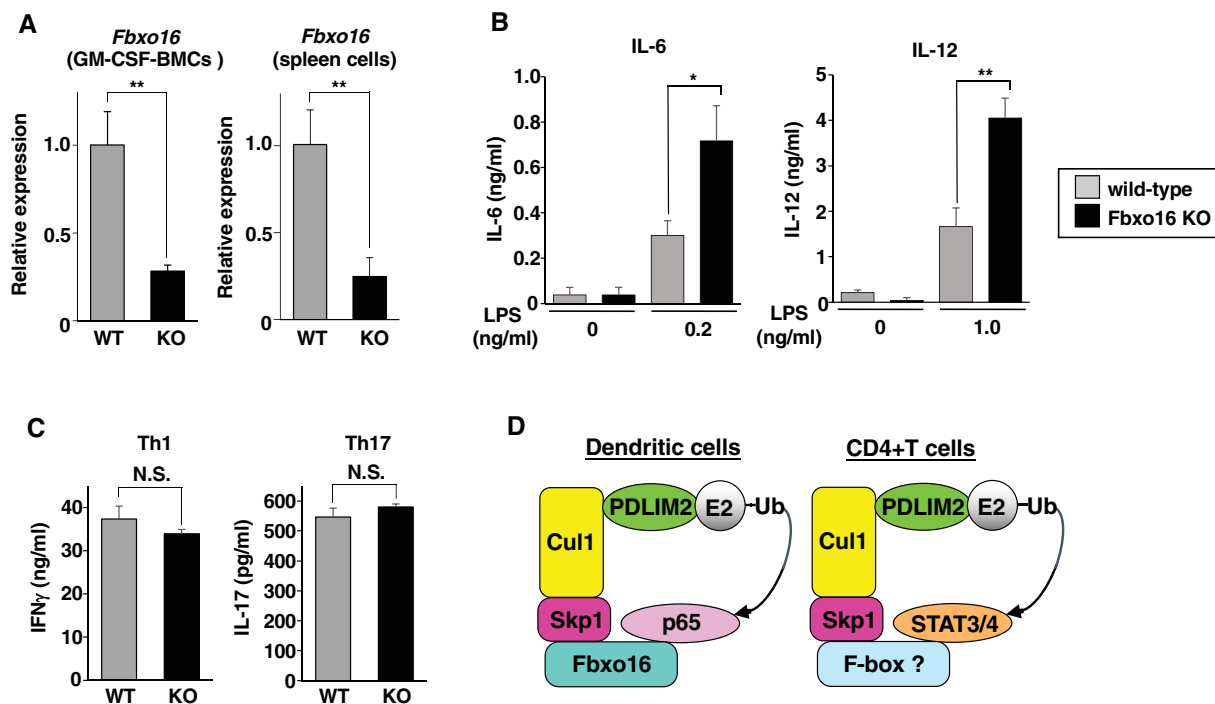


FIGURE 8

Enhanced p65-mediated inflammatory responses, but normal Th1 and Th17 differentiation in Fbxo16-deficient mice. **(A)** Fbxo16 expression in GM-CSF-BMCs and total spleen cells from *Fbxo16*^{+/+} (WT; gray bar) and *Fbxo16*^{-/-} (KO; black bar) mice, analyzed by real-time PCR. **(B)** IL-6 (left) and IL 12 (right) production in culture supernatants of GM-CSF-BMCs from *Fbxo16*^{+/+} and *Fbxo16*^{-/-} mice, stimulated for 24 h with the indicated concentration of LPS and analyzed by ELISA. **(C)** CD4⁺T cells, isolated from the spleen of *Fbxo16*^{+/+} and *Fbxo16*^{-/-} mice, were differentiated under Th1 and Th17-skewing conditions for 4 days and then restimulated with plate-bound anti-CD3 antibody for 24 (h) IFN γ (left) and IL17 (right) production in culture supernatants were analyzed by ELISA. **(D)** The mechanisms by which Fbxo16 in the PDLM2-containing CRL1 complex acts as substrate-recognizing receptor for p65 in dendritic cells, but not for STAT3/4 in CD4⁺T cells. Data are representative of three **(A)**; means \pm SD, **P<0.01), four **(B)**; means \pm SD, *P<0.05, **P<0.01) or three **(C)**; N.S., not significant) independent experiments.

with Cullin 2, Elongin B/C and a RING finger domain-containing protein, Rbx1. In this complex, SOCS1 acts as a substrate-recognizing subunit for p65 and COMMD1 stabilizes the association between SOCS1 and p65 (29).

We have reported for the first time that PDLIM2 is a nuclear ubiquitin E3 ligase mediating polyubiquitination and degradation of the p65 subunit of NF- κ B in the nucleus, thereby negatively regulating inflammatory responses in dendritic cells (11). However, the detailed molecular mechanisms by which PDLIM2 recognizes and polyubiquitinates target proteins remained unclear. In this study, we have demonstrated that PDLIM2 forms a CRL1 complex with Cullin 1 and Skp1 and identified Fbxo16, an F-box protein that belongs to the FBXO subfamily, is the substrate-recognizing subunit of this complex. Fbxo16 binds to all the components of this complex, including Cullin 1, Skp1 and PDLIM2, recruits p65 and then promotes polyubiquitination and degradation of p65 just as PDLIM2 does. Moreover, Fbxo16 deficiency in dendritic cells led to increased nuclear p65 and enhanced TLR-induced production of proinflammatory cytokines, including IL-6 and IL-12, a phenotype identical to PDLIM2-deficient dendritic cells (11). Taking these data together, we concluded that Fbxo16 is the substrate receptor for p65 in PDLIM2-containing CRL1 complex. Notably, this phenotype of Fbxo16 deficiency was evident in GM-CSF BMCs but not in splenic

CD11c+ cells (data not shown). Dendritic cells consist of distinct subsets. The splenic CD11c+ cells are tissue resident DC, whereas GM-CSF BMCs might be equivalent of monocyte-derived DC (inflammatory DC), which can be elicited by infection or inflammation (37). These data suggest that Fbxo16 might be functional in inflammatory DC but not in resident DC. On the other hand, Fbxo16 could not promote polyubiquitination and degradation of either STAT3 or STAT4. Consistently, Fbxo16 deficiency in CD4⁺T cells did not affect IL-6 or IL12-mediated STAT3 or STAT4-dependent Th1 and Th17 cell differentiation, respectively. These data suggest that Fbxo16 is the specific substrate receptor for p65, but not STAT3 or STAT4, in the complex (Figure 8D). We predict that another F-box protein should be responsible for recognizing and recruiting STAT3 and STAT4 in the PDLIM2-containing CRL1 complex, although further study will be needed to clarify this issue.

The LIM domain is thought to be a subtype of a RING finger domain since it is structurally related to a RING finger domain (17). Both the LIM domain and RING finger domains commonly have eight conserved cysteine (Cys) or histidine (His) residues, which are critical for the ubiquitin E3 ligase activity of these domains. We have reported for the first time that the protein containing LIM domain functions as ubiquitin E3 ligase (9). This is clearly evidenced by our result showing that the purified recombinant

PDLIM2 protein synthesized in *E. coli* has autoubiquitination activity *in vitro*, which is a hallmark of ubiquitin E3 ligase activity (9). Moreover, PDLIM2 polyubiquitinates p65 in LIM domain-dependent manner (11). Among a larger LIM protein family, PDLIM2 belongs to a PDZ-LIM protein subfamily that consists of seven members (PDLIM1-7) containing one PDZ domain and one or three LIM domains in the molecule (38). Notably, even though all these PDZ/LIM proteins contain a LIM domain, only PDLIM2, 6 and 7 have ubiquitin ligase activity (15, 39). The RING finger and LIM domains are thought to be an E2 enzyme-recruiting subunit, which facilitates ubiquitin transfer onto the substrate. Although LIM domains of all PDZ/LIM proteins commonly have eight conserved residues of cysteine and histidine, the homology of their amino acid sequence in regions other than in these conserved residues in the LIM domains is relatively low. Possibly due to the structural differences caused by the differences in these amino acid sequences in the LIM domain, only the LIM domains of PDLIM2, 6 and 7 can bind to E2 enzyme and possess ubiquitin E3 ligase activity. Since the LIM domain was originally considered to be protein-protein interaction domain (40), LIM proteins may have different functions depending on the molecules with which they can interact through their LIM domain. In fact, PDLIM4 binds to and recruits protein tyrosine phosphatase through its LIM domain and also binds to STAT3, promoting dephosphorylation of a phosphotyrosine on STAT3, which is essential for its activation, thereby suppressing STAT3-mediated signaling (our unpublished data). Taken together, we hypothesize that not all LIM proteins have ubiquitin E3 ligase activity and a subset of LIM proteins, in which the LIM domain might be highly structurally related to a RING finger domain, should function as ubiquitin E3 ligases.

We have previously reported that PDLIM2 promotes the intranuclear transport of p65 through its PDZ domain and the proteasomal degradation of p65 in the insoluble nuclear compartment through its LIM domain (11). Consistently, a PDZ domain-deletion mutant of PDLIM2 impaired intranuclear transport of p65 but normally polyubiquitinated p65, whereas a LIM domain-deletion mutant of PDLIM2 failed to elicit polyubiquitination and degradation of p65 but could mediate intranuclear transport of p65 to insoluble nuclear compartments. In this study, we have demonstrated that either Fbxo16 knockdown or deletion of its F-box domain not only led to the accumulation of p65 in the insoluble nuclear fraction but also completely restored the PDLIM2-mediated decrease of p65 in the soluble nuclear fraction (Figures 4G, 6E). This can be ascribed to both impaired intranuclear transport of p65 and insufficient p65 degradation in the insoluble nuclear fraction. In contrast, in our previous study, the knockdown of either HSP70 or BAG1 led to the increased p65 protein in the insoluble nuclear fraction but could not restore the PDLIM2-mediated decrease of p65 in the soluble nuclear fraction (14), suggesting that only p65 degradation in the insoluble nuclear compartment was impaired by these knockdowns. This is probably because both HSP70 and BAG1 are essential for facilitating the association of the p65-PDLIM2 complex with the proteasome leading to the degradation of p65 but are not required for the intranuclear transport of p65 to the insoluble nuclear

compartments. Considering that CRL1 complex formation was disrupted by either Fbxo16 knockdown or deletion of the F-box domain from Fbxo16 (Figures 2A, 4E), the complex formation itself might be critical for the PDLIM2-mediated intranuclear transport.

So far, 69 human and 79 murine F-box proteins have been reported (21, 22). These F-box proteins commonly bind to Cullin 1 or Cullin 7 through their F-box domain and should function as substrate-recognizing subunits in the CRL1 or CRL7 complex (19, 20). F-box proteins exert a variety of functions depending on the substrates that they bind to and recruit to the complex. The substrates for many, but not all, F-box proteins have been identified and most of them were found to be the cell cycle regulators or oncogenes, so that the deficiency of these F-box proteins in human and mice enhanced cell proliferation leading to tumorigenesis (41). In contrast, only several F-box proteins, including Fbxw1, Fbxl2, Fbxo6 and Fbxo38 (42–45), have been reported to be involved in the immune regulation. Regarding Fbxo16, previous reports showed that it mediates polyubiquitination and degradation of β -catenin and heterogeneous nuclear ribonucleoprotein L (hnRNPL), both of which regulate signaling pathways leading to cell proliferation and tumor progression (46–48). Forced expression of Fbxo16 in tumor cell lines inhibited cell growth, whereas knockdown of Fbxo16 in these cells resulted in increased β -catenin and hnRNPL protein levels and enhanced tumor cell proliferation. Notably, the association of higher Fbxo16 expression with better prognosis in cancer patients and the attenuated Fbxo16 expression in higher-grade cancer samples were observed in a human cancer database (47, 48). These data suggest that Fbxo16 acts as a tumor suppressor by inhibiting the activity of β -catenin and hnRNPL. However, the role of Fbxo16 in the immune system remained completely unknown. Here we have demonstrated that Fbxo16 is essential for terminating NF- κ B-mediated inflammatory responses by promoting polyubiquitination and degradation of the p65 subunit of NF- κ B as the substrate-recognizing receptor for p65 in the PDLIM2-containing CRL1 complex. This is the first report showing that Fbxo16 can regulate signaling pathway in the immune system. Notably, aberrant and persistent activation of NF- κ B may promote tumor progression (49), so that the activity of Fbxo16 to inhibit NF- κ B activation, which we demonstrated in this study, might be related to the tumor suppressive function of Fbxo16 described above. Fbxo16 could therefore act as the substrate-recognizing receptor for several proteins involved in cell proliferation, including β -catenin, hnRNPL and NF- κ B p65, promotes their degradation and prevents cancer progression (46–48). A recent report showed that Fbxw2 also promotes polyubiquitination and degradation of p65 (50). Although this report did not analyze the complex formation and its role in the immune system, Fbxw2 may be another substrate-recognizing receptor for p65 in the CRL1 complex, thereby regulating NF- κ B-mediated inflammatory responses in dendritic cells.

Persistent activation of NF- κ B is detected at regions of inflammation in certain human diseases, such as inflammatory bowel diseases and rheumatoid arthritis (3, 4). We found that Fbx16 expression in dendritic cells was suppressed by inflammatory stimuli, such as LPS or CpG DNA (Supplementary Figure 8). This attenuated Fbxo16 expression under inflammatory condition may contribute to

constitutive NF- κ B activation leading to inflammatory diseases. We therefore speculate that Fbxo16-deficiency in humans may cause autoimmune diseases and that the Fbxo16/PDLIM2-mediated pathway to terminate NF- κ B activation could be the molecular tool for the development of the new therapy of these diseases.

Data availability statement

The original contributions presented in the study are included in the article/**Supplementary Material**. Further inquiries can be directed to the corresponding author.

Ethics statement

Ethical approval was not required for the studies on humans in accordance with the local legislation and institutional requirements because only commercially available established cell lines were used. The animal study was approved by the Institutional Animal Care and Use Committee (IACUC) of RIKEN Yokohama Branch. The study was conducted in accordance with the local legislation and institutional requirements.

Author contributions

AS-I: Investigation, Writing – review & editing. AJ: Investigation, Writing – review & editing. TT: Conceptualization, Investigation, Writing – original draft, Writing – review & editing.

Funding

The author(s) declare that financial support was received for the research and/or publication of this article. This work was supported by Naito Foundation (TT) and Japan Science and Technology Agency Precursory Research for Embryonic Science and Technology (PRESTO; to TT).

References

- Carroll SL, Pasare C, Barton GM. Control of adaptive immunity by pattern recognition receptors. *Immunity*. (2024) 57:632–48. doi: 10.1016/j.immuni.2024.03.014
- Kawai T, Ikegawa M, Ori D, Akira S. Decoding Toll-like receptors: Recent insights and perspectives in innate immunity. *Immunity*. (2024) 57:649–73. doi: 10.1016/j.immuni.2024.03.004
- Herrington FD, Carmody RJ, Goodyear CS. Modulation of NF- κ B signaling as a therapeutic target in autoimmunity. *J Biomol Screen*. (2016) 21:223–42. doi: 10.1177/1087057115617456
- Balendran T, Lim K, Hamilton JA, Achuthan AA. Targeting transcription factors for therapeutic benefit in rheumatoid arthritis. *Front Immunol*. (2023) 14:1196931. doi: 10.3389/fimmu.2023.1196931
- Plenge RM, Cotsapas C, Davies L, Price AL, de Bakker PI, Maller J, et al. Two independent alleles at 6q23 associated with risk of rheumatoid arthritis. *Nat Genet*. (2007) 39:1477–82. doi: 10.1038/ng.2007.27
- Cleynen I, Vazeille E, Artieda M, Verspaget HW, Szczypiorska M, Bringer MA, et al. Genetic and microbial factors modulating the ubiquitin proteasome system in inflammatory bowel disease. *Gut*. (2014) 63:1265–74. doi: 10.1136/gutjnl-2012-303205
- Balaci I, Spada MC, Olla N, Sole G, Loddo L, Anedda F, et al. IRAK-M is involved in the pathogenesis of early-onset persistent asthma. *Am J Hum Genet*. (2007) 80:1103–14. doi: 10.1086/518259
- Torrado M, Senatorov VV, Trivedi R, Fariss RN, Tomarev SI. Pdlim2, a novel PDZ-LIM domain protein, interacts with α -actinins and filamin A. *Invest Ophthalmol Vis Sci*. (2004) 45:3955–63. doi: 10.1167/iovs.04-0721
- Tanaka T, Soriano MA, Grusby MJ. SLIM is a nuclear ubiquitin E3 ligase that negatively regulates STAT signaling. *Immunity*. (2005) 22:729–36. doi: 10.1016/j.immuni.2005.04.008

Acknowledgments

We thank S. Kato, A. Iyama and S. Noguchi for secretarial assistance, A. Onuma for initial analysis of Fbxo16 function and design of Fbxo16 deficient mice, and P. Burrows for critical reviewing of the manuscript. c-Myc-tagged PDLIM2 expression plasmids and their mutants were provided by M. Grusby (Harvard School of Public Health); The ELAM-1 luciferase reporter construct was provided by D. Golenbock (University of Massachusetts Medical Center).

Conflict of interests

The authors declare that the research was conducted in the absence of any commercial or financial relationships that could be construed as a potential conflict of interest.

Generative AI statement

The author(s) declare that no Generative AI was used in the creation of this manuscript.

Publisher's note

All claims expressed in this article are solely those of the authors and do not necessarily represent those of their affiliated organizations, or those of the publisher, the editors and the reviewers. Any product that may be evaluated in this article, or claim that may be made by its manufacturer, is not guaranteed or endorsed by the publisher.

Supplementary material

The Supplementary Material for this article can be found online at: <https://www.frontiersin.org/articles/10.3389/fimmu.2025.1524110/full#supplementary-material>

10. Loughran G, Healy NC, Kiely PA, Huigsloot M, Kedersha NL, O'Connor R. Mystique is a new insulin-like growth factor-I-regulated PDZ-LIM domain protein that promotes cell attachment and migration and suppresses Anchorage-independent growth. *Mol Biol Cell*. (2005) 16:1811–22. doi: 10.1091/mbc.e04-12-1052
11. Tanaka T, Grusby MJ, Kaisho T. PDLIM2-mediated termination of transcription factor NF- κ B activation by intranuclear sequestration and degradation of the p65 subunit. *Nat Immunol*. (2007) 8:584–91. doi: 10.1038/ni1464
12. Tanaka T, Yamamoto Y, Muromoto R, Ikeda O, Sekine Y, Grusby MJ, et al. PDLIM2 inhibits T Helper 17 cell development and granulomatous inflammation through degradation of STAT3. *Sci Signal*. (2011) 4:ra85. doi: 10.1126/scisignal.2001637
13. Qu Z, Fu J, Ma H, Zhou J, Jin M, Mapara MY, et al. PDLIM2 restricts Th1 and Th17 differentiation and prevents autoimmune disease. *Cell Biosci*. (2012) 2:23. doi: 10.1186/2045-3701-2-23
14. Tanaka T, Shibazaki A, Ono R, Kaisho T. HSP70 is required for PDLIM2-mediated degradation of the p65 subunit of NF- κ B to negatively regulate NF- κ B signaling. *Sci Signal*. (2014) 7:ra119. doi: 10.1126/scisignal.2005533
15. Jodo A, Shibazaki A, Onuma A, Kaisho T, Tanaka T. PDLIM7 synergizes with PDLIM2 and p62/Sqstm1 to inhibit inflammatory signaling by promoting degradation of the p65 subunit of NF- κ B. *Front Immunol*. (2020) 11:1559. doi: 10.3389/fimmu.2020.01559
16. Deshaies RJ, Joazeiro CA. RING domain E3 ubiquitin ligases. *Annu Rev Biochem*. (2009) 78:399–434. doi: 10.1146/annurev.biochem.78.101807.093809
17. Capili AD, Schultz DC, Rauscher III FJ, Borden KL. Solution structure of the PHD domain from the KAP-1 corepressor: structural determinants for PHD, RING and LIM zinc-binding domains. *EMBO J*. (2001) 15:165–77. doi: 10.1093/emboj/20.1.165
18. Metzger MB, Pruneda JN, Kleit RE, Weissman AM. RING-type E3 ligases: master manipulators of E2 ubiquitin-conjugating enzymes and ubiquitination. *Biochim Biophys Acta*. (2014) 843:47–60. doi: 10.1016/j.bbamcr.2013.05.026
19. Sarikas A, Hartmann T, Pan ZQ. The cullin protein family. *Genome Biol*. (2011) 12:220. doi: 10.1186/gb-2011-12-4-220
20. Zhou W, Wei W, Sun Y. Genetically engineered mouse models for functional studies of SKP1-CUL1-F-box-protein (SCF) E3 ubiquitin ligase. *Cell Res*. (2013) 23:599–619. doi: 10.1038/cr.2013.44
21. Jin J, Cardozo T, Lovering RC, Elledge SJ, Pagano M, Harper JW. Systematic analysis and nomenclature of mammalian F-box. *Genes Dev*. (2004) 18:2573–80. doi: 10.1101/gad.1255304
22. Skaar JR, Pagan JK, Pagano M. Mechanisms and function of substrate recruitment by F-box proteins. *Nat Rev Mol Cell Biol*. (2013) 14:3690381. doi: 10.1038/nrm3582
23. Delude RL, Yoshimura A, Ingalls RR, Golenbock DT. Construction of a lipopolysaccharide reporter cell line and its use in identifying mutants defective in endotoxin, but not TNF- α , signal transduction. *J Immunol*. (1998) 16:3001–9. doi: 10.4049/jimmunol.161.6.3001
24. Campanero MR, Flemington EK. Regulation of E2F through ubiquitin-proteasome-dependent degradation: stabilization by the pRB tumor suppressor protein. *Proc Natl Acad USA*. (1997) 94:2221–6. doi: 10.1073/pnas.94.6.2221
25. Popp MW, Maquat LE. Leveraging rules of nonsense-mediated mRNA decay for genome engineering and personalized medicine. *Cell*. (2016) 165:1319–22. doi: 10.1016/j.cell.2016.05.053
26. Kondo T, Kawai T, Akira S. Dissecting negative regulation of Toll-like receptor signaling. *Trends Immunol*. (2012) 33:449–58. doi: 10.1016/j.it.2012.05.002
27. Prescott JA, Mitchell JP, Cook SJ. Inhibitory feedback control of NF- κ B signaling in health and disease. *Biochem J*. (2021) 478:2619–64. doi: 10.1042/BCJ20210139
28. Ryo A, Suizu F, Yoshida Y, Perrem K, Liou YC, Wulf G, et al. Regulation of NF- κ B signaling by Pin1-dependent prolyl isomerization and ubiquitin-mediated proteolysis of p65/RelA. *Mol Cell*. (2003) 12:1413–26. doi: 10.1016/s1097-2765(03)00490-8
29. Maine GN, Mao X, Komarck CM, Burstein E. COMMD1 promotes the ubiquitination of NF- κ B subunits through a cullin-containing ubiquitin ligase. *EMBO J*. (2007) 26:436–47. doi: 10.1038/sj.emboj.7601489
30. Hou Y, Moreau F, Chadee K. PPAR γ is an E3 ligase that induces the degradation of NF- κ B/p65. *Nat Commun*. (2012) 3:1300. doi: 10.1038/ncomms2270
31. Hou Y, Zhang Z, Xu Q, Wang H, Xu Y, Chen K. Inhibitor of growth 4 induces NF- κ B/p65 ubiquitin-dependent degradation. *Oncogene*. (2014) 33:1997–2003. doi: 10.1038/ncr.2013.135
32. Shin C, Ito Y, Ichikawa S, Tokunaga M, Sakata-Sogawa K, Tanaka T. MKRN2 is a novel ubiquitin E3 ligase for the p65 subunit of NF- κ B and negatively regulates inflammatory responses. *Sci Rep*. (2017) 7:46097. doi: 10.1038/srep46097
33. Cao Y, Sun Y, Chang H, Sun X, Yang S. The E3 ubiquitin ligase RNF182 inhibits TLR-triggered cytokine production through promoting p65 ubiquitination and degradation. *FEBS letter*. (2019) 593:3210–9. doi: 10.1002/1873-3468.13583
34. Cong M, Wang Y, Yang Y, Lian C, Zhuang X, Li X, et al. MTSS1 suppresses mammary tumor-initiating cells by enhancing RBCK1-mediated p65 ubiquitination. *Nat Cancer*. (2020) 1:222–34. doi: 10.1038/s43018-019-0021-y
35. Jin J, Lu Z, Wang X, Liu Y, Han T, Wang Y, et al. E3 ubiquitin ligase TRIM7 negatively regulates NF-kappa B signaling pathway by degrading p65 in lung cancer. *Cell Signal*. (2020) 69:109543. doi: 10.1016/j.cellsig.2020.109543
36. Lin X, Tian X, Jiang H, Li W, Wang C, Wu J, et al. Carpine alleviates tendinopathy in mice by promoting the ubiquitin-proteasomal degradation of p65 via targeting the E3 ubiquitin ligase LRSAM1. *Phytomedicine*. (2024) 124:155323. doi: 10.1016/j.phymed.2023.155323
37. Serbina NV, Salazar-Mather TP, Biron CA, Kuziel WA, Pamer EG. TNF/ α /iNOS-producing dendritic cells mediate innate immune defense against bacterial infection. *Immunity*. (2003) 19:59–70. doi: 10.1016/s1074-7613(03)00171-7
38. Te Velthuis AJ, Bagowski CP. PDZ and LIM domain-encoding genes: molecular interactions and their role in development. *ScientificWorldJournal*. (2007) 7:1470–92. doi: 10.1100/tsw.2007.232
39. Ono R, Kaisho T, Tanaka T. PDLIM1 inhibits NF- κ B-mediated inflammatory signaling by sequestering the p65 subunit of NF- κ B in the cytoplasm. *Sci Rep*. (2015) 5:18327. doi: 10.1038/srep18327
40. Bach I. The LIM domain: regulation by association. *Mech Dev*. (2000) 91:5–17. doi: 10.1016/s0925-4773(99)00314-7
41. Zheng N, Zhou Q, Wang Z, Wei W. Recent advances in SCF ubiquitin ligase complex: Clinical implications. *Biochim Biophys Acta*. (2016) 1866:12–22. doi: 10.1016/j.bbcan.2016.05.001
42. Yaron A, Hatzubai A, Davis M, Lavon I, Amit S, Manning AM, et al. Identification of the receptor component of the IkB α -ubiquitin ligase. *Nature*. (1998) 396:590–4. doi: 10.1038/25159
43. Chen BB, Coon TA, Glasser JR, McVerry BJ, Zhao J, Zhao Y, et al. A combinatorial F box protein directed pathway controls TRAF adaptor stability to regulate inflammation. *Nat Immunol*. (2013) 14:470–9. doi: 10.1038/ni.2565
44. Du X, Meng F, Peng D, Wang Z, Ouyang W, Han Y, et al. Noncanonical role of FBXO6 in regulating antiviral immunity. *J Immunol*. (2019) 203:1012–20. doi: 10.4049/jimmunol.1801557
45. Meng X, Liu X, Guo X, Jiang S, Chen T, Hu Z, et al. FBXO38 mediates PD-1 ubiquitination and regulates anti-tumor immunity of T cells. *Nature*. (2018) 564:130–5. doi: 10.1038/s41586-018-0756-0
46. Khan M, Muzumdar D, Shiras A. Attenuation of tumor suppressive function of FBXO16 ubiquitin ligase activates Wnt signaling in glioblastoma. *Neoplasia*. (2019) 21:106–16. doi: 10.1016/j.neo.2018.11.005
47. Paul D, Islam S, Manne RK, Dinesh US, Malonia SK, Maity B, et al. F-box protein FBXO16 functions as a tumor suppressor by attenuating nuclear beta-catenin function. *J Pathol*. (2019) 248:266–79. doi: 10.1002/path.5252
48. Ji M, Zhao Z, Li Y, Xu P, Shi J, Li Z, et al. FBXO16-mediated hnRNPL ubiquitination and degradation plays a tumor suppressor role in ovarian cancer. *Cell Death Dis*. (2021) 12:758. doi: 10.1038/s41419-021-04040-9
49. Taniguchi K, Karin M. NF- κ B, inflammation, immunity and cancer: coming of age. *Nat Rev Immunol*. (2018) 18:309–24. doi: 10.1038/nri.2017.142
50. Ren C, Han X, Lu C, Yang T, Qiao P, Sun Y, et al. Ubiquitination of NF- κ B p65 by FBXW2 suppresses breast cancer stemness, tumorigenesis, and paclitaxel resistance. *Cell Death Differ*. (2022) 29:381–92. doi: 10.1038/s41418-021-00862-4

Frontiers in Immunology

Explores novel approaches and diagnoses to treat immune disorders.

The official journal of the International Union of Immunological Societies (IUIS) and the most cited in its field, leading the way for research across basic, translational and clinical immunology.

Discover the latest Research Topics

[See more →](#)

Frontiers

Avenue du Tribunal-Fédéral 34
1005 Lausanne, Switzerland
frontiersin.org

Contact us

+41 (0)21 510 17 00
frontiersin.org/about/contact

